NASA CR145070

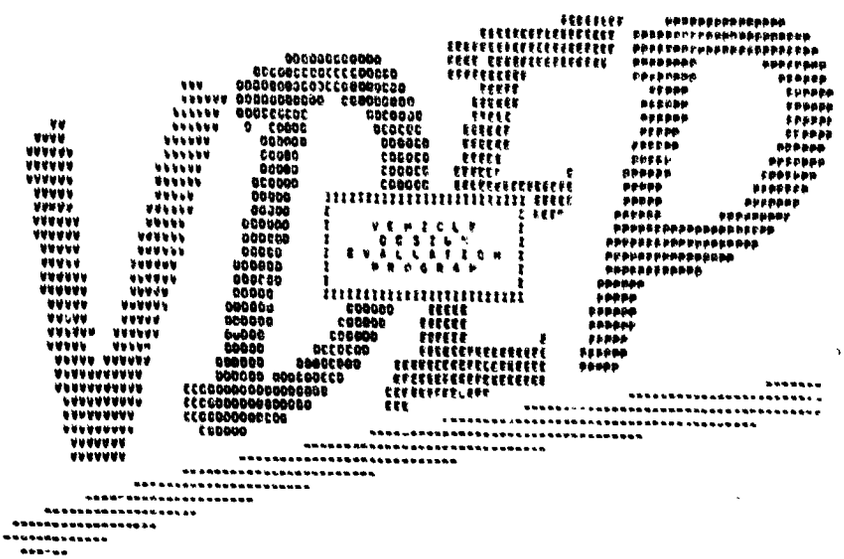

VEHICLE DESIGN EVALUATION PROGRAM

TECHNICAL REPORT

A COMPUTER PROGRAM FOR WEIGHT SIZING, ECONOMIC, PERFORMANCE & MISSION ANALYSIS OF FUEL-CONSERVATIVE AIRCRAFT, MULTIBODIED AIRCRAFT & LARGE CARGO AIRCRAFT USING BOTH JP & ALTERNATIVE FUELS

GENERAL DYNAMICS
Convair Division

NASA CR145070

VEHICLE DESIGN EVALUATION PROGRAM

TECHNICAL REPORT

A COMPUTER PROGRAM FOR WEIGHT SIZING, ECONOMIC, PERFORMANCE & MISSION ANALYSIS OF FUEL-CONSERVATIVE AIRCRAFT, MULTIBODIED AIRCRAFT & LARGE CARGO AIRCRAFT USING BOTH JP & ALTERNATIVE FUELS

B. H. Oman

January 1977

Submitted to

NASA

National Aeronautics and
Space Administration
LANGLEY RESEARCH CENTER
Hampton, Virginia 23665

Prepared Under
Contract NAS1-13285

Prepared by
GENERAL DYNAMICS CONVAIR DIVISION
P.O. Box 80847
San Diego, California 92138

FOREWORD

This report documents the results of a Research and Development study performed under the NASA Contract NAS1-13285. The contract, titled "Computer Program for Weight Sizing, Economic, Performance and Mission Analysis of Fuel-Conservative Aircraft, Multibodied Aircraft and Large Cargo Aircraft Using Both JP and Alternative Fuels", was sponsored by the NASA Langley Research Center with Mr. Owen Schrader as the NASA Project Manager.

The work was accomplished by the Weight/Cost Analysis group of General Dynamics Convair Division, San Diego, California. The Program Manager was B. H. Oman under the administration of Mr. G. V. Smith, Chief of Weight/Cost Analysis, R. E. Martin, Manager of Structures Technology, and J. D. Forest, Director of Structures and Design. Principal contributors to the studies conducted under this contract and the preparation of this report include: W. E. Caddell and W. D. Honeycutt, Mass Properties Analysis; S. K. Pederson and R. J. Bulinski, Mission and Performance Analysis; G. S. Kruse and C. J. Tanner, Structural Analysis; T. F. Reed, G. S. Kruse and S. T. Hitchcock, Part Definition Methodology Development; R. E. Kenyon and J. M. Youngs, Economic Analysis; T. F. Reed and A. R. Stone, Computer Program Development and Implementation.

TABLE OF CONTENTS

TABLE OF CONTENTS (Contd)

TABLE OF CONTENTS (Contd)

TABLE OF CONTENTS (Contd)

TABLE OF CONTENTS (Contd)

LIST OF FIGURES

LIST OF FIGURES (Contd)

LIST OF FIGURES (Contd)

LIST OF FIGURES (Contd)

LIST OF FIGURES (Contd)

LIST OF TABLES

LIST OF TABLES (Contd)

SUMMARY

This report presents the results of a Research and Development Study performed under NASA Contract NAS1-13285. The objective of this study was to expand the capability of the existing NASA Langley Research Center Vehicle Design Evaluation Program (VDEP-II) developed under NASA Contract NAS1-12506 (See Note 1). The three major areas of expansion were: 1) incorporation into the program of a capability to conduct preliminary design studies on subsonic commercial transport type aircraft using both JP and such alternate fuels as hydrogen and methane; 2) incorporation of an aircraft detailed mission and performance analysis capability; and 3) development and incorporation of an external loads analysis capability. The resulting Vehicle Design Evaluation Program (VDEP-III) provides a preliminary design tool that enables the user to perform integrated sizing, structural analysis, and cost trade studies on subsonic commercial transport aircraft. There are two versions of the VDEP-III Program which are designated "Preliminary Analysis VDEP-III" and "Detailed Analysis VDEP-III". Both versions utilize the same vehicle sizing subprogram which includes a detailed mission analysis capability, as well as a geometry and weight analysis for multi-bodied configurations.

The preliminary analysis VDEP-III consists of the vehicle sizing subprogram and a cost analysis subprogram. The vehicle sizing subprogram provides geometry, weight, and balance analysis for aircraft using JP, hydrogen or methane fuels. It has an option of providing first pass performance data or conducting a detailed mission and performance analysis. A mass distribution and moment of inertia analysis is also provided. The cost analysis subprogram integrates first unit manufacturing costs based on Cost Estimating Relationships (CERs), total program costs that includes tooling and engineering, and a return-on-investment analysis based on route structures. The preliminary design VDEP-III program is designed to evaluate and provide trade study data for fuel conservative aircraft, multi-bodied aircraft, and large cargo aircraft using both JP and cryogenic fuels.

The detailed analysis VDEP-III consists of the vehicle sizing subprogram, the external loads subprogram, the structural analysis subprogram, the detail parts subprogram, and the cost analysis subprogram. The vehicle sizing subprogram is the same as that used in the preliminary analysis VDEP-III described in the previous paragraph. The external loads subprogram provides a method for development of steady state load distribution on preliminary aircraft components for specified airplane weights and load factors. The structural synthesis subprogram utilizes a multi-station analysis for aerodynamic surfaces and fuselages to develop theoretical weights and geometric dimensions. The parts definition subprogram utilizes the geometric data from the structural analysis and develops the predicted fabrication dimensions, parts, material raw stock buy requirements and the predicted actual weights. The cost analysis subprogram utilizes detail part data in conjunction with standard hours, realization factors, labor rates, and

---

1 "Computer Program to Assess Impact of Fatigue and Fracture criteria on Weight and Cost of Transport Aircraft," (NAS1-12506) NASA CR 132648, June 1975.

material data to develop the manufacturing costs. The detail cost analysis integrates the detail part developed manufacturing cost with the total program costs, which includes tooling, engineering, and return-on-investment based on airline route structures to provide a complete cost analysis capability.

The computer programs have been written in FORTRAN IV and are designed for use on the CDC 6000 series computers. Several test cases, using data for existing aircraft, were run to check the program results against actual data. It was shown that the program represents an accurate and useful tool for estimating purposes at the preliminary design stage of airframe development. A sample case along with an explanation of program applications and input preparations is presented in the User's Manual.

Table 1 is a summary of the preliminary analysis program version functional capability and Figure 1 is a preliminary analysis program block diagram. Table 2 is a summary of the detail analysis program version functional capability and Figure 2 is a detail analysis program block diagram.

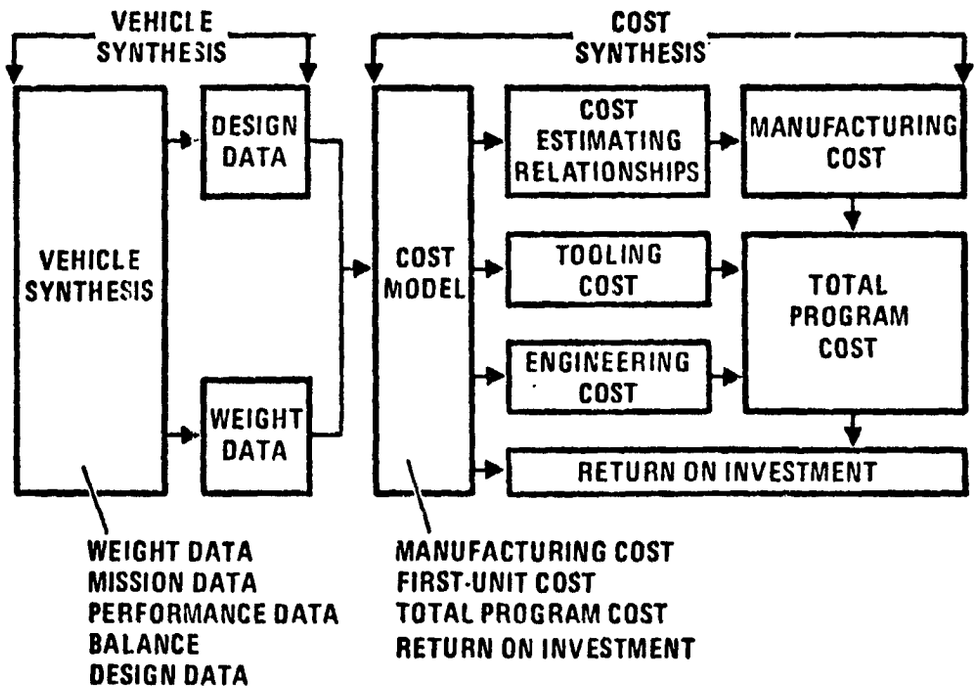

Figure 1. Vehicle Design and Evaluation Program (Preliminary Analysis Version) (VDEP-III) Block Diagram

Table 1. Summary of the Preliminary Analysis Program Version Functional Capability

VEHICLE SYNTHESIS (SIZING)	TOOLING COSTS
AIRCRAFT BALANCE	TOTAL VEHICLE PROGRAM COSTS
MANUFACTURING COST	AIRLINE ROUTE ANALYSIS
ENGINEERING COST	RETURN-ON-INVESTMENT

Table 2. Summary of the Detail Analysis Program Version Functional Capability

VEHICLE SYNTHESIS (SIZING)	MATERIAL COSTS
AIRCRAFT BALANCE	ENGINEERING COSTS
EXTERNAL LOADS	TOOLING COSTS
STRUCTURAL SYNTHESIS	TOTAL VEHICLE PROGRAM COSTS
DETAIL PART DEFINITION	AIRLINE ROUTE ANALYSIS
MANUFACTURING COSTS	RETURN-ON-INVESTMENT

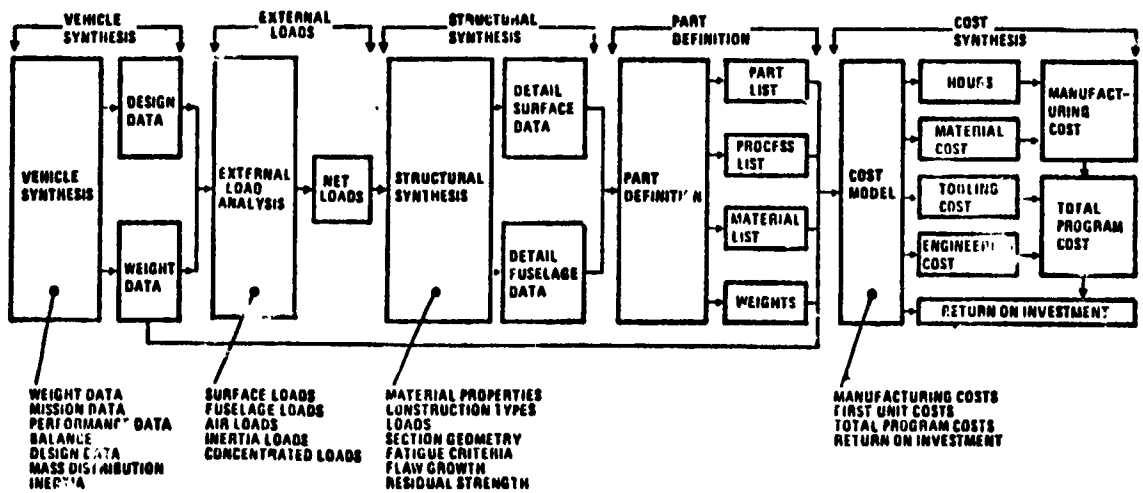

Figure 2. Vehicle Design and Evaluation Program (Detail Analysis Version) (VDEP-II) Block Diagram

SECTION 1

INTRODUCTION

This report presents the results of a research and development study performed under Contract NAS1-13285. The objective of the study was to develop a "Computer Program for Weight Sizing, Economic, Performance and Mission Analysis of Fuel Conservative Aircraft, Multi-Bodied Aircraft and Large Cargo Aircraft Using Both JP and Alternate Fuels".

Its intended use is as a preliminary design analysis tool to enable the user to perform trade-off studies involving subsonic commercial transport type aircraft using both JP and such alternate fuels as hydrogen and methane.

The starting point of the present effort was a computer program developed under NASA Contract NAS2-5718, "Estimation of Airframe Manufacturing Costs", (See Note 1). This program was modified and expanded in a study that analyzed manufacturing and material cost, engineering costs, tooling costs, total vehicle program costs, direct operating costs, airline route analysis, and return-on-investment under NASA Contract NAS1-11343, (See Note 2). A follow-on development expanded the structural synthesis to include a capability to assess the impact of fatigue and fracture criteria in terms of fatigue life, crack growth life and residual strength.

The current study provides an expanded version of the existing vehicle sizing subprogram that incorporated the Combat Aircraft Synthesis Program (See Note 3). The expansion included modifications to account for liquid hydrogen and liquid methane fueled aircraft and multi-bodied configurations. It also included modifications which accounts for mission segments appropriate for transport operations and the generation of propulsion routine engine data for cryogenic fueled systems. This study also includes the development and incorporation of an external loads analysis. The external loads provides an interface between the vehicle sizing subprogram and the structural synthesis subprogram that accounts for changes in external loads associated with vehicle sizing variations.

The detail version of the program generates weight data in four areas. Overall vehicle system weights are derived on a statistical basis as part of the vehicle sizing process.

---

[1] Trelease, R. H., et al, "Estimation of Airframe Manufacturing Costs," Convair Aerospace Report GDCA-BJF71-918, July 1972.

[2] "Computer Program to Perform Cost and Weight Analysis of Transport Aircraft," (NAS1-11343) NASA CR 132362, November 1973.

[3] Bulinski, R. J., "Combat Aircraft Synthesis," General Dynamics Convair Report GDC-ERR-1563, December 1970.

Theoretical weights, actual weights, and the weight of the raw material to be purchased are derived as part of the structural synthesis and part defintion processes based on the computed part geometry. The manufacturing cost analysis, based at the individual detail part level, is made by considering the actual manufacturing operations required to produce that part. A list of shop operations is called out with each detail part, and a series of equations associated with each operation is used to compute the shop hours necessary to make the part. By applying the appropriate labor rates to the calculated hours, the dire and indirect manufacturing labor costs are found. Material costs are computed based or the amount of material required to manufacture each part.

In the short version of the program the vehicle sizing was integrated with the cost estimating relationship (CER) program for the major structural components and subsystems as opposed to the more detail parts definition method. Specifically, the nonrecurring RDT&E portion of the program cost model was modified in the area of initial engineering associated with airframe development. Cost Estimating Relationships (CERs) have been developed to provide a means for generating a theoretical first unit cost for any specific aircraft configuration under study during the preliminary design stage.

Tooling costs are computed as a function of the number of basic tool manufacturing hours, initial sustaining aircraft production rates, and tooling labor rates. Basic tool manufacturing hours are derived as a function of the number of dissimilar parts to be produced, the average number of tools required per dissimilar part, and the average number of hours required to produce each tool.

Total vehicle program costs are computed based on a cost model that was assembled primarily from the work of R. E. Kenyon of General Dynamics/Convair Division (See Note 1). Cost elements that are computed elsewhere in the program are brought across and substituted into the model. A learning-curve approach is utilized to derive costs of a given unit or lot as a function of the first unit cost.

A comprehensive measure of the total economic viability for a commercial transport operation is reflected in the return-on-investment analysis. Direct operating costs are computed using the 1967 Air Transport Association formula updated to 1972 cost levels. Indirect operating costs and return-on-investment are computed by applying aircraft acquisition and direct operating costs to a defined traffic structure. Output includes direct operating costs, indirect operating costs, revenue, load factors, profit, return-on-investment, and fleet size.

These programs provide the user with a Cost Estimating Relationship (CER) method for conducting initial studies, with an option to use the detail method for more in-depth analysis. One advantage provided by the method developed is the capability to make

[1]Kenyon, R. E., "Techniques for Estimating Weapon System Structural Costs," Air Force Report AFFDL-TR-71-74, July 1971.

trade studies from several levels of consideration. For example, weight and cost data can be related directly to key system parameters at the vehicle mission level such as payload, speed, range and landing field length requirements. At the vehicle configuration level, data can be related directly to surface areas, span, sweep, taper, etc., and fuselage length, slenderness, etc. At the major component level comparisons can be made to determine the overall vehicle weight and cost sensitivities at each of these levels, and in this manner the proposed aircraft design may be further and further refined to a high degree of detail. Thus, engineering functions can gain insight into the cost effectiveness of alternate aircraft systems, perform design trade studies, and perform studies to determine the impact of more detailed engineering alternatives with respect to particular aspects of design.

The essential features of the vehicle design evaluation program can be categorized into four major areas: the vehicle synthesis, external loads evaluations, structural synthesis, and parts definition/cost synthesis. The principal functions performed in each of these categories are described in the following paragraphs.

The vehicle synthesis performs the initial sizing of the vehicle using iterative processes to assure compatibility of weights and dimensions with performance and mission requirements. The equations utilized in this process are detailed in Sections 2.0 through 6.0, and each of those sections incorporates a detailed technical discussion. The vehicle synthesis provides data necessary for the other categories in the form of group level weights, vehicle geometry, engine data, detailed arrangement (location) of components, mass distributions, and moments of inertia.

The loads analyses provide shear, moment, and torsion loads at a number of points in each of the major structural components. Separate consideration is given to air loads, inertia loads, aeroelastic effects in wing and tail surfaces, external concentrated loads, etc. The loads are computed for several conditions of flight and aircraft loading configurations in order to obtain the most critical conditions for design. These refined loads data are then provided to the structural synthesis for detailed component analysis. The loads analysis procedures are described in Section 7.0.

The structural synthesis process provides detailed geometry, loads, and weight data for the principal structural elements. The synthesis utilizes a multistation analysis approach that assumes a reasonable structural continuity and a well defined elastic axis. The structural synthesis also has a capability to assess the impact of fatigue and fracture criteria in terms of fatigue life, crack growth life and residual strength. The fatigue life and crack growth life analysis utilizes a flight profile to assess damage for various loading conditions. The residual strength is then determined for flawed structures. The structural synthesis provides the driving parameters for the part definition routines. A detailed technical discussion of the structural synthesis is presented in Section 8.0.

The parts definition/cost analysis portion of the program provides: manufacturing costs based on a consideration of the actual detail parts to be produced and the actual manufacturing and assembly processes required to produce them; material costs based on the type and quantity of material actually purchased; engineering costs based on a statistical treatment of historical data; tooling costs based on the number of parts to be produced; total vehicle program costs based on a cost estimating relationship (CER) approach; and a return-on-investment analysis. A capability has also been added to develop manufacturing costs from Cost Estimating Relationships (CERs) in lieu of the detail parts approach. Except for the total vehicle program cost and the return-on-investment analysis, input to the cost portion of the program is primarily self generated, comprised of either values that have been derived by the preceding synthesis routines or values that are generated internally as needed. A capability has been designed into the program to allow direct input of any parameters for which values are known or for which a constant value is desired. Input to the total vehicle program cost routine is comprized of a series of CER's that are typical of that particular type of analysis. A detailed discussion of the cost computations is presented in Sections 9.0 and 10.0.

SECTION 2

GEOMETRY ANALYSIS

The geometry analysis computes aircraft dimensions, areas, volumes, and miscellaneous dimensional data needed to construct a configuration three view drawing, perform preliminary aerodynamic analyses, estimate design loads, and make preliminary calculations of vehicle structure and component weights. The geometry analysis has been divided into ten major categories which include wing, tails, fuselage, landing gear, engines, nacelles, pylons, general, loads, and cryogenic tankage.

Because of the close interaction between geometry and design weights a loop has been included which derives and iterates design weights as required to maintain consistency of the data.

2.1 DESIGN WEIGHTS. The design weights utilized within this program development are design landing weight, design mission weight, and design maximum weight. Significant vehicle dimensions are derived as a function of imposed load conditions and the various vehicle design weights. The design weights are the vehicle total weights defined by specification and operating requirements that are subsequently used in performance, weight prediction, and loads analysis. Design weights are usually required for combat (design mission), landing, and maximum load. The design weights are derived by modifying the mission takeoff weight and applying safety margin factors as required by specifications. The sizing process is initiated by inputting an initial takeoff weight estimate and computing the design weights. As the sizing iteration progresses the takeoff weight and design weights are updated until the new estimate and the calculated value is within a predetermined tolerance. The design weights are computed by the following equations:

Basic Flight Design Gross Weight

$$W_d = W_{to} - W_{pm} + W_{pd} - k_1 (W_f) + W_{fd}$$

where:

W_{to} = mission takeoff weight

W_{pm} = mission payload weight

W_{pd} = design payload weight

k_1 = percent reduction of mission fuel for flight design weight

W_f = mission fuel weight

W_{fd} = specified (fixed) quantity of design fuel

Maximum Flight Design Gross Weight

$$W_m = k_2 (W_{to} - W_{pm} + W_{pmx} - W_f + W_{fmx})$$

where:

W_{to} = mission takeoff weight

W_{pm} = mission payload weight

W_{pmx} = maximum payload weight

W_f = mission fuel weight

W_{fmx} = maximum capacity fuel weight

k_2 = max. weight over-design factor

Landing Design Gross Weight

$$W_L = k_3 (W_{to} - W_{pm} + W_{pl} - k_4 (W_f) + W_{fl})$$

where:

W_{to} = mission takeoff weight

W_{pm} = mission payload weight

W_{pl} = landing design payload weight

W_f = mission fuel weight

W_{fl} = specified (fixed) quantity of landing fuel

k_3 = landing weight over-design factor

k_4 = percent reduction of mission fuel for design landing weight

The Design Gross Weight Calculation equations are located in Overlay 1,1 Program GEOM.

2.2 WING GEOMETRY. The wing geometry calculations have as their basis a generalized wing configuration description expressed in terms of dimensionless ratios and sizing parameters. The sizing parameters are either wing loading (W/S) or wing area (S_W). The dimensionless ratios include the aspect ratio (AR), the taper ratio (λ), the thickness-to-chord ratio (t/c), and the spar location as percent wing chord.

2.2.1 Wing Dimensional Data.

Wing Area

If the wing area is not fixed (input), it is computed from takeoff weight and wingloading:

$$S_W = \frac{W_{to}}{(W/S)_{to}}$$

where:

S_W = theoretical or reference wing area

W_{to} = mission takeoff weight

$(W/S)_{to}$ = input value of takeoff wing loading.

Wing Span

Wing span is calculated using wing area and aspect ratio:

$$b = \sqrt{AR\ (S_W)}$$

where:

b = aerodynamic span of the wing

S_w = wing reference area

AR = wing aspect ratio

When aspect ratio has not been input, however, an equation is provided to compute aspect ratio in the event the leading edge and trailing edge sweep angles are provided as input. This equation is provided to ensure consistency between leading edge/trailing edge sweep angle and aspect ratio. An equation is also provided to compute the wing quarter chord sweep angle when the leading edge sweep angle is input. These equations are described as follows and are located in Overlay 1,4 Program INGEOM:

Aspect Ratio

$$AR = \left(\frac{1-\lambda}{1+\lambda}\right)\left(\frac{4.0}{TANA_{le} - TANA_{te}}\right)$$

where:

AR = wing aspect ratio

λ = wing taper ratio

$TANA_{le}$ = tangent of the wing leading edge sweep angle

$TANA_{te}$ = tangent of the wing trailing edge sweep angle

Mean Aerodynamic Chord (MAC) Length

$$\bar{C}_w = \frac{4}{3}\sqrt{\frac{S_w}{AR}}\left[1 - \frac{\lambda}{(1+\lambda)^2}\right]$$

$\bar{C}_w$ = wing mean aerodynamic chord

S_w = reference wing area

AR = wing aspect ratio

λ = wing taper ratio

Spanwise Location of MAC

$$y_{\bar{C}_w} = \frac{b}{6}\left[\frac{1+2\lambda}{1+\lambda}\right]$$

$y_{\bar{C}_w}$ = spanwise location of the MAC

b = wing span

λ = wing taper ratio

Wing Chord at Root (Centerline, reference wing)

$$C_r = \frac{2}{1+\lambda}\sqrt{\frac{S_w}{AR}}$$

C_r = wing chord at the root

λ = wing taper ratio

S_w = theoretical wing area

AR = wing aspect ratio

Wing Thickness at the Root (Centerline, reference wing)

$$t_r = (t/c)_r\, C_r$$

t_r = wing thickness at the root

$(t/c)_r$ = wing thickness to chord ratio at the root

C_r = wing chord at the root

Wing Chord at the Tip

$$C_t = C_r\lambda$$

C_t = wing chord at the top

C_r = wing chord at the root

λ = wing taper ratio

Wing Thickness at the Tip

$$t_t = (t/c)_t \, C_t$$

t_t = wing thickness at the tip

$(t/c)_t$ = wing thickness to chord ratio at the tip

C_t = wing chord at the tip

Wing Expanded Root Chord

$$C_{rx} = k_{cr} \, C_r$$

C_{rx} = wing expanded root chord

k_{cr} = coefficient for percent root chord expansion

C_r = wing chord at the root

Wing Chord at Planform Break

$$C_b = C_r \left[1 - \frac{y_b}{b/2} \, (1-\lambda) \right]$$

C_b = wing chord at the planform break

C_r = wing chord at the root

y_b = spanwise location of the wing break

b = wing span

λ = wing taper ratio

Wing Thickness at the Break

$$t_b = (t/c)_b \, C_b$$

t_b = wing thickness at the break

$(t/c)_b$ = thickness to chord ratio at the break

C_b = wing chord at the planform break

Wing Thickness at MAC

$$t_{\bar{c}_w} = t_b - \frac{\left(Y_{\bar{c}_w} - Y_b\right)\left(t_b - t_t\right)}{(b/2 - Y_b)} \qquad \text{(outboard of break)}$$

$$t_{\bar{c}_w} = t_r - \frac{y_{\bar{c}_w}(t_r - t_b)}{Y_b} \qquad \text{(inboard of break)}$$

t_t = wing thickness at tip

$t_{\bar{c}_w}$ = wing thickness at MAC

t_r = wing thickness at root

t_b = wing thickness at break

$y_{\bar{c}_w}$ = spanwise location of MAC from centerline

y_b = spanwise location of break from centerline

b = wing span

Quarter Chord Sweep Angle

$$\Lambda_{0.25} = \text{TAN}^{-1}\left[\text{TAN}\Lambda_{le} - \frac{1}{AR}\,\frac{1-\lambda}{1+\lambda}\right]$$

$\Lambda_{0.25}$ = wing sweep angle at the 25% chord

$\text{TAN}\Lambda_{le}$ = tangent of the wing leading edge sweep angle

AR = wing aspect ratio

λ = wing taper ratio

Wing Sweep at the 50% Chord

$$\Lambda_{0.50} = \text{TAN}^{-1}\left[\text{TAN}\,\Lambda_{0.25} - \frac{C_r\,(1-\lambda)}{2b}\right]$$

$\Lambda_{0.50}$ = wing sweep angle at the 50% chord

$\text{TAN}\Lambda_{0.25}$ = wing sweep angle at the 25% chord

C_r = wing chord at the root

λ = wing taper ratio

b = wing span

Gross Wing Area (including expanded root area)

$$S_g = S_w + y_b\,(C_{rx} - C_b)$$

where:

S_w	=	basic reference wing area
y_b	=	spanwise distance centerline to break
C_{rx}	=	expanded root chord
C_b	=	chord at break

Chord at any Spanwise Location

$$C_\eta = C_r \left[1 - \frac{y_\eta}{(b/2)}\,(1-\lambda)\right] \quad \text{, outboard of break, or}$$

$$C_\eta = C_r \left[1 - \frac{y_\eta}{(b/2)}\,(1-\lambda)\right] + (C_{rx} - C_r)\left[\frac{y_b - y_n}{y_b}\right]$$

inboard of break

where:

$C\eta$	=	chord at any span station η
y_η	=	dimension from center line to span station η
y_b	=	dimension from center line to break
C_r	=	root chord, reference wing
C_{rx}	=	expanded root chord
λ	=	reference wing taper ratio
b	=	wing span

Thickness of any Spanwise Location

$$t_\eta = t_b - \frac{y_\eta - y_b}{(b/2) - y_b}\,(t_b - t_t) \text{ , outboard of break, or}$$

$$t_\eta = t_r - \left(\frac{y_\eta}{y_b}\right)(t_{rx} - t_b) \text{ , inboard of break}$$

where:

t_η = thickness at any span station η

y_η = dimension from centerline to span station η

y_b = dimension from centerline to break

t_{rx} = expanded root thickness

t_b = thickness at break

t_t = thickness at tip

b = wing span

Cross-section Area of Structural Box at any Spanwise Station

$$A_b = 0.864\ (C_\eta)\ (t_\eta)\ (k_{rs}-k_{fs})$$

where:

C_η = wing chord at any span location η

t_η = wing thickness at any span location η

k_{rs} = rear spar location, decimal chord

k_{fs} = front spar location, decimal chord

Volume of Structural Box Between Two Spanwise Stations (per side)

$$V_b = \left(\frac{y_2 - y_1}{6}\right)(A_1 + 4A_m + A_2)$$

where:

y_2 = distance center line to outboard station

y_1 = distance center line to inboard station

A_1 = box cross section at station (1)

A_2 = box cross section at station (2)

A_m = box cross section at station midway between

Cross Section Area of Airfoil at any Spanwise Station

$$A_{cw}\quad \eta_v\ (C_\eta)(t_\eta)$$

where:

C_η = wing chord at any span station η

t_η = wing thickness at any span station η

η_v = unit volume coefficient (See Figure 2-1)

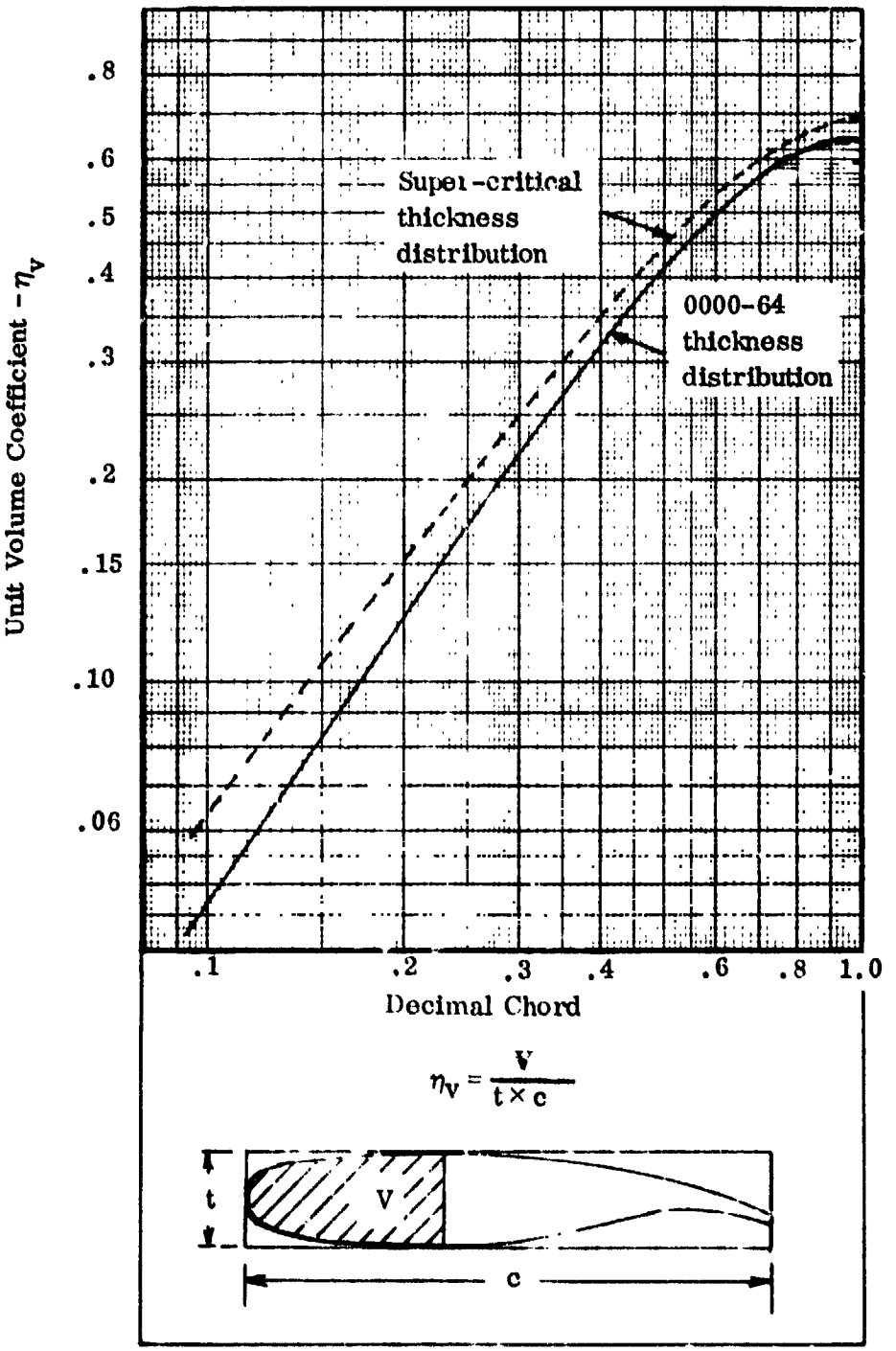

Figure 2-1 Volume Enclosed in an Airfoil

Volume of Total Exposed Wing (outside body width) per airplane

$$V_w = 1/3\ [(y_b - y_1)(A_b + 4A_{m1} + A_1) + (y_t - y_b)(A_b + 4A_{m2} + A_t)]$$

where:

y_1 = dimension centerline to side of body

y_b = dimension centerline to wing break

y_t = dimension centerline to wing tip

A_1 = wing cross section area at span station side of body

A_b = wing cross section area at break

A_{m1} = wing cross section area midway between break and side of body

A_t = wing cross section area at tip

A_{m2} = wing cross section area midway between break and tip

2.3 TAIL GEOMETRY. Tail geometry calculations are made in a manner similar to those of the wing. The major exception is the derivation of the tail areas based on tail volume coefficients and the previously computed tail arms.

Horizontal Tail Area (includes projected area in fuselage)

$$S_h = C_h\ (S_w) \left(\frac{\bar{c}_w}{L_h}\right)$$

where:

C_h = horizontal tail volume coefficient

S_w = reference wing area

$\bar{c}_w$ = wing MAC

L_h = distance from the quarter chord of the wing MAC to that of the horizontal tail MAC

Vertical Tail Area (exposed area. No fuselage buried area.)

$$S_v = C_v\ (S_w) \left(\frac{b}{L_v}\right)$$

where:

C_v = vertical tail volume coefficient

S_w = reference wing area

b = reference wing span

L_v = distance from the quarter chord of the wing MAC to that of the vertical tail MAC.

2.4 FUSELAGE GEOMETRY. A number of options are provided for fuselage types, each having need for different types of dimensional data. Different equations are provided for each. In some cases input values may be used in lieu of calculations.

2.4.1 Commercial Transport Bodies (non-cryogenic fuel).

Body Volume

$$V_b = 1.1\ (V_c + V_e + V_p)$$

where:

V_c = cockpit volume

V_e = equipment volume

V_p = passenger volume

Body Length

$$L_b = \frac{V_b}{0.8(A_{cs})}$$

where:

V_b = body volume

A_{cs} = constant section cross section area

Body Diameter

$$h_b = b_b = \sqrt{\frac{A_{cs}}{.7854}}$$

where:

h_b = body depth

b_b = body width

A_{cs} = constant section cross section area.

Body Wetted Area

$$S_b = 0.8\left(\frac{h_b + b_b}{2}\right)(\pi)\ (L_b)$$

where:

h_b = body depth

b_b = body width

L_b = body length

2.4.2 Military Transport Body (non-cryogenic fuel). The equations are the same as commercial transport bodies except as shown.

Cargo Volume

$$V_c = W_c/3.4$$

where:

W_c = cargo weight

Body Volume

$$V_b = 1.32\ (V_c + V_e + V_C)$$

where:

V_c = cockpit volume

V_e = equipment volume

V_C = cargo volume

Body Length

$$L_b = \frac{V_b}{.714(A_{cs})}$$

where:

V_b = body volume

Body Wetted Area

$$S_b = 0.842\left(\frac{h_b + b_b}{2}\right)(\pi)(L_b)$$

where:

h_b = body depth

b_b = body width

l_b = body length

2.4.3 Combat Aircraft Bodies. Military fighter type aircraft bodies seldom have very simple lines for easy approximation of dimensions. However, it has been shown by W. E. Caddell (Reference 1) that very good statistical correlations exist between body volumes, wetted areas, maximum cross section areas, and the weights of body and contents. (Table 2-1 , Fig. 2-2) Therefore, for this type aircraft the dimensions are derived from volumes which are derived from densities and weights of fuselage and contents.

Table 2-1 Density Comparison

Condition	Gross (1)						Dry (2)						Net (3)					
	Weight		Volume		Density		Weight		Volume		Density		Weight		Volume		Density	
	Kg	(Lbs)	M^3	(Ft^3)	Kg/M^3	(Lbs/Ft^3)	Kg	(Lbs)	M^3	(Ft^3)	Kg/M^3	(Lbs/Ft^3)	Kg	(Lbs)	M^3	(Ft^3)	Kg/M^3	(Lbs/Ft^3)
A3D-2Q	37,648.8	(83,000)	101.9	(3,599)	369.9	(23.1)	26,490.2	(58,400)	82.5	(2,916)	321.1	(20.0)	15,822.5	(34,882)	78.7	(2,780)	201.0	(12.5)
A3J-1	25,222.4	(55,605)	62.8	(2,220)	401.6	(25.0)	16,570.5	(36,531)	52.2	(1,845)	317.4	(19.8	8,189.3	(18,054)	49.2	(1,738)	166.4	(10.4)
A4D-2N	7,250.3	(15,984)	18.6	(658)	389.8	(24.3)	4,782.8	(10,544)	15.6	(551)	306.6	(19.1)	2,552.4	(5,627)	14.8	(523)	172.5	(10.8)
A-4E	7,282.1	(16,054)	18.9	(667)	385.3	(24.1)	4,814.5	(10,614)	15.8	(560)	304.7	(19.0)	2,477.6	(5,462)	15.0	(530)	165.2	(10.3)
RA-5C	29,145.2	(64,253)	74.8	(2,643)	389.6	(24.3)	18,041.0	(39,773)	61.2	(2,162)	294.8	(18.4)	8,298.6	(18,295)	57.7	(2,038)	143.8	(9.0)
A-6A	18,411.2	(40,589)	43.9	(1,551)	419.4	(26.2)	11,144.5	(24,569)	35.0	(1,238)	318.4	(19.8)	4,961.0	(10,937)	32.8	(1,159)	151.3	(9.4)
A-7A	11,371.2	(25,069)	27.4	(972)	415.0	(25.8)	7,810.5	(17,219)	21.8	(771)	358.3	(22.3)	3,657.4	(8,063)	20.3	(718)	180.2	(11.2)
T-38A	5,232.6	(11,536)	14.0	(495)	373.8	(23.3)	3,475.5	(7,662)	11.7	(415)	297.0	(18.5)	1,655.6	(3,650)	11.1	(392)	149.2	(9.3)
F11F-1	9,123.3	(20,113)	20.7	(731)	440.7	(27.5)	6,428.9	(14,173)	17.2	(609)	373.8	(23.3	3,143.4	(6,930)	16.0	(567)	196.5	(12.2)
F9F-8	8,919.6	(19,664)	22.5	(796)	396.4	(24.7)	6,026.5	(13,286)	18.3	(646)	329.3	(20.6)	3,015.5	(6,648)	17.2	(609)	175.3	(10.9)
F4D-1	11,490.6	(25,332)	24.4	(862)	470.9	(29.4)	7,834.6	(17,272)	22.0	(776)	356.1	(22.3)	4,483.9	(9,885)	20.7	(733)	216.6	(13.5)
F8C-1	11,823.5	(26,066)	31.0	(1,094)	381.4	(23.8)	8,081.3	(17,816)	26.3	(929)	307.3	(19.2)	4,158.6	(9,168)	24.9	(879)	167.0	(10.4)
F3U-3	16,933.8	(37,332)	45.4	(1,603)	373.0	(27.3)	10,444.6	(23,026)	37.0	(1,309)	282.3	(17.6)	5,307.6	(11,701)	35.2	(1,243)	150.8	(9.4)
F4H-1	19,254.4	(42,448)	44.3	(1,565)	434.6	(27.1)	13,094.5	(28,868)	36.7	(1,298)	356.8	(22.2)	7,281.2	(16,052)	34.6	(1,224)	210.4	(13.1)
F-4E	20,002.4	(44,097)	44.7	(1,580)	447.5	(27.9)	14,153.2	(31,201)	37.2	(1,315)	380.5	(23.7)	7,963.9	(17,557)	35.0	(1,236)	227.5	(14.2)
F101B	20,599.8	(45,414)	54.4	(1,921)	378.7	(23.6)	14,455.3	(31,868)	46.5	(1,642)	310.9	(19.4)	9,468.0	(20,873)	44.6	(1,575)	212.3	(13.2)
F-102A	12,762.9	(28,137)	44.4	(1,568)	287.4	(17.9)	9,563.7	(21,084)	40.3	(1,423)	237.3	(14.8)	5,729.9	(12,632)	38.9	(1,374)	147.3	(9.2)
F-105D	16,058.3	(35,402)	38.3	(1,353)	419.3	(26.2)	12,038.2	(27,862)	33.9	(1,198)	372.8	(23.3)	6,257.0	(13,794)	31.6	(1,117)	198.0	(12.4)
F-106A	16,266.5	(35,861)	46.8	(1,653)	347.6	(21.7)	11,802.7	(26,020)	41.1	(1,451)	287.2	(17.9)	7,168.2	(15,803)	39.4	(1,392)	181.9	(11.3)
F-111A	34,784.7	(81,086)	76.2	(2,693)	492.7	(30.1)	22,198.7	(48,939)	57.5	(2,032)	386.1	(24.1)	10,234.6	(22,563)	53.2	(1,879)	192.4	(12.0)
F-111B	33,680.7	(74,252)	73.7	(2,604)	457.0	(28.5)	22,161.5	(48,857)	59.6	(2,105)	371.8	(23.2)	9,918.4	(21,866)	55.2	(1,949)	179.7	(11.2)
F-5A	6,110.4	(13,471)	14.5	(514)	421.4	(26.2)	4,391.3	(9,681)	12.3	(436)	357.0	(22.2)	2,277.5	(5,021)	11.6	(409)	196.3	(12.3)
RMS Value						410.86						332.53						183.89
Standard Dev. (%)						10.66						11.64						13.31

Notes: Gross (1) = Full internal - no external
Dry (2) = Gross less fuel
Net (3) = Gross less fuel and structure

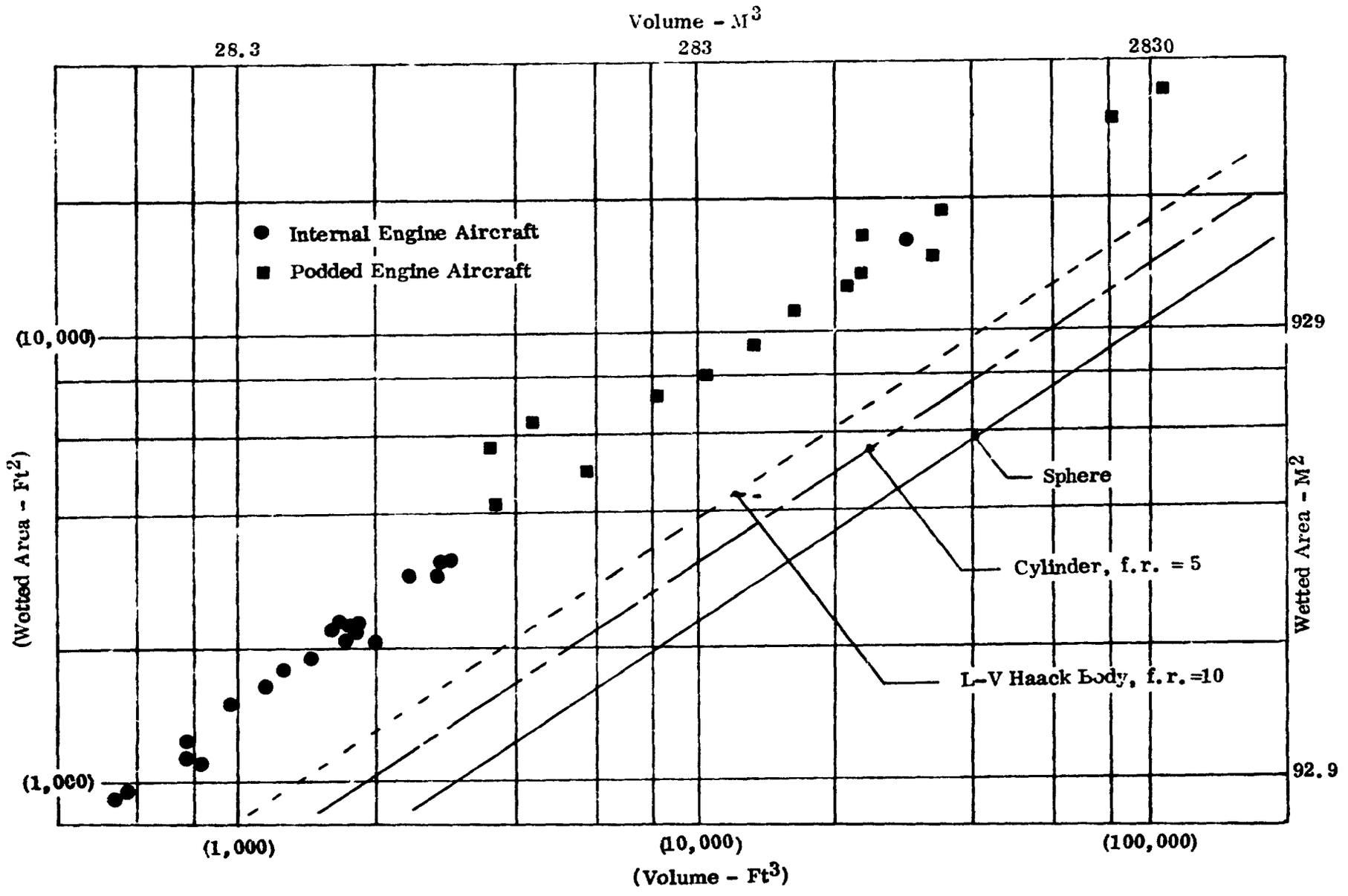

Figure 2-2 Wetted Area/Volume Relationships for Various Body Shapes

Aircraft Gross Volume Required

$$V_a = \left[\frac{W_1 - W_f - W_s}{\rho_0} + \frac{W_f}{\rho_f} + \frac{W_s}{172.8} \right] k_I$$

where:

V_a = gross volume including inlet capture air

W_1 = full internal aircraft weight

W_f = weight of internal fuel

W_s = weight of aircraft total structure

ρ_0 = density of typical fighter aircraft

ρ_f = density of fuel

k_I = factor to account for inlet air volume

Body Volume Required

$$V_b = V_a - V_{wx} - V_{hx} - V_{vx}$$

where:

V_b = gross volume of body

V_a = gross volume of total aircraft

V_{wx} = volume of exposed wing (par. 2.2.1)

V_{hx} = volume of exposed horizontal tail

V_{vx} = volume of exposed vertical tail

Body Length (If input, then input overrides)

$$L_b = k_b \left[\frac{(\gamma_f)^2 (V_a)}{(\pi/4)(0.7)} \right]^{1/3}$$

where:

L_b = body length

V_a = total aircraft gross volume

k_b = calibration constant

γ_f = total aircraft fineness ratio based on total length and equivalent diameter of max cross section.

Body Equivalent Diameter

$$D_{be} = \left[\frac{V_b}{0.7(L_b)(\pi/4)}\right]^{0.5}$$

where:

V_b = body gross volume

L_b = body length

Body Width

$$b_b = \frac{2\,(D_{be})}{(1+k_n)}$$

where:

b_b = body width

D_{be} = body equivalent diameter

k_n = ratio of depth/width

Body Depth

$$h_b = k_n\,(b_b)$$

where:

k_n = ratio of depth/width

b_b = body width

Body Wetted Area

Table 2-2 demonstrates the feasibility of estimating total aircraft wetted areas by calculating the exposed areas of airfoil surfaces and empirically estimating body areas from volumes and lengths only. The equation following is a later development of the same idea for the body, removing a portion of the area covered by wing intersections. The constant 3.309 is that for an idealized Haack body of revolution and a calibration coefficient is provided.

$$S_{bw} = k_c\,(3.309)\sqrt{L_b\,(V_b)} - 2\,(C_b)(t_b)$$

where:

L_b = body length

V_b = body gross volume

C_b = wing chord at side of body

t_b = wing thickness at side of body

k_c = calibration coefficient for non-idealized shape

Table 2-2 Total Aircraft Wetted Areas Can Be Estimated Accurately Using Only Airfoil Surface Geometry & Fuselage Volume Requirements

A/C	Note 1 A_w M^2	A_w (Ft^2)	A_{ht} M^2	A_{ht} (Ft^2)	A_{vt} M^2	A_{vt} (Ft^2)	Other M^2	Other (Ft^2)	A_f* M^2	A_f* (Ft^2)	ΣCalc. Areas M^2	ΣCalc. Areas (Ft^2)	Act. Area M^2	Act. Area (Ft^2)	% Dev.
A3J-1	101.59	(1093.5)	32.23	(346.9)	18.94	(203.9)			124.89	(1344.4)	277.65	(2989)	268.20	(2887)	-3.4
A-4E	37.73	(406.1)	9.09	(97.1)	9.49	(102.1)			50.81	(546.9)	106.12	(1142)	101.63	(1094)	-4.2
RA-5C	108.61	(1169.1)	32.23	(346.9)	18.94	(203.9)			137.48	(1479.9)	297.26	(3200)	287.15	(3091)	-3.4
A-6A	83.53	(899.1)	18.08	(194.6)	11.77	(126.7)			88.03	(947.6)	201.41	(2168)	205.96	(2217)	+2.3
A-7A	57.23	(616.0)	10.63	(114.2)	13.11	(141.1)			69.04	(743.2)	150.01	(1615)	152.63	(1643)	+1.7
T-2B	45.20	(486.5)	13.13	(141.3)	6.87	(74.0)			48.09	(517.7)	113.29	(1220)	116.03	(1249)	+2.4
F11F-1	38.27	(411.9)	8.13	(87.5)	8.31	(89.4)			56.83	(611.7)	111.54	(1200)	106.37	(1145)	-4.6
F4D-1	66.02	(925.9)	—	—	8.69	(93.5)			50.79	(546.7)	145.50	(1566)	140.74	(1515)	-3.3
F-8A	54.77	(589.6)	10.61	(114.2)	13.53	(145.6)			79.63	(857.2)	158.54	(1707)	136.85	(1796)	+5.2
F8U-3	65.72	(707.4)	12.34	(132.8)	14.87	(159.6)	8.69	(93.6)	103.28	(1111.7)	204.90	(2205)	210.88	(2270)	+3.0
F-4E	73.24	(788.4)	15.78	(169.9)	10.83	(116.6)			99.38	(1069.8)	199.23	(2145)	211.81	(2280)	+6.3
F-102A	87.92	(946.4)	--	—	17.97	(193.4)			100.69	(1083.9)	206.58	(2224)	194.16	(2090)	-6.0
F-106A	97.07	(937.2)	—	—	19.69	(212.0)			105.42	(1134.8)	212.18	(2284)	204.01	(2196)	-3.9
F-111A	81.53	(877.6)	28.89	(311.0)	20.91	(225.1)			142.21	(1530.8)	273.54	(2944)	286.32	(3082)	+4.7
Model 44	87.14	(938.0)	28.18	(303.3)	26.36	(283.7)			120.81	(1300.4)	262.49	(2825)	269.41	(2900)	+2.7
F-5A	22.24	(239.4)	6.22	(67.0)	7.78	(83.7)			49.55	(533.4)	85.79	(944)	86.07	(948)	+0.4

Note 1. All aerodynamic surfaces calculated from actual dimensions

*Fuselage wetted area calculated by the equation $A_f = 3.60\ (L_f V_f)^{0.5}$.

The standard deviation error is 4 percent.

2.5 LANDING GEAR GEOMETRY. The dimensions required for computation of landing gear geometry are the length and stroke, and wheel and tire sizes. Unless given, these dimensions are derived from aircraft configuration requirements and landing gear loads. Therefore, calculations of approximate landing gear loads are included in the geometry calculations.

The conditions that establish the oleo length include the location of the mounting point, aircraft ground clearance, and the length requirements to accommodate the oleo stroke. The stroke is established by the landing energy absorption requirements and a landing load factor. The landing load factor and landing weight are used to compute the loads, and the landing stall speed or an approximation is used to establish the kinetic energy to be dissipated through braking.

Main Landing Gear

Length $l_{tm} = k_m l_b$

Stroke $S_m = .1865 \dfrac{(V_s)^2}{(N_L - 1)} < (l_m/3)$

Vertical load $F_{vm} = \left(\dfrac{W_l}{2}\right)(N_L - 1)$

Drag load $F_{dm} = .481\ (F_{vm})$

Stall speed $V_{so} = \dfrac{29}{1.688} \sqrt{\dfrac{(W/S)\left(W_{L/W_{to}}\right)(1 + 3/AR)}{3.86}}$

Brake energy $E_m = \dfrac{W_{to}}{2g}\left(\dfrac{V_{so}^2}{N_{w_m}}\right)$

Wheel diameter $D_{w_m} = 1.224 \sqrt{\dfrac{N_L (W_L)}{N_{w_m}(500)}}$

Wheel flange width $W_{fm} = .863\ D_{wm}$

Tire diameter $D_{tm} = \dfrac{D_{wm}}{1.4} \quad 2(W_{fm})$

Tire width $W_{tm} = W_{tm}$

where:

L_b	= body length
k_m	= input coefficient
V_s	= landing design sink rate (defaults to 10.0)
V_{so}	= landing stall speed
W_L	= landing design weight
W_{to}	= takeoff (max.) gross weight
N_L	= landing design vertical load factor
W/S	= design wing loading
AR	= wing aspect ratio
g	= gravitation acceleration constant = 32.2
N_{wm}	= number of main gear wheels
D_{wm}	= diameter of main wheel
W_{fm}	= flange width of main wheel
D_{tm}	= diameter of main tires

Nose Landing Gear

Length	$L_n = .9\ (L_m)$
Stroke	$S_n = L_n/4.5$
Vertical load	$F_{vn} = .4\ (F_{vm})$
Drag load	$F_{dn} = .481\ (F_{vn})$
Wheel diameter	$D_{wn} = 1.224 \sqrt{\frac{.1(N_L)(W_L)}{N_{wn}(500)}} \geq 8.$
Wheel flange width	$W_{fn} = .863\ (D_{wn})$
Tire diameter	$D_{tn} = \frac{D_{wn}}{1.4} + 2\ (W_{fn})$
Tire width	$W_{tn} = W_{fn}$

where:

L_m = main landing gear length

W_L = landing design weight

N_L = landing design vertical load factor

N_{wn} = number of nose gear wheels

D_{wn} = diameter of nose wheel

W_{fn} = flange width of nose wheel

D_{tn} = diameter of nose gear tire

2.6 POWER PLANT, NACELLE, AND PYLON GEOMETRY

2.6.1 Propulsion Units. The propulsion geometry depends on input values or input dimensions of a reference power plant. Scaling of that reference data is then as follows.

$$k_{eng} = A + B\left(\frac{T_e}{T_{er}}\right)^C$$

$$D_e = D_{er}\sqrt{\frac{T_e}{T_{er}}}$$

$$L_e = L_{er}\sqrt[3]{\frac{T_e}{T_{er}}}$$

where:

k_{eng} = engine scaling coefficient

A = engine scaling curve intercept

B = engine scaling curve slope

C = engine scaling curve exponent

D_e = engine diameter

D_{er} = reference engine diameter

T_e = engine thrust

T_{er} = reference engine thrust

L_e = engine length

L_{er} = reference engine length

Input coefficients are used to determine engine locations at "D" diameters outboard of the side of the body. Other location data are calculated in subroutine CONMAS where concentrated load masses are accumulated.

2.6.2 Nacelles. Nacelle geometry is calculated as a function of engine dimensions and input coefficients.

$L_n = 1.2\ (L_e)$

$D_{nq} = D_e + 1$ (single engine nacelles)

$D_{ng} = (3D_e + 1)/2$ (siamese engine nacelles)

$D_{nq} = L_n/f_n$ (if f_n is input)

$A_{nm} = .7854\ (D_{nq})^2$

$S_n = .9\ (D_{ng})(\pi)(L_n)$

$h_n = D_{nq}$

$b_n = D_{nq}$ (single nacelles)

$b_n = 2(D_e) + 3.$ (siamese nacelles)

where:

L_n = nacelle length

L_e = engine length

D_{nq} = nacelle equivalent diameter

D_e = engine diameter

f_n = nacelle fineness ratio (if input)

A_{nm} = nacelle max. cross section

S_n = nacelle wetted area

h_n = nacelle height

b_n = nacelle width

2.6.3 Pylons. External tank

$L_p = D_t \quad (\leq 4.0)$

$C_{pw} = k_{rs} \quad (C_{wt})$

$C_{pt} = .3 \quad (L_t)$

where:

L_p = pylon length (span)

D_t = tank diameter

C_{pw} = pylon chord length at wing

C_{pt} = pylon chord length at tank

k_{rs} = wing rear spar location, demimal chord

C_{wt} = wing chord at tank location

L_t = external tank length

2.6.4 Pylons. Wing mounted engines

$L_p = D_e$

$C_{pw} = k_{rs} \, (C_{we})$

$C_{pe} = .7 \, (L_e)$

$$S_{pw} = L_p \left(\frac{C_{pw} + C_{pe}}{2} \right) (2 + t_c \, 1.5)$$

where:

L_p = pylon length (span)

D_e = engine diameter

C_{pw} = pylon chord at wing

C_{pe} = pylon chord at engine

C_{we} = wing chord at engine location

L_e = engine length

t_c = pylon thickness ratio

2.7 GENERAL GEOMETRY.

Area of Exposed Wing

$$S_{wx} = \left(\frac{C_s + C_b}{2}\right)(b_i)(2) + \left(\frac{C_b + C_t}{2}\right)(b_o)(2)$$

Wing Wetted Area

$$S_{ww} = S_{wx}\,(2 + (t_{cn})^{1.5})$$

where:

S_{wx} - planform exposed area of the wing

S_{ww} - exposed total wetted area of wing

C_s - wing chord at side of body

C_b - wing chord at planform break

C_t - wing chord at tip

b_i - span per side of inboard section wing

b_o - span per side of outboard section wing

t_{cm} - wing thickness ratio at MAC

Total wetted area is the sum of the various components.

2.8 SIMPLIFIED LOADS. These equations are supplied to provide order of magnitude values used in the "start-up" mode.

Force Coefficient Slopes

$$C_{n_\beta} = 5.7\left[\frac{1.5\,(AR_V)}{1.5\,(AR_V)+2}\right]$$

$$C_{n_\alpha} = \frac{6}{\left(1 + \frac{.6}{\pi\, AR_W}\right)} + 2.15\left(\frac{S_h}{S_w}\right)$$

where:

C_{n_α} - rate of change of normal force coefficient (Z direction) with angle of attack (lift curve slope).

C_{n_β} - rate of change of normal force coefficient (Y direction) with angle of yaw.

AR_v = vertical tail aspect ratio

AR_w = wing aspect ratio

S_h = horizontal tail area (includes projected area in fuselage)

S_w = reference wing area

Gust Load Factor (if greater than maneuver)

$$N_{z_g} = 1.5\,(1 + \Delta^N g)$$

$$\Delta^N g = \frac{\rho/2\, V_g\, U\, C_{n_\alpha}\, K_w}{W/S} \qquad \text{(Ref. MIL-A-8861)}$$

where:

N_{z_g} = ultimate gust load factor

$\Delta^N g$ = limit value of gust increment

ρ = air density in mass units

V_g = velocity for maximum dynamic pressure

U = design gust velocity

C_{n_α} = lift curve slope

$$K_w = \frac{.88\,(u)}{(5.3 + u)}$$

$$u = \frac{W/s}{(\rho/2)(g)(C)(C_{n_\alpha})}$$

W/s = wing loading

g = gravitational acceleration constant

c = average chord of wing

Design Tail Loads

Vertical

$$F_{V_g} = C_{n_\beta} (U) (V_g)(S_v)/841$$

$$F_{V_m} = .22 (C_{n_\beta})(V_m)^2(S_v)/841$$

$$F_{V_U} = 1.5 \text{ (Greater of } F_{V_g} \text{ or } F_{V_m})$$

Horizontal

$$F_{h_g} = C_{n_{\alpha_h}} (U) (V_g) (S_h)/841$$

$$F_{h_m} = .147 (C_{n_{\alpha_h}}) (V_m)^2 (S_h)/841$$

$$F_{h_u} = 1.5 \text{ (Greater of } F_{n_g} \text{ or } F_{h_m})$$

where:

F_{V_g} = vertical tail design gust load, limit

F_{V_m} = vertical tail design maneuver load, limit

F_{V_u} = vertical tail design ultimate load

F_{h_g} = horizontal tail design gust load, limit

F_{h_m} = horizontal tail design maneuver load, limit

F_{h_n} = horizontal tail design ultimate load

C_{N_β} = rate of change of normal force coefficient (Y direction) with angle of yaw.

$C_{n_{\alpha_h}}$ = horizontal tail lift curve slope

V_g = velocity for maximum dynamic pressure

V_m = maximum maneuver velocity

S_v = vertical tail area

S_h = horizontal tail area

U = design gust velocity

2.9 CRYOGENIC STRUCTURES AND TANKAGE. When cryogenic fuel vehicles are being analyzed it is presumed that the low density of the fuel will result in volume requirements such that fuel required will be the actual size determinant. The sizing sequence begins by calculating the fuselage diameter as a function of the internal passenger arrangement (see Figure 2-3).

2.9.1 Fuselage Length Calculations. Figure 2-4 is an illustration of the cryogenic fuselage model on which the analysis is based. Also shown are the sequential steps for calculating the major dimensions. The dimensions L_1 thru L_3 are simply a function of diameter and input fineness ratios as shown on Figure 2-4 . The other dimensions, however, are a function of fuel volume required and the steps are as follows.

1. The desired distribution of the required cryogenic fuel is input as percentages of the total to:

   a. Wing external
   b. Wing internal
   c. Under floor fuselage
   d. Forward fuselage
   e. Aft fuselage

2. The program logic then sizes the tanks accordingly in the sequence shown, but with certain limitations as follows. The internal wing tanks are sized to hold the requested amount. If the wing volume is too small, the residual requirement is added to the forward and aft fuselage tanks. Likewise, if the under floor fuel tanks are to small to contain the requirement, the residual is added to the forward and aft fuselage tanks in equal increments. The sizing of the forward and aft fuselage tanks is then accomplished.

3. The dimensions L_4, L_5 and L_6 of figure 2-4 are then calculated as that sufficient for the volume plus a constant end clearance. In the case of dimension L_6, if the tank volume so dictates, the dimension L_3 is increased as required to maintain side clearance as well.

2.9.2 Cryogenic Fuel Tank Sizing. Two types of cryogenic tanks are provided for: The first is a frustrum of a cone (or cylinder) capped on each end by an elliptical hemispheroidal dome. This type is typified by the forward and aft body tanks in figure 2-4 . A semi-monocoque structure is assumed. This type construction is also used in the external wing tanks except that an aerodynamic fairing completely envelopes the fuel tank.

The second type (figure 2-5) is a three lobe conventional membrane tank as described in reference 2. This type construction is assumed for the internal wing tanks and the fuselage underfloor tanks.

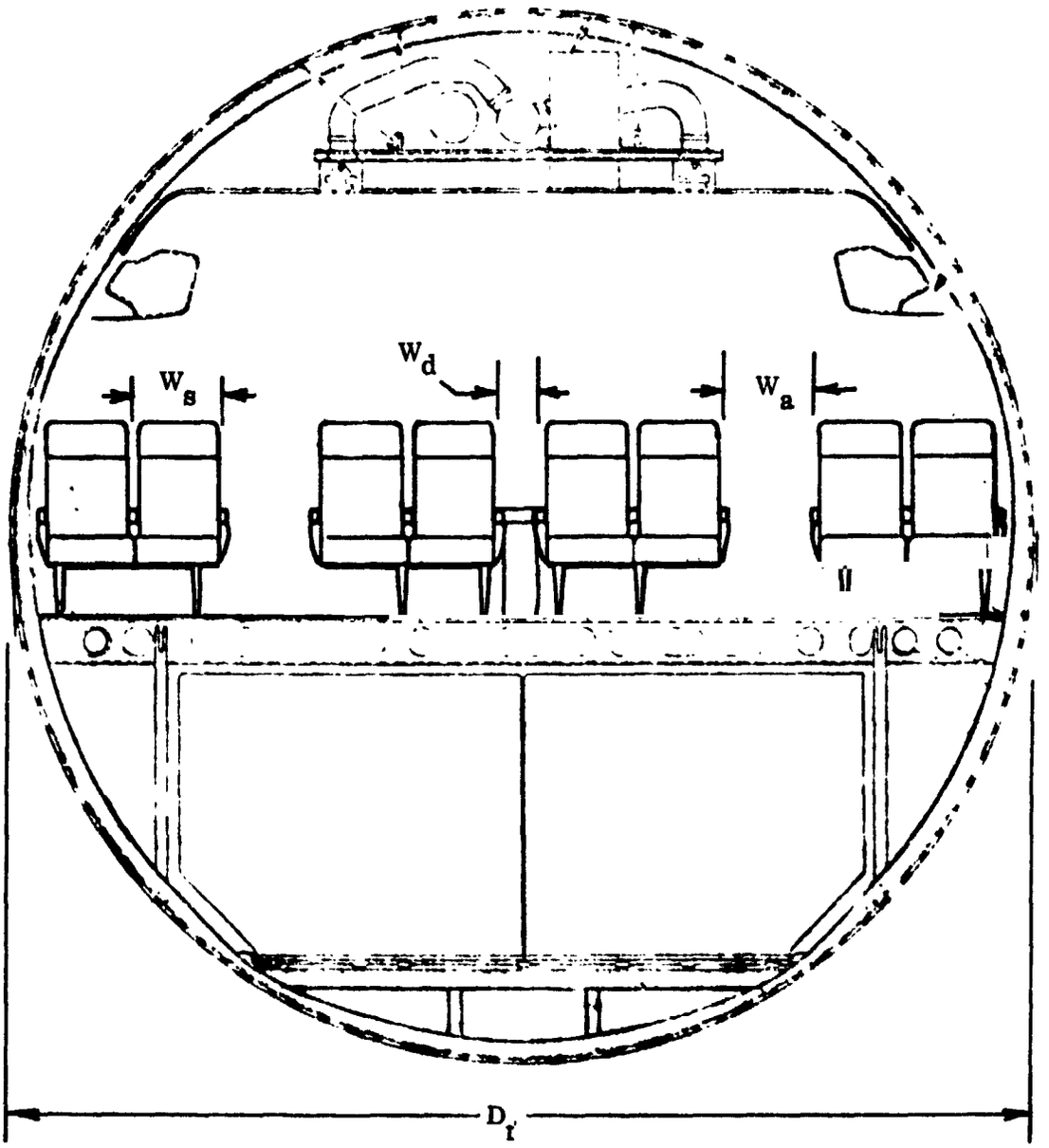

$$D_f = \frac{12 + W_s (N_{pr}) + W_a (N_a) + W_d (N_s)}{12}$$

where

N_{pr}	= number of passengers per row	$W_d = 8$
N_a	= number of aisles provided	$W_s = 22$
N_s	= number of spacers = $N_a - 1$	$W_a = 19$

If $N_{pr} \leq 6$, $N_a = 1$

If $N_{pr} = 7$ to 10, $N_a = 2$

If $N_{pr} \geq 11$, $N_a = 3$

Figure 2-3 Fuselage Width Calculations

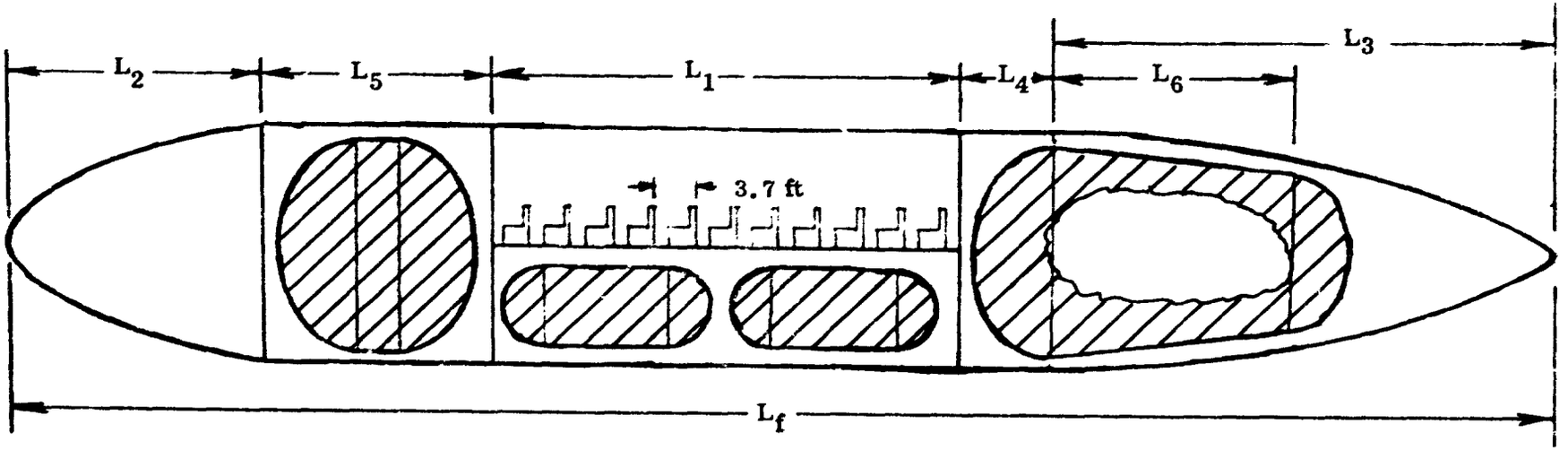

Sizing Sequence:

$L_1 = \frac{N_p}{N_{pr}}$ (3.7) where N_p = total passengers and N_{pr} = seats per row

$L_2 = k_{fn}(D_f)$ where D_f is fuselage diameter and k_{fn} is input nose fineness ratio

$L_3 = k_{fb}(D_f)$ where D_f is fuselage diameter and k_{fb} is input afterbody fineness ratio

L_4 thru L_6 See paragraph 2.9.1

$L_f = \sum (L_1, L_2, L_3, L_4, L_5)$

Figure 2-4 Cryogenic Fuselage Model

Table 2-3 is a directory of which subroutines are used in sizing and weighing of each tank and a paragraph reference telling where the procedures are described. Due to this integrated nature of some of the procedures (weights and geometry together) all the weight equations are described as well.

2.9 Subroutine TDOME. This routine calculates the skin thickness of an elliptical hemispheroidal dome. The thickness is calculated from the basic stress relationship:

$$t = \frac{Pa^2}{2b\sigma}$$

where:

a = radius of dome

b = height of dome

σ = design ultimate stress

P = internal pressure

A minimum gage is assumed to correspond to typical manufacturing gages. A 20% safety factor is also assumed.

2.9.4 Subroutine TFRUS. This routine calculates the equivalent skin/stringer thickness for a frustrum or cylinder. Additionally, a description of the required frames and their spacing is generated. The skin thickness is initially calculated from the equation:

$$t = \frac{PR \cos \alpha}{\sigma}$$

where:

R = largest radius of frustrum

p = internal pressure

σ = design ultimate stress

α = angle of inclination of frustrum sides

A minimum gage is assumed to correspond to typical manufacturing gages. An integral stiffened stringer is assumed with a web thickness equal to twice the skin thickness and a web height equal to thirty times the skin thickness. The stringer spacing is equal to the web height divided by 0.6557. The equivalent skin/stringer thickness (TBAR) is defined as:

Table 2-3 Directory of Routines - Cryogenic Tank Sizing

The weight and geometry of these tanks are computed using these subroutines	(Paragraph)	Fwd Body Tank	Aft Body Tank	Under Floor Tank	Wing Inter. Tank	Wing Exter. Tank
TDOME	2.9.3	X	X			X
TFRUS	2.9.4	X	X	X		X
FUSV	2.9.5	X	X			X
DOMEV	2.9.6	X	X			X
DOMES	2.9.7	X	X			X
FUSS	2.9.8	X	X			X
NOFD	2.9.9	X	X			X
NOFF	2.9.10	X	X			X
TLTT	2.9.11				X	
TLTG	2.9.12			X	X	
TLTW	2.9.13			X	X	
WSUM	2.9.15	X	X	X	X	X
FBT	2.9.14	X				
BBT	2.9.14			X		
ABT	2.9.14		X			
WIT	2.9.14				X	
ETT	2.9.14					X

$$\bar{t} = t_s + \frac{B_w t_w}{B_s}$$

Utilizing these assumptions the material stress is calculated assuming a combined loading condition and employing the Hencky-Von Mises theory:

$$\sigma_{net} = \sqrt{(\sigma_h)^2 + (\sigma_h)(\sigma_a) + (\sigma_a)^2}$$

where:

$$\sigma_h = \frac{pR}{\bar{t} - A_s/B_s} \quad = \text{hoop stress}$$

$$\sigma_a = \sigma_L + \sigma_p + \sigma_m \quad = \text{axial stress}$$

and where:

$$\sigma_L = [\,(k)(W_f)(N_z) / 2\pi (r)(\bar{t})\,]$$

$$\sigma_p = [\,(p)(R)/\,2\,(\bar{t})\,]$$

$$\sigma_m = [\,(W_f)(L)/\,(8)(\pi)(r^2)(\bar{t})\,]$$

W_f = weight of fuel in tank

N_z = flight design load factor

p = pressure

R = largest radius

r = smallest radius

$\bar{t}$ = equivalent skin/stringer thickness

A_s = area of stringer

b_s = stringer spacing

L = length of cylinder/frustrum

The stress in the material is compared to the ultimate stress allowed in the material. If the two values are not within 5% of one another, the skin gage is revised to bring these values within the 5% acceptable limit. If minimum skin gage has been achieved, but this 5% acceptable limit has not, the minimum skin gage takes preference and the material stress will be less than the ultimate stress by more than 5% value.

The frame spacing for this skin/stringer combination is calculated assuming that both the skin and the stringers will buckle at the same time under stress - thus this is theoretically the maximum frame spacing.

$$b_f = \sqrt{\left(\frac{\pi^2 E}{\sigma_{CR}}\right)\left(\frac{Ic}{Ao}\right)}$$

where:

b_f = maximum frame spacing

E = modulus of elasticity

σ_{CR} = buckling stress

Io = skin + stringer area moment of inertia

Ao = skin + stringer cross sectional area

The theoretical frame dimensions are calculated in the following manners:

$$b_c = \left[\frac{(C_f)(W_f)(L)(d_f)^2}{(8)(S_f)(E)(.0135)}\right]^{.25}$$

where:

b_c = frame cap width

C_f = frame stiffness coefficient

W_f = weight of fuel

L = length of cylinder or frustrum

d_f = frame diameter

S_f = frame spacing

E = modulus of elasticity - tension

and

t_c = $b_c/30.0$ = thickness of cap

t_w = $(b_c/60.0)1.30$ = thickness web

h_f = $2.5\ (b_c)$ = frame height

$$I_f = \frac{b_c\ (2\,h_f\,t_c)^3 - (h_f)^3\ (b_c - t_w)}{12} = \text{area moment of inertia of the frame}$$

The number of frame splices is calculated as shown:

N_s = $2\pi r/240$

r = radius of frame

The length of each splice is calculated as:

$$L_s = 4\ (D_f)\ (N_f)$$

where:

D_f = diameter of fastener

N_f = 10 = (number of fasteners)

Then the volume of the splices is:

$$V_s = N_s\ (L_s)\ (2 + b_c + t_c)$$

Additionally, this routine prints out a summary of the skin/stringer geometry and stress data, general frame and splice data and individual frame and splice data.

2.9.5 Subroutine FUSV. This routine calculates the volume of a frustrum of a cone.

$$V_f \quad \frac{h}{6} \left[A_1 + 4A_n + A_2 \right] = \text{volume}$$

where:

A_1 = area at one end

A_2 = area at other end

A_n = area midway between ends

h = length (distance between ends)

2.9.6 Subroutine DOMEV. This routine calculates the volume of an elliptical hemispheroid.

$$V_d = 2/3\ (\pi)\ (r^2)\ (h)$$

where:

V_d = volume of an elliptical hemispheroid

r = radius of an elliptical hemispheroid

h = height of an elliptical hemispheroid

2.9.7 Subroutine DOMES. This routine calculates the surface area of an elliptical hemispheroid.

$$S_d = \pi \left[R^2 + \frac{H^2}{2(A)\ (\text{Log}_e\ (1 + A/1-A))} \right]$$

where:

S_d = surface area of an elliptical hemispheroid

$$A = \frac{1}{R} \sqrt{R^2 + H^2}$$

and:

R = radius of an elliptical hemispheroid

H = height of an elliptical hemispheroid

2.9.8 Subroutine FUSS. This routine calculates the surface area of a frustrum of a cone.

$$S_f = \pi (R_1 + R_2)\sqrt{H^2 + (R_1 - R_2)^2}$$

where:

S_f = surface area of a frustrum of a cone

R_1 = large radius of a frustrum of a cone

R_2 = small radius of a frustrum of a cone

H = height of a frustrum of a cone

2.9.9 Subroutine NOFD. This routine calculates typical non-optimum factors associated with the manufacture of an elliptical hemispherical dome. The non-optimum factors calculated are:

1. Non-optimum factor associated with machining tolerance on dome bulkheads: a manufacturing tolerance of .0381 cm (0.015 inches) is assumed.

2. Non-optimum factor associated with weld lands between gore sections of dome: a constant factor of 1.065 is assumed.

3. Non-optimum factor associated with the pressure discontinuity load on dome

4. Non-optimum factor associated with access cutouts in dome cutout: a circular cutout with a radius of 45.72 CM (18 inches) is assumed. Additionally, the weight increment penalty is assumed to be seven times the weight of the cutout.

5. Non-optimum factor associated with attach ring on dome bulkhead: a constant factor of 1.255 is assumed. This factor is composed of a non-optimum factor for the adapter ring (1.075), for the buildup from the dome/cylinder interface to the ring (1.035), for the extension of stringers from cylinder to ring (1.115) and for the taper roundout from ring to dome (1.03).

2.9.10 Subroutine NOFF. This routine calculates typical non-optimum factors associated with the manufacture of a frustrum of a cone, or a cylinder. The non-optimum factors calculated are:

1 Non-optimum factor associated with manufacturing mismatch tolerance on barrel stringers: a mismatch tolerance of .0381 cm (.015 inches) on each side of the stringer is assumed.

2. Non-optimum factor associated with machining tolerance on stringers in barrel section: a tolerance is assumed (over stress gage) of .0381 cm (.015 inches).

3. Non-optimum factor associated with fillet radius of .3175 cm (0.125 inches) is assumed.

4. Non-optimum factor associated with weld lands between skin panels of barrel section: a maximum panel width of 215.9 cm (85 inches) is assumed to determine number of circumferential welds while the number of longitudinal welds is assumed to be 3 for a circumference of 18.36 meters (60 feet) or less and 4 for any greater circumference.

5. Non-optimum factor associated with step-gaging of barrel skins: a constant factor of 1.07 is assumed (i.e. panel is of constant thickness).

6. Non-optimum factor associated with pressure discontinuity loads on barrel.

7. Non-optimum factor associated with frame pads on barrel.

2.9.11 Subroutine TLTT. This routine computes the skin thickness required for three lobe tanks.

$$t_s = \frac{pa}{2\sigma}$$

where:

p = pressure

a = tank lobe diameter

σ = allowable stress

2.9.12 Subroutine TLTG. This routine calculates the volume of a three-lobe conventional membrane tank. The tank volume is calculated in the following manner:

$$\text{Tank volume} \approx (L-a)\ \frac{a^2}{8}\left\{6\pi - 4\left[\cos^{-1}\left(\frac{N_1-1}{2}\right)+\cos^{-1}\left(\frac{N_2-1}{2}\right)\right]\right.$$

$$\left.+(N_1-1)\sqrt{3+N_1(2-N_1)}+(N_2-1)\sqrt{3-N_2(2-N_2)}\right\}$$

$$+\frac{\pi a^3}{12}\left\{6-\frac{3}{4}\left[(3-N_1)^2+(3-N_2)^2\right]+\frac{1}{8}\left[(3-N_1)^3-(3-N_2)^3\right]\right\}$$

The volume enclosed by the storage void envelope is

$$\text{Void volume} = \frac{1}{2}a^2 L\,(N_1+N_2)$$

The volumetric efficiency is

$$\eta = \frac{\text{Total tank volume}}{\text{Void volume}}$$

Where all variables are as shown in figure 2-5.

2.9.13 Subroutine TLTW. This routine calculates the weight of a three-lobe conventional membrane tank. The tank weight is calculated in the following manner.

$$\omega_w \quad \frac{\pi a^2 \omega_w t}{2}(N_1+N_2)+\frac{atL\omega_w}{2}\left\{6\pi-4\left[\cos^{-1}\left(\frac{N_1-1}{2}\right)+\cos^{-1}\left(\frac{N_2-1}{2}\right)\right]\right.$$

$$\left.+\sqrt{(N_1-1)\,3+N_1(2-N_1)}+\sqrt{(N_2-1)\,3+N_2(2-N_2)}\right\}$$

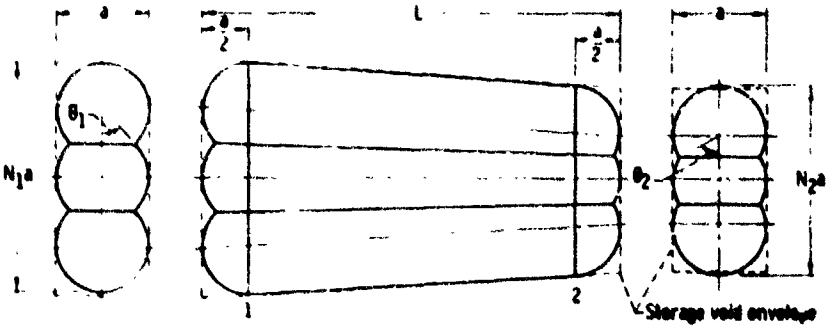

Figure 2-5 Three-lobe Conventional Membrane Tank

where:

ω_w = tank material density

t = tank skin gage

Other symbols as shown on figure 2-5

2.9.14 Weight and Volume Driver Routines. The routines named FBT, BBT, ABT, WIT, and ETT apply to, respectively, the forward body tank, under-floor tanks, aft body tank, wing internal tanks, and the wing external tanks. These routines act only as drivers, calling up the other subroutines which do the calculations. See the directory, table 2-3 , to find where the individual subroutines are discussed.

2.9.15 Subroutine WSUM. This subroutine calculates the insulation weight for cryogenic tanks. It sums the surface areas of tanks previously calculated and multiplies by a thickness and density from input data.

$$W_i = (S_t)\ (t_i)\ (P_i)$$

where:

S_t = total surface area of cryogenic tanks

T_i = insulation thickness

P_i = insulation density

The subroutine also sums the total tank weight to compute the mass fraction.

2.10 REFERENCES

1. Caddell, W. E., "The Use of Aircraft Density in Preliminary Design," SAWE Paper 813, 1970.

2. Chambellan, R. E., Lubonski, J. F., and Bevevino, W. A., "Structural Feasibility Study of Pressurized Tanks for Liquid Methane Fueled Supersonic Aircraft," NASA TN D-4295, December 1967.

SECTION 3

WEIGHT ANALYSIS

This section describes the weight equations that are needed to produce a group weight statement, loadings for computing design weights iteratively, and sufficient data to provide mass distribution used in the loads programs. The equations are relatively simple types that one normally uses in scaling equations where minimal design data is available. The equations are generally empirical but in some cases are based on analytical techniques with empirically derived coefficients. The nomenclature and weight definitions generally follow those of MIL-STD-1374.

3.1 WING WEIGHT. Three wing weight methods are provided, the selection being made by assigning a value (via input) to one of the coefficients. The first method (Green method described in Section 3.1.1) is based on the work of G. G. Green (see Note 1) and takes into account varying amounts of relieving loads and the attendant wing weight reductions. The second method (alternate method described in Section 3.1.2) is a purely empirical procedure based on an extensive regression fit of more than 100 aircraft wings of widely divergent characteristics. Although insensitive to certain design considerations, it has been shown to provide excellent scaling effects for variations in the included parameters, especially when calibrated to a known starting point. The third method (described in Section 3.1.3) is a multi-station analysis with simplified expressions for approximating external loads and allowable stresses. This method also considers concentrated and distributed relieving loads.

3.1.1 The Green Method. This method calculates separately the wing box (with increments for expanded root thickness, etc.), the leading and trailing edge weight, flap weight, and spoiler weight (if used). It uses an equivalent bending stress level based on an approximate bending moment at the side of the body, computed as follows:

Approximate Root Bending Moment

$$M_b = \frac{N_z W_t}{2}\left(\frac{C_p - Y_b}{\cos\Lambda}\right) - \Sigma\left(\frac{Py}{\cos\Lambda}\right)$$

where:

N_z = ultimate flight design load factor

W_t = design takeoff gross weight

C_p = spanwise center of pressure = .43 semi-span

Y_b = span station, side of body

ΣPy = sum of relieving moments

Λ = mid chord sweep angle

[1] Green, G. G., "Derivation of a Formula for Estimating Wing Weight," Consolidated Vultee Aircraft Corporation Report ZW-018, March 1945.

Bending Load Intensity Factor

$$P_c = \frac{M_b}{0.85\,(t_b)(C_b)}$$

where:

M_b = approximate root bending moment

t_b = box thickness at side of body

c_b = box chord at side of body

Equivalent Allowable Bending Stress Level and Coefficient

$$f_e = \frac{63{,}000\,(P_c)}{(P_c + 3000)} \qquad \text{(Figure 3-1)}$$

$$C_2 = \frac{2.215}{(P_c)^{.935}} \qquad \text{(Figure 3-2)}$$

where:

P_c = as defined above

f_e = equivalent allowable bending stress level

C_2 = coefficient

Basic Wing Equation

$$W_{w_{l_e}} = \frac{(3 + r)\ (C_1)\ (Sw)\ (N_z\, w_d)^{.25}}{(3 + r) + \dfrac{C_2 N_z\,(.34L^2)}{t_b}}$$

and

$$W_{w_b} = \frac{(3 + r)\ (C_2)\ (N_z)\ \left[\dfrac{W_d R L^2}{1/R + r} - \sum \dfrac{PY^2_k}{\cos 2\Lambda}\right]}{t_b \left[(3 + r) + \dfrac{C_2 N_z\,(.34L^2)}{t_b}\right]}$$

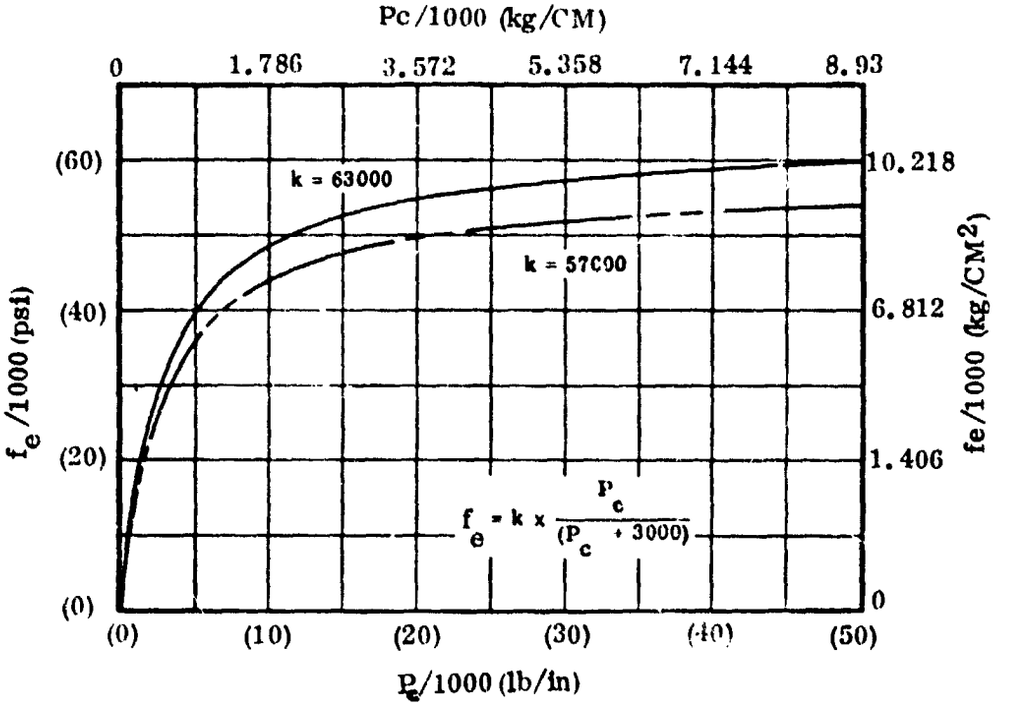

Figure 3-1 Root Bending Stress Versus Chord Loading (Bending Cover)

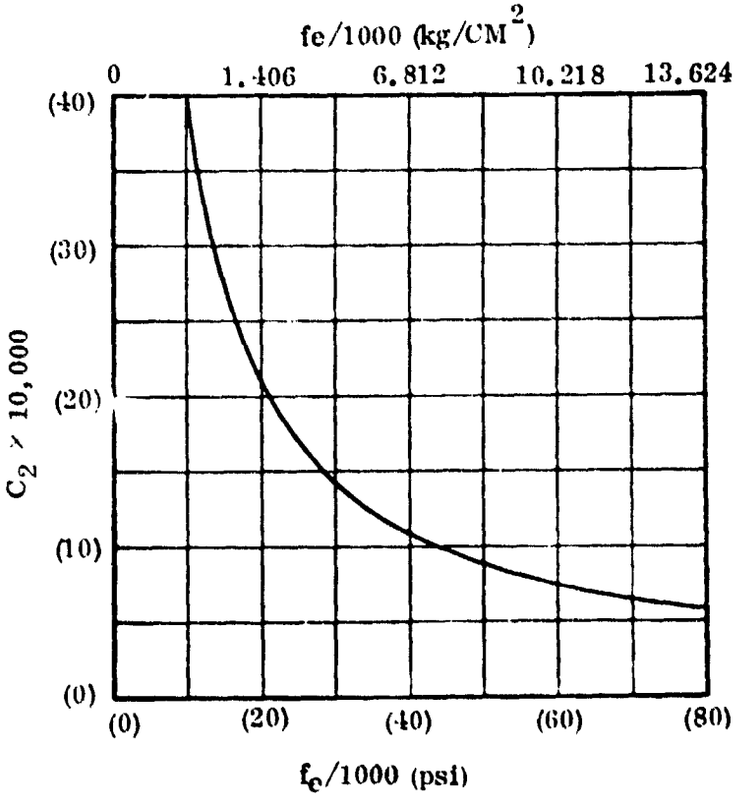

Figure 3-2 Stress Level Coefficient Versus Root Bending Stress

$$W_{b_1} = W_{w_{l_e}} + W_{w_b} = \frac{(3+r)\left[C_1(S_w)(N_z w_d)^{.25} + \frac{C_2(N_z)}{t_b}\left(\frac{w_d R L^2}{1/R+r} - \sum \frac{P Y^2 k}{\cos^2 \Lambda}\right)\right]}{(3+r) + \frac{C_2 N_z}{t_b}(.34\ L^2)}$$

where:

$W_{w_{l_e}}$ = basic leading edge weight

W_{w_b} = basic structural box weight

W_{b_1} = basic wing weight excluding special penalties

S_w = wing area

N_z = ultimate flight design load factor

w_d = flight design gross weight

L = wing semispan/cosine sweep angle (mid-chord)

Λ = mid-chord sweep angle

P = relieving load

Y = spanwise distance to relieving load from centerline

k = thickness coefficient (Figure 3-3)

r = ratio of tip thickness to thickness at side of body

R = ratio of center of pressure location to semispan (Figure 3-4)

t_b = box thickness at side of body

C_1 = input coefficient

C_2 = input coefficient

The basic box structure (w_{wb}) is that calculated by the right side portion of the above equation. In order to compute an increment for expanded root thickness, an equation is provided to approximate the spanwise distribution of the wing box weight:

$$w_{nb} = w_{wb}\left(\frac{2\eta_b}{1+\eta_b}\right)$$

where:

w_{nb} = box weight inboard of the thickness break

w_{wb} = total wing box weight

η_b = decimal semispan of location of break

$$w_{ns} = w_{wb}\left(\frac{2\eta_s}{1+\eta_s}\right)$$

where:

w_{ns} = box weight inboard of side of body

η_s = decimal semispan of location side of body

Expanded Thickness Increment

$$w_{\Delta t} = .5(w_{nb}-w_{ns})\left(\frac{t_s}{t_{sx}} - 1\right) + (w_{ns})\left[\left(\frac{t_s}{t_{sx}}\right)^{.8} - 1\right] \quad \text{(Figure 3-5)}$$

where:

t_s = thickness side of body for basic trapezoid wing

t_{sx} = thickness side of body after thickness expansion

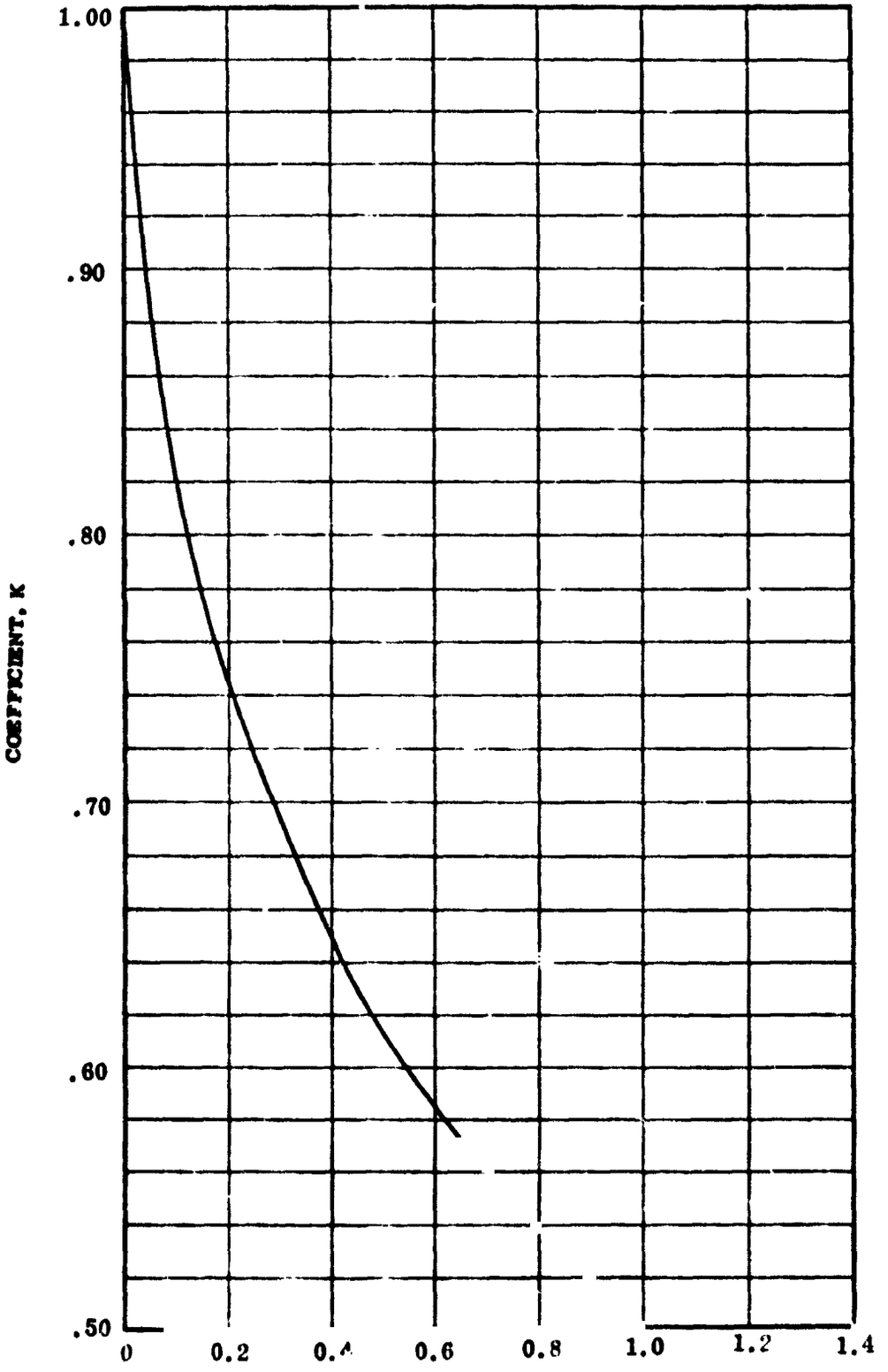

Figure 3-3 Term Accounting for Wing Relieving Loads

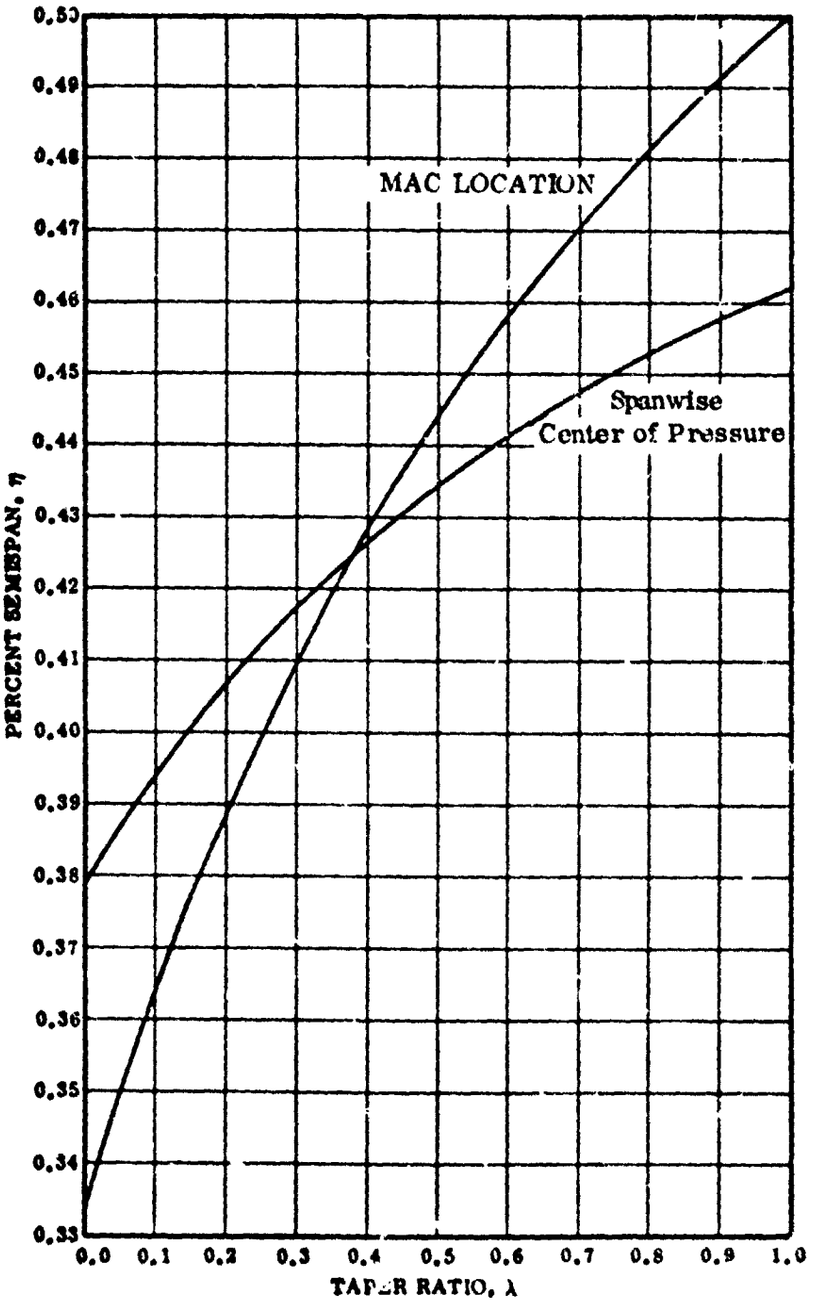

Figure 3-4 R Term of Basic Wing Equation

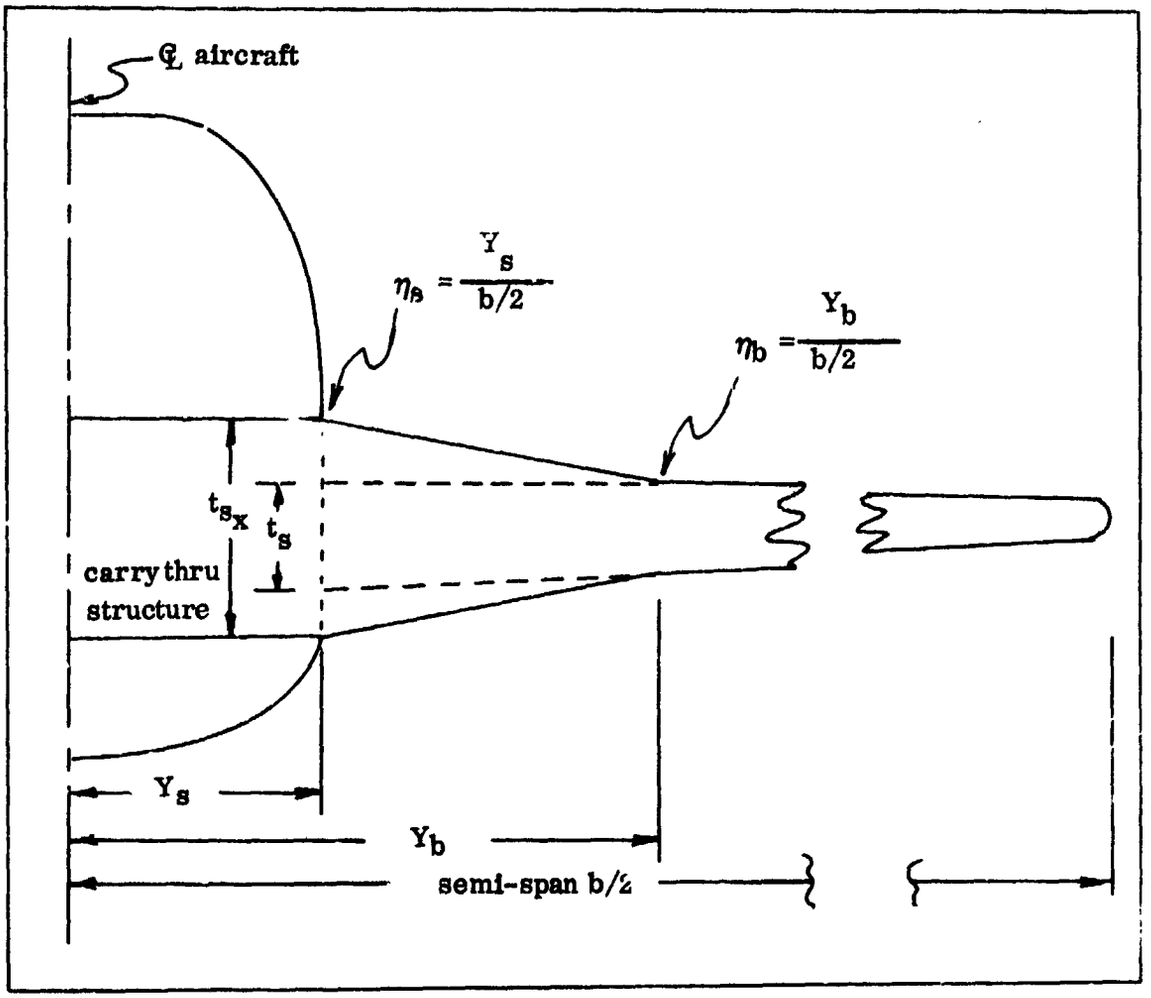

Figure 3-5 Treatment of Expanded Thickness Wing Root

Basic Wing Weight (Including corrections for special penalties)

$$w_{bw} = w_{b1} (k_{p1}) + (k_{p2})$$

where:

w_{bw} = basic wing weight with special penalties

w_{b1} = basic wing weight without special penalties

k_{p1} = input coefficient for special penalties (savings)

k_{p2} = input constant penalty for special features

Secondary Structure Weight

$$w_{s2} = .05\, w_{wb}$$

Flap Weight (Figure 3-6)

$$w_f = k_f \left[\frac{w_T S_f C_f}{S_w (10)^5}\right]^{.57} \left[\frac{1}{(t/c)_f}\right]^{.228} \left[.5 + .3\,\frac{M_f}{.5} + .2\left(\frac{\delta_f}{37}\right)\right]$$

where:

k_f = flap configuration factor

w_T = design takeoff weight

S_f = flap area

C_f = flap chord

S_w = wing area

$(t/c)_f$ = wing thickness ratio at center of flap

M_f = ratio fowler motion to flap chord

δ_f = flap deflection in degrees

The last major element of the above equation was added to provide some weight sensitivity for fowler motion and deflection. The term is based on studies indicating that, based on a flap with 50 percent fowler motion and 37 degree deflection, approximately 30 percent of the weight varies with fowler motion and 20 percent varies with deflection. In addition, differences in flap configuration are accounted for by selections of the coefficient k_f.

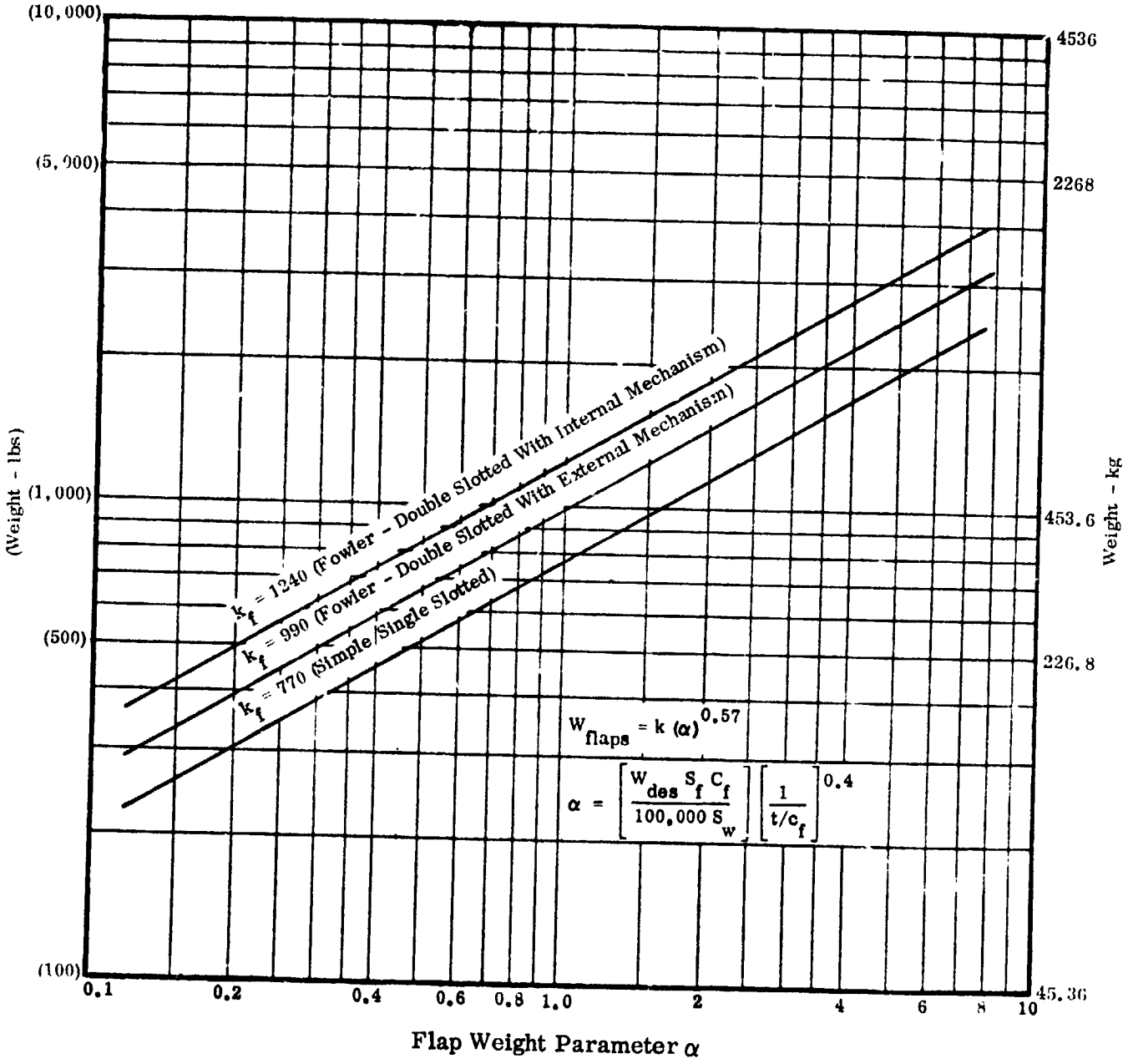

Figure 3-6 Wing Trailing Edge Flap Weight

Leading Edge High Lift Device Weight (Figure 3-7)

$$w_{led} = k_{led} \left[\frac{N_z w_T}{1000 S_w} \right]^{.324} (S_{led})^{1.081}$$

where:

N_z = ultimate maneuver load factor

w_T = design take-off weight

S_w = wing area

S_{led} = area of leading edge high lift device

K_{led} = input coefficient (see Figure 3-7)

Spoiler Weight (Figure 3-8)

$$w_{sp} = k_{sp} \left[\frac{w_T L_{sp}}{1000 S_w} \right]^{.569} [C_{sp}]^{1.139} \left[\frac{1}{(t/c)_{sp}} \right]^{.228}$$

where:

w_T = design takeoff weight

L_{sp} = spanwise length of spoiler

S_w wing area

C_{sp} spoiler chord length

$(t/c)_{sp}$ wing thickness ratio at center of spoiler

k_{sp} input coefficient (Figure 3-8)

Wing Fold Weight

$$k_{fold} \quad \frac{25}{b}$$

$$C_{fold} = C_r \left[1 - k_{fold} (1 - \lambda) \right]$$

$$t_{fold} = t_r \left[1 - k_{fold} (t_r - t_t) \right]$$

$$W_{fold} = 10 (10^{-6}) \left[\frac{N_z W_d b (1 - k_{fold})^{1.5}}{t_{fold}} \right] + 1.0 (C_{fold})^2 (t_{fold})$$

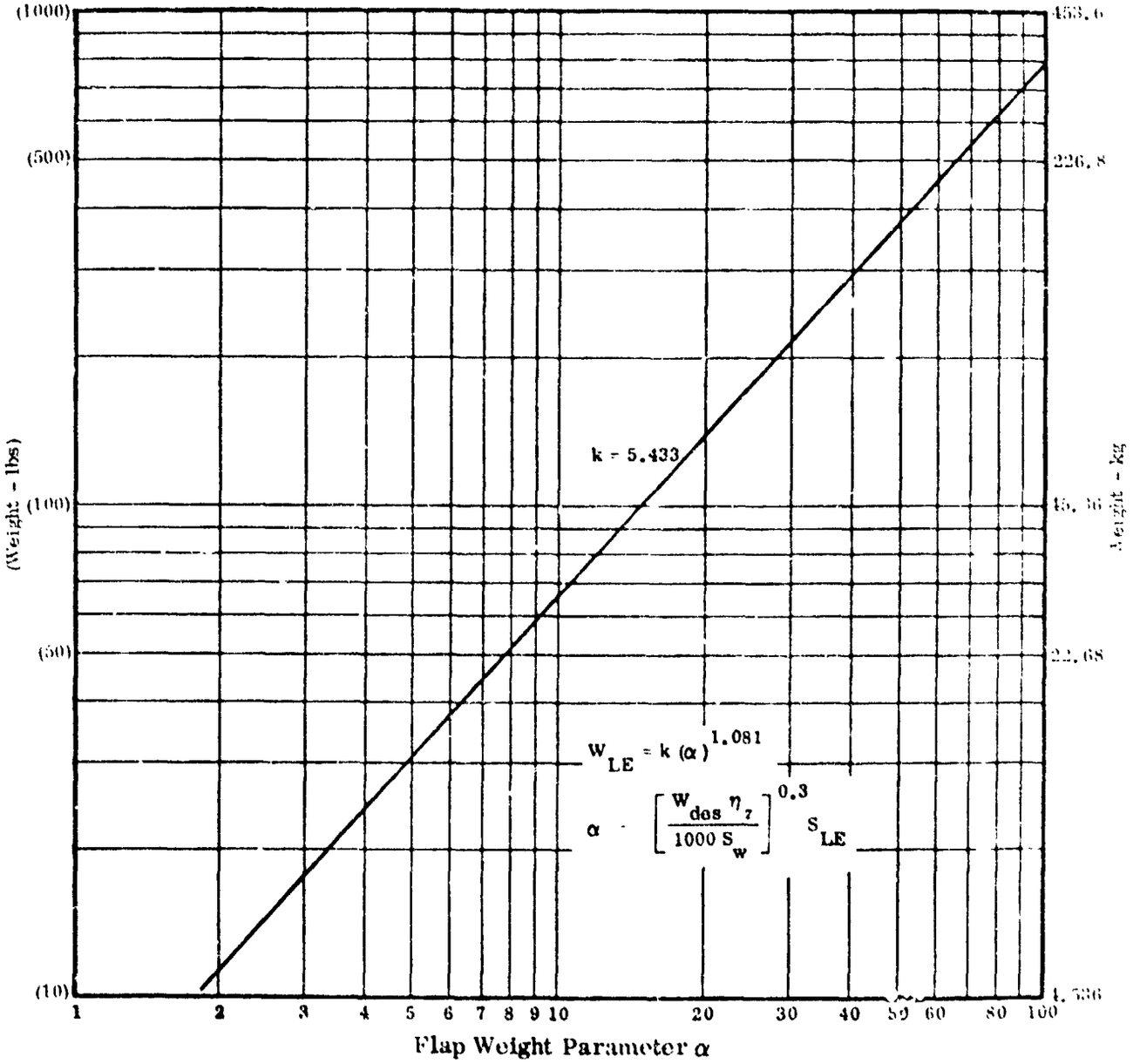

Figure 3-7 Wing Leading Edge Flap Weight

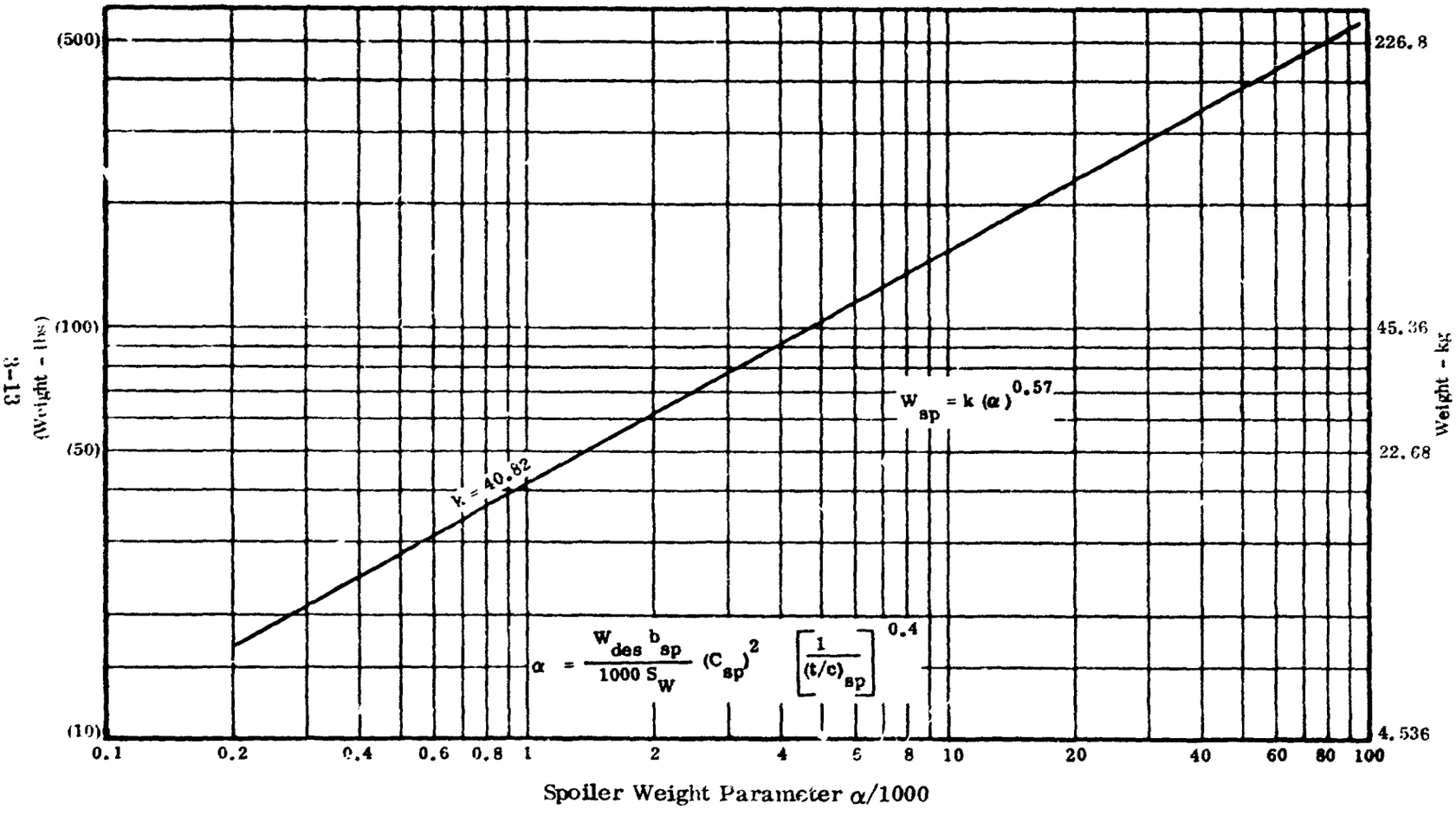

Figure 3-8 Wing Spoiler Weight

where:

k_{fold} = wing fold location, decimal semi-span

b = wing span

C_{fold} = wing chord at the fold line

C_r = wing chord at the root

λ = wing taper ratio

t_{fold} = wing thickness at the fold line

t_r = wing thickness at the root

t_t = wing thickness at the tip

W_{fold} = wing fold weight penalty

N_z = ultimate flight design load factor

W_d = flight design gross weight

Total Wing Weight

$$W_w = W_{bw} + W_{s2} + W_f + W_{led} + W_{sp} + W_{fold}$$

where:

(All values as defined above)

3.1.2 Alternate Wing Weight Equation (Figure 3-9)

$$W_{wa} = k_{wa}\left[\left(\frac{W_d N_z}{1000}\right)^{.52} (S_w)^{.7} (AR)^{.47} \left(\frac{1+\lambda}{t/c}\right)^{.4} (F_\Lambda)\right] + W_{iw}$$

where:

W_d = flight design gross weight

N_z = ultimate flight design load factor

S_w = wing area

AR = wing aspect ratio

λ = wing taper ratio

Figure 3-9 Wing Weight vs α

t/c = wing thickness ratio at the root

k_{wa} = input coefficient (Figure 3-9)

Λ = sweep of wing mid chord line

w_{iw} = input weight increment for any special feature

$$F_{\Lambda} = .3 + .7\left(\frac{1}{\cos \Lambda}\right)$$

3.1.3 Multi-station Analysis Method. This method performs shear and moment computations at each rib station, estimates allowable stresses, computes material required (separately for ribs, box cap material, and shear webs) and integrates the results. The weights of leading and trailing edge items are obtained by an empirical equation. The analysis begins at the tip and integrates inboard. The sequential steps are as follows.

3.1.3.1 Rib Spacing. Rib spacing is calculated as a function of the wing thickness, beginning at the tip (y_1 = semi-span)

$$S_i = \sqrt{(t_{i-1})^2 + 256}$$

where:

t_{i-1} = wing thickness at wing station y_{i-1}

S_i = space between ribs at y_i and y_{i-1}

3.1.3.2 Net Wing Airloads. Net wing airloads are estimated by an expression which assumes a distribution midway between elliptical and planform shape. This distribution is further modified by an empirical expression to account for the inboard shift of the center of pressure of swept wings under load. A "net airloads" empirical expression provides for addition of horizontal tail loads and also relief due to the wing structure weight. (Relieving loads due to concentrated items or distributed fuel are handled separately by analytical procedures.)

$$\ell_n = \frac{(N_d)\,(L_N)\,(f_r)}{b}\left[\frac{2}{\pi}\sqrt{1-\eta^2} + \frac{1}{(1-\lambda)\,(1-\eta)\,(1-\lambda)}\right]$$

where:

ℓ_n = unit airload at span station η

N_d = $N_z\left(\frac{w_d}{w_m}\right)$ = ultimate load factor applied to air load

L_N = $[w_m - .12(w_d)]\ (1 + .0125\ N_z)$ = net max air load

N_z = ultimate vertical load factor at w_{des}

w_d = flight design gross weight

w_m = maximum flight design gross weight

f_Λ = $2 - r_\Lambda + 2\eta(r_\Lambda - 1)$ = sweep unloading factor

r_Λ = $\dfrac{\cos \Lambda_{LE}}{\cos \Lambda_{.425}}$ = relative sweep ratio

η = wing span station, decimal semi-span

λ = wing taper ratio

b = wing span

3.1.3.3 Wing Fuel Relief. Wing fuel relief loads are assumed to be distributed linearly between the inboard and outboard fuel boundaries.

3.1.3.4 Concentrated Relief Loads. Concentrated relief loads are calculated for; (per side in each case) one main landing gear station, if wing mounted, two engine stations, and one external tank station.

3.1.3.5 Shear and Bending Moments. Shear and bending moments are obtained by integration of the preceding loads from the tip inboard to the particular station.

3.1.3.6 Bending Material Weight. Bending material weight is obtained by integration of the following:

$$w_b = 1.449 \sum_{y=b/2}^{y=0} \frac{4(M_i)\ (S_r)\ (\rho)}{.9(t_i)\ (f_b) \cos \Lambda_b}$$

where:

M_i = bending moment at span station y_i

S_r = $y_{i-1} - y_i$ = rib spacing to next outboard rib

ρ = material density

t_i = wing thickness at span station y_i

Λ_b = sweep angle of the 42.5% chord

f_b = allowable bending stress - section average

The allowable bending stresses are developed from the following relationships.

$$t_m = \text{equivalent minimum gage} = .00126\left(\frac{S_r}{\cos \Lambda_b}\right)\left(\frac{1 + (t/c)^2}{t/c}\right)^{.25}$$

$$R = \text{equivalent running load (buckling)} = 60{,}000\ (t_m)$$

$$M_c = \text{applied running load} = \frac{\dot{M}_i}{.9(t_i)\ (.45\ c_i)\ (\cos \Lambda_b)}$$

$$f_b = \frac{60000\ (M_c)}{R + M_c}$$

3.1.3.7 Shear Material Weight. Shear material weight is obtained by integration of the following:

$$w_s = k_s \sum_{y=b/2}^{y=0} \frac{4(V_i)\ (S_r)}{\cos \Lambda_b}$$

where

V_i = shear at span station y_i

S_r = $y_{i-1} - y_i$ = rib spacing to next outboard rib

Λ_b = sweep angle of 42.5% chord

k_s = $40.56\ (10^{-6})/(t/c)^{.5}$

3.1.3.8 Rib Material. Rib material weight is estimated by the following expressions which first estimate a minimum weight based on minimum practical gages and rib dimensions and then adds incremental weights for loads.

$$w_r = 1.841\ (P_g + P_L) = \text{weight of rib}$$

where

P_g = rib geometric weight parameter

P_L = rib load weight parameter

$$P_g = \left[5.568\ (10^{-6})\ (1 + t/c)\ (t/c)^{.25} + 7.584\ (10^{-6})\ (1 + t/c)^2\ (t/c)^{.5}\right] C^3$$

$$P_L = .0304\ (10^{-6})\left[\frac{W_m\ (C)^2}{t_w}\right]$$

where

t/c	=	wing section thickness ratio
w_m	=	maximum design gross weight
c	=	wing chord at that span station
t_w	=	wing max thickness at that span station

Rib weights are calculated individually and integrated over the span from tip to root.

3.1.3.9 Leading and Trailing Edge Material. Leading and trailing edge material is estimated by an empirical expression whose parameters reflect the fact that the complexity of high lift devices (the major contributor) is a function of the span loading of the wing.

$$W_{lt} = .057\ (S_w)\ \left(\frac{W_m}{b}\right)$$

where:

S_w = wing area

W_m = maximum design gross weight

b = wing span

3.2 HORIZONTAL TAIL WEIGHT (Figure 3-10)

$$w_h = .00563\ (C_h)(w_d)^{.6}\ (S_h)^{.469} \left(\frac{AR_h}{\cos^2 \Lambda}\right)^{.539} \left(\frac{1+\lambda}{t/c}\right)^{.692}$$

where:

C_h	=	calibration coefficient input (nominal value 1.0)
w_d		flight design gross weight
S_h	=	horizontal tail area
AR_h	=	horizontal tail aspect ratio
Λ		horizontal tail area mid-chord sweep angle
λ	=	horizontal tail taper ratio
t/c	=	horizontal tail root thickness ratio

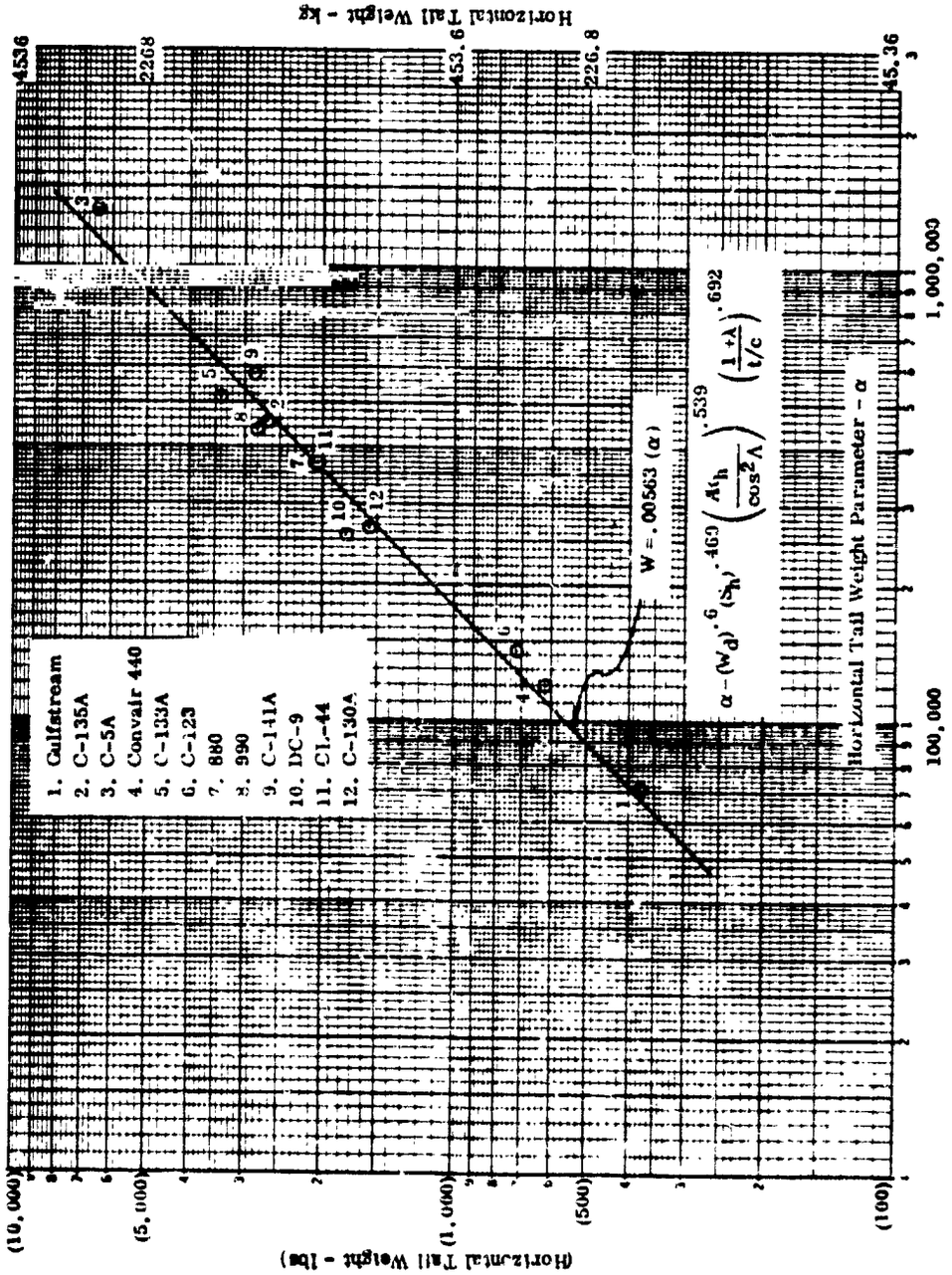

Figure 3-10 Horizontal Tail Weight vs α

ORIGINAL PAGE IS
OF POOR QUALITY

3.3 VERTICAL TAIL WEIGHT (Figure 3-11)

$$w_v = .0909\,(C_v)(w_d)^{.333}\,(S_v)^{.7}\left(\frac{AR_v}{\cos^2 \Lambda}\right)^{.35}\left(\frac{1+\lambda}{t/c}\right)^{.5}(1+\phi)^{.43}$$

where:

C_v = calibration coefficient input (nominal value 1.0)

w_d = flight design gross weight

S_v = vertical tail area

AR_v = vertical tail aspect ratio

Λ = vertical tail mid-chord sweep angle

λ = vertical tail taper ratio

t/c = vertical tail root thickness ratio

ϕ = horizontal tail location, decimal span of vertical tail

3.4 BODY WEIGHT

Body Weight For Nose Gear Catapult

$$W_{nc} = 4.03\,(10^{-6})(W_m)(L_n + 0.2\,h_b)\left(\frac{L_b}{h_b}\right)$$

where:

W_{nc} = body weight for nose gear catapult loads

W_m maximum flight design gross weight

L_n nose landing gear length

h_b = body depth

L_b = body length

Body Weight For Arresting Gear Loads

$$W_{agl} = 36.9\,(10^{-6})\,[\,W_L (V_{so})^2\,]^{0.71}$$

where:

W_{agl} = body weight for arresting gear loads

W_L = landing design gross weight

V_{so} = landing stall speed

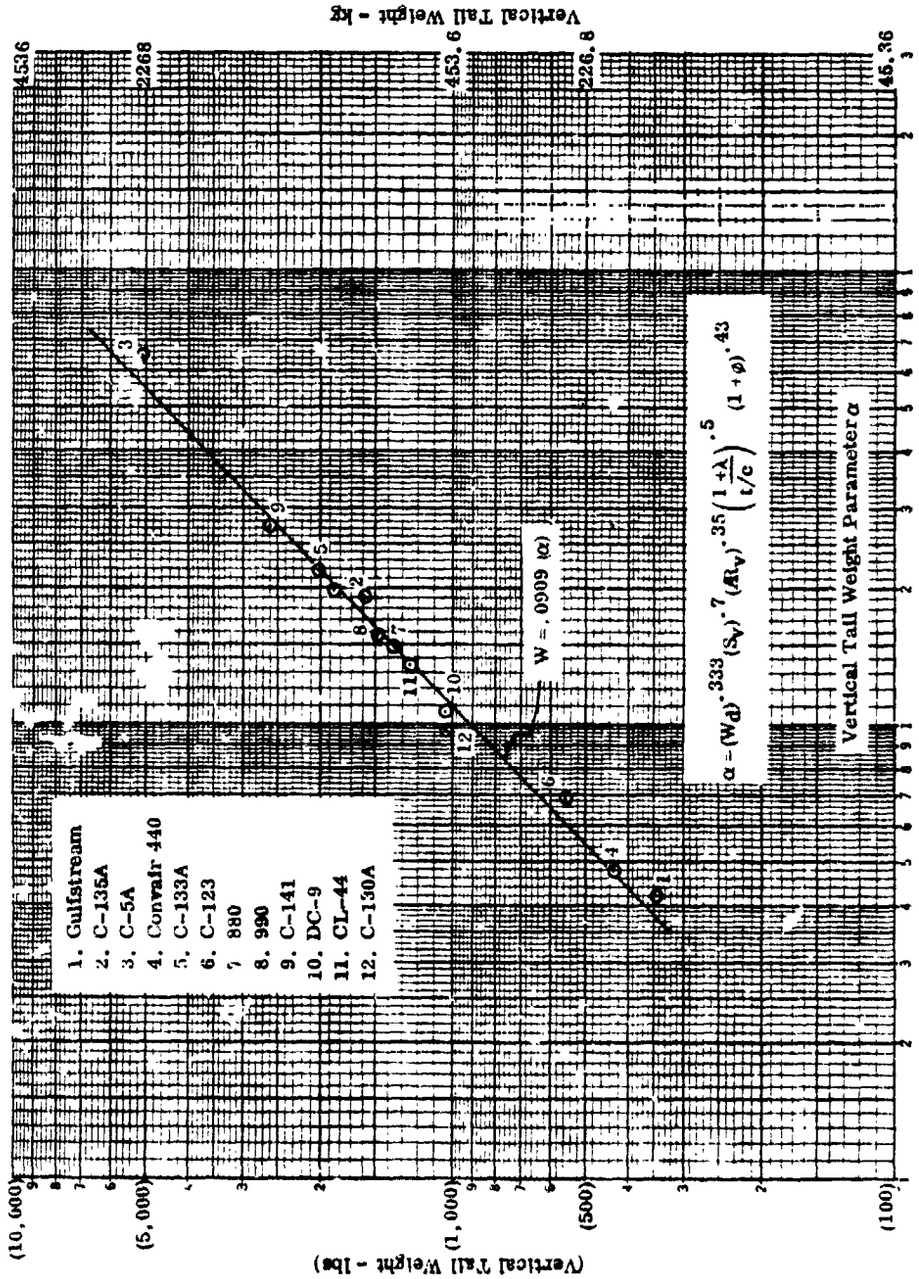

Figure 3-11 Vertical Tail Weight vs α

Total Body Weight (Figure 3-12)

$$W_b = k_b (N_z)^{.52} (W_d)^{.33} (L_b)^{.76} (h_b + b_b)^{1.2} + W_{nc} + W_{agl} + W_{ib}$$

where:

k_b = input coefficient (Figure 3-12)

N_z = ultimate flight design load factor

w_d = flight design gross weight

L_b = body length

h_b = body height

b_b = body breadth

W_{nc} = body weight for nose gear catapult loads

W_{agl} = body weight for arresting gear loads

W_{ib} = input weight increment for any special feature

3.5 LANDING GEAR WEIGHT. Two methods are provided for landing gear weight. A simplified equation requiring no dimensional data is provided for gross scaling. It is shown in Paragraph 3.5.2. A more detailed method, in which several components are calculated separately, is shown in the following paragraph.

3.5.1 Landing Gear Component Weights

Main Landing Gear

Struts $$w_{sm} = .0032 (F_{vm} \times S_m)^{.75} \left(\frac{L_m}{S_m}\right)$$

Drag Braces $$w_{dm} = .0026 (F_{dm})$$

Attachments $$w_{am} = .003 (F_{vm})$$

Brakes $$w_{bm} = .00562 (N_{wm}) (E_m)^{.75}$$

Brake Mechanism $$w_{mbm} = 2.2 \left(\frac{w_{bm}}{N_{wm}}\right)^{.5} (N_{wm})$$

Tires $$w_{tm} = .001 (N_L) (w_L) \text{ - - - [or input]}$$

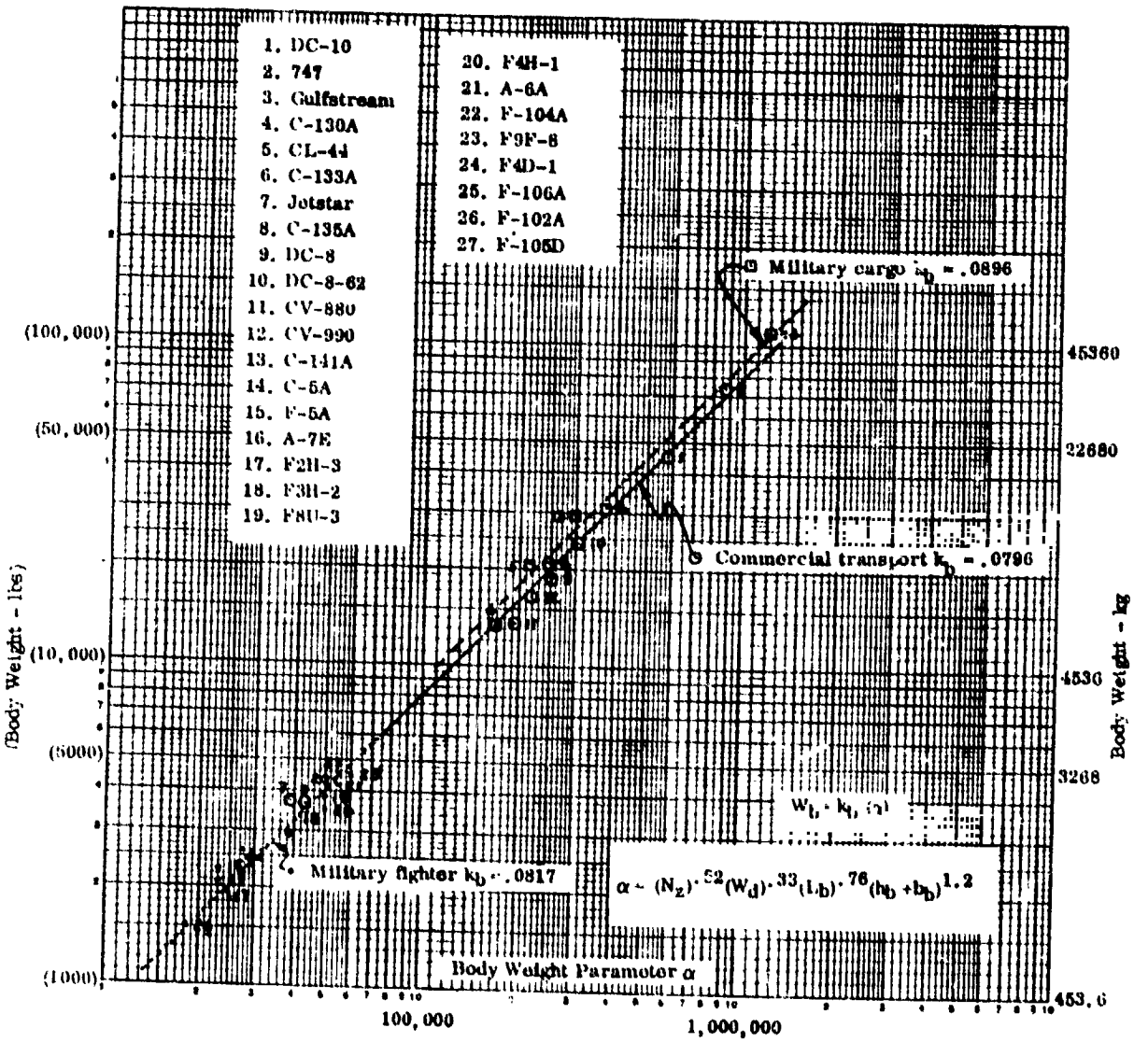

Figure 3-12 Body Weight vs α

Wheels

$$w_{wm} = .07\,(N_{wm})\left[\frac{N_L\,(w_L)}{N_{wm}(1000)}\right]^{.7}(D_{wm})^{1.3}\left(1+\frac{w_{fm}}{40}\right) \text{ - - - [or input]}$$

Retracting Mechanism

$$w_{mm} = .53\left[1.15\,(w_{sm} + w_{am} + w_{dm})\right]^{.66}$$

where:

F_{vm} = ultimate vertical load per main gear
S_m = stroke of main strut
L_m = length of main strut
F_{dm} = ultimate design drag load for strut
N_{wm} = number of main wheels
E_m = brake design energy for wheel
N_L = ultimate landing load factor
w_L = design landing weight
D_{wm} = main wheel bead ledge diameter
w_{fm} = main wheel flange width

Nose Landing Gear

Strut

$$w_{sn} = .0016\,(F_{vn} \times S_n)^{.75}\left(\frac{L_n}{S_n}\right)$$

Drag Brace

$$w_{dn} = .0013\,(F_{dn})$$

Attachments

$$w_{an} = .0015\,(F_{vn})$$

Tires

$$W_{tn} = .0001\,(N_L)\,(w_L) \text{ - - - [or input]}$$

Wheels

$$w_{wn} = .07\,(N_{wn})\left[\frac{.2\,(N_L)\,(w_L)}{N_{wn}\,(1000)}\right]^{.7}(D_{wn})^{1.3}\left(1+\frac{w_{fn}}{40}\right)\text{- - - [or input]}$$

Retracting Mechanism $w_{mn} = .53\,[1.3\,(w_{sn} + w_{an} + w_{dn})]^{.66}$

Catapult Penalty

$$W_{cp} = 0.312\,(L_n) + 0.00223\,(W_m)$$

where:

F_{vn} = ultimate vertical load for nose gear

S_n = stroke of nose gear

L_n = length of nose strut

F_{dn} = ultimate design drag load

N_L = ultimate landing load factor

W_L = landing design weight

W_m = maximum flight design gross weight

N_{wn} = number of nose wheels

D_{wn} = nose wheel bead ledge diameter

w_{fn} = nose wheel flange width

Arresting Gear

$$W_{ag} = 0.05\,(W_L)^{0.75}$$

where:

W_{ag} = arresting gear weight

W_L = landing design weight

3.5.2 Simplified Method, Landing Gear Weight (Figure 3-13)

$$w_{LG} = k_L\,(R_M)^{.21}\,(w_L)^{1.12}$$

ORIGINAL PAGE IS
OF POOR QUALITY

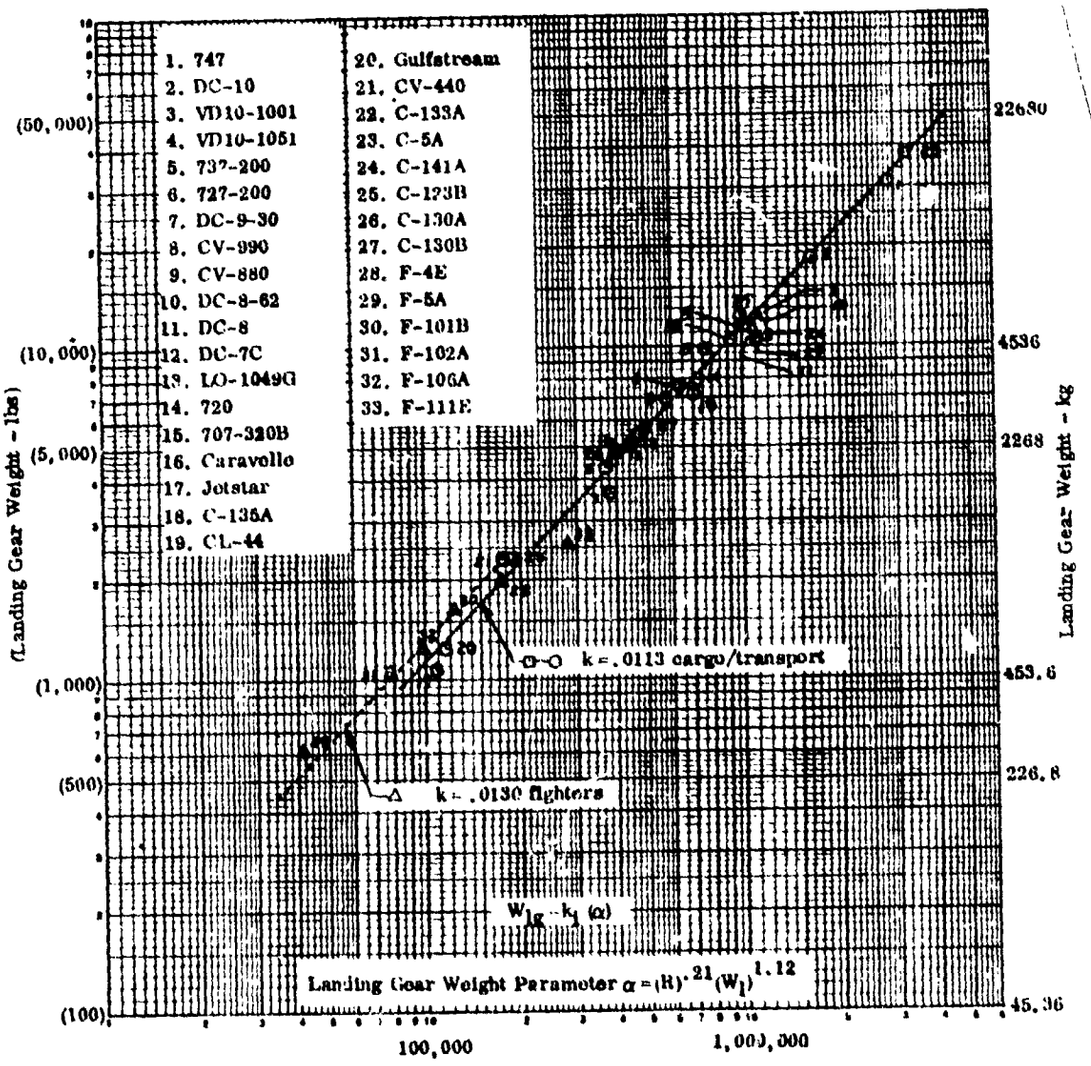

Figure 3-13 Landing Gear Weight vs α

where:

w_L = design landing weight

R_M = ratio of max gross weight to landing weight

k_L = coefficient (Figure 3-13)

3.6 SURFACE CONTROLS WEIGHT. An empirical method is providing for scaling. It depends primarily on size and shape parameters.

$$w_{sc} = k_{sc} \frac{(L_b + b_{ws})(S_w)^{.5}(q)^{.16}}{(AR)^{.85}} \quad \text{(Figure 3-14)}$$

where:

L_b = body length

b_{ws} = wing structural span

S_w = wing area

AR = wing aspect ratio

q = maximum dynamic pressure

The major factor in estimating surface controls weight, however, is identification of the features used to provide control. This can be accounted for only by selection of values for k_{sc}. The types of controls used varies widely from one aircraft to the other. The following list is provided for estimating a value of k_{sc} when a comparable aircraft value is not available. In this application, k_{sc} is the sum of incremental values selected from the following list.

Surface Control System	Δk_{sc}
Flight Controls	
Ailerons	.065
Elevons	.045
Spoilers	.035
Rudder	.035
Elevator	.045
Unit Horizontal Tail	.125
Adjustable Stabilizer	.010
Speed Brakes (separate)	.030
High Lift Systems	
Hinged Flaps	.045
Fowler Flaps	.085
Articulated Flap Vanes	.010
Hinged Leading Edge	.060
Translating Slats	.075
Krueger Flaps (simple)	.055

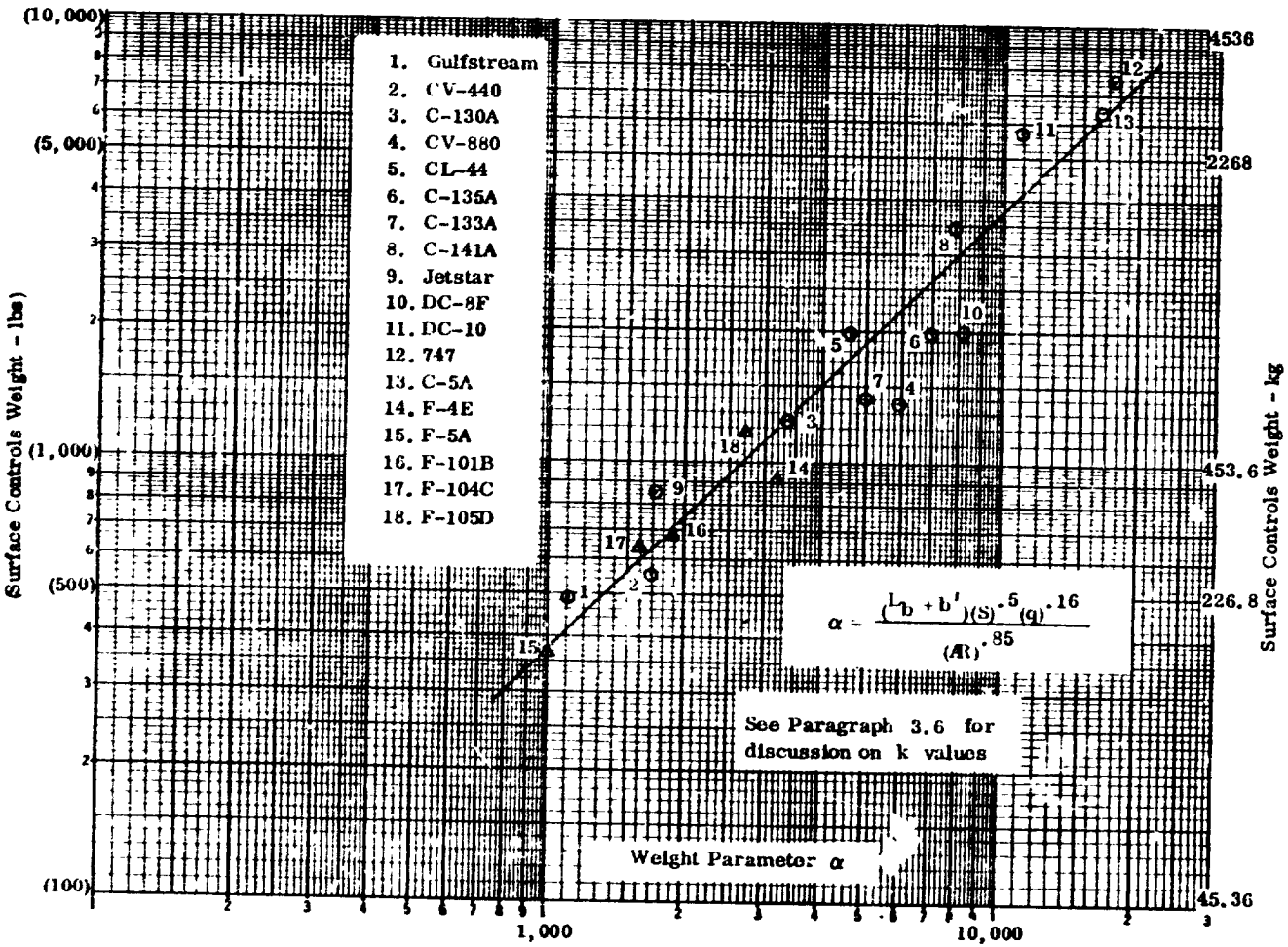

Figure 3-14 Surface Controls Weight vs α

3.7 NACELLES AND PYLONS.

3.7.1 Nacelle Weight. An empirical expression using weight of nacelle contents and nacelle dimensions is used to obtain nacelle weight.

$$w_n = 35.45\ (N_n)\left[\frac{k_E\ (w_{nc})(S_n)\ (R_d)}{10,000}\right]^{.59} \text{ --- } \left[\text{or input}\right]$$

where:

N_n = number of nacelles

w_{nc} = weight of nacelle contents

S_n = wetted area of nacelle surface

R_d = factor for non-circularity; ratio of height to width (or reverse, whichever is greater)

w_{nc} = 1.1 × engine weight (times 2 if siamese engines)

k_e = engine type coefficient

= 1.0 for single subsonic turbo-jet

= 2.33 for single subsonic turbofan

= 2.15 for single supersonic turbo-jet

= 0.32 for siamese subsonic turbo-jet

= 1.00 for siamese subsonic turbo-fan

3.7.2 Pylon Weights. Two empirical equations are provided, one for single engine nacelles and one for siamese engine installation.

Single Engine for Pylon

$$w_p = 24.11\ (N_p)\left[\frac{k_p\ (N_z)\ (w_{nc})\ (L_n)\ (D_n)}{(10)^6 \cos \Lambda_p}\right]^{.952} \left[S_p\right]^{.381}$$

Siamese Engine Pylons

$$w_p = 340.26\ (N_p)\left[\frac{(N_z)\ (w_{nc})\ (S_p)}{10^6\ (\cos\ \Lambda_p)}\right]^{.693}$$

where:

N_p number of pylons for aircraft

N_z = ultimate flight load factor

w_{nc} - weight of nacelle contents

S_p planform area of pylon

L_n nacelle length

D_n nacelle equivalent diameter

Λ_p = sweep of pylon leading edge (measured from vertical)

k_p - 1.46 for commercial transports, 1.0 for military

3.8 PROPULSION SYSTEMS WEIGHT. Engine sizing is accomplished in program GEOM, Overlay (WU, 1, 1). The output from that program defines an engine weight coefficient. The main engine weight is therefore determined by multiplying that coefficient by a reference engine weight. If engine weight is input, that value is used instead.

$$W_e = k_{eng} (W_{R_{eng}})$$

W_e = total engine weight

k_{eng} = engine scaling coefficient

$W_{R_{eng}}$ = reference engine weight

3.8.1 Propulsion Sub-systems. The propulsion systems weights are computed in Overlay (WU, 1, 2) using the following empirical equations. In most cases, provision is made for inputting fixed values which add to or replace that computed by coefficient. These are of the form

$$y = k_1 (x)^a + k_2$$

This form allows the user to input a fixed value by inputting a finite value for k_2 and zero for k_1. It obviously can also be used to vary part of the weight and fix part of the weight. The equations for the various sub-systems are as follows:

Thrust Reversers

$$w_{tr} = N_e [k_1 (T_e/10,000)^{.88} + k_2]$$

Exhaust Systems

$$w_{ex} = k_3 (w_e)^{.52} + k_4$$

Inlet Systems

$$w_{in} = k_5 (w_e)^{.37} = k_6$$

Cooling Systems

$$w_c = k_7 (T_e) (N_e) + k_8$$

Lubricating System

$$w_L = k_9 (w_e)^{.78} + k_{10}$$

Starting Systems

$$w_{st} = k_{11} (w_e)^{.65} + k_{12}$$

Engine Controls

$$w_{ec} = k_{13} [y_e + .3 (L_b)] (N_e) + k_{14}$$

where:

N_e = number of engines

T_e = thrust for engine

w_e = total engine weight

y_e = lateral distance engines from centerline

L_b = body length

$k_1 \cdots k_{14}$ = coefficients

3.8.2 Fuel System Weight. All the fuel system weight is computed in Overlay (WU, 1, 2) except the cryogenic tanks and insulation which is computed in Overlay (WU, 1, 5). Fuel system plumbing, controls, etc. are calculated by one of the three following equations:

JP Fuels

$$w_{fp} = 2.471 (T_e)^{.386} (N_e)^{.625} (N_t)^{.739}$$

LH_2 Fuel

$$w_{fp} = 0.01569\ (T_t)^{.75} + 7.742\ (T_e)^{.38}\ (N_e)^{.825}\ (N_t)^{.739}$$

Methane Fuel

$$w_{fp} = 0.01267\ (T_t)^{.75} + 5.221\ (T_e)^{.38}\ (N_e)^{.825}\ (N_t)^{.739}$$

where:

T_e = thrust per engine

T_t = total thrust

N_e = number of engines

N_t = number of fuel tanks

Explosion Suppressant System

$$w_{es} = k_1\ (w_{fc})$$

where:

w_{fc} weight of fuel in protected cells

k_1 coefficient

3.8.3 Cryogenic Tankage Weight. When cryogenic fuels are used, the volume required for fuel is a major determinant in the vehicle size and shape equations. Therefore both the weight and dimensional calculations are made in the geometry section of the program, paragraph 2.9.

3.9 AIRCRAFT SYSTEMS WEIGHT. Most of the aircraft systems weights are approximated as functions of simple parameters for scaling. Through the use of the equation form

$$w = a \cdot f(P) + b$$

it is also possible to input a fixed value (b) by making the coefficient a = 0.0. Obviously, it also provides for a partially fixed and partially variable form.

Auxiliary Power Unit	$w_a = k_1 (w_E)^{.18} + k_2$
Instruments	$W_I = k_3(.00224)(w_d) + k_4$
Electrical System	$w_e = k_5 (w_{fs} + w_{av})^{.473} + k_6$
Furnishings	$w_{fu} = k_7 (w_{pl}) + k_8 (N_p)^{1.165} + k_9$
Air Conditioning System	$w_{ac} = k_{10}(w_{av}) + k_{11} [(w_b)(N_{sr})]^{.72} + k_{12}$
Anti-icing Systems	$w_{ai} = k_{13} (b_{w2})^{.95} + k_{14}$
Auxiliary Gear	$w_{ax} = k_{15}(w_t) + k_{19}$
Unusable Fuel	$w_{uf} = k_{16} (w_F)$
Engine Oil	$w_o = k_{17} (w_E)^{.26}$
Cryogenic Boil-off	$w_{cb} = k_{18} (w_F)$

where:
- w_E = weight of engines
- w_d = flight design gross weight
- w_{fs} = weigh of fuel system less tanks
- w_{av} = weight of avionics
- w_{pl} = weight of mission payload
- N_p = number of passengers
- w_t = design takeoff weight
- w_b = body width
- N_{sr} = number of passenger seat rows
- b_{w2} = wing span along 50% chord
- w_F = weight of fuel
- k_1-k_{19} = input coefficients

Hydraulic Systems

$$w_n = k_h \left[\left(\frac{S_s q}{1000} \right)^{1.3125} + (L_b + b_{w2})^{1.06125} \right]^{.849} + k_{h}$$

where: S_g = sum of wing, horizontal, and vertical tail areas

q = design maximum dynamic pressure

L_b = body length

b_{w2} = wing span along 50% chord

k_h & k_{hi} = input coefficients

The following items necessary to complete the weights are not computed but must be input as a constant:

Avionics System
Armament and armament provisions
Crew
Oxygen
Survival gear
Miscellaneous, cargo handling, etc.

C-2

SECTION 4

BALANCE ANALYSIS

A preliminary balance calculation is performed in order to properly locate the wing, fuselage, and certain other major masses relative to each other. The locations thus determined establish the general arrangement of the vehicle; that is, the components are located to achieve a balance (operating weight empty cg.) at a designated position relative to the wing. That point is defined by input in the form of percent wing mean aerodynamic chord with a default value of 25 percent. After all detailed geometry is created (Section 2.0) a more detailed balance computation is conducted as a by-product of the mass distribution and moment of inertia calculation(Section 5.0). These more refined data are used in the loads (Section 7.0) and stress analyses (Section 8.0).

4.1 PRELIMINARY BALANCE. The preliminary balance is performed as part of the weight/sizing/balance loop to ensure overall consistency as the iteration closes in on a design. Therefore it is necessary to vary locations of all components as a function of the major dimensions of the vehicle so that wing relocations can be accomplished iteratively.

The program provides for separation of all weight items into two categories, (1) wing and contents and (2) body and contents. The term "and contents" means all items which move (or remain fixed) with that component regardless of where it is actually attached. For example the main landing gear must be located relative to the c.g. which is located relative to the wing. Therefore the main landing gear is included in the "wing and contents" regardless of whether it is to be physically attached to the wing. Table 4-1 lists each mass component and tells how its location is determined for balance calculation purposes. It also shows whether the item moves with the wing or body during sizing iterations. The program uses both wing mounted and/or body mounted power plants, so duplicate handling of those components is provided.

The balance computations are based on moment arms about the aircraft nose (X station = 0 at nose of the aircraft) and outputs the c.g. as inches from the nose. It is also shown as percent of mean aerodynamic chord (MAC). No vertical c.g. computations are made in the preliminary balance since that data is not a major determinant of any of the major characteristics of the aircraft.

Although the Operating Weight Empty c.g. is the point to which wing location is keyed, the program continues and adds in the other components to calculate the c.g. at the Zero Fuel Weight condition and the Maximum Takeoff Weight Condition.

4.2 DETAILED BALANCE CALCULATION. A more detailed balance computation (including vertical c.g.) is conducted as a by-product of the mass distribution and moment of inertia calculations. The process is described in detail in Section 5.0, but in summary form it consists of the following. Each mass item in the body and contents weight is distributed in accordance with a prescribed "shape" and between

certain prescribed limits (body stations). The mass is then "sliced" into one inch slices and accumulated with other mass items similarly distributed. The resultant slice data is then integrated into the appropriate c.g. and moment of inertia data.

The wing and contents weight (also horizontal and vertical tail) is similarly treated except that instead of one inch slices stationwise, the weight is distributed into 9 panels (per side) having equal spanwise dimensions. Certain items are accumulated as concentrated loads (engines, nacelles,etc.). The result is a more refined balance, including vertical c.g.

Table 4-1 Mass Location Data

Mass Items	Location	Note:	Moves with:	
			Wing	Body
Wing Structure	Input as % wing MAC	2	X	
Hor. Tail Structure	Input as % H. T. MAC (located by tail arm)	2	X	
Vert. Tail Structure	Input as % V. T. MAC (located by tail arm)	2	X	
Fuselage Structure	Input as % body length	2		X
Landing gear - main	Input as % wing MAC	2	X	
Landing gear - nose	Input as % body length	2		X
Nacelle Structure	Located relative to engines - see notes	1 & 2	X	X
Surface Controls	Input as % body length	2		X
Auxiliary Power Unit	Input as % body length	2		X
Instruments	Input as % body length	2		X
Hydraulics Systems	Input as % body length	2		X
Electrical group	Input as % body length	2		X
Avionics	Input as % body length	2		X
Armament group	Input as % body length	2		X
Furnishings	Input as % body length	2		X
Air Conditioning	Input as % body length	2		X
Auxiliary Gear group	Input as % body length	2		X
Propulsion Systems	(see notes)	1 & 2	X	X
Unusable Fuel	Input as % body length	2		X
Oxygen	Input as % body length	2		X
Gases	Input as % body length	2		X
Weapons Pylons		2		X
Survival Gear	Input as % body length	2		X
Crew	Input as % body length	2		X
Cryogenic body tanks	Tank cg calculated in geometry routine			X
Cryogenic wing tanks	Tank cg calculated in geometry routine		X	
External cryogenic tanks	Tank cg calculated in geometry routine		X	

Notes:

1. Wing mounted engines are located at input % engine length of the wing leading edge which is calculated from wing geometry and an input span location. Body engines are located as input % body length. Propulsion system items (including nacelles, inlets, thrust reversers, oil, starting system, etc.) are located relative to the engines and primarily as a function of engine dimensions.

2. A provision is also made for inputting a fixed dimension for a balance location of each component.

SECTION 5

MASS DISTRIBUTION & INERTIA ANALYSIS

One of the most critical factors in aircraft design load determination is the weight of the aircraft itself, and how that weight is distributed is of equal importance. This is especially true of the designs in which a significant portion of the weight is carried in or is distributed along the wing. In these cases the loads tend to be partially self cancelling and at least have a minimal effect on critical design conditions. Also, if aeroelastic loads are to be considered, it is quite necessary that the distribution of the mass be known. To accomplish these ends a program was developed that systematically computes the required data using inputs provided from the weights and geometry programs.

5.1 SUMMARY OF PURPOSES. The purposes of this program are to (1) prepare all the mass properties (weights, centers of gravity, and moments of inertia) for the complete aircraft (in four sequentially loaded steps), (2) to distribute the weights in panels or nodes along the body axes and along the span dimension of the wing, horizontal tail and vertical tail, (3) calculate the weights, center of gravity, and moments of inertia of each of these panels/nodes/concentrated loads, and (4) store these data in arrays for access by the loads program AELOADS.

5.2 OUTLINE OF OPERATIONS PERFORMED. The following sequential operations are performed in MIPIMD (the specifics on how these are accomplished are discussed in Section 5.3):

a. All operating weight empty items are distributed into appropriate node/panel masses or into concentrated loads.

b. Separate data arrays are created for the wing, horizontal tail, vertical tail, body, and concentrated loads. The body (and contents) array includes the following data bits for each node:

   (1) Weight

   (2) X - cg

   (3) Y - cg

(4) Z - cg

(5) I_{ox}

(6) I_{oy}

(7) I_{oz}

(8) Fuselage station of forward edge

c. Calls subroutine ISUM which calculates the center of gravity (3 axes) and moments of inertia (three axes plus product X-Z) for the wing and contents, body and contents, horizontal tail and contents, vertical tail and contents, and the total aircraft (operating weight empty).

d. Stores these data in arrays for access by the loads program AELOADS.

e. Builds a maximum centerline load case by calling body fuel distribution (BODFD) and body payload (BODPL), creating arrays for each with the same data shown in subparagraph (b) above.

f. Again calls subroutine ISUM and performs the same operations as subparagraph (c) but for the maximum centerline load case.

g. Builds a full internal loading condition by calling for distribution of wing fuel (WINGDR) and repeating the steps of subparagraphs (b) and (c).

h. Builds a maximum gross weight loading condition by calling up the external fuel and again repeating the steps of subparagraphs (b) and (c).

5.3 MASS DISTRIBUTION EQUATIONS. Table 5-1 shows the disposition of each functional weight item, what procedure was used, and where that procedure is described.

The distribution of weight along the wing is accomplished by subroutine WINGDR which is discussed in paragraph 5.4 . The accumulation of certain items into concentrated masses is accomplished by subroutine CONMAS which is discussed in paragraph 5.5 . The remaining items are distributed in the body according to the following procedures.

Table 5-1 Mass Distribution Map

Functional Weight	Distribution Code				
	(1)	(2)	(3)	(4)	(5)
Wing + 50% surface controls	X				
Hor. tail + 2% surface controls	X				
Ver. Tail + 2% surface controls	X				
Body + 46% surface controls			X		
Nose landing gear				X	
Main landing gear		X			
Nacelles and pylons		X			
Engines and propulsion subsyetems		X			
JP fuel systems				X	
Cryogenic fuel systems less tanks				X	
Cryogenic tanks and insulation - fwd body					X
Cryogenic tanks and insulation - mid body				X	
Cryogenic tanks and insulation - aft body					X
Auxiliary power unit				X	
Instruments - cockpit				X	
Instruments - other					X
Electrical system					X
Hydraulics				X	
Avionics				X	
Armament					X
Furnishings					X
Air Conditioning				X	
Auxiliary gear				X	
Operating items				X	
Body payload				X	
Body fuel - fwd				X	
Body fuel - mid					X
Body fuel - aft				X	
Wing internal fuel	X				
Wing external tanks and pylons		X			
Wing external fuel		X			

Distribution Codes:	Paragraph
(1) Spanwise using WINGDR	5.4
(2) Concentrated load using subrouinte CONMAS	5.5
(3) Subroutine BODY	5.3
(4) Subroutine TRAPD-Rectangular distribution, defined length	5.3
(5) Subroutine TRAPD - Trapezoidal distribution, defined stations	5.3

The body weight is assumed to be distributed in accordance with a shape that is parabolic on each end and trapezoidal (or rectangular) in a mid-section. A separate subroutine (BODY) (Figure 5-1) uses the appropriate dimensions, weight and cg location to derive the equations of distribution that satisfy those requirements. The resultant equations are then used (by subroutine MDB) to distribute weight into one inch segments along the body. The weight thus distributed includes 46 percent of the surface controls weight as well. The remaining surface controls weight is distributed with the wing (50%) and the horizontal and vertical tails (2% each).

Each of the remaining systems weights is distributed separately according to a trapezoidal (or rectangular) distribution as derived by subroutine TRAPD (Figure 5-2). The program supplies the total weight, its center of gravity, and either total length or the stations between which it is to be distributed. If the total length is supplied, the distribution is rectangular on each side of the center of gravity of the item. If the terminating stations are supplied, the subroutine calculates a trapezoidal distribution to satisfy the c.g. defined. The masses are then broken down accordingly and distributed into one-inch segments of the body between the limiting stations defined.

After all distributions have been completed, the body is divided into 30 nodes (29 of equal number of integer inches in length and the remaining length in node 30). All the individual segments are then integrated between the node limits to obtain the necessary mass properties for each node (weight, 3 axis center of gravity, 3 axis moments of inertia, and the fuselage station of the forward edge of the node).

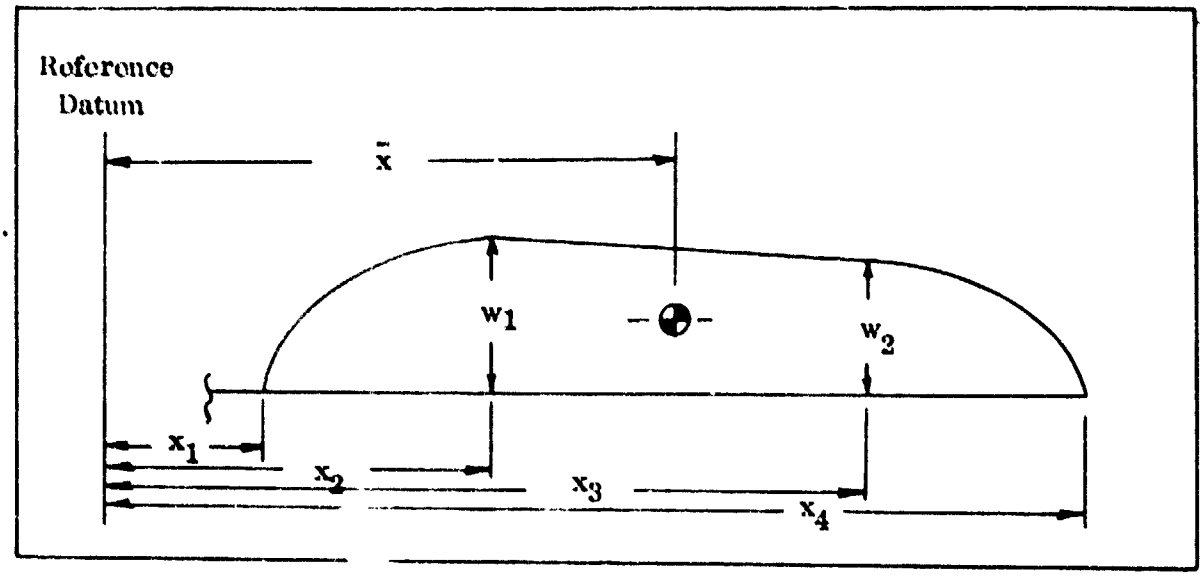

Figure 5-1 . Subroutine BODY Distribution Model

$$w_1 = \frac{w_1}{w_2}(w_2)$$

$$w_2 = \frac{W}{2/3\left(\frac{w_1}{w_2}\right)(x_2 - x_1) + \frac{1}{2}\left(\frac{w_1}{w_2} + 1\right)(x_3 - x_2) + \frac{2}{3}(x_4 - x_3)}$$

$$\frac{w_1}{w_2} = \frac{-C_2 + \sqrt{C_2^2 - 4C_1C_3}}{2C_1}$$

where: $C_1 = \frac{2}{3}(x_2 - x_1)\bar{x} + \frac{1}{2}(x_3 - x_2)\bar{x} - \frac{2}{3}\left|x_1 + .6(x_2 - x_1)\right|(x_2 - x_1)$
$- \frac{1}{2}(x_3 - x_2)x_2 - \frac{1}{6}(x_3 - x_2)^2$

$C_2 = \frac{2}{3}(x_2 - x_1)\bar{x} + (x_3 - x_2)\bar{x} + \frac{2}{3}(x_4 - x_3)\bar{x} - \frac{2}{3}\left|x_1 + .6(x_2 - x_1)\right|(x_2 - x_1)$
$-(x_3 - x_2)x_2 - \frac{1}{2}(x_3 - x_2)^2 - \frac{2}{3}\left|x_3 + .4(x_4 - x_3)\right|(x_4 - x_3)$

$C_3 = \frac{2}{3}(x_2 - x_1)\bar{x} + \frac{1}{2}(x_3 - x_2)\bar{x} + \frac{2}{3}(x_4 + x_3)\bar{x} - \frac{1}{2}(x_3 - x_2)x_2$
$- \frac{1}{3}(x_3 - x_2)^2 - \frac{2}{3}\left|x_3 + .4(x_4 - x_3)\right|(x_4 - x_3)$

w_1 = weight per inch at x_1 inches from reference

w_2 = weight per inch at x_2 inches from reference

W = total weight $= \int_{x_1}^{x_4} w_x \, d_x$

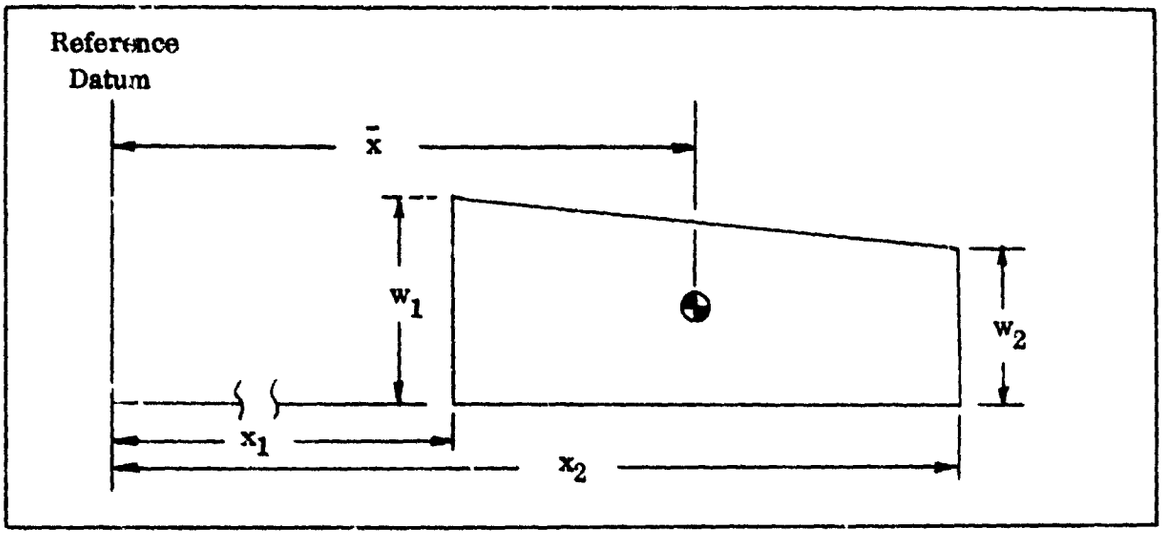

Figure 5-2 Subroutine TRAPD Distribution Model

w_1 = Weight per inch at x_1 inches from reference sta.

w_2 = Weight per inch at x_2 inches from reference sta.

w_x = Weight per inch at any station x.

$$w_1 \quad \frac{w_1}{w_2}(w_2)$$

$$w_2 = \frac{2W}{(x_2 - x_1)\left(\frac{w_1}{w_2} + 1\right)}$$

$$\frac{w_1}{w_2} = \frac{2x_2 + x_1 - 3\bar{x}}{3\bar{x} - 2x_1 - x_2}$$

W = Total weight $= \int_{x_1}^{x_2} w_x \, dx$

5.4 Subroutine WINGDR. This subroutine provides mass distribution data for all airfoil surface structures (wing, horizontal tails, vertical tails) and for fuel or payload housed within the structure and distributed along the span.

5.4.1 Operations performed. The following specific operations are performed:

1. Defines boundaries of panels (Figure 5-3) in such a way as to provide equally spaced panels outboard of the fuselage (numbered from the tip toward the inboard) and, in the case of a wing or horizontal tail, a tenth panel consisting of the carrythrough structure (half) from the side of the body to the centerline.

2. Distributes the weight of the surface structure (plus certain distributed systems weights) into the various panels, assuming that half the weight is distributed in accordance with airload bending parameters and half the weight is a function of geometric size and shape. (Figure 5-4).

3. Calculates and distributes the weight of internal fuel as a function of tank spanwise boundaries and relative incremental volumes of the wing box for each panel.

4. Calculates the x, y, and z center of gravity for each element.

5. Calculates overall dimensions for each element and calls the moment of inertia subroutine (MIPI) for accumulation into the aircraft moment of inertia. (See par. 5.6)

6. Prepares and stores the mass properties data for each panel in appropriate arrays (Figure 5-5).

5.4.2 Equations

5.4.2.1 Structural Weight. One-half the structural weight is distributed in accordance with an empirical equation which approximates the distribution of airload bending material in typical wing structures.

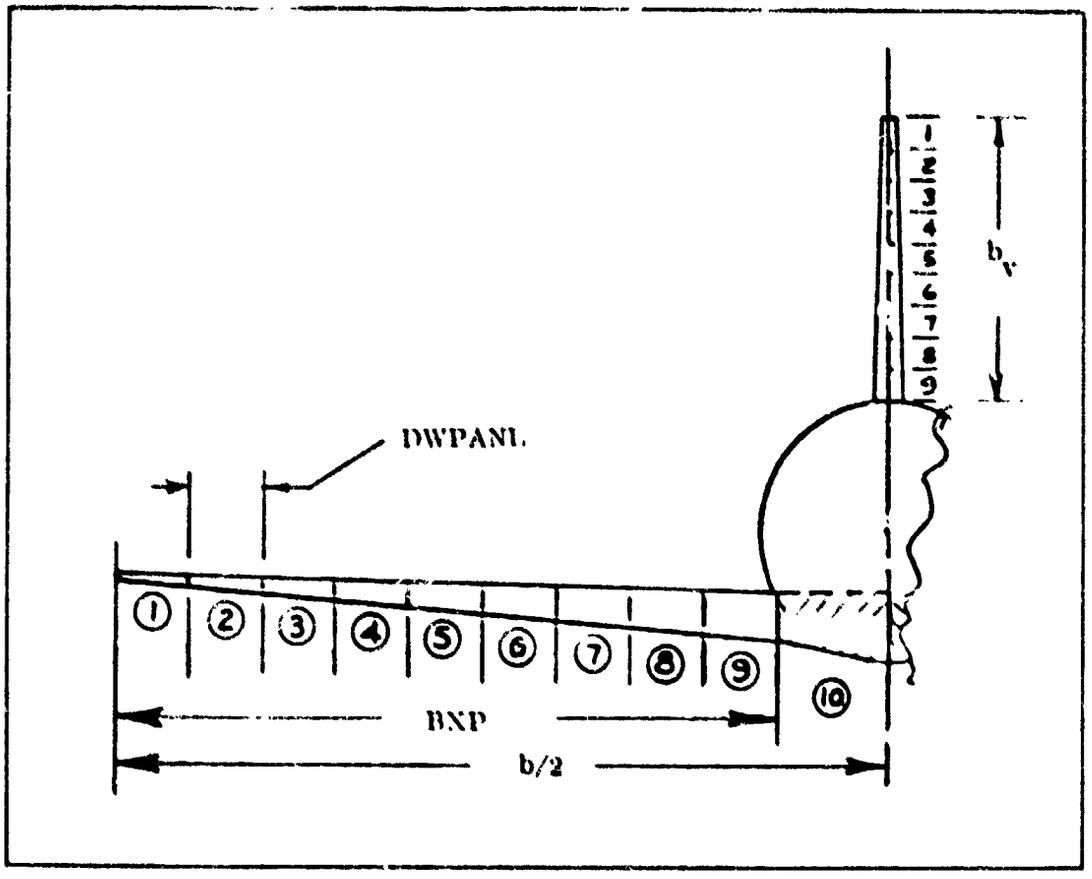

Figure 5-3 Mass Distribution Panel Definitions

Weight	Center of Gravity			Panel No.
	X	Y	Z	
				1
				2
				3
				4
				5
				6
				7
				8
				9
				(10)

Array Names:

Wing structure	PWE(10, 5)
Horizontal tail structure	HS(10, 5)
Vertical tail structure	VS(9, 5)
Wing internal fuel	PWF(9, 5)
Distributed payload	PWP(9, 5)

Figure 5-5 Mass Distribution Arrays

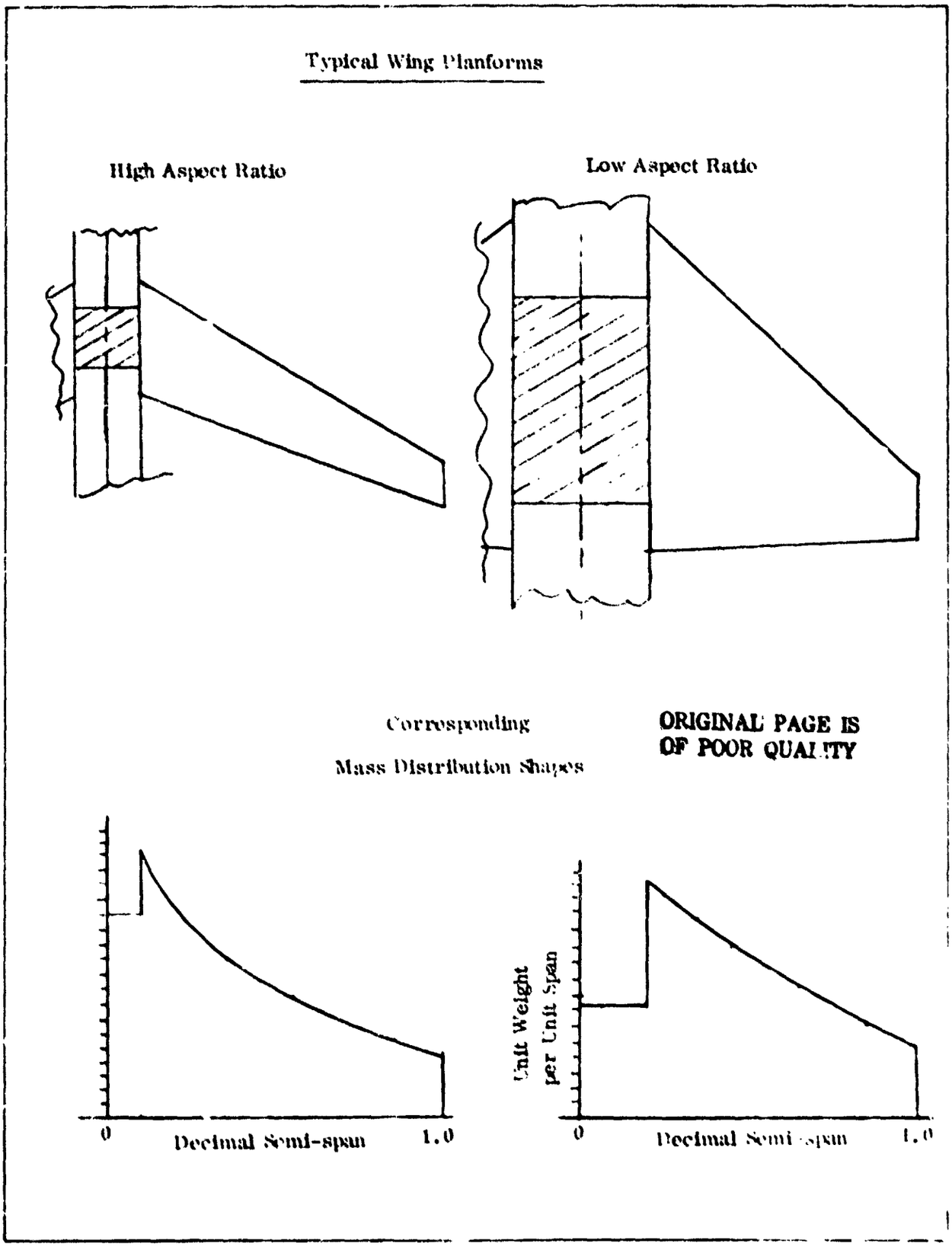

Figure 5-4 Distribution of Wing Weight

$$W_p = \int_{y_2}^{y_1} w_i \, dy \quad \frac{W_s}{2} \left[\frac{(1+\Delta)\eta_1}{(\Delta+\eta_1)} - \frac{(1+\Delta)\eta_2}{(\Delta+\eta_2)} \right]$$

where:

W_p = weight distributed within a panel bounded by span stations y_1 and y_2.

W_i = unit value of spanwise distributed weight at any station.

η = decimal semi-span at any station y.

Δ = constant based on wing external geometry.

$$\Delta = \frac{2C_r}{b} \quad \left(= \frac{C_r}{b} \text{ for vertical tails} \right)$$

C_r = airfoil surface theoretical root chord.

b = airfoil surface span

W_s = structural weight of one side of a wing or horizontal tail, or total weight of a vertical tail. Includes some systems, controls, etc., which are distributed along the span.

The remaining half of the structural weight is assumed to be proportional to the exposed area. The weight is therefore distributed in proportion to the product of the panel width and the average chord. The center of gravity of each panel is assumed to be at mid-span, mid-chord, and mid-thickness of each structural panel.

5.4.2.2 Wing internal fuel weight. The wing fuel weight is distributed between the defined boundaries in proportion to the C-square rule, that is, a constant t/c is assumed and spars are assumed at constant percent chords. Therefore, the fuel cross section dV at any station y is proportioned to the chord times the thickness, and since thickness is C x t/c, then dV is proportional to C squared.

$$W_{f_p} \sim \int dV\, dy \sim \int_{y_2}^{y_1} C^2\, dy$$

where:

W_{f_p} = weight of fuel in one panel element.

dV = differential volume at any station y

y_1 & y_2 = spanwise stations at panel boundaries

C = wing chord at any station y.

The panel definitions are the same as those derived for the wing structure. When fuel boundaries fall between panel edges, actual fuel boundaries establish fuel panel dimensions.

The center of gravity of each fuel element is assumed to be at mid-span, mid-thickness, and at 42.5% chord of each panel element.

5.5 Subroutine CONMAS This subroutine provides for accumulation of certain items into concentrated load elements to be used in the loads program.

5.5.1 Operations Performed. The following specific operations are performed:

1. Utilizes location data from the main program to set up dimensional arrays for computing composite center of gravity of all items accumulated at a given station.

2. Utilizes number of engines on wing and number of pylons to determine arrangements (siamese or single nacelles).

3. Distributes weight of engines, nacelles, pylons, and other power plant related items to the proper stations (Figure 5-6) and separately calculates the center of gravity (3 axes) for each weight used.

4. Accumulates weight and moments for each weight item at each station for determination of net station weight and center of gravity.

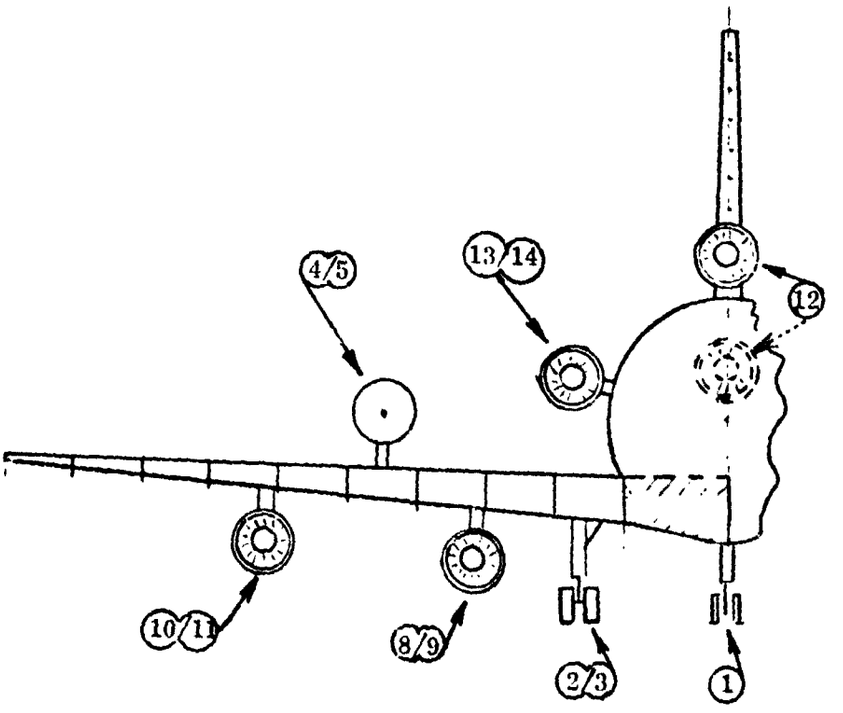

Stations at which certain weight items may be accumulated

Legend

1 Nose gear
2/3 Main gear*
4/5 External fuel tanks
6/7 Not used
8/9 Inboard engines
10/11 Outboard engines
12 Body centerline engine
13/14 Body aft side mounted engines

* Located in body if high wing configuration

Figure 5-6 Concentrated Load Points

5. Calculates dimensional characteristics of each weight component and calls the moment of inertia subroutine (MIPI) for accumulation into the aircraft moment of inertia.

6. Repeats above procedure for external fuel tanks and pylons, nose gear, and main landing gear.

5.5.2 Equations. The mathematics of the problem is simply one of summing weights, calculating areas based on geometry, calculating moments and summing moments. The primary purpose of the subroutine is providing all the logic necessary to satisfy the wide range of configuration options provided.

5.5.3 Related Operations. The logic and equations that assign these concentrated loads to the appropriate wing panel is found in the main program MIPIMD. That program also performs the task of creating the arrays in which the concentrated loads data are stored for use by loads.

5.6 MOMENT OF INERTIA CALCULATIONS. Moment of inertia calculations are accomplished in the program using the basic mathematical relationship:

$$I_R = \Sigma W_i d_i^2 + \Sigma I_{o_i} - \left(\Sigma W_i\right)\left(\frac{\Sigma W_i d_i}{\Sigma W_i}\right)^2$$

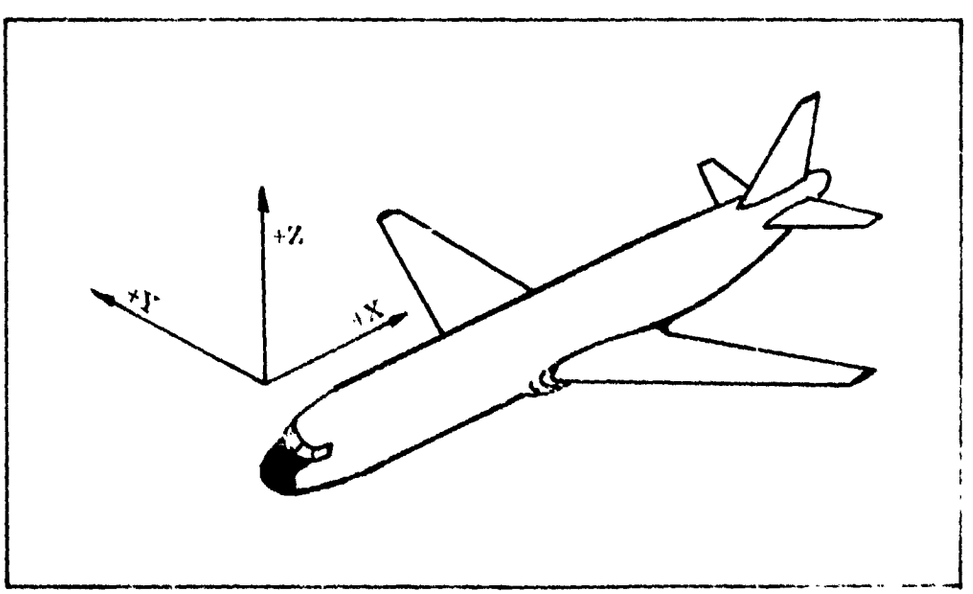

Figure 5-7 Axis Orientation for Balance and Inertia

where:

I_R = moment of inertia of a conglomerate mass about a reference centroidal axis "R"

$\Sigma W_i d_i^2$ = an accumulation of incremental component inertia values each of which is the result of displacement from an arbitrary axis of accumulation that is parallel to but displaced from the reference centroidal axis "R".

ΣI_{o_i} = an accumulation of incremental component inertia values each of which is the inertia of that component about an axis through its centroid and parallel to the reference centroidal axis "R".

$\left(\Sigma W_i\right)\left(\frac{\Sigma W_i d_i}{\Sigma W_i}\right)^2$ = a resolution term expressing the difference between the inertia values about the axis of accumulation and the centroidal axis "R".

W_i = mass of an individual component

d_i = the undirected distance from the centroid of an individual mass to the axis of accumulation.

5.6.1 Scope of Calculation. Moments of inertia are computed about all three mutually perpendicular axes x, y, and z (Figure 5-7). A product of inertia (x-z plane) is also calculated. These values are computed (and output to the loads program) for (1) wing and contents, (2) body and contents, (3) horizontal tails and contents (4) vertical tail and contents, and (5) total aircraft. The above data is repeated for four aircraft loading conditions; (1) operating weight empty, (2) same plus maximum centerline load, (3) same plus maximum internal wing fuel, and (4) maximum gross weight including external fuel.

5.6.2 Depth of Calculation. The inertia resulting from displacement from the c.g. (the $W_i d_i^2$ term) is of course completely accounted for. In order to accurately account for the inertia of each component about its own centroid (the I_{o_i} term), the program breaks down the operating weight empty into approximately 100 elements.

The magnitude of each element is determined by (1) its dimensions relative to the overall airplane and (2) how accurately its inertia can be approximated by any of five standard shapes provided.

Each inertia call statement in the program provides the following data to the inertia routine for each component:

(1) weight

(2) location in 3 axes

(3) orientation relative to 3 axes

(4) appropriate dimensions (up to 3) of each component

(5) location code (wing, body, etc.) for sub-accumulation

(6) shape code directing use of one of the 5 shapes

Figure 5-8 describes the five shapes provided and lists the equations used in the calculations. The orientation code, item (2) above, is provided to orient the shape relative to the aircraft axes.

Subroutine		Shape	Equations
Name	Description		
PA	Surface area of a parabolic shell	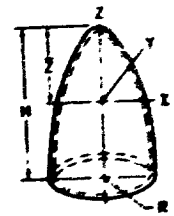	$I_x = I_y = \left(\frac{W}{28H^2}\right)\left[\frac{P(12H^4 + 6R^2H^2 - R^4 + R^2)}{P - R^3}\right]$ $\left(\frac{-W}{168H^2}\right)\left[\frac{P(6H^2 - R^2 + R^2)}{P - R^3}\right]^2$ $I_z = \frac{WR^2}{18H^2}\left[\frac{P(6H^2 - R^2 + R^2)}{P - R^3}\right]$ $I_z = \frac{WR^2Z}{H}$ OR
RP	Solid rectangular prism	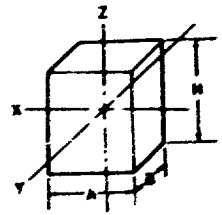	$I_x = \frac{W}{12}(B^2 + H^2)$ $I_y = \frac{W}{12}(A^2 + H^2)$ $I_z = \frac{W}{12}(A^2 + B^2)$
DM	Surface area of an elliptical hemispheroidal shell (or hemispherical)	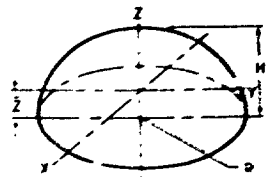	$K = R \cdot \log_e\left[\frac{R - \sqrt{R^2 - H^2}}{H}\right]\left[\frac{R^2}{\sqrt{R^2 - H^2}}\right]$ $I_z = \frac{WR^2}{2(R^2 - H^2)}\left[\frac{4R^2 - 2H^2}{2} - \frac{R^3}{K}\right]$ $I_x = I_y = \frac{W}{4(R^2 - H^2)}\left[\frac{4R^4 - 2R^2H^2 - 2H^4}{2} - \frac{R^3(R^2 - 2H^2)}{K} - \frac{16H^2(R^2 - H^2)^2}{9K^2(R^2 - H^2)}\right]$
BOX	Hollow four sided box open on both ends	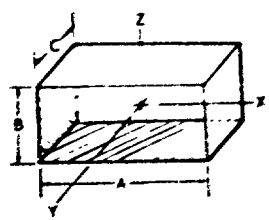	$I_x = \frac{W}{12}\left[C^2 + B^2\left(\frac{2A + B}{A + B}\right)\right]$ $I_y = \frac{W}{12}\left[A + B\right]^2$ $I_z = \frac{W}{12}\left[C^2 + A^2\left(\frac{2B + A}{B + A}\right)\right]$
FU	Surface area of a frustrum of a cone (also cylinder)	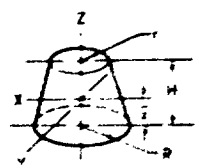	$I_x = I_y = \frac{W}{2}(R^2 + r^2) - \frac{Wh^2}{18}\left[1 + \frac{2Rr}{(R + r)^2}\right]$ $I_z = \frac{W}{2}(R^2 + r^2)$

Figure 5-2 Inertia Shapes and Equations

SECTION 6

MISSION/PERFORMANCE ANALYSIS

The purpose of the mission analysis routine is to determine the relationship between aircraft fuel volume and mission performance capability. By appropriately varying an iteration option, one of the following calculations may be performed:

1. Determine the fuel required and appropriate aircraft geometry to fly a fixed mission.
2. Determine the fuel required by a fixed geometry aircraft to fly a fixed mission.
3. Maximize any single radius segment of a mission profile for a fixed geometry aircraft carrying a fixed quantity of fuel.
4. Maximize any single loiter segment of a mission profile for a fixed geometry aircraft carrying a fixed quantity of fuel.

The routine is comprised of the following mission segments: Takeoff, Climb, Acceleration, Cruise, Loiter, Combat, Descent, Deceleration, Landing and Reserves. Through the use of input parameters, these segments may be linked together in any desired manner to form a mission profile. In addition, there are several different approaches to each of the individual segments. For example, the cruise segment may be performed at a fixed speed and altitude, or at optimum conditions.

In order to fly a given mission, the program is dependent on aerodynamics, propulsion, geometry and weights data. The propulsion data is generated external to the program and is accessed by an internal interpolation routine. Aerodynamics and weights data are calculated internally through the use of empirical equations derived from historical data. Geometric characterizations are input to the program and are iterated internally so as to remain compatible with the available fuel volume of the aircraft.

The function of the performance analysis routine is to evaluate the performance characteristics of a fixed geometry aircraft. That aircraft may have evolved from the iterative process of the mission analysis routine or may have had its origin directly through input data. In either case, the following performance parameters may be calculated:

1. Specific excess power at various speeds, altitudes and load factors.
2. Sustained maneuver load factor at various speeds and altitudes.
3. Maximum speed at various altitudes.
4. Maximum ceiling for a specified rate of climb at various speeds.
5. Takeoff distance for a specified power setting and high lift configuration at various gross weights.

6. Landing distance for a specified high lift configuration at various gross weights.

The resulting values can be compared to the desired performance capability for each parameter and provide the user with insight as to how to change the aircraft geometry to meet those desired capabilities. With the exception of a few input values to define the flight conditions at which the performance parameters are to be calculated, the performance analysis routine uses the same input data as specified for the mission analysis routine.

6.1 TECHNICAL DATA BASE. In order to carry out a mission/performance analysis on a given aircraft design, it is necessary to define the aerodynamic, propulsion, geometry and weight characteristics of that design. Each of these technical functions is carried out in a separate subroutine of the program. A cursory description of each of these routines is given in the following sections, with appropriate reference documents identified, should the reader desire more detail.

6.1.1 AERO (Clean Configuration Aerodynamics). The aerodynamic estimation procedures for the zero flap, clean wing configuration are divided into two segments. The first segment is intended primarily for combat type aircraft and is thoroughly described in Reference 1. The second segment deals with transport type aircraft and will be further discussed herein.

The methods selected, in both segments, are those which provide a reasonable degree of drag estimation accuracy and, at the same time, make use of dimensional data available from empirically derived sizing relationships. Particular attention has been given to achieving good drag estimates for the range of lift coefficients and speeds which are normally significant in the determination of mission fuel requirements. The aerodynamic subroutine is actually divided into two parts: entry AEROZ, which computes all parameters which are independent of mach number or angle of attack, thus conserving computer time; and AERO, which computes lift and drag at specified speed, altitude and angle of attack conditions, using parameters defined by AEROZ.

The major differences in the aerodynamic estimation procedures used for combat and transport type aircraft are the minimum drag equations for wing and tail surfaces and bodies of revolution. Compressibility effects and drag due to lift characteristics are determined in substantially the same manner for both types of aircraft.

The minimum drag contribution for wing and tail surfaces for transport type aircraft is found, in terms of equivalent flat plate area (f), from the relation:

$$f_{\substack{\text{wing}\\ \text{or}\\ \text{tail}}} \quad C_f \left[1 + k_s \, (t/c) + 60 \, (t/c)^4 \right] S_{wet} \qquad (1)$$

where,

C_f = flat plate skin friction coefficient = $0.455/(\text{Log } R_N)^{2.58}$

ks = supervelocity factor (determined by the data of Figure 6-1 as a function of maximum t/c location)

t/c = maximum thickness to chord ratio of wing or tail surfaces

S_{wet} = wetted surface area of respective wing or tail surface

R_N = Reynolds number (function of characteristic length of wing or tail surface)

The equivalent flat plate area of a streamlined body of revolution may be determined from the relationship:

$$f_{fus} = C_f S_{wet_B} \left[1 + 0.001 (L/D)_B + 1.5 (D/L)_B^{3/2} + 7 (D/L)_B^3\right] \quad (2)$$

where,

C_f = flat plate skin friction coefficient = $0.455/(\text{Log } R_N)^{2.58}$

S_{wet_B} = body wetted area (ft^2)

$(L/D)_B$ = body fineness ratio (length/diameter)

R_N = Reynolds number based on body length

The second term of equation (2) accounts for the boundary layer thickness increase for wrapping a flat plate into a cylinder. The third term accounts for supervelocity and the fourth term pressure drag.

The drag of fuselages having highly upswept afterbodies is not adequately predicted by equation (2). Reference 2 shows correlations of these type fuselages which resulted in the following relationship for fuselage drag:

$$f_{fus} = C_f S_{wet_B} \left[1 + 0.001 (L/D)_B + 1.5 (D/L)^{3/2}\right] \quad (3)$$

$$+ 0.007 A_\pi \left\{ \underbrace{\left[6 (D/\ell)^{5/2} - 1\right]}_{\text{contraction effect}} + 5.2 (Y/D) \underbrace{\left[1.4 - (D/\ell)^4 K_\ell\right]}_{\text{camber effect}} \right\}$$

where,

A_m	body maximum cross sectional area (ft^2)
Y/D	afterbody camber radio
ℓ/D	afterbody contraction ratio
K_ℓ	lateral contraction factor 1.0 for no contraction (beaver tail) 0.0 for total contraction

It should be noted that the contraction and camber terms shown in equation (3) replace the pressure drag term 7 $(D/L)_B^3$ of equation (2). Figure 6-2 presents a schematic of the fuselage geometry to which equation (3) applies.

Summing the equivalent flat plate areas of the various components, and providing the necessary component interference factors, the subsonic minimum drag buildup for a multiple body transport configuration may be expressed as follows:

$$C_{D_{min_{sub}}} = \left[\left(f_{fus}(l_f) \times N_{fus}(l_f) \times facif(l_f)\right) + \left(f_{pyl}(l_p) \times N_{pyl}(l_p) \times facip(l_p)\right) + \left(f_{wing} \times faciw\right) + \left(f_{hort} \times facih\right) + \left(f_{vert} \times faciv\right) + \left(f_{can} \times faici\right) + \left(f_{nac} \times Q_N \times facin\right) + f_{camber} + f_{misc}\right] \Big/ S_w \quad (4)$$

where,

f_{fus}	fuselage equivalent flat plate area (ft^2)
l_f	index representing type of fuselage 1, 2 or 3
N_{fus}	number of each type of fuselage
facif	interference factor for each type of fuselage
f_{pyl}	pylon equivalent flat plate area (ft^2)
l_p	index representing type of pylon 1, 2, 3 or 4
N_{pyl}	number of each type of pylon
facip	interference factor for each type of pylon
f_{wing}	wing equivalent flat plate area (ft^2)
faciw	interference factor for wing
f_{hort}	horizontal tail equivalent flat plate area (ft^2)

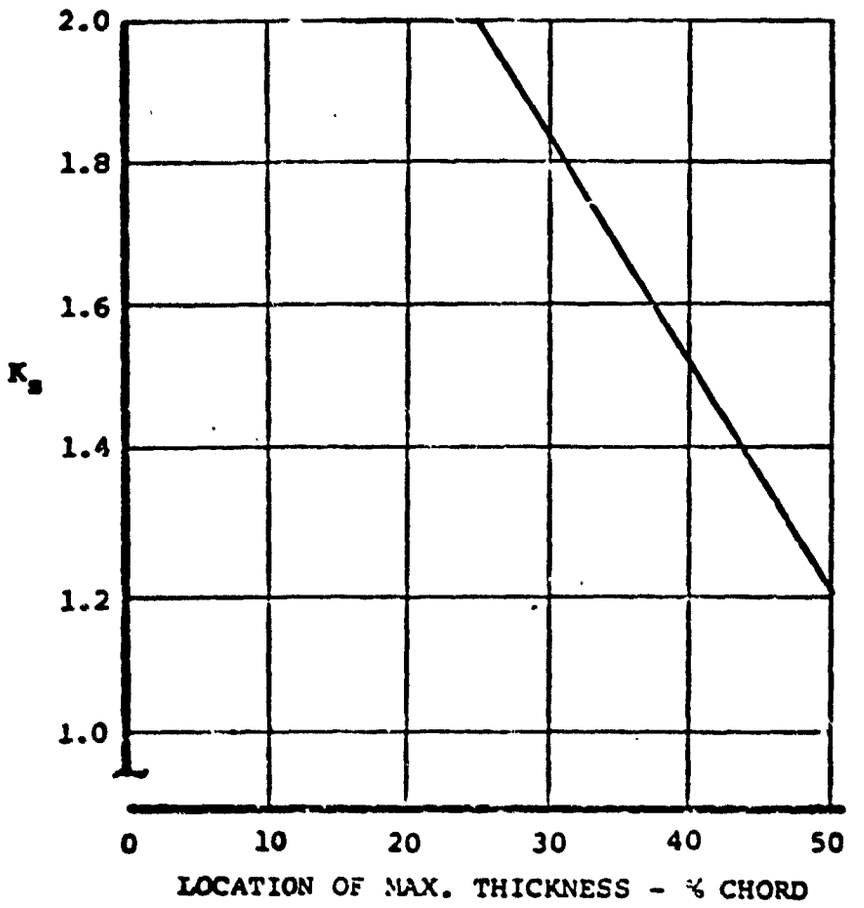

Figure 6-1 Supervelocity Factor

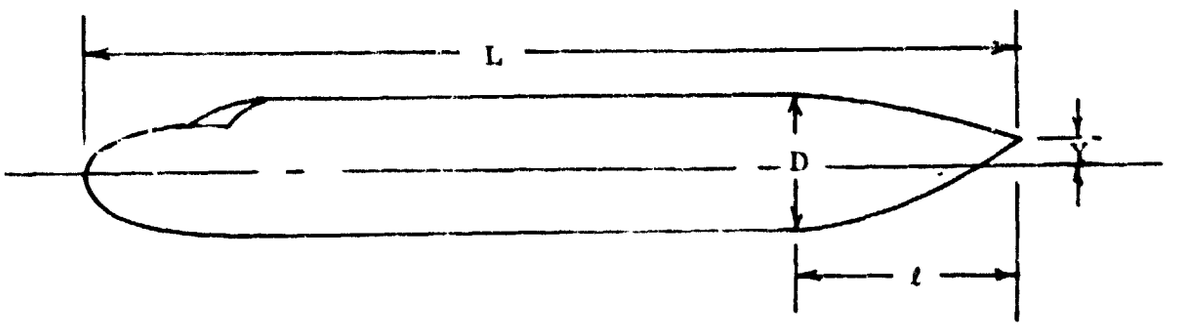

Figure 6-2 Fuselage Afterbody Geometry

facth = interference factor for horizontal tail

f_{vert} = vertical tail equivalent flat plate area (ft^2)

faciv = interference factor for vertical tail

f_{can} = canopy equivalent flat plate area (ft^2)

facic = interference factor for canopy

f_{nac} = nacelle equivalent flat plate area (ft^2)

Q_N = number of nacelles

facin = interference factor for nacelles

f_{camber} = camber drag expressed as equivalent flat plate area (ft^2)

f_{misc} = miscellaneous drag expressed as equivalent flat plate area (ft^2)

S_w = reference wing area (ft^2)

The three (3) types of fuselages and four (4) types of pylons are determined by input parameters rather than being pre-set in the program. Thus, the user may define a very sophisticated multibody configuration.

6.1.2 AEROHL (High Lift Aerodynamics)

6.1.2.1 Lift Characteristics. The maximum lift characteristics of a configuration having both leading and trailing edge high lift devices is determined from the general equation of Reference 3.

$$C_{L_{max}} = \frac{S_w'}{S_w}\left[C_{L_{max_o}} + \Delta C'_{L_{max_{LE}}} + \Delta C'_{L_{max_{TE}}}\right] \qquad (5)$$

where,

S_w = reference wing area of clean wing

S_w' = extended wing area, including leading and trailing edge high lift devices

$C_{L_{max_o}}$ = maximum lift coefficient of the clean wing (i.e., without any high lift devices)

$\Delta C'_{L_{max_{LE}}}$ = increment in maximum lift due to deflection of a leading edge high lift device. This increment is measured without a trailing edge device.

$\Delta C'_{L_{TE}}$ = increment in maximum lift due to deflection of a trailing edge flap system. This increment may be measured with or without a leading edge device.

The clean wing maximum lift characteristics may be found from the equation:

$$C_{L_{max_o}} = \left(\frac{C_{L_{max}}}{C_{\ell_{max}}}\right) C_{\ell_{max_o}} + \Delta C_{L_{max}} \tag{6}$$

The factor $C_{L_{max}}/C_{\ell_{max}}$ is used to correct the section maximum lift coefficient at M = 0.2 for finite wings, including the effects of leading edge sweep angle and airfoil nose shape. It is computed by a curve fit of the data given in Reference 4 in the form

$$\frac{C_{L_{max}}}{C_{\ell_{max}}} = A - B\,\Delta y' \tag{7}$$

where

$$\Delta y' = \begin{cases} 0; & \Delta y < 1.4 \\ \Delta y - 1.4; & 1.4 \leq \Delta y \leq 2.5 \\ 1.1; & \Delta y > 2.5 \end{cases}$$

Δy is determined from Figure 6-3 and terms A and B in Figure 6-4 as a function of leading edge sweep angle.

$C_{\ell_{max_o}}$ is the section maximum lift coefficient and is found from the equation:

$$C_{\ell_{max_o}} = \left(C_{\ell_{max}}\right)_{base} + \left(\Delta C_{\ell_{max}}\right)_{camber} \tag{8}$$

where $\left(C_{\ell_{max}}\right)_{base}$ and $\left(\Delta C_{\ell_{max}}\right)_{camber}$ are shown in Figures 6-5 and 6-6 as a function of airfoil nose shape, location of maximum thickness and camber.

The increment $\Delta C_{L_{max}}$ due to Mach number is given in Figure 6-7 , taken from Reference 5, as a function of leading edge sweep (Λ_{LE}), Δy, and Mach number.

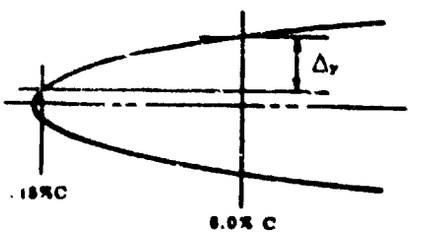

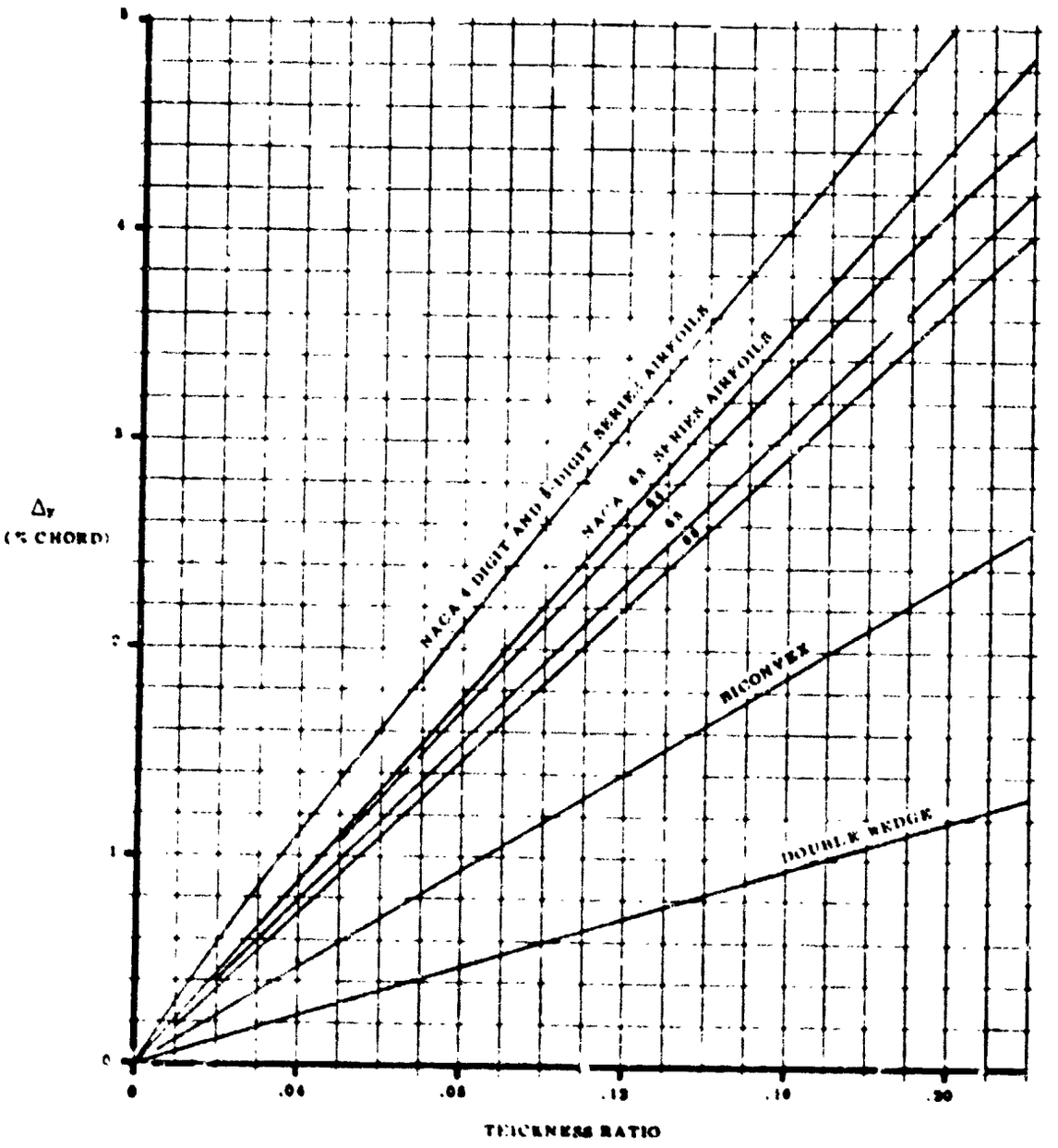

Figure 6-3 Variation of Leading-Edge Sharpness Parameter With Airfoil Thickness Ratio

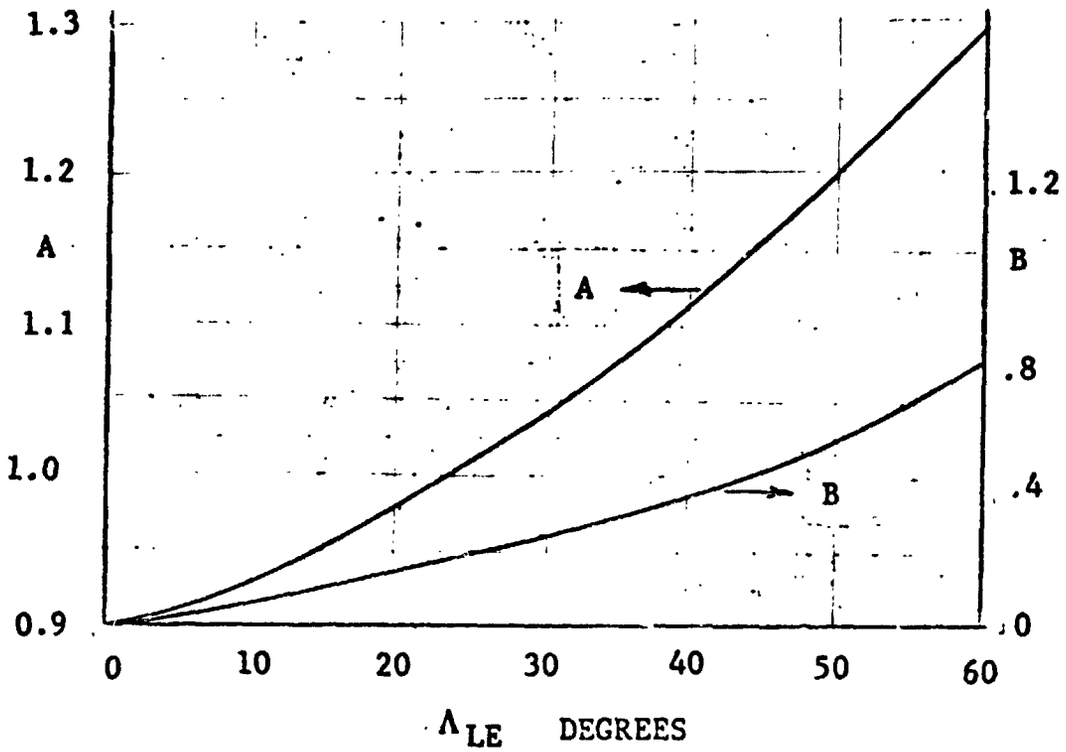

Figure 6-4 Factors for Determining Subsonic Maximum Lift

The contribution of leading edge devices to the maximum lift coefficient is found using the relationship:

$$\Delta C'_{L_{max_{LE}}} = \Delta C'_{\ell_{max_{LE}}} \cdot K_{b_{LE}} \left(\frac{C'_{L_\alpha}}{C'_{\ell_\alpha}} \right) \qquad (9)$$

$\Delta C'_{\ell max_{LE}}$ is the two dimensional increment in maximum lift coefficient and is defined as

$$\Delta C'_{\ell_{max_{LE}}} = C_{\ell_{\delta_{LE_{max}}}} \cdot 0.75\eta_{max} \cdot \eta_\delta \cdot \delta_H \qquad (10)$$

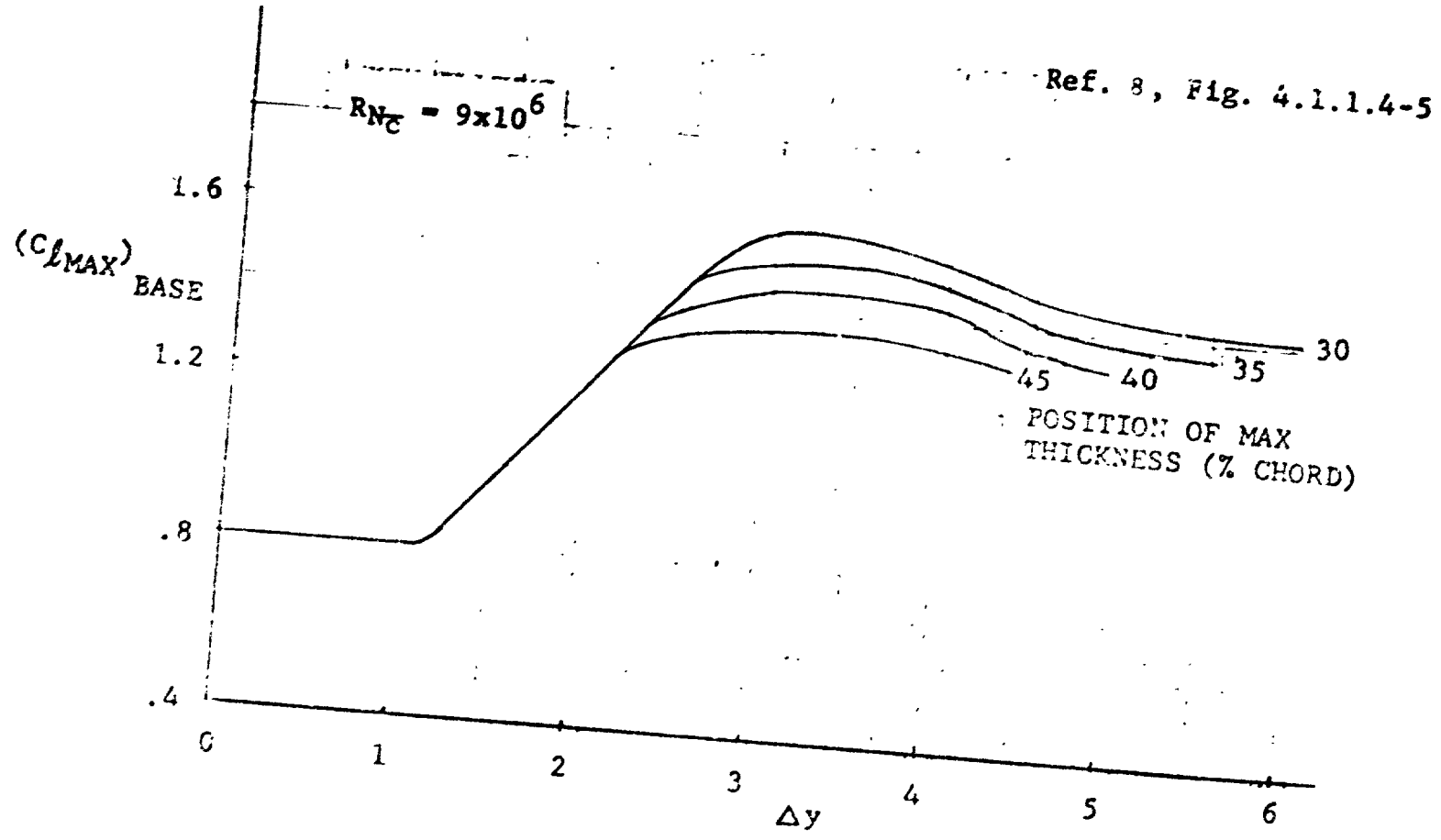

Figure 6-5 Section Maximum Lift for Uncambered Airfoils

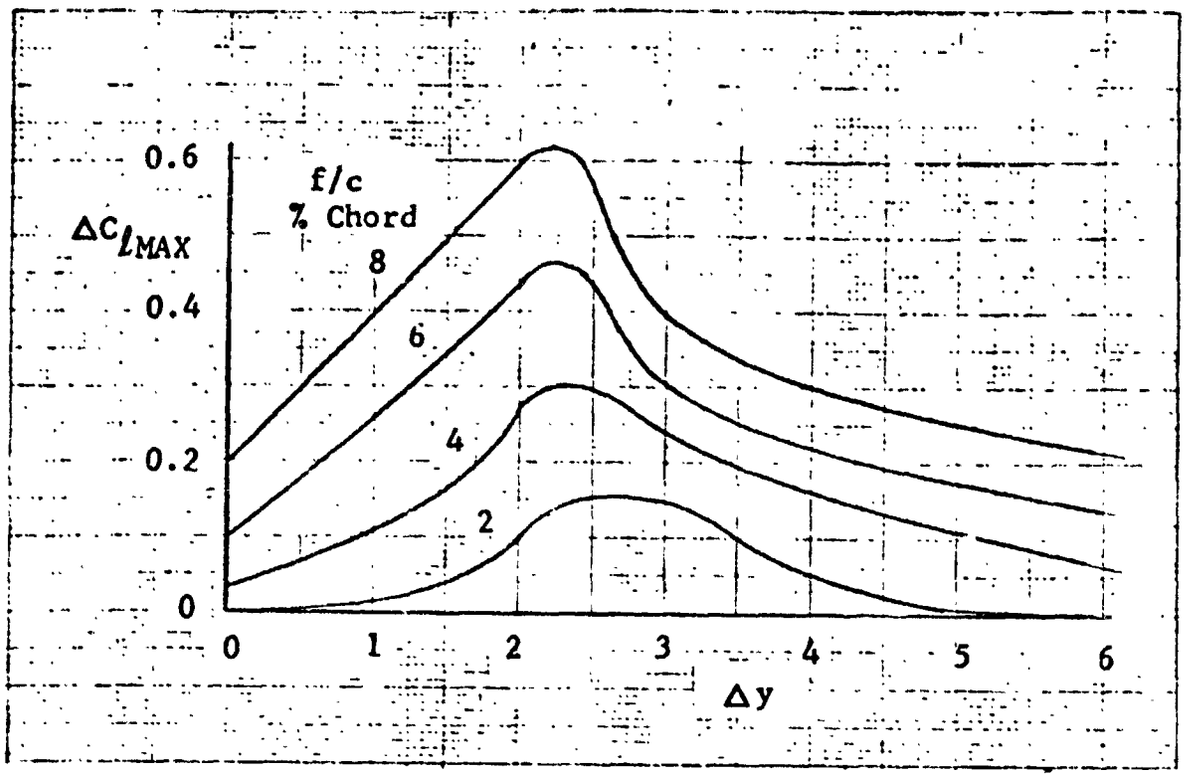

Figure 6-6 Effect of Airfoil Camber on Maximum Lift

$C_{l_{\delta_{LE_{max}}}}$ is presented in Figure 6-8 as a function of $C_{LE}/_{c'}$, where $C_{l_{\delta_{LE_{max}}}} = 2 \sin \theta_{LE}$ and $\cos \theta_{LE} = 1 - 2 \left(C_{LE}/_{c'}\right)$. $C_{LE}/_{c'}$ is the ratio of leading edge device chord to the extended wing chord due to both leading and trailing edge devices.

η_{max} is the maximum lift efficiency for leading edge devices and is given in Figure 6-9 as a function of the ratio of leading edge radius to wing thickness for leading edge flaps, slats and kruegers; both curved and flat.

η_δ is a leading edge device deflection angle correction factor and is presented in Figure 6-10 as a function of leading edge deflection angle, δ_H, for flaps, slats and kruegers.

$K_{b_{LE}}$ is the leading edge partial span factor, and is shown in Figure 6-11 as a function of the ratio of leading edge device span to wing span $\left(b_{LE}/_{b}\right)$.

The term C'_{L_α} is the three-dimensional lift curve slope from the equation:

$$C'_{L_\alpha} = (2\pi\, AR') \Bigg/ \left[2 + \sqrt{\left(\frac{AR'\beta}{k}\right)^2 \left(1 + \frac{\tan^2 \Lambda'_{c/2}}{\beta^2}\right) + 4} \right] \qquad (11)$$

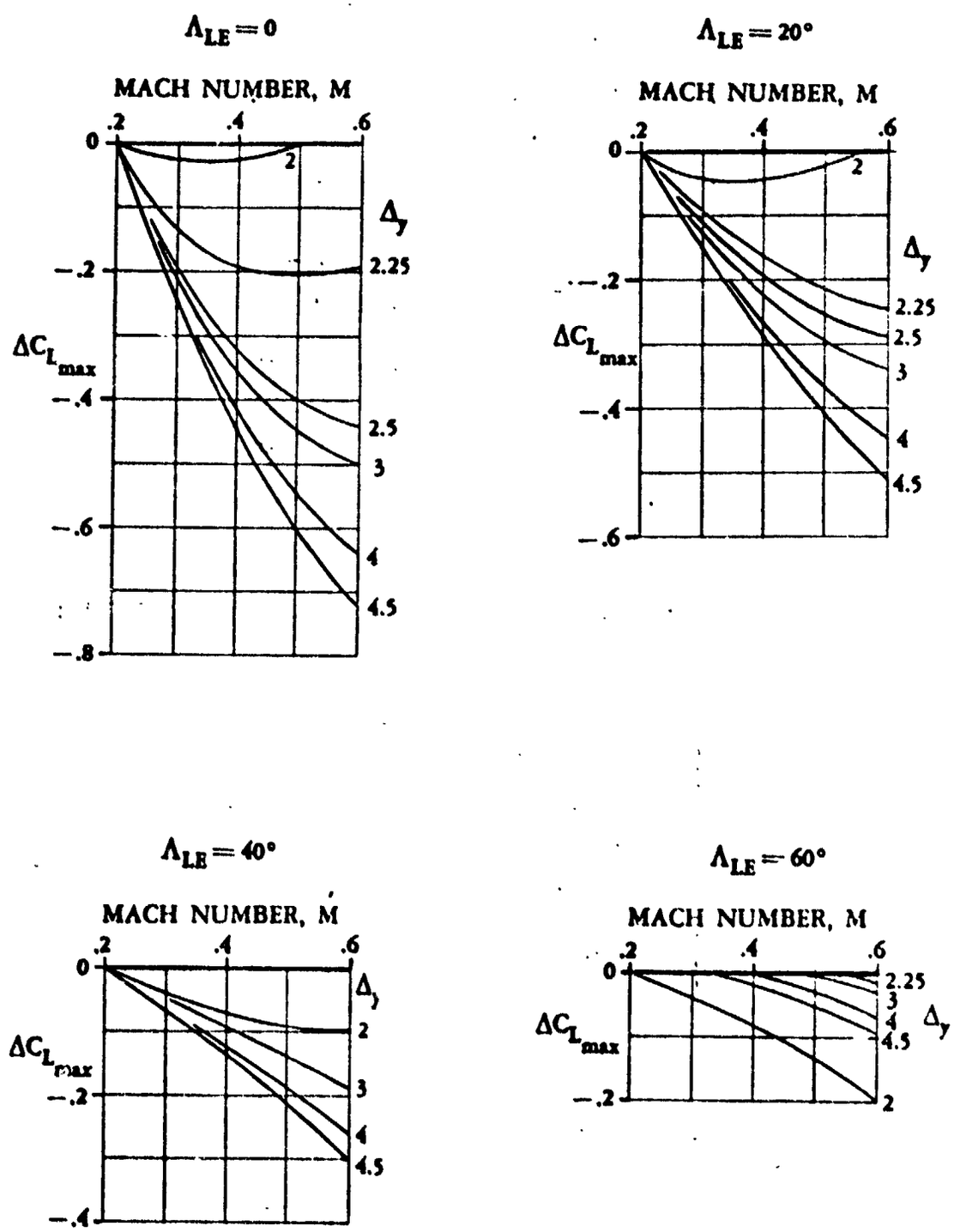

Figure 6-7 Mach Number Correction for Maximum Lift

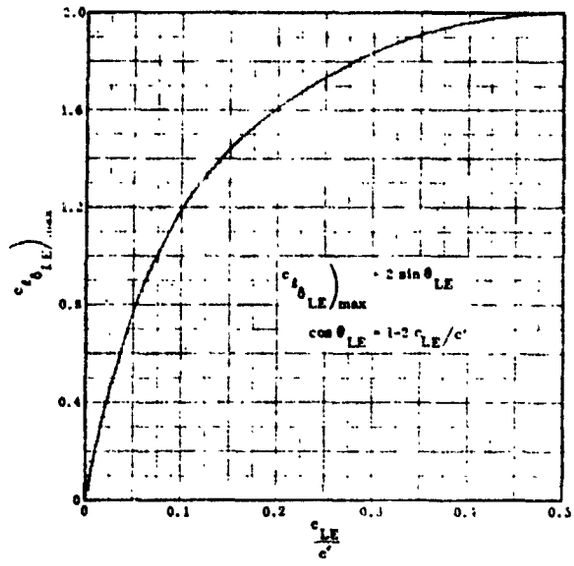

Figure 6-8 Leading Edge Flap Maximum Lift Effectiveness

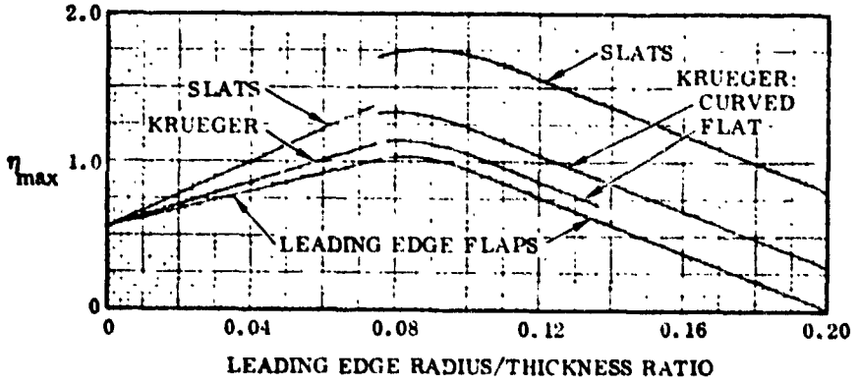

Figure 6-9 Maximum Lift Efficiency for Leading Edge Devices

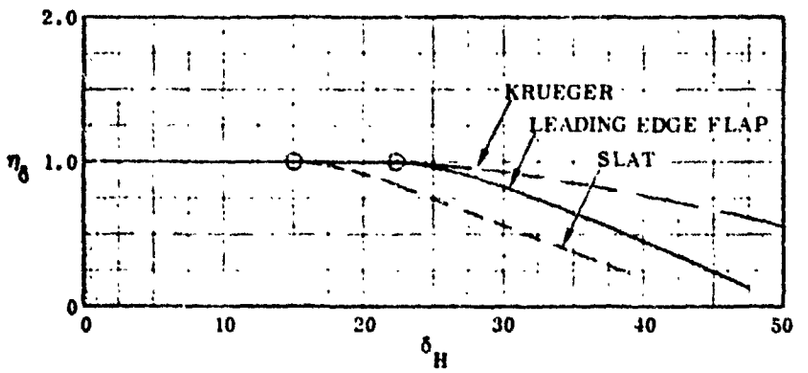

Figure 6-10 . Leading Edge Device Deflection Angle Correction Factor

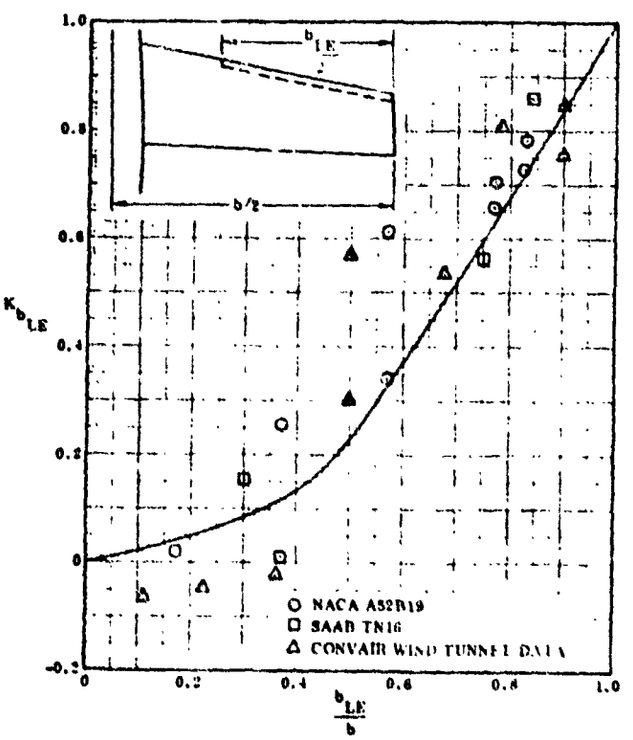

Figure 6-11 Leading Edge Device Maximum Lift Span Factor

where,

AR' = wing aspect ratio for extended leading and trailing edge devices

$\Lambda'_{c/2}$ = mid-chord wing sweep with both leading and trailing edge devices extended

$\beta = \sqrt{1 - M^2}$

M = Mach number

$k = C_{\ell'_\alpha} / (2\pi/\beta)$

$C_{\ell'_\alpha}$ is the section lift curve slope and is found from the equation

$$C_{\ell'_\alpha} = C_{\ell'_{\alpha th}} \frac{1.05}{\beta} \left(\frac{C_{\ell_\alpha}}{C_{\ell_{\alpha th}}} \right) \tag{12}$$

$C_{\ell'_{\alpha th}}$ is based on the Kutta-Joukowski hypothesis of finite velocity at the trailing edge and is calculated from the relationship:

$$C_{\ell'_{\alpha th}} = 2\pi + 4.7\, t/c \left(1 + 0.00375\, \phi_{TE}\right) \tag{13}$$

where

t/c = thickness to chord ratio

ϕ_{TE} = total trailing edge angle (deg)

The term $\left(C_{\ell_\alpha} / C_{\ell_{\alpha th}} \right)$ is a Reynolds number dependent correction factor for boundary layer displacement effects. It is presented in Figure 6-12 as a function of Reynolds number and the trailing edge angle ϕ_{TE}.

The maximum lift coefficient increment due to extended trailing edge devices is determined by the equation

$$\Delta C_{L'_{max_{TE}}} = \Delta K_{b_o} \left(\frac{C_{L'_\alpha}}{C_{\ell'_\alpha}} \right) K_{max}\, \Delta C_{\ell'_{max_{TE}}} \tag{14}$$

ΔK_{b_o} is the partial span flap factor defined as

$$\Delta K_{b_o} = K_{b_{outboard}} - K_{b_{inboard}}$$

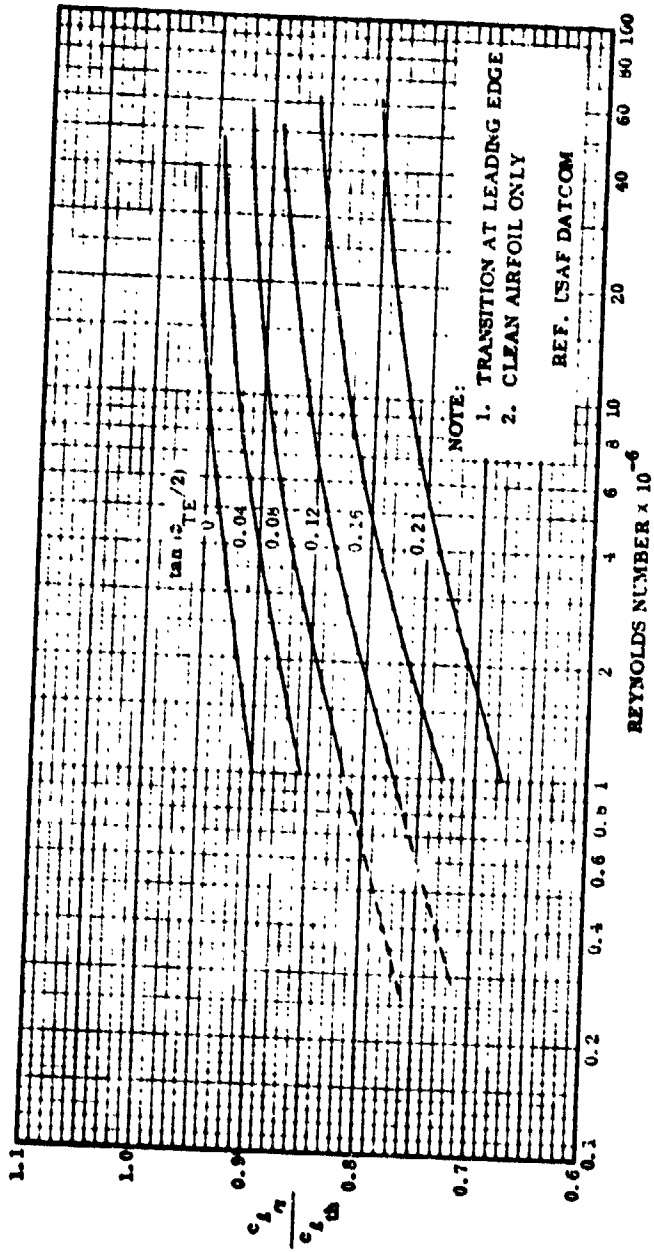

Figure 6-12 Two-Dimensional Life Curve Slope Correction for Reynolds Number

where,

$K_{b_{outboard}}$ = the value at the outboard edge of the flap

$K_{b_{inboard}}$ = the value at the inboard edge of the flap

$Kb_{outboard}$ and $Kb_{inboard}$ are presented in Figure 6-13 as a function of the ratio of flap edge location to wing span and of wing taper ratio.

$C_{L'_\alpha}$ is the three-dimensional wing lift curve slope as given by equation (11) and $C_{\ell'_\alpha}$ is the section lift curve slope found by equation (12).

K_{max} is a correlation factor based on the type of leading edge configuration.

$$K_{max} = \begin{cases} 1.0 & \text{for a slat or Krueger leading edge} \\ 1.21 & \text{for a clean leading edge} \end{cases}$$

$\Delta C_{\ell'_{max_{TE}}}$ is the increment in section maximum lift coefficient due to trailing edge flaps and is determined from the equation

$$\Delta C_{\ell'_{max_{TE}}} = \sum_{i=1}^{I} \eta_{S_{I_i}} C_{\ell_{\delta_i}} \delta_{f_i} \left(\frac{\Delta C_{\ell_{max}}}{\Delta C_{\ell_{\alpha=0}}} \right)_i \qquad (15)$$

where,

i = is the 1st, 2nd, 3rd, etc., flap segment

I = total number of flap segments

η_{S_I} is the slotted flap turning efficiency factor. The values for η_{S_I} are presented in Figures 6-14 , -15 and -16 for single, double and triple slotted flaps, respectively. The data is presented as a function of flap deflection angle (δ_f) and total trailing edge angle (Φ_{TE}).

C_{ℓ_δ} is the flap segment lift effectiveness and is shown in Figure 6-17 as a function of the flap chord ratio (C'_f/c'). Figure 6-18 provides a schematic definition of the geometry terms involved in a trailing edge flap system for lift estimation purposes.

$$\left(\frac{\Delta C_{\ell_{max}}}{\Delta C_{\ell_{\alpha=0}}} \right) = 1 - \frac{\theta_f}{\theta_f + \sin\theta_f} \left[1 + \frac{\text{Log}_e \left| \sin \frac{1}{2}(\Lambda + \theta_f) / \sin \frac{1}{2}(\Lambda - \theta_f) \right|}{\theta_f \tan \Lambda/2} \right] \qquad (16)$$

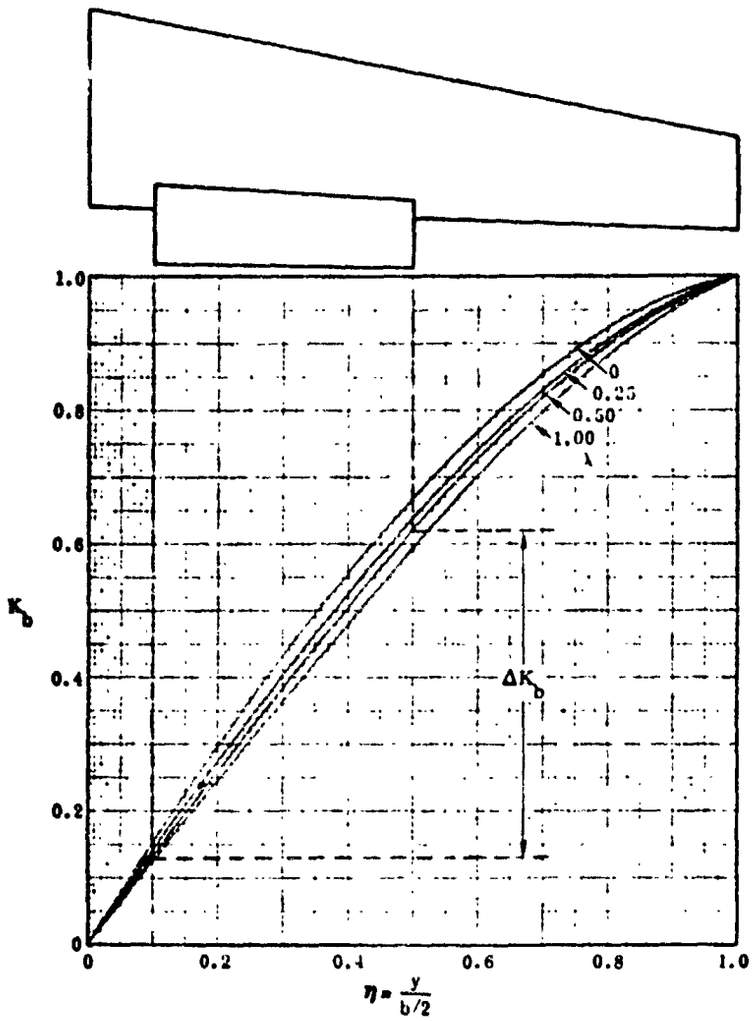

Figure 6-13 Partial-Span Flap Factors

where,

$\cos \theta_f = 1 - 2\,(C'_f/c')$

$\cos X = 2\,(X_s/c') - 1$

X_s/c' = the separation point — the location of which depends on the leading edge configuration. For a clean leading edge, separation is assumed at the leading edge (i.e., $(X_s/c') = 0$). For leading edge high life devices, separation is assumed to be at the knee of the leading edge device (i.e., (X_s/c') C'_f/c').

Figure 6-19 presents the variation of $\left(\frac{\Delta C_{\ell_{max}}}{\Delta C_{\ell_\alpha}}\right)_0$ with flap chord ratio (C'_f/c') and the separation point location (X_s/c').

The lift coefficient at a given angle of attack for a high lift system is determined from the equation

$$C_L = \frac{S'_w}{S_w} \left[C_{L\alpha}' \left(\alpha - \Delta\alpha_T - \Delta\alpha \right) + C'_{L_o} \right] \tag{17}$$

where $\Delta\alpha_T$ is the effect of wing twist given by

$$\Delta\alpha_T = \left(\frac{\Delta\alpha_o}{\theta} \right) \theta \tag{18}$$

$\frac{\Delta\alpha_o}{\theta}$ is the change in wing zero lift angle of attack due to a unit change in linear wing twist and is presented in Figure 6-20 as a function of quarter chord sweep angle (Λ c/4), aspect ratio (AR) and taper ratio (λ).

C_{L_o}' is the lift coefficient at zero angle of attack with high lift devices extended. It is found from the relation

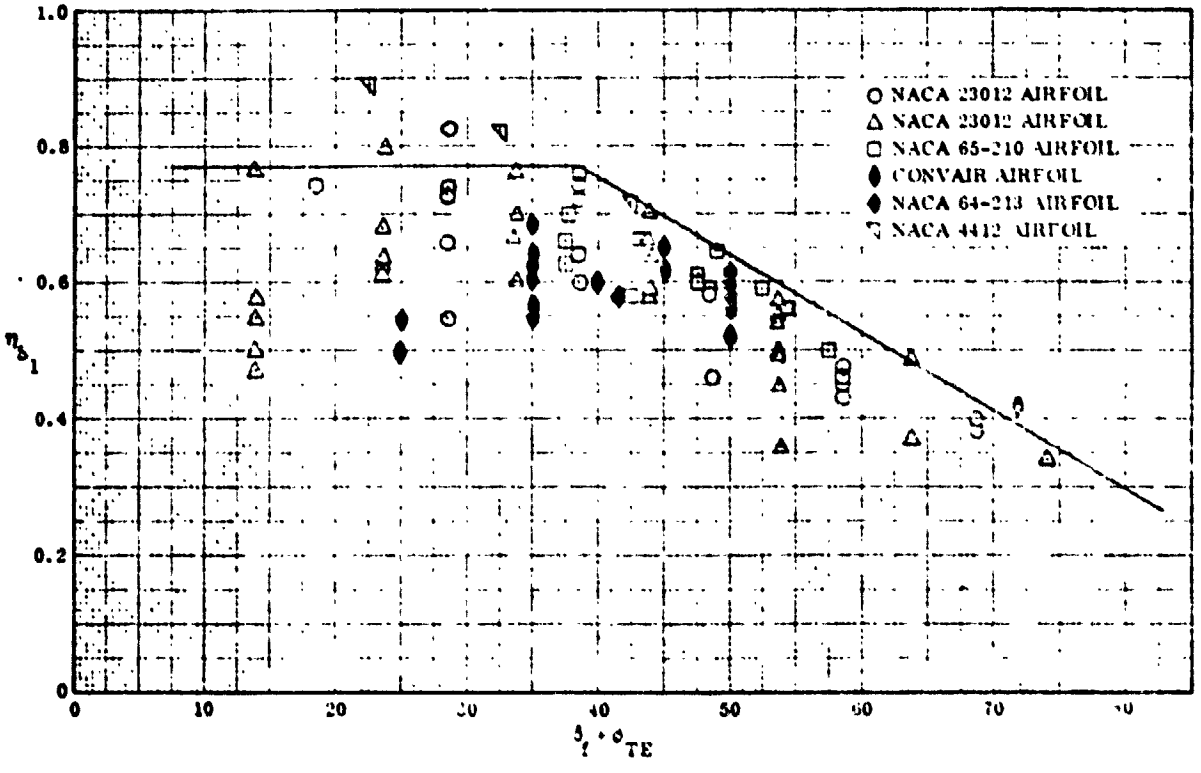

Figure 6-14 Turning Efficiency of Single-Slotted Flaps

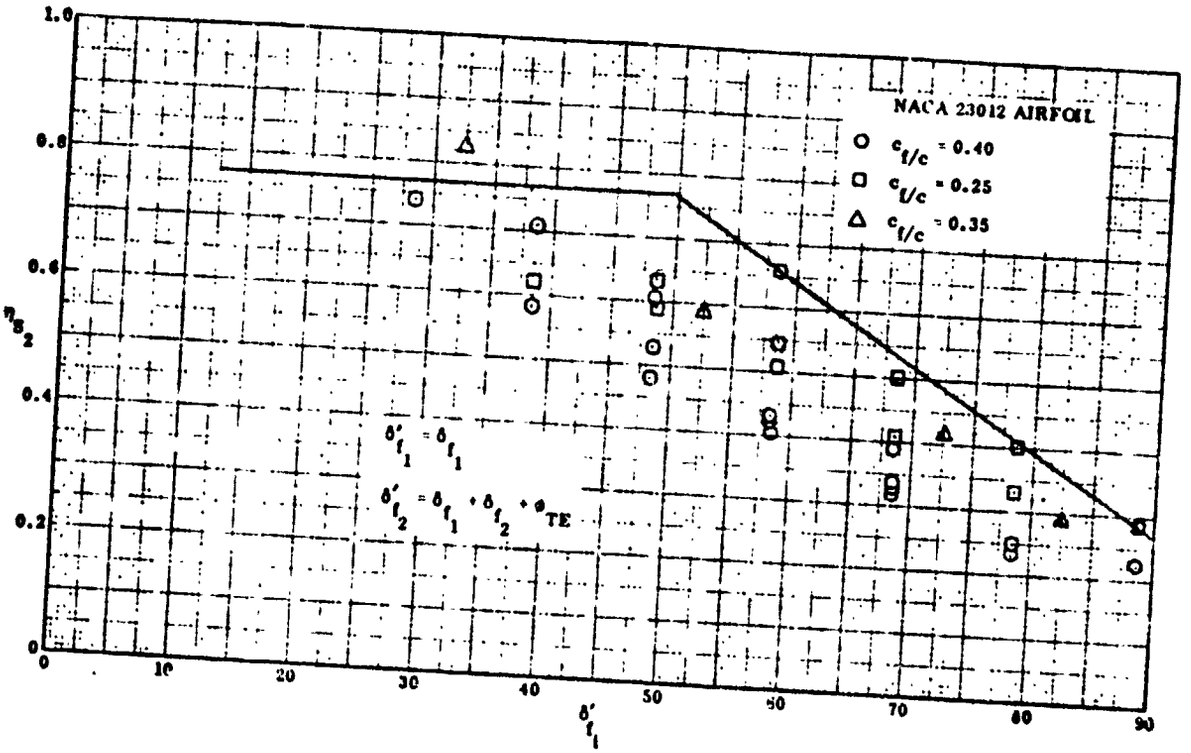

Figure 6-15 Turning Efficiency of Double-Slotted Flaps

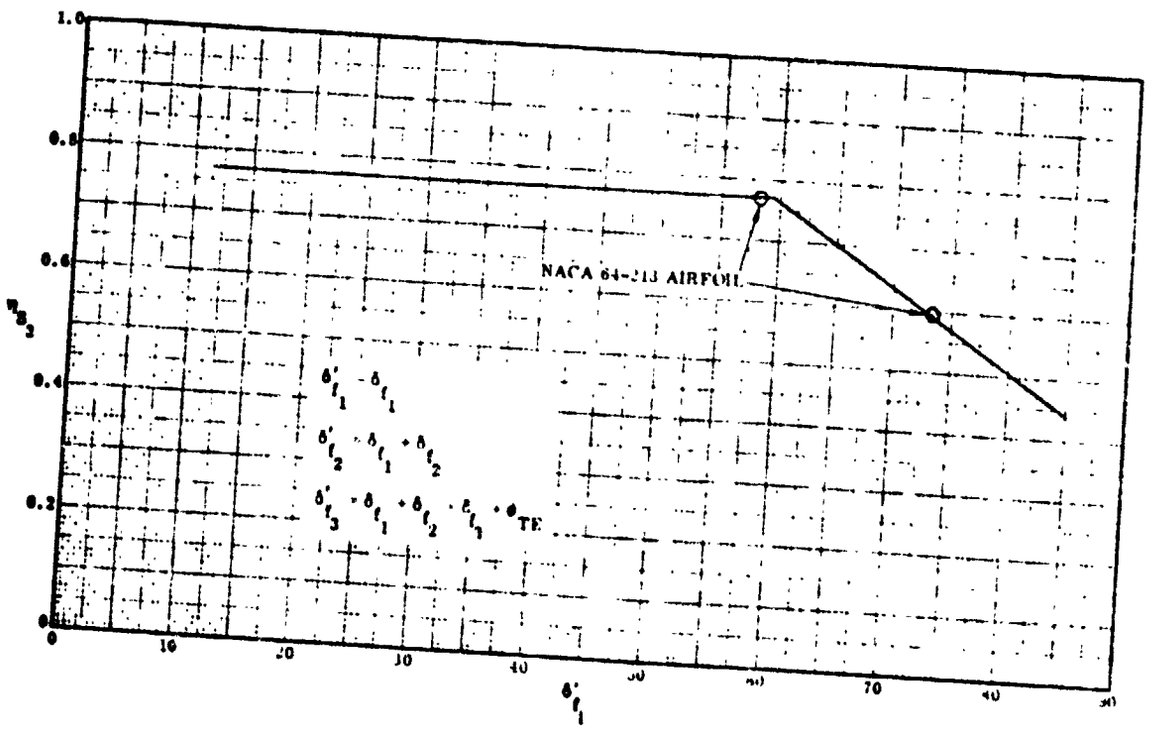

Figure 6-16 Turning Efficiency of Triple-Slotted Flaps

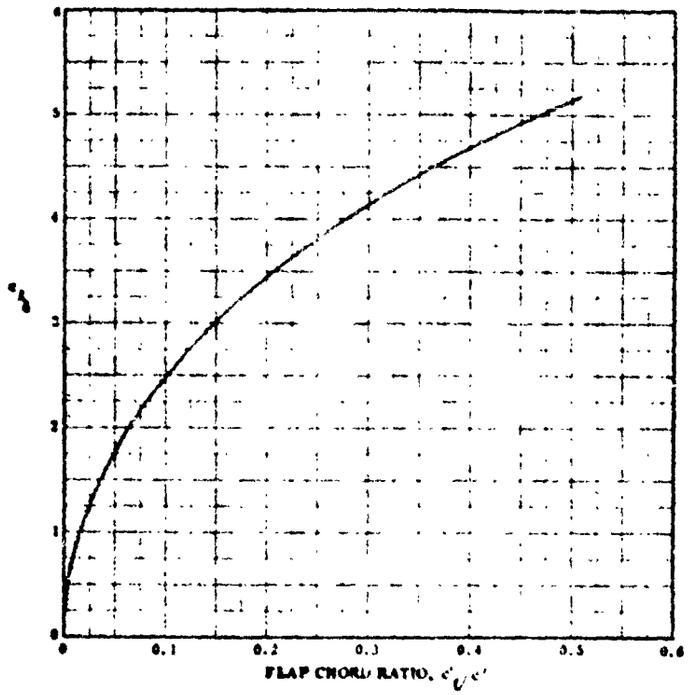

Figure 6-17 Theoretical Lifting Effectiveness of Trailing-Edge Flaps

$$C_{L'_o} \quad \frac{S_w}{S_{w'}} \; C_{L_\alpha} \alpha_{o_L} + \Delta C_{L'_o} \tag{19}$$

where the clean wing lift curve slope (C_{L_α}) is found from the equation:

$$C_{L_\alpha} \quad \frac{2\pi AR}{2 + \sqrt{\left(\frac{AR\beta}{\kappa}\right)^2 \left(1 + \frac{\tan^2 \Lambda_{c/2}}{\beta^2}\right) + 4}} \tag{20}$$

and α_{o_L} is an inputted value of the clean wing angle for zero lift. $\Delta C_{L_o}{}'$ is the incremental lift at zero angle of attack due to high lift devices, and is calculated as follows:

$$\Delta C_{L'_o} = \left[\Delta C_{l_o} \left(\frac{C_{L_\alpha}}{C_{l_\alpha}}\right) K_c K_b\right] \tag{21}$$

where:

K_b = flap lift factor (Figure 6-13)

K_c = flap chord factor (Figure 6-21)

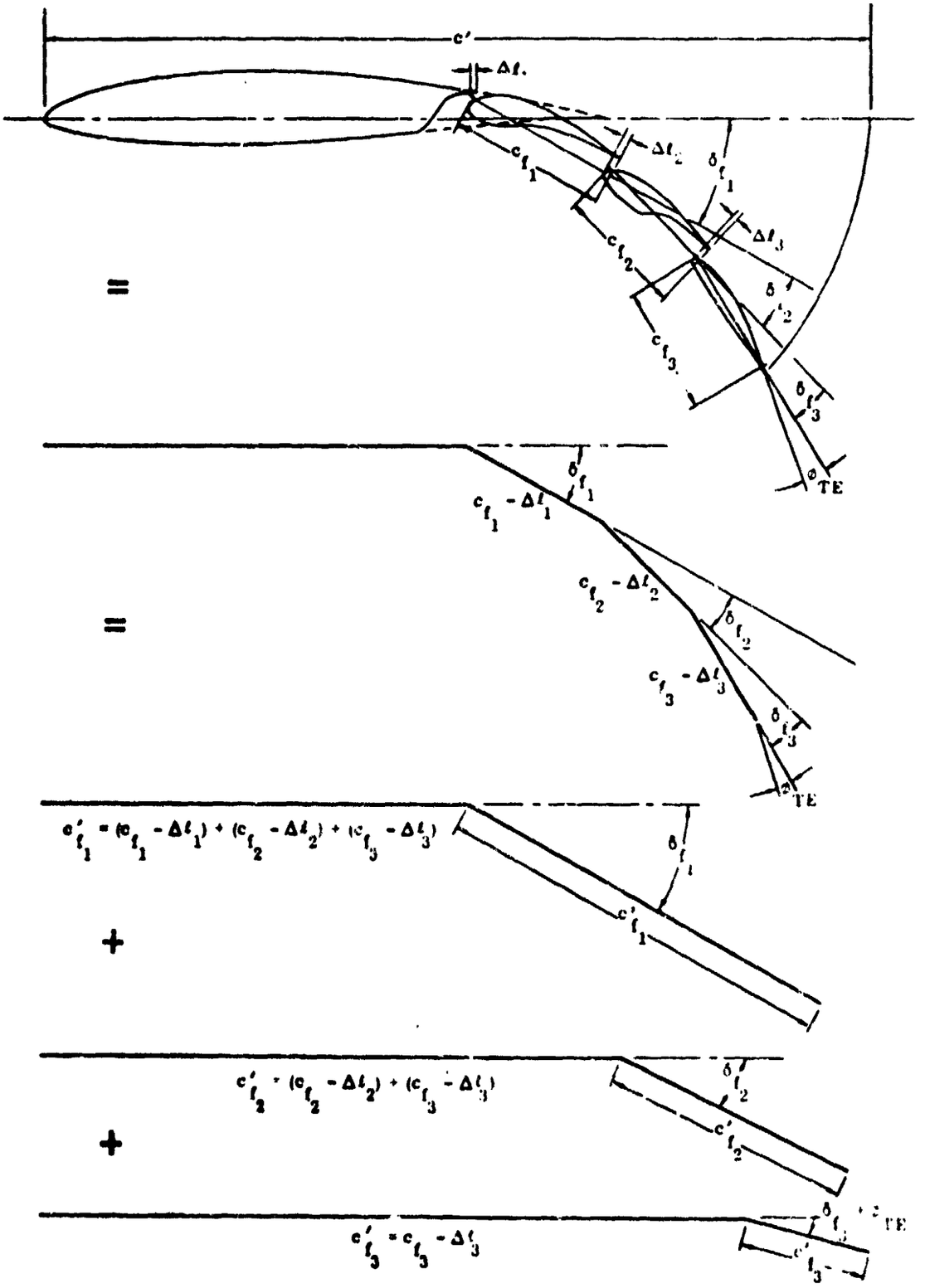

Figure 6-18 **Principle of Superposition Theory and Extended Slotted-Flap Geometry**

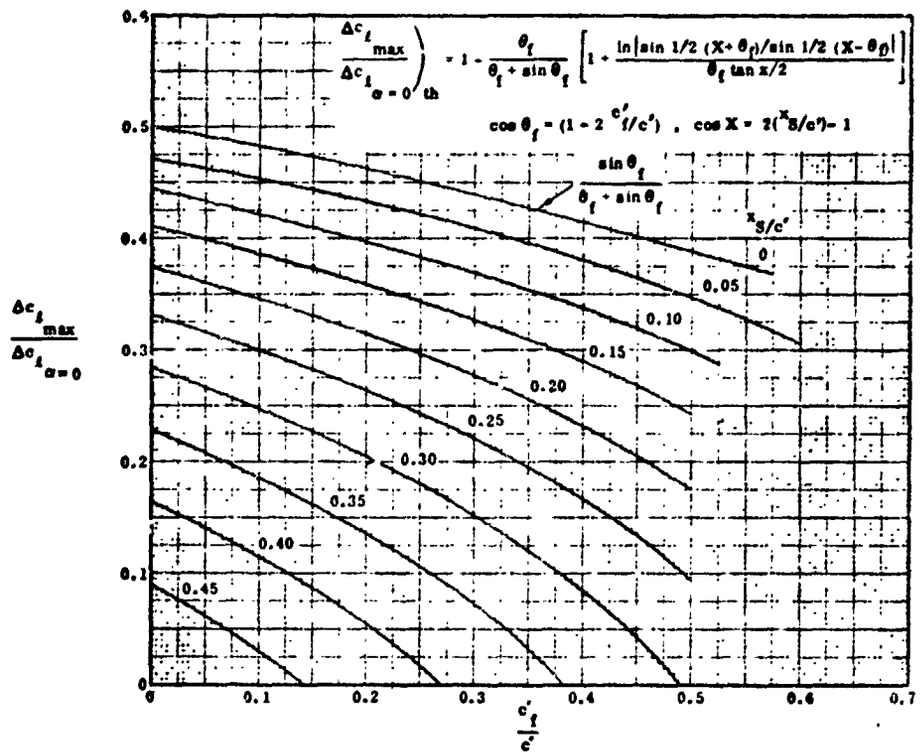

Figure 6-19 Increment in Maximum Lift Coefficient for Trailing-Edge Flaps

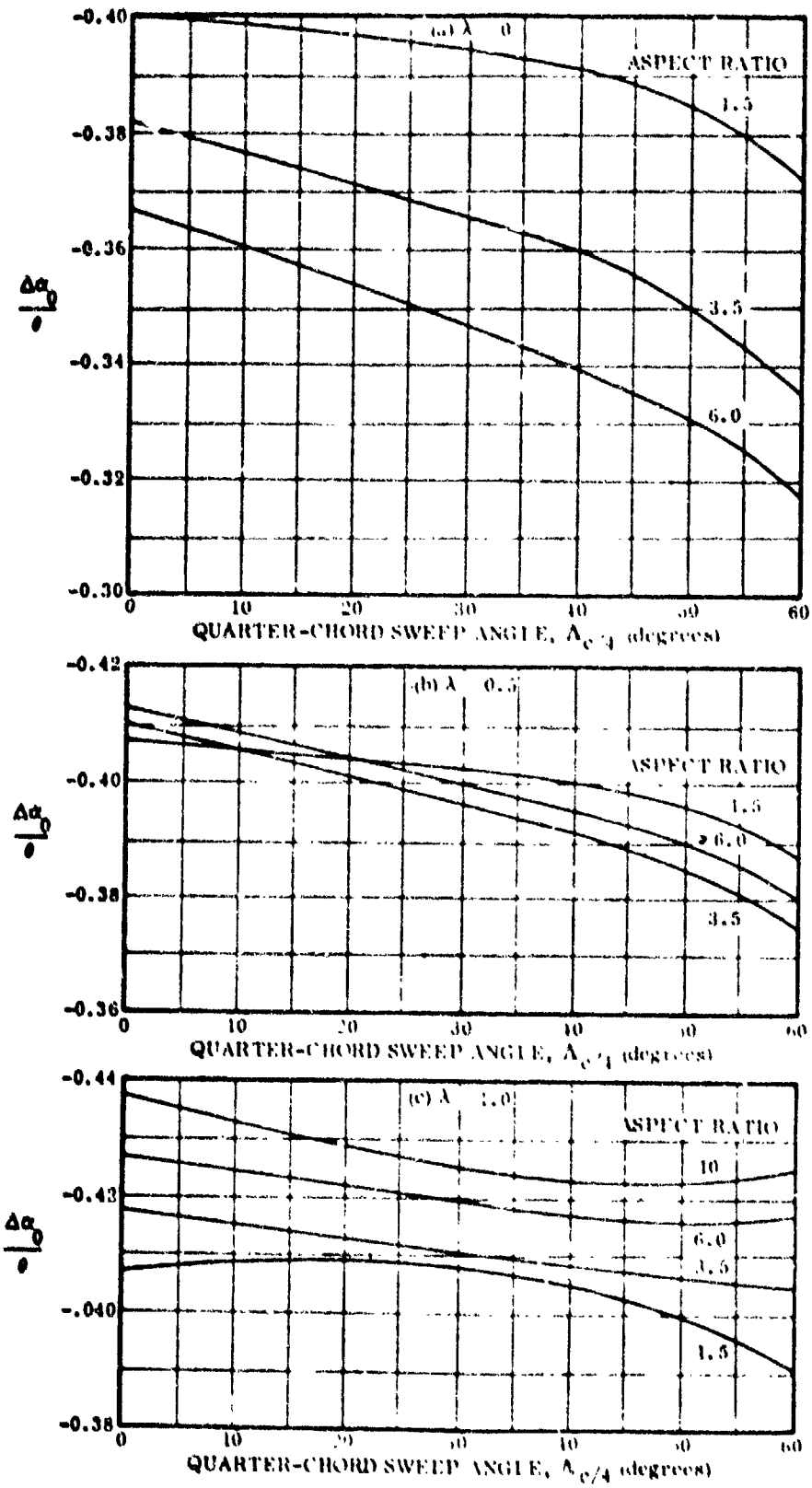

Figure 6-20 Effect of Linear Twist on Wing Angle of Attack for Zero Lift

where,

$$\Delta C_{\ell_o} \quad \sum_{i=1}^{I} \eta_{S_i} \; C_{\ell_{\delta_i}} \; \delta_{f_i}$$

i = the 1st, 2nd, 3rd, etc., flap segments

I = the total number of flap segments

η_{S_i} = slotted flap efficiency factor (Figure 6-14 through 6-16.)

C_{ℓ_δ} = flap segment lift effectiveness (Figure 6-17)

δ_f = flap segment deflection angle (deg)

The lift curve slope ratio $\left(C_{L_\alpha} / C_{\ell_\alpha}\right)$ is found from Reference 4 to be:

$$\frac{C_{L_\alpha}}{C_{\ell_\alpha}} = \frac{AR}{2 + \sqrt{4 + \left(\frac{Sw}{Sw'}\right)^2 \left(\frac{AR}{\cos \Lambda c/2}\right)^2}} \qquad (22)$$

The flap chord factor K_a is plotted in Figure 6-21 as a function of AR and c_f/c and the flap lift factor (K_b) was shown in Figure 6-13 as a function of taper ratio λ and spanwise location η y/b/2.

Δ_α, in equation (17), is a term to account for non-linearities in the lift curve.

If $\alpha < (\alpha max - 2\Delta\alpha max)$

$\Delta_\alpha = 0$

If $\alpha > (\alpha_{max} - 2\Delta\alpha_{max})$

$$\Delta\alpha = \left(\frac{\alpha - \alpha_{max} + 2\Delta\alpha_{max}}{2\Delta\alpha_{max}}\right)^2 \Delta\alpha_{max}$$

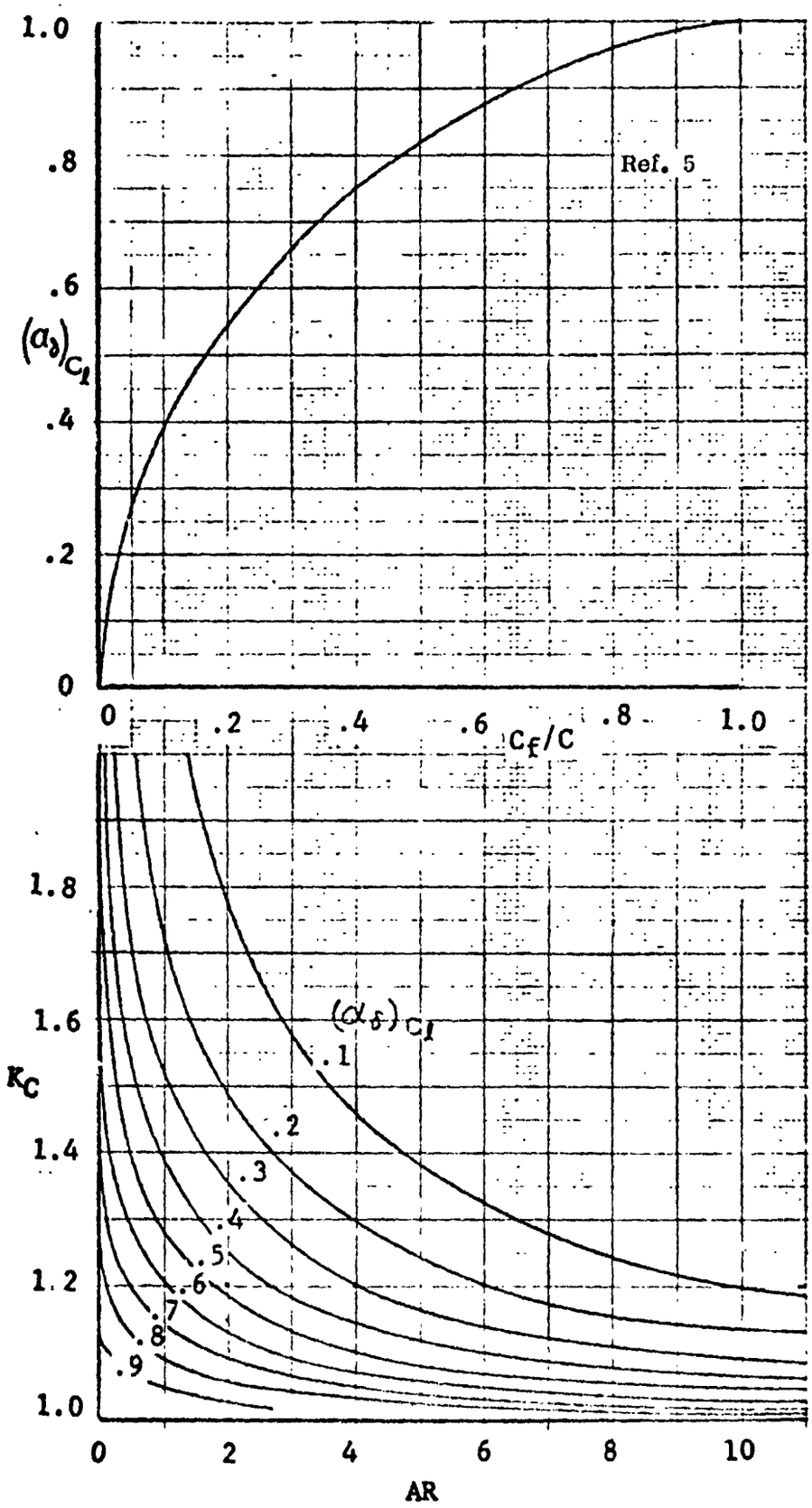

Figure 6-21 Flap C[illegible]l Factor

where,

$$\alpha_{max} = \frac{C_{L_{max}} \frac{Sw}{Sw'} - C'_{L_o}}{C'_{L_\alpha}} + \Delta\alpha_T + \Delta\alpha_{max} \qquad (23)$$

$\Delta\alpha_{max}$ is the angle of attack increment from the angle at $C_{L_{max}}$ based on the lift curve slope (C'_{L_α}) from equation (11), to the actual angle for $C_{L_{max}}$ (α_{max}). Figure 6-22 presents typical values for $\Delta\alpha_{max}$ as a function of leading edge sweep angle Λ_{LE} and leading edge parameter Δ_y.

In order to determine angle of attack (α) as a function of lift coefficient, equation (17) may be rewritten in the form:

$$\alpha = \frac{C_L \frac{Sw}{Sw'} - C'_{L_o}}{C'_{L_\alpha}} + \Delta\alpha_T + \Delta\alpha \qquad (24)$$

Thus, it may be shown that if $\left[\frac{C_L \frac{Sw}{Sw'} - C'_{L_o}}{C'_{L_\alpha}} + \Delta\alpha_T\right] < (\alpha_{max} - 2\Delta\alpha_{max})$

$$\Delta\alpha = 0$$

On the other hand, if $\left[\frac{C_L \frac{Sw}{Sw'} - C'_{L_o}}{C'_{L_\alpha}} + \Delta\alpha_T\right] > (\alpha_{max} - 2\Delta\alpha_{max})$

$$\Delta\alpha = \alpha_{max} - \left[\frac{C_L \frac{Sw}{Sw'} - C'_{L_o}}{C'_{L_\alpha}} + \Delta\alpha_T\right]$$

$$- 2\sqrt{\alpha_{max}\Delta\alpha_{max} - \Delta\alpha^2_{max} - \Delta\alpha_{max}\left[\frac{C_L \frac{Sw}{Sw'} - C'_{L_o}}{C'_{L_\alpha}} + \Delta\alpha_T\right]}$$

6.1.2.2 Drag Characteristics. The drag characteristics of a configuration having both leading and trailing edge high lift devices are determined from the equation:

$$C_D = C_{D_{min}} + \left[\frac{C_L - C_{L_b} - \Delta C_L)_{\text{due to flaps}}}{\pi A Re'}\right]^2 \qquad (25)$$

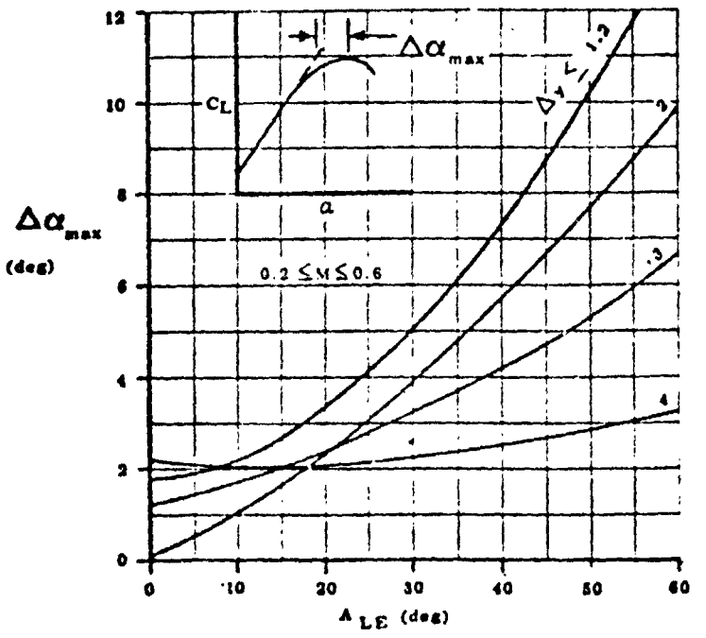

Figure 6-22 Angle-of-Attack Increment for Subsonic Maximum Lift of High-Aspect-Ratio Wings

and

$$C_{D_{min}} = C_{D_{min_{clean}}} + \Delta C_{D_{LG}} + \Delta C_{D_{FLAPS}} + \Delta C_{D_{SLATS}} + \Delta C_{D_I} \qquad (26)$$

where,

$C_{D_{min_{clean}}}$ = minimum drag coefficient of clean configuration

$\Delta C_{D_{LG}}$ = incremental drag due to landing gear

$\Delta C_{D_{FLAPS}}$ = incremental drag due to trailing edge flaps

$\Delta C_{D_{SLATS}}$ = incremental drag due to leading edge slats

ΔC_{D_I} = incremental induced drag due to increasing the lift coefficient at zero angle of attack by extending the trailing edge flap

The incremental profile drag coefficient of a trailing edge flap is defined by the equation from Reference 6.

$$\Delta C_{D_{FLAPS}} = \Delta C_{D_{P_{MIN_{TE}}}} = \left(\Delta C_{D_{P_{TE}}}\right)_{C'_f/c' = .25} \frac{S_{flapped}}{S_{Ref}}$$

$$X \left(\frac{\Delta C_{D_{P_{TE}}}}{\Delta C_{D_{P_{TE}}}\Big)_{C'_f/c' = .25}} \right) \tag{27}$$

The term $\Delta C_{D_{P_{TE}}}\Big)_{C'_f/c' = .25}$ is found from Figure 6-23 as a function of the equivalent flap angle ($\delta_{f_{EQ}}$).

$$\delta_{f_{EQ}} = \delta_{f_1} + \frac{a\delta_2}{a\delta_1} \delta f_2 \tag{28}$$

where,

δ_{f_1} = deflection angle of the first flap segment

δ_{f_2} = deflection angle of the last flap segment

a_δ = change in section zero lift angle of attack due to flap deflection

A schematic of the trailing edge flap geometry for drag purposes is presented in Figure 6-24. Curves of a_δ are given in Figures 6-25 and 6-26 for single and double slotted flap systems, respectively, as a function of flap chord ratio C'_f/c' and flap deflection angle δ_f. Note, from Figure 6-24, that a triple slotted flap must be expressed in terms of a double slotted system in order to use the a_δ curves of Figure 6-26.

$\dfrac{\Delta C_{D_{P_{TE}}}}{\Delta C_{D_{P_{TE}}}\Big)_{C'_f/c' = .25}}$ is the term to correct the flap profile drag increment to other values of C'_f/c' and is presented in Figure 6-23 as a function of flap chord ratio C'_f/c'.

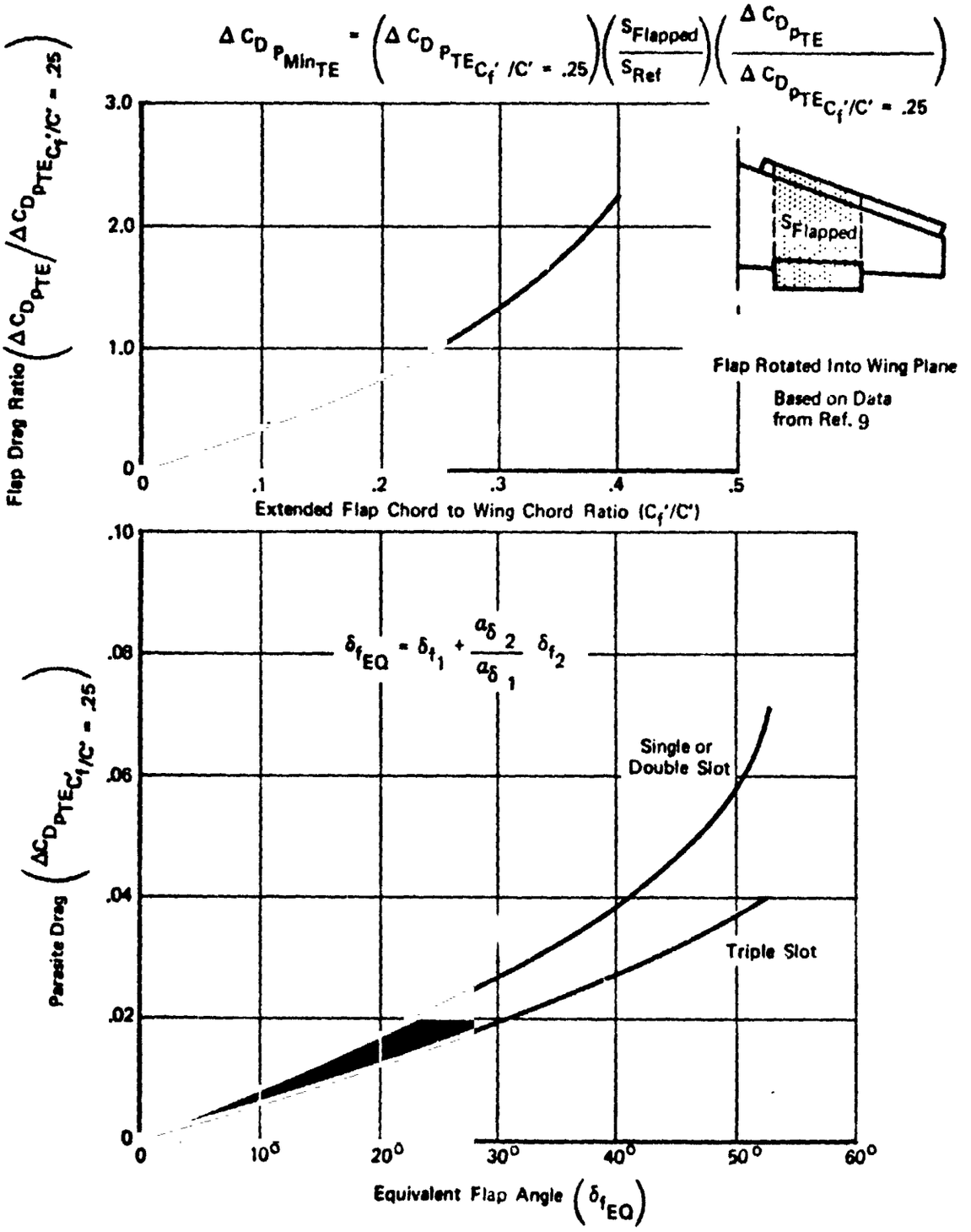

Figure 6-23 *Parasite Drag of Trailing Edge Flaps*

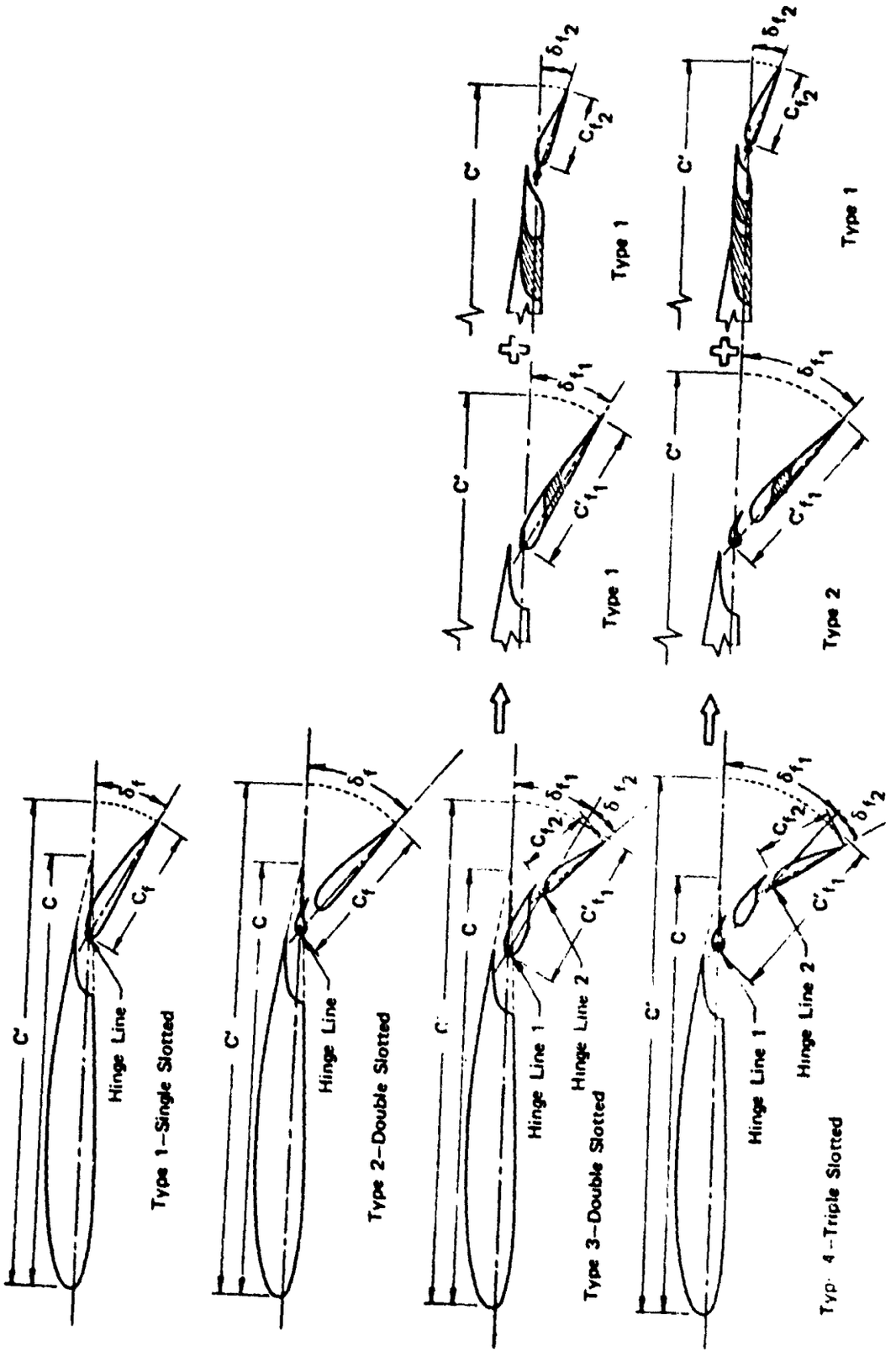

Figure 6-24 *Multi-Element Flap Nomenclature*

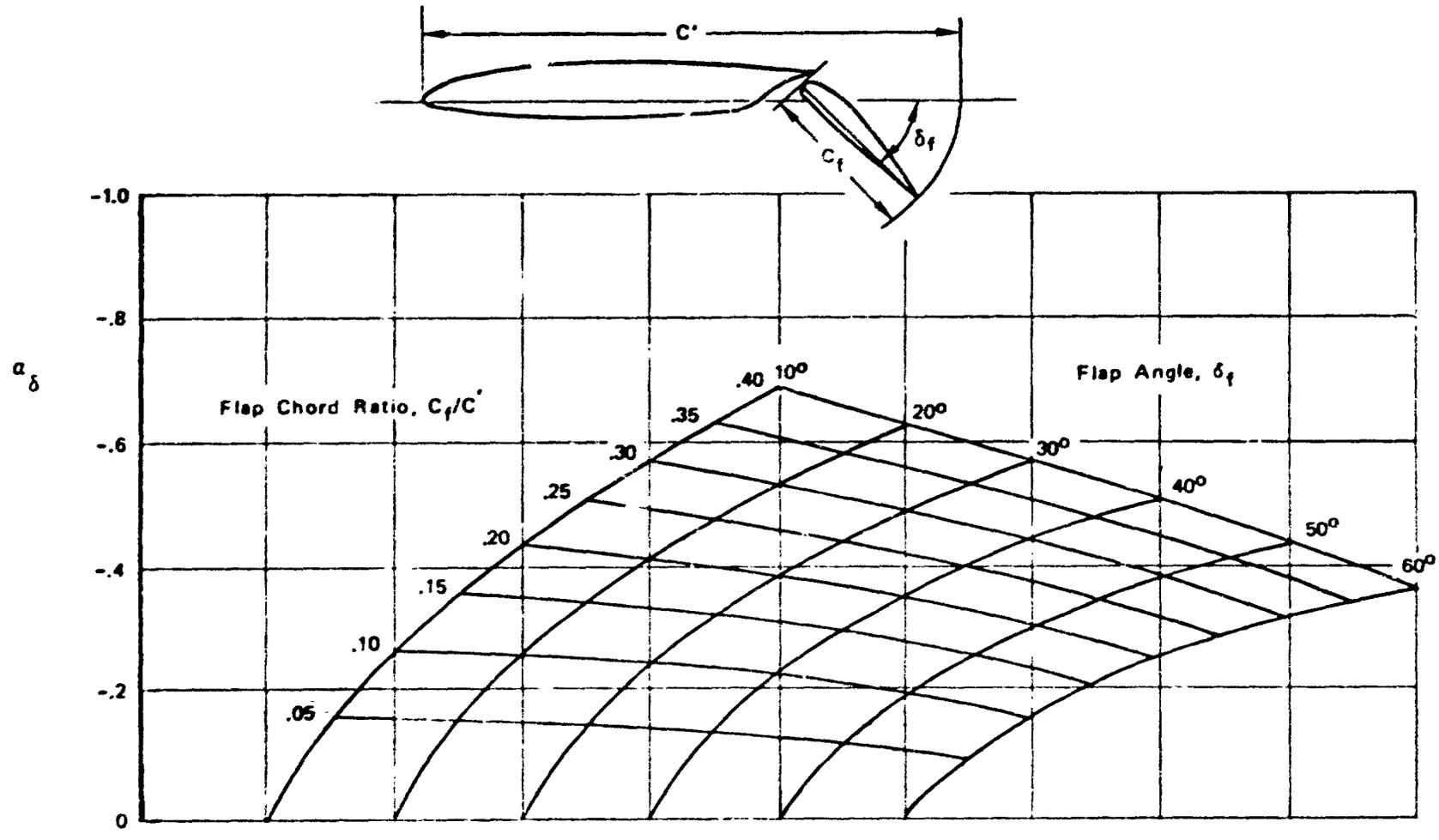

Figure 6–25 *2-D Flap Effectiveness, Single-Slotted Flap*

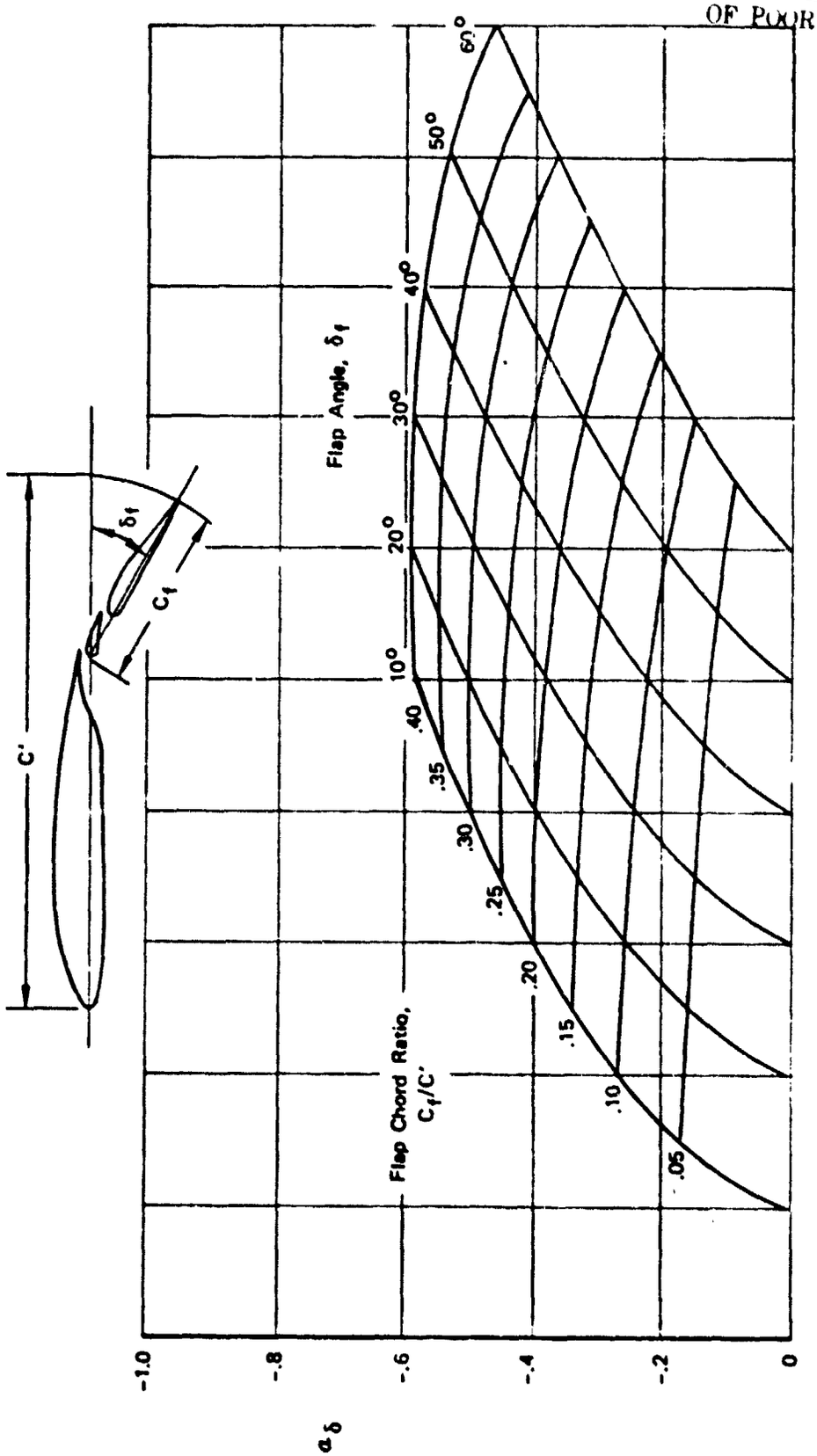

Figure 6-26 *2-D Flap Effectiveness, Double-Slotted Flap*

$S_{flapped}$ represents the area of the wing encompassed by the inboard and outboard edges of the trailing edge flap, with the leading and trailing edges rotated into the plane of the wing chord as shown in Figure 6-23 .

The profile drag coefficient due to leading edge devices is derived from the equation

$$\Delta C_{D_{SLATS}} = 0.154 \frac{S_{LE}}{Sw} \tag{29}$$

where S_{LE} is the planform area of the leading edge device.

The value of ΔC_{D_I} is determined from the equation of Reference 4.

$$\Delta C_{D_I} = K_A K_f \frac{\left(\Delta C_{L_o}\right)^2}{\pi AR} \tag{30}$$

where K_A and K_f, shown plotted in Figure 6-27 , are factors which account for the non-elliptical span loading of partial span flaps. K_f is presented as a function of b_c/b and $(b_c + b_f)/b$, where b is the wing span, b_f the flap span, and $b_c/2$ the distance between the wing centerline and the inboard edge of the flap. K_A is presented as a function of b_c/b and $AR/2\pi$.

ΔC_{L_o} is the incremental lift coefficient due to flaps at zero angle of attack and is determined from equation (21), where

$$\Delta C_{L_o} = \Delta C'_{L_o} \frac{Sw'}{Sw} \tag{31}$$

The induced drag due to deflecting trailing edge flaps is given by the term

$$\left[\frac{\left(C_L - C_{L_b} - \Delta C_L \right)_{\text{due to flaps}}}{\pi A Re'} \right]^2$$ of equation (25).

The term e' is the span efficiency factor for determining polar shape and is given by the equation:

$$e' = e \frac{S'_w}{S_w}$$

where e is the clean airplane polar factor. C_{L_b} is the lift coefficient for minimum drag of the clean airplane polar, while the increment in minimum drag due to the flap is determined from the Equation:

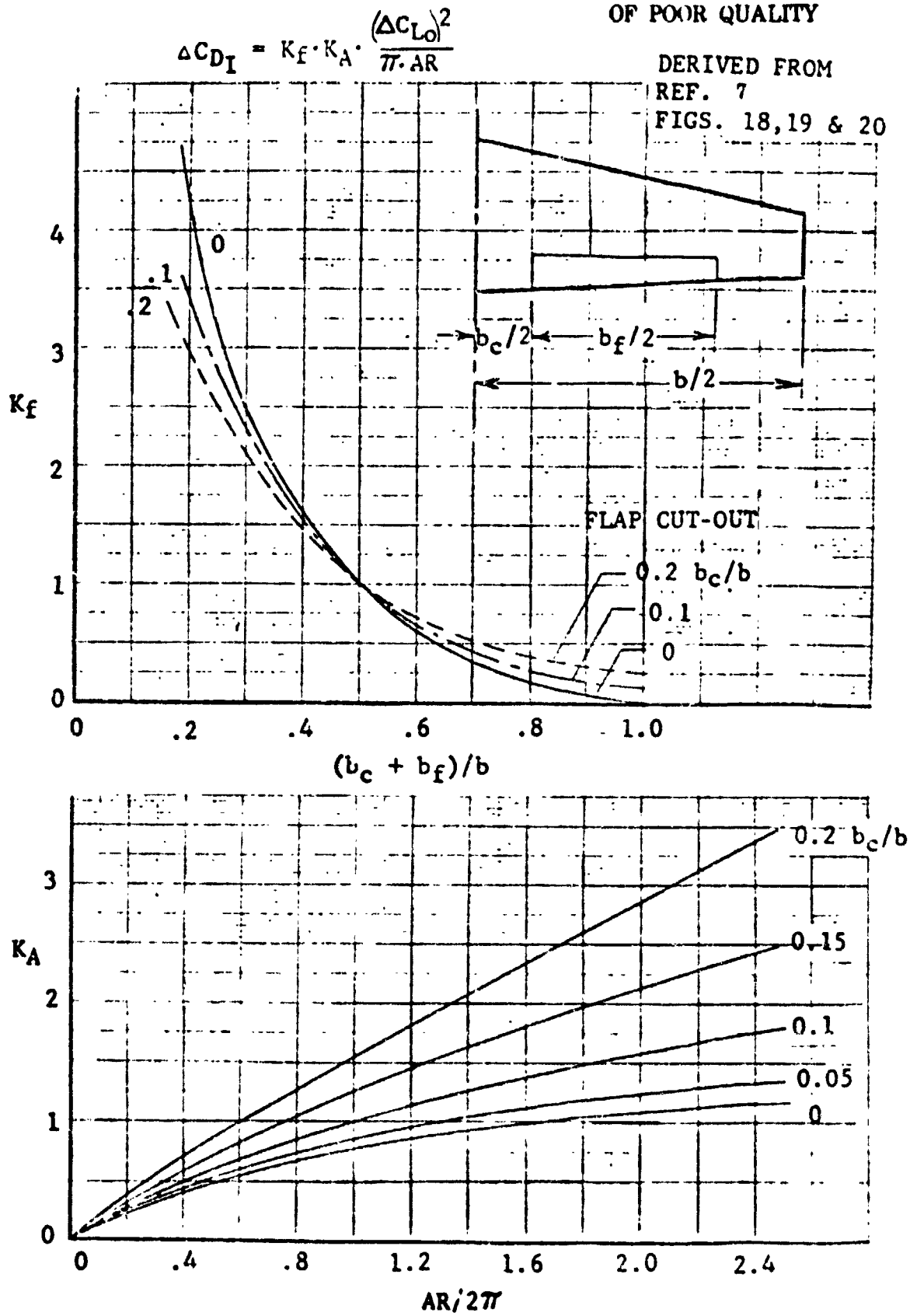

Figure 6-27 Flap-Induced Drag Factors

$$\Delta C_L\Big)_{\text{due to flaps}} = \frac{\left(1 - \frac{1}{\pi AR K}\right)\left(\Delta C_{L_o}\right)}{1 + 1.16\left(\frac{C_{L_\alpha}}{C_{\ell_\alpha}}\right)(0.5 - C_f/c)} \qquad (32)$$

6.1.3 PROPUL (Propulsion Characteristics). This routine computes engine thrust and fuel flow characteristics at a designated flight condition. Required input for the routine consists of thrust and fuel flow data as a function of speed, altitude and power setting. Using a table look-up procedure, the program searches through the matrix of input data and interpolates for the desired engine characteristics by using the hyperbolic curve fit routine of subroutine PROP4.

It should be noted that the program expects the input engine data to have already been corrected for installation losses. There is no existing capability in the program for calculating these losses. This is not a serious drawback so long as the sizing exercise is restricted to a particular engine/airframe installation concept. However, as soon as the installation concept significantly changes, a new engine data deck must be provided.

In order to make the propulsion routine applicable to hydrogen or methane type fuels, the fuel flow characteristics of the input JP engine deck are ratioed by the lower heating value of JP fuel divided by the lower heating value of hydrogen or methane. The appropriate heating values of these three types of fuel are given as follows:

JP	18,400 Btu/lb
Methane	21,350 Btu/lb
Hydrogen	51,590 Btu/lb

Thus, it is seen that the fuel flows for an engine burning hydrogen or methane fuel will be lower than with JP fuel.

6.1.4 GEOM (Geometry Definition). Complete and accurate geometric data, insofar as possible, are generated for use in drag estimation and weight estimation by a geometry subroutine. A relatively small amount of generalized data is required as input.

This routine is intended to reduce or remove the requirement for making many drawings and the hand computation of geometric data required by drag and weight estimation methods. This is more fully described in Section 2.0.

6.1.5 WEIGHTS (Component Weight Estimation). Design weights used in performance analysis, as well as a component weight breakdown, is provided by the weights

subroutine. The routine was designed and developed to provide accuracy and flexibility of application. Accuracy is obtained by use of substantiative equations and, considering the design stage in which the program is meant to be used, accuracy is considered good. Flexibility is achieved by using more than one equation or method, selecting the most appropriate by controlling the input data. This routine is more fully described in Section 3.0.

6.2 MISSION PERFORMANCE. As previously discussed, mission performance is divided into ten flight regimes: takeoff, climb, acceleration, cruise, loiter, combat, descent, deceleration, reserve, and landing. Takeoff, combat and landing are represented by fuel allowance calculations only while reserve depicts a percentage of total fuel. Actual flight performance is calculated for the other flight regimes, using equations of motion.

Calculated flight performance is determined by similar procedures for each of the flight regimes. Equations of motion are solved for the required unknown (e.g., angle of attack), and the required flight condition is derived. For example, cruise can be calculated either at given constant conditions (fixed speed and altitude) or at optimum conditions (e.g., speed for maximum specific range). Integration of various parameters over the applicable increment (e.g., an altitude increment in the case of a climb) is handled by the Gill integration procedure, which was specifically developed for efficient computer use. Termination occurs when a specified condition is reached.

For each mission segment, the number of operating engines, the type of atmosphere, the aerodynamic configuration, and an airplane weight increment can be specified. Thus, each of these parameters can be changed at definite points in the mission by specifying them for each segment.

For ease of use and understanding by a using engineer, each flight segment is represented in the program by a separate subroutine. Since different missions will vary in the way of a given flight segment is to be performed (climb, for instance, can be at maximum rate-of-climb speed or at a given speed-altitude schedule), several options may exist within a given subroutine. The desired option is indicated by use of an input index, with each index representing an alternate way of flying a given mission segment.

A more detailed description of each mission segment is given in the following sections.

6.2.1 Takeoff. For a given (inputted) speed, altitude, and power setting, the fuel flow is determined from subroutine PROPUL (Section 6.1 3) and the airplane weight, fuel used, and time are adjusted accordingly for a given time allowance.

6.2.2 Climb. There are four separate climb options available in the program. These options differ in the manner of performing the climb: at maximum rate-of-climb speed, or at a given speed-altitude schedule; and in the way in which the climb is terminated — at a given altitude, or at the optimum cruise altitude.

6.2.2.1 Calculates Climb at Speed for Maximum Rate-of-Climb, Terminates Climb at a Given Altitude. At an initial starting altitude, the maximum-rate-of-climb and the accompanying speed are determined from subroutine MAXRCV (Section 6.4.2) for zero acceleration. Both are than recalculated at an incremented altitude, with the airplane weight for the second altitude being estimated by the fuel flow obtained for the flight condition at the first altitude.

$$W @ h_2 = W @ h_1 - \text{Fuel Flow} @ h_1 \left(\frac{\Delta H}{R/C @ h_1} \right)$$

where:

$W @ h_2$ = airplane weight at altitude h_2

$W @ h_1$ = airplane weight at altitude h_1

ΔH = incremental climbing altitude $(h_2 - h_1)$

$R/C @ h_1$ = airplane rate-of-climb at altitude h_1

A tangential acceleration is then calculated, based on accelerating from the velocity for maximum rate-of-climb at the first altitude to that at the second altitude.

$$a_t = \frac{\left(V_{\text{max R/C @ } h_2} - V_{\text{max R/C @ } h_1} \right) \left(R/C_{\text{max @ } h_2} - R/C_{\text{max @ } h_1} \right)}{\Delta H \ \text{Log}_e \left(\frac{R/C_{\text{max @ } h_2}}{R/C_{\text{max @ } h_1}} \right)}$$

where:

$V_{\text{max R/C @ } h_2}$ = airplane velocity for maximum rate-of-climb at altitude h_2

$V_{\text{max R/C @ } h_1}$ = airplane velocity for maximum rate-of-climb at altitude h_1

The speeds and max R/C's are then recalculated, and the procedure is iterated until the change in rate-of-climb (due to the change in acceleration) decreases to within a specified tolerance.

The time, distance, fuel, weight, altitude, and velocity are then integrated over an altitude increment using subroutine MSNINTG (Section 6.4.9) and the above procedure is repeated until the given final altitude is reached.

6.2.2.2 Calculates Climb at Speed for Maximum Rate-of-Climb, Terminates Climb at Optimum Cruise Altitude. The procedure for calculating the climb in this routine is the same as that described for the previous routine, except for the manner of termination. An altitude is determined, which will provide the maximum value of specific range in cruise flight, and is designated as the optimum cruise altitude. This altitude is determined by using subroutine MAXSRH (Section 6.4.5).

Since the optimum cruise altitude changes as the airplane weight changes (due primarily to fuel consumption), it is recomputed when the climb approaches its termination. An optimum altitude is calculated at the start of the climb, and when the climb is computed to this height, the optimum cruise altitude is determined once more, at the then reduced airplane weight. The climb is then continued to this new termination altitude.

6.2.2.3 Calculates Climb at a Given Speed-Altitude Schedule, Terminates Climb at a Given Altitude. The fixed speed-altitude schedule is input by the climb subroutine.

The speed can be in terms of either velocity (knots), or Mach number. Up to five segments can be represented for a given climb (i.e., the schedule can be divided into five parts), with different segments in differing speed terms if required (e.g., a Mach altitude schedule segment followed by a velocity-altitude segment). The schedule can be either linear, or a hypervolic curve fit (KABD) (see Section 6.4.13).

For a given altitude, initially the starting altitude, the climb speed is taken from the speed-altitude schedule. The airplane flight parameters are calculated, including rate-of-climb, using subroutine FEQMA (Section 6.4.1) at the current climb weight. This is repeated at an incremented altitude with the airplane weight estimated as

$$W @ h_2 = W @ h_1 - \text{Fuel Flow } @ h_1 \left(\frac{\Delta H}{R/C @ h_1} \right)$$

The tangential acceleration necessary at the initial altitude is calculated, which will enable the velocity at the second altitude to be reached.

$$a_T = \frac{\left(V @ h_2 - V @ h_1\right)\left(R/C @ h_2 - R/C @ h_1\right)}{\Delta H \log_e \left(\frac{R/C @ h_2}{R/C @ h_1} \right)}$$

where:

a_T = airplane tangential acceleration required at altitude h_1 to obtain desired velocity at altitude h_2

The rates-of-climb are then recalculated, and the procedure is iterated until the change in rate-of-climb (due to the change in acceleration) decreases to within a specified tolerance.

The time, distance, fuel, weight, altitude, and velocity are then integrated over an altitude increment using subroutine MSNINTG (Section 6.4.9), and the above procedure is repeated until the given final altitude is reached.

6.2.2.4 Calculates Climb at a Given Speed — Altitude With Velocity Given as Equivalent Airspeed, Terminates Climb at a Given Altitude. The procedure for calculating the climb in this routine is the same as that described for the previous routine, except that the velocity-altitude schedule is given in terms of equivalent airspeed rather than true airspeed.

6.2.3 Acceleration. There are two alternate acceleration routines available in the program. One terminates at a given final speed and the other terminates at an optimum cruise speed.

6.2.3.1 Calculates Acceleration to a Given Final Speed. The initial speed can be either the current mission velocity or a fixed input velocity. The tangential acceleration is calculated for the given power setting using subroutine FEQMA (Section 6.4.1) and integration of time, distance, fuel, weight, and velocity is done with respect to a velocity increment using subroutine MSNINTG (Section 6.4.9). The acceleration is terminated when a given (inputted) speed is reached.

6.2.3.2 Calculates Acceleration to an Optimum Cruise Speed. At the current or given (input) altitude, an optimum cruise speed, providing a maximum value of specific range, is determined using subroutine MAXSRV (Section 6.4.3). The tangential acceleration is calculated for a given power setting using subroutine FEQMA (Section 6.4.1) at the starting velocity, which can be either the current speed or a given (input) speed. Time, distance, fuel, weight, and velocity are then integrated over a velocity interval using subroutine MSNINTG (Section 6.4.9) and the procedure is repeated until the previously determined optimum cruise speed is reached.

6.2.4 Cruise. The program is capable of calculating cruise characteristics for two flight conditions· at a given speed and altitude, and at an optimum speed and altitude.

6.2.4.1 Calculates Cruise at Given Speed and Altitude. The current values of speed and altitude are taken as fixed cruise conditions if input values are not provided. Checks are made against the maximum altitude boundary (for the given minimum ceiling rate-of-climb and maximum cruise power setting), the minimum velocity (determined by the maximum allowable flight angle of attack), and the maximum velocity (using the maximum cruise power setting) by using subroutines CEILING, MINVEL, and MAXVEL (see Sections 6.4.6 , 6.4.7 , 6.4.8).

The flight conditions at the cruise speed and altitude are determined by using subroutine FEQMA (Section 6.4.1), solving for angle of attack and power setting, with zero flight path angle. Time, distance, fuel, and weight are then integrated over a weight increment using subroutine MSNINTG (Section 6.4.9), and the procedure is repeated until the accumulated total distance equals the given cruise radius.

6.2.4.2 Calculates Cruise at Optimum Speed and Given Altitude. The current value of altitude is taken as the fixed cruise condition if no input value is provided. A check is made against the maximum altitude boundary (for the given minimum ceiling rate-of-climb and maximum cruise power setting, using subroutine CEILING, see Section 6.4.6).

The optimum cruise speed, providing the maximum specific range, is determined (using subroutine MAXSRV, see Section 6.4.3), and flight conditions are calculated (using subroutine FEQMA, see Section 6.4.1), solving for the angle of attack and the power setting. This is done for the initial airplane cruise weight, and for an incremented weight. The tangential acceleration at the initial weight and speed is then estimated, and the flight conditions recomputed.

$$\Delta t = \frac{-\Delta W}{\text{Fuel Flow}}$$

where:

Δt = cruise time increment required to burn ΔW amount of fuel

ΔW = fuel weight consumed during cruise

$$a_T = \frac{V_2 - V_1}{\Delta t}$$

where:

V_2 = airplane speed at final cruise weight

V_1 = airplane speed at initial cruise weight

This procedure is repeated until the change in specific range (due to the change in acceleration) decreases to within a given tolerance. Time, distance, fuel, weight, and velocity are then integrated over a weight interval (using subroutine MSNINTG, see Section 6.4.9). The above procedure is then iterated until the accumulated total distance equals the given cruise radius.

6.2.4.3 Calculates Cruise at Optimum Speed and Altitude. The optimum cruise speed and altitude are determined, providing a maximum value of specific range using subroutine MAXSRH (Section 6.4.5). This is done at the initial cruise weight and an incremented weight. An estimated rate-of-climb and tangential acceleration are then estimated at the initial weight, based on reaching the optimum speed and altitude for the incremented weight.

$$\Delta t = \frac{-\Delta W}{\text{Fuel Flow}}$$

$$R/C = \frac{h_2 - h_1}{\Delta t}$$

$$a_T = \frac{V_2 - V_1}{\Delta t}$$

$$\gamma = \arcsin \frac{R/C}{V_1}$$

The above procedure is repeated until the change in specific range, due to changing values of rate-of-climb and tangential acceleration, decreases to within a given tolerance.

Time, distance, fuel, weight, altitude, and velocity are integrated over a weight interval using subroutine MSNINTG (Section 6.4.9). The entire process is then iterated until the accumulated total distance equals the given cruise radius.

6.2.4.4 Calculates Cruise at Given Speed and Altitude, for Given Fuel Usage. The procedure for calculating the cruise in this routine is the same as that described in Section 6.2.4.1 ; except for the manner of termination. The cruise is terminated when the accumulated total fuel used equals a given fuel usage value.

6.2.4.5 Calculates Cruise at Optimum Speed and Given Altitude, for Given Fuel Usage. The procedure for calculating the cruise in this routine is the same as that described in Section 6.2.4.2; except for the manner of termination. The cruise is terminated when the accumulated total fuel used equals a given fuel usage value.

6.2.4.6 Calculates Cruise at Optimum Speed and Altitude, for Given Fuel Usage. The procedure for calculating the cruise in this routine is the same as that described in Section 6.2.4.3; except for the manner of termination. The cruise is terminated when the accumulated total fuel used equals a given fuel usage value.

6.2.5 Descent. There are two ways of calculating descent in the present program: for a given speed-altitude schedule, where speed is given in terms of either true or equivalent airspeed.

6.2.5.1 Calculates Descent at a Given True Airspeed — Altitude Schedule at a Given Descent Rate. Descent performance is determined by integrating over an altitude increment for a given descent rate and for a given true airspeed-altitude schedule. The descent is terminated when a given final altitude or equivalent airspeed is determined. The power setting is limited to idle during descent. Should this limit be reached prior to termination of the descent, the descent rate is reduced accordingly, holding the speed-altitude schedule as defined.

6.2.5.2 Calculates Descent at a Given Equivalent Airspeed-Altitude Schedule at a Given Descent Rate. The procedure for calculating descent in this routine is the same as that described for the previous routine, except that the speed-altitude schedule is given in terms of equivalent airspeed rather than true airspeed.

6.2.6 Deceleration. This routine calculates deceleration performance to a given final speed by integrating over a speed increment. The final speed is limited to the minimum velocity.

6.2.7 Loiter. The program is limited to the calculation of loiter at optimum speed and given altitude. The current altitude is used for loiter unless an input value is provided. A check is made against the maximum altitude boundary (for the given minimum ceiling rate-of-climb and the maximum loiter power setting, using subroutine CEILING, see Section 6.4.6).

The optimum loiter speed, providing maximum endurance (minimum fuel flow), is determined (using subroutine MAXENV, see Section 6.4.4) at the initial loiter weight and an incremented weight. The tangential acceleration at the initial weight and speed is estimated, and the flight conditions are computed (using subroutine FEQMA, see Section 6.4.1).

$$\Delta t = \frac{-\Delta W}{\text{Fuel Flow}}$$

$$a_T = \frac{V_2 - V_1}{\Delta t}$$

This procedure is repeated until the change in endurance, due to the change in acceleration, decreases to within a given tolerance. Time, fuel, weight, and velocity are integrated over a weight interval (using subroutine MSNINTG, see Section 6.4.9), and the above procedure is repeated until the given loiter time is equaled.

6.2.8 Combat. For a given (inputted) speed, altitude, and power setting, the fuel is determined from subroutine PROPUL (Section 6.1.3) and the airplane weight, fuel used, and time are adjusted accordingly for a given time allowance.

6.2.9 Reserve. A fuel reserve is calculated based on a given (inputted) value of percentage of total fuel used. It is used to increment the current airplane weight and the mission fuel used as follows:

$$\Delta \text{fuel} = \frac{\% \text{ reserve}}{1-\% \text{ reserve}} \text{Fuel}_{(\text{current})}$$

$$\text{Fuel} \quad \text{Fuel}_{(\text{current})} + \Delta \text{ fuel}$$

$$W = W_{\text{current})} - \Delta \text{ fuel}$$

6.2.10 Landing. For a given (inputted) speed, altitude and power setting, the fuel flow is determined from subroutine PROPUL (Section 6.1.3) and the airplane weight, fuel used and time are adjusted accordingly for a given time allowance.

6.2.11 Iterate. A correctly sized airplane (in terms of gross weight) carries sufficient fuel aboard to equal the mission fuel requirement. If this is not the case, the airplane size must be re-estimated, and the mission recalculated.

For the first iteration, the airplane weight estimate is based on the difference between the mission fuel and the fuel on board, and a weight growth factor.

$$GW_{\text{takeoff}_2} \quad GW_{\text{takeoff}_1} + (\text{Fuel Mission} - \text{Fuel Aboard}) \, f_{W/F}$$

where:

GW_{takeoff_2} = estimated takeoff weight for succeeding iteration

GW_{takeoff_1} = computed takeoff weight for synthesized fuel requirements

$f_{W/F}$ = gross weight-to-fuel growth factor.

Thus, for example, if the fuel carried by the airplane is 1000 pounds short of the mission fuel requirement, and a growth factor of 1.5 is assumed, the airplane weight would become 1500 pounds greater for the next cycle.

For successive iterations the fuel and airplane weights for the last two previous iterations are used linearly to estimate the proper airplane size.

$$GW \quad GW_2 - \Delta Fuel_2 \left(\frac{GW_2 - GW_1}{\Delta Fuel_2 - \Delta Fuel_1} \right)$$

where:

$\Delta Fuel_2$ = the difference between the required mission fuel and the fuel carried on board, as calculated in the last sizing iteration

$\Delta Fuel_1$ = the differences between the required mission fuel and the fuel carried on board, as calculated in the next to the last sizing iteration

6.2.12 Mission. This routine controls the mission calculation by coordinating the sequence in which the various mission segments are executed. It also contains the iterative logic to assure that the cruise, descent, and deceleration segments are properly matched such that the total mission range requirement is satisfied. For example, if the total mission range required is 3000 nautical miles, the program will cruise until that total range is satisfied. Then, if a descent and/or deceleration segment immediately follows the cruise, the added range contribution will be added to the 3000 nautical miles already flown. The program then returns to cruise with a first guess as to what portion of the 3000 nautical miles should be consumed during cruise and what portion during descent and/or deceleration. This process is continued until the required range is properly distributed between the cruise, descent and deceleration segments. Range contributions from segments prior to cruise are not affected by this iteration, but are included in the total mission range calculation. It should be noted that this iterative process will not be activated if a mission segment other than descent or deceleration follows immediately after cruise. Thus, a cruise, loiter, descent, deceleration sequence will not result in a proper total range calculation.

6.3 PERFORMANCE ANALYSIS. As previsouly discussed, the performance routine will calculate the following performance parameters specific excess power, sustained maneuver load factor, maximum speed, maximum ceiling, takeoff and landing distance. These calculations are carried out in subroutine PERFORM. It should be noted that input values such as engine power setting, gross weight, percentage of fuel carried, atmospheric conditions, aerodynamic configuration, number of engines, etc., are held constant for the first four parameters. For example, if the power setting is specified as intermediate, the specific excess power, sustained maneuver load factor, maximum speed and ceiling will all be calculated at intermediate power. Takeoff and landing power settings may be independently set.

These performance parameters are calculated in a straightforward manner by solving the equations of motion for a fixed geometry aircraft. The normal procedure is to size the aircraft to perform a specified mission by running the Mission Performance routine and then determine the performance characteristics of that aircraft. Generally speaking, the resulting first cut performance will not satisfy the requirements. Thus, significant design parameters such as wing area and engine scale factor need to be

appropriately varied until a configuration is found which satisfies the desired performance characteristics as well as the mission requirements.

The program may also be used without first running the mission performance routine. A known, fixed geometry configuration may be input and its resulting performance characteristics determined without any regard for the aircraft's mission capability.

The individual performance parameters are discussed in the following sections.

6.3.1 Specific Excess Power. The specific excess power capability of a fixed geometry aircraft is determined from the equation

$$SEP = \frac{(T - D)\,V}{W}$$

where, SEP = Specific Excess Power

T = Thrust

D = Drag

V = Velocity

W = Weight

In order to carry out the calculation it is necessary to define the engine power setting, gross weight, percentage of fuel carried, atmospheric conditions, aerodynamic configuration, number of engines, Mach number, altitude and normal load factor for which data is desired. Given this information, the program calls subroutines PROPUL (Section 6.1.3), AERO (Section 6.1.1), ATMOS (Section 6.4.1), and FEQMA (Section 6.4.1).

It should be noted that SEP's can be calculated at several flight conditions during one run by defining the appropriate matrix of Mach numbers, altitudes and normal load factors desired.

6.3.2 Sustained Maneuver Load Factor. Sustained maneuver load factor means that load factor perpendicular to the flight path which the aircraft is able to pull at a fixed power setting without changing the flight path velocity. This means basically that the aircraft thrust and drag must be equal.

In order to carry out the calculation, it is necessary to specify the Mach number and altitude at which data is desired. The engine power setting, gross weight, percentage of fuel carried, atmospheric conditions, aerodynamic configuration and number of engines are set equal to the values used in calculating specific excess power as described in Section 6.3.1 .

Given this information, the program calls subroutine PROPUL (Section 6.1.3), AERO (Section 6.1.1), ATMOS (Section 6.4.11) and FEQMA (Section 6.4.1).

6.3.3 Maximum Speed. This routine determines the maximum speed capability of a fixed geometry aircraft at various altitudes. Therefore, the only additional inputs required for this calculation are the altitudes at which data is desired. The engine power setting, gross weight, percentage of fuel carried, atmospheric conditions, aerodynamic configuration and number of engines are set equal to the values used in the specific excess power and sustained load factor calculations.

Given the above information, the program calls subroutines MAXVEL (Section 6.4.8), PROPUL (Section 6.1.3), AERO (Section 6.1.1), ATMOS (Section 6.4.11), and FEQMA (Section 6.4.1), in an iterative fashion until the equations of motion are satisfied such that the normal load factor is one and the tangential acceleration is zero.

6.3.4 Ceiling. This routine determines the maximum ceiling capability of a fixed geometry aircraft at various speeds for a given minimum rate of climb. Required input for this routine consists of a specified rate of climb and a matrix of speeds for which ceiling data is desired. The engine power setting, gross weight, percentage of fuel carried, atmospheric conditions, aerodynamic configuration and number of engines are the same as those used in the specific excess power, sustained load factor and maximum speed calculations.

Given this information, the program calls subroutines CEILING (Section 6.4.6), PROPUL (Section 6.1.3), AERO (Section 6.1.1), ATMOS (Section 6.4.11), MAXRCV (Section 6.4.2), and FEQMA (Section 6.4.1).

6.3.5 Takeoff. The program contains two different procedures for calculating the takeoff distance over a 10.668 M (35-ft) obstacle - one being empirical and the other semi-analytical. Through input, the user can dictate the use of either or both procedures.

6.3.5.1 Empirical Procedure. The empirical procedure consists of determining takeoff distance as a function of span loading (W_{TO}/b^2) and static thrust to weight ratio for an engine out condition $\left(T_{STO}\ (Ne - 1)/W_{TO}\right)$. W_{TO} is the maximum aircraft takeoff gross weight, b is the wing span, T_{STO} is the sea level, standard day static thrust and Ne is the number of engines. Figures 6-28 and 6-29 present the required runway distance, in meters (feet), for a two- and four-engine aircraft, respectively. Results for a three-engine configuration are found by averaging the two- and four-engine results. It should be noted from these figures that the range of empiricism is fairly narrow. Thus, results obtained outside this range should be viewed with suspicion. Another drawback to the use of Figures 6-28 and 6-29 is that the high lift system needed to obtain these takeoff distances remains undefined. The data shown is based on aircraft whose high lift systems have been individually optimized, and are therefore all different. Advantages of using this empirical procedure include the fact that the required climbout flight path angle, γ_2, has been satisfied through selection of the proper high

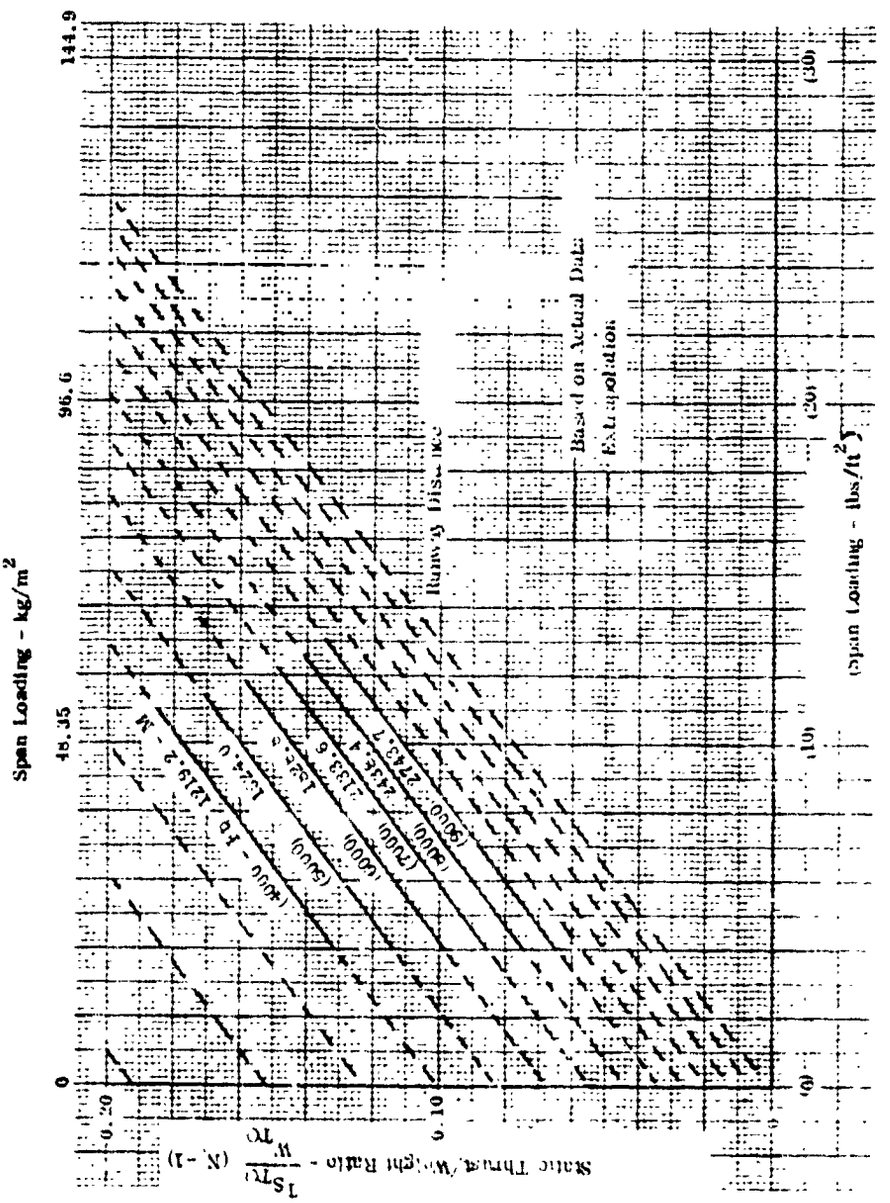

Figure 6-28 Empirical Takeoff Distance — 2-Engine Aircraft

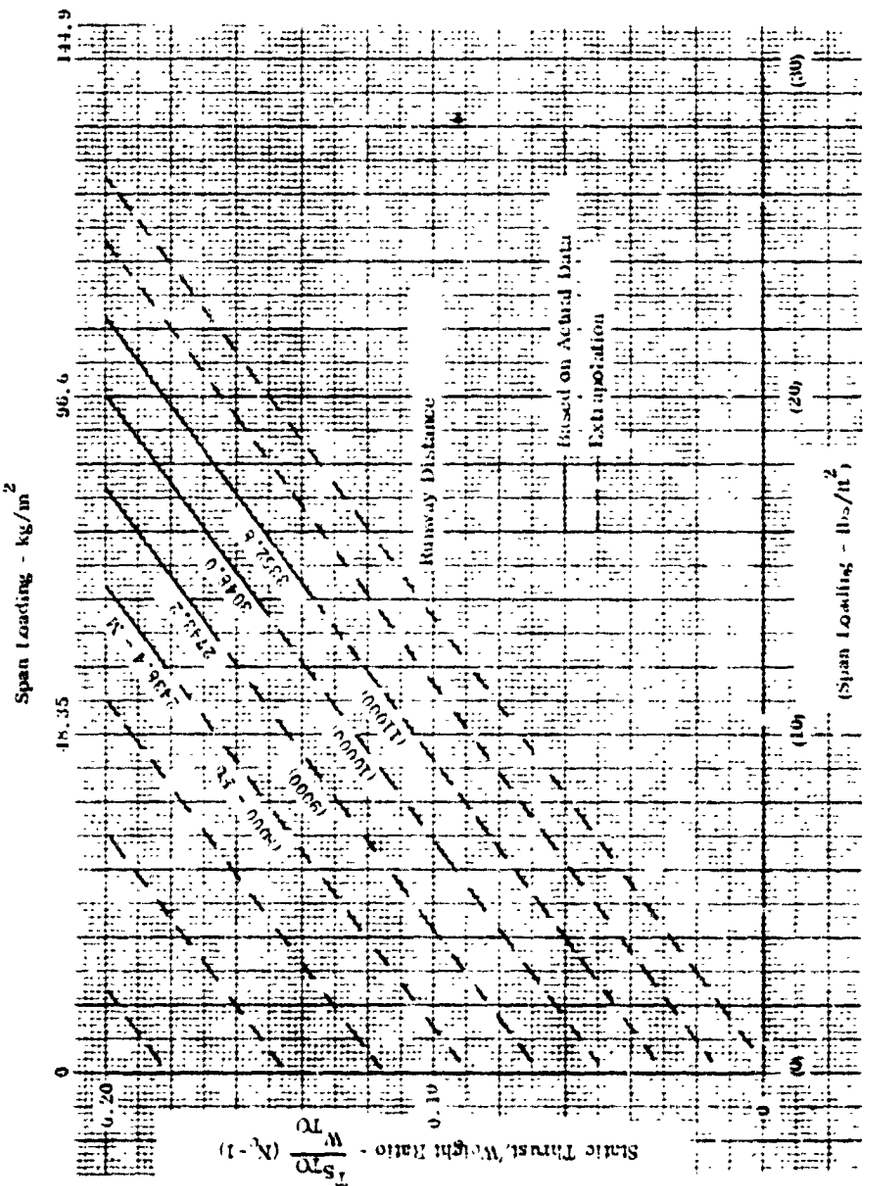

Figure 6-29 Empirical Takeoff Distance — 4-Engine Aircraft

lift system. As will be discussed in the semi-analytical approach, this eliminates the necessity of reiterating the program to satisfy the climbout requirement. Another advantage of the empirical procedure is to negate the need for calculating a takeoff maximum lift coefficient $C_{L_{max_{TO}}}$. In summary, the empirical procedure allows the user to get a first approximation of takeoff distance without having to calculate $C_{L_{max}}$ or reiterate the program to meet the climbout flight path requirement.

6.3.5.2 Semi-Analytical Procedure. The semi-analytical procedure is considerably more complicated than the empirical procedure. In essence, the procedure goes as follows:

1. The user selects the takeoff high lift configuration through input variables.
2. For the selected high lift geometry, the program calculates $C_{L_{max_{TO}}}$ using the high lift estimation procedures of Section 6.1.2 .
3. $C_{L_{CAR_{TO}}}$ is defined as $C_{L_{max_{TO}}}/0.9$.
4. The velocity $V_{S_{CAR_{TO}}}$ is determined from the equation

$$V_{S_{CAR_{TO}}} = \sqrt{\frac{2W}{C_{L_{CAR_{TO}}} \rho Sw}}$$

where,

W = aircraft weight

ρ = air density

Sw = reference wing area

5. A minimum flight speed during second segment climb is defined as $V_{2_{min}} = 1.2\ V_{S_{CAR_{TO}}}$.
6. The climbout flight path angle, γ_2, is calculated at the velocity $V_{2_{min}}$ using the lift and drag characteristics of the takeoff flap configuration.
7. The associated takeoff distance over a 10.668M (35-ft) obstacle is determined from Figure 6-30 as a function of the parameter $W^2/\sigma Sw T C_{L_{TO}}$ (Reference 8).

where,

σ = ratio of air density at altitude to that at sea level

T = sea level static thrust at takeoff power setting

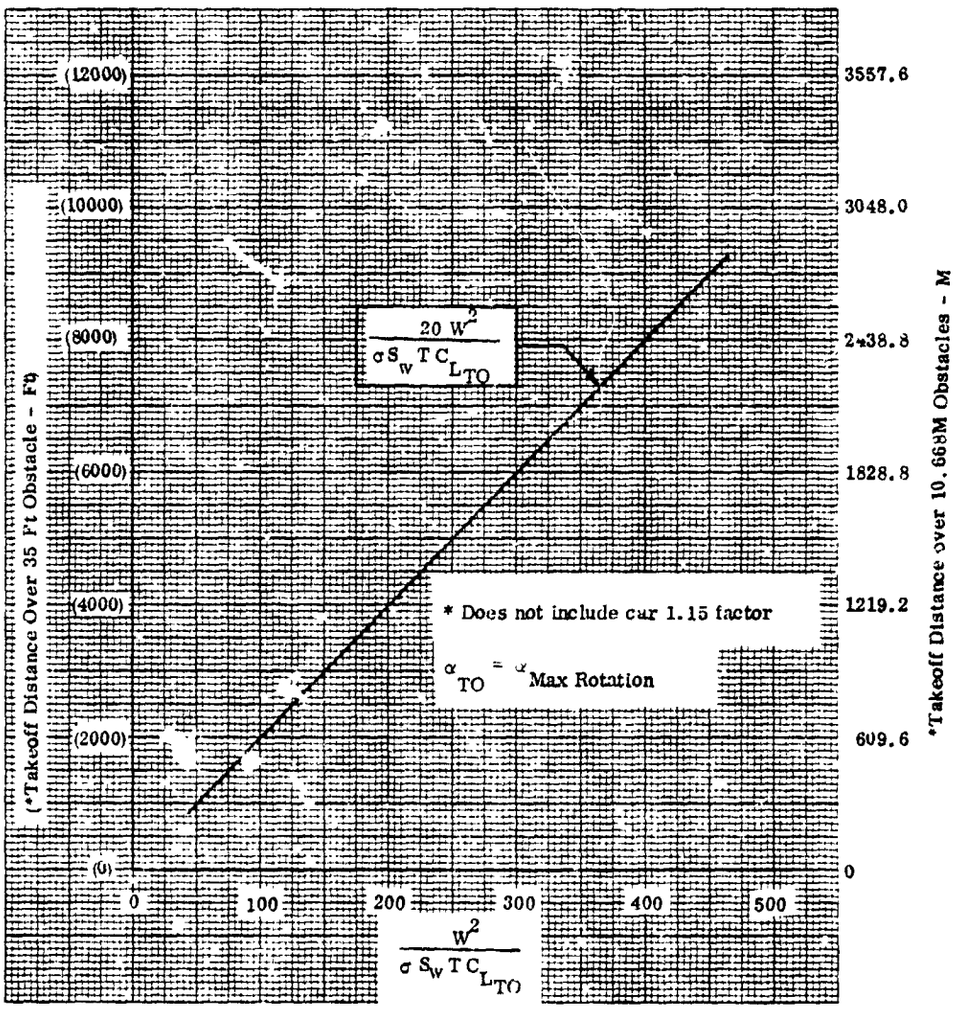

Figure 6-30 Semi-Analytical Takeoff Distance

$C_{L_{TO}}$ lift coefficient corresponding to maximum takeoff rotation angle.

8. The takeoff distance is multiplied by the 115 percent CAR factor.

At this point, the user compares the results with the flight path angle and takeoff distance requirements. If these requirements are not satisfied, the flap configuration should be revised and the procedure repeated. The procedure is thus an iterative one, which requires a knowledgeable user to properly revise the flap configuration as necessary.

6.3.6 Landing. As in takeoff performance, the program can determine landing performance in either one or both of the following ways: through an empirical procedure or through a semi-analytical procedure.

6.3.6.1 Empirical Procedure. The empirical procedure is, by far, the simpler of the two methods. The program merely determines an approach speed as a function of wing span loading (W_{TO}/b^2) from Figure 6-31 and then determines the required landing distance over a 15.24M (50-ft) obstacle from Figure 6-32 as a function of the approach speed. The approach speed is seen in Figure 6-31 to also be a function of the type of flap system (i.e., single, double or triple slotted) and the number of engines (two or four). The approach speed for a three-engine configuration is determined by averaging the two- and four-engine results. Note, also, that the single and double slotted data have been assumed identical. All data is based on configurations having optimized flap systems so as to meet the landing approach gradient requirements. Thus, the empirical procedure allows the user to get a first cut estimate of landing distance without having to specifically identify a high lift system or the associated aerodynamic coefficients.

6.3.6.2 Semi-Analytical Procedure. The semi-analytical procedure is considerably more complicated than the empirical procedure. A general outline of the method is as follows:

1. The user selects a landing high lift system through input variables.
2. Using the aerodynamic high lift procedures of Section 6.1.2 , the program calculates $C_{L_{max_L}}$ for the selected high lift system.
3. $C_{L_{CAR_L}}$ is defined as $C_{L_{max_L}}/0.9$.
4. Following the requirement that the approach stall speed shall be less than or equal to 1.1 times the landing stall speed

$$C_{L_{app}} = C_{L_{CAR_L}} / 1.21$$

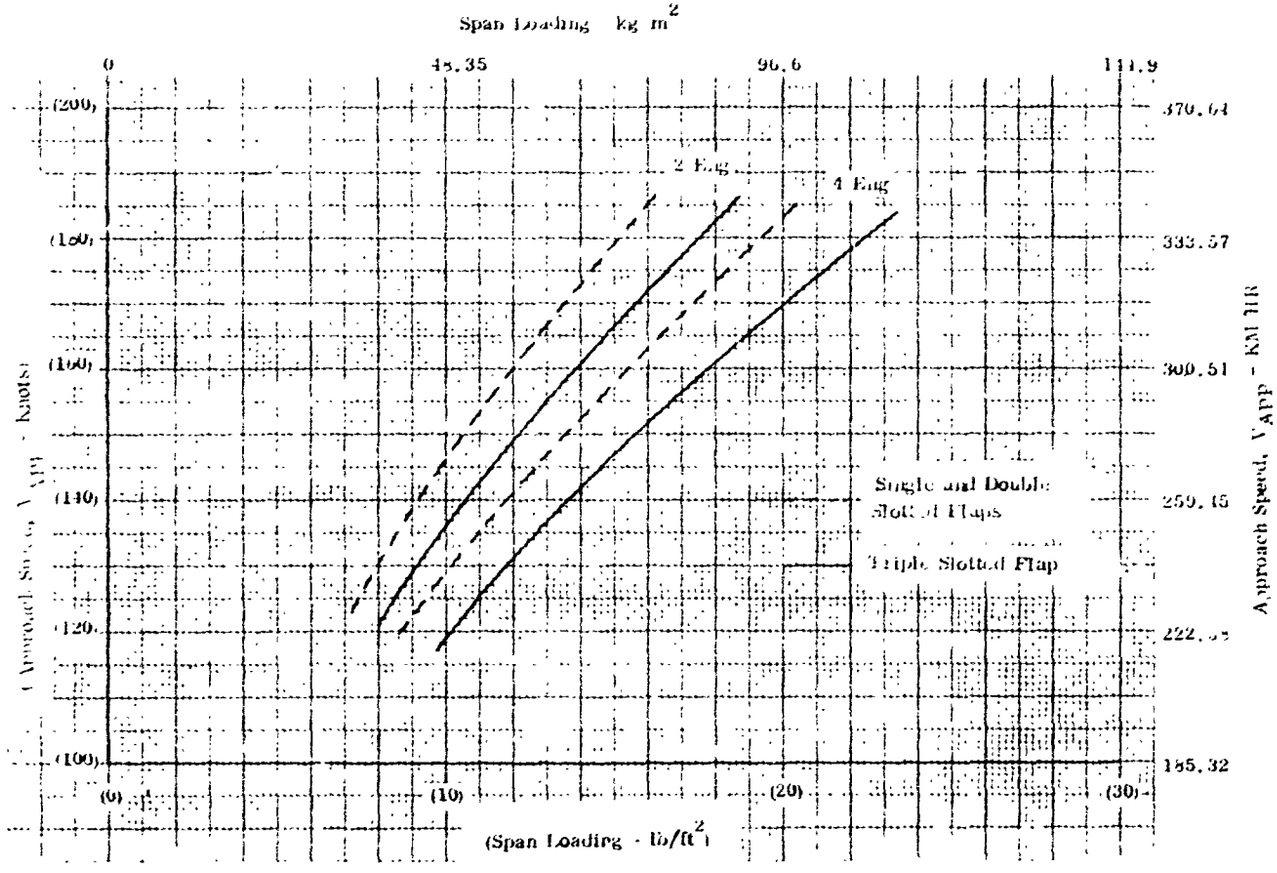

Figure 6-31 Approach Speed Estimate for Empirical Method

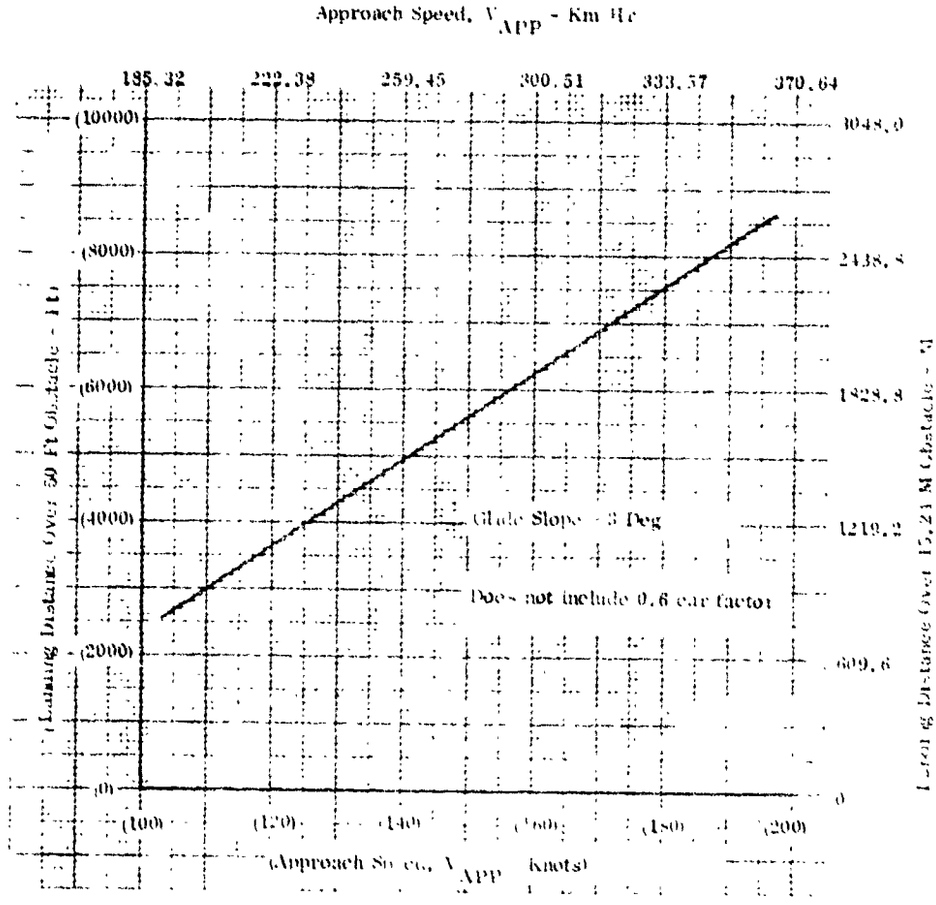

Figure 6-32 Empirical Landing Distance

5. For an initial defined airplane weight (W), a landing stall speed is calculated as

$$V_{S_{CAR_L}} \sqrt{\frac{2W}{\rho C_{L_{CAR_L}} Sw}}$$

where,

ρ = air density

Sw = reference wing area

$C_{L_{CAR_L}}$ = maximum lift coefficient for landing based on Civil Air Regulation (CAR) requirements

6. Since CAR regulations require the approach speed to be greater than or equal to 1.3 times the landing stall speed

$$V_{app} \geq 1.3 \; V_{S_{CAR_L}}$$

7. The landing distance over a 15.24M (50-ft) obstacle is found from Figure 6-33 as a function of the parameter W/σ SW $C_{L_{CAR_L}}$ (Reference 8). The data assumed a touchdown speed of 1.15 $V_{S_{CAR_L}}$ and a constant ground deceleration of 7 ft/sec^2.

8. The distance obtained from Figure 6-33 is divided by 0.6 to abide by CAR regulations.

Having found the landing distance over a 15.24M (50-ft) obstacle for the landing flap condition, the program proceeds to determine the approach flight path angle in the following manner.

9. The user defines a new high lift configuration during approach through input variables.

10. Using the high lift aerodynamic procedures of Section 6.1.2 , the program calculates $C_{L_{CAR_A}} = \frac{C_{l_{max_A}}}{0.9}$ for the approach high lift system.

11. The CAR maximum lift coefficient for the approach high lift system $\left(C_{L_{CAR_A}}\right)$ is then compared to the required lift coefficient for approach based

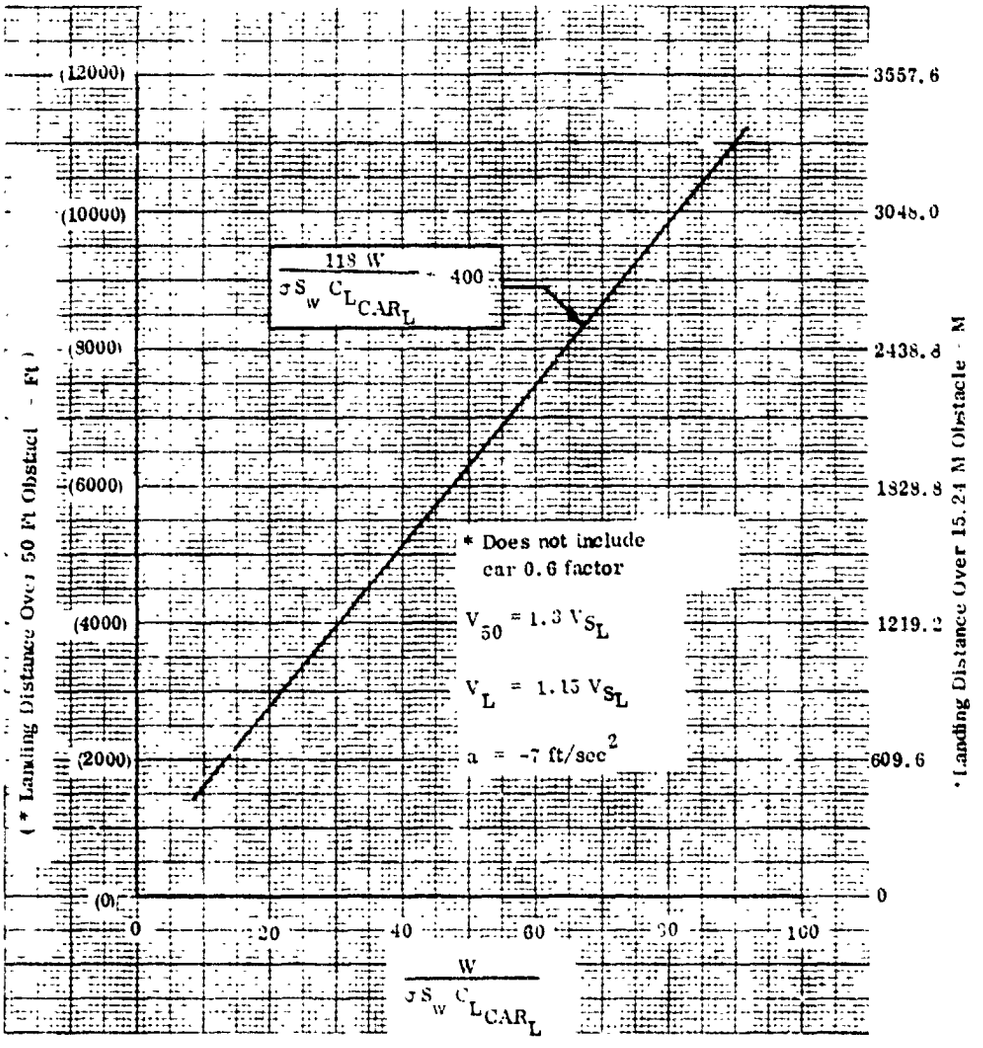

Figure 6-33 Semi-Analytical Landing Distance

on the landing high lift system $\left(C_{L_{app}} = 1.21\, C_{L_{max_L}} / 0.9\right)$. If $C_{L_{CAR_A}} < C_{L_{app}}$ the approach high lift system is set to the next set of input variables (Step 9). If $C_{L_{max_A}} > C_{L_{app}}$ the approach flight path angle γ_{app} is calculated using the approach velocity (V_{app}) and high lift system aerodynamics.

12. The approach high lift system is set to the next set of input variables and Steps 9 through 11 are repeated.

13. When the program exhausts the list of approach high lift systems, it returns to Step 5, resets a new airplane landing weight and proceeds through Step 12 again.

In essence, a landing distance is calculated for a given landing high lift system and a given landing weight. The program then allows the user to input numerous combinations of approach high lift systems so as to satisfy the CAR requirement that $V_{app} \geq 1.3\, V_{S_{CAR_L}}$. If this requirement is met, or if the list of input configurations is exhausted, the program will begin the process over for a new value of landing weight.

6.4 SUPPLEMENTARY ROUTINES. Certain functional routines such as solving the flight equations of motion, optimizing a given parameter (e.g., speed for maximum specific range), integration, and data storage, have been divided into separate subroutines for more efficient computer usage. These supplementary mission routines are described in the following sections.

6.4.1 FEQMA (Force Equals Mass Times Acceleration). This routine solves two dimensional equations of motion and calculates accelerations due to propulsion and aerodynamic forces, iterating when necessary to define up to two unknowns (e.g., angle of attack).

The routine solves the Newtonian equations of motion in order to determine the basic mission flight conditions. Up to two unknowns may be determined. Three optional routines have been programmed, depending on which parameters are unknown. Each type of flight condition (i.e., whether climb, acceleration, or cruise) defines the unknowns, and therefore also defines the option required.

For all options, certain flight and airplane parameters must be defined. These are speed, altitude, airplane weight, number of operating engines, and the thrust line incidence.

Option 1 determines angle of attack and flight path angle, given a power setting, normal load factor, and tangential load factor. It is applicable to climbing flight conditions.

Given these parameters, the atmospheric, propulsive, and aerodynamic parameters are determined, at first for assumed (current) values of angle of attack and flight path angle, and the component forces derived. A flight path angle is then calculated, based on the required tangential acceleration, and the component forces recomputed.

$$\gamma = \text{arc sin}\left(\frac{F_{tangential}}{W} - G_T\right)$$

$$F_{lift} = F_{normal} - W\cos\gamma$$

$$F_{drag} = F_{tangential} - W\sin\gamma$$

where:

G_T = the desired tangential load factor

$F_{tangential}$ = component sum of aerodynamic and thrust force tangential to flight path

W = airplane weight on current iteration

The desired normal acceleration is obtained next by iteration, thus solving for angle of attack. A Newton-Raphson linear extrapolation procedure is used to zero the parameter (and estimating angle of attack)

$$G_N - G_{normal\ calculated}$$

where, G_N is the desired normal load factor,

$$G_{normal\ calculated} = \frac{F_{lift}}{W} + 1.$$

With a new estimate of angle of attack, the above procedure is repeated, and the iteration continues until the parameter

$$\frac{G_N - G_{normal\ calculated}}{G_N}$$

reduces to zero within a given tolerance.

Following completion of this iteration, the airplane accelerations and rate-of-climb are computed.

Accelerating flight is represented by the second option, which solves for angle of attack and tangential acceleration. The parameters required are power setting, flight path angle, and normal load factor. As for the previous option, the atmospheric, propulsive, and aerodynamic parameters are determined, and component forces calculated. Angle of attack is iterated to provide the required normal load factor, using the Newton-Raphson procedure as described under option one. Again, once the iteration is completed, the airplane accelerations and rate-of-climb are computed.

Option three is applicable to cruise and loiter conditions, where angle of attack and power setting are solved for given values of flight path angle, and normal and tangential accelerations. Atmospheric conditions and aerodynamic lift and drag are determined as before, using the current angle of attack for the initial estimate. A thrust required is computed by solving the force equation normal to the flight path, so as to eliminate the ram drag term

$$\text{Thrust}_{\text{Required}} = \frac{\left(G_N - 1. + \cos(\gamma)\right) W - \text{Lift}}{\sin(\alpha + i_T)}$$

where:

lift = airplane aerodynamic lift force

α = airplane angle of attack

The power setting, ram drag, and fuel flow are determined using the propulsion routine. The component forces, normal and tangential to the flight path, are then calculated, using expressions previously presented. The angle of attack is iterated, using the Newton-Raphson method as previously described, to obtain the desired tangential acceleration. When this is completed, airplane accelerations and rate-of-climb are computed.

6.4.2 MAXRCV (Maximum Rate-of-Climb Speed). This routine determines the maximum rate-of-climb, and the accompanying speed, at any given altitude, being used when calculating a max R/C climb, or a ceiling.

For a given power setting, and/or given normal and tangential load factors, the flight conditions, including rate-of-climb, are calculated at three velocities. The three values of R/C are then examined; if R/C increases with increasing velocity, the velocities are incremented positively, and the rates-of-climb recalculated; if R/C increases with decreasing velocity, the velocities are incremented negatively, and the rates-of-climb recalculated; if the R/C data indicates a minimum value (R/C for the lowest and the highest velocities are both larger than that for the middle velocity), an informative statement is outputted, the velocities are incremented positively, and the rates-of-climb recalculated; if, and when, the R/C data indicates a maximum value (the R/C

for the middle velocity being higher than that for the other two), it is curve fit quadratically, and the maximum rate-of-climb speed derived from the curve fit. Once the maximum R/C speed has been defined, it is checked against given minimum allowable speed and Mach number, and the greatest value is retained. Checks are then made against the minimum flight speed (maximum allowable flight angle of attack) and the maximum velocity (using the maximum allowable power setting).

6.4.3 MAXSRV (Maximum Specific Range Speed). This routine is used to determine the optimum cruise speed, by calculating the maximum specific range at a given altitude.

For a given required rate-of-climb, and for given normal and tangential load factors, the flight conditions are calculated at three velocities, including the specific range,

$$SR = \frac{V}{\text{fuel flow}}$$

where:

V = airplane velocity

fuel flow = fuel consumption rate

The three values of specific range are then examined; if SR increases with increasing velocity, the velocities are incremented positively, and the specific ranges recalculated; if SR increases with decreasing velocity, the velocities are incremented negatively, and the specific ranges recalculated; if the SR data indicates a minimum value (SR for the lowest and the highest velocities are both larger than that for the middle velocity), an informative statement is outputted, the velocities are incremented positively, and the specific ranges recalculated; if, and when, the SR data indicates a maximum value (the SR for the middle velocity being higher than that for the other two), it is curve fit quadratically, and the desired optimum cruise speed derived from the curve fit. The desired cruise speed can be defined as that producing some percentage of maximum specific range; in this case two velocities are derived, the higher velocity always being chosen. Once the optimum cruise speed has been defined, it is checked against given minimum allowable speed and Mach number, and the greatest value is retained. Checks are then made against the minimum flight speed (maximum allowable flight angle of attack) and the maximum velocity (using the maximum allowable power setting).

6.4.4 MAXENV (Maximum Endurance Speed). This routine derives a desired optimum loiter speed, by determining the maximum endurance, and the accompanying speed, at any given altitude.

For a given required rate-of-climb, and for given normal and tangential load factors, the flight conditions are calculated at three velocities, and the endurance is defined as

$$EN \quad \frac{1}{\text{fuel flow}}$$

The three values of endurance are then examined; if EN increases with increasing velocity, the velocities are incremented positively, and the endurances recalculated; if EN increases with decreasing velocity, the velocities are incremented negatively, and the endurances recalculated; if the EN data indicates a minimum value (EN for the lowest and the highest velocities are both larger than that for the middle velocity), an informative statement is outputted, the velocities are incremented positively, and the endurances recalculated; if, and when, the EN data indicates a maximum value (the EN for the middle velocity being higher than that for the other two), it is curve fit quadratically and the desired optimum loiter speed derived from the curve fit. The desired loiter speed can be defined as that producing some percentage of the maximum endurance; in this case two velocities are derived, the higher velocity always being chosen. Once the optimum loiter speed has been defined, it is checked against given minimum allowable speed and Mach number, and the greatest value is retained. Checks are then made against the minimum flight speed (maximum allowable flight angle of attack) and the maximum velocity (using the maximum allowable power setting).

6.4.5 MAXSRH (Maximum Specific Range Altitude). The optimum cruise altitude is found by determining the maximum specific range. The maximum specific range, and the accompanying speed, is found at three altitudes. The three values of specific range are then examined; if SR increases with increasing altitude, the altitudes are incremented positively, and the maximum specific ranges redetermined; if SR increases with decreasing altitude, the altitudes are incremented negatively, and the maximum specific ranges redetermined; if the SR data indicates a minimum value (SR for the lowest and highest altitudes are both higher than that for the middle altitude), an informative statement is outputted, the altitudes are incremented positively, and the maximum specific ranges redetermined; if, and when, the SR data indicates a maximum value (the SR for the middle altitude being higher than that for the other two), it is curve fit quadratically, and the maximum specific range altitude derived from the curve fit. This altitude is then compared to the maximum altitude boundary of the airplane (based on the minimum ceiling rate-of-climb and the maximum engine power setting), and the lower altitude of the two chosen.

6.4.6 CEILING (Altitude Boundary). This routine checks altitude boundary and, if exceeded, calculates the maximum allowable altitude.

At any given altitude, the maximum rate-of-climb is determined, using the applicable maximum engine power setting. If this max R/C is less than the allowable minimum ceiling rate-of-climb, the altitude at which the minimum R/C is attainable is determined by an iterative procedure. This iterative procedure uses a Newton-Raphson linear extrapolation method to estimate the desired altitude, thus requiring data for only two altitudes at a time.

6.4.7 MINVEL (Minimum Speed Boundary). This routine calculates the minimum speed flight boundary for a given specific condition by solving the equations of motion.

The velocity of the airplane is found which solves the equations of motion with the angle of attack at the maximum allowable for flight. Three flight conditions can be specified; fixed power setting and tangential acceleration, with flight path angle variable (e.g., climbing flight), fixed power setting and flight path angle, with tangential acceleration variable (e.g., an acceleration), or fixed tangential acceleration and flight path angle, with power setting variable (e.g., cruise or loiter flight).

For the first option, with flight path angle as a variable (given power setting and a tangential load factor), the following procedure applies:

At given conditions of speed, altitude, and normal load factor, the atmospheric conditions, the propulsive thrust and fuel flow, and the aerodynamic lift and drag are determined. The vector force sums are calculated as follows:

$$F_{normal} = \text{Lift} + \text{Thrust} \sin(\alpha_t)$$

$$F_{tangential} = \text{Thrust} \cos(\alpha_t) - \text{drag} - \text{ram drag}$$

where:

α_t = the angle of attack of the thrust vector

thrust = total installed engine thrust

drag = airplane aerodynamic drag

Ram drag = drag force generated by engine intake system

The airplane flight path angle is calculated for the given tangential load factor,

$$\gamma = \arcsin \frac{F_{tangential}}{W - G_{tangential}}$$

where:

$G_{tangential}$ = tangential load factor

and the excess force vectors in the lift and drag direction are,

$$F_{lift} = F_{normal} - W \cos \gamma$$

$$F_{drag} = F_{tangential} - W \sin \gamma$$

The velocity is then iterated to provide the given normal load factor, the normal load factor available being calculated as,

$$G_{\text{normal calculated}} = \frac{F_{\text{lift}}}{W} + 1$$

The Newton-Raphson linear extrapolation procedure is used to zero the parameter

$$G_{\text{normal}} - G_{\text{normal calculated}}$$

where G_{normal} is the required given normal load factor.

The above procedure is repeated until the parameter,

$$\frac{G_{\text{normal}} - G_{\text{normal calculated}}}{G_{\text{normal}}}$$

reduces to a given tolerance.

For the second option, with tangential acceleration as a variable (given power setting and flight path angle), the procedure below is followed:

The atmospheric, propulsion, and aerodynamic parameters are defined as before, and the normal and tangential force vectors are also calculated. Since the flight path angle is given, the excess forces in the lift and drag direction can be calculated as

$$F_{\text{lift}} = F_{\text{normal}} - W \cos \gamma$$
$$F_{\text{drag}} = F_{\text{tangential}} - W \sin \gamma$$

The velocity is then iterated as before to provide the required normal load factor.

For the third option, with power setting as a variable (given tangential acceleration and flight path angle), the procedure as follows:

$$\text{Thrust required} = \frac{\left(G_{normal} - 1 + \cos\gamma\right) W - \text{Lift}}{\sin(\alpha_t)}$$

The resulting force vector sums are,

$$F_{normal} = \text{Lift} + \text{Thrust} \sin(\alpha_t)$$
$$F_{tangential} = \text{Thrust} \cos(\alpha_t) - \text{drag} - \text{ram drag}$$
$$F_{lift} = F_{normal} - W \cos\gamma$$
$$F_{drag} = F_{tangential} - W \sin\gamma$$

The velocity is then iterated to provide the given tangential load factor, the load factor available being calculated as,

$$G_{\text{tangential calculated}} = \frac{F_{drag}}{W}$$

The Newton-Raphson linear extrapolation procedure is used to zero the parameter

$$G_{tangential} - G_{\text{tangential calculated}}$$

where $G_{tangential}$ is the required given tangential load factor.

The above procedure is repeated until the parameter,

$$\frac{G_{tangential} - G_{\text{tangential calculated}}}{G_{tangential}}$$

reduces to a given tolerance.

For all three options the airplane accelerations and rate-of-climb are calculated after iteration for the desired variables is complete.

$$a_{normal} = \frac{G_Z F_{lift}}{W}$$

$$a_{tangential} = \frac{G_Z F_{drag}}{W}$$

$$a_X = a_T \cos\gamma - a_N \sin\gamma$$
$$a_Z = a_N \cos\gamma + a_T \sin\gamma$$
$$R/C = V \sin\gamma$$

where G_Z is the acceleration due to gravity.

6.4.8 MAXVEL (Maximum Speed Boundary). This routine calculates the maximum speed flight boundary for a given specific condition by solving the equations of motion.

The velocity of the airplane is found which solves the equations of motion with a given maximum power setting. Two flight conditions can be specified: a fixed flight path angle with tangential acceleration set to zero (maximum speed for acceleration), and a given fixed flight path angle and tangential acceleration (cruise or loiter). In each of the above, angle of attack is variable.

For the first option, given a fixed flight path angle and setting the tangential acceleration to zero, the following procedure is used.

At given values of altitude, power setting, and normal load factor, the current velocity, the atmospheric conditions, the propulsion thrust and fuel flow, and the aerodynamic lift and drag are determined The vector force sums are calculated as

$$F_{normal} = \text{Lift} + \text{Thrust} \sin(\alpha_t)$$

$$F_{tangential} = \text{Thrust} \cos(\alpha_t) - \text{drag} - \text{ram drag}$$

$$F_{lift} = F_{normal} - W \cos\gamma$$

$$F_{drag} = F_{tangential} - W \sin\gamma$$

where α_t is the angle of attack of the thrust vector.

The angle of attack is then iterated to provide the given normal load factor, the normal load factor available being calculated as,

$$G_{normal\ calculated} = \frac{F_{lift}}{W} + 1$$

The Newton-Raphson linear extrapolation procedure is used to zero the parameter

$$G_{normal} - G_{normal\ calculated}$$

where G_{normal} is the required given normal load factor. This procedure is repeated until the parameter,

$$\frac{G_{normal} - G_{normal\ calculated}}{G_{normal}}$$

reduces to a given tolerance.

The velocity is also iterated to provide the given tangential load factor, the tangential load factor available being calculated as,

$$G_{tangential\ calculated} = \frac{F_{drag}}{W}$$

The Newton-Raphson linear extrapolation procedure is used to zero the parameter

$$G_{tangential} - G_{tangential\ calculated}$$

where $G_{tangential}$ is the required given tangential load factor.

The entire procedure above is repeated until the parameter,

$$\frac{G_{tangential} - G_{tangential\ calculated}}{G_{tangential}}$$

reduces to a given tolerance.

For the second option, given a flight path angle and a tangential acceleration, the procedure is the same as for the first option.

Following determination of the maximum speed for the given flight condition, the airplane accelerations and rate-of-climb are calculated,

$$a_{normal} = \frac{G_Z F_{lift}}{W}$$

$$a_{tangential} = \frac{G_Z F_{drag}}{W}$$

$$a_X = a_T \cos\gamma - a_N \sin\gamma$$
$$a_Z = a_N \cos\gamma + a_T \sin\gamma$$
$$R/C = V \sin\gamma$$

where G_Z is the acceleration due to gravity.

6.4.9 MSNINTG and GILL (Integration Techniques). The integration technique uses the method of S. Gill (Reference 9), which was specifically derived for efficient use of electronic computers. Furthermore, calculation of the required derivatives has been generalized so that a performance routine has only to define required indexes, counters, and parameters.

Eight parameters can be integrated; time, distance, fuel, weight, altitude, velocity, flight path angle, and altitude. Integration can be done with respect to any one of these parameters. The chosen parameters are defined by the mission segment performance subroutines (i.e., climb, acceleration, cruise, loiter, or combat). The GILL integrating routine requires four passes to accomplish the integrating step:

Pass One — takes derivatives at the start of the integration interval and predicts conditions at the middle of the interval;

Pass Two — takes derivatives based on predicted conditions at the mid-interval, combined with derivatives from the first pass, and repredicts conditions at the mid-interval;

Pass Three — takes derivatives based on latest estimate of mid-interval conditions, combined with derivatives from the first two passes, and predicts end-of-interval conditions; and

Pass Four — takes derivatives based on end-of-interval conditions, combined with derivatives from previous passes, and calculates conditions at the end of the interval.

6.4.10 MSTORE (Mission Data Storage and Expendable Fuel Tank Release). The mission performance data, as it is calculated, is stored in a bi-dimensional array, so that the data may be recalled and outputted when required. The capability to restore parameter values to the previous integration step is available by the entry RESTORE. This is utilized by the mission performance routines when, for example, a termination value is exceeded after an integration step is completed, and the integrating interval is decreased. When a problem during an integration step occurs, such as the climb rate becoming negative, the entry RESET will reset the parameter values to those at the beginning of the current integration step.

Adjustment of airplane weight and aerodynamics, based on fuel usage, is also handled by this subroutine. This is normally required when disposing of external fuel tanks during the mission.

6.4.11 ATMOS (Atmospheric Data). This routine calculates atmospheric data for a 1962 ICAO standard day, a MIL-STD-210A tropical day, or a constant ambient temperature.

Three alternate atmospheres are available. The standard day atmospheric conditions are computed as outlined in Reference 10. The tropical day atmosphere is computed using the procedure set forth in Reference 11 (MIL-STD-210A). For a constant temperature atmosphere, the procedure for standard day atmosphere is followed, except that the temperature is the value input.

6.4.12 QUAD (Quadratic Curve Fit). This routine is used to fit data computed by the program for extrapolation, interpolation, or optimization purposes.

Given three x,y, points the coefficients of a quadratic curve fit are calculated, giving

$$Y = a X^2 + b X + c$$

The X value for the minimum or maximum value of the curve (first derivative equal to zero) is also calculated

$$X_{ROOT} = \frac{b}{2a}$$

This routine is used by several subprograms in order to determine maximum or minimum values for a parameter (e.g., max R/C, max SR, etc.).

6.4.13 KABD (Hyperbolic Curve Fit Evaluation). This routine is used to evaluate data which is input in the form of curve fit coefficients. The evaluating equation is depicted by the equation

$$Y = \frac{k}{X - a} + b + dX$$

where k, a, b and d are the inputted coefficients. Using this equation, and dependent variable Y can be evaluated at the independent variable X.

6.4.14 NWRP 2 (Newton-Raphson Linear Extrapolation Procedure). This routine linearly extrapolates from two pairs of X, Y, values, and derives the X value for a zero Y.

$$X = \frac{(X_2 - Y_2)(X_2 - X_1)}{(Y_2 - Y_1)}$$

For most iterative procedures, the parameters can be adjusted so that the desired value is zero.

6.5 SIMPLIFIED PERFORMANCE ANALYSIS

The purpose of the simplified performance analysis is to approximate the performance, propulsion and loads data required for the quick-look vehicle sizing integration cycle. The subroutine (RULES) is designed to provide wing loadings, thrust-to-weight ratios, fuel weights, and gust load factor. The takeoff weight is updated in the weight subroutine during the iteration cycle. The equations are segregated into five groups, including the data for takeoff and landing condition, climb condition, cruise condition, design condition, and a gust load approximation.

Data developed for the takeoff and landing condition includes lift and drag coefficient, wing loadings, and thrust-to-weight ratio. The wing loading is derived from the landing field length requirement, lift and drag coefficient, and assumed deceleration rates. The lift coefficient is computed as a simple function of aspect ratio. The drag coefficient is computed as a simple function of aspect ratio. The drag coefficient is computed from an equivalent skin friction drag coefficient and aircraft wetted area. The thrust-to-weight ratio is derived from takeoff thrust requirements for the landing field length specified. The equations are:

Maximum Lift Coefficient

$$C_{L_{max}} = \frac{k_{C_{L_{max}}}}{1 + \frac{3}{AR})}$$

where

$C_{L_{max}}$ = maximum lift coefficient

$k_{C_{L_{max}}}$ = lift coefficient scaling factor

AR = wing aspect ratio

The lift coefficient scaling factor ($k_{C_{L_{max}}}$) is equalized to the baseline wing configuration. Then as the baseline wing aspect ratio is varied the effect on $C_{L_{max}}$ will be accounted for in the resizing operation. The value for the lift coefficient scaling factor is obtained from the equation:

$$k_{C_{L_{max}}} = C_{L_{max}} \left(1 + \frac{3}{AR}\right)$$

where

$k_{C_{L_{max}}}$ = lift coefficient scaling factor

$C_{L_{max}}$ = maximum lift coefficient for baseline wing

AR = wing aspect ratio for baseline wing

Coefficient of Lift - Landing

$$C_{L_{land}} = 0.75 \left(C_{L_{max}}\right)$$

where

$C_{L_{land}}$ = coefficient of lift @ landing

$C_{L_{max}}$ = calculated maximum lift coefficient

Coefficient of Drag - Equivalent Profile

$$C_{D_o} = 1.1 \left(C_{D_f}\right)\left(\frac{S_{wet}}{S_W}\right)$$

where

C_{D_o} = coefficient of drag - equivalent profile

C_{D_f} = coefficient of skin friction (Typ. value = 0.003)

S_{wet} = aircraft total wetted area

S_W = theoretical wing area

Wing Loading - Landing

$$\left(\frac{W}{S}\right)_{land} = \frac{C_{L_{land}}(\sigma)(a)}{420}\left[\frac{L_{field}}{1.67} - GOH_{min}\left(\frac{C_{L_{land}}}{C_{D_o} + \frac{k_{GE}\left(C_{L_{land}}\right)^2}{\pi(AR)(e)} + \frac{SW}{10^4}}\right)\right]$$

where

$\left(\frac{W}{S}\right)_{land}$ = wing loading @ landing

$C_{L_{land}}$ = coefficient of lift @ landing

σ = air density ratio @ field altitude

a = landing deceleration

L_{field} = landing field length

GOH_{land} = minimum ground object height

$C_{L_{land}}$ = coefficient of lift @ landing

C_{D_o} = coefficient of drag-equvalent profile

k_{GE} = ground effect factor on wing loading @ landing (Typ. value = 0.5)

AR = wing aspect ratio

e = wing efficiency factor (Typ. value = 0.8)

S_W = theoretical wing area

Wing Loading - Takeoff

$$\left(\frac{W}{S}\right)_{TO} = \left(\frac{W}{S}\right)_{land}\left(\frac{W_{TO}}{W_{land}}\right)$$

where

$\left(\frac{W}{S}\right)_{TO}$ = wing loading @ takeoff

$\left(\frac{W}{S}\right)_{land}$ = wing loading @ landing

W_{TO} = gross takeoff weight

W_{land} = landing design weight

Coefficient of Lift - Takeoff

$$C_{L_{TO}} = 0.65\ (C_{L\,max})$$

where

$C_{L_{TO}}$ = coefficient of lift @ takeoff

$C_{L_{max}}$ = maximum lift coefficient

Thrust-to-Weight Ratio - Takeoff

$$\left(\frac{T}{W}\right)_{TO} = \frac{24.09\left(\frac{W}{S}\right)_{TO}}{C_{L_{TO}}\,(L_{TO})\,(\sigma)}$$

where

$\left(\frac{T}{W}\right)_{TO}$ = thrust-to-weight ratio @ takeoff

$\left(\frac{W}{S}\right)_{TO}$ = wing loading @ takeoff

$C_{L_{TO}}$ = coefficient of lift @ takeoff

L_{TO} = takeoff field length

σ = air density ratio @ field altitude

Data developed for climb conditions include lift-to-drag ratio, thrust-to-weight ratio, speed, distance, time and fuel weights. The thrust-to-weight ratio is computed for a sustained angle of climb requirement, and then the greater value of $(T/W)_{TO}$ or $(T/W)_{climb}$ is used to size the engines. The fuel weight is derived from computations that assume a climb at best lift-to-drag ratio to a specified altitude and reserve for 45 minutes of cruise. The average specific fuel consumptions for climb and cruise are input. The equations are:

Lift-to-Drag Ratio - Maximum

$$\left(\frac{C_L}{C_D}\right)_{max} = 0.5 \left[\frac{\pi\,(e)\,(AR)}{C_{D_o}}\right]^{0.5}$$

where

$\left(\frac{C_L}{C_D}\right)_{max}$ = maximum lift-to-drag ratio $[(L/D)_{max}]$

e = wing efficiency factor (Typ. value = 0.8)

AR = wing aspect ratio

C_{D_o} = coefficient of drag - equivalent profile

Thrust-to-Weight Ratio - Climb

$$\left(\frac{T}{W}\right)_{climb} = \frac{0.085 + \frac{1}{\left(\frac{C_L}{C_D}\right)_{max}}}{\sigma_{climb}}$$

where

$\left(\frac{T}{W}\right)_{climb}$ = thrust-to-weight ratio for climb

$\left(\frac{C_L}{C_D}\right)_{max}$ = maximum lift-to-drag ratio $[(L/D)_{max}]$

σ_{climb} = average air density ratio for climb

Climb Speed

$$V_{climb} = 12.16 \left[\frac{\left(\frac{W}{S}\right)_{TO}}{\sigma_{climb}\left(\frac{C_L}{C_D}\right)_{max} C_{D_o}} \right]^{0.5}$$

where

V_{climb} = climb speed

$\left(\frac{W}{S}\right)_{TO}$ = wing loading @ takeoff

σ_{climb} = average air density ratio for climb

$\left(\frac{C_L}{C_D}\right)_{max}$ = maximum lift-to-drag ratio $[(L/D)_{max}]$

C_{D_o} = coefficient of drag - equivalent profile

Climb Distance

$$D_{climb} = \frac{ALT}{0.122\ (6080)}$$

where

D_{climb} = climb distance

ALT = climb altitude

Climb Time

$$t_{climb} = \frac{D_{climb}}{V_{climb}}$$

where

t_{climb} = climb time to altitude

D_{climb} = climb distance

V_{climb} = climb speed

Fuel Weight - Climb

$$W_{fuel_{climb}} = W_{TO} \left(\frac{T}{W}\right)_{climb} (SFC_{climb})(t_{climb})$$

where

$W_{fuel_{climb}}$ = weight of climb fuel

W_{TO} = gross takeoff weight

$\left(\frac{T}{W}\right)_{climb}$ = thrust-to-weight ratio for climb

SFC_{climb} = specific fuel consumption for climb

t_{climb} = climb time to altitude

Fuel Weight - Reserve

$$W_{fuel_{rs}} = SFC_{cr} \quad (0.3) \left(\frac{T}{W}\right)_{TO} (0.75) (W_{land})$$

where

$W_{fuel_{rs}}$ = weight of reserve fuel

SFC_{cr} = specific fuel consumption for cruise

$\left(\frac{T}{W}\right)_{TO}$ = thrust-to-weight ratio @ takeoff

W_{land} = landing design weight

Data computed for cruise conditions include aircraft weight, thrust, speed, lift and drag coefficients, and fuel weight. The fuel weight for the cruise condition is derived for a calculated thrust and an input value of cruise specific fuel consumption. The equations used to develop cruise data are:

Cruise Weight

$$W_{cr} = W_{TO} - W_{fuel_{climb}} - \frac{W_{fuel_{cr}}}{2}$$

where

W_{cr} = cruise weight

W_{TO} = gross takeoff weight

$W_{fuel_{climb}}$ = weight of climb fuel

$W_{fuel_{cr}}$ = weight of cruise fuel

Cruise Thrust

$$T_{cr} = 0.3 \ (W_{cr})(\frac{T}{W})_G$$

where

T_{cr} = cruise thrust

W_{cr} = cruise weight

$(\frac{T}{W})_G$ = the greater value of thrust-to-weight ratio for takeoff or climb

Cruise Speed

$$V_{cr} = \frac{1}{1.687} \left[\frac{T_{cr} + \left((T_{cr})^2 - \frac{4 \ (C_{D_o}) \ (W_{cr})^2}{\pi \ (e) \ (AR)} \right)^{0.5}}{\sigma_{cr} \ (\rho_o)(C_{D_o}) \ (S_W)} \right]^{0.5}$$

where

V_{cr} = cruise speed

T_{cr} = cruise thrust

C_{D_o} = coefficient of drag - equivalent profile

W_{cr} = cruise weight

e = wing efficiency factor (typ. value = 0.8)

AR = wing aspect ratio

σ_{cr} = air density ratio @ cruise altitude

ρ_o = sea level standard air density

S_W = theoretical wing area

Cruise Speed - Maximum

$$V_{cr_{max}} = 0.8\,[\,29(518.7 - 0.00357\,(ALT))^{0.5}\,]$$

where

$V_{cr_{max}}$ = maximum cruise speed

ALT = climb altitude

Coefficient of Lift - Cruise

$$C_{L_{cr}} = \frac{295\left(\frac{W}{S}\right)_{TO}}{\sigma_{cr}(V_{cr})^2}$$

where

$C_{L_{cr}}$ = coefficient of lift @ cruise altitude

$\left(\frac{W}{S}\right)_{TO}$ = wing loading @ takeoff

σ_{cr} = air density ratio @ cruise altitude

V_{cr} = cruise speed

Coefficient of Drag - Cruise

$$C_{D_{cr}} = C_{D_o} + \frac{\left(C_{L_{cr}}\right)^2}{\pi\,(e)\,(AR)}$$

where

$C_{D_{cr}}$ = coefficient of drag @ cruise altitude

C_{D_o} = coefficient of drag - equivalent profile

$C_{L_{cr}}$ = coefficient of lift @ cruise altitude

e = wing efficiency factor (Typ. value = 0.8)

AR = wing aspect ratio

Lift-to-Drag Ratio - Cruise

$$\left(\frac{C_L}{C_D}\right)_{cr} = \frac{C_{L_{cr}}}{C_{D_{cr}}}$$

where

$\left(\frac{C_L}{C_D}\right)_{cr}$ = lift-to-drag ratio @ cruise altitude

$C_{L_{cr}}$ = coefficient of lift @ cruise altitude

$C_{D_{cr}}$ = coefficient of drag @ cruise altitude

Fuel Weight - Cruise

$$W_{fuel_{cr}} = (W_{zero} + W_{fuel_{climb}} + W_{fuel_{rs}})(10^{x-1})$$

where

$W_{fuel_{cr}}$ = weight of cruise fuel

W_{zero} = zero fuel weight

$W_{fuel_{climb}}$ = weight of climb fuel

$W_{fuel_{rs}}$ = weight of reserve fuel

and

$$x = \frac{RANGE - D_{climb}}{2.3\left(\frac{C_L}{C_D}\right)_{cr}\left(\frac{V_{cr}}{SFC_{cr}}\right)}$$

where

x = cruise fuel coefficient

RANGE = total range

D_{climb} = climb distance

$\left(\frac{C_L}{C_D}\right)_{cr}$ = lift-to-drag ratio @ cruise altitude

V_{cr} = cruise speed

SFC_{cr} = specific fuel consumption for cruise

C-3

Data developed for design conditions include the total fuel weight, design wing loading, and design thrust-to-weight ratio. The equations are:

Total Fuel Weight

$$W_{fuel} = W_{fuel_{climb}} + W_{fuel_{cr}} + W_{fuel_{rs}}$$

where

W_{fuel} = weight of total fuel

$W_{fuel_{climb}}$ = weight of climb fuel

$W_{fuel_{cr}}$ = weight of cruise fuel

$W_{fuel_{rs}}$ = weight of reserve fuel

Design Wing Loading

$$\left(\frac{W}{S}\right)_{Des} = \left(\frac{W}{S}\right)_{TO}$$

where

$\left(\frac{W}{S}\right)_{Des}$ = design wing loading

$\left(\frac{W}{S}\right)_{TO}$ = wing loading @ takeoff

Design Thrust-to-Weight Ratio

$$\left(\frac{T}{W}\right)_{Des} = 1.05 \left(\frac{T}{W}\right)_{TO}$$

where

$\left(\frac{T}{W}\right)_{Des}$ = design thrust-to-weight ratio

$\left(\frac{T}{W}\right)_{TO}$ = thrust-to-weight ratio @ takeoff

The loads data required for the weight prediction equations consists primarily of gust load factors. Approximations for this data are derived in the performance subroutine, and then updated and expanded in the loads portion of the geometry subroutine. The gust load factor is derived from the wing geometry and the cruise speed. The wing is assumed rigid and the effective lift curve slope is approximated as a function of the wing aspect ratio and horizontal tail area. The equations are:

Wing Normal Force Curve Slope

$$C_{N_{\alpha_w}} = \left[\frac{6}{1 + \frac{6}{(AR)}}\right] + 2.15 \left[\frac{S_H}{S_w}\right]$$

where

$C_{N_{\alpha_w}}$ = wing normal force curve slope

AR = wing aspect ratio

S_H = horizontal tail area

S_w = theoretical wing area

Aircraft Inertia Factor - Gust Alleviation

$$U = \frac{2\left(\frac{W}{S}\right)_{Des}}{0.0765\,(\sigma_{cr})\,(C_{N_{\alpha_w}})\,(\overline{C}_w)}$$

where

U = inertia factor for gust alleviation

$\left(\frac{W}{S}\right)_{Des}$ = design wing loading

σ_{cr} = air density ratio @ cruise altitude

$C_{N_{\alpha_w}}$ = wing normal force curve slope

$\overline{C}_w$ = wing mean aerodynamic chord

Gust Response Factor

$$K = 0.88 \left(\frac{U}{U + 5.3} \right)$$

where

K = gust response factor

U = inertia factor for gust alleviation

Incremental Gust Load Factor

$$\Delta N_Z = \frac{0.2006 \, (V_{cr}) \, (C_{N_{\alpha_w}}) \, (\sigma_{cr})^{0.5} (K)}{2 \left(\frac{W}{S} \right)_{Des}}$$

where

ΔN_Z = incremental gust load factor

V_{cr} = cruise speed

$C_{N_{\alpha_w}}$ = wing normal force curve slope

σ_{cr} = air density ratio @ cruise altitude

K = gust response factor

$\left(\frac{W}{S} \right)_{Des}$ = design wing loading

Ultimate Gust Load Factor

$$N_{Z_G} = 1.5 \, (1 + \Delta N_Z)$$

where

N_{Z_G} = ultimate gust load factor

ΔN_Z = incremental gust load factor

6.6 REFERENCES

1. Bulinski, R. J. "Combat Aircraft Synthesis Program Aerodynamics Subroutine," General Dynamics Convair Division TN-70-DP-01, December 1970.

2. Anon., LIT System Planning Study, Vol. II, Vertol Division, Boeing Company, 1967.

3. Anon., STOL Tactical Aircraft Investigation, Vol. II, Design Compendium, General Dynamics Convair Division, GDCA-DHG73-001, 1973.

4. Schemensky, R. T., "Development of an Empirically Based Computer Program to Predict the Aerodynamic Characteristics of Large Aircraft, Vol. I, Empirical Methods, "General Dynamics Convair Aerospace Division, AFFDL-TR-73-144, November 1973.

5. Finck, R. D., "USAF Stability and Control DATCOM," McDonnell Douglas Corporation, Douglas Aircraft Division, October 1960, Revised January 1974.

6. Runciman, W. J., Letsinger, G. R., Ray, B. F., and May, F. W., "STOL Tactical Aircraft Investigation, Volume II, Part 1, Aerodynamic Technology: Design Compendium, Vectored Thrust Mechanical Flaps," The Boeing Company, AFFDL-TR-73-19, May 1973.

7. Young, A. D., "The Aerodynamic Characteristics of Flaps," Royal Aircraft Establishment, Farnborough, England. RAE Report No. Aero. 2185, February 1947.

8. Weirich, Robert L., "Analytical Determination of the Takeoff Performance of Some Representative Supersonic Transport Configurations," NASA TN D-2308, 1964.

9. S. Gill, "A Process for the Step-by-Step Integration of Differential Equations in an Automatic Digital Computing Machine," Cambridge Philosophical Society Proceedings, Volume 47, Part 1, January 1951.

10. U.S. Standard Atmosphere, 1962 ICAO Standard Atmosphere to 20 Kilometers, December 1962, U.S. Government Printing Office, Washington D. C.

11. Military Standard, Climatic Extremes for Military Equipment, MIL-STD-210A, August 2, 1957, U.S. Government Printing Office, Washington, D. C.

SECTION 7

EXTERNAL LOADS ANALYSIS

Net limit design loads for the fuselage and aerodynamic surfaces are produced by the external loads program. Net loads are computed by combining aerodynamic loading with loads due to inertia forces and landing gear reactions. The resulting loads data are in the form of shears, bending moments and torsion loads at a number of stations along each component as shown in Figure 7-1. The loads data in this form can be used directly by the structural synthesis program, APAS, described in Section 8.0.

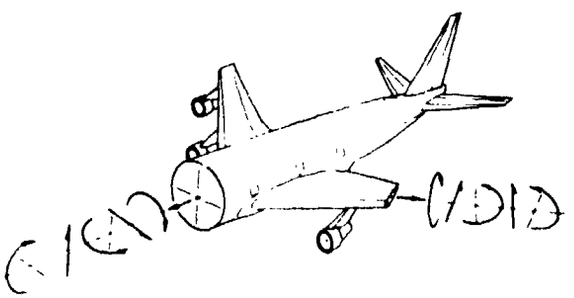

Figure 7-1. External loads

The loads program consists of two basic modules: 1) the aerodynamic surface loads module, AELOADS; and 2) the fuselage loads module, BODLOD. The wing load analysis includes a steady state aeroelastic capability, which can account for structural deformation under load. Loads for wing and horizontal and vertical stabilizers are computed with this module. The fuselage loads are computed by the BODLOD module. Fuselage aerodynamic loads are calculated for a unit angle of attack and a unit dynamic pressure. Inertia loads for the fuselage are determined for unit translational and rotational acceleration. Fuselage net loads are obtained by forming linear combinations of the unit conditions. The angle of attack and load factor from the corresponding wing condition are used as multiplication factors.

The symbols used in the loads analyses are too numerous to be repeated following every equation in the following paragraphs. For convenience, they are grouped together and defined as follows:

Symbol	Definition
AR_w	aspect ratio of wing
b	wing span
$C_{D_{E_\alpha}}$	external store drag coefficient variation with α (per degree)
C_{L_α}	coefficient of lift variation with angle of attack (per degree)
$C_{L_{\alpha_o}}$	coefficient of lift at zero angle of attack
$C_{L_{E_o}}$	coefficient of lift of an external store at zero angle of attack

Symbol	Definition
$C_{L_{F_o}}$	coefficient of lift of the fuselage at zero angle of attack
$C_{L_{E_\alpha}}$	variation of external store lift coefficient with angle of attack
$C_{L_{F_\alpha}}$	variation of fuselage lift coefficient with angle of attack
$C_{L_{I_\alpha}}$	variation of wing carry-through lift coefficient with angle of attack
$C_{L_{WF_\alpha}}$	variation of the complete wing-fuselage lift coefficient with angle of attack
C_{m_α}	aerodynamic moment coefficient variation with angle of attack
$C_{m_{\alpha_o}}$	aerodynamic bending moment coefficient about wing quarter chord at the mean aerodynamic chord for zero angle of attack
$C_{m_{E_o}}$	external store aerodynamic moment coefficient at zero angle of attack
$C_{m_{F_o}}$	fuselage aerodynamic moment coefficient at zero angle of attack.
$C_{m_{E_\alpha}}$	external store aerodynamic moment coefficient variation with angle of attack
$C_{m_{F_\alpha}}$	fuselage aerodynamic moment coefficient variation with angle of attack
$C_{m_{I_\alpha}}$	variation of wing carry-through aerodynamic moment coefficient with angle of attack
$C_{m_{WF_\alpha}}$	variation of total wing-fuselage combination aerodynamic moment coefficient with angle of attack
$C_{m_{O_T}}$	total section moment coefficient at section quarter chord

Symbol	Definition
c	local chord parallel to plane of symmetry
$\bar{c}$	wing mean geometric chord
c_{m_o}	wing section pitching-moment coefficient
c_ℓ	wing segment lift coefficient
ds	incremental length along wing elastic axis
EI	effective value of product of modulus of elasticity and wing section beam bending moment of inertia
GJ	effective value of product of shear modulus of elasticity and wing section polar moment of inertia
h	semispan of horseshoe vortex
I_X	airplane rolling moment of inertia
I_Y	airplane pitching moment of inertia
L_i, L_n	total aerodynamic lift on wing segment i or segment n
L_{EO}	total aerodynamic lift on external store
L_F	fuselage lift in presence of wing, $\left[C_{L_{F_O}} + \left(C_{L_F}\right)_\alpha \alpha_r\right] qS$
ℓ	loading per unit of span perpendicular to plane of symmetry
M	applied bending moment, also Mach number
M_{ea}	total net wing bending moment about an axis perpendicular to the wing elastic axis
M_{eo}	aerodynamic bending moment exerted on an external store about an axis through the store aerodynamic center perpendicular to the fuselage center plane.
m	moment due to unit pitching moment (see Section 7.1.3) also combined compressibility/thickness correction factor (see Section 7.1.8)
m_o	two-dimensional lift-curve slope per radian, including compressibility effects, for sections parallel to plane of symmetry
n_z	airplane load factor, positive when inertia loads are downward

Symbol	Definition
P_T	balancing tail load, positive upward
q	dynamic pressure, $\rho V^2/2$
r	radial distance from vortex core
S	wing area
T	wing torque about airplane pitch axis
T_{ea}	wing torque about wing elastic axis
t	torque about wing elastic axis due to unit pitching moment (see Section 7.1.3)
V	true free-stream velocity
V_Z	vertical component of the free stream velocity
ΔV_Z	the overvelocity, total vertical velocity in the presence of the fuselage minus V_Z
W	airplane gross weight
w_r	wash velocity induced by line vortex at perpendicular distance r from vortex line, positive for downwash
$\left(\frac{w}{V}\right)_{3c/4}$	downwash angle at three-quarter-chord point induced for vortex system representing wing and its spanwise lift distribution
X_{tail}	x-axis coordinate of the horizontal tail aerodynamic load center
XC4	local quarter-chord-position along x-axis
$\bar{X}C4$	quarter-chord-position of the wing mean aerodynamic chord along the x-axis
XCG	location of the vehicle center of gravity along the x-axis
XDE	difference between angle-of-attack type and elevator type horizontal tail load center positions along the x-axis
XE	location of aerodynamic load center of external store along the x-axis
X_{fus}	x-axis coordinate of the fuselage lift center of pressure
X_{WF}	x-axis coordinate of the neutral point location of the wing-fuselage combination

Symbol	Definition
x_T	streamwise distance from pitch reference axis to center of pressure of balancing tail load, positive when center of pressure is to rear of pitch reference axis
x	streamwise distance from pitch reference axis to bound portion of horseshoe vortex, positive when vortex is to rear of pitch reference axis
x_A	streamwise distance from pitch reference axis to airplane center of gravity, positive when center of gravity is to rear of pitch reference axis
$\bar{x}$	streamwise distance from pitch reference axis to $\bar{c}/4$ line positive when $\bar{c}/4$ line is to rear of pitch reference axis
$\bar{Z}C4$	waterline or z-axis location of the mean aerodynamic chord quarter-chord point
ZCD_{fus}	waterline or z-axis location of the fuselage drag load
ZCD_{tail}	waterline or z-axis location of the tail drag load
ZF	waterline or z-axis location of the external store drag load
α	angle of attack, also vortex segment angle (see Figure 7-4)
α_t	final angle of attack of section zero-lift line with respect to local free-stream direction $\alpha_r + \alpha_g + \alpha_s$, radians (see Figure 7-3)
α_g	change in section angle of attack due to aerodynamic twists and due to all structural twists associated with a flexible wing, which are not accounted for by the α_s term, radians (see Figure 7-3)
α_r	angle of attack of root-section zero-lift line, radians (see Figure 7-3)
α_s	change in section angle of attack due to wing lift distribution acting on a flexible wing ($\alpha_s = 0$ for a rigid wing), radians (see Figure 7-3)
α_T	change in section angle of attack due to built-in structural twist or jig twist
$\alpha_{ol_{body\ sect}}$	the zero lift line angle of attack of the wing segment lying inside of the fuselage, with respect to its chord line
$\alpha_{inc\ fus}$	fuselage incidence angle with respect to the root section

Symbol	Definition
$\alpha_{inc\ tail}$	horizontal tail incidence angle with respect to fuselage reference line
$\alpha_{oL_{sect}}$	clean wing section zero-lift-line angle relative to its chord line
$\alpha_{oL_{root}}$	root wing section zero-lift-line angle of attack relative to its chord line positive for chord line above lift line
β	vortex segment angle (see Figure 7-4), also compressibility correction factor (see Section 7.1.8), also upwash angle forward of the wing (see Section 7.2.1)
Γ	strength of line vortex
ΔC_{D_E}	incremental drag coefficient of external store
$\Delta C_{D_{fus}}$	incremental drag coefficient of fuselage
$\Delta C_{D_{tail}}$	incremental drag coefficient of tail
δ_{fl}	flap deflection
δ_{sl}	slat deflection
δ_{sp}	spoiler deflection
ϵ	external store number (see Section 7.1.5), also downwash angle aft of the wing (see Section 7.2.1)
η	fraction of wing semispan
η_f	fraction of fuselage length
Θ	vortex reference angle (see Figure 7-5), also aircraft pitching angle
$\ddot{\Theta}$	aircraft pitching acceleration
κ	function describing the variation of the upwash angle in front of the wing (see Section 7.2.1)
Λ	wing leading edge sweep angle
$\Lambda_{c/4}$	wing sweep angle measured at the quarter chord

Symbol	Definition
Λ_{ea}	wing sweep angle measured at the wing elastic axis
ρ	fluid density
ρ_0	air density at sea level
ρ_h	air density at altitude
φ	vortex reference angle (see Figure 7-5)
$\left\{\frac{\alpha}{\delta_{fl}}\right\}$	flap effectiveness
$\left\{\frac{\alpha}{\delta_{sl}}\right\}$	slat effectiveness
$\left\{\frac{\alpha}{\delta_{sp}}\right\}$	spoiler effectiveness
$\frac{\partial \varepsilon}{\partial \alpha}$	rate of change of the upwash angle forward of the wing with respect to angle of attack
$\frac{\partial \varepsilon}{\partial \alpha}$	rate of change of the down wash angle att of the wing with respect to angle of attack

Matrix Notation

$[\ ]$	square matrix, elements of which are designated by use of subscripts; for example, element a_{ij} is in ith row and jth column
$[\ ]$	row matrix
$\{\ \}$	column matrix
$[^{0}]$	diagonal matrix, which is a square matrix in which all elements are zeros except those on the principal diagonal a_{11}, a_{22}, a_{33},... a_{nn}
$[E_{\alpha}]$	external store influence matrix for zero angle of attack at wing root (see Section 7.1.5)

Matrix Notation (Continued)

$[E_\alpha]$	external store influence matrix, alpha dependent portion (see Section 7.1.5)
[FMM]	unit bending moment structural influence matrix (see Section 7.1.5)
[FMT]	unit torsion moment structural influence matrix (see Section 7.1.5)
[I]	identity matrix; that is, diagonal matrix in which diagonal elements are equal to unity
$[S_1]$	aerodynamic-induction or downwash matrix in which elements a_{ij} relate downwash angle at station i to unit running lift at station j on wing
$[S_2]$	elasticity matrix in which element a_{ij} relate changes in streamwise angle of attack at station i to unit running lift at station j on wing
$[S_f]$	fuselage image-vortex matrix relating image downwash effects at station control points to unit running lifts
$[S_\alpha^o]$	fuselage "overvelocity" matrix

7.1 AERODYNAMIC SURFACE LOADS. This section presents the method used for computing the steady-state span load distribution on an elastic aerodynamic surface for specified airplane weights and load factors. The method is based on a modification of the Weissinger L method (References 1 through 5). The theory, originally developed for subsonic flow, is valid for supersonic flight provided the flow over the surface is subsonic. This is the case for swept wings that operate in the low supersonic Mach number range, where the shock cone lies ahead of the leading edge and no other shocks are generated on the wing.

Because equations for subsonic flow have been used for supersonic flow with varying degrees of success, this extended use of subsonic equations is discussed in Reference 6. Although the supersonic equations are derived from hyperbolic relationship and subsonic equation from elliptic relationship, the end results are surprisingly similar providing the section lift curve slopes and centers of pressure for the desired Mach number are used and if the aerodynamic influence matrix has a reduced region of influence compatible with the Mach angle. It includes the effects of external stores, and fuselage on the spanwise loading.

The program performs the symmetric balance and then distributes the shears, moments, and torques over the vehicle for each condition. It may be used for preliminary sizing of structural capability by first considering the rigid case. The program calculates the EI's from a series of assumptions based upon current design practices and the calculated bending moment of the rigid case. This first approximation of the EI's and GJ's is recycled once more as an elastic case. The recycled results are satisfactory for the initial structural design.

The inclusion of the effects of flexibility in the solution of the spanwise airload distribution applied to a wing of arbitrary plan form and stiffness distribution requires a simultaneous solution of equations that contain both the aerodynamic influence functions and the structural influence functions.

The effects of fuselage and engine pods on the spanwise loading must be taken into account; also the total lift on each of the external stores must be considered simultaneously in order to determine the wing loading at a specified load factor. A method for including such effects without recourse to iterative procedures for steady state flight conditions is provided. The equations are derived so that the spanwise airload distribution can be expressed in matrix form in terms of influence coefficients for aerodynamic induction and structural deflection in a manner similar to that employed in Reference 7.

The basic method outlined in this section includes details of the various derivations, the expansion of the basic equations to include fuselage interference and store load effects, and a method for obtaining compressibility corrections. In the development of the method, certain assumptions that are common to airfoil theory apply, namely:

1. The flow is potential; that is, boundary-layer effects, separation, and compressibility shocks are absent or neglibible.
2. The wing thickness is small.
3. A stagnation point exists at the wing trailing edge.
4. The angles of attack α are small so that $\tan \alpha \approx \alpha$ (where α) is measured in radians) and $\cos \alpha \approx 1$.
5. All drag-load effects, except those due to engine pods and stores, are neglected entirely in determining the deformations of the wing used in obtaining the equilibrium spanwise airload distribution.

With regard to the structure, the following assumptions are made:

1. Camber changes arising from twisting and bending of the wing are neglected.
2. The elastic twist of the control surface is the same as that of the adjoining wing structure.
3. The angles of structural deflection Θ are small so that $\tan \Theta \approx \sin \Theta \approx \theta$ (where Θ is measured in radians) and $\cos \Theta \approx 1$.
4. Although the angle-of-attack changes, including those due to bending and torsional deformations of the wing, are accounted for in the determination of the equilibrium spanwise airload distribution on the wing, this final airload distribution is applied to the geometry of the undeflected wing in computing the bending and torsional moments.

7.1.1 Method of Analysis. The equations of equilibrium must be satisfied for any given flight condition to provide the desired load factors and rotational accelerations.

For the symmetric flight condition two equations of equilibrium are used; the summation of the vertical forces and the summation of the pitching moments must be zero. The vertical forces include wing lift, fuselage lift, the tail load, external store lift forces, and the vertical inertia forces. The pitching moments include moments due to the vertical forces and also due to, fuselage drag forces, external store drag forces, tail drag forces, engine thrust forces, aerodynamic moments on the wing, fuselage and external stores, and the moment due to rotational pitch acceleration.

The fundamental problem involved in the aeroelastic solution is the development of a series of equations that relate the spanwise lift distribution for an arbitrary wing plan form to the elastic properties of the wing, and to the attitude of the wing under the influence of aerodynamic and inertia loading.

The wing is divided by streamwise cuts into slices as shown in Figure 7-2. The aerodynamic and elastic properties are assumed to be constant on the slice and to have the

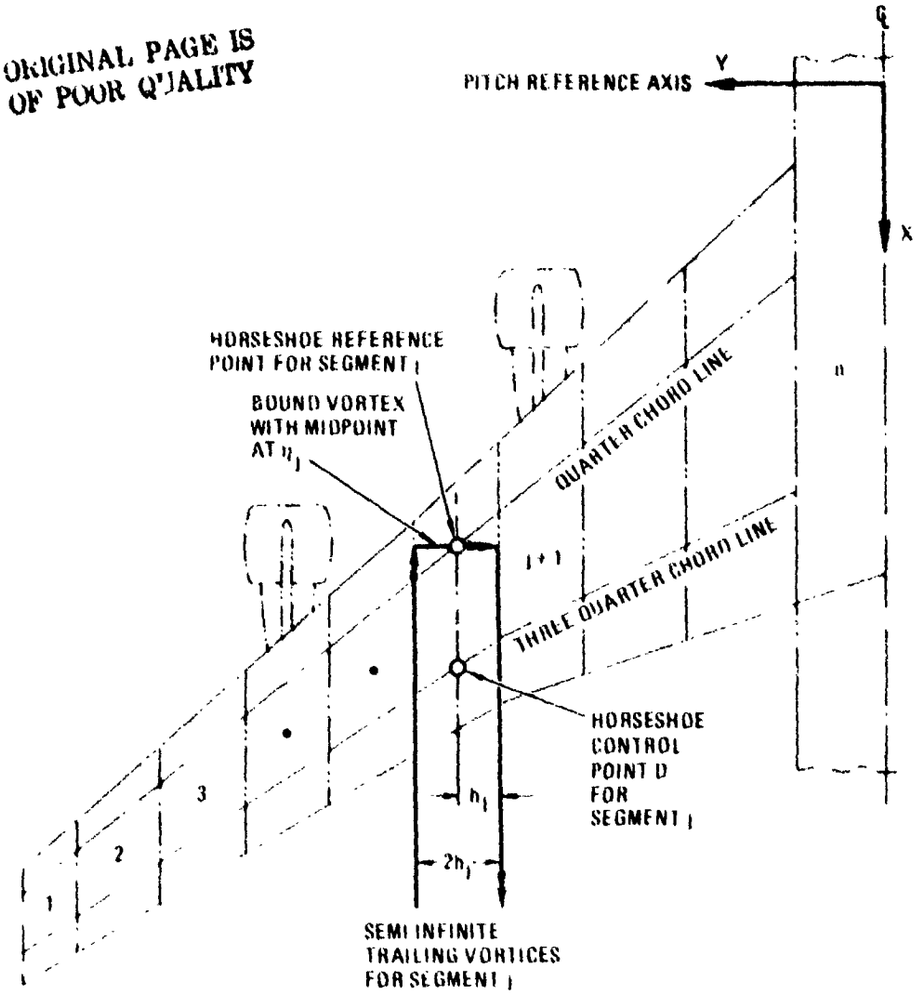

Figure 7-2 Typical Vortex Locations and Locations of Pertinent Points on an Arbitrary Wing Plan Form

properties associated with a section at the center of the slice. The problem is now to develop a series of equations that relate the spanwise lift distribution to the properties and attitude of the individual sections that form the wing.

If the two-dimensional wing section is considered first, the following relationships for lift and downwash behind an airfoil are available from most standard textbooks on aerodynamics:

Kutta-Joukowsky Relationship

$$\ell = \rho V \Gamma \tag{1}$$

where:

$$\Gamma = \int w_r \, ds \quad \text{circulation} \tag{1a}$$

ρ = fluid density

V velocity

$$\ell = \text{span loading} \quad m_o \rho \alpha_f \frac{V^2}{2} c \tag{2}$$

$$w_r = \frac{\Gamma}{2\pi r} \tag{3}$$

The circulation Γ is taken to be such that, at a specified distance r behind the lifting line, the resultant of the downwash velocity w_r and the flight velocity V is parallel to the section zero-lift line; that is, no flow exists normal to the zero-lift line at this point. Then

$$\frac{w_r}{V} = \alpha_f \tag{4}$$

and from equations (1) and (2),

$$\Gamma = m_o \alpha_f \frac{V}{2} c \tag{5}$$

Substituting equation (5) into equation (3) results in:

$$w_r = \frac{m_o \, c/2}{2\pi \, r} \alpha_f V \tag{6}$$

or

$$\frac{w_r}{V} = \frac{m_o}{2\pi} \frac{c/2}{r} \alpha_f \tag{7}$$

In order to satisfy equation (4), the expression $\frac{m_o}{2\pi} \frac{c/2}{r}$ in equation (7) must be equal to 1.0. Since the theoretical section two-dimensional lift-curve slope is equal to 2π, r must equal c/2, which is the distance between the lifting line and the three-quarter-chord point.

In the development of the method presented in this report, equation (7) is always used in the form:

$$\left(\frac{w}{V}\right)_{3c/4} = \frac{m_o}{2\pi}\alpha_f \tag{8}$$

This simplification requires that the section lift-curve slope m_o be the two-dimensional value (i.e., the value of the lift-curve slope for an unswept two-dimensional wing) and that the location of the downwash control point D (see Figure 7-2) be one-half of the local streamwise chord to the rear of the quarter-chord point, or at 3c/4.

The essential difference between a two-dimensional wing and a wing of finite aspect ratio arises from the nonuniform spanwise loading that produces the trailing vortices of the finite-aspect-ratio wing. The equations presented thus far are considered to apply to the finite-aspect-ratio wing when the effects of all the vortices, both bound and trailing, have been taken into account. The starting vortex is, however, ignored.

Equation (8) in matrix form is:

$$\left\{\frac{w}{V}\right\}_{3c/4} = \left[\frac{m_o}{2\pi}\right]\{\alpha_f\} \tag{9}$$

This matrix relation represents a series of equations, each applicable to a particular station on the semispan of the wing. The values of $\left(\frac{w}{V}\right)_{3c/4}$, every one of which is affected by the bound and trailing vortices at all of the wing stations, can be evaluated from:

$$\left\{\frac{w}{V}\right\}_{3c/4} = \frac{1}{4\pi V}[S_1]\{\Gamma\}$$

which, in combination with equation (1), results in:

$$\left\{\frac{w}{V}\right\}_{3c/4} = \frac{1}{8\pi q}[S_1]\{\ell\} \tag{10}$$

or

$$= \frac{1}{8\pi}[S_1]\{c_\ell c\} \tag{10a}$$

The $[S_1]$ matrix in these equations is the aerodynamic influence matrix, which is derived in Section 7.1.2.

Combining Equations (9) and (10) gives:

$$\left\{\frac{w}{V}\right\}_{3c/4} = \frac{1}{8\pi q}[S_1]\{\ell\} = \left[\frac{m_o^o}{2\pi}\right]\{\alpha_f\} \tag{11}$$

$$\left[\frac{1}{4qm_o^o}\right][S_1]\{\ell\} = \{\alpha_f\} \tag{12}$$

or

$$\left[\frac{1}{4m_o^o}\right][S_1]\{c_\ell c\} = \{\alpha_f\} \tag{12a}$$

The series of equations represented by the matrix equation (12) expresses, for any given dynamic pressure, the relationship between the spanwise variation of running lift $\{\ell\}$, the final section angles of attack $\{\alpha_f\}$, and the spanwise variation of the two-dimensional section lift-curve slope $[m_o^o]$. The effects of wing plan-form geometry are accounted for through the elements of the $[S_1]$ matrix. The section lift-curve slope is expressed in the general form, m_o, to permit substitution of actual values when available from scaled-model tests or to permit correction for compressibility effects as described in Section 7.1.8.

The final angle-of-attack variation across the span $\{\alpha_f\}$ can be considered to be composed of three essential parts (see Figure 7-3).

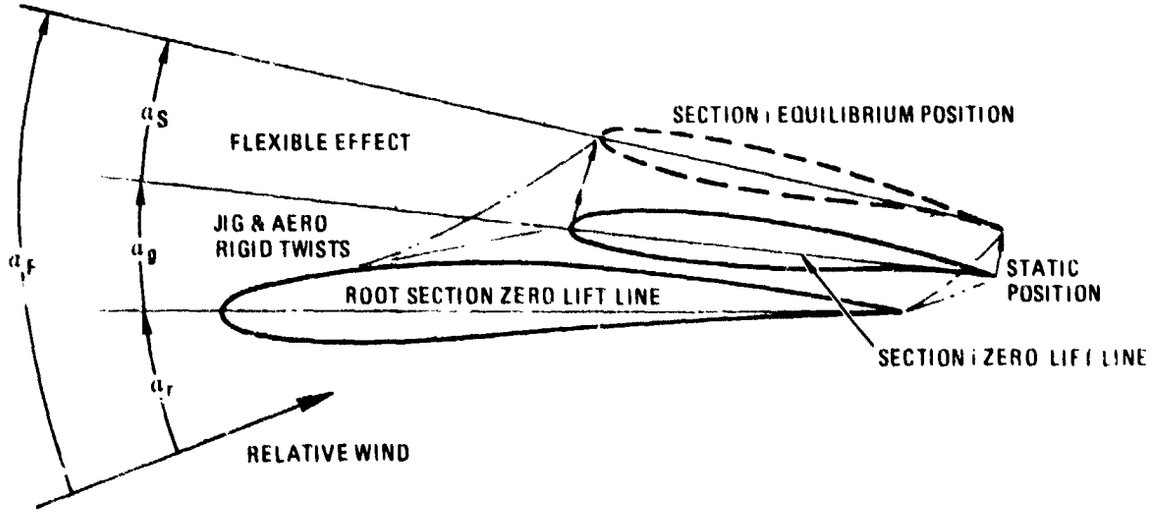

Figure 7-3 Angle-of-Attack Definitions and Sign Convention

$$\{\alpha_f\} = \{\alpha_r\} + \{\alpha_g\} + \{\alpha_s\} \tag{13}$$

For a wing free of external stores, the $\{\alpha_s\}$ component of the angle of attack caused by structural deflection of a flexible wing due to the section lifts acting at the section aerodynamic centers is linearly related to the matrix $\{\ell\}$ by an expression derived in Section 7.1.3, as:

$$\{\alpha_s\} = [S_2]\{\ell\} \tag{14}$$

The wing geometry and stiffness are accounted for in the structural influence matrix $[S_2]$. This matrix is based on loadings associated with stations that are parallel to the airplane plane of symmetry.

The $\{\alpha_g\}$ component of $\{\alpha_f\}$ is composed of built-in (jig) twist, apparent or aerodynamic twists such as those due to interference, control deflection, and angular velocities, and all structural twists of an elastic wing that are not accounted for in the $\{\alpha_s\}$ matrix.

Although equation (12) is general, it is not useful in the form given for determining the lift distribution on a flexible wing since a component of the $\{\alpha_f\}$ matrix is itself a function of the lift. If $\{\alpha_s\}$ is therefore expressed as in equation (14), equations (12) and (13) may be combined so as to express the load distribution on a flexible wing in terms of wing root angle of attack $\{\alpha_r\}$ and any combination of the $\{\alpha_g\}$ twists as:

$$\left[\left[\frac{o}{4qm_o}\right][S_1] - [S_2]\right]\{\ell\} = \{\alpha_r\} + \{\alpha_g\} \tag{15}$$

By considering the airplane to be in equilibrium as regards vertical forces and pitching moments, two additional equations may be written as:

$$2[2h]\{\ell\} + P_T - n_z W = 0 \tag{16}$$

for equilibrium of vertical forces, and

$$-2[2hx]\{\ell\} + 2q[2hc^2]\{cm_o\} - P_T x_T + n_z W x_A = 0 \tag{17}$$

for equilibrium of pitching moments about the pitch axis.

Equations (15), (16), and (17) are the basic equations for a flexible wing airplane. They may be solved simultaneously for the spanwise variation of running lift $\{\ell\}$, the root section angle of attack, α_R, and the balancing tail load, P_T, as functions of any design values of speed, gross weight and load factor.

These basic equations have been altered to include: 1) the effects of forces on the fuselage; 2) the effects of forces on external stores; 3) the interference effects on the exposed wing loading due to the presence of the fuselage and external stores; and 4) the effect of pitching acceleration. The altered equations are presented as equations (18), (19), and (20). These are the equations used by the program to perform the aeroelastic solution of the wing and fuselage with external stores. The additional terms, which appear in these equations, are derived in following sections.

The unknowns, which are solved for simultaneously in the symmetric aeroelastic equations (18), (19), and (20), are the loading distribution $\{c_\ell c\}$ at each strip, the wing root angle of attack α_r, and the balancing tail load p_T.

Angle of Attack at Each Strip

$$\{\alpha_f\} = (\alpha_r) + \{\alpha_g\} + \{\alpha_s\} \tag{18}$$

where:

$$\{\alpha_f\} = \left[[I] - qS\,[E_\alpha] + \left[\frac{\Delta V_z}{V_z}\right]\right] \times \left[\frac{1}{4m_o}\right] \times \left[[S_1] + [S_f]\right] \times \{c_\ell c\}$$

$$\{\alpha_s\} = \int_o^\eta \frac{m\,M\,ds}{EI} + \int_o^\eta \frac{t\,T\,ds}{GJ} = q\,[S_2] \times \{c_\ell c\}$$

$$\{\alpha_g\} = \left[\frac{\Delta V_z}{V_z}\right] \times (\alpha_r) + \alpha_\tau + (\alpha_{oL_{root}}) - \left\{\alpha_{oL_{sect}}\right\}$$

$$+\left(\left(\alpha_{inc_{fus}}\right) + \left(\alpha_{oL_{root}}\right)\right)\left[\frac{\Delta V_z}{V_z}\right]\left\{\frac{\alpha_{oL_{body\ sect}} + \alpha_{inc_{body}}}{\alpha_{oL_{root}} + \alpha_{inc_{fus}}}\right\} + \left\{\frac{\alpha}{\delta_{fl}}\right\}\delta_{fl} + \left\{\frac{\alpha}{\delta_{sp}}\right\}\delta_{sp}$$

$$+ \left\{\frac{\alpha}{\delta_{sl}}\right\}\delta_{sl} + \left\{\alpha_{g_{II}}\right\}$$

$$\left\{\alpha_{g_{II}}\right\} = qS\left\{[E_o]'\right.$$

$$\left. + [m]\left[\frac{2h}{\cos\Lambda}\right]\left[\frac{1}{EI}\right]\left\{-n_z\left\{\frac{M_{ea}}{n_z}\right\} - \ddot{\theta}\left\{\frac{M_{ea}}{\ddot{\theta}}\right\} + 2q\,[CMS]\left\{C_{m_{O_T}}\right\}\right\}\right.$$

$$+ [t] \left[\frac{2h}{\cos\Lambda}\right]^{o} \left[\frac{1}{GJ}\right]^{o} \left\{ n_z \left\{\frac{T_{ea}}{n_z}\right\} + \ddot{\theta} \left\{\frac{T_{ea}}{\ddot{\theta}}\right\} + 2q\,[CTS] \left\{C_{m_{O_T}}\right\} \right\}$$

and

$$[CMS] = \begin{bmatrix} \cdot c_1^2 h_1 (\sin \Lambda_1)/2 & 0 & 0 \\ -c_1^2 h_1 \sin \Lambda_2 - c_2^2 h_2 (\sin \Lambda_2)/2 & & 0 \\ \vdots & \ddots & \\ -c_1^2 h_1 \sin \Lambda n & & -c_n^2 h_n (\sin \Lambda_n)/2 \end{bmatrix}$$

$$[CTS] = \begin{bmatrix} c_1^2 h_1 (\cos \Lambda_1)/2 & 0 & 0 \\ c_1^2 h_1 \cos \Lambda_2 \; c_2^2 h_2 (\cos \Lambda_2)/2 & & 0 \\ \vdots & \ddots & \\ c_1^2 h_1 \cos \Lambda n & & c_n^2 h_n (\cos \Lambda_n)/2 \end{bmatrix}$$

Vertical Force on Both Wings

$$\underline{\text{wings}}$$
$$4\,|qh| \times \{c_\ell c\} + 2qS \sum_1^n \left(C_{L_{E_\alpha}}\right)_n \times \underline{\text{stores}} \left[\frac{1}{4m_o}\right] \times [S_1 + S_f] \times \{c_\ell c\} + \underline{\text{fuselage}} \; qSC_{L_{F_\alpha}} \alpha_r + \underline{\text{tail}} \; P_T$$

$$= \underline{\text{inertia}} \; n_z W - qS\left(C_{L_{F_o}} + C_{L_{F_\alpha}} \left(\alpha_{\substack{\text{inc} \\ \text{fus}}} + \alpha_{\substack{\text{oL} \\ \text{root}}}\right)\right) - \underline{\text{fuselage}} \; 2qS \sum_1^n \left(C_{L_{E_o}}\right)_n \underline{\text{stores}} \qquad (19)$$

Moments on Both Wings at $\bar{c}/4$

$$-4\,|qh|\,(XC4-\bar{X}C4)\,\{c_\ell c\} - 2\,qS\sum_1^n \Bigg[\underbrace{\left(C_{L_{E_\alpha}}\right)_n}_{\text{wings}}(XE-\bar{X}C4) + \underbrace{\left(C_{D_{E_\alpha}}\right)_n}_{\text{stores}}(\bar{Z}C4-ZE)$$

$$-\bar{c}\left(C_{M_{E_\alpha}}\right)_n\Bigg]\times\left[\frac{1}{4\,m_o}\right]\times\,[S_1+S_f]\times\{c_\ell c\} + qS\Bigg(\underbrace{C_{L_{F_\alpha}}}_{\text{fuselage}}(\bar{X}C4-Xfus) + C_{M_{F_\alpha}}\bar{c}$$

$$-\underbrace{C_{L_{\alpha_{tail}}}\left(1-\frac{d\epsilon}{d\alpha}\right)(XDE)}_{\text{tail}}\Bigg)\times\alpha_r - \underbrace{(X\,tail-XC4-XDE)\times P_T}_{\text{tail}} =$$

$$\underbrace{I_Y\ddot{\theta}}_{\text{inertia}} - n_z\,W\,(XCG-\bar{X}C4) - 4q\,[hc^2]\underbrace{\left\{C_{m_o}\right\}}_{\text{wing }C_{m_o}}$$

$$+\,qS\Bigg(C_{L_{F_o}} + \underbrace{\left(C_{L_{F_\alpha}}\right)\left(\alpha_{\substack{inc\\fus}} + \alpha_{oL_{root}}\right)}_{\text{fuselage}}\Bigg)\times(Xfus-\bar{X}C4)$$

$$-qS\Bigg(C_{M_{F_o}} + \underbrace{\left(C_{M_{F_\alpha}}\right)\left(\alpha_{\substack{inc\\fus}} + \alpha_{oL_{root}}\right)}_{\text{fuselage}}\Bigg)\bar{c} + \Delta C_{D_{fus}}\underbrace{(\bar{Z}C4-ZCD_{fus})}_{\text{fus drag}}$$

$$+\,\Delta C_{D_{tail}}\underbrace{(\bar{Z}C4-ZCD_{tail})}_{\text{tail drag}} + 2\,qS\sum_1^n\Bigg(\left(C_{L_{E_o}}\right)_n(XE-\bar{X}C4) - \left(C_{M_{E_o}}\right)_n\bar{c}$$

$$+\left(\Delta C_{D_E}\right)_n(\bar{Z}C4-ZE)\Bigg) + qS\,\underbrace{C_{L_{\alpha_{tail}}}\times\alpha_{\substack{inc\\tail}}}_{\text{tail}}\times XDE \qquad (20)$$

The method outlined in this report includes several items that are of practical interest in the design of a wing for aeroelastic effects and sufficiently extensive in scope that almost any type of airplane configuration may be considered. The program runs sufficiently fast to be useful both in preliminary design studies and is as accurate as the input data for final design.

Matrix formulation of the problem has particular merit for such a general treatment since discontinuities in angles or masses due to either special aerodynamic or structural features can readily be included.

For these reasons only a few general guides, which might be considered for successful application of the method, are given.

For m_0 equal to 2π, equation (12) will give essentially the same results as those given by the Weissinger L-method of Reference 8, which is valid for wings of arbitrary plan form and having flat-plate, circular-arc, or parabolically cambered airfoil sections (References 9, 10, and 11).

The treatment of compressibility effects used in this report, wherein each wing section is permitted to have its own compressibility correction, differs from the Prandtl-Glauert method in that the wing plan form is not distorted; instead, the angles of attack are altered as indicated by equation (11). The treatment adopted has the merit of considerable saving in time for equal or better accuracy since only one $[S_1]$ matrix is required for all Mach numbers. The methods of obtaining compressible values of m_0 are described in Section 7.1.8.

7.1.2 Aerodynamic Influence Matrix. The derivation of the aerodynamic influence matrix $[S_1]$ proceeds as follows:

Biot-Savart Law of Vorticity

This law was applied to the bound vortex and the trailing vortices at each wing strip to calculate the aerodynamic influence functions:

$$w_p \quad \frac{\Gamma(\cos\alpha - \cos\beta)}{4\pi R}$$

where α and β are the angles between the direction of the vortex segment and lines joining the ends of the segment to the control point (Figure 7-4). The control point in this theory is located at the 0.75c location of each strip. w_p is the velocity induced normal to the plane of the wing.

A plane view of the geometry of a typical horseshoe vortex on the left-hand wing is given in Figure 7-5, in which distances and angles are considered positive as indicated

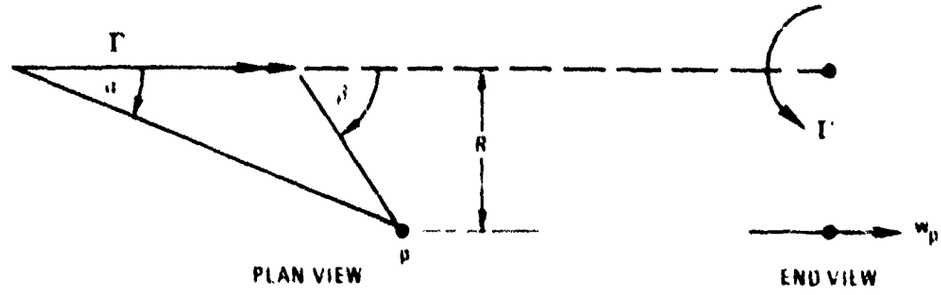

Figure 7-4 Definition of Vortex Segment Angles

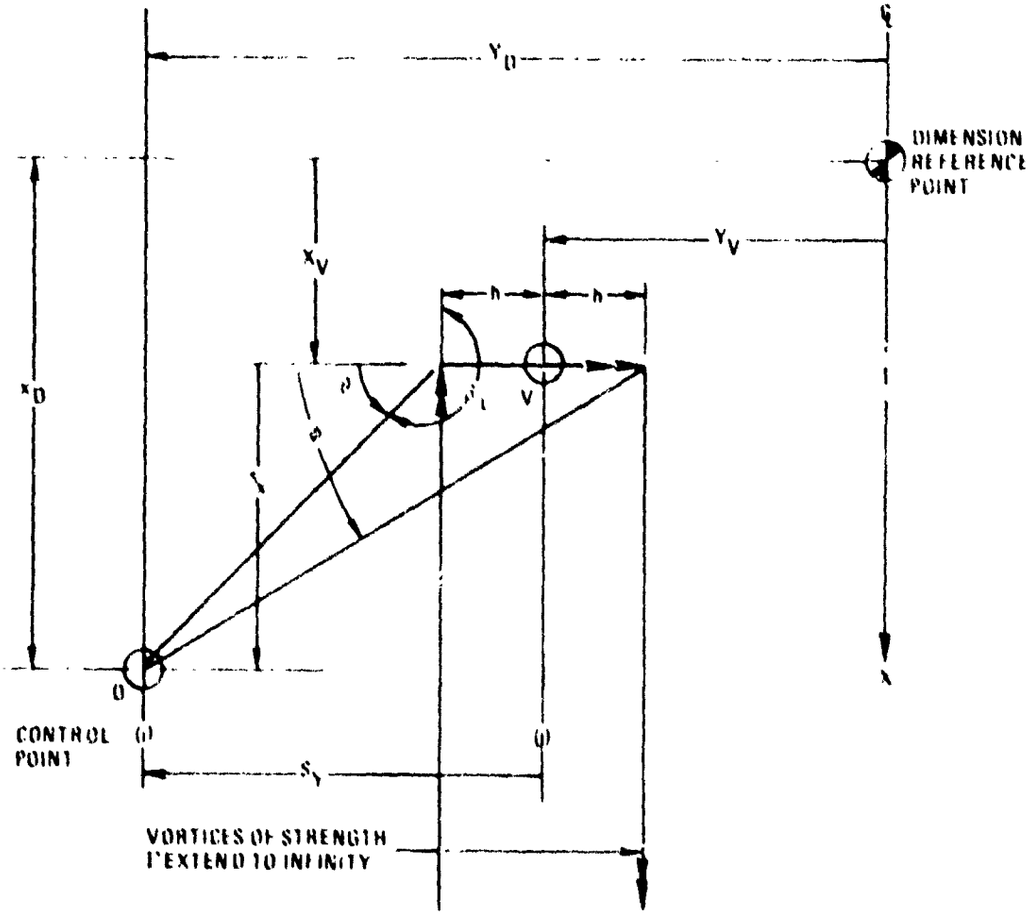

Figure 7-5 Plan View Geometry for Typical Horseshoe Vortex

and the sense of the circulation of the elements of the horseshoe vortex is given by the right-hand moment rule.

The points V and D are a typical horseshoe reference point and a typical control point, respectively. In the program, the subscript i is used for point D and subscript j for point V.

The incremental downwash velocities induced by a single horseshoe vortex, if downwash velocities are considered as positive, are:

(1) For the left-hand trailing vortex the relations:

$$R = -(s_y - h)$$

TAIL: $\alpha = 0°$ at $-\infty$ $\quad \cos\alpha = 1$

NOSE: $\beta = 270° - \theta$ $\quad \cos\beta = -\sin\theta$

are substituted into the general relation

$$w_L = \frac{\Gamma(\cos\alpha) - (\cos\beta)}{4\pi R}$$

to obtain the incremental downwash velocity

$$w_L = \frac{\Gamma(1 + \sin\theta)}{4\pi (s_y - h)}$$

(2) From the right-hand trailing vortex where

$$R = s_y + h$$

TAIL: $\alpha = 90° - \phi$ $\quad \cos\alpha = \sin\phi$

NOSE: $\beta = 180°$ at $+\infty$ $\quad \cos\beta = -1$

the incremental downwash velocity is:

$$w_R = \frac{\Gamma(\sin\phi + 1)}{4\pi (s_y + h)}$$

(3) From the bound vortex where

$$R = s_x$$

TAIL: $\alpha = 180° - \theta$ $\quad \cos\alpha = -\cos\theta$

NOSE: $\beta = 180° - \phi$ $\quad \cos\beta = -\cos\phi$

the incremental downwash velocity is:

$$w_B = \frac{\Gamma (\cos \delta - \cos \theta)}{4\pi s_x}$$

The total downwash velocity at a typical control point due to a complete single horseshoe is then:

$$w = w_L + w_R + w_B$$

$$\frac{\Gamma}{4\pi}\left(-\frac{1+\sin\theta}{s_y - h} + \frac{1+\sin\delta}{s_y + h} + \frac{\cos\delta - \cos\theta}{s_x}\right)$$

Substitution of the identities

$$s_y - h = \frac{s_x \cos\theta}{\sin\theta}$$

$$s_y + h = \frac{s_x \cos\delta}{\sin\delta}$$

into the preceding equation yields:

$$w = \frac{\Gamma}{4\pi s_x}\left(\frac{1+\sin\delta}{\cos\delta} - \frac{1+\sin\theta}{\cos\theta}\right)$$

As indicated in Figure 7-6 the control points are assumed to be located on the left semispan of the wing so that θ_L and δ_L represent the pertinent angles for a horseshoe located on the left semispan and θ_R and δ_R represent the pertinent angles for the corresponding horseshoe on the right semispan, then for a typical control point

$$K_L = \frac{1}{4\pi s_x}\left(\frac{1+\sin\delta_L}{\cos\delta_L} - \frac{1+\sin\theta_L}{\cos\theta_L}\right)$$

$$K_R = \frac{1}{4\pi s_x}\left(\frac{1+\sin\delta_R}{\cos\delta_R} - \frac{1+\sin\theta_R}{\cos\theta_R}\right)$$

$$k = 4\pi (K_L + K_R)$$

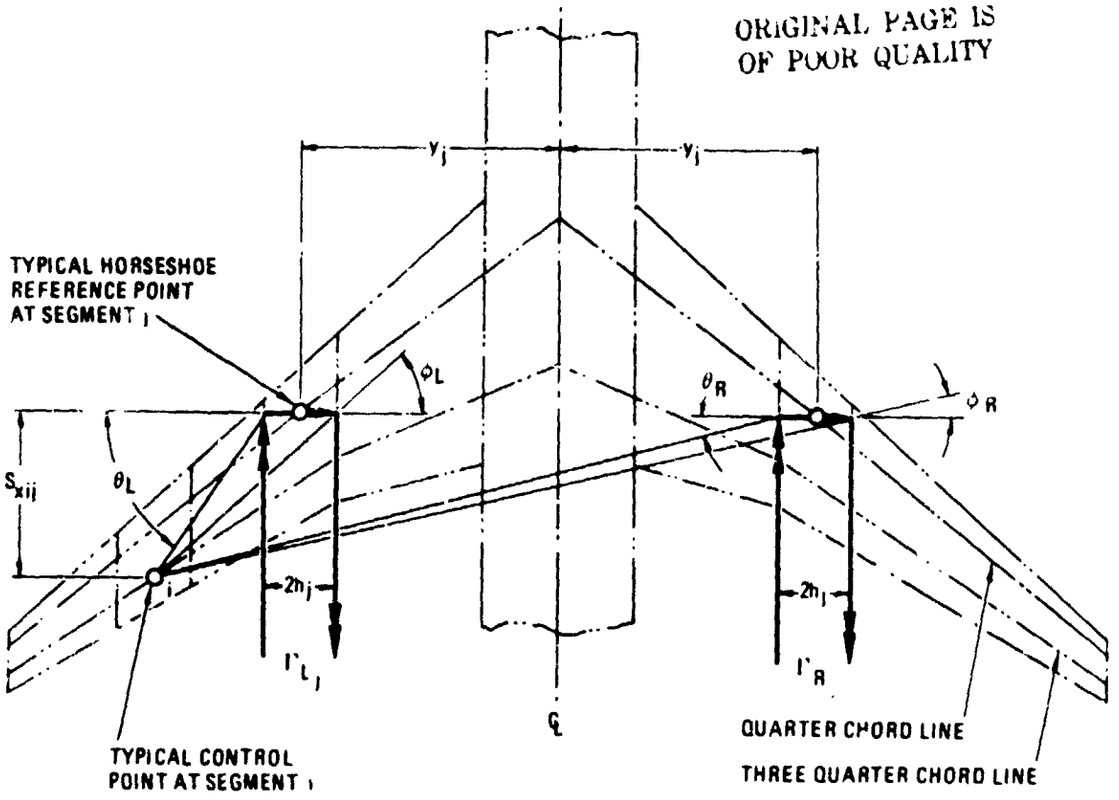

Figure 7-6 Typical Horseshoe Vortex Control Points

so that in the $[S_1]$ or downwash matrix each element k is computed from the equation:

$$k \quad \frac{1}{s_x}\left(\frac{1+\sin\phi_L}{\cos\phi_L} - \frac{1+\sin\theta_L}{\cos\theta_L} + \frac{1+\sin\phi_R}{\cos\phi_R} \mp \frac{1+\sin\theta_R}{\cos\theta_R}\right)$$

The upper sign is to be used for symmetrical spanwise airload distributions, and the lower sign can be used for antisymmetrical spanwise airload distributions. Note that

$$\sin\phi = \frac{x_D - x_V}{\sqrt{\left(x_D - x_V\right)^2 + \left(y_D - y_V + h\right)^2}}$$

$$\cos\phi = \frac{y_D - y_V + h}{\sqrt{\left(x_D - x_V\right)^2 + \left(y_D - y_V + h\right)^2}}$$

$$\sin \vartheta = \frac{x_D - x_V}{\sqrt{\left(x_D - x\right)^2 + \left(y_D - y_V - h\right)^2}}$$

$$\cos \theta = \frac{y_D - y_v - h}{\sqrt{\left(x_D - x_v\right)^2 + \left(y_D - y_V - h\right)^2}}$$

The $[S_1]$ matrix therefore is computed from the matrix equation, since $[S_1]$ is equal to $[k_{ij}]$.

$$[S_1] = \left[\frac{1}{s_x}\left(\frac{1 + \sin \phi_L}{\cos \phi_L} - \frac{1 + \sin \theta_L}{\cos \theta_L} \pm \frac{1 + \sin \phi_R}{\cos \phi_R} \mp \frac{1 + \sin \theta_R}{\cos \theta_R}\right)\right]$$

where the upper sign is used for symmetric flight conditions and the lower sign can be used for antisymmetrical conditions.

$$X_i = x_i + 1/2\ c_i$$

$$Sx_{ij} = X_i - x_j$$

$$\text{Sin } \phi_L = (X_i - x_j)/[(X_i - x_j)^2 + (y_i - y_j + h_j)^2]^{1/2}$$

$$\text{Sin } \phi_R = (X_i - x_j)/[(X_i - x_j)^2 + (y_i + y_j + h_j)^2]^{1/2}$$

$$\text{Cos } \phi_L = (y_i - y_j + h_j)/[(X_i - x_j)^2 + (y_i - y_j + h_j)^2]^{1/2}$$

$$\text{Cos} \phi_R = (y_i + y_j + h_j)/[(X_i - x_j)^2 + (y_i + y_j + h_j)^2]^{1/2}$$

$$\text{Sin } \theta_L = (X_i - x_j)/[(X_i - x_j)^2 + (y_i - y_j - h_j)^2]^{1/2}$$

$$\text{Sin } \theta_R = (X_i - x_j)/[(X_i - x_j)^2 + (y_i + y_j - h_j)^2]^{1/2}$$

$$\text{Cos } \theta_L = (y_i - y_j - h_j)/[(X_i - x_j)^2 + (y_i - y_j - h_j)^2]^{1/2}$$

$$\cos\theta_R \quad (y_i + y_j - h_j)\left[(X_i - x_j)^2 + (y_i - y_j - h_j)^2\right]^{-1/2}$$

Digital programming makes extensive use of integer subscripts (alphabetic characters i through n) in performing repeated operations. For comparison with the text, the following identities are stated:

$$x_D \quad X_i$$

$$x_V \quad x_j$$

$$y_D \quad y_i$$

$$y_V \quad y_j$$

$$h \quad b_j$$

$$s_x \quad S_{x_{ij}}$$

where the jth station produces the effect and the ith station is the location where the effect of the jth station is being calculated.

Since the $[S_1]$ matrix is used in equation (12):

$$[S_1]\{\ell\} \quad \left[4q m_\infty^{\circ}\right]\{\alpha_i\}$$

the elements of the $[S_1]$ matrix are seen to be influence coefficients relating the incremental downwash angle at each control point to the intensity of the running lift over each increment of the semispan of the wing. In general, all the elements in the principal diagonal of the $[S_1]$ matrix will always be positive and those elements not in the principal diagonal will always be negative because the velocities were considered as positive downward and wash velocities from a horseshoe vortex are downward only in the region behind the bound vortex and between the trailing vortices of that horseshoe.

7.1.3 Structural Influence Matrix $[S_2]$. The structural influence matrix relates the deformation of the structure to the bending and torsional stiffness properties and to the applied bending and torsional moments. It is derived by an application of Castigliano's theorem.

A part of the general Castigliano Theorem was used that related the twisting of a structure to the applied bending and torsional moments by means of virtually applied moments. Structural properties are represented by the EI and GJ terms.

$$\alpha_s = \int \frac{m\ M\ ds}{EI} + \int \frac{t\ T\ ds}{GJ}$$

where:

α_s = Elastic angle of attack change due to bending and torsional moments (M, T) along the elastic axis resulting from the series of loads $\{L\}$

m = Beam bending moment per unit pitching moment applied at the station at which α_s is to be determined

t = Torsional moment around the elastic axis per unit pitching moment

ds = Incremental distance along elastic axis

EI = Effective beam stiffness around the axis of the bending moments M and m

GJ = Effective torsional stiffness around the axis of the torsional moments T and t

The stations on the wing for which the angle-of-attack changes α_s are to be computed are those on the centerline of each horseshoe vertex.

The above equation can be written in matrix form as:

$$\{\alpha_s\} = [m]\left[\frac{2h}{\cos \Lambda}\right]\left[\frac{1}{EI}\right]\{M\} + [t]\left[\frac{2h}{\cos \Lambda}\right]\left[\frac{1}{GJ}\right]\{T\}$$

The elements of [m] and [t] are:

$m_{ij} = 0$ for $i > j$

$m_{ij} = -(\sin \Lambda_j)/2$ for $i = j$

$m_{ij} = -\sin \Lambda_j$ for $i < j$

$t_{ij} = 0$ for $i > j$

$t_{ij} = (\cos \Lambda_j)/2$ for $i = j$

$t_{ij} = \cos \Lambda_j$ for $i < j$

where the rows are designated in the program by i and the columns by j.

At the nth strip, the general form for the wing lift is:

$$L_n \quad 2\, h_n \ell_n$$

where ℓ_n is the magnitude of the loading and $2\, h_n$ is the span of the strip.

The general form of the bending and torsion moments are:

$$M_n = M_{x_n} \cos \Lambda_n - M_{y_n} \sin \Lambda_n$$

$$T_n \cdot M_{y_n} \cos \Lambda_n + M_{y_n} \sin \Lambda_n$$

where M_{x_n} rolling moment at the elastic axis point around the longitudinal axis through the local elastic axis reference point due to the total lift of all vortices outboard of this point. M_{y_n} pitching moment at the elastic axis point around the lateral axis through the local elastic-axis reference point due to the total lift of all vortices outboard of this point.

The following equations are developed with the aid of the geometry depicted in Figure 7-7.

$$\{M\} \quad \left[\left[\cos^{o} \Lambda\right] \left[r_1\right] - \left[\sin^{o} \Lambda\right] [u]\right] \{L\}$$

$$\{T\} \quad \left[\left[\sin^{o} \Lambda\right] \left[r_2\right] + \left[\cos^{o} \Lambda\right] [u]\right] \{L\}$$

where the elements of diagonal matricies $[\cos^{o} \Lambda]$ and $[\sin^{o} \Lambda]$ are given by

$$(\cos \Lambda)_{ij} \quad \begin{matrix} \cos (\Lambda_i) & \text{for } i \quad j \\ 0 & \text{for } i \neq j \end{matrix}$$

$$(\sin \Lambda)_{ij} \quad \begin{matrix} \sin (\Lambda_i) & \text{for } i \quad j \\ 0 & \text{for } i \neq j \end{matrix}$$

elements of the matrix [u] are given by

$$U_{ij} = \quad 0 \qquad \text{for } i \leq j$$

$$\cdot \; e_j - \sum_{k}^{i-1} \ell_k \qquad \text{for } i > j$$

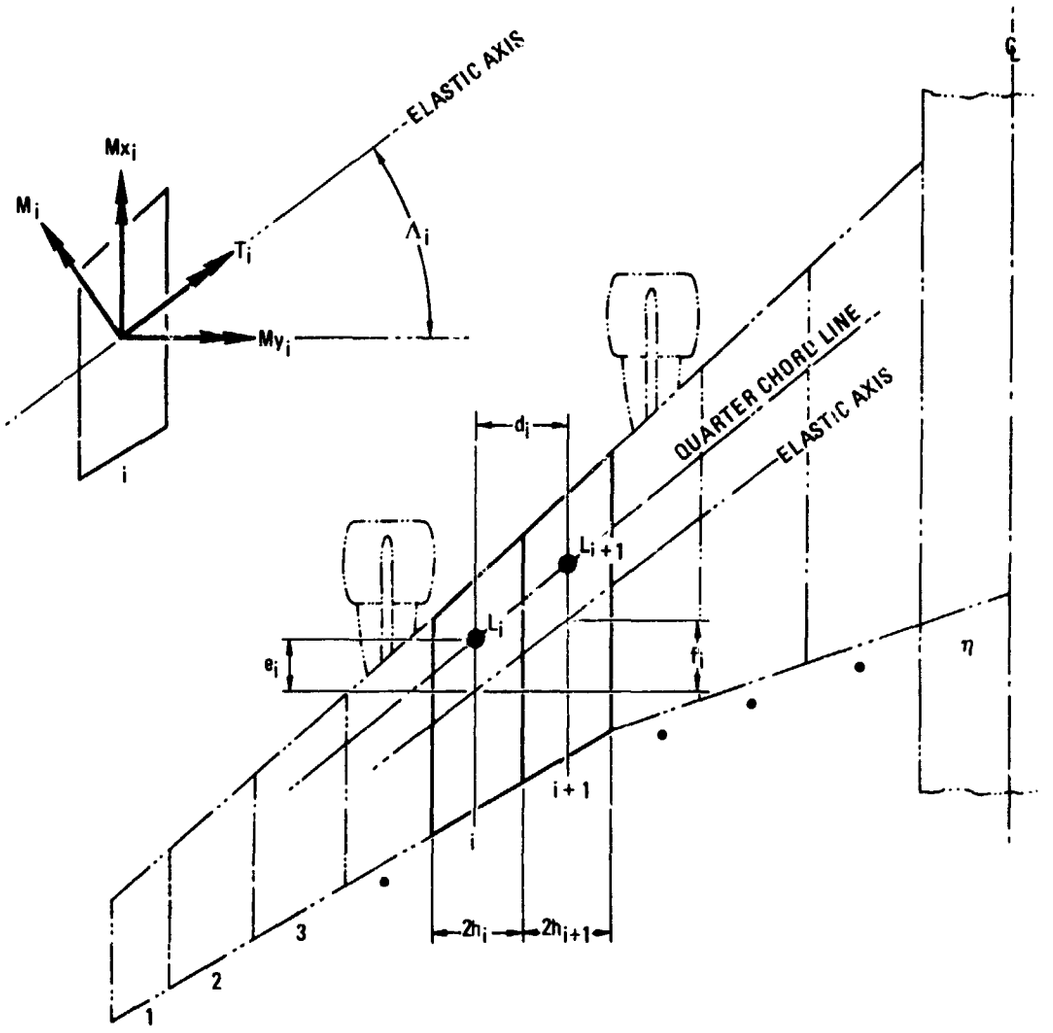

Figure 7-7 Wing Segment Geometry and Moment Sign Convention

and the elements of $[r_1]$ and $[r_2]$ are given by

$$(r_1)_{ij} = \frac{h_i}{4\cos^2(\Lambda i)} - \frac{e_i \tan(\Lambda i)}{2} \qquad \text{for } i = j$$

$$(r_2)_{ij} = \frac{e_i}{2\tan(\Lambda i)} \qquad \text{for } i = j$$

$$(r_1)_{ij} = (r_2)_{ij} = 0 \qquad \text{for } i < j$$

$$= \sum_{k=j}^{i-L} d_k \qquad \text{for } i > j$$

If we let

$$[S_2] = [m]\left[\frac{2h}{\cos \Lambda}\right]\left[\frac{1}{EI}\right]\left[[\cos \Lambda]\,[r_1] - [\sin \Lambda]\,[u]\right][2h]$$

$$+ [t]\left[\frac{2h}{\cos \Lambda}\right]\left[\frac{1}{GJ}\right]\left[[\sin \Lambda]\,[r_2] + [\cos \Lambda]\,[u]\right][2h]$$

then

$$\{\alpha_s\} = [S_2]\,\{\ell\} - q\,[S_2]\,\{c_\ell c\}$$

Note that, except for the structural properties EI and GJ, all terms of $[S_2]$ are functions of geometry and station spacing.

This represents the most general form for the $[S_2]$ matrix, and each element a_{ij} of this matrix represents the angle-of attack change in radians at station i due to the structural deflection of the wing caused by a unit loading at station j. In effect, the $[S_2]$ matrix is an array of influence coefficients, and the elements of this matrix may be computed according to the above equation, or, when an actual wing is available, they may be obtained by load deflection tests of that wing.

7.1.4 Fuselage Image Vortex Matrix $[S_f]$. An image vortex system lies inside the fuselage. It was first considered in Reference 12. This image vortex system induces a flow that is a first approximation to that necessary to satisfy the condition that there be zero velocity normal to the fuselage.

The fuselage is assumed to be of circular cross section, of constant diameter, and infinitely long.

The individual images of the wing trailing vortices can be shown to be located on a straight line joining the axis of the fuselage with the axis of the particular wing trailing vortex at a distance, R_2, from the fuselage centerline such that:

$$R_2 \quad \frac{(RF)^2}{R_1}$$

where RF is the fuselage radius and R_1 is the distance from the fuselage axis to the trailing vortex.

Similarly, the bound vortices, connect to the trailing vortices in the transverse plane of the particular wing bound vortex being represented.

Here, again, the Biot-Savant Law of Vorticity is applied, but in a three-dimensional situation.

Figures 7-8 and 7-9 show the geometry of the left and right fuselage image vortices relative to the wing.

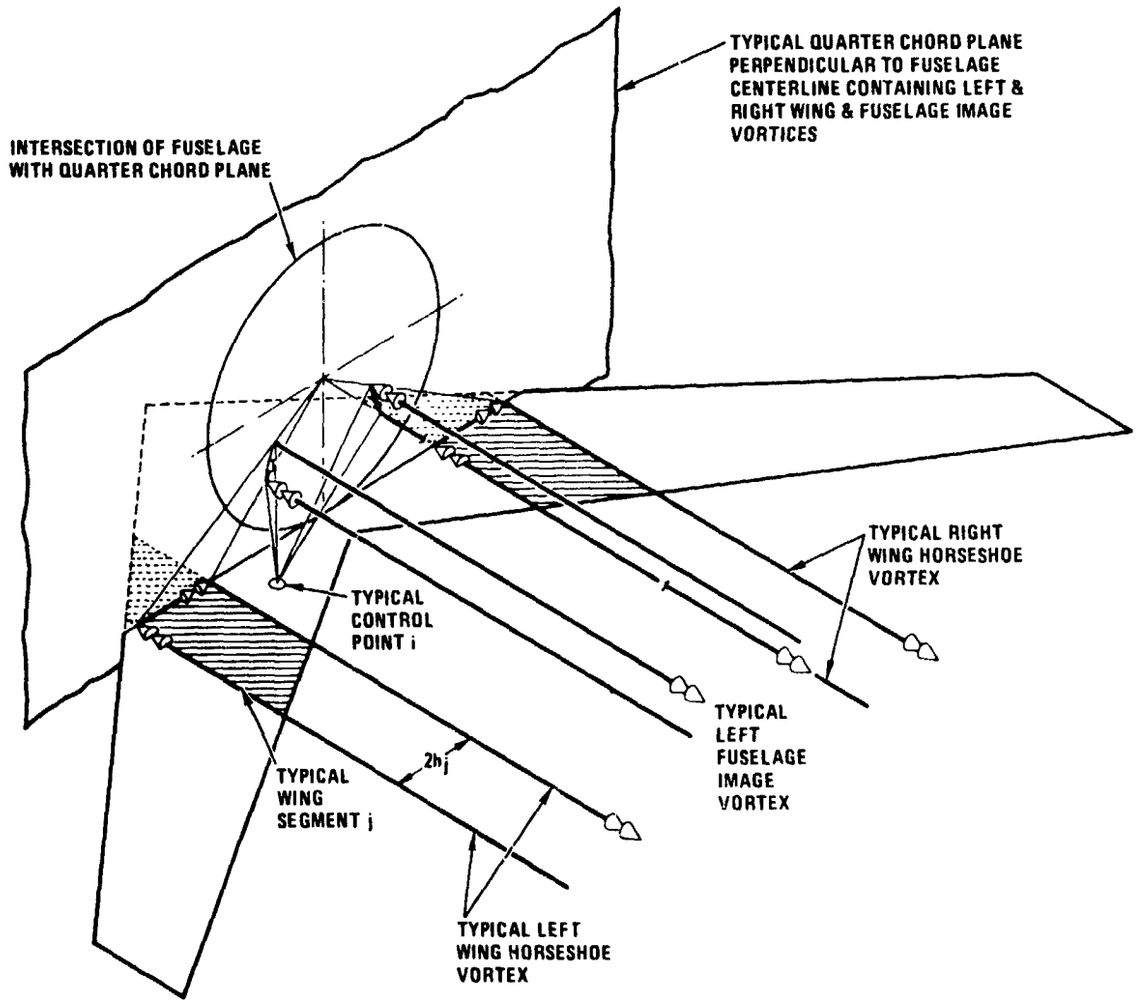

Figure 7-8 Typical Wing Strip Vortex System

Consider first the downwash on the ith control point of the left wing due to the fuselage image vortex caused by the jth vortex on the left wing. For the vortex elements $\infty a'$, $a'b'$, and $b'\infty$:

$$W_{\infty a'} = - (1 + \cos \lambda') (Y_i - Y_{a'})/(A')^2$$

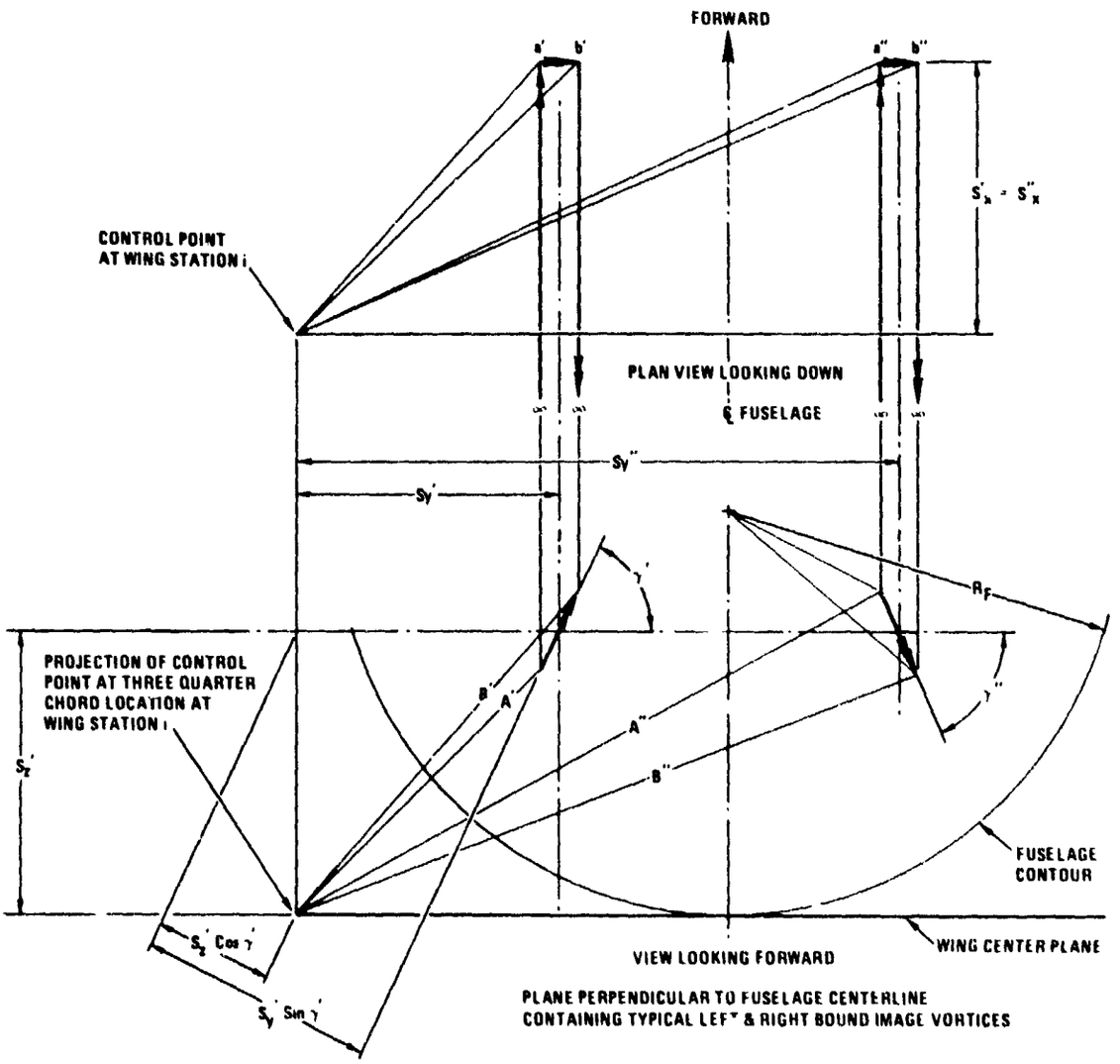

Figure 7-9 Fuselage Image Vortex Geometry

$$W_{a'b'} = (\cos\phi' - \cos\theta')\left(X_i + \frac{1}{2}C_i - X_j\right)\cos\gamma'/(D')^2$$

$$W_{b'\infty} = (1 + \cos\mu')(Y_i - Y'_b)/(B)^2$$

The combined effect is the sum of the elements.

$$(W')_{ij} = W_{\infty a'} + W_{a'b'} + W_{b'\infty}$$

Next, consider the downwash on the ith control point of the left wing due to the fuselage image vortex caused by the jth vortex on the right wing. The vortex elements are ∞a", a"b", and b"∞.

$$W_{\infty a''} = -(1 + \cos \lambda'')\,(Y_i + Y'_b)/(A'')^2$$

$$W_{a''b''} = (\cos \phi'' - \cos \theta'')\,(X_i + \frac{1}{2} C_i - X_j) \cos \gamma'/(D'')^2$$

$$W_{b''\infty} = (1 + \cos \mu'')\,(Y_i + Y_a')/(B'')^2$$

$$(W'')_{ij} = W_{\infty a''} + W_{a''b''} + W_{b''\infty}$$

The following geometric relations apply in solving the above equations.

$$Y_a'' = -Y_b'$$

$$Y_b'' = -Y_a'$$

$$Z_a'' = Z_b'$$

$$Z_b'' = Z_a'$$

$$\alpha' = \text{ARC TAN}\,(Z_j/(Y_j + h_j)),\ -\pi/2 < \alpha' < \pi/2$$

$$\beta' = \text{ARC TAN}\,(Z_j/(Y_j - h_j)),\ -\pi/2 < \beta' < \pi/2$$

$$R_{1a} = Z_j/\sin \alpha'_i$$

$$R_{1b} = Z_j/\sin \beta'_j$$

$$R_{2a}' = \frac{(RF)^2}{R_{1b}}$$

$$R_{2b}' = \frac{(RF)^2}{R_{1a}}$$

$$YAP = Y_a' = R_{2a}' \cos \beta'$$

$$ZAP = Z_a' = R_{2a}' \sin \beta'$$

$$YBP = Y_b' = R_{2b}' \cos \alpha'$$

$$Z_b' = R_{2b}' \sin \alpha'$$

$$(A')^2 = (Y_i - Y_a')^2 + (Z_i - Z_a')^2$$

$$(A'')^2 = (Y_i + Y'_b)^2 + (Z_i - Z_b')^2$$

$$(B')^2 = (Y_i - Y_b')^2 + (Z_i - Z_b')^2$$

$$(B'')^2 = (Y_i + Y_a')^2 + (Z_i - Z_a')^2$$

$$S_x' = S_x'' = X_i + \frac{1}{2} C_i - X_j$$

$$S_y' = Y_i - (Y_a' + Y_b')/2$$

$$S_y'' = Y_i + (Y_a' + Y_b')/2$$

$$\gamma' = -\gamma'' = \text{ARC TAN } \left[(Z_a' - Z_b')/(Y_a' - Y_b')\right], \; -\pi/2 < \gamma < \pi/2$$

Note that: $\cos \gamma'' = \cos \gamma'$

$$(D')^2 = (S_x')^2 + (S_y' \sin \gamma' - S_z' \cos \gamma')^2$$

$$(D'')^2 = (S_x')^2 - (S_y'' \sin \gamma' + S_z' \cos \gamma')^2$$

$$\cos \lambda' = S_x'/[(A')^2 + (S_x')^2]^{1/2}$$

$$\cos \lambda'' = S_x'/[(A'')^2 + (S_x')^2]^{1/2}$$

$$\cos \mu' = S_x'/[(B')^2 + (S_x')^2]^{1/2}$$

$$\cos \mu'' = S_x'/[(B'')^2 + (S_x')^2]^{1/2}$$

$$\cos \theta' = \left\{[(A')^2 + (S_x')^2 - (D')^2]/[(A')^2 + (S_x')^2]\right\}^{1/2}$$

$$\cos \theta'' = \left\{[(A'')^2 + (S_x')^2 - (D'')^2]/[(A'')^2 + (S_x')^2]\right\}^{1/2}$$

$$\cos \phi' = \left\{[(B')^2 + (S_x')^2 - (D')^2]/[(B')^2 + (S_x')^2]\right\}^{1/2}$$

$$\cos \phi'' = \left\{[(B'')^2 + (S_x')^2 - (D'')^2]/[(B'')^2 + (S_x')^2]\right\}^{1/2}$$

Finally

$$[S_f] \quad (w')_{ij} + (w'')_{ij}$$

The downwash on the wing due to the image vortex system in the fuselage becomes:

$$\left\{\frac{w}{V}\right\} = \frac{1}{4\pi V}[S_f]\{\Gamma\} \quad \frac{1}{4q(2\pi)}[S_f]\{\ell\}$$

$$= \frac{1}{4m_o}[S_f]\{c_\ell c\} \tag{12a}$$

7.1.5 External Stores Matrices $\{E_\alpha\}$ and $\{E_o\}$. The following equations are solved for each external store that is attached to the wing. Since external stores characteristically induce concentrated loads into the wing structure, their effect occurs only over the part of the wing between the centerline and the point of attachment.

j = number of the wingstrip which contains the external store; the wingstrip nearest the wing tip is Number 1.

i = number of wingstrip where E_α and E_o are being calculated.

$$L_{EO} = qS\left[C_{L_{E_O}} + \left(C_{L_E}\right)_\alpha \alpha_{f_E}\right]$$

$$M_{EO} = qSc\left[C_{m_{E_O}} + \left(C_{m_E}\right)_\alpha \alpha_{f_E}\right]$$

The lift and moment on the external store L_{EO} and M_{EO} are located with respect to Point ϵ by the dimensions y_ϵ and x_ϵ as shown in Figure 7-10.

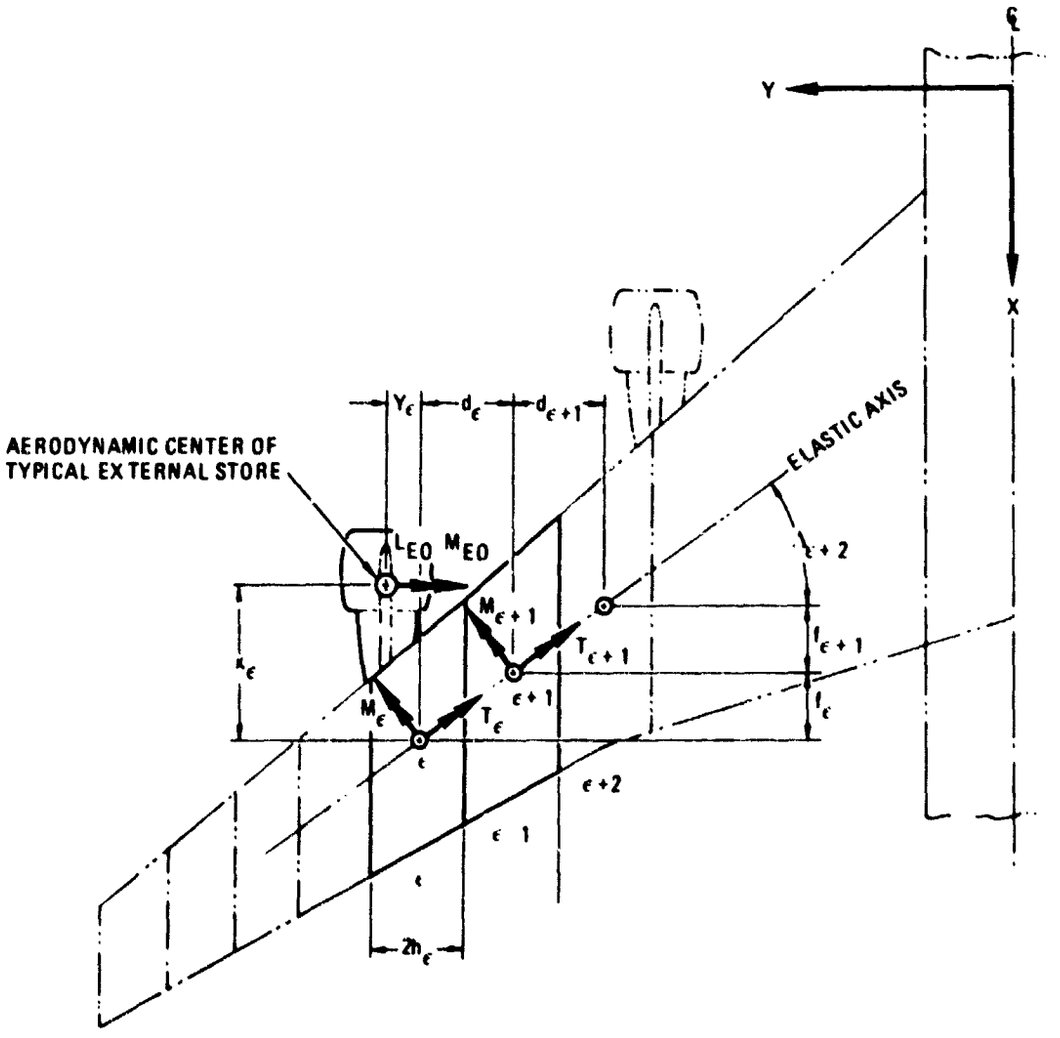

Figure 7-10 Typical External Store Geometry

$$\left\{M_E\right\} = qS\left\{\left\{X_{2M}\right\} C_{L_{E_O}} + \left\{X_{2M}\right\}\left(C_{L_{E_\alpha}}\right)\alpha_{f_E} - \left[\sin \overset{o}{\Lambda}\right]\left\{I_E\right\} \bar{c}\, C_{m_{E_O}}\right.$$

$$\left. - \left[\sin \overset{o}{\Lambda}\right]\left\{I_E\right\} \bar{c} \left(C_{m_{E_\alpha}}\right) \alpha_{f_E}\right\}$$

$$\left\{T_E\right\} = qS\left\{\left\{X_{2T}\right\} C_{L_{E_O}} + \left\{X_{2T}\right\}\left(C_{L_{E_\alpha}}\right)\alpha_{f_E} + \left[\cos \overset{o}{\Lambda}\right]\left\{I_E\right\} \bar{c}\; C_{m_{E_O}}\right.$$

$$\left. + \left[\cos \overset{o}{\Lambda}\right]\left\{I_E\right\} \bar{c}\left(C_{m_{E_\alpha}}\right)\alpha_{f_E}\right\}$$

where,

$$\left\{X_{2M}\right\} = \left\{\left[\cos \overset{o}{\Lambda}\right]\{R\} - \left[\sin \overset{o}{\Lambda}\right]\{U\}\right\}$$

$$\left\{X_{2T}\right\} = \left\{\left[\sin \overset{o}{\Lambda}\right]\{R\} + \left[\cos \overset{o}{\Lambda}\right]\{U\}\right\}$$

$$\{R\} = \begin{Bmatrix} 0 \\ 0 \\ 0 \\ Y_\epsilon \\ Y_\epsilon + d_\epsilon \\ Y_\epsilon + d_\epsilon + d_{\epsilon+1} \\ Y_\epsilon + d_\epsilon + d_{\epsilon+1} + d_{\epsilon+2} \end{Bmatrix} \qquad \left\{I_E\right\} = \begin{Bmatrix} 0 \\ 0 \\ 0 \\ 1 \\ 1 \\ 1 \\ 1 \end{Bmatrix}$$

$$\{U\} = \begin{Bmatrix} 0 \\ 0 \\ 0 \\ X_\epsilon \\ X_\epsilon - f_\epsilon \\ X_\epsilon - f_\epsilon - f_{\epsilon+1} \\ X_\epsilon - f_\epsilon - f_{\epsilon+1} - f_{\epsilon+2} \end{Bmatrix}$$

Now let

$$\left\{K_{1M}\right\} = \left\{X_{2M}\right\} C_{L_{E_O}} - [\sin \overset{o}{\Lambda}]\left\{\left\{I_E\right\} \bar{c}\, C_{m_{E_o}} - \{P\} C_{D_{E_O}}\right\}$$

$$\left\{K_{2M}\right\} = \left\{X_{2M}\right\} C_{L_{E_\alpha}} - [\sin \overset{o}{\Lambda}]\left\{\left\{I_E\right\} \bar{c}\, C_{m_{E_\alpha}} - \{P\} C_{D_{E_\alpha}}\right\}$$

$$\left\{K_{1T}\right\} = \left\{X_{2T}\right\} C_{L_{E_O}} + [\cos \overset{o}{\Lambda}]\left\{\left\{I_E\right\} \bar{c}\, C_{m_{E_o}} - \{P\} C_{D_{E_O}}\right\}$$

$$\left\{K_{2T}\right\} = \left\{X_{2T}\right\} C_{L_{E_\alpha}} + [\cos \Lambda]\left\{\left\{I_E\right\} \bar{c}\, C_{m_{E_\alpha}} - \{P\} C_{D_{E_\alpha}}\right\}$$

The moment arm about the elastic axis of the drag (or thrust) due to external stores is:

$$(P)_i = 0 \qquad , i < j$$

$$= Z_i - Z_\epsilon \qquad , i \geq j$$

$$(I_E)_i = 0 \qquad , i < j$$

$$= 1 \qquad , i \geq j$$

Let

$$[FMM] = [m]\left[\frac{\overset{o}{2h}}{\cos \Lambda}\right]\left[\overset{o}{\frac{1}{EI}}\right]$$

$$[FMT] = [t]\left[\frac{\overset{o}{2h}}{\cos \Lambda}\right]\left[\overset{o}{\frac{1}{GJ}}\right]$$

The final set of stores equations are as follows:

$$\left\{E_\alpha\right\} = [FMM]\left\{K_{2M}\right\} + [FMT]\left\{K_{2T}\right\}$$

$$\left\{E_O\right\} = [FMM]\left\{K_{1M}\right\} + [FMT]\left\{K_{1T}\right\}$$

7.1.6 EI and GJ Estimation Procedure. The aeroelastic solution requires values of EI and GJ for each section of the wing. Since these values are often not available during preliminary vehicle design, a method has been provided for estimating them.

A rigid solution is performed for a worst-case symmetric loading condition. Based on the bending moment, BM, at each section of the wing from the rigid solution and certain structural configuration assumptions, values of EI and GJ are calculated. These in turn are used in the elastic solution for the remaining loading conditions. The estimating technique is an emperical method based on historical data taken from aluminum winged aircraft.

Implicit assumptions in the method are: 1) No large cross section areas are unstiffened. 2) The structure ahead of the front spar and aft of the rear spar is noneffective. 3) Wing torque is ignored. 4) Only the symmetric case is used to size the EI's and GJ's; consideration of the asymmetric case will usually cause some modifications. 5) Present day structural design practice results in wings sufficiently stiff that the preliminary and final EI's and GJ's will be within five percent because of the similarity of rigid and elastic load distributions.

The equations used to calculate the estimates of EI and GJ for at any wing section are presented below.

$$EI_i = E \cdot (1.5\ BM_i \cdot h_{eq_i})/(f_C + f_T)$$

where:

E = the modulus of elasticity of the wing material

BM_i = the bending moment as section i, the 1.5 factor adjusts the bending moment to account for the ultimate load factor

h_{eq_i} = the equivalent height of the structural box at section i given by

$$h_{eq_i} = 0.91\ (t/c)_i\ C_i$$

where:

$(t/c)_i$ = the wing thickness ratio at section i

C_i = the wing chord at section i

f_{c_i} = the allowable compression stress for the wing material at section i

f_{t_i} = the allowable tension stress for the wing material at section i

f_C and f_T are calculated based on the applied axial loading intensity, Nx. The curves presented in Figure 7-11 represent curve fits to historical data gathered for aluminum airplanes.

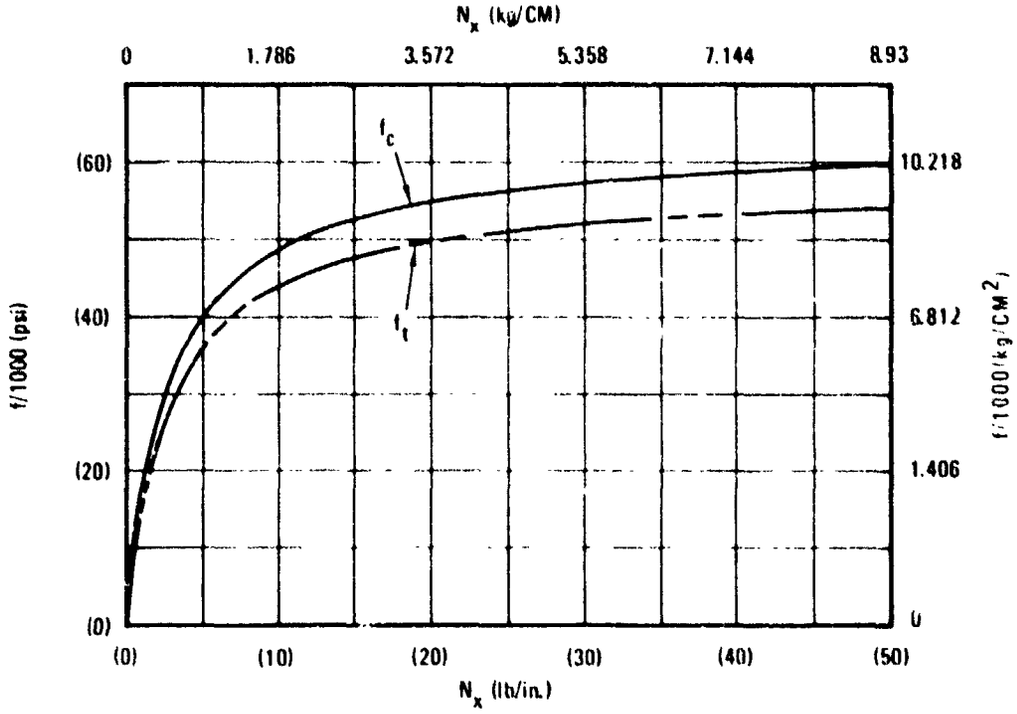

Figure 7-11 Allowable Stress Versus Applied Load Intensity

$$f_c \quad 63,000 \frac{Nx}{(Nx + 3,000)}$$

$$f_t \quad 57,000 \frac{Nx}{(Nx + 1,000)}$$

The equivalent load intensity at section i is calculated from the following equation:

$$Nx_i \quad BM_i/(h_{eq_i} C_{b_i})$$

where:

C_{b_i} the chordwise distance between the front and rear spar at wing section i

The average skin thickness, t_{SK_i}, in the torsion box at section i, bounded by the front and rear spars is approximated by the following equation, which assumes that 60 percent of the total cross section is used to support wing twist with a factor of safety of 1.5.

$$t_{SK_i} = (1.5)\ (0.60)\ Nx_i/f_{c_i}$$

The polar moment of inertia of the section, J_i is calculated based on the average skin thickness by the following equation:

$$GJ_i = [4\ C_J\ (C_i t_i)^2/(Ci/t_{SK_i})]\ G$$

where:

C_J = the torsional constant calculated as shown in Figure 7-12

t_i = the wing thickness as section i

G = the material shear modulus

7.1.7 Gust Load Factors. Specification MIL-A-8861 (ASG) 18 May 1960 is used to determine the gust load factors. The following equations are programmed in the subroutine GUST, which is called when needed by the subroutine SYBAL.

$$n_z = 1 \pm \frac{\rho_o\ V_e\ Ud_e\ m\ K_w}{2\ W/S}$$

where:

ρ_o = density of air at sea level

ρ_h = density of air at altitude

σ = ρ_h/ρ_o

V = airspeed (EAS) V (TAS) $\sqrt{\sigma}$

U_{d_o} = gust velocity (EAS)

m = slope of curve of C_{N_A} versus α for airplane with flexible wing, 1/radian

W = weight

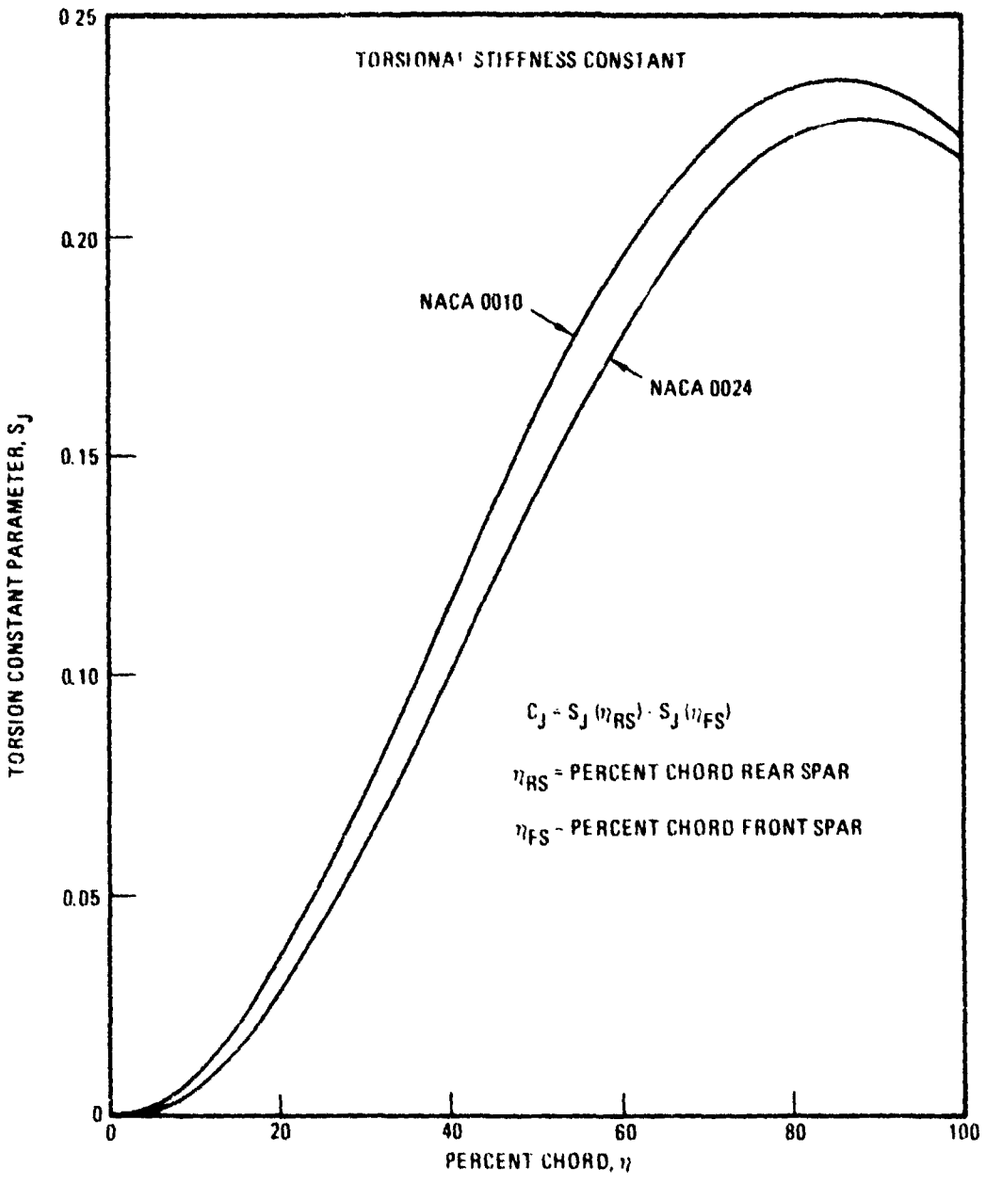

Figure 7-12 Torsional Stiffness Constant

S = wing area

C_{av} = average wing chord = area/span

g = acceleration due to gravity

μ = $(2W/S)/(g\, C_{av}\, m\rho_h)$, non-dimensional

K_W = gust factor

$$K_{W_{Subsonic}} = (0.88\mu)/(5.3 + \mu)$$

$$K_{W_{Supersonic}} = (\mu^{1.03})/(6.95 + \mu^{1.03})$$

The positive gust load factor is identified as VNZGP and the negative one as VNZGN in the program. Each appears as VNZ in the printout of the symmetric balance input data whenever the gust condition is calculated.

7.1.8 Effects of Compressibility and Thickness. The effect of compressibility can be expressed in terms of Mach number, M, and the sweep angle of the quarter chord, $\Lambda_{c/4}$.

Let:

$M \cos \Lambda_{c/4} \leq 0.90$ be the subsonic case

$0.90 < M \cos \Lambda_{c/4} < 1.091$ be the transonic case

$M \cos \Lambda_{c/4} \geq 1.091$ be the low supersonic case

For the subsonic case, the compressibility correction factor, β, is given by:

$$\beta = 1/\sqrt{1 - (M \cos \Lambda_{c/4})^2}$$

For the transonic case,

$$\beta = 1/\sqrt{1 - (0.90)^2} = 2.29$$

For the low supersonic case,

$$\beta = 1/\sqrt{(M \cos \Lambda_{c/4})^2 - 1}$$

A fairly good correction for thickness at M = 0 is $(2\pi - 4\ t/c)$. Combining the above effects, the combined compressibility/thickness correction factor, m, is:

$$m = (2\pi - 4\ t/c)\ \beta$$

where t/c is the wing thickness ratio

Table 7-1 provides the Mach number at which the transition takes place for two wing sweep angles.

Table 7-1 Transition Mach Numbers

$\Lambda_{c/4}$	Subsonic	Transonic	Supersonic
0°	M = 0.90	$0.90 < M \leq 1.091$	$M > 1.091$
20°	M = 0.96	$0.96 < M < 1.16$	$M > 1.16$

7.2 FUSELAGE AERODYNAMIC LOADS. This section describes the method for calculating the stick-fixed longitudinal stability of a wing-fuselage configuration with unswept or swept wings at subcritical Mach numbers. The stability parameters estimated by the method show reasonable agreement with the experimental values for the 23 configurations used in the comparison. For the wing carry-through section no theory was available for predicting the loading; therefore, the loading was obtained from curves based on experiment. The experimental lift-curve slope of the wing carry-through section calculated in terms of the carry-through area appears to be consistent about a value of 0.055 per degree. The method has been used to calculate the neutral points of 23 configurations. The agreement between experimental and calculated values has generally been better than ±0.04 and is considered to be good especially for such a large variety of wing plan forms. The method for calculating fuselage aerodynamic loads is described in detail in Reference 13. The pertinent sections, which aid in the understanding of the method, are included in this report.

7.2.1 Method of Analysis. The stick fixed neutral point of a wing-fuselage configuration is defined as the center of gravity location for which the slope of the curve of airplane pitching moment coefficient against lift coefficient dC_M/dC_L is zero. In order to estimate the neutral point of a configuration it is necessary to determine the additional loading and pitching moment of the configurations. In order to determine these quantities the configuration is separated into its principal parts and the additional loading of these parts is calculated. The resultant forces and pitching moments contributed by each part are presented in coefficient form as values of C_{L_α} and C_{M_α} respectively.

In the present method, the configuration is separated into the following three parts: 1) the external wing; 2) the fuselage fore and aft of the wing-fuselage juncture; and 3) the wing carry-through section (see Figure 7-13). Hereafter, the part of the fuselage fore and aft of the wing-fuselage juncture is referred to as the "fuselage." The carry-through is considered rectangular in shape; its length is equal to the length of the wing-fuselage intersection chord and its width is the average width of the carry-through section. It is important to note, however, that whenever the total wing area is considered in this method the center-section area is the area indicated by the dotted lines in Figure 7-13. The lift and moment coefficients for the principal parts are calculated in terms of the total wing area. The moment reference point is taken as the quarter-chord point of the mean aerodynamic chord of the total wing.

Complete Configuration

Calculation of $C_{L_{WF_\alpha}}$ - Obtain $C_{L_{WF_\alpha}}$ as a sum of the lift-curve slopes of the principal parts:

$$C_{L_{WF_\alpha}} = C_{l_{\alpha_o}} + C_{L_{F_\alpha}} + C_{L_{I_\alpha}}$$

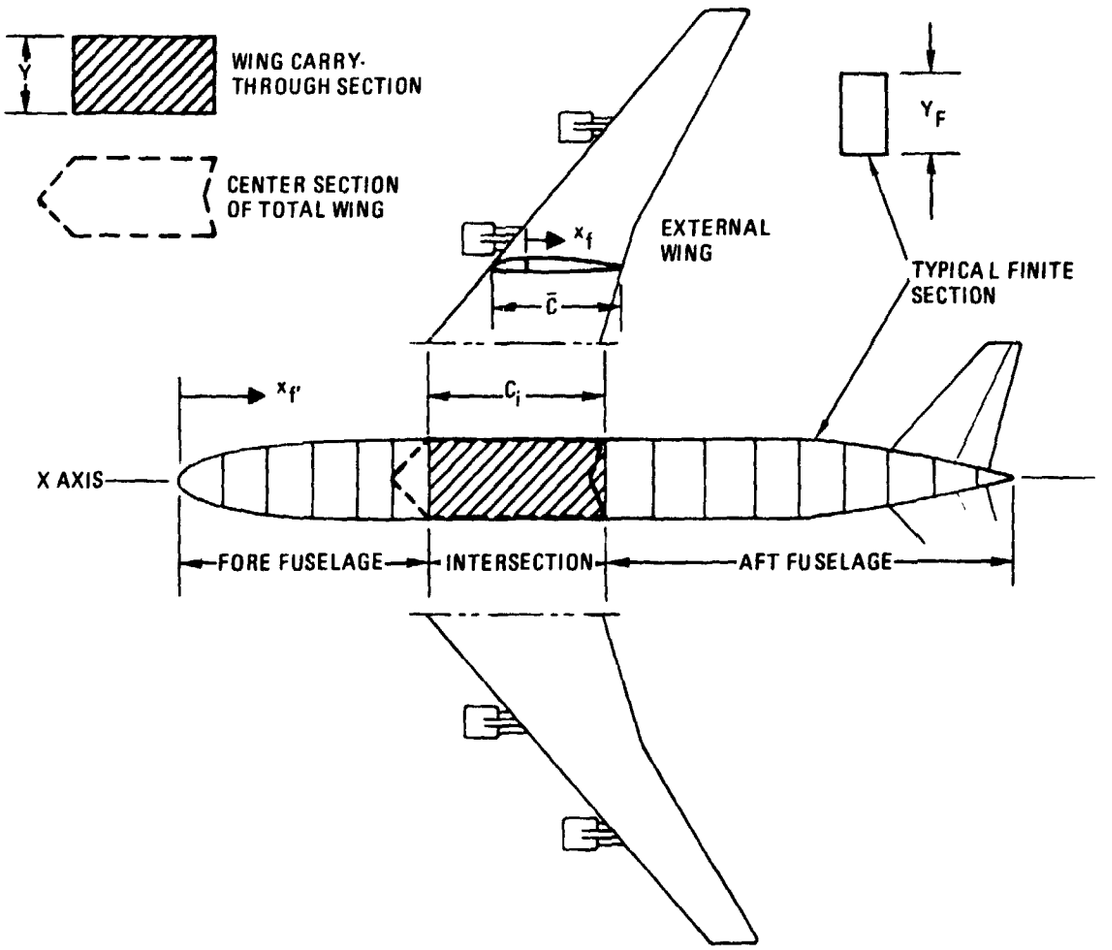

Figure 7-13 Wing-Fuselage Configuration — Principal Parts

Calculation of $C_{m_{WF_\alpha}}$ - Determine $C_{m_{WF_\alpha}}$ by summing up the pitching-moment-curve slopes of the principal parts:

$$C_{m_{WF_\alpha}} = C_{m_{\alpha_o}} + C_{m_{F_\alpha}} + C_{m_{I_\alpha}}$$

Calculation of neutral-point location - Obtain the neutral-point location with respect to the reference axis, expressed as a fraction of the mean aerodynamic chord of the wing by the relation:

$$\frac{C_{m_{WF_\alpha}}}{C_{L_{WF_\alpha}}} = \frac{x_{WF}}{\bar{c}}$$

For swept wing configurations the loading on the fuselage and wing carry-through sections are much the same as for unswept configurations. However, since the wing carry-through section for swept wings is located farther from the neutral point of the configuration, the longer moment arm results in a large pitching moment contribution. The lift contribution of the wing carry-through section, therefore, must be determined as accurately as possible in order to determine satisfactorily the pitching moment contribution. Thus the assumption that the fuselage lift can be taken as equal to the lift of the center section of an isolated wing no longer applies and the lift and moment contributions to both the fuselage and the wing carry-through sections must be obtained. In general, the method used herein is to estimate the load distribution on the fuselage and the load on the external wing by theoretical methods, whereas for the carry-through section it is necessary to develop curves based on available experimental data for predicting the loading and the aerodynamic center. The theoretical values that were used in calculating the wing stability parameters were obtained from Reference 14. That reference was used because it presented a readily available uniform source of information and showed fairly good agreement when checked with experiment. The subroutine KAPPA in the program was derived from Reference 14.

The present method for determining the values of C_{L_α} and C_{M_α} of the fuselage is based on Multhopp's method in Reference 15. Good agreement is found to exist between Multhopp's method and experimental data on the fore and aft sections of the fuselage as is shown in Figure 7-14. The experimental fuselage sectional loading was obtained from unpublished pressure distribution measurements on a wing-fuselage configuration. For the fuselage section adjacent to the wing, large disagreement can be seen between theory and experiment. The large difference in loading on the sections immediate to the wing was caused by the wing, and in the present method this difference in loading is considered to be part of the wing carry-through loading.

Calculation of $C_{L_{F_\alpha}}$ - The contribution of the fuselage to lift curve slope $C_{L_{F_\alpha}}$ is determined as follows:

Obtain the contribution to lift-curve slope of the fore and aft fuselage sections by a graphical integration of the following formula, which was derived from Formula (3.3) of Reference 15:

$$C_{L_{F_\alpha}} = \frac{\pi}{180\,S}\left[\int_0^{X_{LE}} \left(\frac{d\left(\frac{\pi}{2} Y_f \frac{2\,d\beta}{d\alpha}\right)}{dx_f}\right) dx_f + \int_{X_{TE}}^{L_f} \left(\frac{d\left(\frac{\pi}{2} Y_f^{\,2} \frac{d\beta}{d\alpha}\right)}{dx_f}\right) dx_f\right]$$

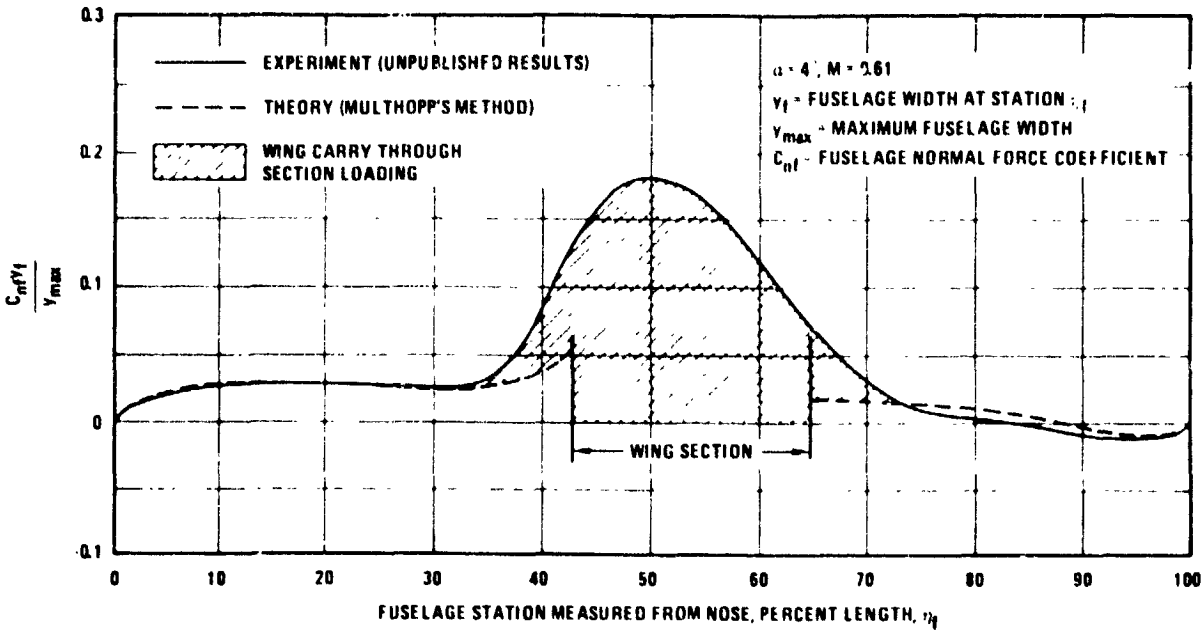

Figure 7-14 Experimental and Theoretical Fuselage Sectional Loading

where Y_f is the width of fuselage at any station. The fuselage plan form is divided into a finite number of sections as shown by Figure 7-13. For each of these sections the parameter $\left(\frac{\pi}{2} Y_f^2 \frac{d\beta}{d\alpha}\right)$ is calculated and plotted against its fuselage longitudinal station x_f'. The measured slope $\left(\frac{d\left(\frac{\pi}{2} Y_f^2 \frac{d\beta}{d\alpha}\right)}{dx_f}\right)$ at each of these stations is proportional to the slope of the sectional lift coefficient $C_{l_{f_\alpha}}$ (per radian) of that station.

For the fuselage stations ahead of the wing, values of $d\beta/d\alpha$ are obtained from the following formula:

$$\frac{d\beta}{d\alpha} = 1 + \kappa \frac{C_{L_w}}{AR_w} \frac{180}{\pi}$$

which is the variation in local airflow with angle of attack for the fuselage alone plus the additional variation caused by the presence of the wing. The parameter κ is noted to be expressed as a function of the distance forward of the intersection quarter chord $c_j/4$ as shown by Figure 7-15. For the fuselage sections behind the wing, values of $d\beta/d\alpha$ are obtained from the variation of downwash with angle of attack $d\epsilon/d\alpha$ by the formula:

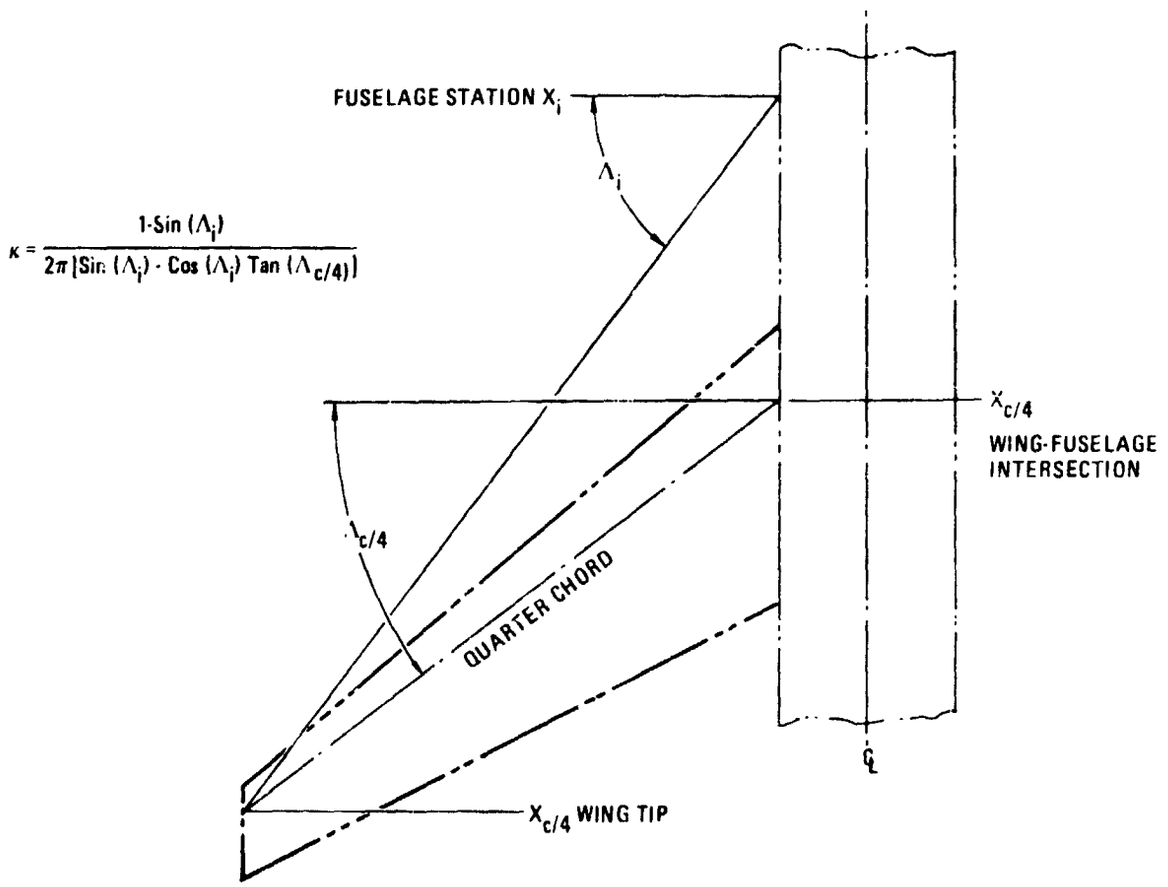

Figure 7-15 Wing-Fuselage Intersection Geometry for Aerodynamic Parameter κ

$$\frac{d\beta}{d\alpha} = 1 - \frac{d\epsilon}{d\alpha}$$

Calculation of $C_{m_{F_\alpha}}$ - The contribution of the fuselage to pitching moment curve slope $C_{m_{F_\alpha}}$ is as follows:

Obtain the contribution of the fore and aft fuselage sections to pitching moment curve slope by a graphical integration of the following formula, which was derived from Formula (3.7), Reference 15.

$$C_{m_{F_\alpha}} = \frac{1}{57.3\,S_w\,\bar{c}} \left[\int_0^{LE} \left(\frac{d\left(\frac{\pi}{2} Y_f^2 \frac{d\beta}{d\alpha}\right)}{dx_f} \right) x_f \cdot dx_f + \int_{TE}^{L_f} \left(\frac{d\left(\frac{\pi}{2} Y_f^2 \frac{d\beta}{d\alpha}\right)}{dx_f} \right) x_f \cdot dx_f \right]$$

where x_f is the longitudinal distance measured from the quarter chord of the mean aerodynamic chord to a finite fuselage station.

7.2.2 Correlation of Results. The method has been used to determine the static longitudinal stability of the 23 wing-fuselage configurations and the results are presented and compared with the experimental results in Figures 7-16 through 7-18. A comparison between the experimental and calculated values of lift-curve slopes is presented in Figure 7-16. The calculated values show some disagreement with experiment, however, the disagreement was found to result mostly from low values of $C_{L_{W_\alpha}}$ (theoretical) for wings with approximately 45° sweep angle.

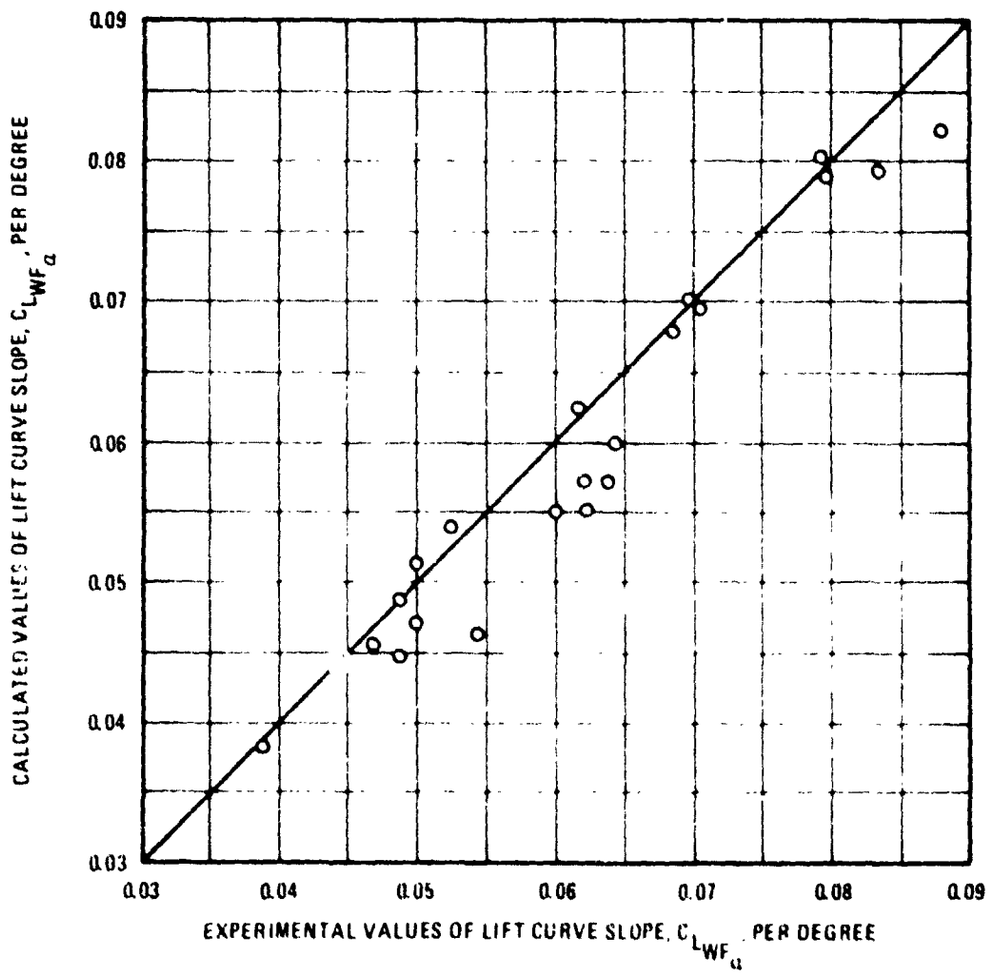

Figure 7-16 A Comparison Between Experimental and Theoretical Values of $C_{L_{WF_\alpha}}$ for Wing-Fuselage Combinations

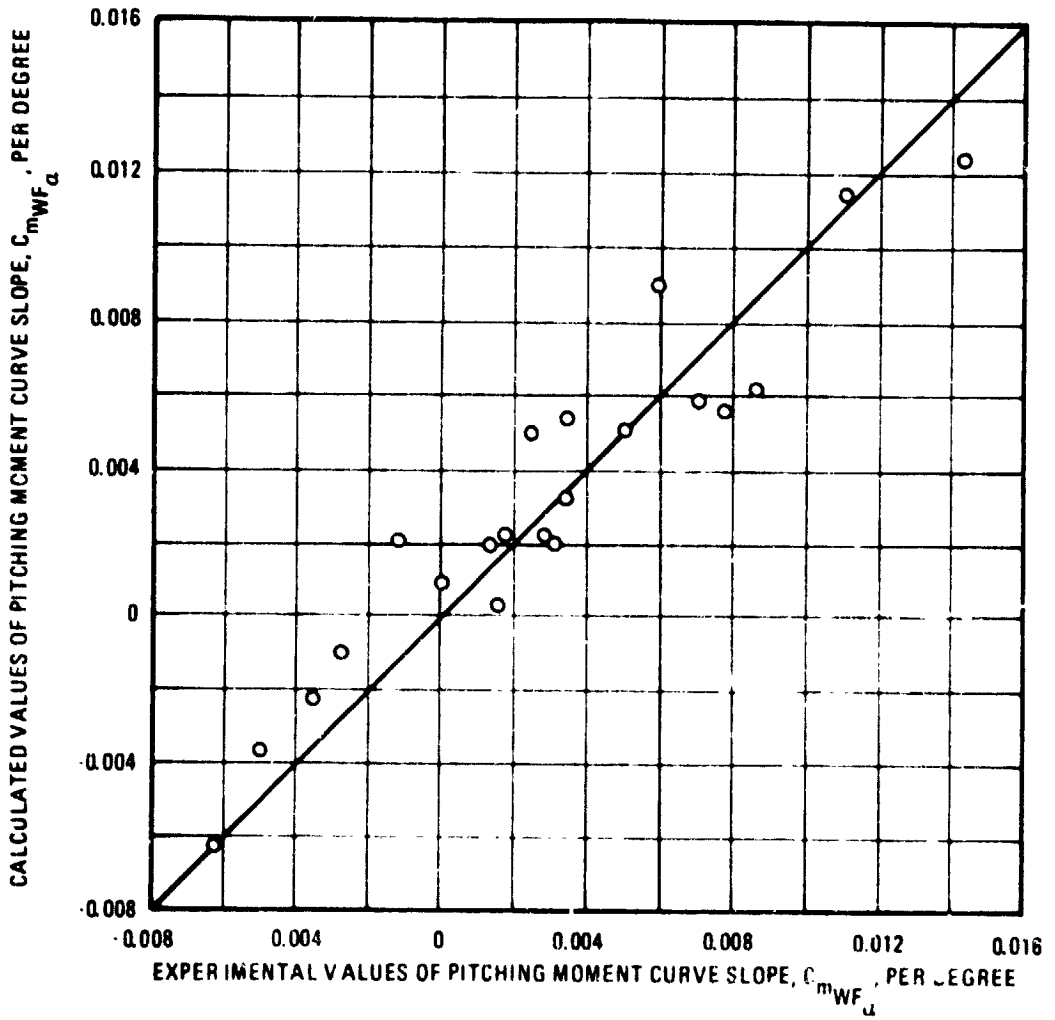

Figure 7-17 A Comparison Between Experimental and Theoretical Values of $C_{m_{WF\alpha}}$ for Wing-Fuselage Combinations

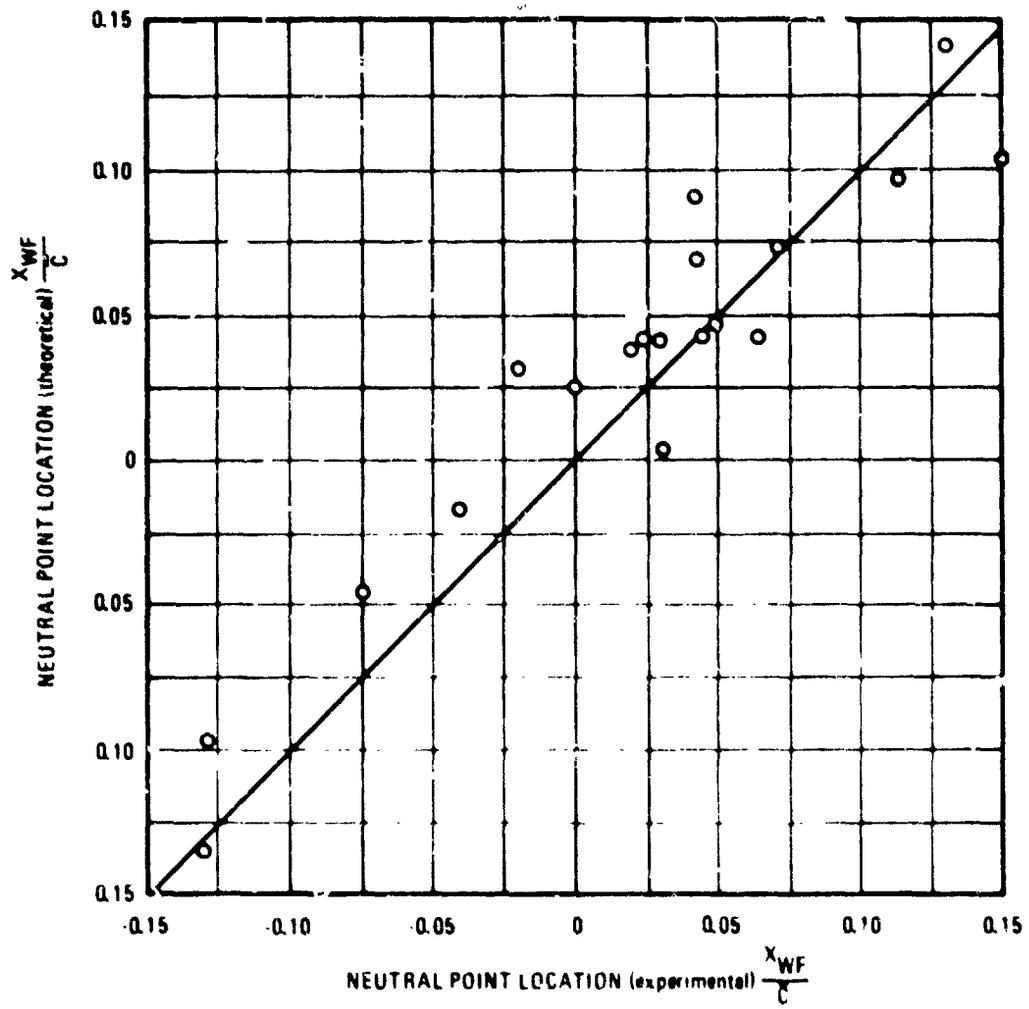

Figure 7-18 A Comparison Between Experimental and Calculated Stick Fixed Neutral Points for Wing-Fuselage Combinations

A comparison between the experimental and the calculated values of pitching-moment-curve slopes for the configurations is presented in Figure 7-17. The results of the calculations show reasonable agreement with the experimental values. The disagreement that exists, however, can be traced primarily to the disagreement in lift-curve slopes and to the limitations in estimating the aerodynamic-center location for some of the lift contributing parts. Calculation of the aerodynamic center location of the wing carry-through section shows that there are probable Reynolds number effects that have not been considered in the method.

A comparison between the experimental and calculated neutral points for the various configurations is presented in Figure 7-18. The agreement, which is generally better than ±0.04, is considered to be good, especially for such a large variety of wing plan forms. The accuracy with which the aerodynamic center and the lift-curve slope of the wing can be determined to a large extent determines the accuracy of the neutral-point location for a wing-fuselage configuration.

7.2.3 Program Description. The program of Reference 16 is based directly on the theory and experimental data of Reference 13. All curves and table look-ups have been expressed in equation form. The following subroutine summary indicates how the large variety of fuselage shapes are treated mathematically. The effect of wing vorticity on the fuselage characteristics is treated with the aid of the subroutine KAPPA.

Subroutine Summary

1. SHAPE - This subroutine provides the coefficients of a parabolic curve fit through any set of three adjacent points. The first step searches through an abscissa array until the input abscissa is properly positioned. A parabola is ther defined by the nearest three points, providing coefficients A, B, and C for the equation:

$$y = AX^2 + BX + C$$

2. KAPPA - Strength of the wing up wash (ahead of the wing), or down wash (behind the wing) is computed here.

3. HIT - Given the values of A, B, and C from SHAPE, this subroutine is used to compute the ordinate of the desired function.

$$y = AX^2 + BX + C$$

4. SLP - Using the coefficients A and B from SHAPE, this subroutine is used to compute the slope (or derivative) of the desired function.

$$\left(\frac{\partial y}{\partial x}\right) = 2.0\,AX + B$$

7.2.4 Fuselage Unit Inertia Loads. The fuselage unit inertia loads differ from the treatment of the wing inertia loads in that they are calculated separately and for unit translatory and rotary accelerations. The wing solution treated both aerodynamic and inertia loads with a set of simultaneous solutions for the balanced vehicle.

The fuselage unit inertia loads of this section are derived with the aid of the digital program described in Reference 16. These fuselage inertia loads are applied to the balanced vehicle with the aid of n_z and $\ddot{\theta}$ from the wing solution performed in program AELOADS.

The following text was taken from Reference 16 to aid in understanding the scope of this part of the overall program. The main program and each subroutine are discussed in the following paragraphs. The sign convention and geometry data are presented in Figures 7-19 and 7-20.

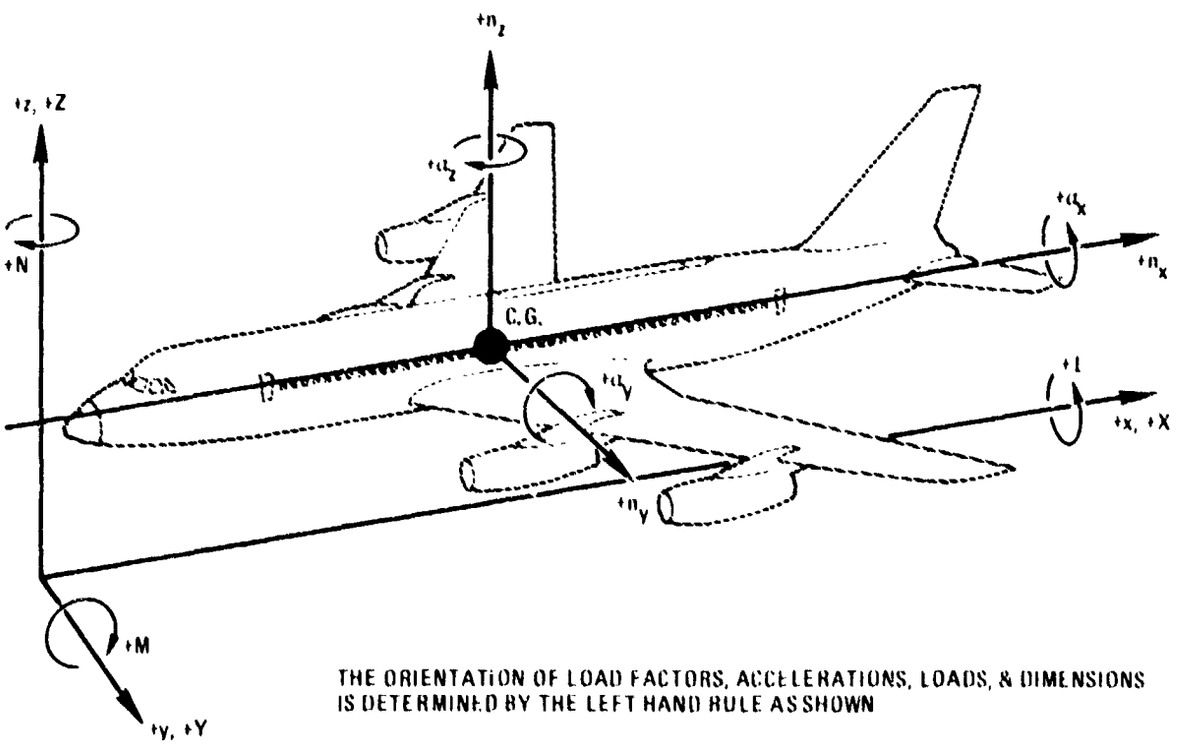

Figure 7-19 Nomenclature and Sign Convention

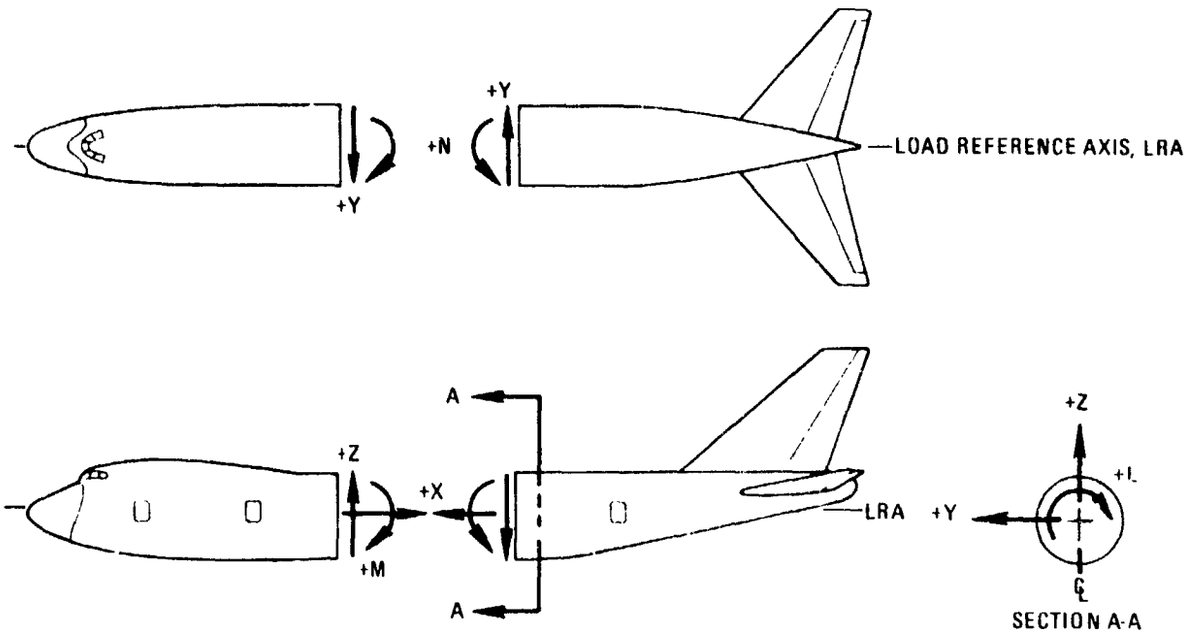

Figure 7-20 Fuselage Sign Convention

Main Program

This program controls the subprogram usage and provides the logic for building the airplane configuration. The following options are available for configuration development and may be used separately or in any combination:

fuselage + contents + fixed useful load

fuselage fuel

fuselage payload (internal bomb load, cargo, etc.)

add vertical tail/s to fuselage

add horizontal tail/canard to fuselage

add wing to fuselage

add engine/s to fuselage

add external store/s to fuselage

Inertia loads are stored in the array E(I, J, K) where:

I = fuselage station at which loads are calculated

J = 1 load due to n_x

J = 2 load due to n_y

J = 3 load due to n_z

J = 4 load due to α_x

J = 5 load due to α_y

J = 6 load due to α_z

K = 1 X shear

K = 2 Y shear

K = 3 Z shear

K = 4 L moment (torsion)

K = 5 M moment (vertical bending)

K = 6 N moment (side bending)

For example, E(3, 4, 2) would be the Y shear (K = 2) due to roll acceleration, α_x, (J = 4) at the fuselage station represented by I = 3. The values for each element of E(I, J, K) are calculated in the various subprograms.

Subroutine UNITL

UNITL is used to calculate the inertia forces, shears, and moments resulting from distributed weight (slice) data. Slice data is read in this subprogram. Shear and moment data are stored in the array XYZLMN(I, J, K). "I" refers to the fuselage stations that separate the slice data. "J" and "K" are the same as those described in the main program for E(I, J, K).

Subroutine INTPOL

This routine is used to interpolate for shears and moments at the output fuselage stations located in the array FUSSTA(I). FUSSTA is read by the main program. The resulting interpolated data are stored in OUTPUT(I, J, K). "I" = the output fuselage stations. J and K are the same as those for E(I, J, K) described in the main program.

Subroutine ULOADS

Inertia loads due to concentrated mass items that utilize a single attach point are calculated in ULOADS. Fuselage shears and moments for components such as the horizontal tail or canard would be calculated in this routine. These loads are stored in the array CILODS(I, J, K). I, J, and K are the same as those described in subroutine INTPOL.

Subroutine PLOADS

This routine calculates the fuselage inertia loads due to the wing. The resulting shears and moments are stored in the array DPCILS(I,J,K). I,J, and K are the same as those in subroutine INTPOL.

Subroutine ENGINE

Inertia loads due to fuselage mounted engines are calculated in subroutine ENGINE. Engine loads are applied to the fuselage through the attach points. Inertia load distributions are stored in the array CONLOD(I,J,K). Engine attach loads are written from this routine.

Subroutine STORE

STORE is used to calculate the inertia loads for externally mounted fuselage stores and for vertical tails with two attach points. Shears and moments are stored in the array STORES (I,J,K). External store loads are written from this routine.

Subroutine DATA

The fuselage inertia loads for the complete airplane that are stored in E(I,J,K) are written from subroutine DATA. When the variable IPUNCH has a value of 1, E(I,J,K) is punched on cards. The center-of-gravity and weight of each component are printed next.

7.2.5 Fuselage Net Loads. The methods and techniques presented in the fuselage net loads module consist of basic matrix operations. These operations facilitate the process of combining airload and inertia load data to obtain net load distributions. The two computer programs contained in this module do not calculate any new information or data that are part of the net loads. The input data for these routines contain all of the required information.

The fuselage net loads computer program contains a procedure for forcing the sum of the moments to zero at the nose of fuselage. The moment is eliminated by applying a couple at the wing attach points.

Data output from the other modules are required input for this routine. The types of data required from the other modules are summarized below:

Aerodynamic Data Module

Unit shear, bending moment, and torsion distributions due to angle-of-attack, alpha fuselage = 0, carry-over load from horizontal rail and vertical tail, side-slip angle, rudder deflection, etc.

Fuselage stations for these unit airload distributions. (All distributions must be based on these stations.)

Inertia Loads Module

Inertia load distributions for $n_x = n_y = n_z = 1g$, and $\alpha_x = \alpha_y = \alpha_z = 1$ rad/sec^2.

One set is required for each gross weight to be used.

Fuselage stations for these inertia distributions. (These stations are used for net loads calculations.)

Coordinates of attach points for wing, horizontal tail or canard, and vertical tail.

Inertia parameters n_y, n_z, α_x, α_y, α_z, gross weight, and c.g. location.

After these data are available, values for both distributed and concentrated airloads may be calculated.

Distributed airloads are those due to pressure loadings resulting from angle-of-attack, zero lift, etc.

Concentrated airloads are those airloads on the wing and tails that are applied to the fuselage through the attach points of these components.

7.3 REFERENCES

1. Gray, W. L. and Schenk, K. M., "A Method for Calculating the Subsonic Steady-State Loading on an Airplane with a Wing of Arbitrary Planform and Stiffness," NACA TN 3030, December 1953.

2. "Application of Lifting Line Theory to Aircraft Aeroelastic Loads Analysis," General Dynamics/Convair Report No. GDC-ERR-AN-1128, February 1968.

3. Schindel, L. H., "An Evaluation of Procedures for Calculating Aerodynamic Loads," AFFDL-TR-65-18, May 1965.

4. Borland, C. J., "Methods of Calculating Aerodynamic Loads on Aircraft Structures," AFFDL-TR-66-37, August 1966.

5. Blackwell, J. A., Jr., "A Finite Step Method for Calculation of Theoretical Load Distribution for Arbitrary Lifting - Surface Arrangements at Subsonic Speeds," NASA TND-5335, 1969.

6. Bisplinghoff, R. L., Ashley, Holt, and Halfman, Robert L. "Aeroelasticity," 1955.

7. Diederich, Franklin W., "Calculation of the Aerodynamic Loading of Swept and Unswept Flexible Wings of Arbitrary Stiffness," NACA Report No. 1000 (Supersedes NACA TN No. 1876), 1950.

8. Weissinger, J., "The Lift Distribution of Swept-Back Wings," NACA TM No. 1120, 1947.

9. Falkner, V. M., "The Calculation of Aerodynamic Loading on Surfaces of Any Shape," British A. R. C., R. & M. No. 1910, 1943.

10. Mutterperl, William, "The Calculation of Span Load Distributions on Swept-Back Wings," NACA TN No. 834, 1941.

11. Wieghardt, Karl, "Chordwise Load Distribution of a Simple Rectangular Wing," NACA TM No. 963, 1940.

12. Lennertz, J., "On the Mutual Reaction of Wings and Body," NACA TM No. 400, 1927.

13. McLaughlin, Milton D., "Method of Estimating the Stick-Fixed Longitudinal Stability of Wing-Fuselage Configurations Having Unswept or Swept Wings," NACA RM L51J23, January 1952.

14. De Young, John, and Harper, Charles W., "Theoretical Symmetric Span Loading at Subsonic Speeds for Wings Having Arbitrary Plan Form," NACA Report 921, 1948.

15. Multhopp, H., "Aerodynamics of the Fuselage," NACA TM 1036, 1942.

16. Curry, A. L. and Minter, E. A., "Preliminary Airframe Structural Design Load Prediction Techniques for Military Aircraft," Air Force Report AFFDL-TR-73-157, December 1973.

SECTION 8

STRUCTURAL SYNTHESIS

The Structural Synthesis uses two separate and independent procedures to develop component geometry and weight data. The primary structure is analyzed by the automated structural analysis procedure described in Section 8.1 . The secondary structure is defined and sized by an independent analysis procedure that develops geometry and weight data for the parts definition process and is described in Section 8.2 .

8.1 PRIMARY STRUCTURE. The Structural Synthesis procedure for primary structure is known as APAS (Automated Predesign of Aircraft Structure). This procedure was initiated under a company sponsored IRAD Program (Reference 1) and further developed under NASA Contracts NAS1-11343 (Reference 2) and NAS1-12506 (Reference 3). This section describes the technical approach used in the synthesis procedure for analysis of primary structure.

The APAS Analysis Procedure is applicable to any closed section beam like structure, and is typical of the procedure used in the early design phase of aircraft structure. The overall approach makes use of a point design/analysis/redesign process which is iterated until an acceptable design is produced.

The program accepts up to six external static strength loading conditons. Each condition consists of a set of three forces and three moments (PX,PY,PZ,MX,MY,MZ), for up to twenty stations along the structure. An accurate representation of geometry is permitted by defining discrete nodes on the contour of the surface. Any convenient reference axis may be adopted. Internal computations automatically transfer the loads to the section elastic axis. The internal distribution of loads is calculated by a multicell box beam analysis subroutine. Complex bending stresses are found using the assumption that plane sections remain plane (i.e., MC/I). Torsional moment is assumed to have a T/2A distribution and direct shear is presumed to follow a VQ/I distribution.

If fatigue or crack growth analyses are to be performed six additional loading conditions are required. These are used in conjunction with a flight profile to generate a unique stress spectra at each analysis point. In the current version of APAS, the flight profile for medium range operation of a large commercial transport is built into the program.

Analysis routines are used to find the allowable stresses; these together with the applied stresses from the internal loads solution are used to compute margins of safety. These routines provide for several different kinds of construction and reflect the failure modes to which the components are susceptible. Buckling, crippling and net tension are typical failure modes.

A special symmetry grouping feature permits the user to constrain selected panels to be alike. This technique provides a means by which fuselage centerplane symmetry can be respected without duplicating reversible loading conditions. It is often desirable to make

adjacent panel elements identical for ease in manufacturing. This can be accomplished with symmetry grouping also.

The optimization procedure is a two step process. Design synthesis proceeds systematically from station to station in discrete steps, at rib or frame locations. In the first phase of the synthesis process, a set of initial member size estimates are adjusted by iterative steps until each element has a zero margin of safety or until a minimum gage constraint is encountered. The second phase seeks to maximize margins of safety by refinement of element geometry while holding structural weight constant. When this has been accomplished the design is recycled through phase one to further refine structural weight. This logic is repeated until satisfactory convergence is obtained for static strength load conditions, or the input iteration limit is encountered.

This optimized design is then successively checked for fatigue life, crack growth and residual strength criteria. If any criteria is not met the structure is augmented at that point and a new pass is made through static strength, fatigue, crack growth, and residual strength analyses. Iteration continues until all criteria are met.

It is important to recognize that margin of safety maximization rather than weight minimization on the second phase permits use of unconstrained function optimization methods. Optimization methods have been the subject of previous research at Convair. A Fletcher, Powell, Davidon technique is used in this program.

Major advantages of this approach are: member sizes can be constrained to lay within practical limits of material sizes and manufacturing capability; multiple failure modes may be taken into consideration for each structural element; and, positive margins of safety are always maintained so that a satisfactory design - from the strength point of view if not the weight - is available at the completion of each iteration.

The overall program is modular to permit modifications or additions to the element routines with minimum impact on the total system.

8.1.1 Nodal Geometry. The geometry of each component, (fuselage, wing, horizontal and vertical stabilizer) is represented by the coordinates of a set of nodes at each of the various stations along the component. This nodal geometry describes the shape of the component which is used for the computation of section properties and internal loads. The analysis procedure uses linear interpolation between control stations to determine required nodal information. Nodal information at a control station consists of X and Y coordinates for each node.

The fuselage is represented by up to 20 nodes at analysis stations selected by the user. The nodes are located at user selected intervals around the fuselage. However, when APAS is used in the integrated mode with parts definition it is restricted to 18 nodes at 20 degree intervals around the fuselage with a maximum of 10 analysis stations. Nodal geometry for a typical transport fuselage is presented in Figuge 8-1 . Nodes are numbered starting at the top centerline and proceeding clockwise looking aft.

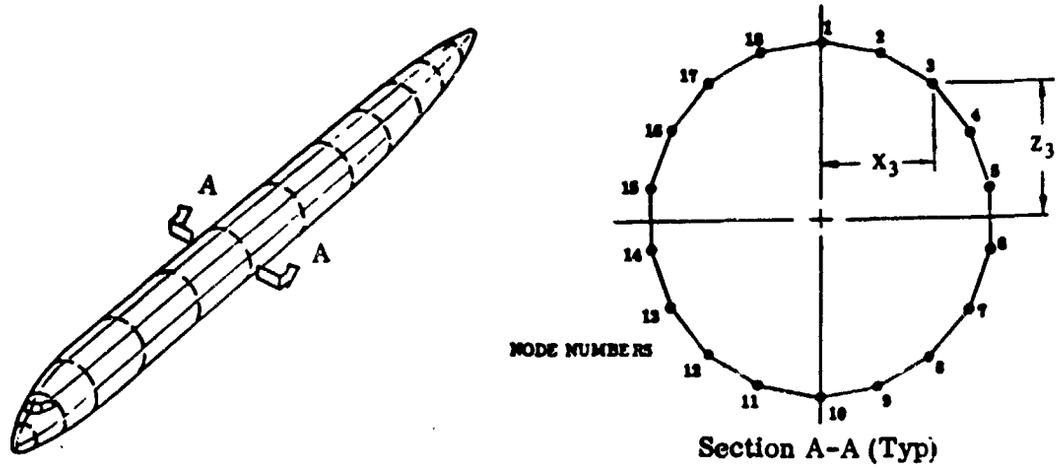

Figure 8-1 Fuselage Nodal Geometry

The wing, horizontal and vertical stabilizer are represented by 30 nodes at analysis stations selected by the user. The aerodynamic surfaces, like the fuselage, are restricted to 10 nodes at each of 10 analysis stations when APAS is used in the integrated mode with parts definition. The nodal geometry describes the box structure for a surface with up to 5 spars. The nodes are numbered beginning at the upper sparcap of the front spar and proceeding clockwise to the lower front sparcap. A typical surface nodal geometry is presented in Figure 8-2 .

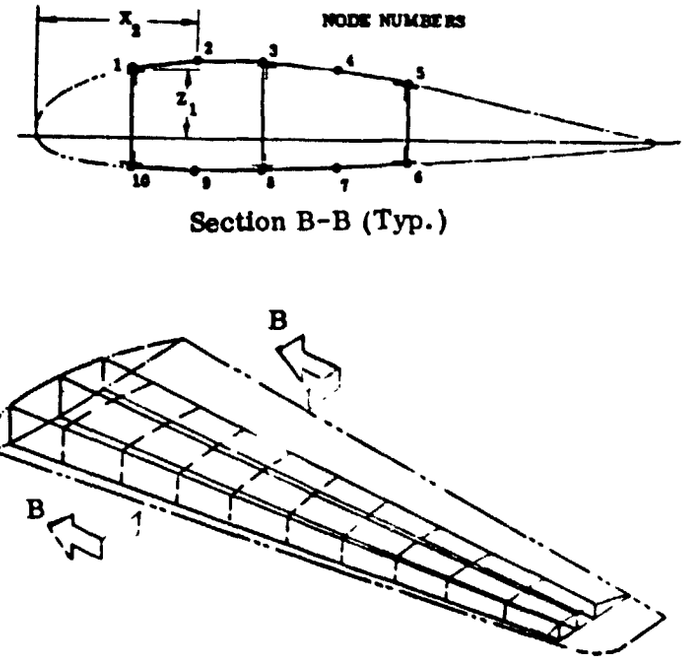

Figure 8-2 Aerodynamic Surface Nodal Geometry

8.1.2 Structural Elements. Structural elements include skin panel, spar webs and spar caps. Each element is described by a type number and from one to eight dimension variables. The dimension variables are of two types, thickness variables and non-thickness variables, such as stiffener spacing, stiffener height, corrugation angle, etc. In general, non-thickness variables may have either equality or inequality constraints imposed, whereas thickness variables may have equality or lower bound inequality constraints imposed.

The structural synthesis program provides an analysis procedure for twelve types of panel elements as presented in Figure 8-3 . The stiffeners on panel types one through nine are assumed to be oriented parallel to the elastic axis of the structure. The 0 degree ply of panel type 12 is also assumed to be parallel to the elastic axis.

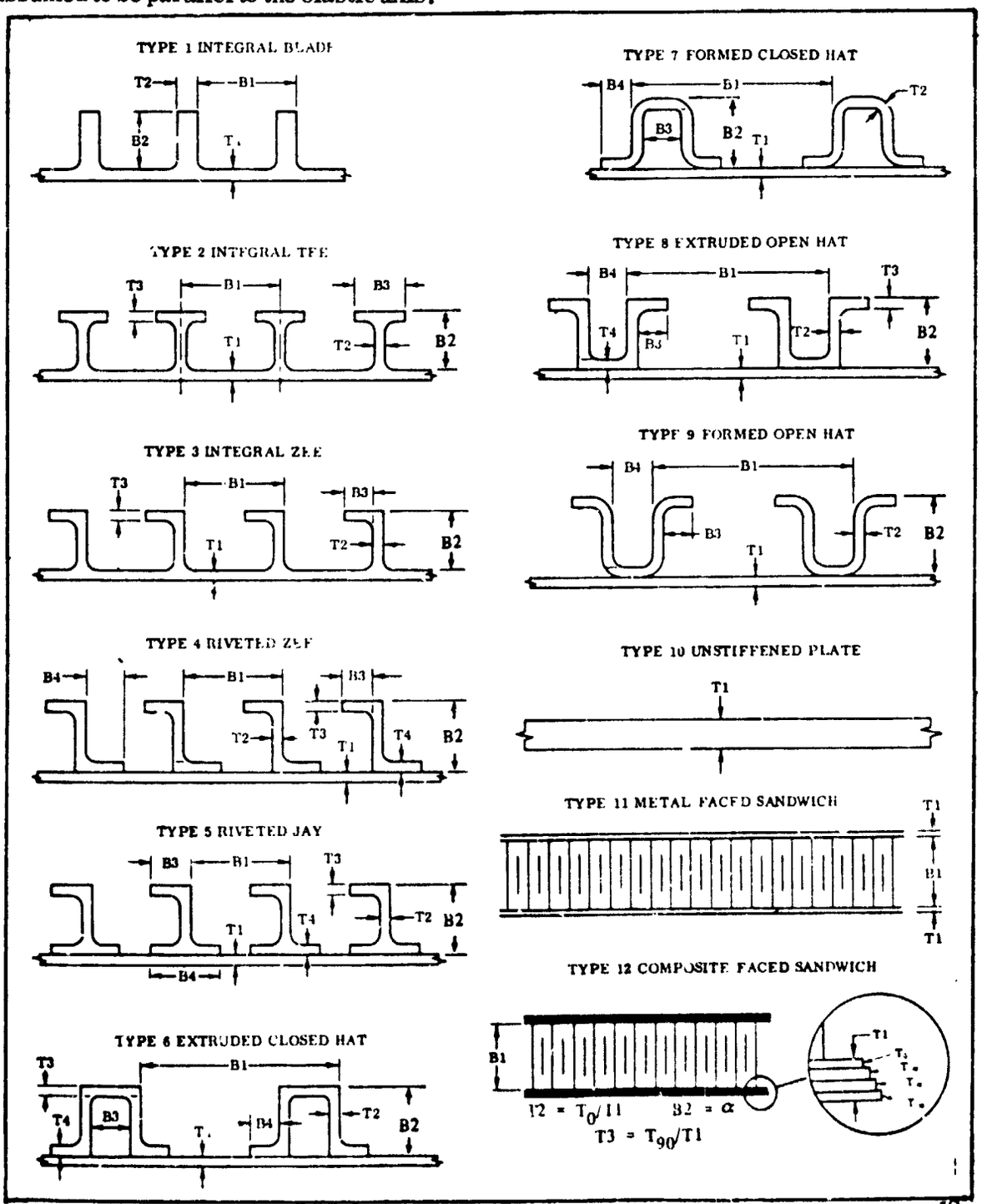

Figure 8-3 Skin Panel Elements

The structural synthesis program provides an analysis procedure for seven types of "spar web" elements. Four of these are truss type elements, two are stiffened webs and the remaining one is a corrugated web. These elements are presented in Figure 8-4 . "Spar Web" elements are assumed to resist only shear and crushing loads, the axial stiffness of these elements is assumed to be zero for the purpose of computing section properties.

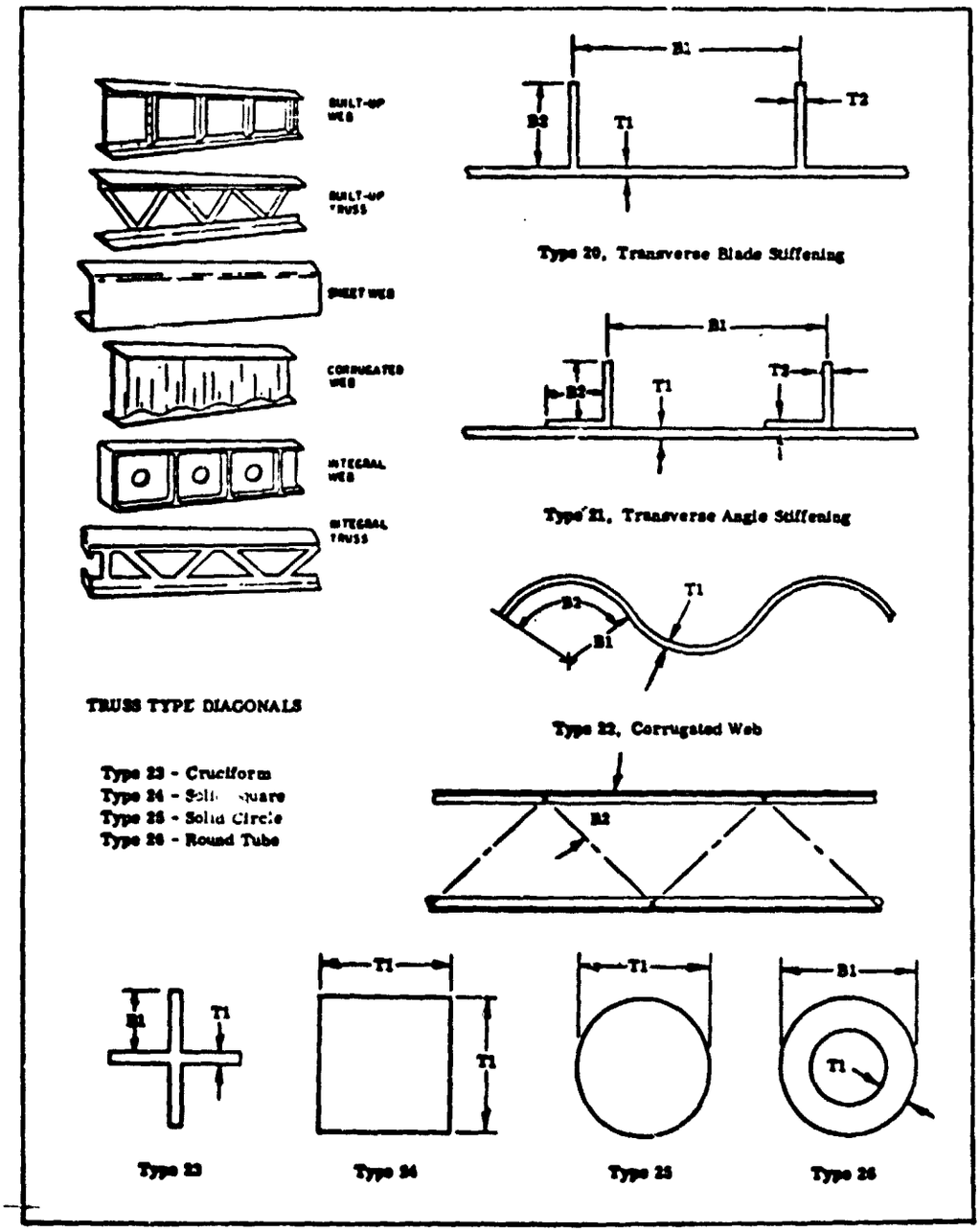

Figure 8-4 Spar Web Elements

An analysis procedure for four types of spar cap elements is currently available. They include integral tee and angle and riveted tee and angle as shown in Figure 8-5 .

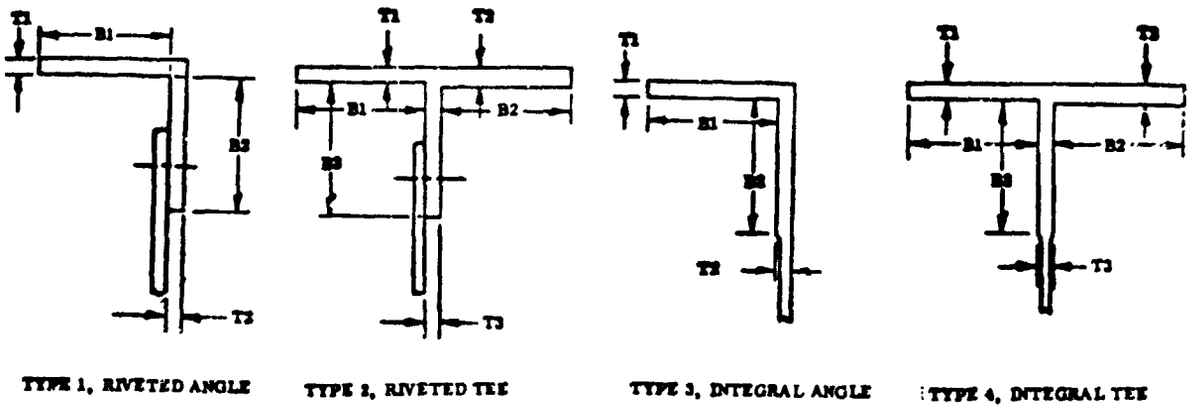

Figure 8-5 Spar Cap Elements

8.1.3 Ribs. The types of ribs available within the program are presented in Figure 8-6. The ribs are comprised of caps and webs or truss elements. Rib caps are sized to react a moment at the rear spar due to the loading on the surface aft of the rear spar. Rib webs are sized to carry shear and to support crushing loads.

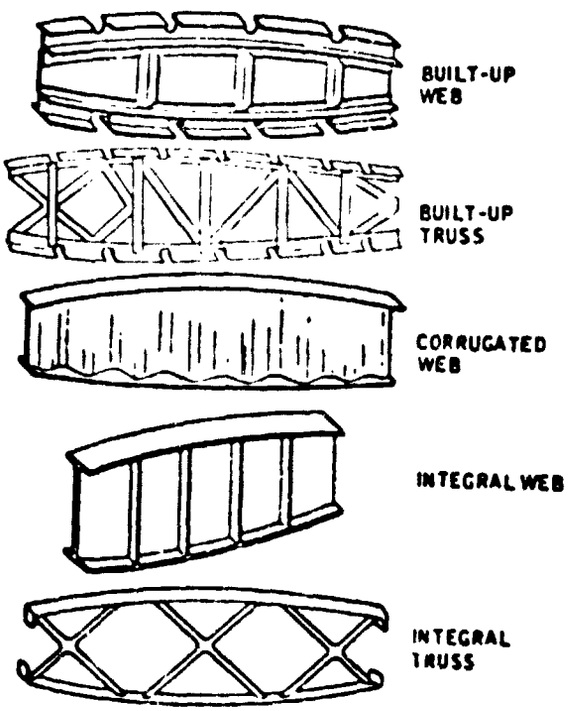

Figure 8-6 Ribs

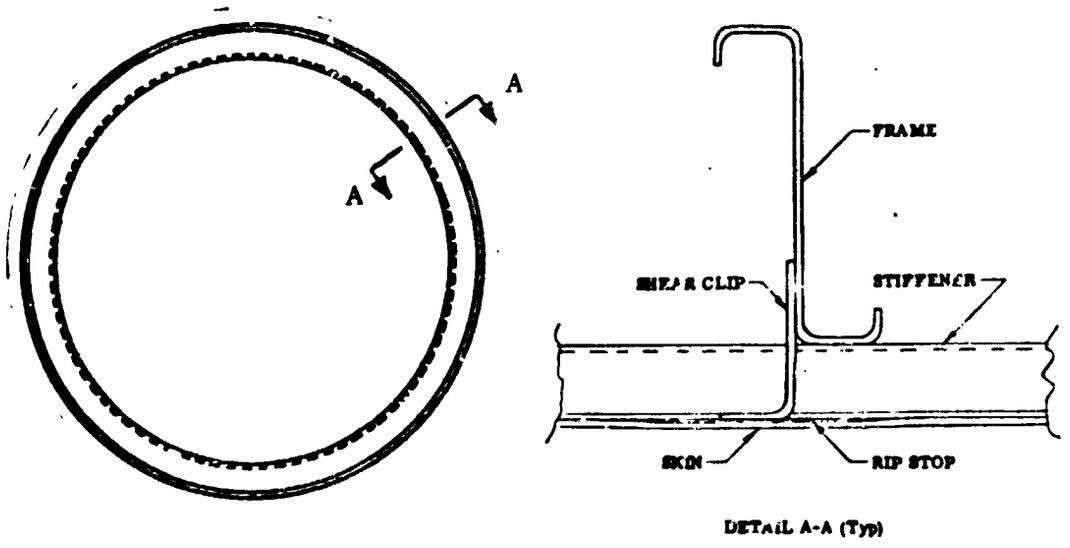

Figure 8-7 Typical Ring Frame

8.1.4 Frames. A typical ring frame is shown in Figure 8-7 . The frames are sized so that the outer flange clears all of the skin stiffeners. The inner flange is maintained at 14 cm (5.5 inches) from the outer skin contour. The frame is sized using Shanley's criteria to set a minimum frame bending stiffness. If the frame thickness determined by this criteria is less than minimum gage, it is set at minimum gage.

$$EI = \frac{C_f M D^2}{L}$$ Shanley's criteria (Reference 4 ,

where:

EI = frame bending stiffness

M = maximum resultant fuselage bending moment, $\sqrt{M_x^2 + M_z^2}$

D = fuselage diameter

L = frame spacing

C_f = fit coefficient (.00025)

8.1.5 Flight Profile and Load Spectrum. The fatigue load spectrum defines the number of times that incremental loads of given magnitudes are encountered during the design life of the aircraft. Experimental data is available which defines the probable magnitudes and frequency of occurrence of these incremental loads as a function of aircraft type, configuration parameters and flight parameters.

The configuration and flight parameters are defined using a typical flight profile, which is divided into segments. Parameters are averaged for each segment, and these average values are used in finding the incremental loads. See Figures 8-8 and 8-9 .

The typical flight profile used for fatigue and flaw growth analysis is based on medium range operation of a contemporary transport aircraft.

The parameter values for each segment are listed in Table 8-1 . The segments are divided into subsegments, with each subsegment representing a particular magnitude of incremental load. Using the segment parameters and the subsegment load, frequency of occurrence of the incremental load is found for each subsegment using the methods and information in Reference 5 .

For gust loads, curves showing gust velocity vs frequency of occurrence are found in Reference 5 , Figure C13-32 through C13-37. From Reference 5 , Page C13-24,

$$\Delta g = m S V_e U_{de} K_g \rho_o/(2W)$$

For speeds below critical Mach number:

$$K_g = \frac{.88\mu_g}{5.3+\mu_g} \qquad \mu_g = \frac{2W}{mgcS\rho}$$

where

- Δg = incremental load factor
- m = slope of lift curve
- S = wing area
- V_e = equivalent airspeed
- U_{de} = derived gust velocity
- K_g = gust alleviation factor
- ρ_o = air density at sea level
- W = aircraft weight
- μ_g = aircraft mass ratio
- g = acceleration of gravity
- c = mean geometric wing chord
- ρ = air density

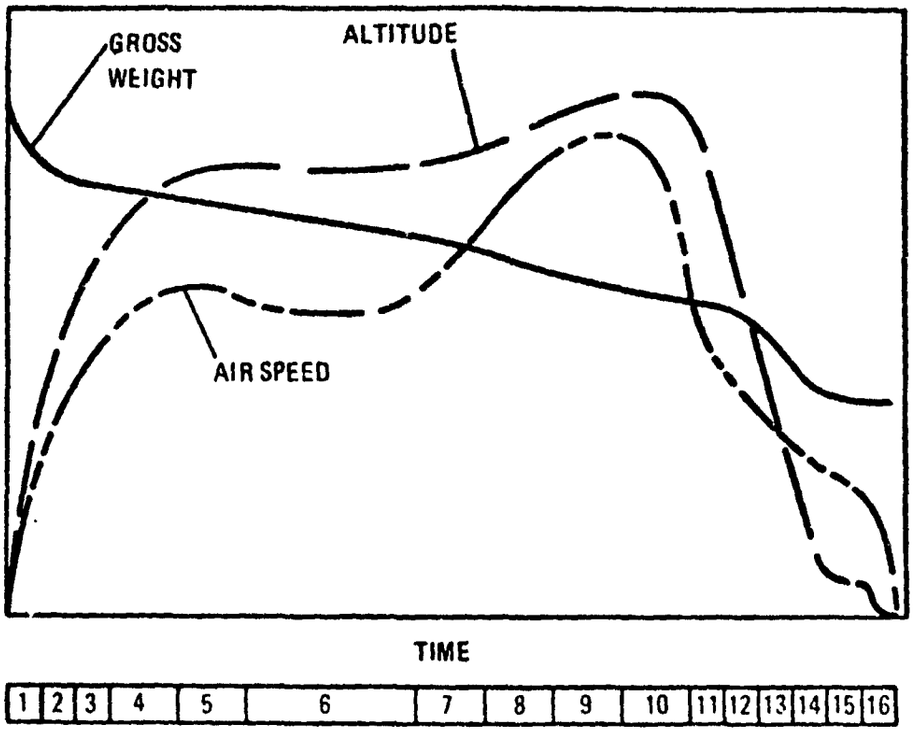

Figure 8-8 Typical Flight Profile

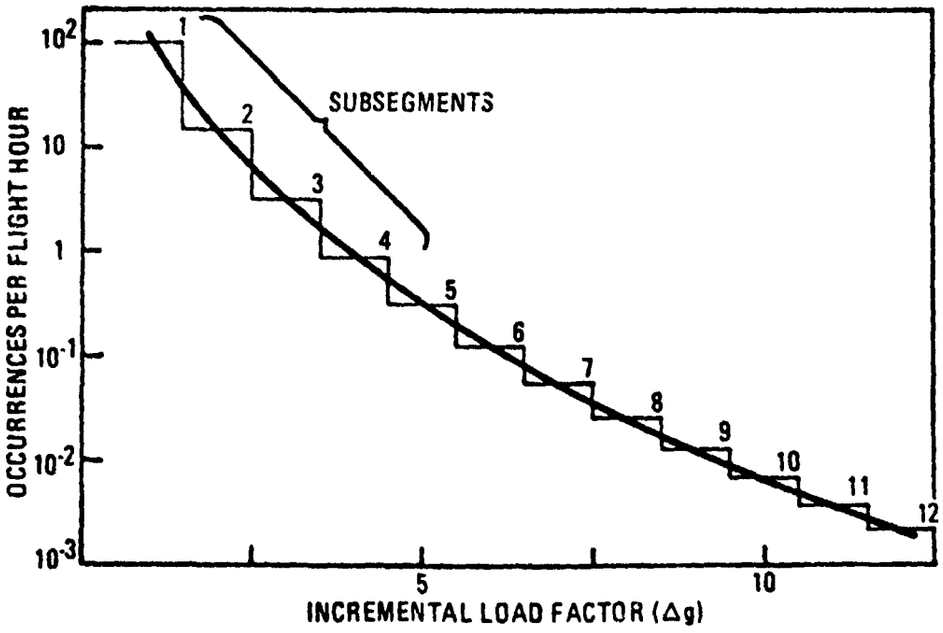

Figure 8-9 Typical Segment Load Frequency Curve

solving for U_{de}

$$U_{de} = \frac{\Delta g}{m S V_e \bar{K}_g \rho_o/(2W)}$$

U_{de} is then calculated for each subsegment, and the curves of Figure C13-37 are used to find the frequency of occurrence.

For maneuver loads, Figure C13-41 of Reference 5 shows incremental load factor vs frequency of occurrence. For taxi loads, Figure C13-46 of Reference 5 shows incremental load factor vs frequency of occurrence. Incremental load factor vs frequency of occurrence for landing loads was averaged from data for two commercial transport aircraft.

The resulting fatigue load spectrum is shown in Table 8-2 . The number of cycles is based on 10,000 flights. The variation between cycles and flights is linear, so that linear ratioing of cycles and design life is valid.

Table 8-1 Typical Transport Flight Profile

	Segment Description	Gross Weight		Altitude		Eqev. Airspeed		Mach	Distance	
		Kg (10^3)	Lbs (10^3)	M (10^3)	FT (10^3)	Km Hr	Knots	No.	Km	Miles
	1. Taxi; Takeoff Run; Landing Roll	162.5	358.3	S.L.	S.L.	-	-	-	-	-
Maneuver Segments	2. Climb (Flaps Down 25°)	159.8	352.2	0-1.52	0-5	413.3	223	0.355	13.12	8.15
	3. Climb	159.8	352.2	1.52-3.05	5-10	463.3	250	0.435	20.13	12.51
	4. Climb	159.8	352.2	3.05-6.1	10-20	630.1	340	0.684	76.49	47.53
	5. Climb	159.8	352.2	6.1-10.67	20-35	591.2	319	0.836	242.52	150.70
	6. Cruise	154.9	341.4	10.67	35	505.9	273	0.850	636.61	395.58
	7. Descent	152.1	335.4	10.67-6.1	35-20	591.2	319	0.836	85.76	53.29
	8. Descent	152.1	335.4	6.1-3.05	20-10	630.1	340	0.684	53.64	33.33
	9. Descent (Flaps Down 15°)	152.1	335.4	3.05-1.52	10-5	463.3	250	0.435	37.74	23.45
	10. Descent (Flaps Down 50°)	152.1	335.4	1.52-0	5-0	413.3	223	0.355	22.71	14.11
Gust Segments	11. Climb (Flaps Down 25°)	159.8	352.2	0-1.52	0-5	413.3	223	0.355	13.12	8.15
	12. Climb	159.8	352.2	1.52-3.05	5-10	463.3	250	0.435	20.13	12.51
	13. Climb	159.8	352.2	3.05-6.1	10-20	630.1	340	0.684	76.49	47.53
	14. Climb	159.8	352.2	6.1-10.67	20-35	591.2	319	0.836	242.52	150.70
	15. Cruise	154.9	341.4	10.67	35	505.9	273	0.850	636.61	395.58
	16. Descent	152.1	335.4	10.67-6.1	35-20	591.2	319	0.836	85.76	53.29
	17. Descent	152.1	335.4	6.1-3.05	20-10	630.1	340	0.684	53.64	33.33
	18. Descent (Flaps Down 15°)	152.1	335.4	3.05-152	10-5	463.3	250	0.435	37.74	23.45
	19. Descent (Flaps Down 50°)	152.1	335.4	1.52-0	5-0	413.3	223	0.355	22.71	14.11
	20. Landing	151.8	334.7	S.L.	S.L.	237.2	128	-		-

Table 8-2 Typical Transport Fatigue Spectrum - Cycles per 10,000 Flights

SUBSEGMENT		1	2	3	4	5	6	7	8	9	10	11	12	13	14	15	16
SEGMENT NO.	LOAD TYPE •	Δ g .10	Δ g .15	Δ g .20	Δ g .25	Δ g .30	Δ g .35	Δ g .40	Δ g .45	Δ g .50	Δ g .60	Δ g .70	Δ g .80	Δ g .90	Δ g 1.00	Δ g 1.10	Δ g 1.20
1	2-2	2349957		249957		15070		882		43							
2	2-1	246970		10867		823		120		26	8	3	1	.4			
3	2-1	11700		5212		834		199		54	17	7	3	1	.6		
4	2-1					6990		2502		951	336	190	90	45	24	14	8
5	2-1	100467		13700		3014		685		196	60	24	11	6			
6	2-1	113023		8417		1236		283		75	25						
7	2-1	48446		5921		1211		296		85	28	11	5	2			
8	2-1					6060		2083		833	333	159	79	42	22	12	7
9	2-1			13794		2468		558		156	52	20	8	4	2	.9	
10	1-1	486552		22397		1987		282		61	18	7	3	1			
11	1-1	4320	1328	448	151	51	18	7	3	2							
12	1-1	6630	2039	688	231	78	28	11	5	2							
13	1-1	25191	7747	2614	879	295	106	42	19	9							
14	1-1	79871	24564	8288	2788	934	347	132	59	30							
15	1-1	209657	64480	21757	7318	2453	882	347	154	77							
16	1-1	28244	8686	2931	986	330	119	47	21	10							
17	1-1	17665	5433	1833	617	207	74	29	13	6							
18	1-1	12428	3822		434	145	52	21	9	5							
19	1-1	7478	2300	[illegible]	261	87	31	12	6	3							
20	3-2				508.	7030.	1500.			845.		104.		13.			

• 1-1 MANEUVER
3-2 LANDING IMPACT
2-2 TAXI
2-1 GUST

8.1.6 External Loads. Net limit loads due to the air load, inertia loads and landing gear loads of various flight and ground conditions may be input directly or provided by the integrated loads program described in Section 7.0.

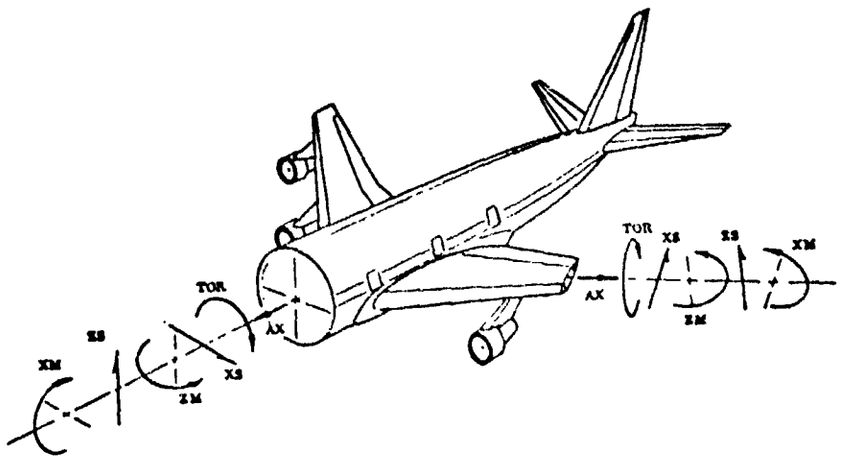

Figure 8-10 External Loads Sign Convention

The loading conditions are separated into two groups. The first group consists of from one to six conditions. These conditions are specified by the user and are used to size the structure so as to preclude static strength failures and to meet residual strength requirements. The second group consists of the six conditions listed in Table 8-3 . These conditions are used to define the fatigue stress spectrum described in Section 8.1.9.

Table 8-3 Fatigue Spectrum Loading Conditions

Condition Number	Description
1	1G Taxi
2	1G Level Flight
3	2G Vertical Gust
4	2G Maneuver
5	1G Landing Impact
6	Maximum Pressure (Fuselage)

Each loading condition defines the six components of load (AX, XS, ZS, TOR, XM, ZM) at up to twenty stations along the structure. The sign convention used is presented in Figure 8-10 . A typical fuselage loading condition is illustrated in Figure 8-11. Steps in the loading curves are represented by repeating stations with the two

different load component values. The reference axis used for input loads is the centerline for fuselages and a line midway between the front and rear spars for aerodynamic surfaces.

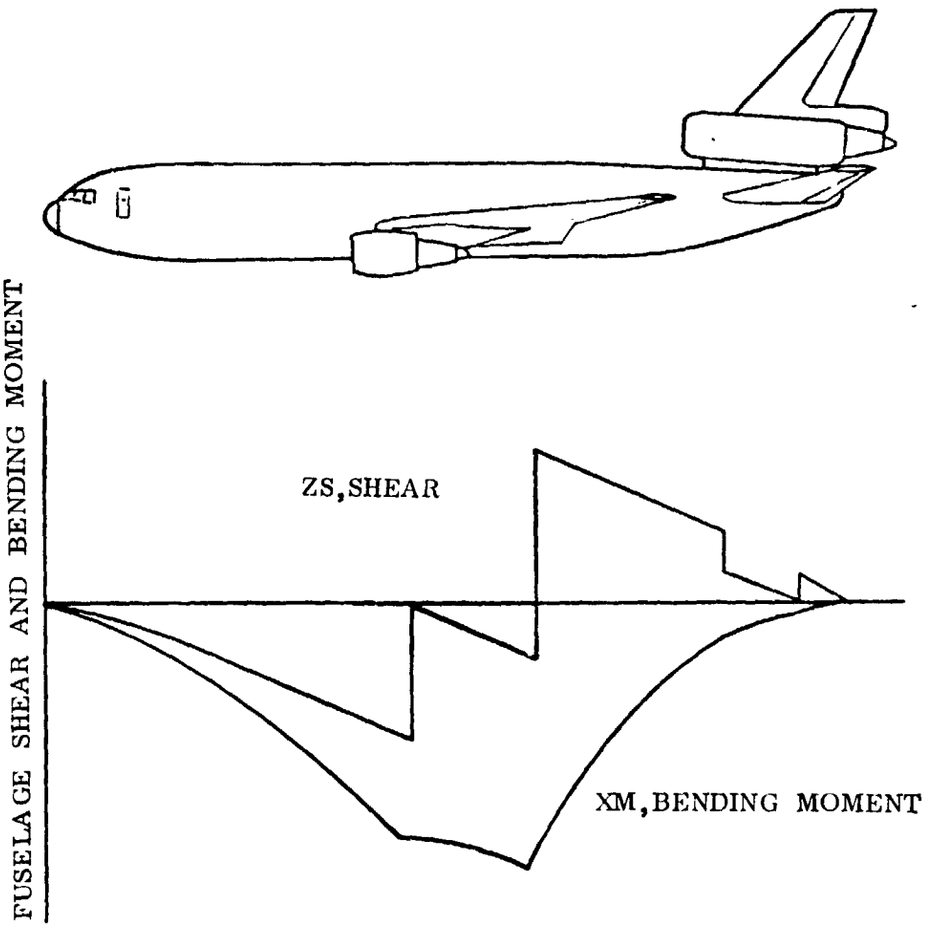

Figure 8-11 **Typical Fuselage Load Condition**

8.1.7 Structural Design Procedure. The structural design procedure starts with the input design, then through a series of design analysis and redesign iterations produces a final design. The iteration process continues until the lightest weight design which satisfies design criteria and constraints is found.

The design analysis involves the comparison of applied stresses and allowable stresses. The internal load solution described in Section 8.1.9 is used to calculate the applied stresses. The box beam internal load solution was selected instead of a finite element solution in order to keep computer execution time at an acceptable level. This selection restricts this procedure to relatively clean beam-like structures. However, decoupling of internal loads from one station to the next is basic to the box beam theory. Hence, the overall design problem is reduced to a series of cross-section design problems at any number of desired locations along the structure.

The procedure used to design the cross section is a two part procedure. The first part, the section sizing procedure, adds or subtracts material from the structural elements of the cross section in order to produce a zero margin or minimum gage design. The second part employs a non-linear programing technique to minimize the "criticality" of each element while maintaining a constant weight design. This element optimization procedure is then iterated with the section sizing procedure until the design converges. Convergence occurs when two successive iterations produce a change in weight that is within a specified tolerance, or the input iteration limit is encountered.

During the section sizing portion of the design process, only the thickness variables are changed. Figure 8-12 illustrates a typical cross-section design problem.

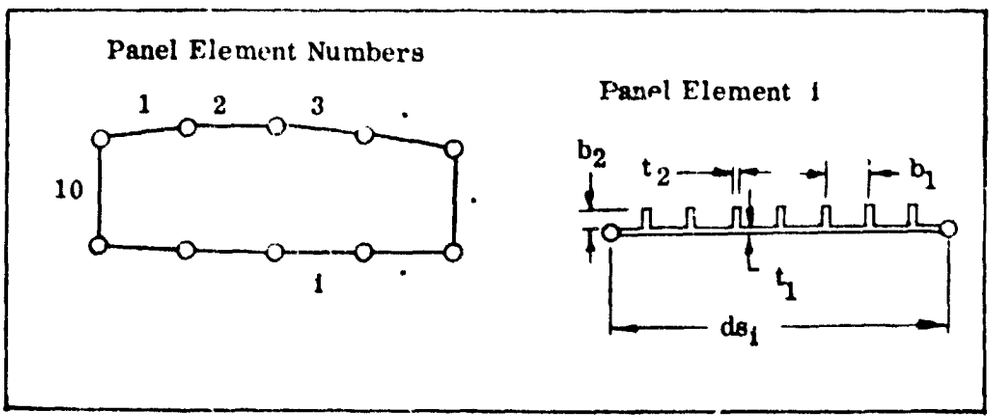

Figure 8-12 Typical Cross Section

The section sizing procedure sizes the structure based on design criteria such as static strength, stability, service life, and residual strength.

The procedure used to size the structure is:

a. Analyze the structure as it is defined by the input data.

b. Predict new skin thickness and stiffener area based on the analysis results.

c. Re-analyze the structure as predicted in b.

Steps b. and c. are iterated until the minimum weight structure satisfying the design criteria is found. During this process, material is added or removed from the panel such that the design proportions produced in the optimization phase are maintained.

The equivalent thickness ($\bar{t}$) of a structural panel is computed:

$$\bar{t} = t_{sk} + \frac{\rho_{st}}{\rho_{sk}} \cdot \frac{A_{st}}{B_{st}}$$

where: t_{sk} - skin thickness

A_{st} - stiffener area

B_{st} - stiffener spacing

ρ_{st} - stiffener material density

ρ_{sk} - skin material density

The technique employed in step b. to predict the new $\bar{t}$ is described below. The new $\bar{t}$ is predicted by passing a parabola through three points on a plot of $\bar{t}$ versus margin of safety, MS. The points are (TBAR = 0, MS = -1), ($\bar{t}_i$, MS t_i), ($\bar{t}_{i+1}$, MS ($\bar{t}_{i+1}$), see Figure 8-13. The new $\bar{t}$ is found by solving for the proper root of the resulting equation. The process is started by assuming the slope at $\bar{t} = 0$ to be 0 for the first iteration.

The object of the element optimization procedure is to adjust detail dimensions of an element so as to make the most efficient use of the material while maintaining a given weight. As an example refer again to Figure 8-12 . The panel element shown contains four design variables t_1, t_2, b_1 and b_2.

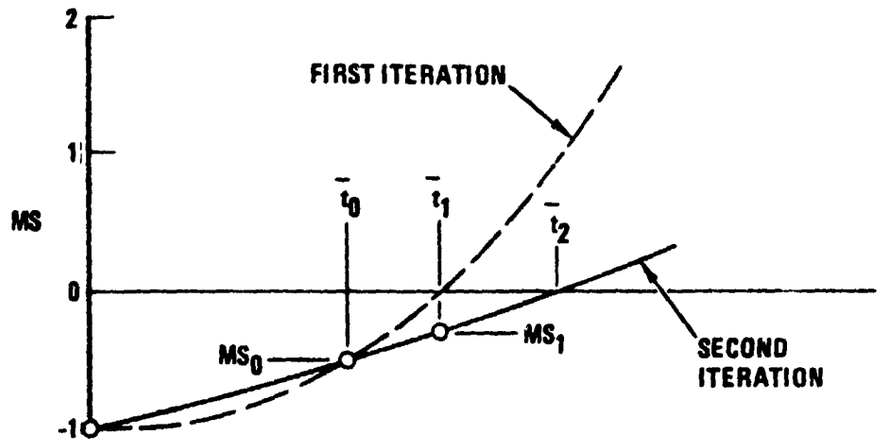

Figure 8-13 Section Sizing Procedure

The object is to find the optimum set, i.e., that set which represents the "least critical" panel possible. Since this procedure requires that $\bar{t}$ remain constant, there are only three independent design variables. Given any three variables the fourth is found by solving the following equation for the appropriate variable.

$$\bar{t} = t_1 + t_2 b_2 / b_1$$

The "least critical" design is defined as that design for which the following criticality parameter is a minimum

$$P = \sum_{\ell=1}^{L} \sum_{j=1}^{J} F(MS_{\ell,j}) + \sum_{m=1}^{M} F(MC_m)$$

where

ℓ denotes the failure mode
j denotes the loading condition
m denotes the sub element of each panel element

MS = margin of safety

MC = side constraint margin e.g., $(t_m - tmin_m)/tmin_m$

$$F(x) = \frac{1}{x} \qquad x > \epsilon$$

$$F(x) = \frac{1}{\epsilon}\left[\frac{x}{\epsilon}\left(\frac{x}{\epsilon} - 3.\right) + 3.\right] \qquad x \leq \epsilon$$

where

$$\epsilon = 10^{-5}$$

A typical plot of the criticality function, F, is illustrated in Figure 8-14.

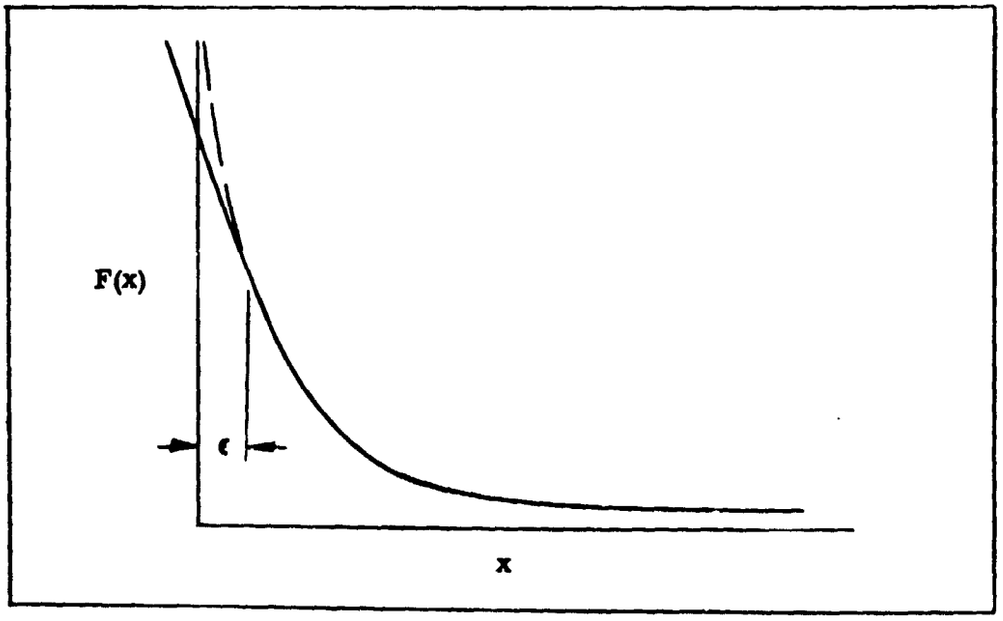

Figure 8-14 Criticality Function

There are a number of techniques available to minimize P, the method used by APAS is the Fletcher-Powell-Davidon, unconstrained minimization technique (Ref. 6). P is the objective function and $[t_2, b_1, b_2]$ is the design variable vector for the example problem. Optimization is performed on each element of the cross section in order to minimize weight.

8.1.8 Structural Element Symmetry Groups. A symmetry group is a group of structural elements which have identical designs. When a number of structural elements are placed into the same symmetry group only one design is produced. The design of the

element respects all of the margins of safety for all of the elements in the group. This technique provides a means by which fuselage centerplane symmetry can be respected without duplicating reversible loading conditions. It is often desirable to make adjacent panel elements identical for ease in manufacturing. This can be accomplished with symmetry grouping also. Since the use of symmetry groups reduces the number of independent design variables of the structure it can be of significant use in reducing execution time and should be employed wherever possible.

8.1.9 Structural Analysis. This section presents the techniques used to calculate the applied stresses, including the fatigue stress spectrum and the methods used to calculate margins of safety for static strength, fatigue, flaw growth, and residual strength criteria.

The internal loads analysis is based on classical box beam theory (Reference 5). The assumptions made are; plane sections remain plane under the action of bending moments and axial loads, cross sections are free to warp when torque is applied, and the structure obeys a linear elastic stress-strain law.

The axial stresses are made up of stresses due to axial loads and stresses due to bending moments. The equation used to calculate the axial stresses is,

$$\sigma = \frac{M_x I_{xz} - M_z I_{xx}}{I_{xx} I_{zz} - I_{xz}^2}(x-\bar{x}) + \frac{M_z I_{xz} - M_x I_{zz}}{I_{xx} I_{zz} - I_{xz}^2}(z-\bar{z}) + \frac{P}{A}$$

where,

M_x = Net bending moment about a horizontal axis passing through the centroid

M_z = Net bending moment about a vertical axis passing through the centroid

P = Axial load

x, z = Coordinates of the element, see Figure 8-15

$\bar{x}, \bar{z}$ = Coordinates of the centroid, see Figure 8-15

$I_{xz}, I_{xx}, I_{zz}, A$ = Section properties

The shear stresses resist the external shear forces and the torque applied to the section. Under the basic assumptions the shear flow is calculated using a VQ/I distribution for the shear forces. The resultant applied torsion is due to the applied torque and the couples resulting from shifting the shear forces XS and ZS to the shear center. This net torsion is resisted internally by a shear flow which is distributed according to a T/2A distribution. In the case of multiple cell structures, such as multi-spar wings, the cells are assumed to have equal twisting angles. For a further description of the method see Paragraph 17.9 thru 17.11 of Reference 7 .

Section properties of the cross section of the wing or fuselage are calculated at each station where structural sizing is performed. These properties are used to calculate the internal loads distribution and to provide stiffness information. In order to simplify the calculation of section properties the following assumptions are made: (1) the material which resists bending moments is assumed to be smeared uniformly between nodal points, (2) only the skin and shear webs are effective for resisting shear loads and torsion. The following equations are used to calculate section properties. (See Figure 8-15)

$$A = \int da$$

$$\bar{x} = \frac{1}{A} \int x\,da$$

$$\bar{z} = \frac{1}{A} \int z\,da$$

$$I_{xx} = \int z^2 da - A \cdot \bar{z}^2$$

$$I_{zz} = \int x^2 da - A \cdot \bar{x}^2$$

$$I_{xz} = \int xz\,da - A \cdot \bar{x} \cdot \bar{z}$$

$$J = 4A_T^2 / \oint ds/t$$

where,

x, z are the coordinates of the incremental area da

A is the total area of the cross-sectional material

$\bar{x}, \bar{z}$ are the coordinates of the centroid of A

I_{xx} is the moment of inertia of A taken about an x axis passing through the centroid

I_{zz} is the moment of inertia of A taken about a z axis passing through the centroid

I_{xz} is the product of inertia of A with respect to the centroid

J is the torsional stiffness constant

A_T area enclosed by the cross section

ds incremental distance along the box contour

t thickness of the shear resisting material associated with ds

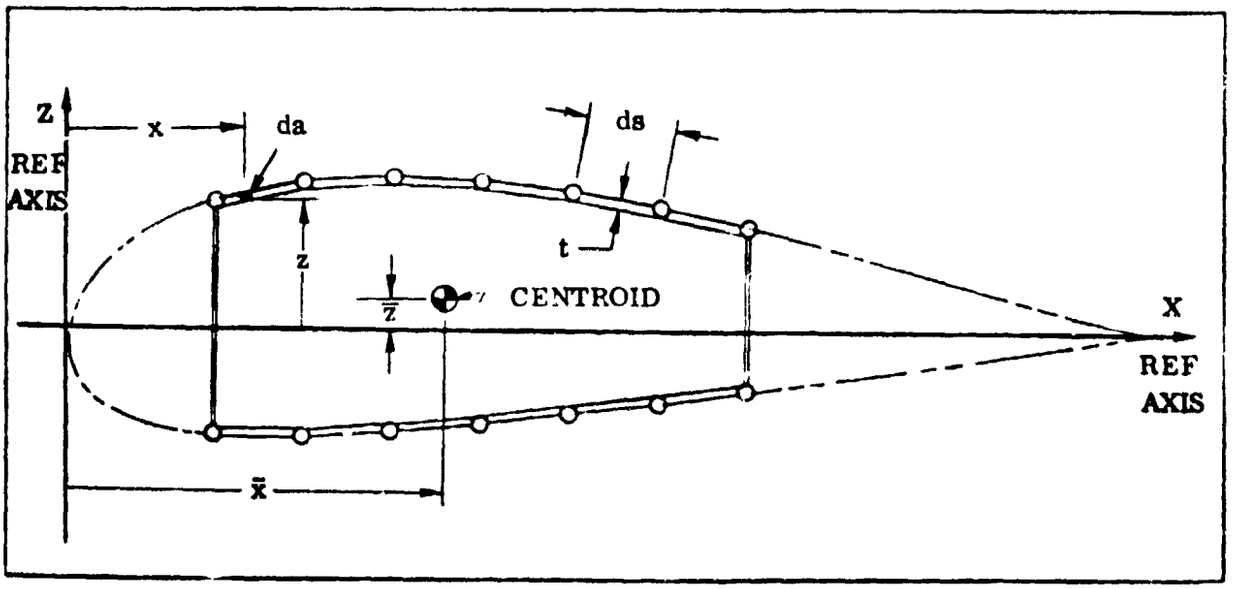

Figure 8-15 Typical Wing Section

The depth of the static strength analyses performed is consistent with typical pre-design stress analyses. The analytical techniques and their sources are described in the following paragraphs. The failure modes included are summarized in Table 8-4. The margins of safety are computed for each failure mode and uses these values to direct structural design optimization. The critical failure mode margin of safety is included in the computer output for each element and load condition.

Table 8-4. Panel Element Failure Modes

Failure Mode	Panel Construction Type (see Figure 8-3)											
	1	2	3	4	5	6	7	8	9	10	11	12
Local Buckling	•	•	•	•	•	•	•	•	•			
Diagonal Tension	•	•	•	•	•	•	•	•	•			
Crippling	•	•	•	•	•	•	•	•	•			
Inter-Rivet Buckling and Wrinkling				•	•	•	•	•	•			
Panel General Instability										•	•	•
Wide Column Buckling	•	•	•	•	•	•	•	•	•			
General Yielding	•	•	•	•	•	•	•	•	•	•	•	
Distortion Energy Theory	•	•	•	•	•	•	•	•	•	•	•	
Maximum Fiber [illegible] Laminate												•

Local Buckling (Compression and Shear)

Critical local buckling stresses for compression and shear loading are computed by using Equations 8-1 and 8-2, respectively. These equations were obtained from Reference 5.

Compression Buckling

$$F_{cr} = \frac{\pi^2 k_c E}{12 (1 - \nu_e^2)} \left(\frac{t}{b}\right)^2 \qquad (8\text{-}1)$$

where: F_{cr} - critical compression buckling stress

k_c - compression buckling coefficient

E - modulus of elasticity

ν_e - elastic Poisson's ratio

t - thickness

b - short dimension of plate or loaded edge

Shear Buckling

$$F_{scr} = \frac{\pi^2 k_s E}{12 (1 - \nu_e^2)} \left(\frac{t}{b}\right)^2 \qquad 8\text{-}2$$

where: F_{scr} - critical shear buckling stress

k_s - shear buckling coefficient

b - short dimension of plate

The buckling coefficient in Equations 8-1 and 8-2 is dependent on the aspect ratio of panel length/width and panel edge fixity. The aspect ratio is assumed to to be large and the corresponding asymptotic value of the buckling coefficient for the appropriate edge fixity is used. Typical values of shear and compression buckling coefficients for various edge fixity conditions are shown in Figure 8-16. The actual coefficients used for each available type of stiffened skin panel construction are shown in Figure 8-17.

For some flight vehicle designs, it may be a requirement that buckling of the skin panels is not permitted up to a specified percent of limit load. The program has the capability to handle this design criterion. Both shear and compression buckling are considered. The interaction equation used to combine the effects of shear and compression was taken from Reference 5 and is presented below:

$$R_c + R_s^2 = 1.0 \qquad (8\text{-}3)$$

where: R_c - applied compression stress/compression buckling stress

R_s - applied shear stress/shear buckling stress

The associated margin of safety equation is:

$$M.S. = \frac{2}{R_c + \sqrt{R_c^2 + 4 R_s^2}} - 1 \qquad (8\text{-}4)$$

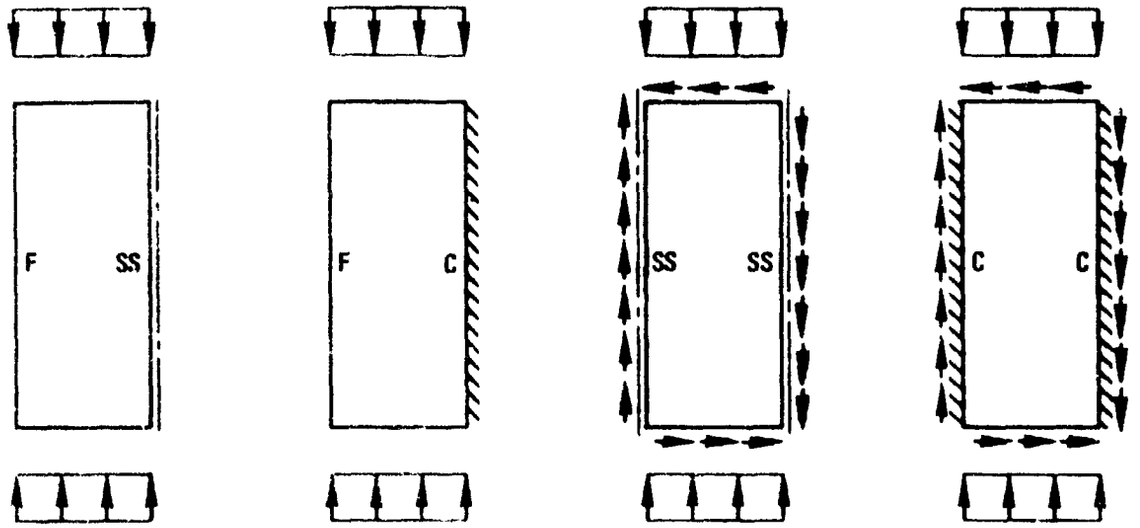

Figure 8-16. Shear (k_s) and Compression (k_c) Buckling Coefficients for Various Edge Fixities

Diagonal Tension Analysis

Maximum allowable panel shear stresses are determined by using the relationship shown in Figure 8-18. Parameters F_s and F_{su} are the maximum allowable shear and the material ultimate shear, respectively. Parameter F_{scr} is critical shear stress at which shear buckling initiates. The equation used to compute F_{scr} is described in the local buckling failure mode section.

Crippling

The method for the crippling analysis used was taken from Reference 8. The crippling strain for the combination of stiffener and effective skin is computed by the following equation:

$$\epsilon_{cc} = \left[\frac{\Sigma b_n t_n f_{ccn}}{\Sigma b_n t_n E_n} \right] \qquad (8\text{-}5)$$

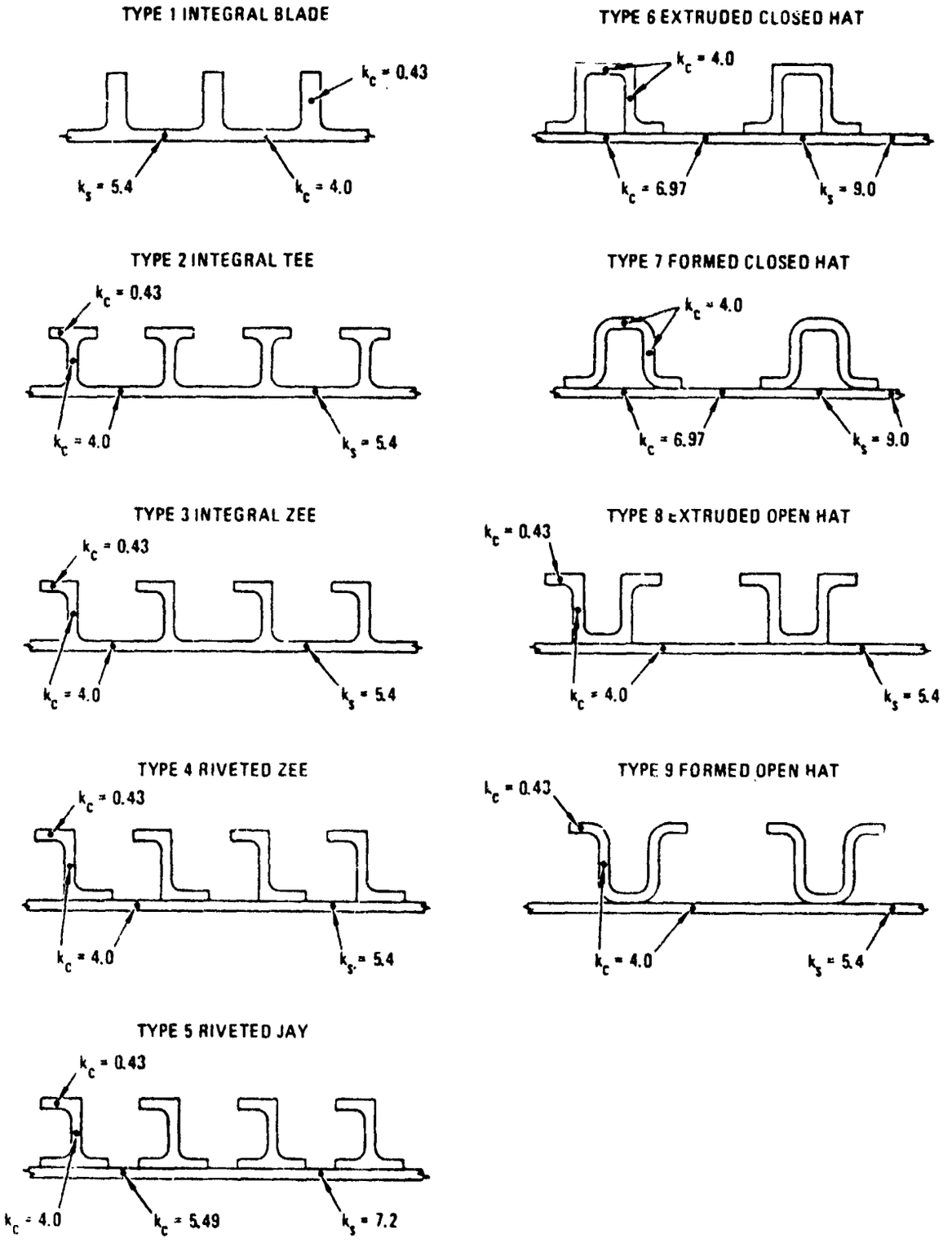

Figure 8-17. Compression and Shear Buckling Coefficients for Each Skin Panel Construction Type

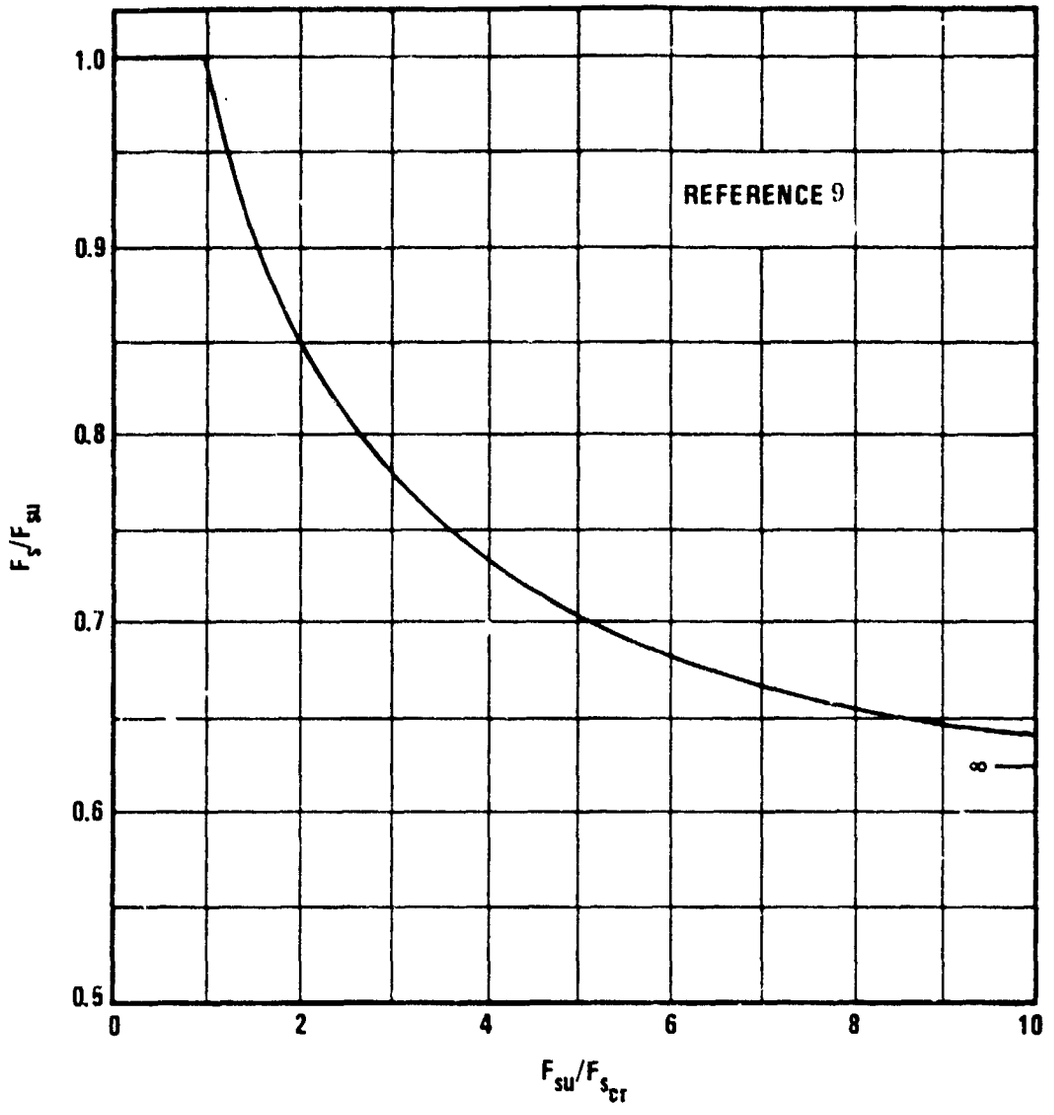

Figure 8-18. Diagonal Tension Chart

where: ϵ_{cc} - crippling strain for section

E_n - modulus of elasticity of element n

b_n - effective element width

t_n - element thickness

f_{ccn} - element crippling stress

The element crippling stress (f_{ccn}) is obtained from Figure 8-19.

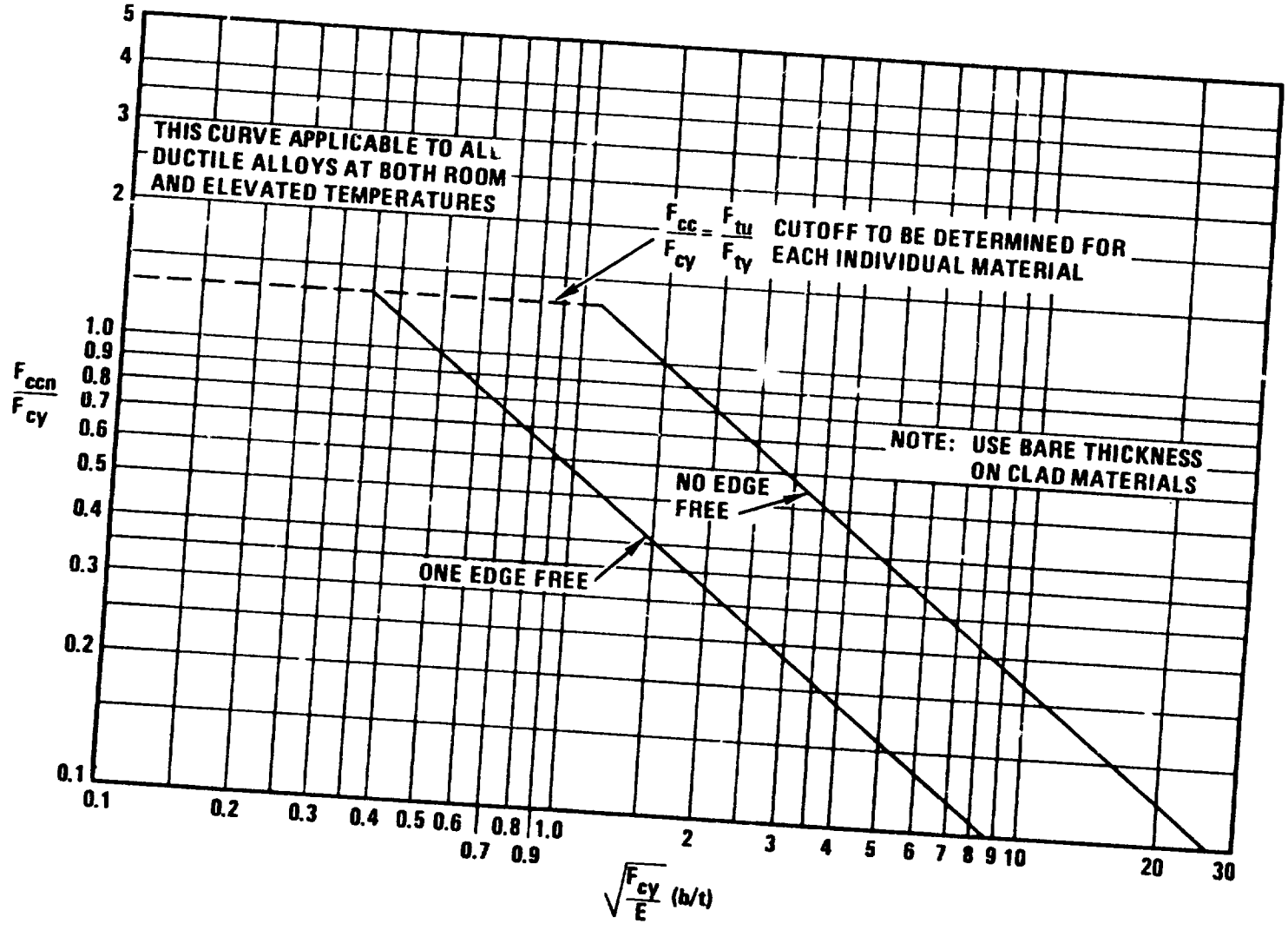

Figure 8-19. Nondimensional Crippling Curves

Inter-Rivet Buckling and Sheet Wrinkling

Inter-rivet buckling involves a failure of the skin between rivets. When both the skin and the stiffener fail, it is known as a wrinkling failure. The program checks for both of these failure modes using the methods taken from Reference 5. Inter-rivet buckling strain is computed using the following equation:

$$\epsilon_{ir} = \frac{C\pi^2}{12\,(1-\upsilon_e^2)}\left(\frac{t_s}{P}\right)^2 \qquad (8\text{-}6)$$

where: ϵ_{ir} - inter-rivet buckling strain

C - end fixity (C equals 4, for all cases)

t_s - skin thickness

P - rivet pitch

E - modulus of elasticity

υ_e - Poisson's ratio

Rivet pitch spacing is set equal to four times the rivet diameter for all cases. The rivet diameter for each case is selected based on skin thickness according to Table 8-5.

Table 8-5. Rivet Diameter Versus Skin Thickness cm, (inches)

Skin Thickness (t_s)		Rivet Diameter	
0.000	(0.000)	0.318	(0.1250)
0.064	(0.025)	0.397	(0.1563)
0.127	(0.050)	0.476	(0.1875)
0.318	(0.125)	0.635	(0.2500)
0.635	(0.250)		

Sheet wrinkling strain is computed using the equation presented below:

$$\epsilon_w = \frac{k_w\,\pi^2}{12\,(1-\upsilon_e^2)}\left(\frac{t_s}{b_s}\right)^2 \qquad (8\text{-}7)$$

where: ϵ_w - wrinkling strain

k_w - wrinkling coefficient

t_s - skin thickness

b_s - stringer spacing

The empirical wrinkling coefficient (k_w) is a function of the effective rivet offset and local geometry. The effective rivet offset is determined using Figure 8-20 and is used in Figure 8-21 to evaluate the wrinkling coefficient.

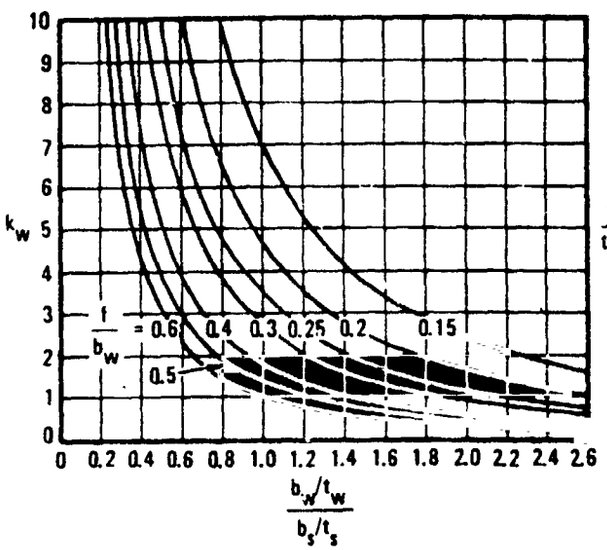

Figure 8-20. Experimentally Determined Values of Effective Rivet Offset

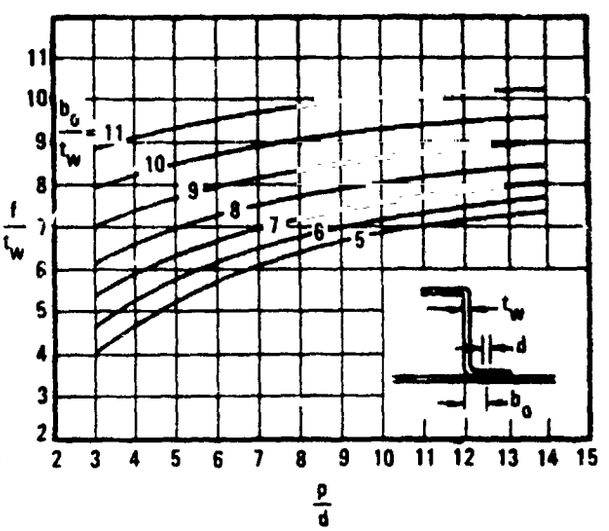

Figure 8-21. Experimentally Determined Coefficients for Failure in Wrinkling Mode

Panel General Instability

This section is a description of the analysis used to calculate general instability allowables for panel types 10, 11, and 12 (see Figure 8-3). This analysis procedure was taken from Reference 10. Design formulas are used to provide conservative estimates of the buckling allowables.

The moments of inertia and stiffnesses in both directions are calculated for a plate or sandwich panel in the conventional manner. See Figure 8-22 for sign convention used in the development of the design equations for buckling.

$$D_{11} = E_x I_y/(1 - \upsilon_{xy} \upsilon_{yx}) \quad (8\text{-}8)$$

$$D_{22} = E_y I_y/(1 - \upsilon_{xy} \upsilon_{yx}) \quad (8\text{-}9)$$

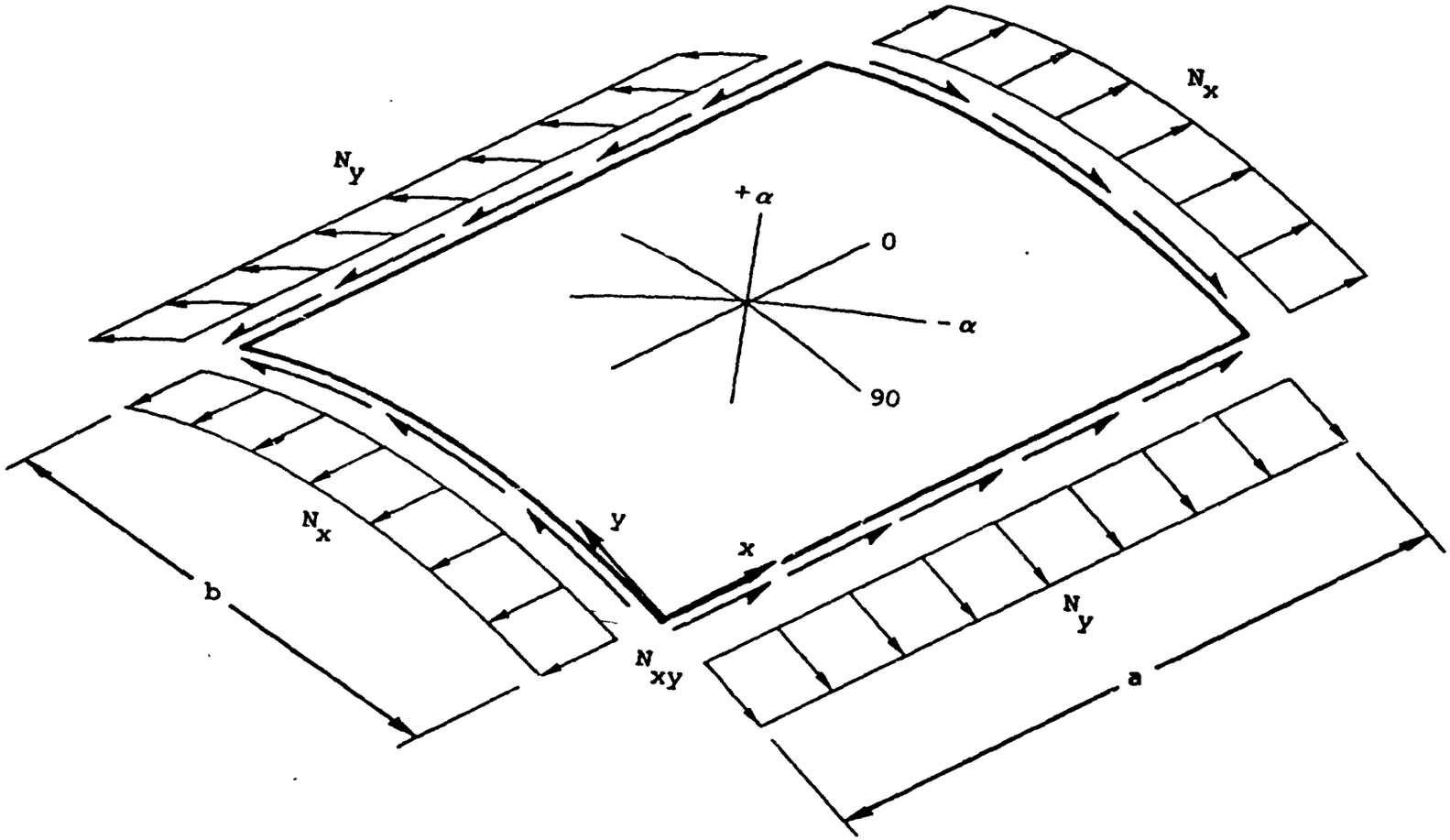

Figure 8-22. Panel Configuration

$$D_{12} = D_{11}\, \upsilon_{yx} \tag{8-10}$$

$$D_{66} = G_{xy}\, I_x \tag{8-11}$$

The shear buckling of a simply supported orthotropic plate can be reasonably estimated with the following formula

$$N_{xy_{cr}} = C_3 \sqrt[4]{D_{11}\, D_{22}^3} \,/\, b^2 \tag{8-12}$$

where: $$C_1 = (b/a) \sqrt[4]{D_{11}/D_{22}} \tag{8-13}$$

$$C_2 = (D_{12} + 2D_{66}) / \sqrt{D_{11}\, D_{22}} \tag{8-14}$$

$$C_3 = 32.8 + 20\, C_2 + 14.2\, (C_1)^{2.4} + 24.8\, C_2\, C_1^2 \tag{8-15}$$

No simple correction for the effect of curvature on the shear buckling allowable is available at present.

The buckling allowable for a flat, simply-supported, orthotropic plate under biaxial loads may be found using the following method. Given a ratio

$$\alpha = N_x/N_y \tag{8-16}$$

the allowable in the axial direction may be expressed by

$$(N_{x_{cr}})_{panel} = \frac{\pi^2 \left[D_{11}\, (m/a)^2 + 2\, (D_{12} + 2D_{66})(n/b)^2 + D_{22}\, (n/b)^4 (a/m)^2 \right]}{1 + \alpha\, (an)^2 \,/\, (bm)^2} \tag{8-17}$$

where m and n are possible half-wave numbers into which the panel may buckle in the x and y directions, respectively. This formula is evaluated for the first five modes in each direction, and the minimum value is chosen. The allowable $N_{y_{cr}}$ is obtained similarly.

An estimate for the correction due to curvature on the compressive buckling allowable is obtained as described in Reference 7. The buckling allowable of the full cylinder from which the panel was cut is added to the flat plate allowable as obtained above. For an orthotropic cylinder, the cylinder buckling allowable is approximated as

$$(N_{x_{cr}})_{cylinder} = \frac{1}{2} \sqrt{E_x E_y}\; t^2 \,/\, \left[R \sqrt{3\, (1 - \upsilon_{xy}\, \upsilon_{yx})} \right] \tag{8-18}$$

where t and R are the thickness and radius of the cylinder, respectively.

The ratios of the applied loads to the allowables are formed:

$$R_s = N_{xy} / N_{xy_{cr}} \tag{8-18}$$

$$R_x = N_x / \left[(N_{x_{cr}})_{panel} + (N_{x_{cr}})_{cylinder} \right] \tag{8-19}$$

$$R_y = N_y / N_{y_{cr}} \tag{8-20}$$

The buckling margin of safety for each panel is calculated from the interaction equation

$$M.S. = \left[\frac{2}{R_x + R_y + \sqrt{(R_x + R_y)^2 + 4 R_s^2}} \right] - 1 \tag{8-21}$$

The above analysis is brief and offers various degrees of approximation, depending on the complexity of the section being analyzed. For construction with orthotropic flat panels, they provide excellent estimates for the buckling allowables of simply supported panels. With the addition of curvature, it provides somewhat less accurate allowables.

Wide Column Buckling

This section is a description of the analysis used to calculate the general instability allowables for panel types 1 through 9, (see Figure 8-3).

Wide column buckling analysis of multi-rib structures assumes that the cover panel behaves as a simply supported column. The ribs, oriented perpendicular to the load, are assumed to provide the continuous simple supports. The effect of spar support at the unloaded edges of the column is ignored in this analysis. The method used for wide column analysis was taken from Reference 5 and is described below.

The relationship between critical column strain versus slenderness ratio (L'/ρ) is shown in Figure 8-23.

For large values of slenderness ratio, a form of the Euler column equation applies:

$$\epsilon_c = \frac{\pi^2}{(L'/\rho)^2} \tag{8-22}$$

where: ϵ_c - column failing strain

(L'/ρ) - slenderness ratio (effective length/radius of gyration)

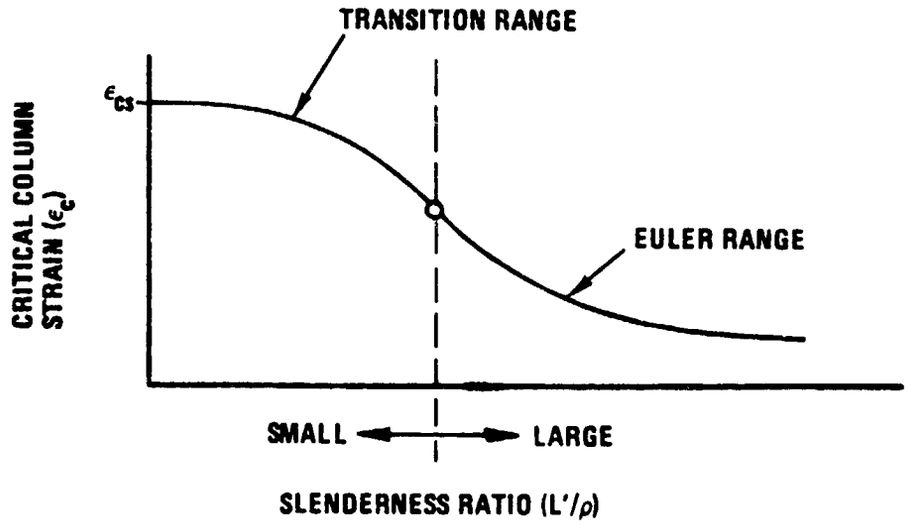

Figure 8-23. Critical Column Strain Versus Slenderness Ratio (L'/ρ)

For small values of slenderness ratio, the critical column strain transitions from the crippling strain to the Euler critical column strain. The following parabolic approximation is used to represent this transition.

$$\epsilon_c = \epsilon_{cs}\left[1 - \left(1 - \frac{\epsilon_{cr}}{\epsilon_{cs}}\right)\left(\frac{\epsilon_{cr}}{\epsilon_E}\right)\right] \qquad (8\text{-}23)$$

where: ϵ_c - column critical strain

ϵ_{cs} - crippling strain

ϵ_{cr} - buckling strain for column cross-section

ϵ_E - Euler column strain

Equation 8-23 applies for $\epsilon_c > \epsilon_{cr}$. Yield strain ($\epsilon_y$) is substituted for ϵ_{cr}, when $\epsilon_{cr} > \epsilon_y$.

General Yielding

To ensure that elastic stress conditions exist up to limit load for each structural design, the program compares element tensile or compressive stresses to material yield for all loading conditions.

Distortion Energy Theory

The distortion energy theory (Hencky - Von Mises theory, Reference 11) is another failure mode criterion used in the analysis. This theory is based on the assumption

that failure occurs when the distortion energy corresponding to the principal stress components equals the distortion energy at failure for the maximum allowable axial stress. This failure criterion is defined by Equation 8-24:

$$\sigma_1^2 - \sigma_1 \sigma_2 + \sigma_2^2 = \sigma_{max}^2 \qquad (8\text{-}24)$$

The boundary curve defined by Equation 8-24 for all possible combinations of principal stresses is shown in Figure 8-24. Any principal stress combination that falls outside this boundary curve represents a negative margin of safety.

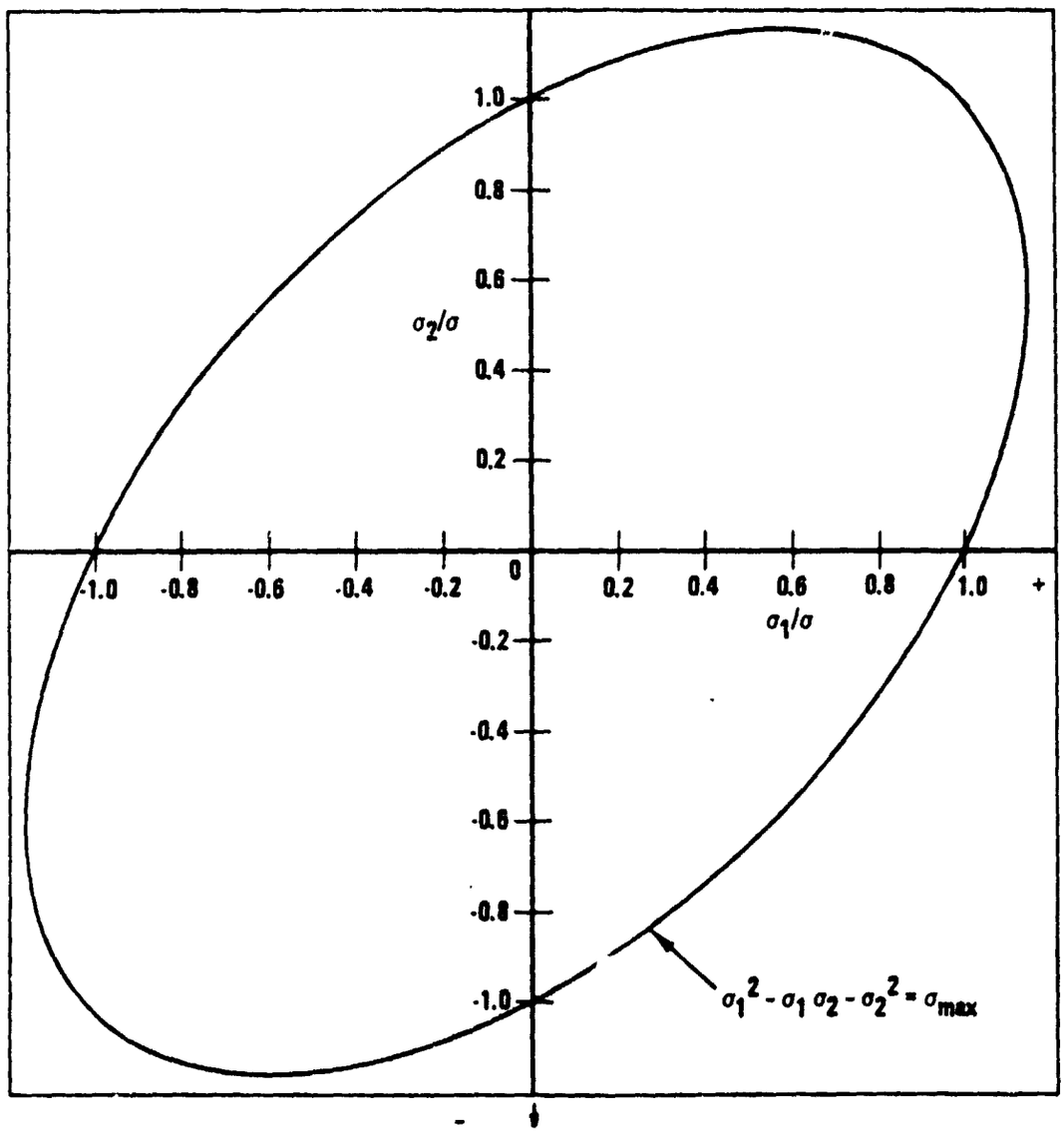

Figure 8-24. Distortion Energy Theory

Laminate Analysis

The composite panels (construction type 12) are specially orthotropic; if the panel is of sandwich construction, it is assumed that the core supplies no in-plane stiffness but is perfectly rigid in the out of plane direction, and that each of the composite faces carries one-half of the applied in-plane loads.

The laminate analysis is designed to find the strains in the 0°, 90°, and $\pm\alpha°$ plies. The laminate longitudinal, transverse and shear strains, ϵ_x, ϵ_y, and ϵ_{xy} respectively, are calculated using the laminate in-plane constitutive matrix, [A], and the applied running loads, N_x, N_y, and N_{xy}, as shown in Figure 8-22.

$$\begin{Bmatrix} \epsilon_x \\ \epsilon_y \\ \epsilon_{xy} \end{Bmatrix} = [A^{-1}] \begin{Bmatrix} N_x \\ N_y \\ N_{xy} \end{Bmatrix} \tag{8-25}$$

The laminate strains are rotated using the transformation matrix, [T], for each ply angle in the laminate. These strains are used for computing the margins of safety.

The margins of safety for failure of a laminate of orthotropic materials are computed by using the six allowable failure strains of the basic lamina material and the orientation angle of each ply in the laminate. The strains are:

+ ϵ_{11}, tension in the 11 direction

+ ϵ_{22}, tension in the 22 direction

+ ϵ_{12}, positive shear

- ϵ_{11}, compression in the 11 direction

- ϵ_{22}, compression in the 22 direction

- ϵ_{12}, negative shear

The laminate strains are calculated and then transformed to coincide with each ply material axis system as shown in Figure 8-25. The transformed strains are then compared with the appropriate allowable strains and three margins of safety are obtained for each ply, for each loading condition.

The minimum margin from all of the plies then becomes the final margin for the ultimate strain failure mode of the laminate. The equation used for each margin of safety is:

$$\text{M.S.} = \frac{\epsilon_{PSAL}}{\epsilon} - 1 \tag{8-26}$$

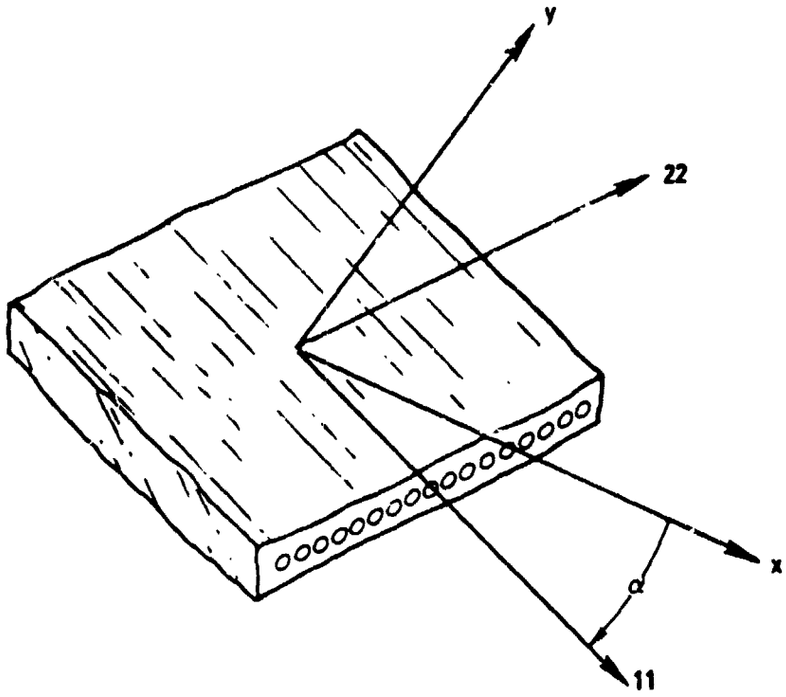

Figure 8-25. Coordinate Transformation for the α Ply

where ϵ_{PSAL} is the ultimate strain allowable and ϵ is the applied strain.

The fatigue stress spectrum is based on the flight profile and load spectrum discussed in Section 8.1.5. It is made up of a group of minimum and maximum stresses and the number of applications expected during the design life. This spectrum is used for the fatigue analysis and the flaw growth analysis of the element discussed in this section.

Minimum and maximum stresses are calculated for each subsegment of the fatigue spectrum (see Table 8-2). These stresses are calculated from the segment constant stress σ_c and the segment alternating stress σ_a.

$$\sigma_{min} = \sigma_c - \Delta g \cdot \sigma_a \tag{8-27}$$

$$\sigma_{max} = \sigma_c + \Delta g \cdot \sigma_a \tag{8-28}$$

The value of σ_c and σ_a are in general different for each segment and are calculated by forming linear combinations of the stress due to the fatigue spectrum conditions (see Table 8-3).

$$\sigma_{cj} = \sum_{i=1}^{6} c_{ij}\, \sigma_i \tag{8-29}$$

C-4

$$\sigma_{aj} = \sum_{i=1}^{6} a_{ij}\,\sigma_i \qquad (8\text{-}30)$$

where i denotes the fatigue spectrum condition number and j denotes the segment number. The constants c_{ij} and a_{ij} are based on the flight profile (see Table 8-1) and are stored within the program.

The ground-air-ground (G-A-G) cycle shown in Figure 8-26 is not defined in Section 8.1.5. It dominates fatigue damage and flaw growth in many areas of the structure of transport aircraft. This stress excursion is due in part to the difference between the groundborne load distribution and the airborne distribution, and in part to cabin pressurization. A G-A-G spectrum is calculated automatically within the program at each analysis point. The G-A-G cycle is defined as the maximum stress excursion between the peak inflight stress (e.g., the maximum gust occurring in that flight) and the peak/valley groundborne stress (e.g., the maximum taxi Δg). Several high peaks of cyclic loads, such as those due to gust encounters in stormy weather, tend to occur on the same flight. It would therefore be conservative to use all peak loads expected in the total aircraft life in building the G-A-G spectrum. To avoid this overconservatism a frequency factor is introduced, which has the effect of skipping over some of the peak loads. A frequency factor equal to two is considered appropriate for transport aircraft. Thus, every other peak is included in the G-A-G spectrum. Frequency factor is a user input.

A unique stress spectrum is generated for each structural element based on the local stress history and is used for the fatigue analysis and flaw growth analysis also reported

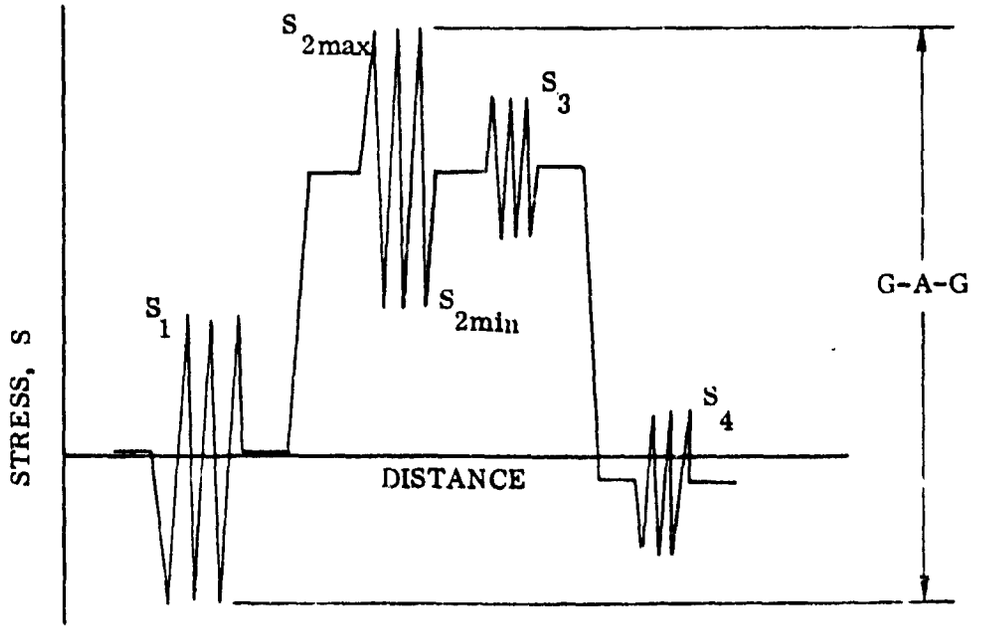

Figure 8-26. Simplified Flight Profile

in this section. No provision is currently available for changing the load profile; however, additional load spectra can be incorporated into the existing program with very little programming effort.

Fatigue damage is defined as the ratio of the number of applied stress cycles, n, of a given stress magnitude to the number of allowable stress cycles, N, of the same stress magnitude. Miner's Rule (Reference 12) is the basis of fatigue damage analysis performed by the subroutine, PRODAM. Under this concept, fatigue damage is assumed to be linearly cumulative, and fatigue failure is assumed to occur when the damage summation equals unity.

$$\text{Fatigue Damage} = \frac{n_1}{N_1} + \frac{n_2}{N_2} + \frac{n_3}{N_3} + \cdots \frac{n_m}{N_m} \qquad (8\text{-}31)$$

$$\text{Fatigue Failure} = \sum_{i=1}^{m} \frac{n_i}{N_i} = 1 \qquad (8\text{-}32)$$

To facilitate the analysis, S-N curves are plotted from test data for several values of stress ratio, R. Allowable cycles for each subsegment are read from the curves as shown in Figure 8-27.

where,
$$R = \frac{S_{min}}{S_{max}} \qquad \text{(Also see Figure 8-26)} \qquad (8\text{-}33)$$

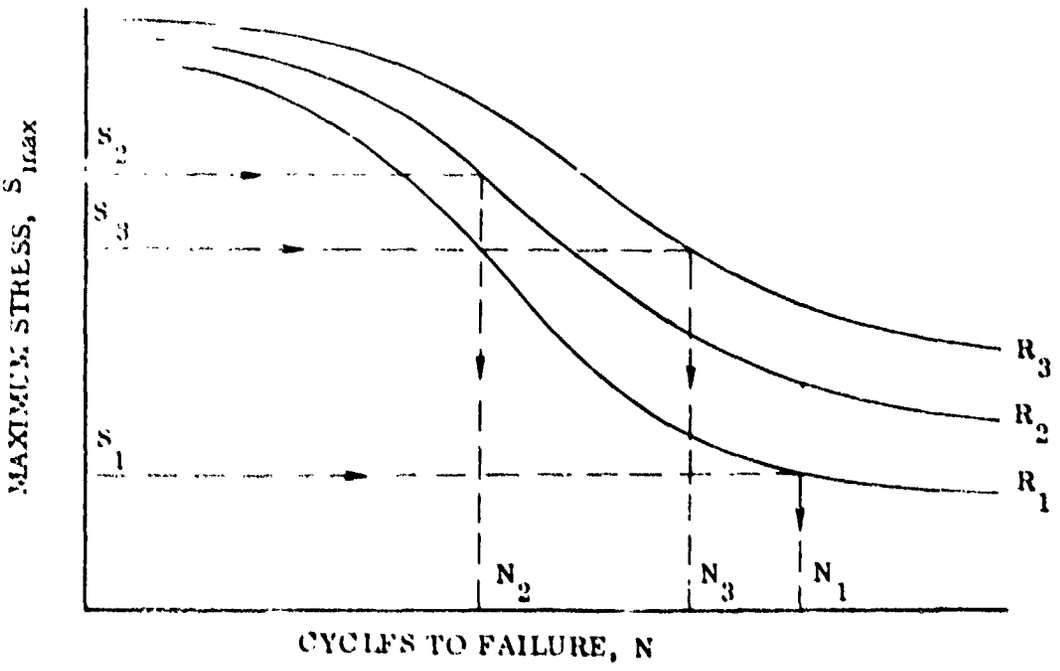

Figure 8-27. Fatigue Damage Determination

A review of previous General Dynamics programs and other sources did not produce nearly enough component S-N data to fill the required data bank indicated by Table 8-6. Much of the data reviewed was generated for specific configurations and load spectra. Manufacturers usually test splices and other fatigue critical details but seldom develop S-N curves for typical structure and spectra. Even less data is published because component test results are frequently considered proprietary or sensitive to a particular project.

Table 8-6 Availability of Fatigue Data

Material	Fabrication Method	Wing Box	Fuselage	General Structure	Coupon S-N
Aluminum	Riveted	◒	◒	◒	●
	Integral	◒	○	◒	
	Bonded	○	○	○	
	Welded	○	○	○	
Titanium	Riveted	○	○	○	●
	Integral	◒	○	◒	
	Bonded	○	○	○	
	Welded	○	○	○	
Graphite/ Epoxy	Riveted	○	○	○	◒
	Integral	○	○	○	
	Bonded	○	○	○	
Boron/ Epoxy	Riveted	○	○	◒	◒
	Integral	○	○	○	
	Bonded	○	○	◒	

○ = No data

● = Complete data

In some cases the component data was incomplete. To facilitate extrapolation, curves of stress vs. stress ratio at constant cycle values were plotted from the original data. Expanded S-N curves were then drawn based on the extrapolated data. For the many cases where component data was not available, reduction factors were applied to unnotched coupon data for the appropriate material. A complete set of data was generated by this method. However, S-N curves plotted from this data did not show the trends and consistency expected. Anomalies in the component data due to inconsistent test parameters were still present in the expanded S-N curves. A complete and consistent set of S-N curves for all required component types could not be obtained with this approach.

Subsequently, a second method, Reference 13, for plotting S-N curves from limited data was employed. More reliance is placed on unnotched coupon data, and competent fatigue strength factors are plotted versus life to ensure that smooth and consistent S-N curves are generated. The component S-N curves used for fatigue analysis were generated by this method, and are presented in Figures 8-28 thru 8-38 . All curves are normalized to the net section static strength, S_g. These curves provide fatigue data for all of the component construction types currently allowed in the structural synthesis module.

Figure 8-28 S-N Curves for Riveted or Integral Aluminum Components

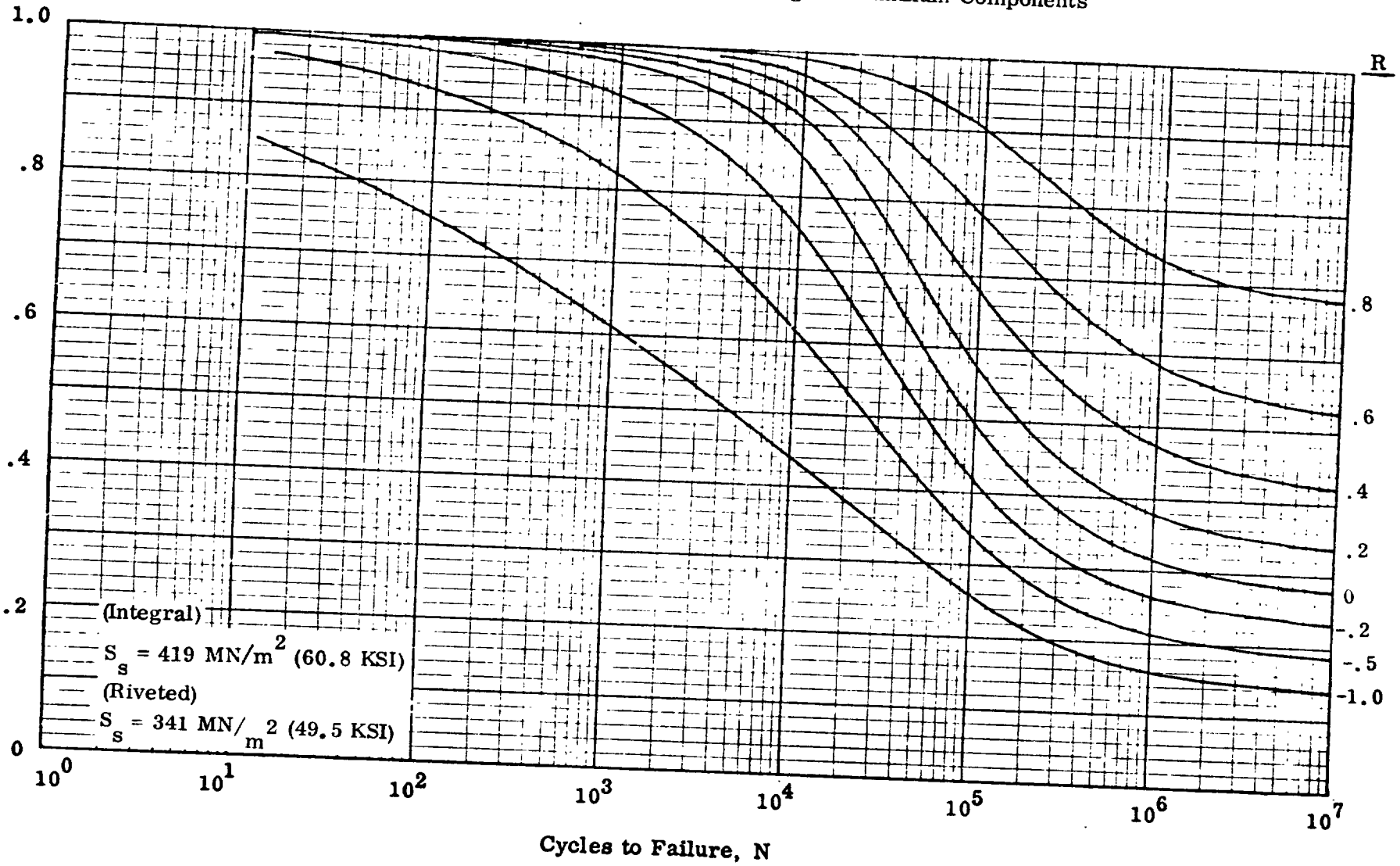

Figure 8-29 S-N Curves for Spot Welded Aluminum Components

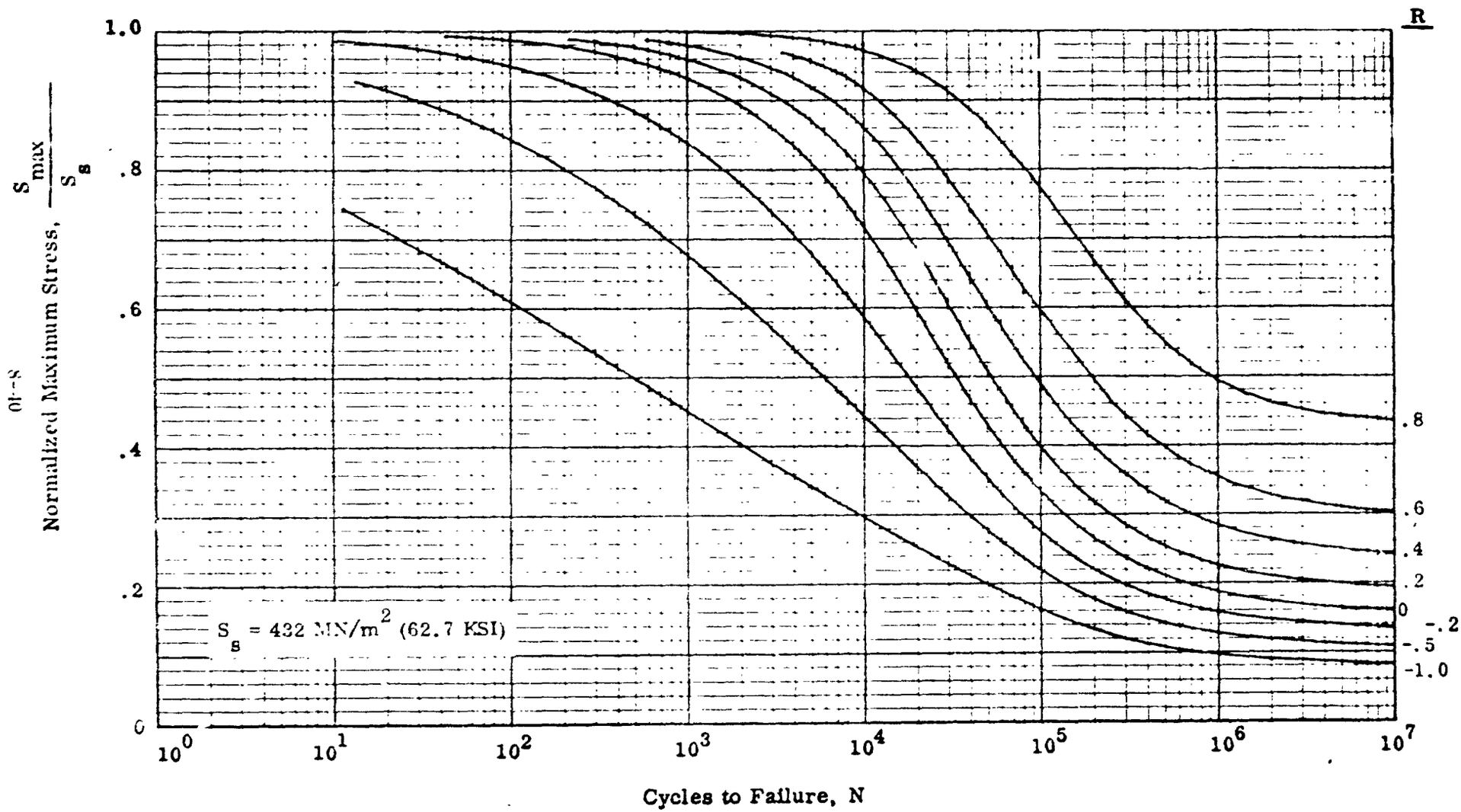

Figure 9-30 S-N Curves for Bonded Aluminum Components

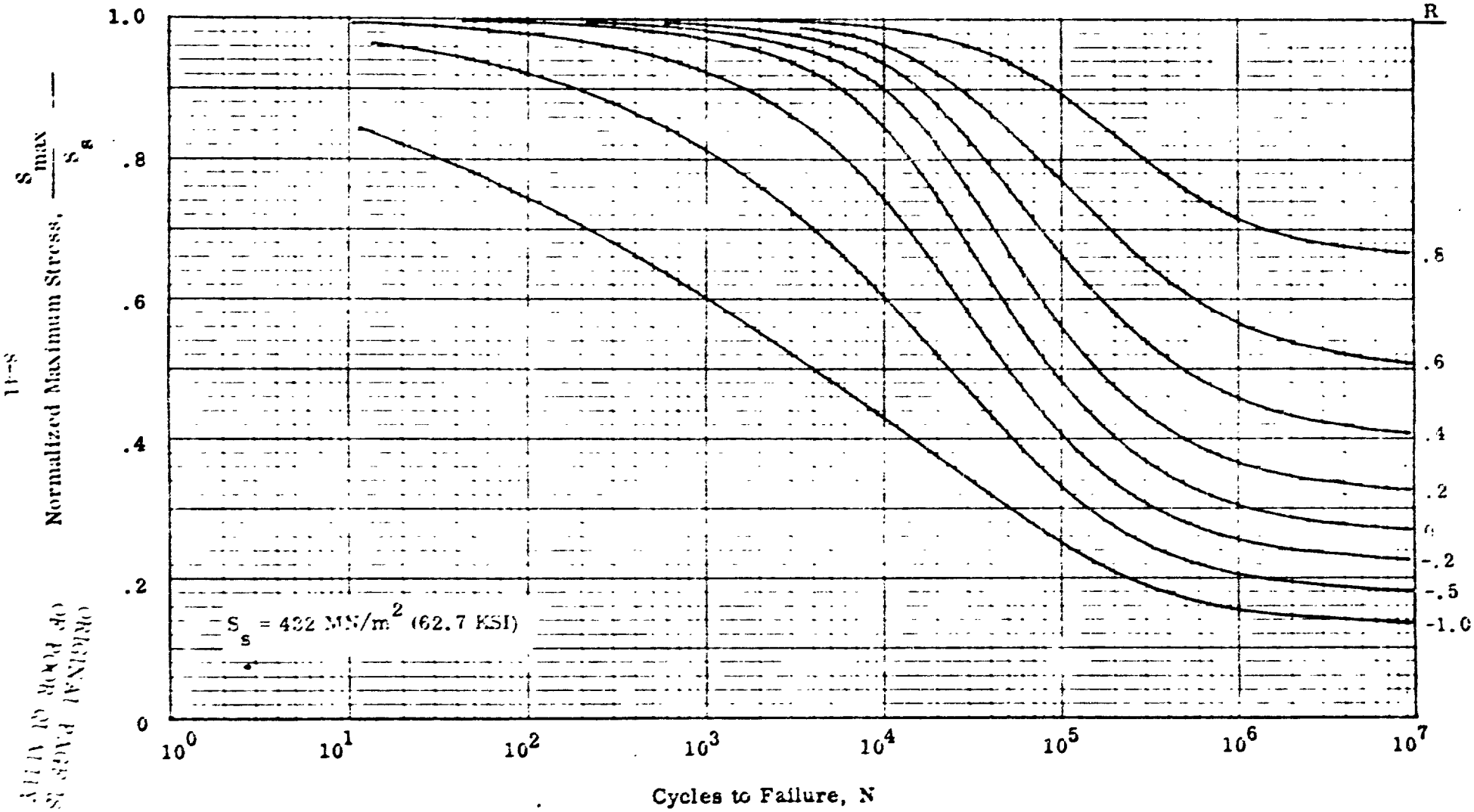

Figure 8-31 S-N Curves for Riveted Titanium Components

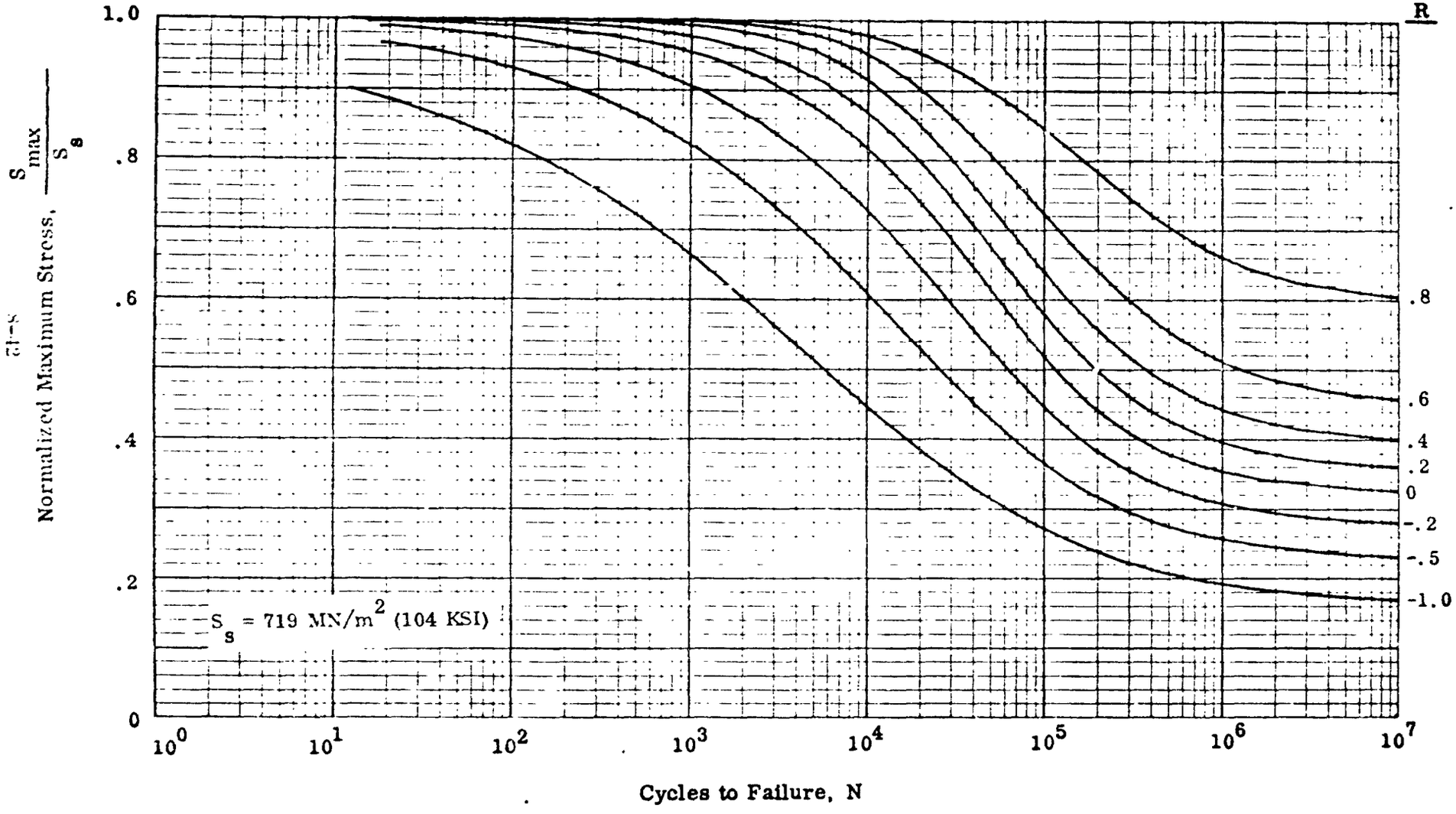

Figure 8-32 S-N Curves for Integral Titanium Components

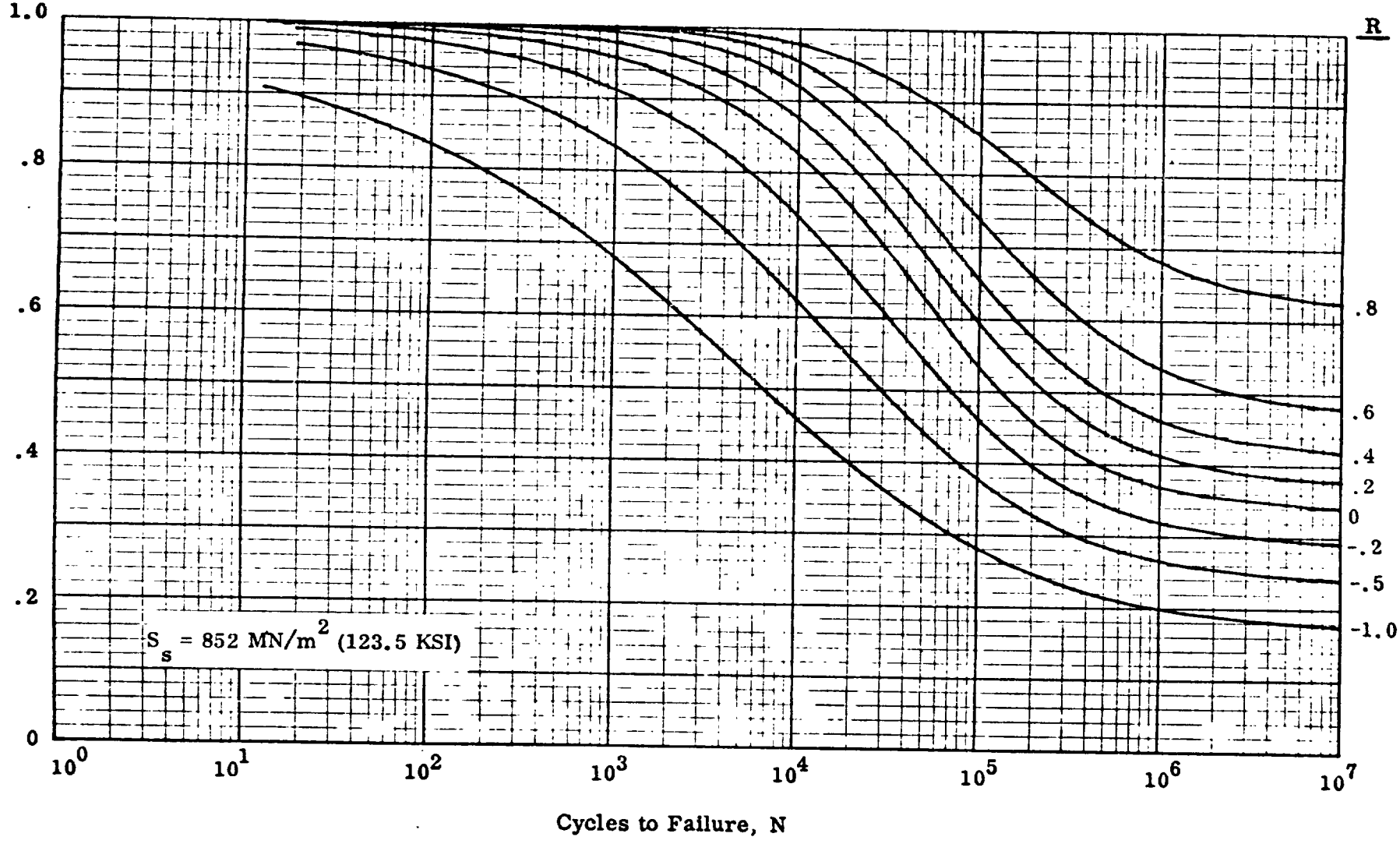

Figure 8-33 S-N Curves for Spot Welded Titanium Components

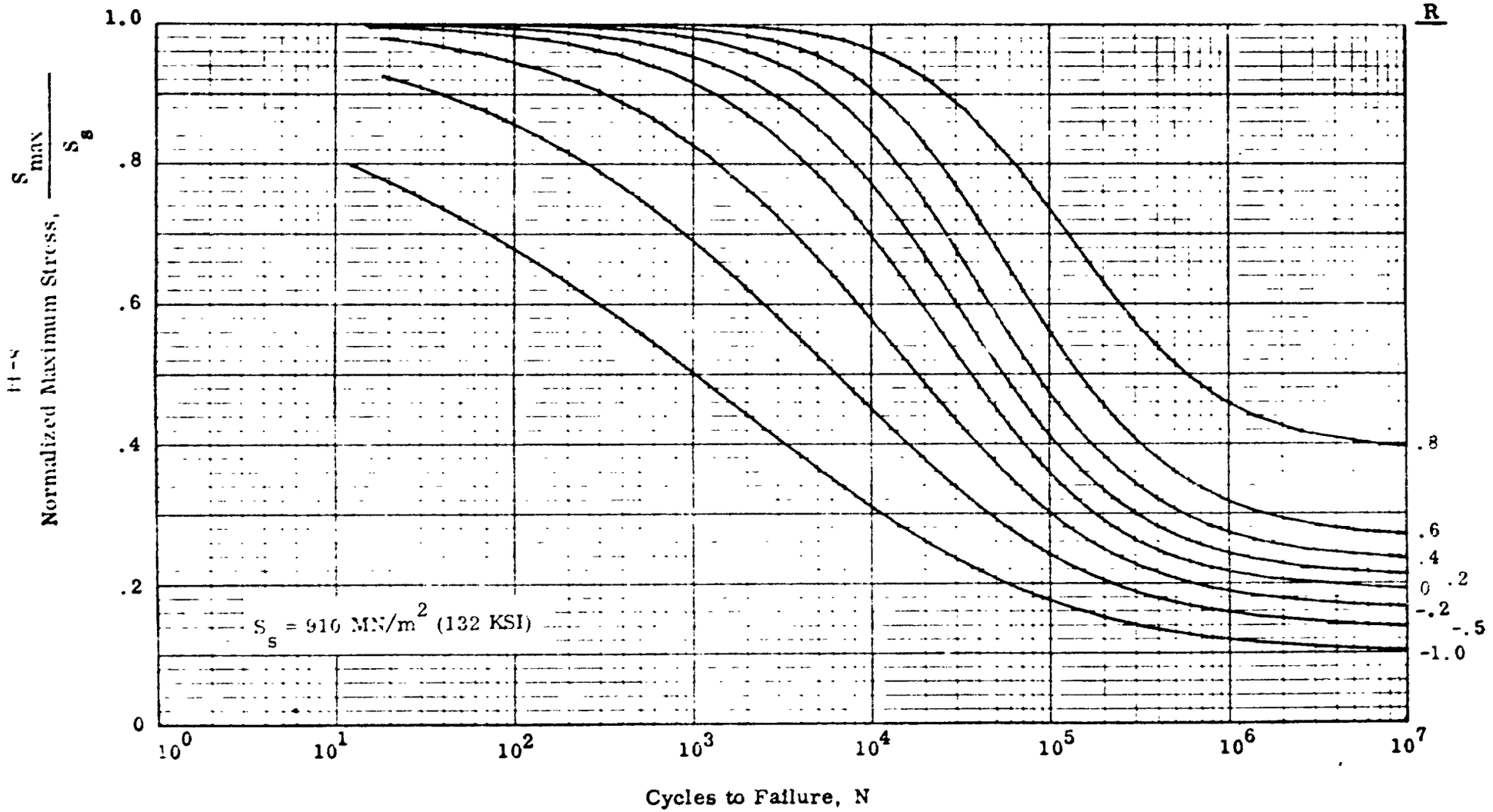

Figure 8-34 S-N Curves for Bonded Titanium Components

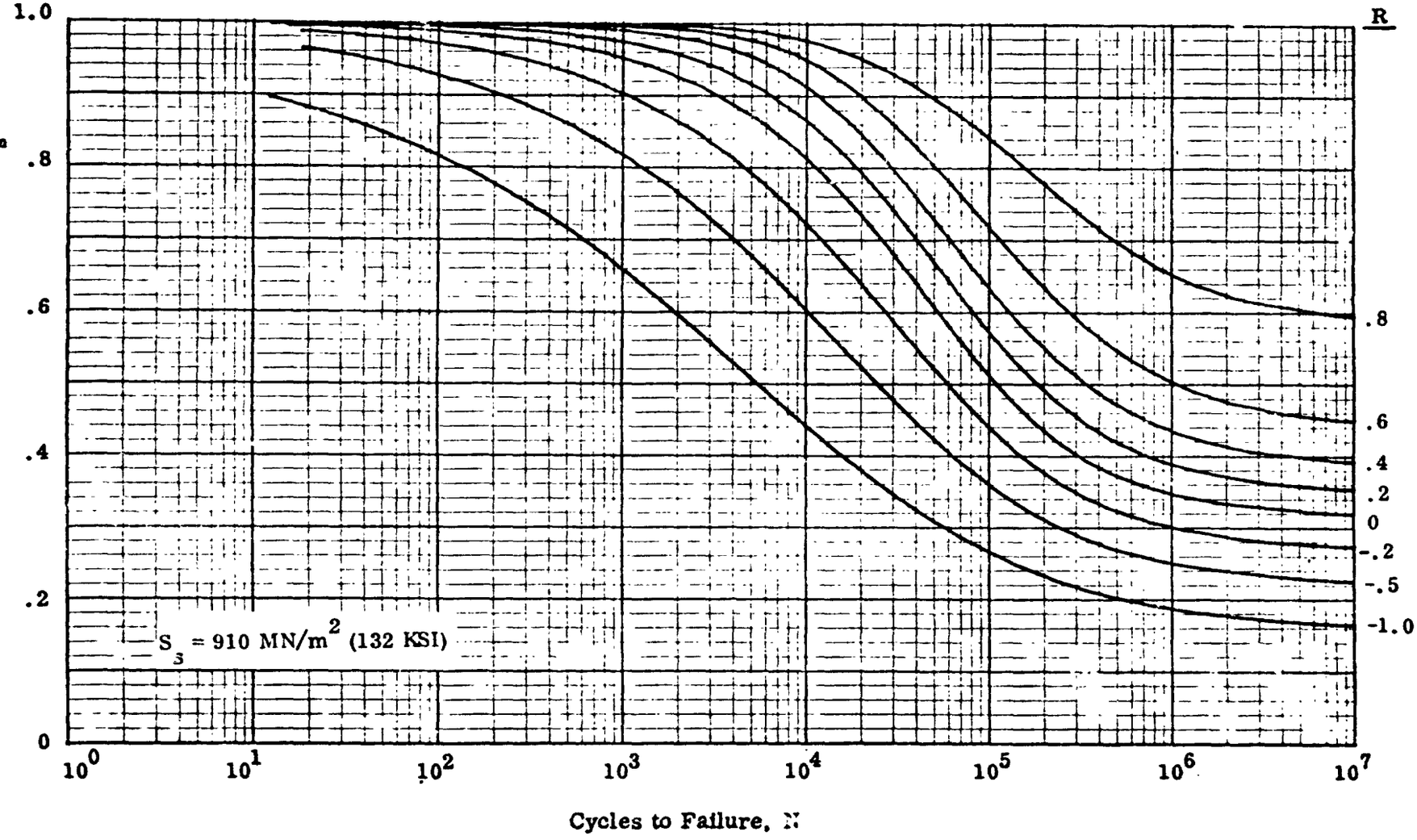

Figure 8-35 S-N Curves for Riveted Graphite/Epoxy, 0/±45/90, Components

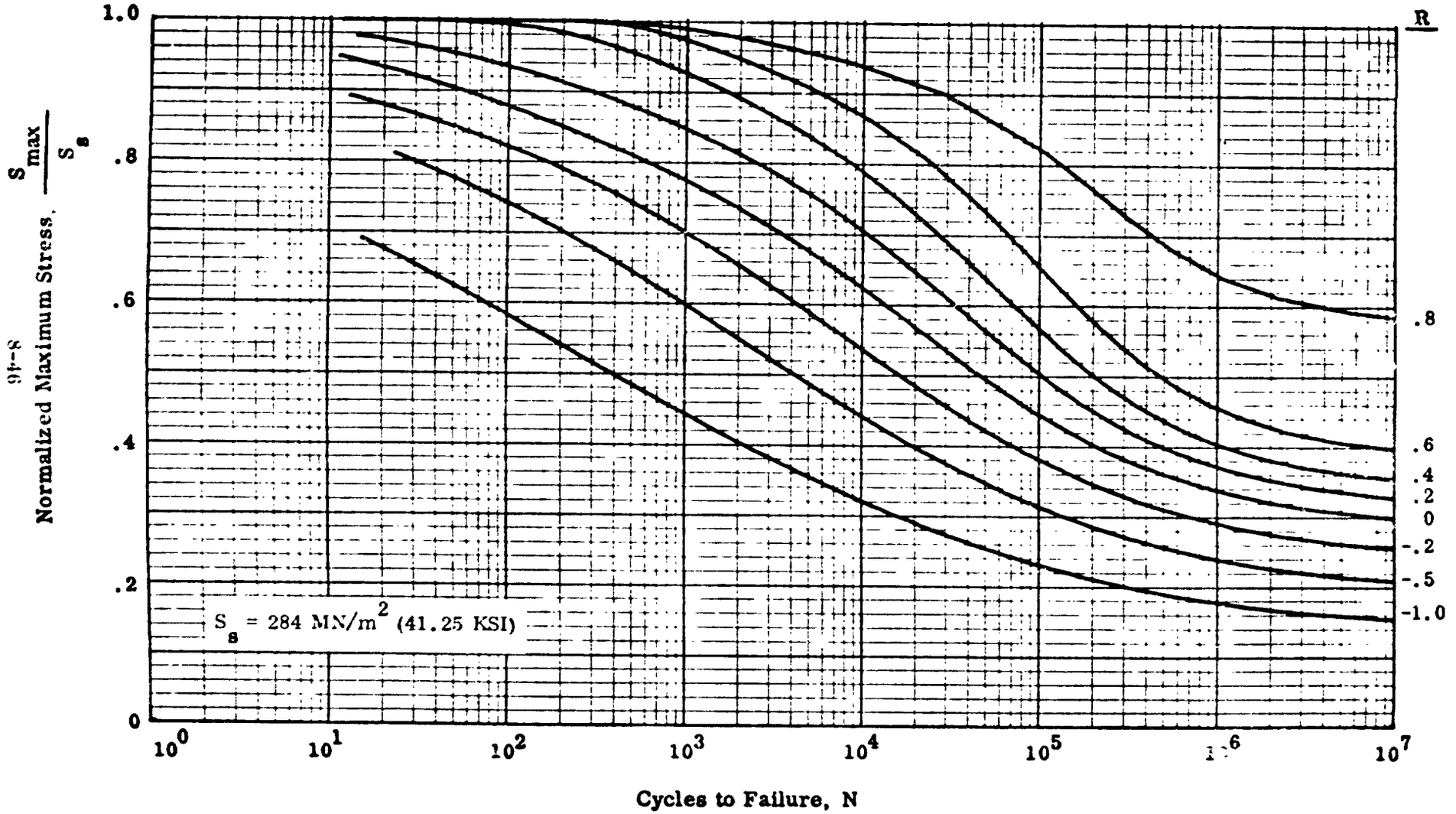

Figure 8-36 S-N Curves for Integral or Bonded Graphite/Epoxy, $0/\pm45/90$, Components

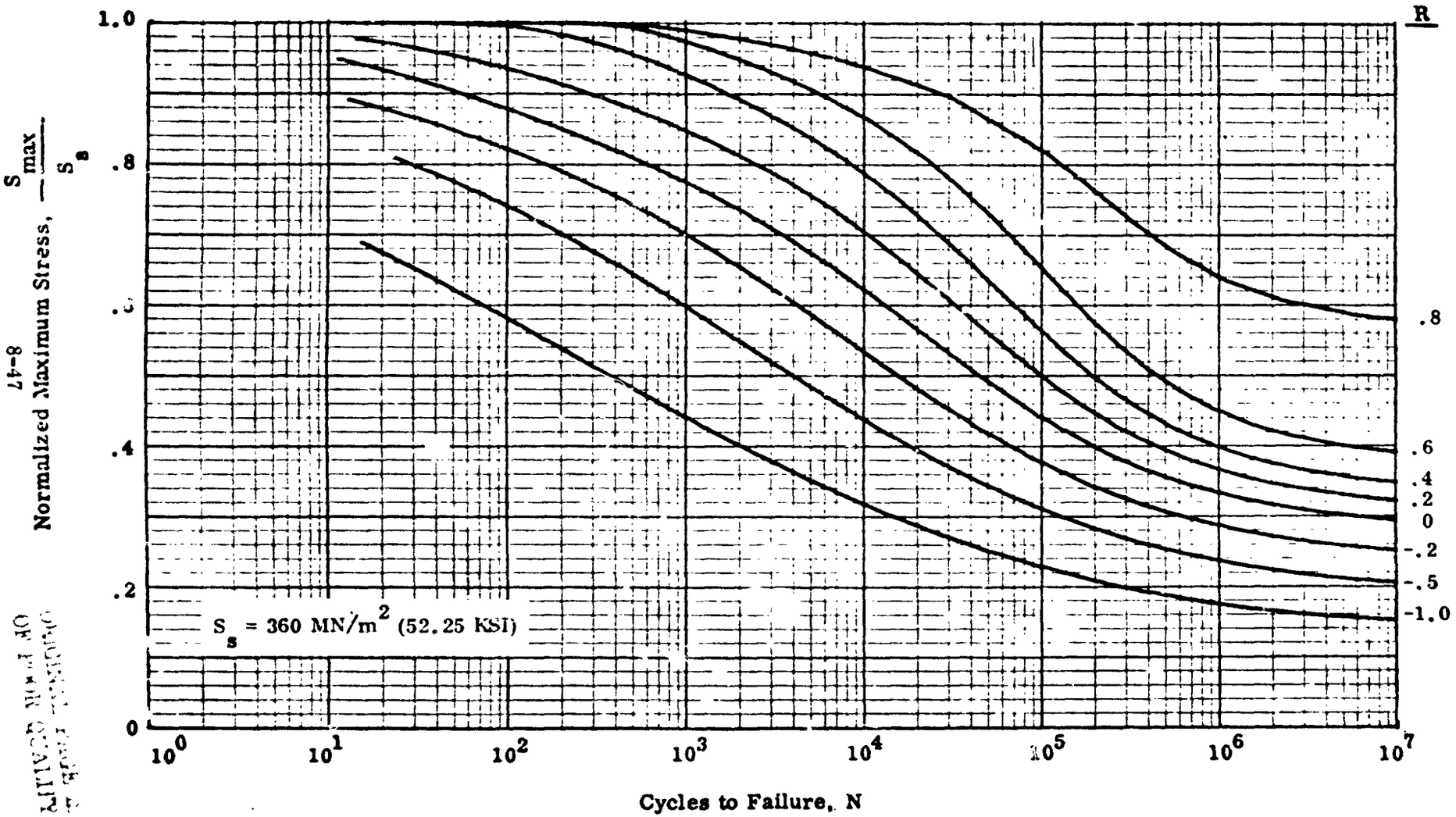

Figure 8-37 S-N Curves for Riveted Boron/Epoxy, 0/±45/90, Components

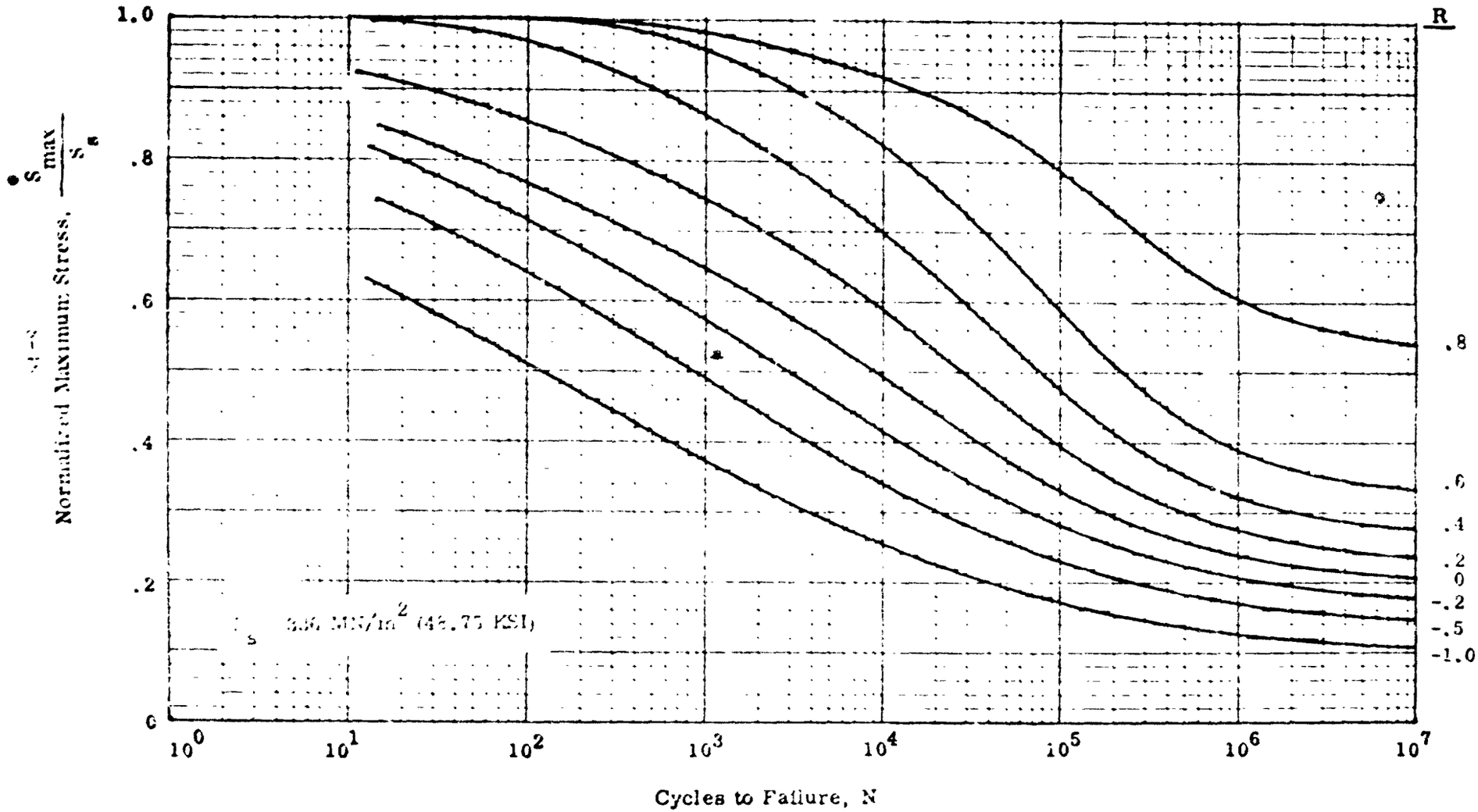

Figure 8-38 S-N Curves for Integral or Bonded Boron/Epoxy, 0/±45/90, Components

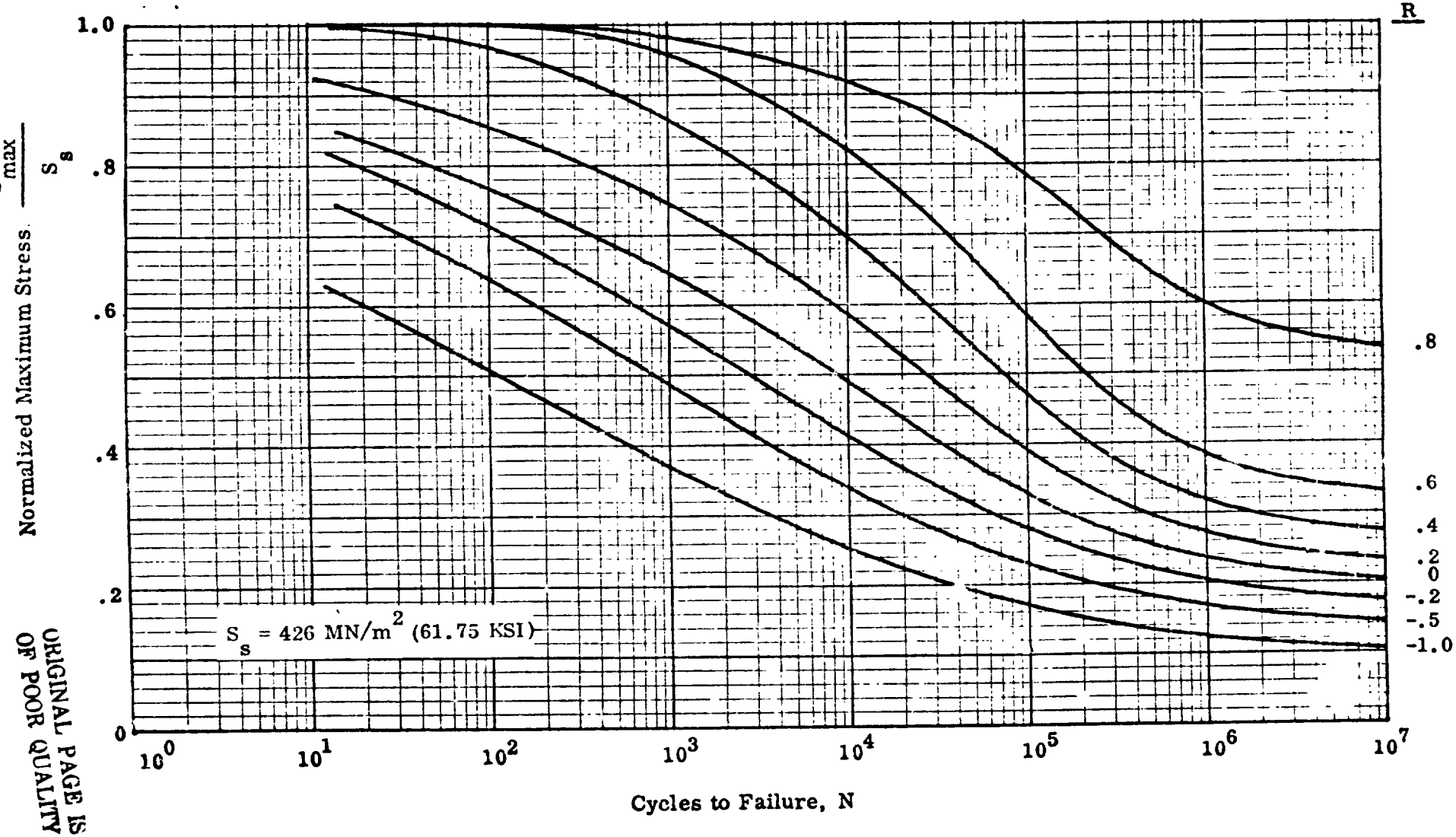

Data from constant life cuts of these curves is stored in the program. An interpolation routine is used in the program to retrieve allowable cycles from the stored data.

This rather simple approach is widely used in fatigue life predictions of transport aircraft. The more severe load spectra of fighter type aircraft produce more significant residual stresses at points of stress concentration and may warrant a more sophisticated analytical treatment.

Regarding the data for the composite materials (boron/epoxy and graphite/epoxy), it must be realized that an infinite variety of laminates is possible. Each lay-up will have different fatigue characteristics. A pseudo isotropic lay-up, 0/±45/90, was selected for this program because it is a common lay-up and some fatigue data was available.

The flaw growth analysis presented in the following paragraphs represents the procedure used in the VDEP Program. The flaw growth analysis predicts how a through the thickness crack grows under the influence of a fatigue load spectrum. The growth analysis is based on an integration technique presented in Reference 3. The technique currently used is conservative, making no provision for growth retardation effects due to spectrum loading.

Crack growth predictions are usually based on the integration of empirical growth rate laws. The integration techniques range from simple cycle by cycle summations to more sophisticated techniques involving high powered numerical methods. Cyclic growth rate equations are usually expressed as functions of the stress intensity factor range, ΔK, the cyclic stress ratio, R, and certain empirical constants determined from tests data.

$$\frac{da}{dN} = F\ (\Delta K\ ,\ R,\ \text{empirical constants})$$

where $\frac{da}{dN}$ is the cyclic growth rate.

The stress intensity factor range, ΔK, is a measure of the change in the intensity of the stress field near the tip of the crack, (see Figure 8-39).

$$\Delta K = \lambda(a)\,\Delta\sigma\sqrt{\pi a} = K_{max} - K_{min}$$

where,

$\Delta\sigma$ range of the remotely applied cyclic stress

a half crack length

$\lambda(a)$ correction factor which accounts for geometric effects

The amount of growth, Δa, which occurs during one cycle of applied stress can be predicted using a growth rate equation, i.e.,

$$\Delta a = f(\Delta K, R, \text{empirical constants})$$

After a load cycle is applied the new crack length is longer by Δa at each tip. The ΔK calculated for the next load cycle is then based on the new crack size. Crack growth can in this way be predicted for cyclic loading. This process is cumbersome if the number of load cycles is very large.

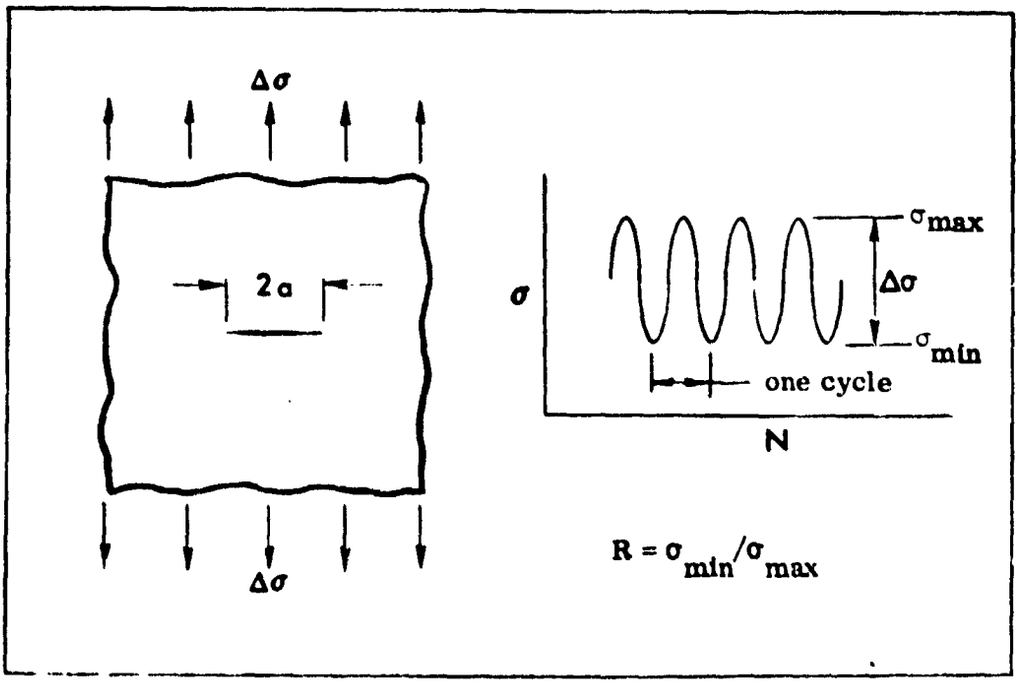

Figure 8-39 Fatigue Crack Loading

Crack growth analysis of transport aircraft often involves millions of cycles of applied loads during service life. Computer routines written to predict flaw growth based on the method just described were found to be too slow to use for this program. A technique based on averaging the cyclic growth rates during a flight and then performing the integration on a flight by flight basis was developed. A curve of average flight crack growth rate da/dF versus crack length is obtained for the specific crack geometry and load spectrum. Such a curve is obtained by summing the growth rates due to each of the load cycles in the spectrum and then dividing by the number of flights represented by the spectrum. By performing this process at various crack sizes a curve can be constructed as shown in Figure 8-40 .

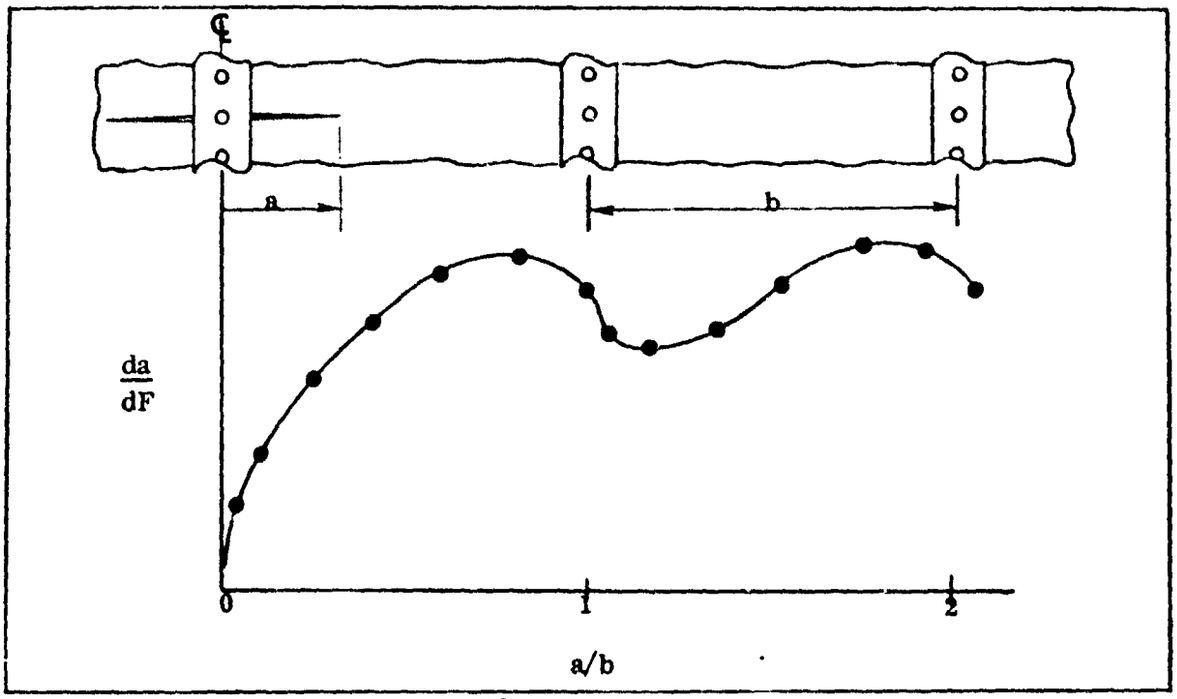

Figure 8-40 Flight by Flight Growth Rate

The inverse of this curve, i.e. dF/da, is integrated numerically over the desired crack interval. A technique based on the Erdogan growth rate equation was developed in order to simplify and automate the procedure needed to generate the da/dF curves.

Erdogan growth rate equation:

$$\frac{da}{dN} = C K_{max}^{m} \Delta K^{p} \qquad (8\text{-}34)$$

where C, m, and p are empirical constants determined from constant amplitude crack growth tests.

Since $K_{max} = \frac{\Delta K}{1-R}$

$$\frac{da}{dN} = \frac{C(\Delta K)^{m+p}}{(1-R)^{m}} \qquad (8\text{-}35)$$

The average flight growth rate at any crack size a is then,

$$\frac{da}{dF} = \frac{1}{M} \sum_{i=1}^{N_s} C \frac{(\Delta K_i)^{m+p}}{(1-R_i)^{m}} \qquad (8\text{-}36)$$

where,

$$\Delta K_i = \lambda(a)\, \Delta\sigma_i \sqrt{\pi a} \qquad (8\text{-}37)$$

$$R_i = \sigma_{min_i} / \sigma_{max_i} \qquad (8\text{-}38)$$

$$\Delta\sigma_i = \sigma_{max_i} - \sigma_{min_i} \qquad (8\text{-}39)$$

N_s = Total number of cycles contained in the spectrum.

M = Number of flights represented by the spectrum.

Rewriting Equation 8-36 , assuming the change in a to be small in N_s cycles.

$$\frac{da}{dF} = C\left(\lambda(a)\sqrt{\pi a}\right)^{m+p} \cdot \frac{1}{M} \sum_{i=1}^{N_s} \frac{(\Delta\sigma_i)^{m+p}}{(1-R_i)^{m}} \qquad (8\text{-}40)$$

Now define $\bar{\sigma}$ as

$$\bar{\sigma} \equiv \left[\frac{1}{N_s} \sum_{i=1}^{N_s} \frac{(\Delta\sigma_i)^{m+p}}{(1-R_i)^{m}}\right]^{\frac{1}{m+p}} \qquad (8\text{-}41)$$

The application of N/M cycles of $\bar{\sigma}$ with an R value of 0, will produce the growth which is equivalent to the growth caused by the actual load cycles of an average flight.

$$\frac{da}{dF} = \frac{N_s}{M} C \left[\lambda(a) \bar{\sigma} \sqrt{\pi a} \right]^{m+p} \qquad (8\text{-}42)$$

The number of flights required to grow a crack from a_i to a_{i+1} can be found by solving the differential equation. Equation 8-42 is separable and can be written in integral form as shown by Equation 8-43 .

$$\Delta F = \frac{M}{N_s C \bar{\sigma}^{m+p}} \int_{a_i}^{a_{i+1}} \frac{da}{[\lambda(a)\sqrt{\pi a}]^{m+p}} \qquad (8\text{-}43)$$

The closed form solution to Equation 8-43 can become exceedingly complex and perhaps impossible depending on the form of $\lambda(a)$. The simplest form of $\lambda(a)$ which is useful leads to the following choice.

$$\lambda(a) = \lambda_o + \lambda_i a \quad \text{for} \quad a_i \le a \le a_{i+1} \qquad (8\text{-}44)$$

Equation 8-44 represents a linear approximation to λ on an interval containing both a_i and a_{i+1}. λ_i and λ_o are the slope and intercept of this linear approximation. Even with this simple form, the closed form of the solution is not practical. Numerical integration techniques must be applied to find the solution. Since $\lambda(a)$ has been chosen to be linear in a, the following form of Equation 8-42 can be written.

$$\Delta F = \frac{M}{N_s C[\bar{\sigma}\lambda(a^*)]^{m+p}} \int_{a_i}^{a_{i+1}} \frac{da}{(\sqrt{\pi a})^{m+p}} \qquad (8\text{-}45)$$

where

$$a_i \le a^* \le a_{i+1}$$

Performing the integration in Equation 8-45 leads to the following solution.

$$\Delta F = \frac{2M}{N_s \cdot C[\bar{\sigma}\lambda(a^*)]^{m+p} \cdot (m+p-2)} \left[a_i^{(2-m-p)/2} - a_{i+1}^{(2-m-p)/2} \right] \qquad (8\text{-}46)$$

where

$$m+p \neq 2$$

The error of integration introduced is dependent on the selection of a*. If a* is chosen to be equal to a_i then the error is

$$E = \left| \left[\frac{\lambda(a^*)}{\lambda(a_i)} \right]^{m+p} - 1 \right| \qquad (8\text{-}47)$$

Since ($a_i \leq a^* \leq a_{i+1}$) the maximum possible error is introduced when $a^* = a_{i+1}$.

$$E_{max} = \left| \left[\frac{\lambda(a_{i+1})}{\lambda(a_i)} \right]^{m+p} - 1 \right| \qquad (8\text{-}48)$$

The greatest potential error can be limited to some prescribed error $E^* > 0$ by proper selection of a_{i+1}.

$$\left| \left[\frac{\lambda_o + \lambda_1 \cdot a_{i+1}}{\lambda_o + \lambda_1 \cdot a_i} \right]^{m+p} - 1 \right| < E^* \qquad (8\text{-}49)$$

An operator H is introduced so that the absolute value bars can be removed.

$$\frac{\lambda_o + \lambda_1 \cdot a_{i+1}}{\lambda_o + \lambda_1 \cdot a_i} < (1 + HE^*)^{1/(m+p)} \qquad (8\text{-}50)$$

Where,

$H = 1$ for $\lambda_1 > 0$

$= -1$ for $\lambda_1 < 0$

Solving Equation 8-50 for a_{i+1} results in the following

$$a_{i+1} = (HE^* + 1)^{1/(m+p)} \cdot \left[\frac{\lambda_o}{\lambda_1} + a_i \right] - \frac{\lambda_o}{\lambda_1} \qquad (8\text{-}51)$$

where $\lambda_1 \neq 0$

For the case where $\lambda_1 = 0$ the value of a_{1+1} may be set to the largest value of a for which the linear approximation to λ is valid, in which case the integration is exact.

The following equation is used to supply the (λ_o/λ_1) term for values of λ supplied at two crack sizes.

$$\frac{\lambda_o}{\lambda_1} = \frac{\lambda_j \cdot a_{j+1} - \lambda_{j+1} \cdot a_j}{\lambda_{j+1} - \lambda_j} \qquad (8\text{-}52)$$

where (a_j, a_{j+1}) is the interval over which the λ function is to be linearized and λ_j and λ_{j+1} are the values of λ at a_j and a_{j+1} respectively.

The foregoing procedure is applicable to any flaw geometry for which the stress intensity correction factors, λ, are known. The program currently contains factors for a wide range of stiffened panels with through cracks. Curves for L(a) and λ(a) for the case of a crack extending equally on both sides of a riveted stiffener (illustrated in Figure 8-41) are stored within the program in the form of data tables. For further there information concerning the derivation of these curves the reader is referred to Reference 14.

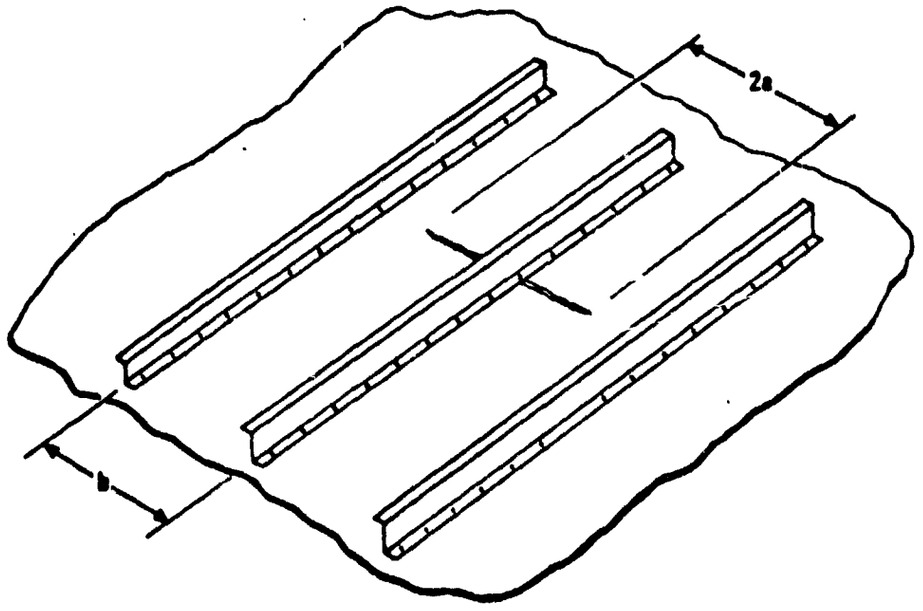

Figure 8-41 Stiffened Panel Crack Geometry

The program currently contains 75 sets of data for L(a) and λ(a) covering a wide range of stiffener spacing and percent stiffening, including cases for broken stiffeners. Figure 8-42 presents a typical set of curves. Linear interpolation is used to determine L(a) and λ(a) curves for cases which lie between data sets. These curves are used for all riveted-stiffener plate combinations, (e.g., panel types 4 through 9 of Figure 8-3).

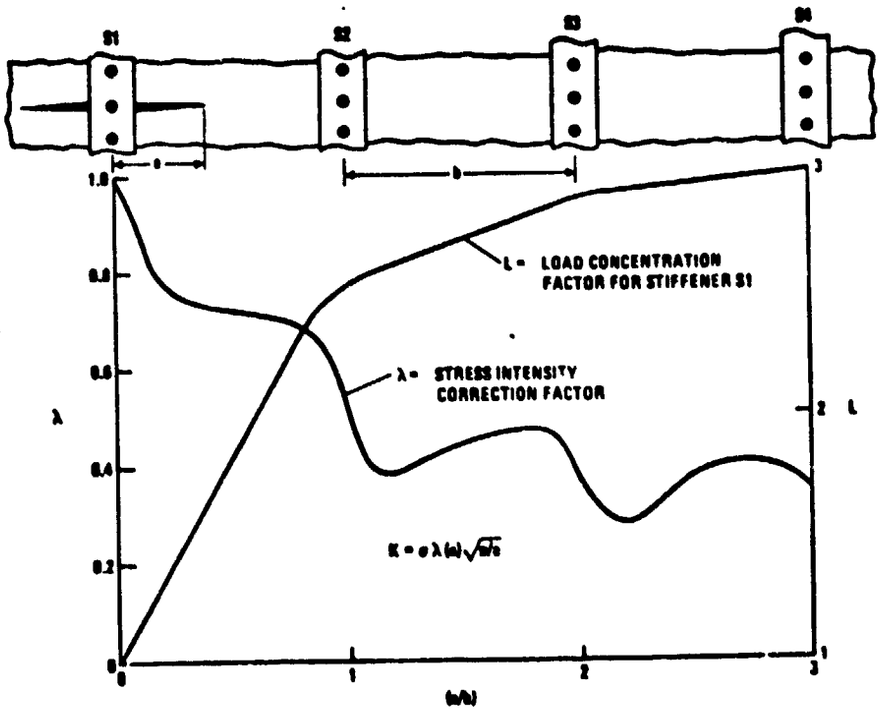

Figure 8-42 Stiffened Panel Stress Intensity Correction Factors

For the case of integral construction (e.g., panel types 1, 2, and 3), the panel is treated as a flat plate without stiffeners with a thickness equal to $\bar{t}$ (i.e., $\lambda(a) = 1.0$).

The residual strength analysis determines the failing strength of a damaged panel. Damage consists of skin cracks and broken stiffeners. The residual strength of a damaged panel is defined as the maximum stress level which can be applied to the panel without the crack growing unstably to failure. Unstable crack growth occurs when the applied stress intensity factor, K, exceeds the fracture toughness of the skin material, K_C.

Unstable crack growth is allowed to occur at stress levels below the residual strength of a panel as long as the crack growth eventually arrests at a larger crack size. Whenever stress level of the most highly loaded stiffener exceeds the ultimate tensile strength of the stiffener, it fails, and the applied stress intensity factors of the skin are recalculated to reflect the broken stiffener.

Figure 8-43 illustrates a typical example of the residual strength analysis procedure. The curves shown are generated by calculating the gross panel stress which causes stiffener failure and the gross panel stress which cause unstable crack growth. Equations 8-53 and 8-54 are used for these calculations.

$$\sigma_{or_{\text{(unstable crack growth)}}} = \frac{K_C}{\lambda(a)\ \sqrt{\pi\, a}} \qquad (8\text{-}53)$$

$$\sigma_{or\ \text{(stiffener failure)}} = \frac{F_{tu}}{L(a)} \qquad (8\text{-}54)$$

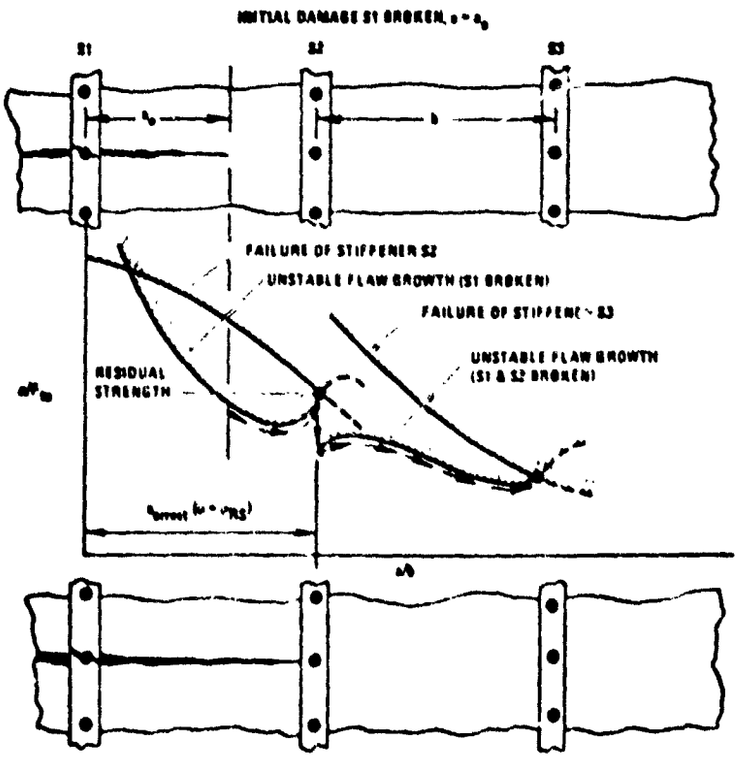

Figure 8-43 Typical Example of Residual Strength Analysis

8.2 SECONDARY STRUCTURE. The analysis procedure for secondary structure is for the leading edge, trailing edge, and tips for the aerodynamic surfaces. The fuselage secondary structure (floors, doors, and windows) is based on statistical data and is included in Section 9.2.

8.2.1 Tip, Leading and Trailing Edge Analysis. The leading edge, trailing edge, and tip synthesis modules provide the capability to analyze the aerodynamic surface structural components that are not considered as part of the structural box. The leading edge is defined as being forward of the front spar and includes the fixed position of the leading edge and the leading edge high lift devices (slats). The trailing edge is defined as being aft of the rear spar and includes the fixed trailing edge, foreflaps, flaps, ailerons, rudder, elevator, and spoilers. The tip is defined as that structure outboard of the structural box tip closing rib.

The synthesis includes a definition of part geometry and a detailed stress analysis that determines gages, accounts for material types, and sets minimum gage constraints. The geometry routines provide dimensional input to the stress analysis routines. The geometry and stress routines output includes part size and weight, as well as parameters for the part definition and cost routines. A generalized flow of the leading edge, trailing edge, and tip subprogram is shown in Figure 8-44 .

The analysis utilizes nine geometry routines, three stress analysis routines, six supporting routines, and two calling routines. The geometry routines are for flaps, aileron, rudder, elevator, slat location, slats, fixed leading edge, and spoilers.

The stress analysis routines include foreflap, spoiler, and one which analyzes the flaps, ailerons, slats, rudder, and elevator. The supporting routines derive dimensions, material properties, and general analysis. A discussion of these routines is included in the following paragraphs.

The flap geometry routine provides flap planform dimensions and locations from input data. The flap types considered are simple flaps, and single-slotted and double-slotted flaps. In the case of single or double slotted flaps the foreflap dimensions are computed in addition to the main flap dimensions. The driving parameters in determining flap dimensions are the flap area to wing area ratio, flap chord to wing chord ratio, and flap inboard chord. If the area ratio is input the flap length will be set to give required flap area. The flap length will be truncated at the wing tip or the inboard edge of the aileron. The flap chord is set by the ratio of flap chord to wing chord. If the ratio is zero the chord is assumed to be 85% of the distance aft of the rear spar. If the flap chord is input, the value of flap chord to wing chord ratio will be computed for use in determining flap dimensions. The inboard edge of the flap is located at the side of the fuselage. Flap geometry output consists of inboard and outboard chords, span stations of the flap inboard and outboard edges, and the flap length.

The aileron geometry routine provides aileron planform dimensions and locations from input data. The outboard edge of the aileron is assumed to be at the wing tip and the

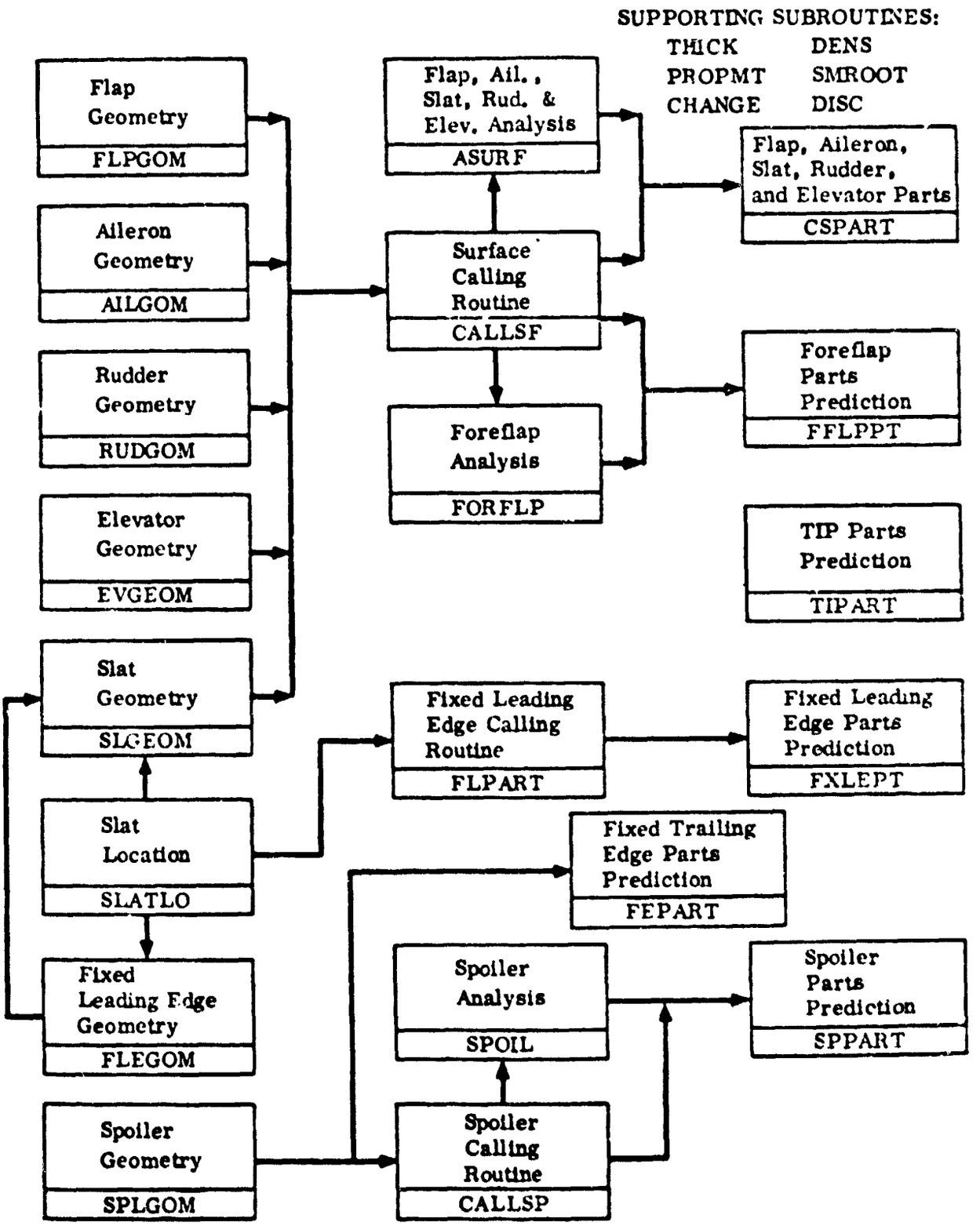

Figure 8-44 Leading Edge and Trailing Edge Synthesis Routine

inboard edge is truncated at the side of the body if the inboard location is not specified. The aileron chord is computed as 10% greater than the trailing edge length. If the outboard edge location of the aileron is input the length will be set to provide the required aileron area. Aileron geometry output consists of inboard and outboard chords, span stations of the aileron inboard and outboard edges, and the aileron length.

The rudder geometry routine provides rudder planform dimensions and locations from input data. The rudder extends from the body to the vertical stabilizer tip. The rudder chord value is set equal to 90% of the theoretical chord length aft of the vertical stabilizer rear spar location. Rudder geometry output consists of inboard and outboard chords, span stations of the rudder inboard and outboard edges, and the rudder length.

The elevator geometry routine provides elevator planform dimensions and locations from input data. The elevator extends from the body to the horizontal stabilizer tip. The elevator chord value is set equal to 90% of the theoretical chord length aft of the horizontal stabilizer rear spar location. Elevator geometry output consists of inboard and outboard chords, span stations of the elevator inboard and outboard edges, and the elevator length.

The slat geometry routine comprises two separate operations. The first locates the inboard and outboard ends of the slats and defines the slat length. The inboard location is set at 45.7 cm (1.5 ft) outboard of the side of the body. The outboard location includes 91.4 cm (3.0 ft) of clearance for each wing mounted engine pylon. The second operation determines the individual slat lengths, chords, and inboard and outboard stations for two and four engine aircraft. The slat analysis for a two-engine configuration provides three options for slat segment location: 1) inboard only, 2) outboard only, 3) outboard only, 4) inboard and center, 5) center and outboard, and 6) inboard, center, and outboard. The specific slat chord lengths are computed as a function of the slat chord to wing chord ratio. However, if the ratio is not input a value of 0.0735 is used. This is an average value for typical transport aircraft.

The fixed leading edge geometry routines provide planform dimensions and locations for the wing, horizontal stabilizer, and vertical stabilizer leading edges. The horizontal and vertical stabilizer leading edges start at the body and end at the tip. The leading edge chord is input as the total distance forward of the front spar. The wing has two types of fixed leading edges; under-slat and between-slat. The leading edges extend from the side of the body to the tip, the appropriate type being used as a function of the slat locations. The between-slat type extends the full distance forward of the front spar and the under-slat type assumes a chord equal to 8% of the wing chord. Fixed leading edge geometry output consists of the lengths and chords of each type of edge.

The spoiler geometry routine provides spoiler planform dimensions and locations from input data. If the spoiler area is input the spoiler will be resized to the area output from the aircraft sizing routine. If the area is not input the user must provide the inboard and outboard edge locations as well as the spoiler chord to wing chord ratio. If the spoiler chord to wing chord ratio is not input it is assumed to be 0.15. The spoiler inboard edge is assumed to be at the side of the body and the outboard edge is computed. The outboard edge is truncated at the wing tip or at the edge of the aileron. Spoiler geometry output consists of inboard and outboard chords, span stations of spoiler inboard and outboard edges, and the spoiler length.

The fixed trailing edge geometry routine assumes a total length from the body to the tip for wings, horizontal stabilizers, and vertical stabilizers. The fixed trailing edge chord is computed as a function of the total trailing edge length and the surfaces involved. The lower surface chord is computed as 6.8% of the trailing edge length if there are flaps and 10% if there are ailerons, rudders, or elevators. The upper surface chord is computed as 29.6% of the trailing edge length for flaps only. It is set equal to the spoiler chord if there are flaps and spoilers, and equal to 10% of the trailing edge length for ailerons, rudder, or elevators. If there are no control surfaces the fixed trailing edge extends from the rear spar to the aft edge of the wing, horizontal stabilizer, or vertical stabilizer.

The spoiler analysis produces structural member thicknesses and desired rivet patterns. The planform geometry is obtained from the spoiler geometry output. Member thicknesses are computed and adjusted to standard gages. Cross-sectional geometry is shown in Figure 8-45 . The front spar is a bent-up sheet metal zee, the two ribs (at each support) are bent-up sheet, and the skins are sheet metal over a full depth honeycomb core.

The spoiler analysis accounts for external and internal loads. The external loads for transport aircraft are normally those loads which the spoiler actuator produces. In this analysis the spoiler external load is assumed to be 68 N-m (600 lb-in) of hinge torque per running inch, limit. This is comparable to the 990 loading condition. The internal load analysis subdivides the total spoiler area into the smallest number of segments (individual surfaces) where all segments are equal in length and not longer than 152 centimeters (60 inches). The segments are supported at each end and all torque is taken by the inboard support. The spoiler is analyzed as a simple beam. The point of maximum bending moment is determined, and the bending moment and spar depth computed. All spoiler bending moment is taken by the spar and effective skin. The bending section (Figure 8-45) is assumed symmetrical, and the tension and compression stresses are equal to:

$$F = \frac{M\,(d/2)}{I} \qquad (8\text{-}55)$$

where

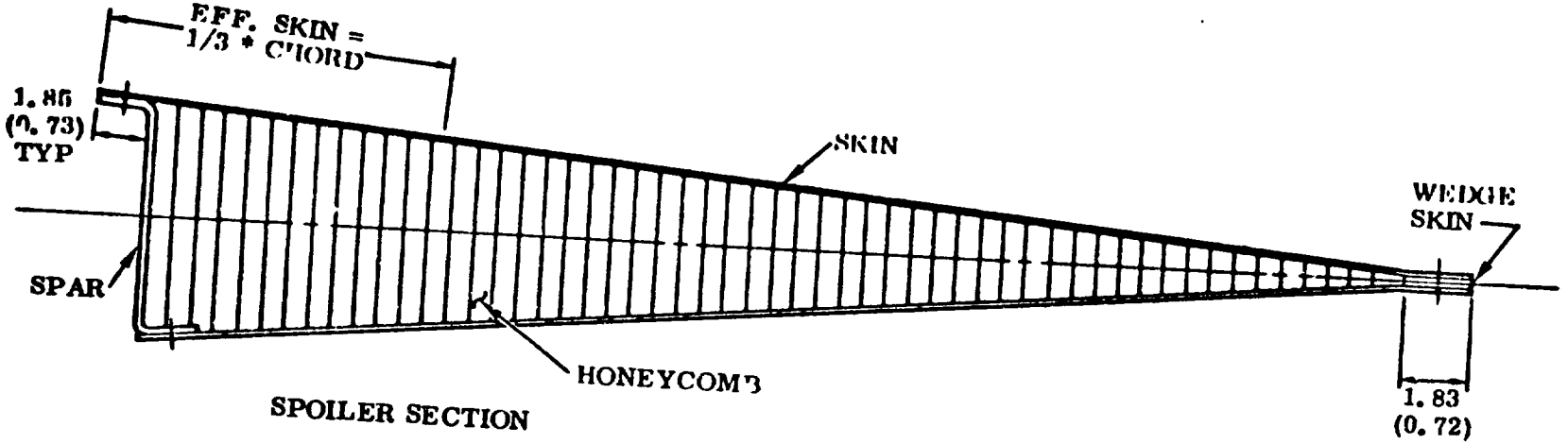

SPOILER SECTION

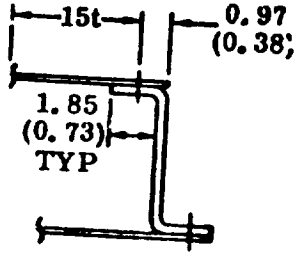

HINGE RIB SECTION

DIMENSIONS IN CENTIMETERS (INCHES)

Figure 8-45 Spoiler Geometry

F bending stress

d contour depth at spar

M bending moment

I section moment of inertia

The compression buckling allowable is:

$$F_{cs} = 0.56\, F_{cy} \left[\left(\frac{2t^2}{A} \right) \left(\frac{E}{F_{cy}} \right)^{0.5} \right]^{0.85}$$ (Reference 5, Equation C7.4) (8-56)

where

F_{cs} = compression buckling allowable

F_{cy} = compressive yield allowable

t = material thickness

A = cap area (= 1.73t)

E = material elastic modulus

The spar cap sheet thickness is sized so that the stress level is equal to or less than the larger of the compression buckling allowable or 80% of the ultimate tensile allowable.

The inboard rib is analyzed for bending at the front spar. Since all torque is taken at this rib, the bending moment is equal to the total spoiler torque about the spar. The section (Figure 8-45) is symmetrical and the tension, compression, and compression buckling stresses are computed the same as shown for the spar.

The skin thickness is based on skin shear flow at the inboard hinge where all spoiler torque is reacted about the spar. Since the skin is supported by the honeycomb core, the shear allowable is based on the ultimate shear stress times a rivet factor of 0.8.

Approximate material properties are selected for each part analyzed. The analysis determines the material thicknesses as a minimum required thickness and then rounds the value of the next larger standard gage. A minimum gage of 0.051 cm (0.020 in.) and a maximum gage of 0.635 cm (0.250 in.) are set as constraints. The standard sheet gages used are summarized in Table 8-7 .

The number of rivet holes (representing the actual number of rivets needed) and the hole sizes are output. The quantity and size of the rivets is based on a F 2A shear flow analysis at the inboard rib. The rivets are sized based on the protruding head shear allowables at a spacing of four times the shank diameter. The number of holes

Table 8-7 Standard Sheet Gages

cm	in.	cm	in.
0.051	0.020†	0.180	0.071
0.064	0.025	0.203	0.080
0.081	0.032	0.229	0.090
0.091	0.036	0.254	0.100
0.102	0.040	0.318	0.125
0.114	0.045	0.406	0.160
0.127	0.050	0.483	0.190
0.160	0.063	0.635	0.250‡

† minimum ‡ maximum

is equal to the number of rivets. That is, the holes are counted for only one member. When two rows of rivets are required, an additional amount of spar or rib cap width is output, but the additional area is not used to resize the cap.

The foreflap analysis produces the structural member dimensions and desired rivet patterns. The planform geometry is obtained from the foreflap geometry output. Member thicknesses are computed and then adjusted to standard gages. A typical foreflat cross section is shown in Figure 8-46 . The front spar is bent-up sheet metal channel and is sized by a loads analysis. The leading edge skin and rib thicknesses are fixed at 0.127 cm (0.050 in.). The honeycomb box factor is set at 1 and assumes an allowable shear stress of 110 N/cm^2 (160 psi). The box skin thickness is assumed to be 0.051 cm (0.020 in.).

The foreflap spar analysis accounts for external and internal loads. The external applied loads are derived from the general formula:

$$W \quad S\, C_n \left(\frac{V^2}{295}\right) \qquad (8\text{-}57)$$

where

W = total surface load

S total surface area

C_n normal lift coefficient

V design speed

The average pressure, ultimate, is applied to the foreflap uniformly and is computed from the transposed form:

$$P_{ave} \quad \frac{W}{S} \quad 1.5 \left(\frac{C_n V2}{295}\right) \qquad (8\text{-}58)$$

where

P_{ave} average ultimate surface pressure and for the foreflap

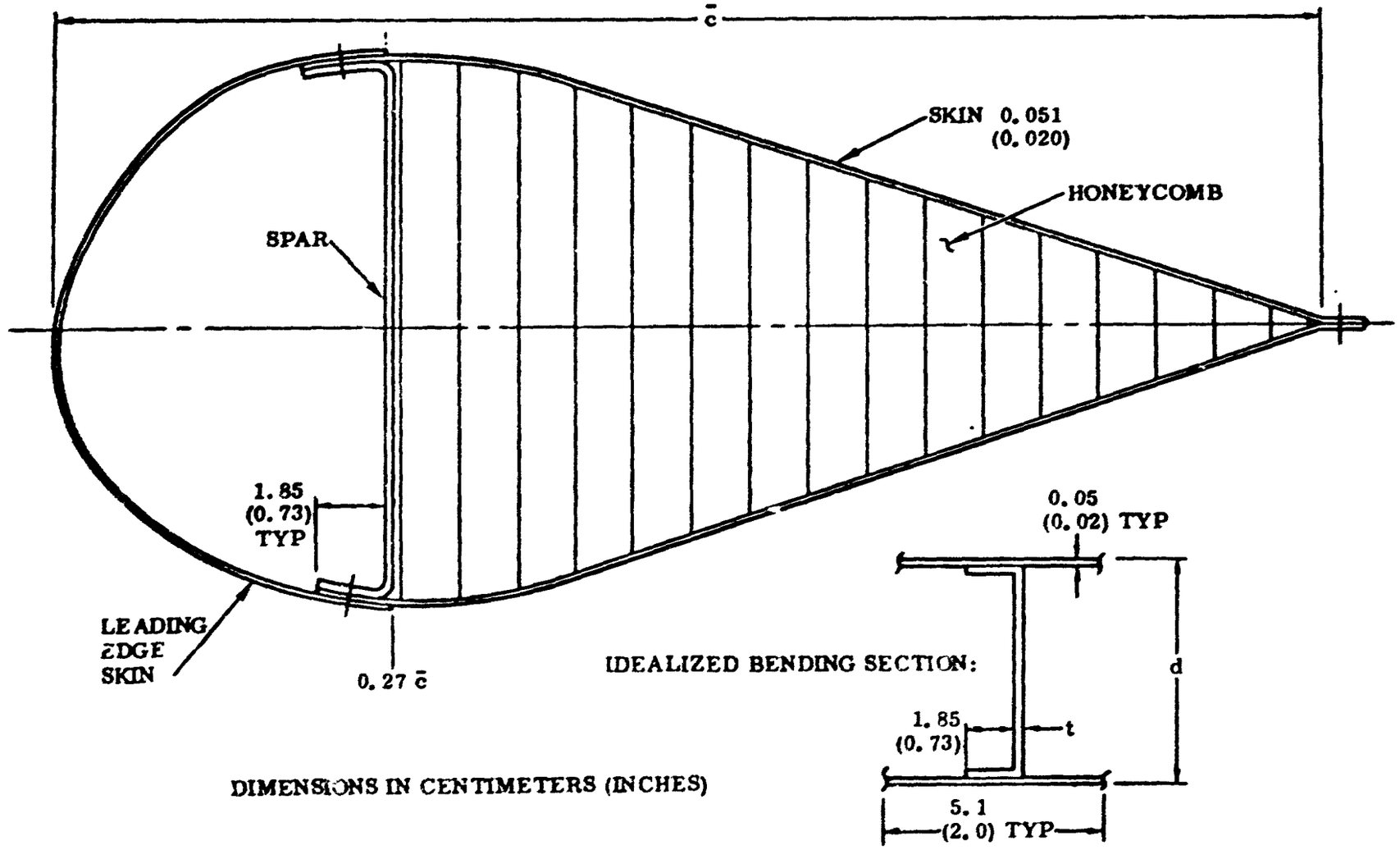

Figure 3-46 Foreflap Geometry

C_n = 4.0

V = 1.75 V_s, where V_s = stall speed

The internal load analysis subdivides the total surface length into a number of equal length segments (individual surfaces) each with a length equal to or less than 457 cm (180 in.). If the individual segment length turns out to be greater than 356 cm (140 in.), three hinge supports are assumed. One is in the center and two are located 15% of the surface length from each end. If the individual surface length is less than or equal to 356 cm (140 in.), two hinge supports are assumed, each 28% of the surface length from each end.

The vertical shear, bending moment, and torque about the front spar are calculated at each hinge. The torque is calculated at each end of the surface segment and is assumed to vary linearly between the ends. The torque is reacted at each hinge using the same formulae used to calculate shear reactions. The foreflap bending is assumed to be taken by the spar and associated skin as shown in Figure 8-46 . The bending stress can be computed from Equation 8-55 , and the compression buckling allowable stress can be computed from Equation 8-56 . Spar thickness is sized to be the minimum necessary so that the stress level is equal to or less than the larger of the compression buckling allowable or 80% of the ultimate tensile allowable.

All rivet patterns are assumed to be comprised of a single row of 0.65 cm (0.25 in.) diameter rivets spaced at two diameters. The output number of holes is equal to the number of rivets. However, each rivet is accounted for in only one part of the joint. Adjustment of material thicknesses to a standard gage is accomplished in the same manner as discussed for the spoiler.

The analysis of the flaps, ailerons, slats, rudder, and elevators produces the structural member dimensions and the desired rivet patterns. The planform geometry is obtained from the specific control surface geometry output, and the member thicknesses are computed and then adjusted to standard gages. The control surfaces are assumed to have the geometry shown in Figure 8-47 . The front spar has extended caps and a sheet metal web, and the rear spar is a bent-up sheet. Both the leading edge skin and the main box skin are sheet metal. The trailing edge consists of a full-depth honeycomb core with a single piece of sheet metal forming both upper and lower skins. The airload ribs and the leading edge ribs are bent-up metal. There is a leading edge rib at each airload rib span station. The hinge ribs consist of extruded spar caps and a sheet metal web with bent-up flanges to pick up front and rear spars.

Appropriate material properties are selected for the analysis of each part. Thicknesses are fixed for the leading edge skin and ribs, airload ribs, rear spar, and trailing edge skin as follows:

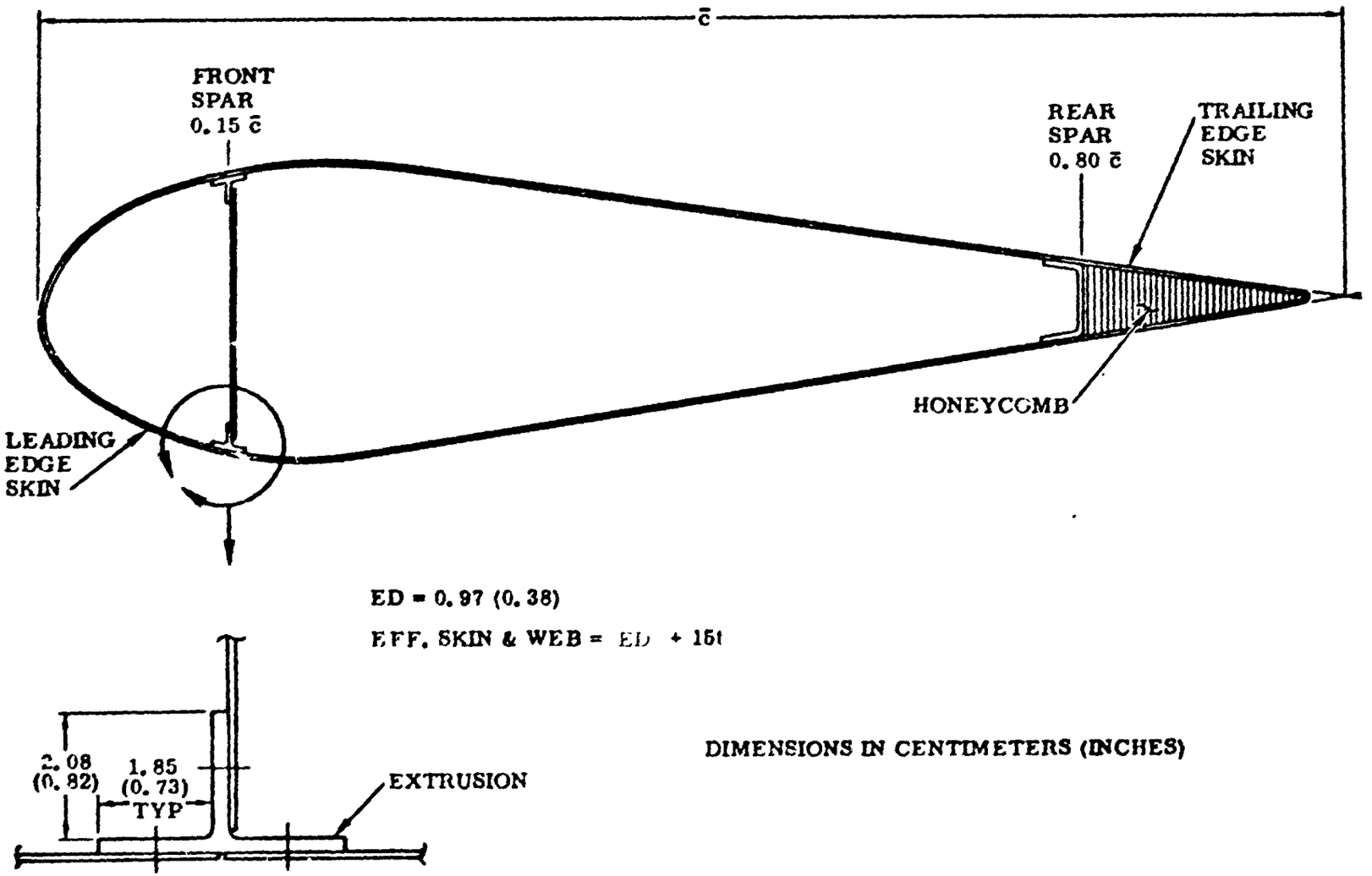

Figure 6-47 Typical Geometry for the Flaps, Slats, Ailerons, Rudder, and Elevators

Part	Thickness
Leading edge skin	Same as box skin
Leading edge ribs	Same as airload ribs
Airload ribs	One gage heavier than skin
Rear spar	One gage heavier than skin
Trailing edge skin	Minimum gage

The analysis for the remaining parts determines the material thicknesses in terms of a minimum required thickness and then rounds the value to the next larger standard gage. Standard sheet gages are summarized in Table 8-7 , and standard gages for extrusions in Table 8-8 .

Table 8-8 Standard Extrusion Gages

cm	in.	cm	in.
0.127	0.050†	0.318	0.125
0.160	0.063	0.395	0.156
0.198	0.078	0.478	0.188
0.239	0.094	0.635	0.250‡

† minimum ‡ maximum

The parts sized by a loads analysis include the basic skins, spar webs, spar caps, hinge rib caps, hinge rib webs, and the trailing edge honeycomb. The analysis accounts for both the internal and external loading conditions. The applied external loads are normal (to the surface) loads only. For the wing surfaces (flaps, ailerons, and slats) these normal loads are derived from the general formulae of Equations 8-57 and 8-58 .

For flaps,

$V \quad 1.75\ V_S$ (Ref. MIL-8860, Para. 6.2.3.9), where V_S = stall speed

$C_n \cdot 1.6$

For slats,

$V \cdot 1.75\ V_S$

$C_n \quad 3.0$

For ailerons, rudders, and elevators, V is derived from

$$N_Z\ W = C_{L_{Max}}\ S_{Wing}\ \frac{V_a^2}{295}$$ (MIL-8860, Para. 3.2.2.2);

or transposing:

$$V_a = V = \frac{295\ N_z\ W}{C_{L_{Max}}\ S_{Wing}}$$

where

N_z = maximum normal load factor

W = aircraft gross weight

$C_{L_{Max}}$ = maximum lift coefficient

S_{Wing} = wing area

V_a = aileron design speed

For ailerons,

C_n = 1.6

For rudders and elevators,

C_n = 1.3

The average pressure, P_{ave}, is applied to the control surface as a chordwise triangular distribution with the center of pressure at the 33% chord aft of the leading edge. If the design speed is equal to or greater than Mach 1, the center of pressure for the aileron, rudder, or elevator is assumed to be at the 47% surface chord. Spanwise running surface loads are therefore proportional to surface chord.

The internal load analysis subdivides the total surface length into a number of equal length segments (individual surfaces) each with a length equal to or less than 457 cm (180 in.). If the individual segment length is 356 cm (140 in.) or less, two hinge supports are assumed, located 28% of the total length from each end. If the segments are greater than 356 cm (140 in.), three hinge supports are assumed. One is located in the center and two are located 15% of the total length from each end. The vertical shear, bending moment, and torque about the front spar are calculated at each hinge. Torque is calculated at each end of the surface segment and is assumed to vary linearly between the ends. For flaps and slats, torque is reacted at each hinge using the same formulae used to calculate shear reactions. For ailerons, rudders, and elevators all torque is reacted at the inboard (or lower) hinge.

The skin thickness is computed based on skin shear flow, and the allowable stresses are fixed as a function of rib spacing. Since the hinge rib number and locations are fixed, rib spacing is determined for each bay between hinge ribs by equally spacing airload ribs. For a given skin thickness, rib spacing can be determined from Figure 8-48 . This curve is a typical design curve for sonic fatigue requirements associated

with the preliminary design phase of aircraft analysis. For practical considerations, a minimum rib spacing of 7.6 CM (3.0 in.) has been incorporated into the computer program analysis logic.

An analysis is made of the inboard panel of the bay with the maximum rib spacing assuming maximum skin shear flow exists there. Allowables are determined for an incomplete diagonal-tension panel utilizing NACA TN 2661, (Reference 15). The critical buckling stress is computed from $F_{S_{CR}} = K_{ss} E (t/d)^2$ where K_{ss} is from figure 12 of NACA TN 2661 (Reference 15). The diagonal tension factor, K, is derived from Equation 27 of NACA TN 2661 (Reference 15). Then the allowable shear stress can be determined as a function of K utilizing the 40-degree curve of Figure 19 (a) of NACA TN 2661 (Reference 15). The skin is sized so that the maximum shear stress does not exceed the allowable, and so that the ratio of the maximum to the critical shear stress does not exceed 5.

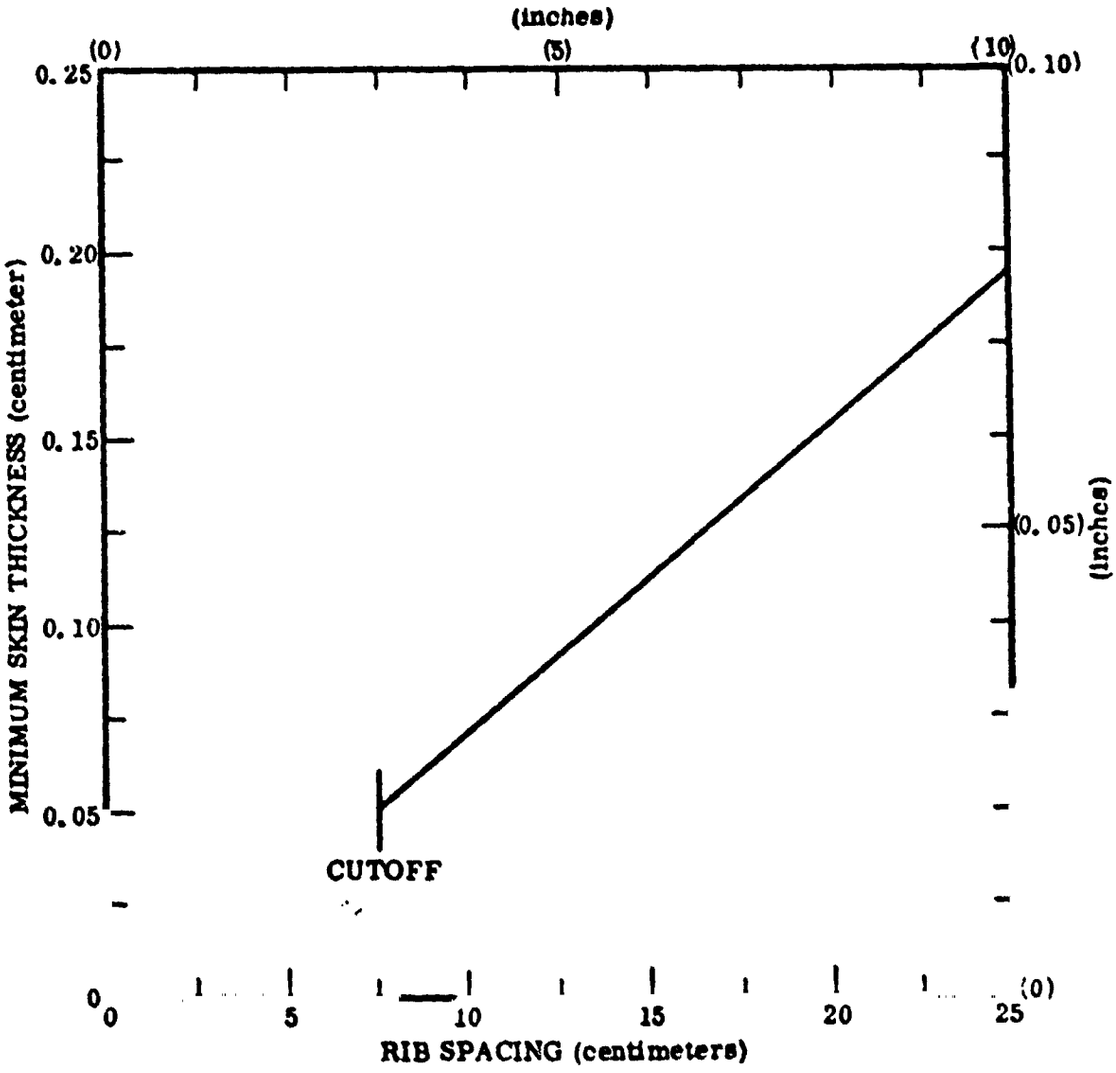

Figure 8-48 Sonic Fatigue Curve

The spar web thickness is determined using the maximum spar shear flow. The analysis is made using either the panel at the inboard end of the surface segment or the panel just outboard of the inboard hinge, which ever has the greatest ratio of spar height to rib spacing. An incomplete diagonal-tension analysis is made like that made for the skin.

All the flap bending moment is taken by the front spar caps and associated skin and spar web. The critical bending location is at the hinge where the ratio of bending moment-to-spar depth is largest. The effective spar section is as shown in Figure 8-47 .

This bending section is symmetric; therefore, tension and compression stresses are equal and may be computed from Equation 8-55 .

$$F = \frac{M\,(d/2)}{I}$$

d = contour depth at spar

The compression buckling allowable,

$$F_{cs} = 0.67\,F_{cy}\left[\frac{3\,t^2}{A}\left(\frac{E}{F_{cy}}\right)^{0.5}\right]^{0.40}$$ (Reference 5 , Equation C7.5)

where

F_{cs} = compression buckling allowable

F_{cy} = compressive yeild allowable

t = material thickness

A = cap area ($= 1.46\,t^2 + 0.82t$)

E = material elastic modulus

The spar cap is assumed to be an extrusion with a constant section thickness sized so that the stress level is equal to or less than the larger of the compression buckling allowable or 80% of the ultimate tensile allowable.

For all surface types, hinge ribs are assumed to have the same part thickness as the inboard hinge. The rib cap is sized by the rib bending moment at the front spar, which is equal to the surface torque (about front spar) at the inboard hinge. The generalized effective rib section is considered to be the same as the spar section. The compression buckling allowable stress equation is the same as that used for the

spar. The rib cap is assumed to be an extrusion, and the constant section thickness is sized in the same manner as the spar cap. The web thickness is sized to be adequate for the inboard hinge rib shear flow,

$$Q = \frac{T}{2A}$$

Q = inboard hing shear flow

T = torque reacted by the inboard hinge

A = inter-spar box area at the inboard hinge

The shear buckling stress is calculated for a web panel at the front spar assuming a panel aspect ratio of 2.

$$F_{SCR} = 5.9\ E \left(\frac{t}{h/2}\right)^2$$

where

F_{SCR} = shear buckling stress

E = material elastic modulus

t = material thickness

h = front spar height at rib

The web thickness is sized so that the shear stress level is equal to or less than the larger of the shear buckling stress or 80% of the ultimate shear allowable.

The assumed honeycomb type and size has a shear allowable of 110 N/cm^2 (160 lb/in^2). A factor is developed that indicates how much heavier, than the basic core, the actual core must be. The factor, K_{core}, is based on the core shear due to trailing edge airload,

$$f_s = \frac{(0.2\ P_{max})\ (0.2\ chord)}{2d}$$

where

f_s = core shear

P_{max} = maximum airload

chord = chord length

d = contour height at rear spar

and

$K_{core} = f_s/160$

Rivet sizes and numbers are calculated using the shear flows that sized the skin, spar web, and hinge rib web. Rivet shear values are used as the allowables and a rivet spacing of four diameters is assumed.

Q		No. of		Spacing	
N/cm	lb/in	Rows	Rivet	cm	in.
0 to 1359	(0 to 776)	1	4AD	1.27	(0.50)
1360 to 1671	(777 to 954)	1	5AD	1.59	(0.625)
1672 to 2755	(955 to 1573)	1	6DD	1.91	(0.75)
2756 to 3427	(1574 to 1957)	2	5DD	1.59	(0.625)
3428 and above	(1908 and above)	2	6DD	1.91	(0.75)

In the output the number of holes is equal to the number of rivets; each rivet hole is accounted for in only one part of the joint. When two rows of rivets are required, an additional spar or rib cap width is output. This additional area is not used to resize the cap.

8.3 REFERENCES

1. Kruse, G. S., and Peterson, L. M., "Automated Structural Sizing Techniques for Aircraft and Aerospace Vehicle Structures", General Dynamics/Convair Report GDCA-ERR-1748, December 1972.

2. "Computer Program to Perform Cost and Weight Analysis of Transport Aircraft," (NAS1-11343) NASA CR 132362, November 1973.

3. "Computer Program to Assess Impact of Fatigue and Fracture Criteria on Weight and Cost of Transport Aircraft," (NAS1-12506) NASA CR 132648, June 1975.

4. Shanley, F. R., "Weight-Strength Analysis of Aircraft Structures", Dover Publications, Inc., New York, N. Y., March 1960.

5. Bruhn, E. F., "Analysis and Design of Flight Vehicle Structures", Tri-State Offset Co.. Cincinnati, Ohio, 1965.

6. Fletcher, R., and Powell, M. J. D., "A Rapidly Convergent Descent Method for Minimization", The Computer Journal, Vol. 6, April 1963 - January 1964.

7. Peery, D. J., "Aircraft Structures", McGraw-Hill Book Company, New York, N. Y., 1950.

8. "Astronautics Structures Manual," NASA Marshall Space Flight Center.

9. List, G. R., "F-111 Design Allowables," General Dynamics Fort Worth Report FZS-12-141.

10. Blackmon, C. M., and Eisenmann, J. R., "Advanced Composite Fuselage Section Optimization," General Dynamics Report FZM-5686, June 1976.

11. Miner, M. A., "Cumulative Damage in Fatigue," Journal of Applied Mechanics, Volume 12, No. 3, September 1945.

12. Miner, M. A., "Cumulative Damage in Fatigue", Journal of Applied Mechanics, Vol. 12, No. 3, Sept. 1945.

13. Kruse, G. S., Tanner, C. J., and Wilson, P. J., "Fatigue and Fracture Mechanics Technology - Analysis," General Dynamics/Convair Report CASD-ERR-74-052, December 1974.

14. Poe, C. C., Jr., "Stress-Intensity Factor for a Cracked Sheet with Riveted and Uniformly Space Stringers," NASA TR-R-358, Washington, D. C., May 1971.

15. Kuhn, P., Peterson, J., and Levin, L., "A Summary of Diagonal Tension Part 1 - Methods of Analysis," NACA TN 2661, May 1966.

SECTION 9

PARTS DEFINITION

Detail parts definition methods have been developed to predict a generalized detail parts listing based on the output from the structural synthesis analysis. The resultant parts listing provides a complete breakdown of an airframe structure into its most elementary components. This listing of detail parts then represents the basis of a weight and manufacturing cost analysis procedure. As part of this procedure each detail part is looked at individually and analyzed in terms of its weight, cost to manufacture and cost of material.

A sequence of assembling the detail parts is also modeled. The weight and costs corresponding to each step of the assembly process are included in the computations. Thus, the weight and costs of the complete airframe structure can be obtained by summing the values for the individual parts, and adding in the elements associated with the assembly.

The detail parts associated with the fuselage and aerodynamic surfaces are defined and analyzed in the part definition subprograms that are driven by the structural synthesis. The part definition routines associated with the structural box define the surface geometry in terms of minimum gages, rib type and location, flange width, fastener size, etc. A breakdown is made of major components into detail parts. The logic parameters are defined for process listings and the cost analysis. These routines also define and size the leading edge, trailing edge, and tip geometry and weights.

The part definition routines associated with the fuselage shell define geometry in terms of frame stations, barrel stations, frame segment perimeters, etc. A breakdown is made of major components into detail parts. The logic parameters are defined for process listings and the cost analysis. A separate accounting is made for the fuselage penalty items (bulkheads, windows, floors, doors, etc.) not included in the fuselage structural synthesis subprogram.

The airframe actual weight and the material purchase weight are computed within the part definition subprogram. Detail part weights are summed to build up the subcomponents into subassemblies, and subassemblies into major components, etc., to derive the complete airframe assembly weight.

The actual weight reflects the actual weight of the finished part. It is computed based on the actual geometry of the finished part, and accounts for design, manufacturing, and assembly considerations that would normally go into producing a real part. Figure 9-1 illustrates the different concepts involved in determining the idealized or theoretical weight and the practical or actual weight. The former is based on the output from the structural synthesis routines, and the latter on the detail part definition routines.

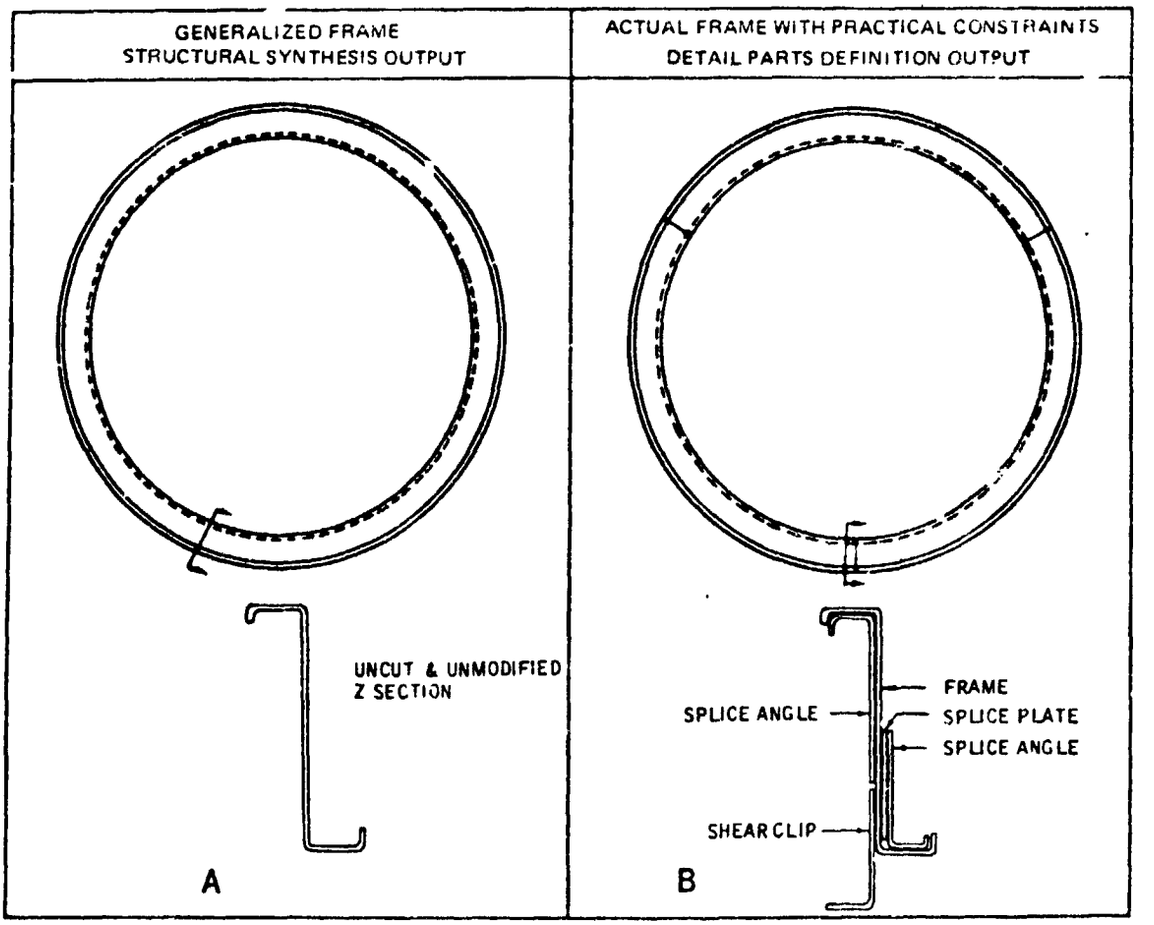

Figure 9-1 Representative Difference Between Theoretical and Actual Body Frames

The material purchase weight is the weight of raw material stock that must be purchased in order to be able to manufacture a part of actual weight. Calculation of the material purchase weight uses the same terms as the actual weight but includes allowances for material removed during manufacturing. Operations resulting in the loss of material include the initial material cut off from the raw stock, initial cutting to size, trimming, milling, turning, drilling, etc. Figure 9-2 illustrates the difference in actual and material purchase weight for an integrally stiffened skin panel. Extruded plate is purchased. From the constant dimensions of the plate a skin panel with varied skin thickness and stiffener dimensions is machined corresponding to the varied load conditions over the surface of the skin.

9.1 AERODYNAMIC SURFACES. The parts definition associated with the aerodynamic surfaces is subdivided into two parts. The first part deals with the structural box and the second with the leading edge, trailing edge, and tips. The leading edge is deinfed to include all items located forward of the front spar, the trailing edge includes

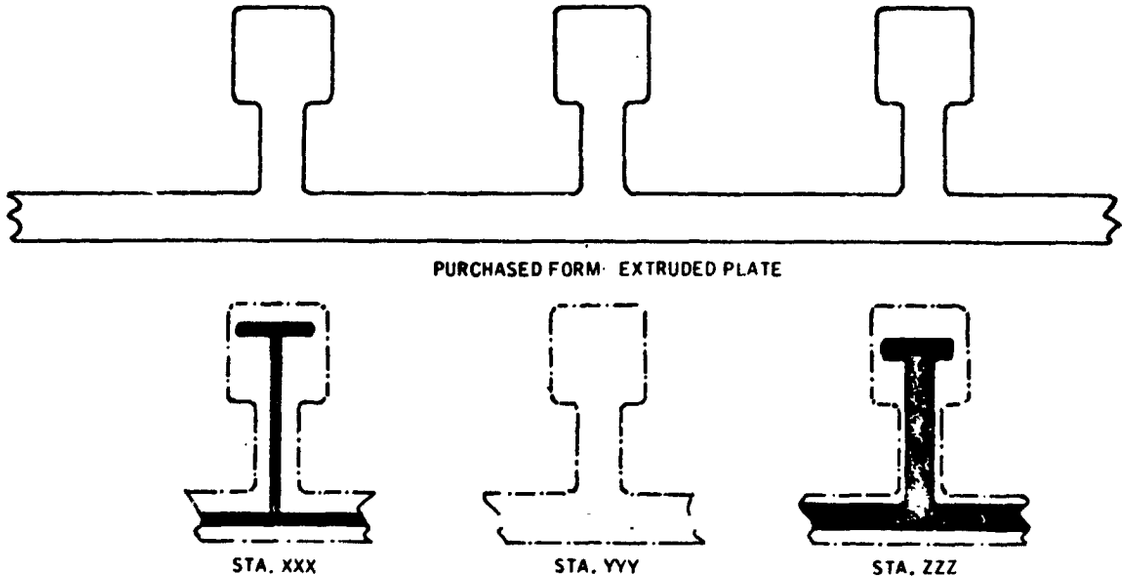

Figure 9-2 Representative Difference Between Material Purchased and Finished Form of Skin Panels

all items aft of the rear spar, and the tip includes all items outboard of the structural box tip closing rib.

The parts definition of the structural box encompasses the covers, spars, and ribs. The construction modes available are skin-stringer, multi-web, and full depth sandwich. The construction modes are built-up from a combination of skin panels, spars, and ribs. The structural synthesis program analyzes twelve panel configurations, five spar types, and five rib types, and transfers dimensional data to the parts definition subprogram. The parts definition program generates detail part data on four panel configurations, two spar types, and one rib type. A summary of the available skin panel configurations, spar types and rib types within the structural synthesis and parts definition subprograms are shown in Figure 9-3 .

The part definition material properties include three metallic and three composites. The metallic material properties stored as a function of temperature are for aluminum, titanium and steel. The composite material properties stored as a function of temperature are for boron-epoxy, boron-aluminum, and graphite-epoxy.

The parts definition subprogram develops data for the leading edge, trailing edge and tips in addition to the structural box. Dimensional data for the detail parts are derived in the structural synthesis and each component that is analyzed is then broken down into a series of detail parts in the detail part subprogram. The components include flaps, foreflaps, ailerons, rudders, elevators, slats, spoilers, fixed leading edge, fixed trailing edge, and tips. The aerodynamic surface parts definition analysis is discussed in detail in the following sections.

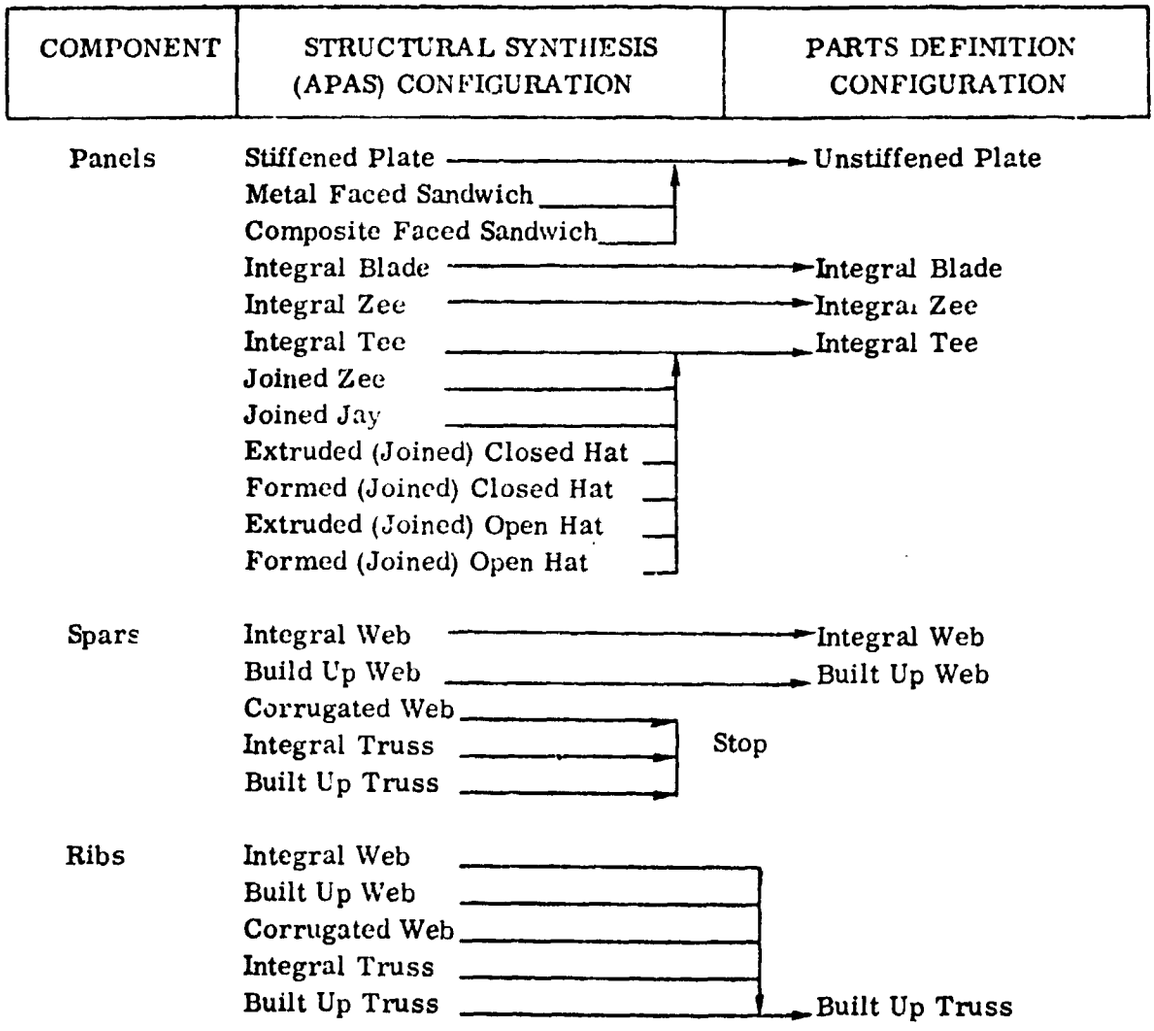

Figure 9-3 Summary of Structural Synthesis and Parts Definition Configurations

9.1.1 Skin Panel Parts Definition. The skin panel part definition model has four panel types. A summary of the panel concepts currently available in the parts definition is presented in Figure 9-4 .

Each of the lifting surface cover panels is assumed to be a complete (integral) assembly by itself. There are no other detail parts associated with the panels at this stage. Subassembly operations accounted for in the panel analysis are the spanwise and chordwise panel splices. Assembly of the complete box structure, as illustrated in Figure 9-5 , is accounted for in the structural box parts definition process.

Input to the panel parts definition routine includes variables from both the lifting surface geometry and the structural synthesis routine. Input from the structural synthesis process is comprised of panel cross section dimensions of each control station.

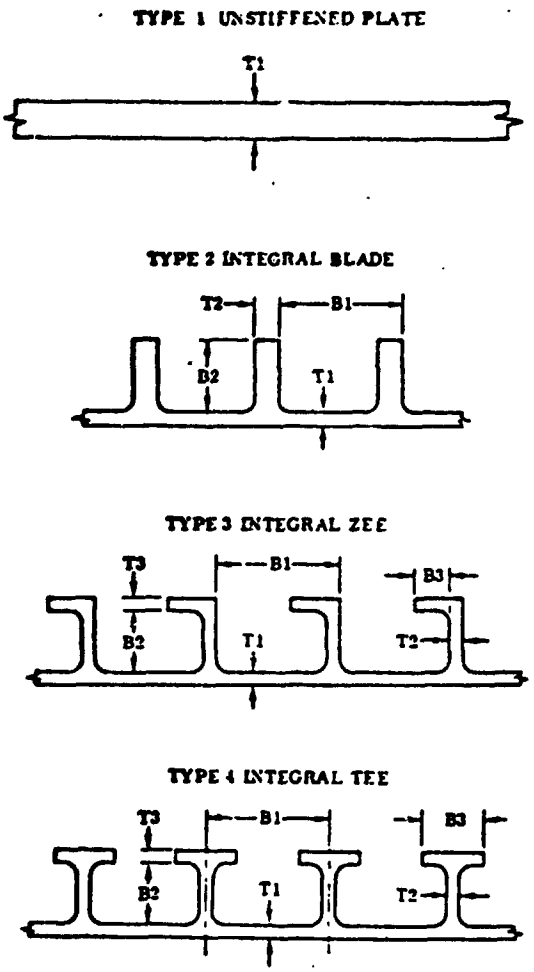

Figure 9-4 Lifting Surface Cover Panel Options for the Parts Definition

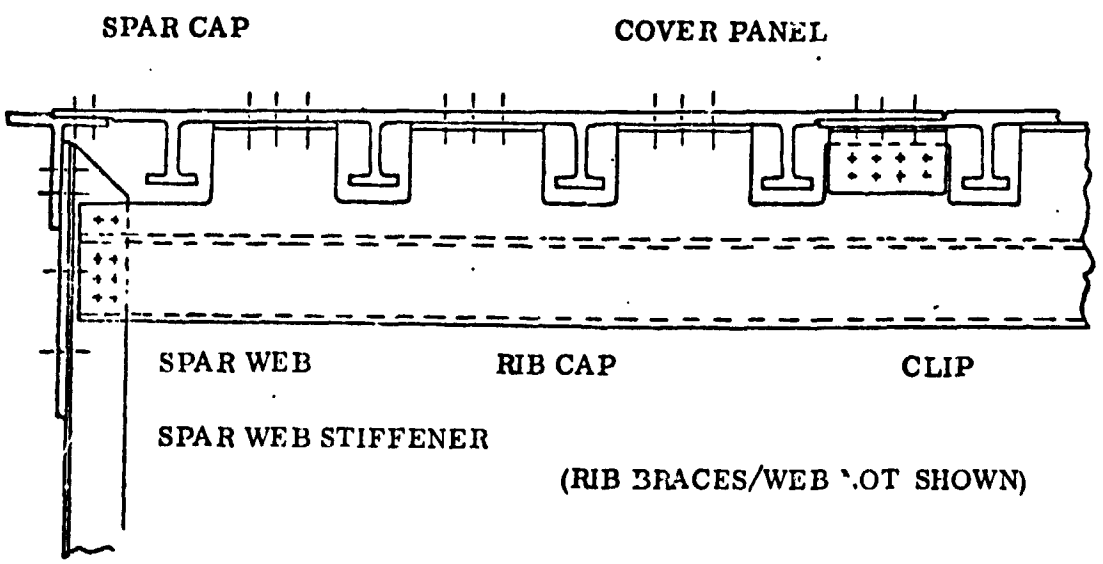

Figure 9-5 Typical Mode of Attachm for a Lifting Surface Cover Panel

Additional input from the geometry routine includes the number and location of the control stations, and the number of control station nodes. User supplied input accounts for specifying a panel type with an option for also defining a maximum allowable panel length.

As part of the parts definition process the semi-span is divided into a number of constant length panels. In the absence of a user specified panel length, a maximum length of 10.06 m is assumed. Panel widths are assumed to be defined by the node locations, which in turn are defined in the lifting surface geometry routine. A constant number of panels are assumed across the surface in both a spanwise and a chordwise direction.

Panel cross section dimensional data is computed at the actual panel endpoints by a linear interpolation of the geometry at adjacent control stations. The reference geometry of a typical panel in terms of the program Fortran variables is illustrated in Figure 9-6 . Corresponding detailed dimensions for the various panel types are presented in Figure 9-4 . The panels are assumed to be spliced, using an overlap joint, in both the spanwise and chordwise directions, to form a complete cover ready for attachment to a spar and rib box structure.

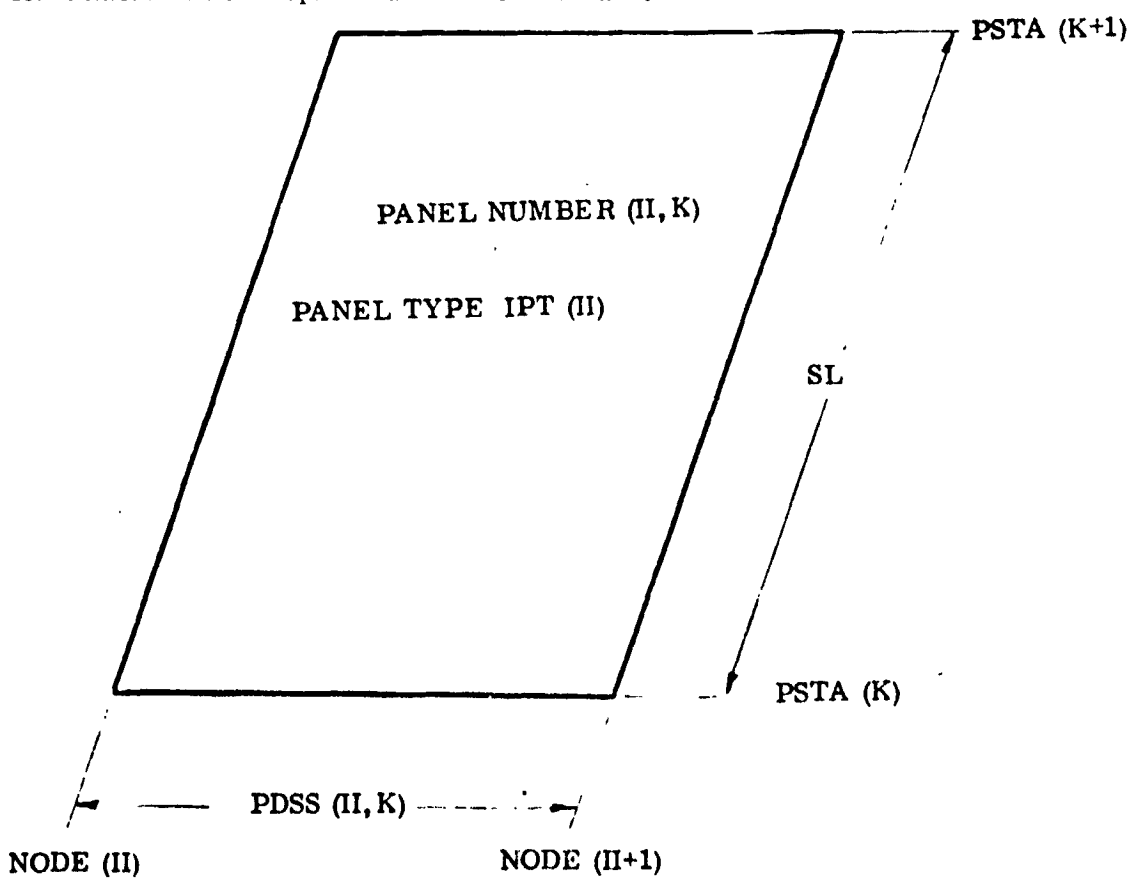

Figure 9-6 Typical Lifting Surface Panel Arrangement With Corresponding Fortran Variables

Panel weights are computed at three different levels of consideration. A theoretical weight is computed directly from the output of the structural synthesis routines. The theoretical weight is the weight of the basic, idealized structural element. It represents an optimum value that is based on geometry of a component sized simply for load carrying capability. Real world manufacturing and assembly constraints are not considered. Typical features not accounted for are: flanges to serve as attachment points, clearance allowances, material widths for edge distance requirements, joint load path continuity, etc.

The actual weight reflects the actual weight of the finished part. It is computed based on the actual geometry of the finished part, and accounts for all design, manufacturing, and assembly considerations that would normally go into producing a real part. The material purchase weight is the weight of raw material stock that must be purchased in order to be able to manufacture a part of actual weight. Calculation of the material purchase weight uses the same terms as the actual weight but includes allowances for material removed during manufacturing. Losses occurring between the time the material is purchased and its being utilized to produce a useful part (including losses due to design changes, part duplication, spoilage, waste, overbuy, etc.) are accounted for in the cost analysis portion of the program. Actual manufacturing operations which result in the loss of material include the initial material cut off from the raw stock, initial cutting to size, trimming, milling, turning, drilling, etc. Figure 9-7 illustrates the difference due to fabrication in actual and material purchase weights for the cover panel arrangements which are available.

The general form of the equation used to compute cover panel weight is:

$$\text{weight} = \frac{\text{panel length}}{6} * (\text{area}_1 + \text{area}_2 + 4 * \text{area}_{12}) * \text{density}$$

where area_1 and area_2 are the cross sectional areas at the panel ends, and area_{12} is the cross sectional area at the panel midpoint. The panel midpoint dimensional data needed to compute area_{12} is obtained by a linear interpolation of dimensional data at the panel ends.

The optimum weight for each panel is computed utilizing the dimensions output from the structural synthesis routines directly. The actual weight computation utilizes the dimensions output by the structural synthesis with extra allowances made for manufacturing and assembly clearance requirements, edge distance requirements, flange widths for attachment, fillets, standard and minimum gages, etc. For the current cases involving integrally machined cover panels a minimum gage of .081 cm is assumed for the outer skin portions of the panel which are to be riveted during assembly. Minimum gage for the remaining portions of the panel are specified by the user and are accounted for in the structural synthesis. For the unstiffened plate configuration the thickness of the skin is increased to the nearest standard material stock gage. Because the panels are integrally machined, there are no stiffener attachment flange

width requirements or fastener edge distance requirements during assembly to consider. Fillets with a .635 cm radius are added to the stiffener corners.

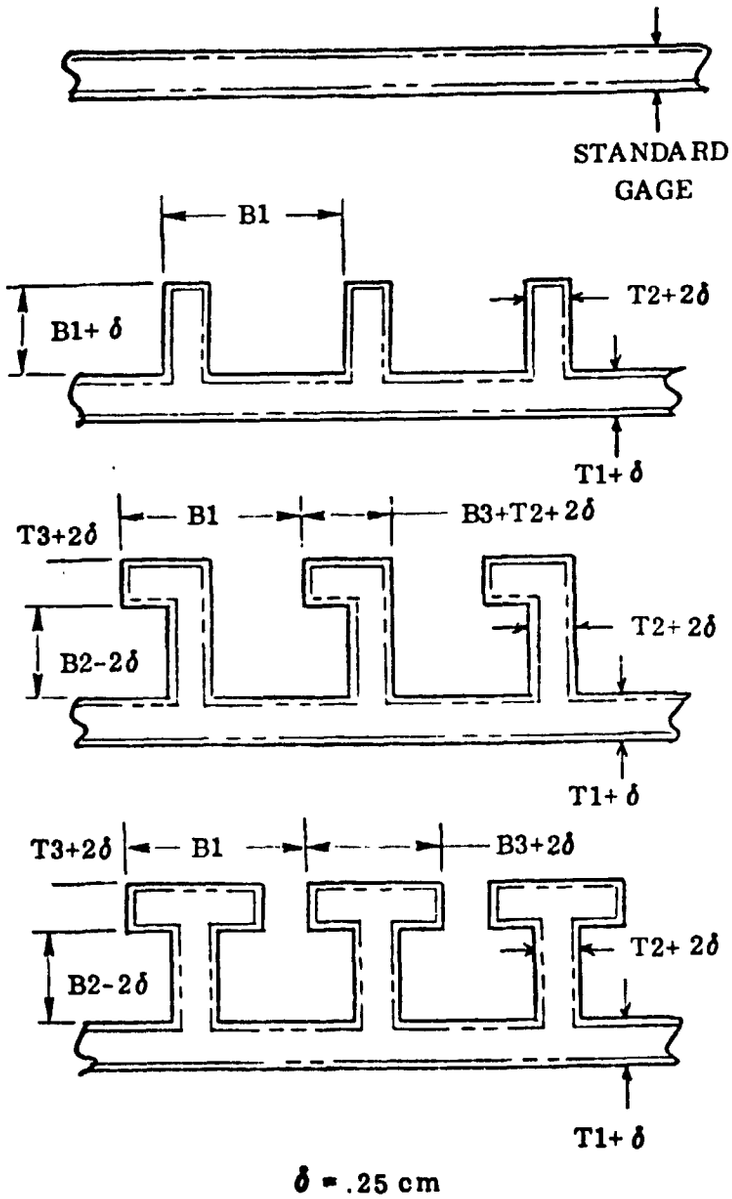

Figure 9-7 Purchased Material Forms for Lifting Surface Cover Panel

Material purchase weights are computed based on an assumed raw material stock form of either flat plate or extruded flat plate. Constant dimensions are assumed

for the raw material stock. The actual cover panel is assumed to be machined from the raw material stock with skin thickness and stiffener dimensions corresponding to the varied load conditions occurring on different parts of the surface. A constant (linear) rate of taper of panel dimensions is assumed between panel endpoints. Weight of the purchased raw material is computed by using the dimensions of the center, root panel, and adding an allowance to account for machining losses. A single size of raw material stock is assumed for each surface and all panels for that surface are assumed to be machined from this. The assumed raw material forms are illustrated in Figure 9-7.

The next step in the analysis procedure is a manufacturing cost computation. For each detail part defined by the parts definition process, a corresponding sequence of manufacturing operations is automatically specified. This list represents those processes which are required to produce the part in the shop. Each process is represented by an equation from which a calculation is made to determine the number of labor hours required for that process during production of the part. These hours plus corresponding labor rates, overhead rates, and efficiencies form the basis of determining manufacturing cost.

9.1.2 Spar Part Definition. The spar configurations include integrally machined and built-up spar arrangements. Each arrangement uses either an angle or a tee cap. A summary of spar configurations currently available in the parts definition analysis is presented in Figure 9-8.

Input to the spar parts definition routines include variables from both the lifting surface geometry and the structural synthesis routine. Input from the structural synthesis process is comprised of spar cap and web cross section dimensions at each control station. Additional input from the geometry routine includes basic surface geometry, the number and location of the control stations, and the number of ribs associated with the surface. User supplied input encompasses the rib and spar types, and the total number of spars. A minimum of two spars, a front and rear, is assumed in the absence of an input. A maximum of five spars are allowed.

The program analyzes each spar of a surface individually. The true length of the spar is computed by assuming a structural box extending from airplane centerline to the surface tip, minus 30.48 cm allowed for attachment of a tip cap. No separate carry through structure inside the fuselage shell is accounted for. The spars are assumed

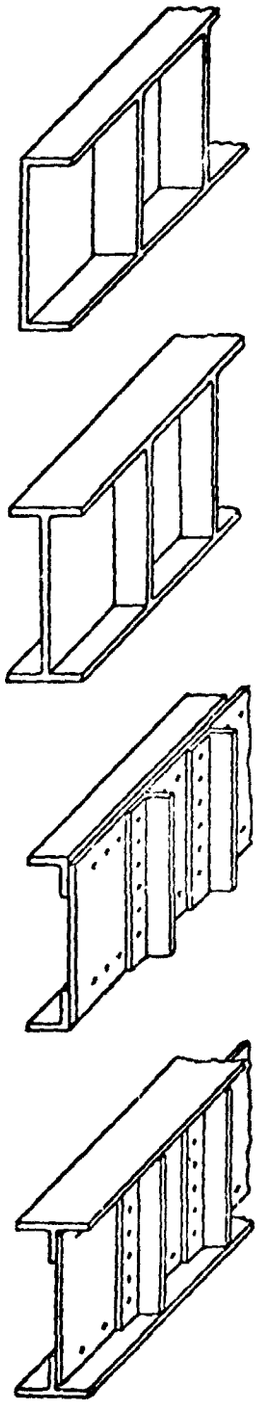

Integral Angle/Integral Blade

Integral Tee/Integral Blade

Joined Angle/Joined Angle

Joined Tee/Joined Angle

Figure 9-8 Summary of the Spar Configurations Currently Available in the Parts Definition Routines

to run along constant percent chord lines, and are divided into a number of segments if necessary to attain the full spar length. Maximum segment length may be input by the user. In the absence of an input integrally machined spars are assumed to have a maximum segment length of 4.115 m and builtup spar segments a maximum length of 8.230 m.

Each spar segment is then analyzed separately. Basic elements comprising the spar segment include the caps, web, web stiffeners, and rib stiffeners. Additional spar parts include splice plates for splicing segments, fittings for attachment of leading and trailing edge components, and assembly fasteners.

The structural synthesis process provides basic dimensions for caps, web, and web stiffeners at each control station. Dimensions for the spar segment cap and web ends are derived by interpolation between adjacent control stations. A constant rate of taper of cap and web dimensions is assumed between segment endpoints. Web stiffener dimensions are assumed constant along the length of the segment, and equal to those dimensions arrived at by interpolation at the inboard end of the segment.

Optimum weights for the caps, webs, and web stiffeners are computed utilizing interpolated structural synthesis dimensions. The general form of equation is the same as that used for the cover panels. The program next adjusts these dimensions to account for actual manufacturing considerations. In particular, flange sizes are checked to see that they are large enough to allow for proper clearances, edge distances, fastener spacing, etc. The thicknesses of components fabricated from sheet stock are readjusted to the next higher standard material gage, joint overlaps are checked, etc. Actual weights are then computed using the revised dimensions.

Material weight for the integrally machined spar segment are computed by assuming a solid bar of material with dimensions slightly greater than the maximum spar external dimensions to account for cutoff and machining of the segment. The built-up spar is assumed to be comprised of extruded caps, sheet webs, and bent-up sheet web stiffeners. Material weights for each of these elements are computed using the actual weight computation dimensions plus allowances for machining, cutoff, etc.

One spar web splice plate is assumed for each spar segment except the last one. Splice plates are sized to fit on the spar web inside the spar cap flanges. The width is derived by assuming a total of four fastener rows across the splice with appropriate clearances, spacing, and edge distances. Thickness is set equal to the spar web thickness. The optimum weight is set equal to the actual weight in this case since the plate is sized initially by functional logic and not the structural synthesis. Material weight is computed by assuming fabrication from flat sheet stock with a thickness equal to the next higher standard sheet gage. Extra length and width of 5.08 cm are added to the actual dimensions to account for initial cutting size.

Rib stiffeners are specified along the spar web at each rib attachment point if the local web stiffener spacing is greater than 30.48 cm. These stiffeners serve as attachment clips for the rib webs and are not utilized if truss type ribs are present. One set of rib stiffeners are specified for external spars, and two sets (one on each side of the spar web) for interior spars.

Rib stiffeners are assumed to be bent-up angles with a thickness and riser height equal to those of the web stiffeners. They are sized for an attachment flange width carrying a single row of fasteners. Length is set equal to the web height. Optimum weight is again set equal to the actual weight. Material weight is computed by assuming fabrication from the next higher standard sheet gage. The length and width are increased by 5.08 cm and 2.54 cm respectively, for the material weight computation.

Fittings are specified on the exterior spars for attachment of the leading and trailing edge elements. These fittings attach to spar web stiffeners directly and to the adjacent skin panels through a clip and doubler arrangement. Each machined fitting has associated with it two clips and two doublers.

Fittings are sized on the basis of the local spar height. A generalized fitting design is assumed and the actual weight is computed by deriving dimensions in proportion to the spar height. Appropriate dimensions and attachment flanges are checked for fastener allowances and readjusted if necessary. Optimum weight is again set equal to the actual weight. Material weight is computed by assuming the fitting to be machined from a block of thick plate. The dimensions of the block are assumed to be those of the maximum fitting dimensions in each direction with an additional (5.08 cm on the length, 2.54 cm on the width, and a 1.27 cm on the thickness).

The two doublers associated with each fitting are assumed to be cut from .160 cm sheet. The length and width are computed as a function of the fitting size with minimum values set for four rows of four fasteners each. Optimum weight is set equal to actual weight. Material weight is computed with an additional 5.08 cm added to the length and width dimensions.

The two clips associated with each fitting are assumed to be short pieces cut from a tee shaped extrusion. The length and riser height are computed as a function of fitting size. The base flange is sized to carry a single row of fasteners along each side of the riser. The thickness of both the base flange and the riser is assumed to be .127 cm. Optimum weight is set equal to actual weight. Material weight is computed by assuming 5.08 cm of additional length plus an allowance for the material removed from the riser.

The total number of assembly fasteners required is computed by summing the number of fasteners necessary to assemble each detail part as it is looked at individually. The following assembly operations are accounted for: attachment of the segment spar

caps to the web, splicing the webs to attain a full length spar, attachment of the web and rib stiffeners to the web, attachment of the doublers and clips to the skin panels, and attachment of the fittings. The appropriate assembly operations are bypassed for the case of an integrally machined spar.

No changes were made to the manufacturing process listings or to the manufacturing cost analysis portion of the program during this effort. Spar detail parts are assumed to use those process listings previously specified for similar parts. It is recommended that future refinements include the addition of new structural configuration alternatives, but also an updated and expanded process listing for the concepts currently available.

9.1.3 Rib Part Definition. A single rib configuration representing a built-up truss is available in the parts definition. All other rib types available in the structural synthesis revert to a built-up truss rib when the program reaches the parts definition process.

The assumed arrangement of the rib is illustrated in Figure 9-9 . Detail parts include the upper and lower (or left and right) caps, 45 degree angle braces, right angle braces, skin panel attachment clips, and assembly fasteners. The rib cap is assumed to be comprised of an extruded modified jay section with cutouts to allow for passage of the skin panel spanwise stiffeners. The rib caps are attached directly to the skin panels along the length of the caps except where spanwise skin panel splices occur. Here, clips are specified for attachment of the rib cap to the skin panel. The clips are assumed to be short pieces of extruded angle, and the number of clips associated with each rib is set equal to the number of spanwise panel splices.

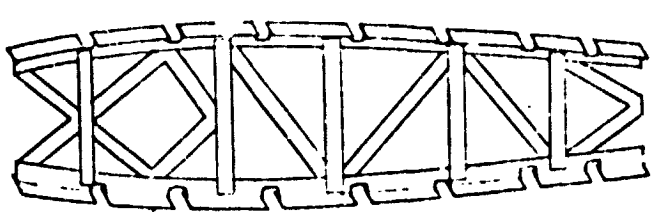

Figure 9-9 Assumed Arrangement of a Builtup Truss Type of Rib

The number of angle braces is computed by assuming a brace angle of 45 degrees with a single right angle brace between adjacent 45 degree angle braces. The braces are assumed to be extrusions with a cruciform section. Fasteners are required for attachment of the braces and clips to the rib cap, and attachment of the rib cap to the skin panels and spars. Aluminum, steel, or titanium fasteners are available in the program.

Input to the rib parts definition routine includes variables from both the lifting surface geometry and structural synthesis routines. The required geometry data includes the number and location of the control stations, the number of control station nodes, the number of ribs (up to a maximum of 100 are allowed per semi-span), rib spacing, and surface span. The structural synthesis provides at each control station the rib cap area and length, brace area and weight, and the structural box average height. Panel cross section dimensions (and panel type) are also required at each control station to determine the rib cap cutout size for clearance of panel stiffeners.

Ribs are sized by the structural synthesis routine at each control station. The rib parts definition routine derives an actual spanwise rib location based on the specified rib spacing. The dimensions of the actual ribs are obtained by interpolating dimensions between the control stations. Each actual rib is then analyzed individually.

9.1.4 Structural Box Parts Definition. To be able to predict manufacturing costs based on the actual work to be performed, a complete list of required parts must be generated. A parts definition procedure was developed that calls out a list of detail parts when a structural component such as a wing spar or a body frame is specified by the structural synthesis routines. Each detail part is used, in turn, to call out a list of the associated manufacturing processes and the raw material stock necessary to produce that part.

The part list library was established in the following manner. A model component such as the structural box of the C-5A vertical stabilizer was selected and a complete part listing of the model component was obtained. Additional parts were added to those of the model component to account for variations in the mode of construction. The example components were used as a checklist to ensure that all detail parts were accounted for; they were not intended to serve as models to develop statistical part prediction factors. An example of a component part listing for a skin-stringer type of vertical stabilizer is presented in Table 9-1 . Illustrated are the type and form of the data utilized to develop the part list library. The figure reflects the number of dissimilar parts and total pieces making up each component and gives the relative weights.

The parts list developed for the program is in a more generalized form than that shown in Table 9-1 . Instead of having separate front, intermediate, and rear upper and lower spar caps, for example, the program defines one general spar cap.

However, the specific dimensions are determined separately for each location by the spar sizing procedure in the structural synthesis routines. In this way the actual dimensions change for various locations and types of spar caps, but the general shape remains the same. Table 9-2 is a summary of the parts buildup available in the program for aerodynamic surfaces.

Table 9-1 Example of a Component Part Listing

AIRFRAME ELEMENTS	WEIGHT (kg)	WEIGHT (lb)	DISSIMILAR PARTS	TOTAL PIECES
Horizontal Tail	[2,643.1]	[5,814.9)]	[2,287]	[4,528]
Basic Structure	[2,068.9]	[4,529.6)]	[1,366]	[2,975]
Center Section	[449.0]	[987.8)]	[99]	[163]
Upper Caps & Covers				
Front Spar Cap	2.8	(6.4)	3	3
Intermediate Spar Cap	11.5	(25.4)	3	3
Rear Spar Cap	30.4	(66.8)	3	3
Interspar Cover	41.0	(90.1)	4	4
Joints, Splices, & Fast.	12.0	(26.4)	17	42
Lower Caps & Covers				
Front Spar Cap	2.8	(6.4)	1	2
Intermediate Spar Cap	11.5	(25.8)	-	2
Rear Spar Cap	30.4	(66.8)	2	2
Interspar Cover	40.0	(87.9)	4	4
Joints, Splices, & Fast.	13.1	(28.9)	18	45
Spar Web & Stiffeners				
Intermediate Spar	6.5	(14.4)	1	1
Joints, Splices & Fast.	1.0	(2.1)	-	-
Interspace Ribs	69.0	(151.9)	21	30
Pivot Fitting Installation	170.7	(375.6)	6	6
Pitch Trim Actuator Fitting	3.9	(8.5)	16	16
Outer Section	[1,609.9]	[3,541.8)]	[1,367]	[2,812]
Upper Caps & Covers				
Front Spar Cap	25.9	(56.9)	3	4
Rear Spar Cap	40.9	(90.0)	6	6
Interspar Cover	467.2	(1,027.8)	23	24
Joints, Splices, & Fast.	18.8	(41.4)	26	88
Lower Caps & Covers				
Front Spar Cap	25.4	(55.8)	4	4
Rear Spar Cap	39.5	(86.8)	4	6
Interspar Cover	419.3	(922.5)	12	12
Joints, Splices, & Fast.	18.5	(40.6)	46	81
Spar Web & Stiffeners				
Front Spar	56.4	(124.0)	77	118
Rear Spar	98.4	(216.7)	101	149
Joints, Splices, & Fast.	16.8	(36.9)	1	2
Interspar Ribs	167.8	(369.1)	297	754
Leading Edge				
Cover	35.6	(78.3)	21	32
Ribs	11.2	(24.7)	49	98
Auxiliary Spars	6.4	(14.0)	5	20
Joints, Splices & Fast.	5.1	(11.2)	5	10

The actual part prediction is done by establishing the functional dependency between the parts available on the parts list and the specified mode of construction or the structural configuration. For example, if a skin-stringer mode of construction is specified, the structural synthesis routine calls out and sizes the appropriate spars, ribs, and cover panels. The parts definition routines then specify each detail part making up these components. The form of the functional logic used to break down each component further is shown in the following example for a vertical stabilizer, which assumes the selection of a truss-type, built-up rib, a built-up web type of spar, and an integral skin-stringer skin.

A truss-type, built-up vertical stabilizer rib is basically composed of left and right (upper and lower) caps, truss-type braces, clips for skin attachment, and fasteners. An assumed angle of 45 degrees is used to calculate the number of cross braces, which is then equal to the rib chord divided by the average rib depth. The number of right-angle braces is equal to the number of 45-degree braces minus one. The number of clips required is equal to the number of 45-degree braces minus one. The number of clips required is equal to the number of skin panels specified minus one, assuming the panels overlap and that the edges of the forward and aft panels attach to spar clips instead of rib clips. The number of fasteners required for skin attachment is derived as a function of the number of rows of fasteners needed and a typical fastener spacing, for aluminum, say four times the fastener diameter. Figure 9-10 shows a root chord section of the C-5A vertical stabilizer, illustrating the construction of the rear spar, cover panels, and the lower rib. Figure 9-11 illustrates the actual truss-type rib configuration used in the C-5A vertical stabilizer compared to the truss-type rib generated functionally by the parts definition routine.

A built-up web-type vertical stabilizer spar consists of left and right (upper and lower) caps on each side of a web, which is stiffened longitudinally by left and right (upper and lower) rails. Various types of stiffeners are attached laterally across the web, including actuator and rib stiffeners plus the basic web stiffeners. Actuator and hinge support fittings and miscellaneous doublers, clips, and shims complete the parts list.

To the basic spar structure of caps, rails, and web, the program adds a rib stiffener at each rib station and one web stiffener for each rib. One doubler and doubler stiffener are required at the root of the front spar. The program also calls out two miscellaneous stiffeners and seven skin attachment clips for the front spar, and two hinge support fittings and one actuator support fitting for the rear spar. The callout for four actuator stiffeners (two each of two kinds for an actual total of four) has as its basis four actuator/hinge ribs required in a typical control surface (rudder) installation. The spar fasteners required are calculated based on the number of fasteners needed to fasten the caps, rails, and stiffeners to the web. The cap-to-web fasteners are assumed to run along the length of the spar in two rows for each cap. The rail-to-web fasteners are also assumed to run the length of the spar, but in only one row per rail instead of two. A typical spacing of four times the fastener diameter is used. The various stiffener-to-web fastener requirements are calculated based on the number of each kind of stiffener needed and the average

length of each stiffener, which is assumed equal to the average spar depth. A portion of a rear spar similar to the type being discussed is shown in Figure 9-10 .

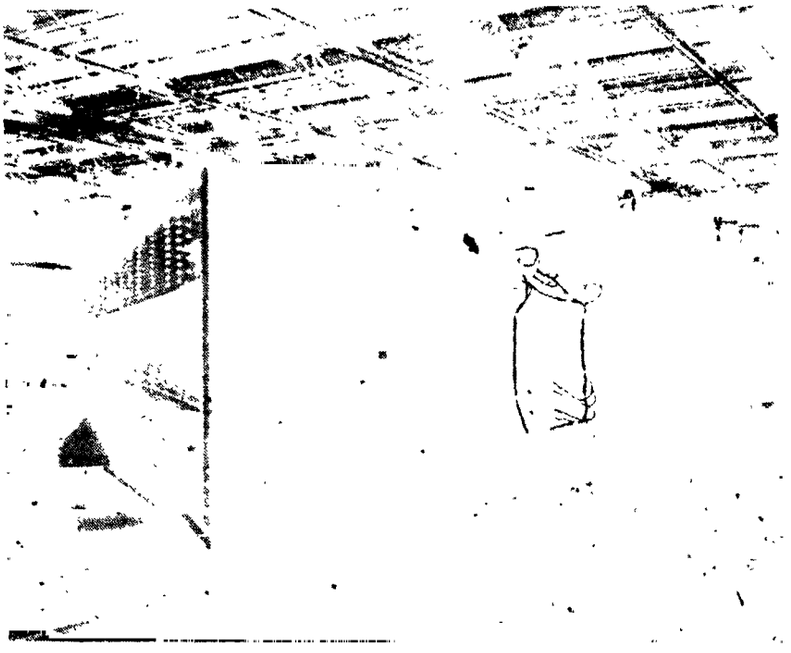

Figure 9-10 Root Chord Section of the C-5A Vertical Stabilizer

The various fastener diameters used in calculations are derived on the basis of material thickness. Average thicknesses for the skin panel and spar web are calculated within the parts-listing subroutine; the skin and rib fastener diameters are based on the average skin thickness, and the spar fastener diameters are based on the average web thickness. Actual values of diameter are called from a table located on the BLOCK DATA portion of the program, which lists values of diameter corresponding to a given skin thickness.

The number of skin panels required for each side of the vertical stabilizer is calculated by assuming a maximum skin panel width of 50.8 CM (20 inches); hence, the number of panels is equal to the rib chord divided by 20. The corresponding number of lengthwise panel stiffeners is calculated based on the stiffener spacing, which is called from the structural synthesis portion of the program. The skin fasteners required are calculated as the number of fasteners needed to splice the overlapping skin panels together along their lengths using two rows of fasteners along each splice. The skin panel assembly shown in Figure 9-12 is the type discussed, and an individual panel is shown in greater detail in Figure 9-13 .

The variables used in the parts definition routines, such as rib chord, average rib depth, number of skin panels, and fastener diameters, are generated as output by the

structural synthesis routines and act as input for the subsequent part definition routines. There is no direct input to the parts definition routines. Three material types are currently available in the parts definition routines: aluminum, titanium, and steel. Note that eight material choices were available in the structural synthesis routines, including the three available in the parts definition routines. A material form is defined for all the structural components, as listed in Table 9-3 . The program retains the capability of adding any number of additional material and material form choices at a future date.

Table 9-2 Parts Summary: Aerodynamic Surfaces

SPARS (FRONT & REAR)
CAPS
WEBS
RAILS
RIB STIFFENERS
WEB STIFFENERS
ACTUATOR STIFFENERS
DOUBLERS
DOUBLER STIFFENERS
ACTUATOR SUPPORTS
HINGE SUPPORTS
CLIPS
SHIMS
FASTENERS
RIBS (STANDARD, CLOSING, HINGE, AND ACTUATOR/HINGE)
CAPS
BRACES
CLIPS
FASTENERS
SKIN PANELS
SKINS
FASTENERS
FASTENERS

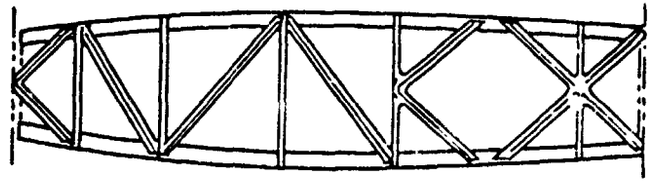

ACTUAL TRUSS-TYPE RIB FROM C-5A VERTICAL STABILIZER

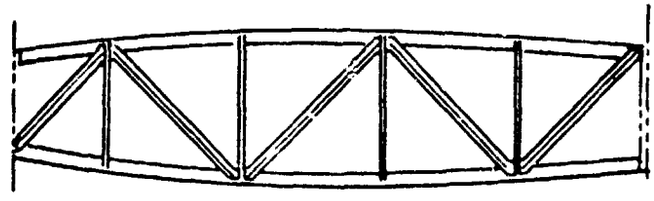

FUNCTIONALLY GENERATED TRUSS-TYPE RIB FROM PARTS DEFINITION ROUTINE

Figure 9-11 Example of an Actual Truss-Type Rib Compared to one Generated Functionally by the Parts Definition Routines

Table 9-4 is a summary of some of the primary structural concepts available in the parts definition procedure. Note that the selections available in the parts definition procedure do not always correspond to the selections available in the structural synthesis routines, i.e., the number of spars presently available in the parts definition routines is two, while any number of spars may be called out in the structural synthesis routines. Provision has been designed into the program for the future addition of several alternate concepts.

9.1.5 Tip, Leading and Trailing Edge Part Definition. The tip, leading edge, and trailing edge part definition routines define the detail parts making up the fixed leading edge, fixed trailing edge, slats, flaps, foreflaps, control surfaces (spoilers, ailerons, rudder, and elevators), and tips. The data that is generated includes the number of

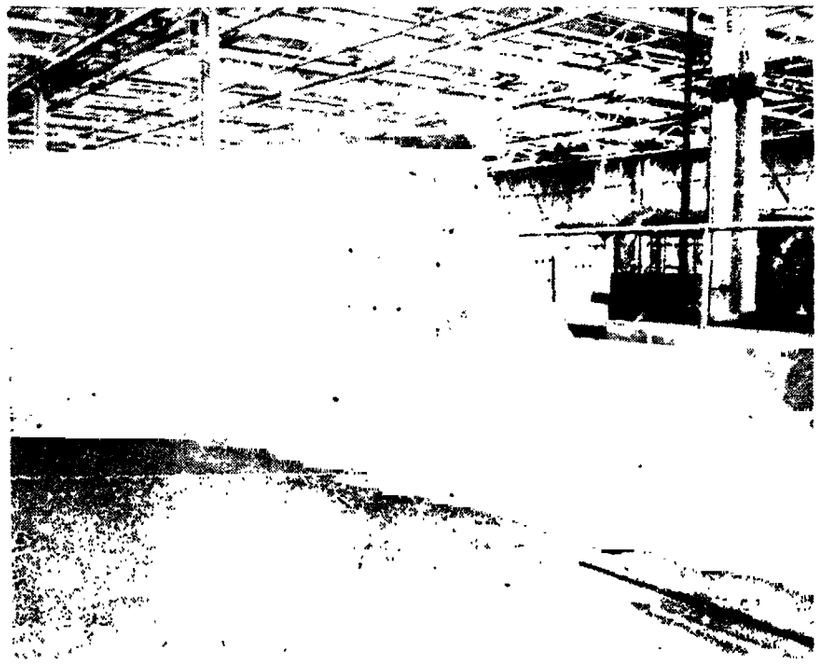

Figure 9-12 Integral Skin Stringer Panel Assembly

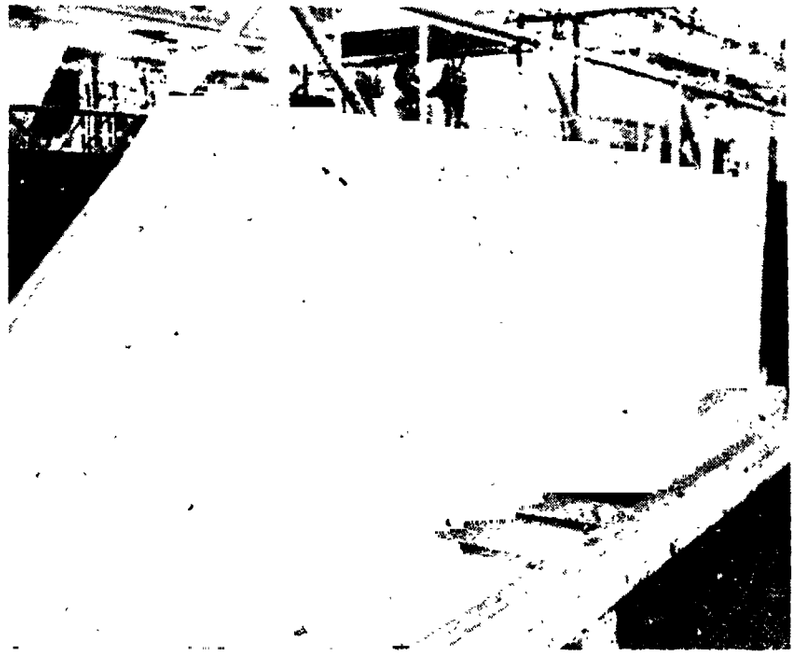

Figure 9-13 Individual Integrally Stiffened Skin Panel

parts, part dimensions, weight, and cost parameters. The parts definition derives its input from previous geometry and analysis subroutines.

The fixed leading edge segments, as defined by the geometry subprogram, are divided into a number of 152-cm (60-in.) sections with one shorter section. If the segment is 152 cm or less, only one section is assumed. The under-slat leading edge is made of two skins spliced at the nose with an extruded angle (chafing strip). The between-slat leading edge has a one piece skin; the skin perimeter is assumed equal to 2.5 times the fixed leading edge chord. The upper skin of the under-slat segment utilizes a factor of

Table 9-3 Summary of the Available Material Forms and the Corresponding Material Form Index

Material Form Index	Material Form	Typical Part References
1	Flat plate	Spar webs
11	 extruded plate	Cover panels
21	 extrusion	Spar caps
22	 extrusion	Spar rails
23	 extrusion	Rib caps, spar hinge/actuator supports, frames, longerons, intercostals
24	 extrusion	Rib and actuator stiffeners
25	 extrusion	Doubler stiffeners, miscellaneous stiffeners
26	 extrusion	Rib braces
27	 extrusion	Web stiffeners
44	Flat sheet	Shear clips, splice plates, ripstops, doublers, straps, spar doublers, clips, shims
81	Aluminum fastener	Fastener
82	Titanium fastener	Fastener
83	Steel fastener	Fastener

1.5 and the lower skin a factor of 1.0. The skin thickness is set at 0.102 cm (0.040 in.) with the chafing strips and edge member thicknesses set at a 0.152 cm (0.060 in.). The ribs are spaced at 25.4-cm (10-in.) increments, and the rib height is assumed to be 0.85 times the rib chord length. The ribs are made of bent-up 0.102-cm (0.040-in.) sheet with lightening holes. The rib-to-skin fasteners are 0.40 cm (5/32-in.) diameter

rivets spaced at 1.91-cm (0.75-in.) intervals. The chafing strip rivets are 0.40 cm (5/32 in.) in diameter spaced at 1.59-cm (0.625-in) intervals, and the edge member-to-skin rivets are 0.48 cm (3/16 in.) in diameter spaced at 3.81 cm (1.5 in.).

The fixed trailing edges for the wings, horizontal stabilizer, and vertical stabilizer, illustrated in Figure 9-14 , are assumed to be comprised of flat sheet skins and bent-up sheet ribs. All skins are 0.08-cm (0.037-in.) thick and, like the fixed leading edge, are defined in terms of 152-cm (60-in.) segments. The ribs are spaced at 25.4-cm (10-in.) increments and are constructed of bent-up 0.102 cm (0.040-in.) sheet with a 1.85-cm (0.73-in.) flange on each edge. Lightening holes are spaced at 3.8-cm (1.5-in.) intervals and have a diameter of 0.375 times the local chord. The skins attach along the forward edge and along each rib with 0.40-cm (5/32-in.) diameter rivets spaced at four diameters.

Table 9-4 Summary of Structural Concepts Available Through the Parts Definition Procedure

	Primary Mode	Alternate Mode
Spar construction	Built-up web	Integral web*
Rib construction	Built-up truss	Integral truss*
Skin construction	Integral skin-str	Built-up skin-str*
Frame construction	Built-up	Extruded*
Number of spars	Two	Input*
Number of ribs	Calc	Input
Number of lifting surface skins	Calc	None
Number of fusclage skins	Calc	Input
Number of frames	Calc	None
Number of frame segments	Calc	Input
Number of fuselage barrels	Calc	Input
Spar locations	Input	None
Rib locations	Calc	Input
Fuselage longeron spacing	Calc	Input
Fuselage frame spacing	Calc	None
Fuselage barrel lengths	Calc	Input

*Alternate mode to be added at a future date

The spoiler, illustrated in Figure 9-15 , is assumed to be comprised of a spar, skins, honeycomb core, and a wedge shaped skin closure. The parts definition process defines the dimensions, and the rivet sizes and quantities based on the spoiler stress analysis. The material weight assumes 2.5 cm (1.0 in.) added to the length and width dimensions of the sheet flat pattern, and to all dimensions of the full-depth honeycomb core. The material weight of the core includes 0.5 kg/m^2 (0.1 lb/ft^2) for adhesive.

The parts definition for the foreflap (Figure 9-16) derives the dimensions, and the rivet sizes and quantities from the foreflap stress analysis. The upper, lower, and leading edge skins have material weights calculated assuming 2.5 cm (1.0 in.) of additional material on all sides. The leading edge skin width, or cross-section periphery, is set equal to 2.64 times leading edge chord. Foreflap cross-sectional area aft of the spar is calculated as

$$\text{Area} = (\text{spar height}) \times (\text{chord length aft of spar}) \times 0.698$$

This formula provides the basis for computing the honeycomb core and closing rib weights. Material weight for the core is based on maximum dimensions plus 2.5 cm (1.0 in.). Closing rib material weight is based on flat pattern dimensions plus 2.5 cm (1.0 in.) on each side.

The parts definition process for the flaps, ailerons, rudders, elevators, and slats (Figure 9-17) derives the dimensions, and rivet sizes and quantities from the control surface stress analysis. The surface skins are assumed to be made in three pieces. The inboard and outboard skins are assumed to have a length equal to 28% of the surface length and the center 44% of the surface length. The leading edge skin width (periphery of leading edge cross section) is calculated from the following:

$$\text{Inboard skin width, INSWI} = K\left[\frac{2\,(DCSWI) - .28\,(DCSWI - DCSWO)}{2}\right](.15)$$

$$\text{Center skin width, DNSWC} = K\left[\frac{2\,(DCSWI) - (DCSWI - DCSWO)}{2}\right](.15)$$

$$\text{Outboard skin width, DNSWO} = K\left[\frac{DCSWO + DCSWI - .72\,(DCSWI - DCSWO)}{2}\right](.15)$$

where

K = 2.98 for slats

= 2.57 for other surfaces

DCSWI = inboard chord length of surface

DCSWO = outboard chord length of surface

Computation of the front spar and hinge rib cap material weight assumes an additional 5.1 cm (2.0 in.) on the extrusion length. Rear spar material weight assumes an additional 1.27 cm (0.5 in.) on all sides of the flap pattern dimensions. Material weight for the skins is computed as the actual weight plus 1.27 cm (0.5 in.) of additional material on all edges. Of the total skin rivets 32% are assumed to be in each of the inboard and outboard skins, and 36% in the center skin.

Airload ribs are bent-up sheet metal and material weight is based on the flat pattern dimensions plus an additional 2.5 cm (1.0 in.) in both length and width. Theoretical and actual rib weights assume lightening holes with diameter equal to 75% of average rib height spaced at 1-1/2 diameters.

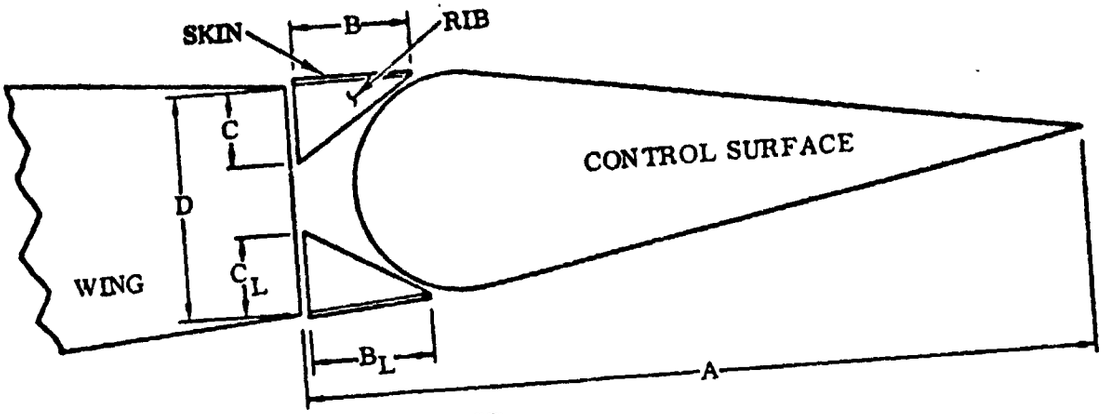

D = 0.85 (MAX. WING THICKNESS)

C = LESSOR OF B OR D/2

C_L = LESSOR OF B OR D/2

LOCATION	B	B_L
AT FLAP (NO SPOILER)	0.296A	0.068A
AT FLAP (INBD./OUTBD. OF SPOILER)	SPOILER CHORD	0.068A
AT AILERON	0.10A	0.10A
AT RUDDER/ELEVATOR	0.10A	0.10A

INBOARD OF AILERON (NO FLAP)

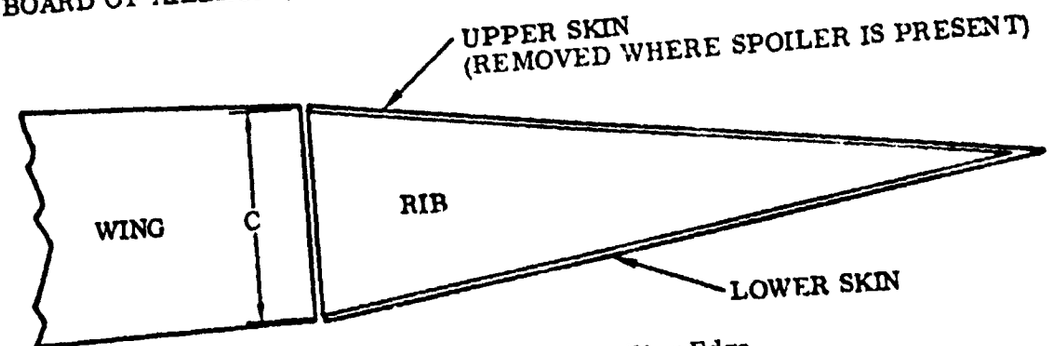

Figure 9-14 Fixed Trailing Edge

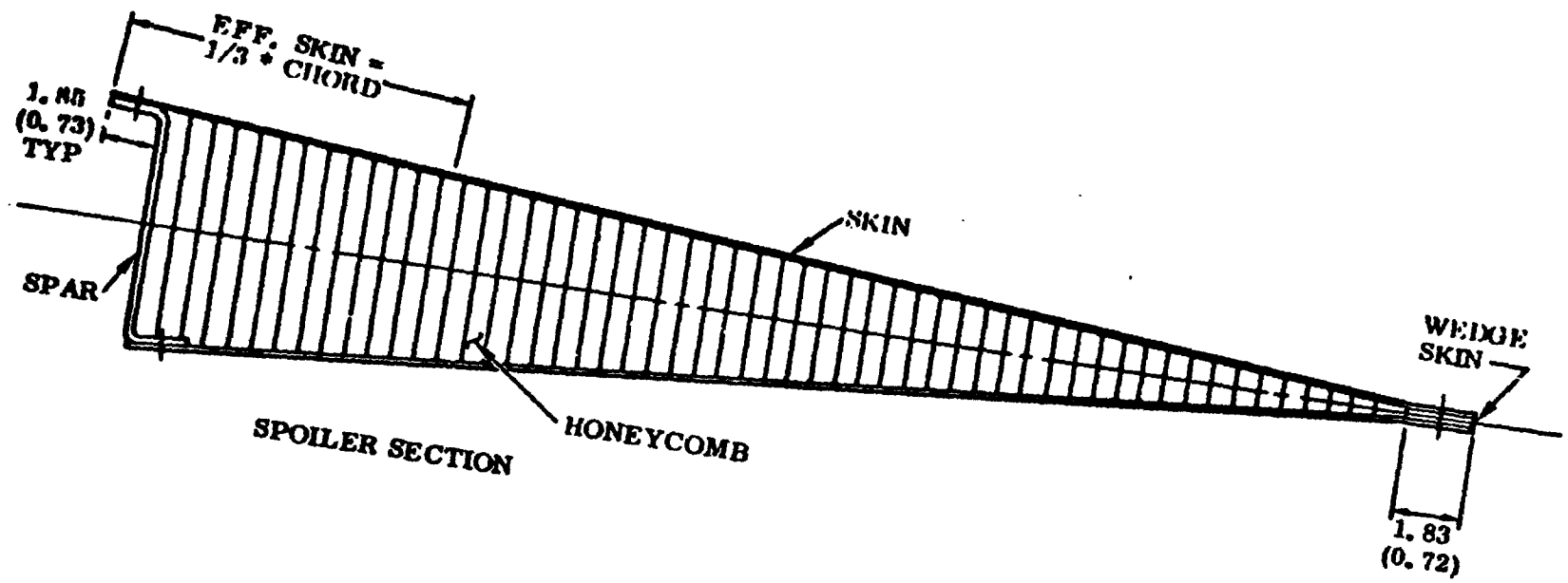

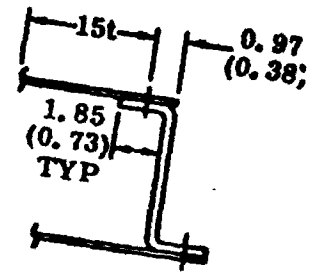

DIMENSIONS IN CENTIMETERS (INCHES)

Figure 9-15 Spoiler Geometry

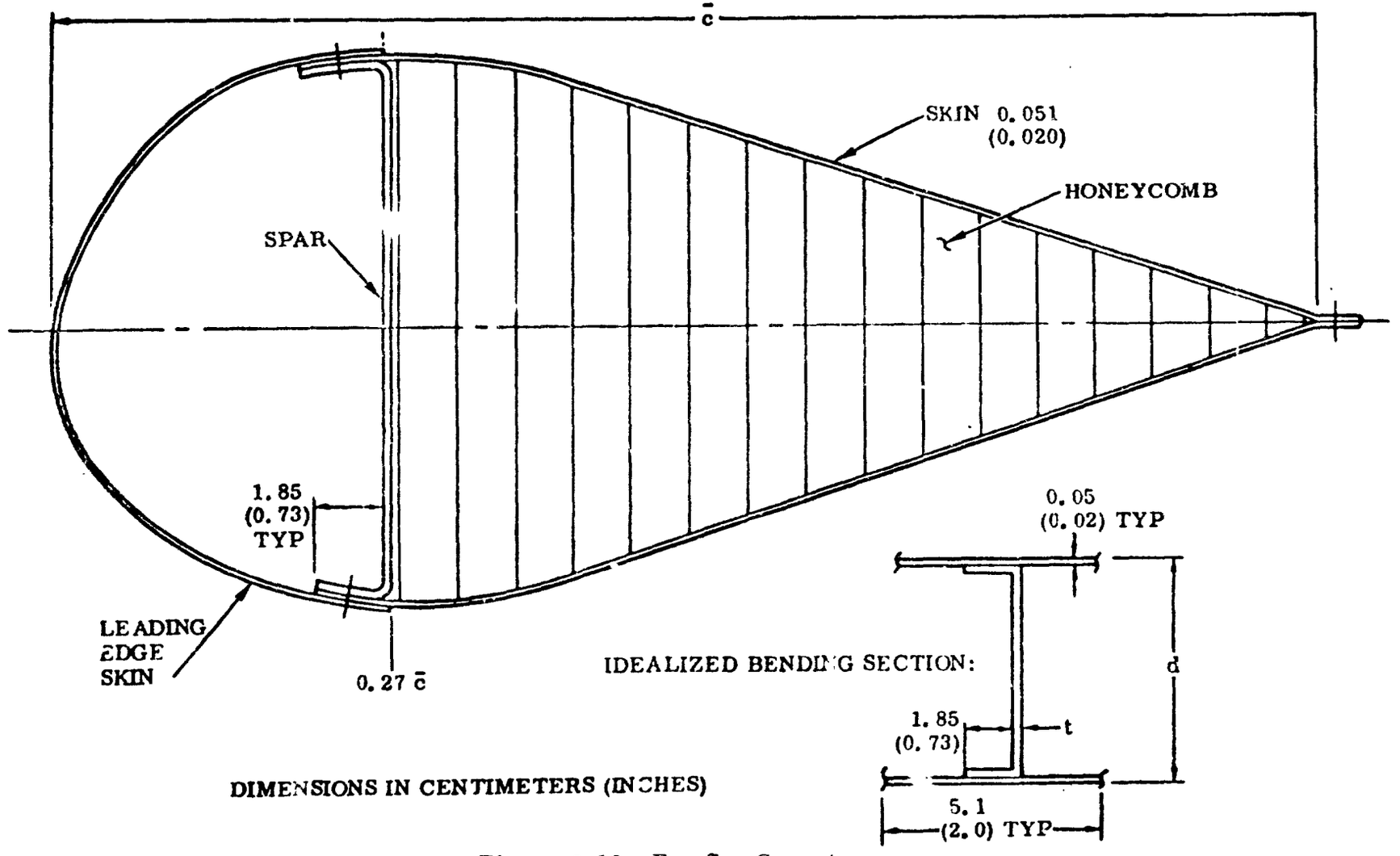

Figure 9-16 Foreflap Geometry

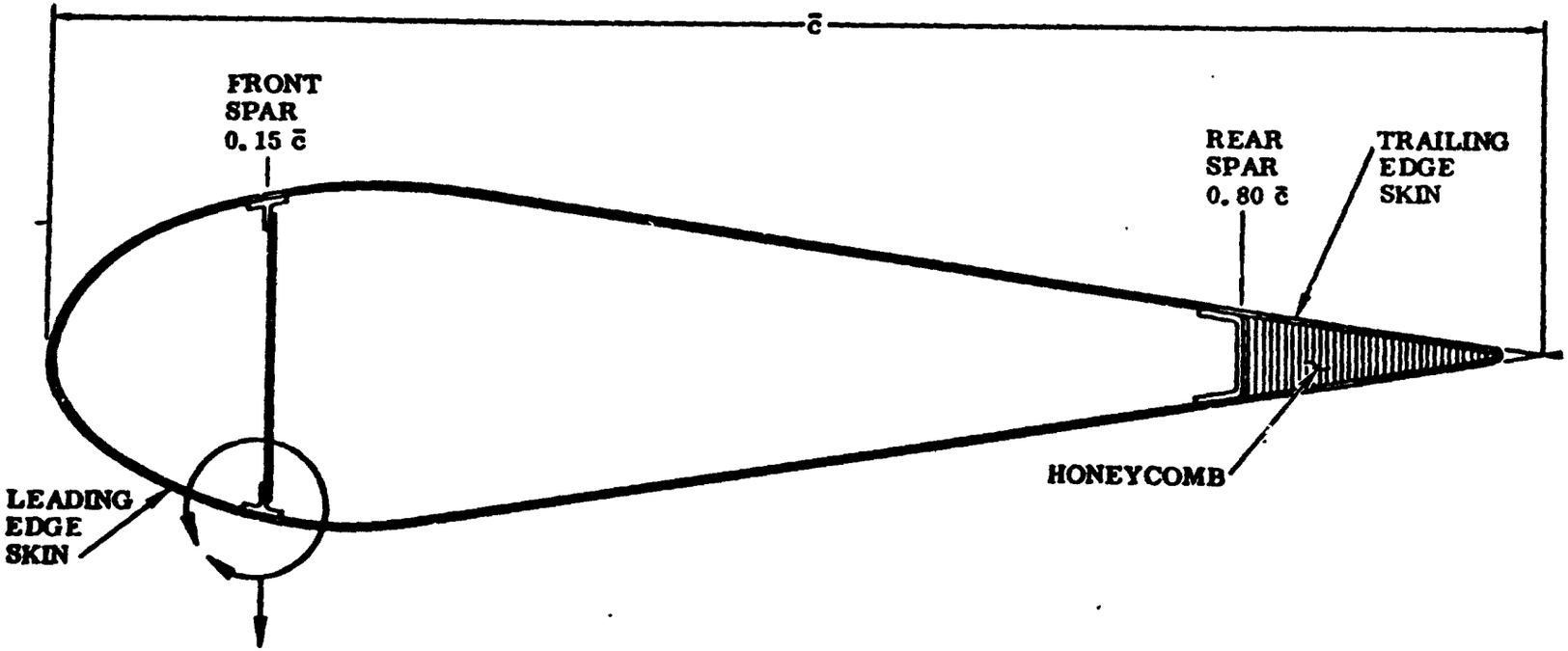

ED = 0.97 (0.38)

EFF. SKIN & WEB = ED + 15t

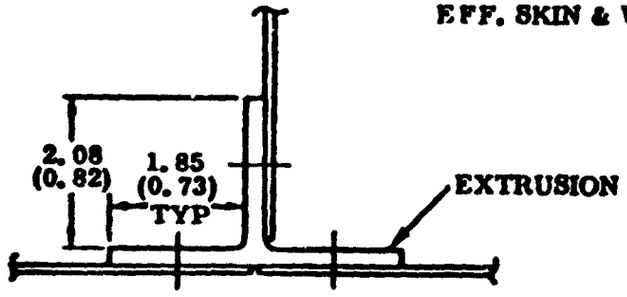

DIMENSIONS IN CENTIMETERS (INCHES)

Figure 9-17 Typical Geometry for the Flaps, Slats, Allerons, Rudder, and Elevators

The nose ribs are assumed to be parabolic. Material weight is based on 2.5 cm (1.0 in.) added to the length and width of the flat pattern dimensions. Each rib contains one lightening hole with a diameter equal to 75% of the smaller rib chord length or 84.5% of rib height. The hinge rib webs are a solid web with no lightening holes. Material weight is calculated assuming 1.27 cm (0.5 in.) of additional material on all edges. The honeycomb trailing edge wedge theoretical weight is computed as the theoretical weight times the honeycomb core factor from the stress analysis routines. Material weight is computed assuming a honeycomb block with dimensions equalling the largest web dimensions plus 2.5 cm (1.0 in.) and adhesive weight.

The parts definition process for the tip assumes the geometry and part dimensions shown in Figure 9-18 . Actual weight for the skin is computed from:

$$WT = 30\ (0.032)\ (\text{TIP CHORD})\ (\text{DENSITY})$$

The material weight for all sheet metal parts assumes an additional 2.5 cm (1.0 in.) of material on both the length and the width. All attachments assume a single row of 0.48-cm (3/16-in.) diameter rivets spaced at four diameters.

9.2 FUSELAGE SHELL PART DEFINITION. The structural synthesis routines produce general fuselage geometry at each control station. Data generated for each station includes barrel perimeter, frame spacing, panel cross-section dimensions, panel stiffener spacing, etc. The parts definition routines take the output from the fuselage structural synthesis and derive the detail parts sufficient to construct the complete basic fuselage shell structure.

The first step in the parts definition process is to develop the geometry data to a greater degree of detail. Data output from the structural synthesis for various control stations are interpolated to provide data for actual fuselage stations. The following geometry data are derived:

a. Fuselage frame spacing and frame stations.

b. Fuselage barrel lengths and number of barrels.

c. Barrel perimeters.

d. Complete frame cross-section geometry and perimeters.

e. Frame segment length and number of segments.

f. Panel width and number of panels around circumference.

g. Complete panel cross-section geometry.

h. Window cutout dimensions

The structural synthesis derives frame spacing at given control stations. This spacing may vary from station to station. The parts definition places a frame at the first control station, and frames between the midpoints of adjacent control stations are given

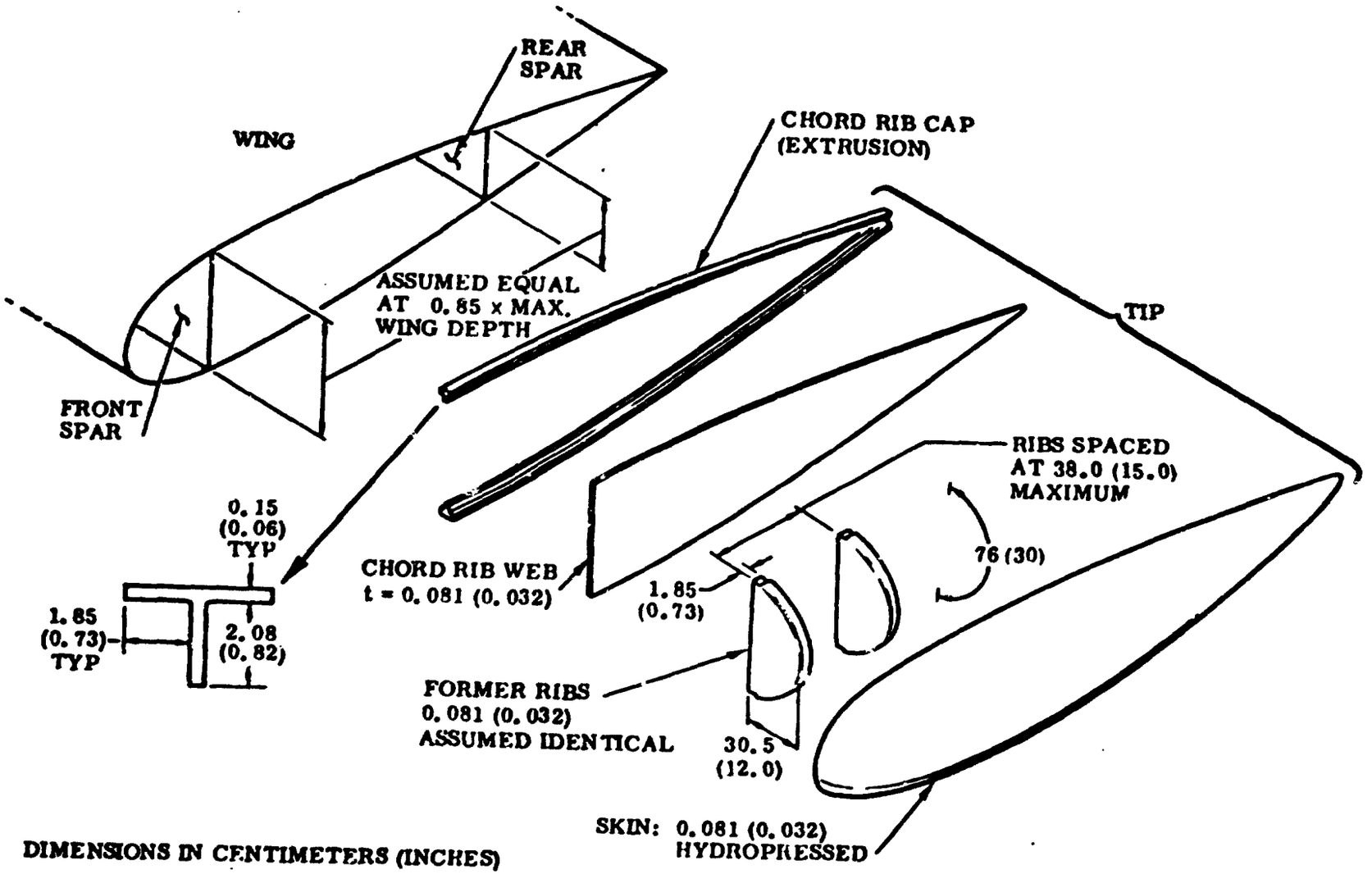

Figure 9-18 Wing Tip

the spacing of the nearest control station. A frame is placed at the first and last control station (aircraft nose and tail) only if its perimeter is not zero. Perimeters for each frame station are computed by interpolating between control station perimeters. The number of frame segments may be input or computed. In the absence of an input two segments are assumed for a maximum control station barrel perimeter of less than 1143 cm (450 in.). Otherwise three segments are used.

The fuselage barrel length is initially determined by either user input (barrel length or number of barrels) or by dividing the fuselage into equal barrel lengths. A maximum length of 1006 cm (33 ft.) is allowed. The nose and tail barrels are half the length of the others. Barrel lengths are then adjusted to fall halfway between frame stations. Barrel perimeters are computed by interpolating control station perimeters from the structural synthesis.

The number of panels or panel length ratios may be input by the user. For computation of skin panel width the fuselage cross section is broken up at nodes into individual panels. If the entire cross section is one "symmetry group" (all the same construction and subject to the same structural synthesis geometry constraints), it is broken up into an even number of panels with a width at the largest control station perimeter of 226 cm (89.1 in.). If more than one "symmetry group" occurs at a given cross section, panel widths are defined such that only one "symmetry group" is contained in a given panel. All cross sections are assumed to have the same number of panels (minimum of 4 and maximum of 10), and all panel end points are on the same node. Panel lengths are assumed to be equal to the barrel lengths except for the nose and tail barrels where the effect of fuselage taper is accounted for. The end width of each panel is computed, and a mid-height panel on each side of the fuselage is designated for containing windows. Panel end cross-section dimensions (Figure 9-19) and average cross-section dimensions are computed by interpolating between control stations.

The actual parts definition process is comprised of four steps. First, the complete skin panel assembly is derived: the corresponding parts are skin, stringers, and ripstops. Second, the complete frame assembly is derived, comprised of frame segments, frame splice angles, shear clips, and shear clip splice plates. Third, the parts necessary to assemble each fuselage barrel section are derived, including internal and external longitudinal skin panel splices, intercostals, and intercostal clips. And fourth, the parts required to assemble the barrel sections into a complete fuselage shell are derived: stringer splices, barrel finger splices, barrel strap splices, and splice plates. For each detail part originated, a theoretical weight, an actual weight, and a raw material purchase weight is computed. Fasteners are accounted for as each group of parts is brought together to form an assembly.

A typical skin panel assembly is illustrated in Figure 9-20 . The structural synthesis routines optimize the shell structure at individual control stations. This normally produces different quantities of stringers (or risers) at each station. Transport aircraft always have a constant number of fuselage stringers because of the difficulty of

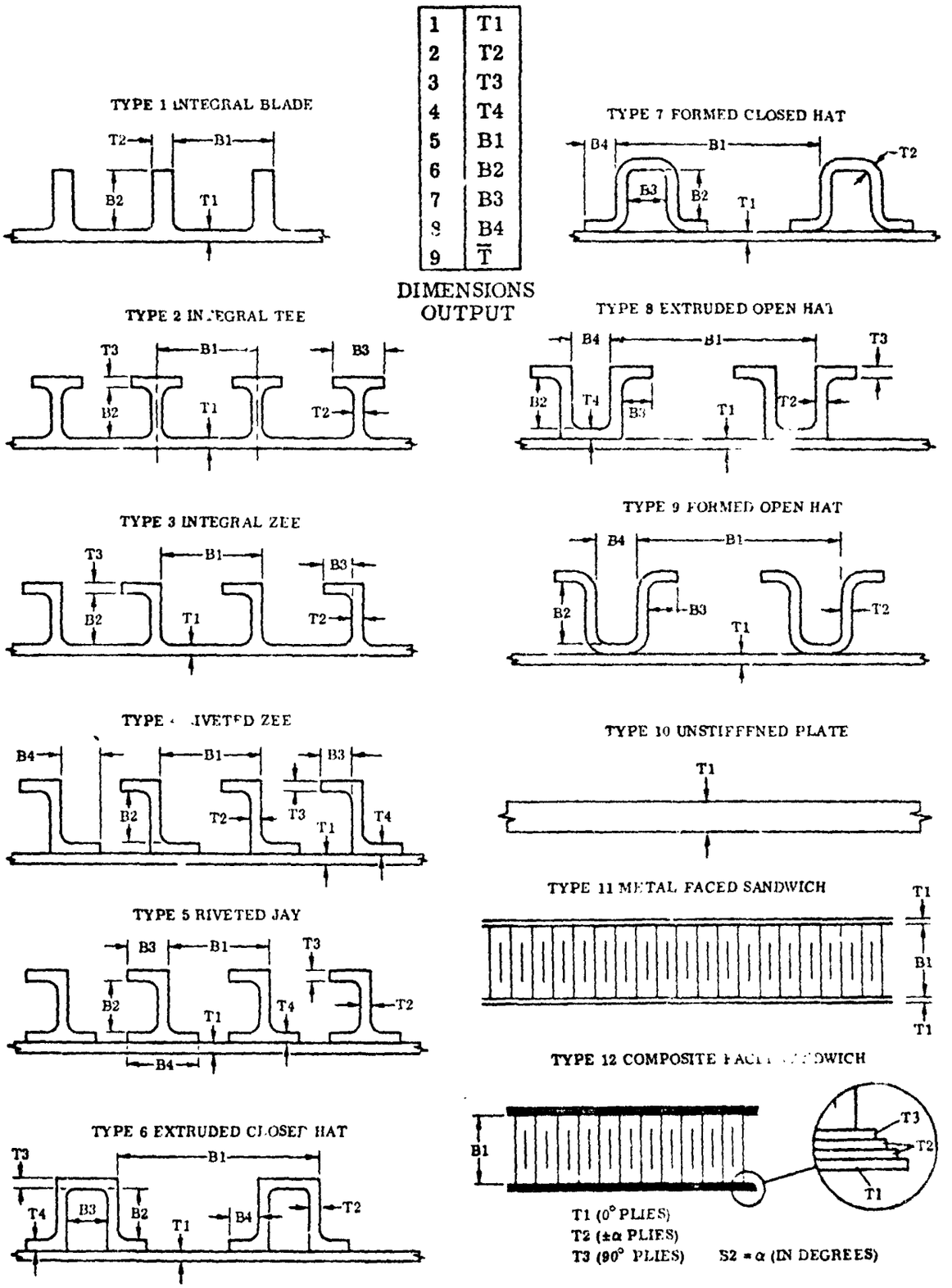

Figure 9-19 Panel Element Geometry

transferring discontinued stringer loads to adjacent stringers. Therefore, a constant number of stringers is assumed for a given panel at any station location. For each panel a maximum number of stringers is determined by dividing the panel width by the stringer spacing at each end of each barrel. This number is used for that panel at all fuselage station locations.

Windows are assumed located in the specified mid-height panels between each frame for all but the nose and tail barrel sections. Window cutout dimensions are computed as follows. Width is assumed equal to 50% of the local frame spacing with a maximum width of 64 cm (25 in.) specified. Height is assumed equal to 1.35 times the window width. The arrangement of a typical window is presented in Figure 9-21 .

The theoretical and actual weights for the integrally stiffened skin panel are computed using an average panel length, average panel width, and equivalent flat plate thickness averaged for each end of the panel. The material weight can be expressed in terms of the maximum cross sectional area of the largest end of the panel with an additional 0.25 cm (0.10 in.) of material added on all sides of the cross section to account for machining.

For skin-stringer skin panels the skins and stringers are considered separately. The theoretical skin weight is based on the average of the tapered skin thicknesses. Actual weight is based on a standard sheet gage shown in Table 9-5 , which is equal to or larger than the maximum thickness of a given panel. Both theoretical and actual weights account for window cutouts. Material weight assumes a standard sheet gage, and average panel lengths and widths with an additional 5.1 cm (2.0 in.) of material along all the edges.

Table 9-5 Standard Sheet Gages

cm	in.	cm	in.
0.081	(0.032)	0.203	(0.080)
0.091	(0.036)	0.229	(0.090)
0.102	(0.040)	0.254	(0.100)
0.114	(0.045)	0.318	(0.125)
0.127	(0.050)	0.406	(0.160)
0.160	(0.063)	0.483	(0.190)
0.180	(0.071)	0.635	(0.250)

Theoretical stringer weight assumes a tapered stringer. Actual weight assumes a constant section stringer with the dimensions of the end with the largest cross-sectional area. The material weight for extruded stringers utilizes the same cross-sectional area as the actual weight computation, but assumes an additional 5.1 cm (2.0 in.) of length for cutoff. For sheet metal stringers, the actual weight is based on a standard sheet gage equal to or larger than the maximum stringer thickness. The material weight is calculated in the same manner as the actual weight with an additional 2.5 cm (1.0 in.) of flat stock on the width and 5.1 cm (2.0 in.) on the length.

Thick plate skin panels and sandwich panel face sheets are assumed to be tapered sheet or plate. Theoretical and actual weights are based on the tapered material thicknesses. Material weight assumes the maximum thickness and an additional 5.1 cm (2.0 in.) added to the panel length and width. The honeycomb core for the sandwich panel is treated in a like manner.

Table 9-6 Rivet Sizes

Component Thickness		Rivet Diameter	
cm	in.	cm	in.
		0.318	(0.125)
0.091	(0.036)		
		0.396	(0.156)
0.114	(0.045)		
		0.478	(0.188)
0.318	(0.125)		
		0.635	(0.250)
0.381	(0.150)		
		0.792	(0.312)
0.508	(0.200)		
		0.953	(0.375)

Skin panel assembly assumes rivet sizes based on the skin thickness, as shown in Table 9-6 . For integrally stiffened panels the panel average skin thickness is used to choose rivet diameter. For skin-stringer constructions the standard sheet gage is used. For plate and sandwich constructions the maximum total skin thickness is used.

Ripstops are thin sheet metal doubler straps (often made of titanium) that lie on the skin under each frame. Their purpose is to stop fuselage skin fatigue cracks from growing. They are assumed to have the same thickness as the skin and a length equal to the panel width. Ripstop width is determined by fastener spacing and edge distance requirements. Ripstop-to-skin rivets consist of three rows, as shown in Figure 9-20 , spaced at four diameters. The fourth row is supplied by the frame shear clip-to-skin rivets called out in the frame parts definition analysis. Stringer-to-skin rivets are placed in one or two rows as depicted in Figure 9-20 . Rivets are spaced at four diameters pitch.

A typical frame assembly is illustrated in Figure 9-22 . The frame cross-sectional area is computed using loads and materials property data from the structural synthesis routines. An expression for the frame cross-sectional area is as follows (Reference 1).

$$\left[\frac{C_f * D^2 * M}{K_4 * E_F * L}\right]^{1/2}$$

where

D = Shell diameter (use body width)
M = Fuselage bending moment (use maximum value from structural synthesis)
L = Frame spacing (from parts definition geometry computations)
C_f = Coefficient (use 0.0000625 from Ref. 1)
K_4 = Shape parameter (use 5.4 from Ref. 1)
E_F = Frame modulus of elasticity (from structural synthesis)

The computed frame area is used to derive the frame dimensions by an iterative technique. Frame height and flange width dimensions are sized based on fastener spacing and edge distance requirements (Figure 9-22) with a minimum frame thickness of 0.102 cm (0.040 in.) specified. The computed (or minimum) frame thickness is used to determine theoretical weight, while a standard gage equal to or greater than the computed

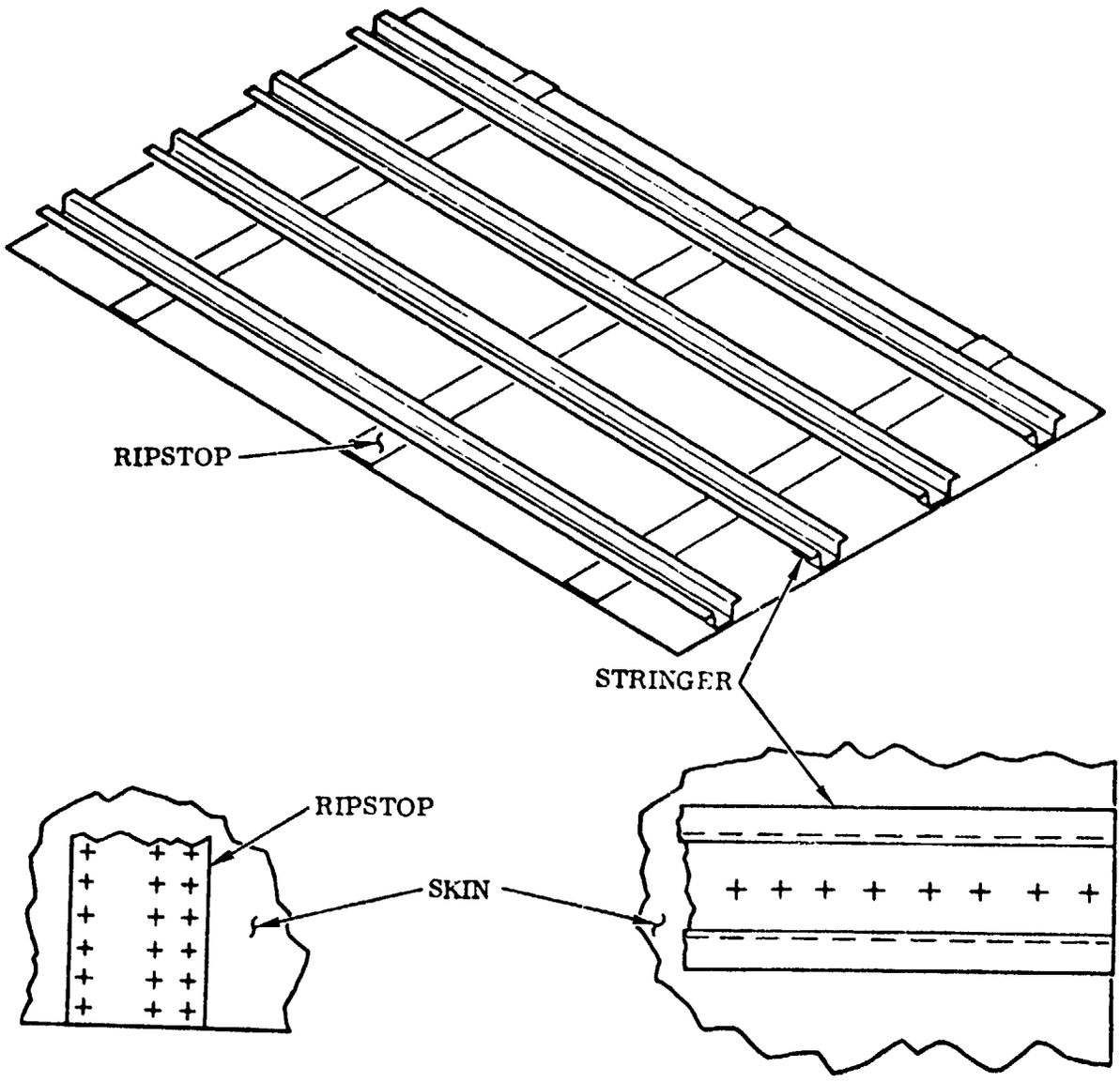

Figure 9-20 Skin Panel Assembly

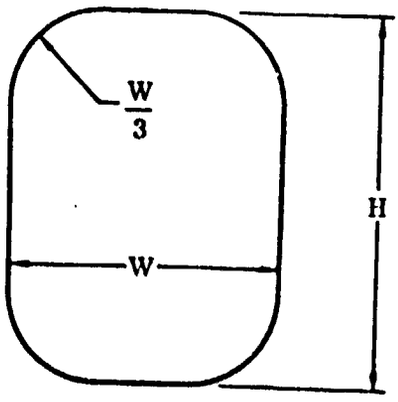

$W = 0.60 * \text{FRAME SPACING}$

$H = 1.35 * W$

$\text{AREA} = H * W - \frac{W^2}{9}(4-\pi)$

Figure 9-21 Typical Window Arrangement

frame thickness is used to determine actual weight. The material weight computation assumes a standard gage with 5.1 cm (2.0 in.) of additional width and a length equal to the frame segment length plus 10.2 cm (4.0 in.).

It is assumed that there are two shear clips per frame segment, which attach the frames to the skin. The long shear clip is equal to the frame segment length minus the length of two stringer spacings. The short shear clip spans the frame splices, and is two stringer spacings long. Shear clip cutouts for stringers are derived on the basis of the largest computed value for stringer height and width. Thickness is assumed to be equal to the frame thickness. Theoretical and actual weights are computed in the same manner as for frames; material weight is computed assuming a standard gage and 2.5 cm (1.0 in.) of additional width and 5.1 cm (2.0 in.) of additional length.

Shear clips are spliced together with a shear clip splice plate (Figure 9-21) that is assumed to have the same thickness as the shear clip. The length and width are sized for picking up a single row of four rivets. Two frame splice angles (Figure 9-21) are assumed for each frame segment splice. These angles nest inside the frame at the splice and are assumed to be the same thickness as the frame. The length of the angles is made equal to a stringer spacing plus a stringer width.

Frame thickness is used to size all the fasteners required in the frame assembly (Table 9-6). One row of fasteners is assumed through the shear clips into the frames, and two fasteners are assumed to attach each stringer to a frame. A single row of fasteners from the skin through the shear clip is assumed. Typical fastener spacing has been defined as four diameters.

The detail parts required to splice the skin panel and frame assemblies into a barrel section include internal and external longitudinal panel splices, frame stabilizing intercostals, and intercostal clips. The assembly is illustrated in Figure 9-23 .

The external panel splice is a flat plate splice running the length of the skin panel (which is equal to the length of the barrel). The width is 10 fastener diameters and the thickness is set equal to the skin thickness. Theoretical and actual weights are assumed to be equal. Material weight is computed assuming 1.3 cm (0.5 in.) of additional width and 10.2 cm (4.0 in.) of additional length.

The internal panel splice is scalloped with fingers, but is synthesized as a straight-edged plate with an equivalent width of 26 skin fastener diameters. The actual weight is assumed equal to the theoretical weight, which is based on a standard sheet gage equaling or exceeding 40% of the skin thickness. Material weight assumes 10.2 cm (4.0 in.) of additional length and 5.1 cm (2.0 in.) of additional width. The internal splice is assumed to be attached to the skin with the equivalent of four rows of fasteners spaced at four diameters. The two middle rows also pick up the external splice on the skin exterior.

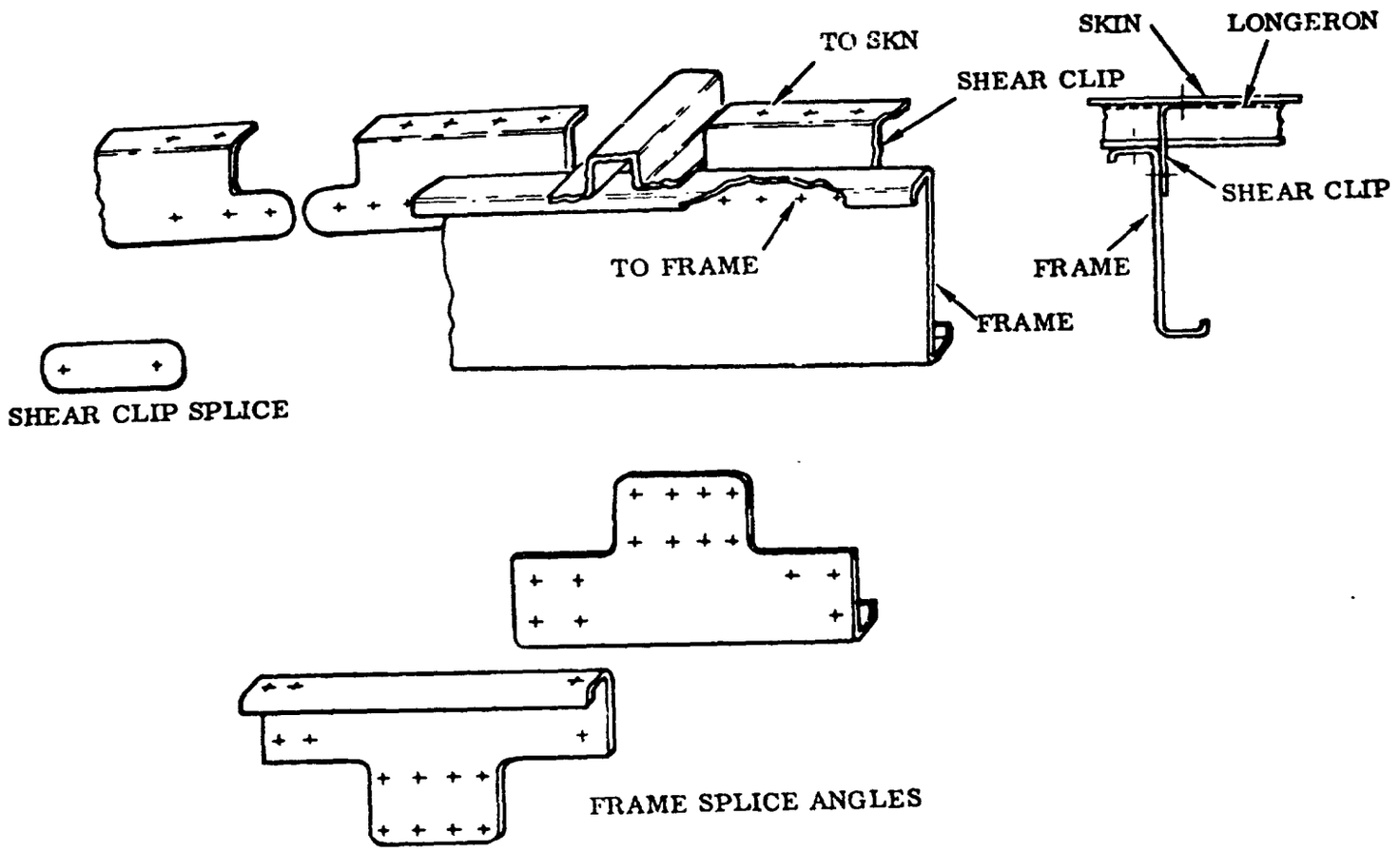

Figure 9-22 Frame Parts

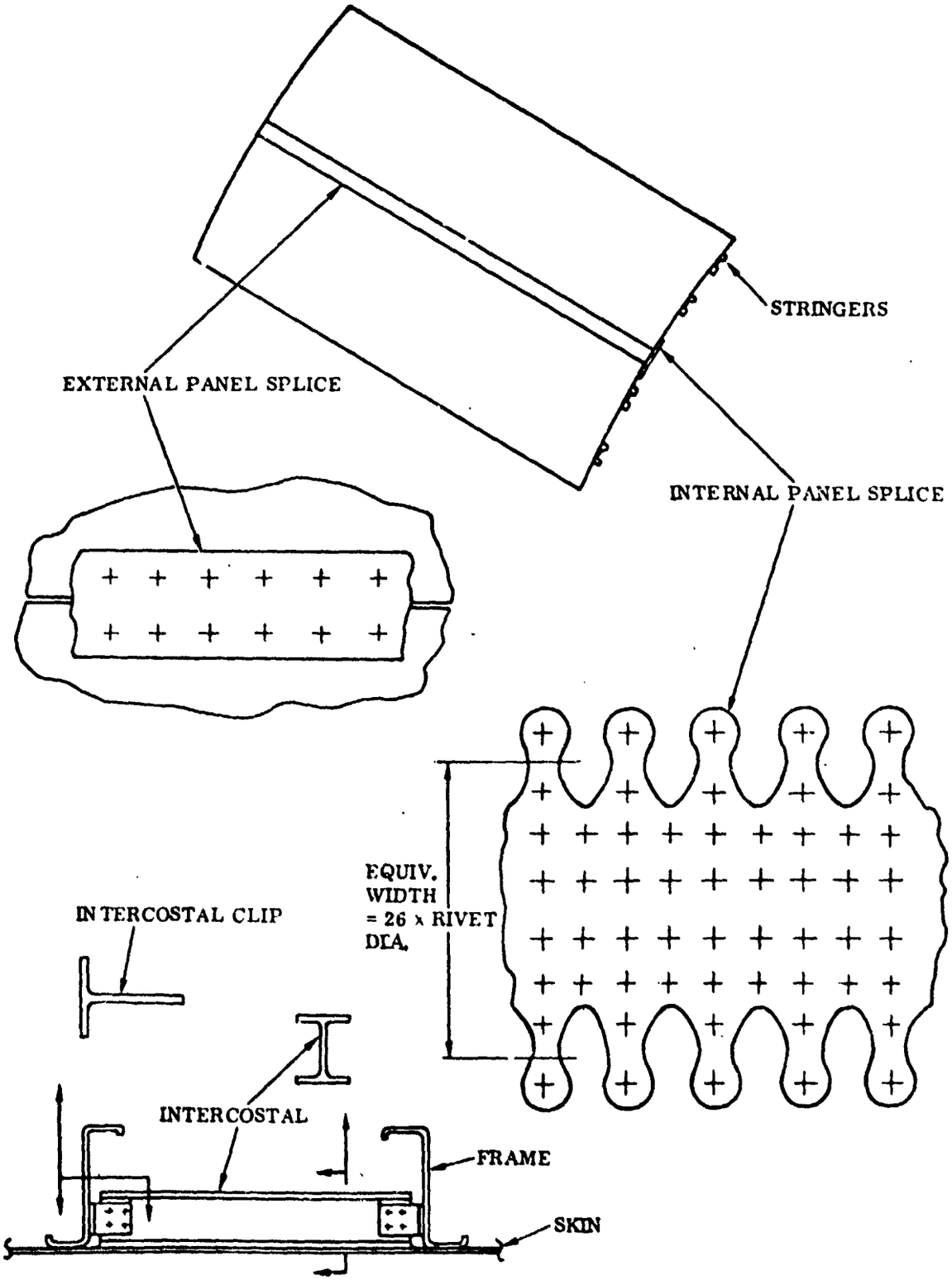

Figure 9-23 Barrel Parts

Intercostals are extruded I-sections located in every other frame bay between stringers and spaced five stringers apart. Their length is equal to the frame spacing minus a clearance of 1.0 cm (0.4 in.). Height of the intercostal section is assumed to be 40% of the intercostal height. Theoretical and actual weights are based on a thickness equal to the maximum fuselage skin thickness. Material weight is computed assuming the same cross-sectional area and an additional 5.1 cm (2.0 in.) of length. Intercostal to skin fasteners are assumed to be comprised of two rows of skin fasteners spaced at four diameters.

Two extruded tee clips attach each intercostal to frames. The length of each extruded clip is such that it fits between the intercostal flanges (Figure 9-23) with a total clearance of 0.38 cm (0.15 in.). The height of the clip measured from the frame toward the intercostal is set equal to the length. The flange against the frame has a width equal to eight fastener diameters. Thickness is assumed equal to the intercostal thickness for all weight computations. Intercostal clips are attached using frame fasteners, six through the frame and four through the intercostal.

The detail parts required to splice the barrel sections into a complete fuselage section include stringer splices, barrel finger splices, barrel strap splices, and splice plates. The assembly is illustrated in Figure 9-24 . The stringer splice cross sections are shown in Figure 9-25.

9.3 FUSELAGE PENALTY ANALYSIS. The treatment of fuselage penalty items encompasses windows, doors (landing gear and side loading) and floors. The analysis is comprised of a statistically based actual weight computation and a unitized manufacturing cost computation. The values derived for fuselage penalty weights and costs are added to those of the basic fuselage shell (which are determined from a structural synthesis/parts definition analysis) to obtain total fuselage data.

Window weights are computed as a function of the total glass area required for the specified number of windows. Individual window area is computed from the assumed window geometry illustrated in Figure 9-21 . Windows are assumed located between each frame for all but the nose and tail barrel sections, and hence, the number of windows is equal to twice the number of frames in those barrel sections minus two. Following is the equation used to compute the total window weight penalty (Reference 2).

$$WNDWWT = 10.0 * AGL$$

where

WNDWWT = Window weight and AGL = Total glass area

Doors are assumed to include nose and main landing gear doors, and side loading cargo and passenger doors. Nose landing gear door weight is computed as a function of the maximum dynamic pressure and the total door area. Main landing gear weight and side loading door weight are computed as a function of the total door area alone. The following equations are used for the weight computations (Reference 2).

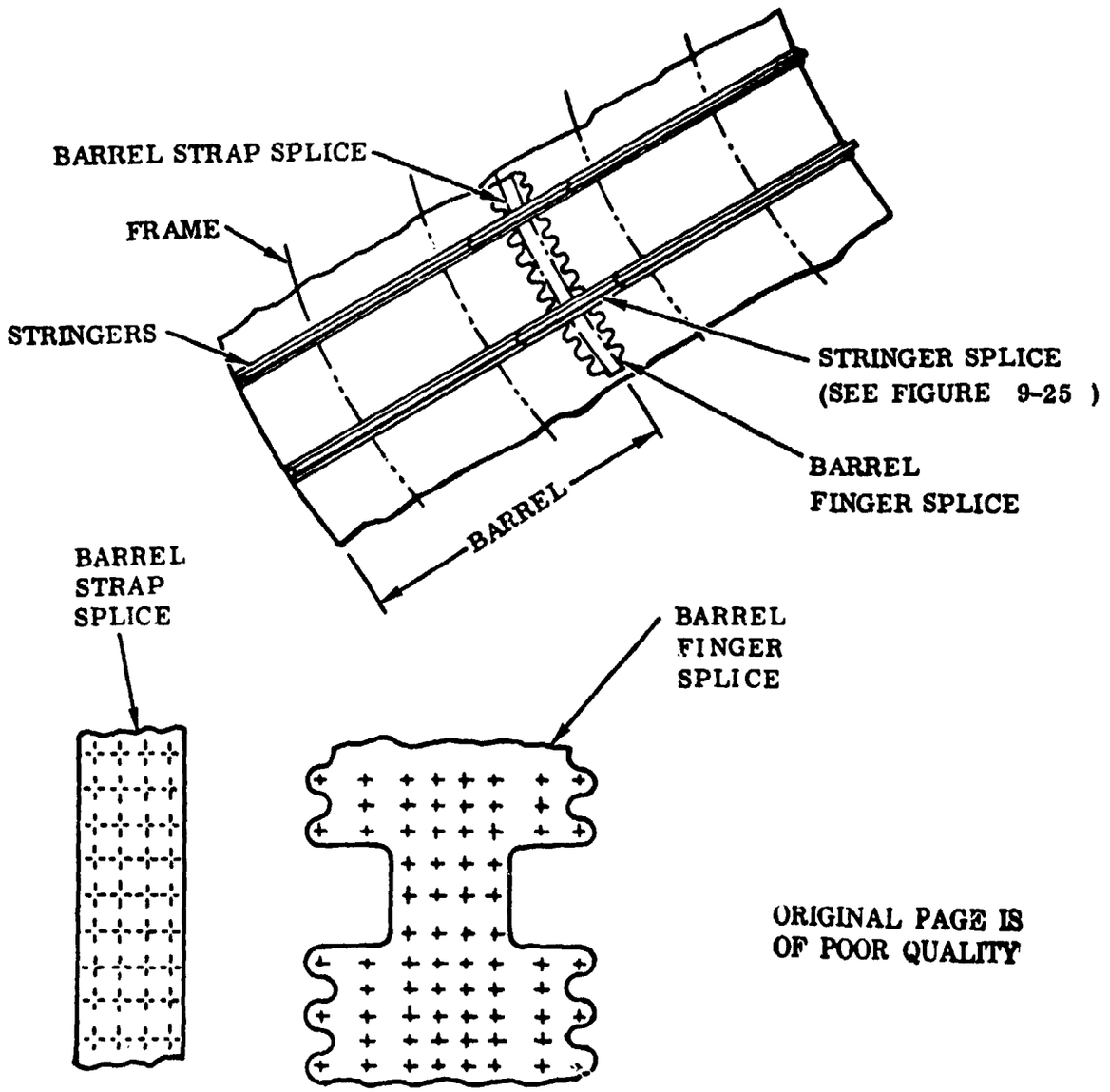

Figure 9-24 Barrel Splice Parts

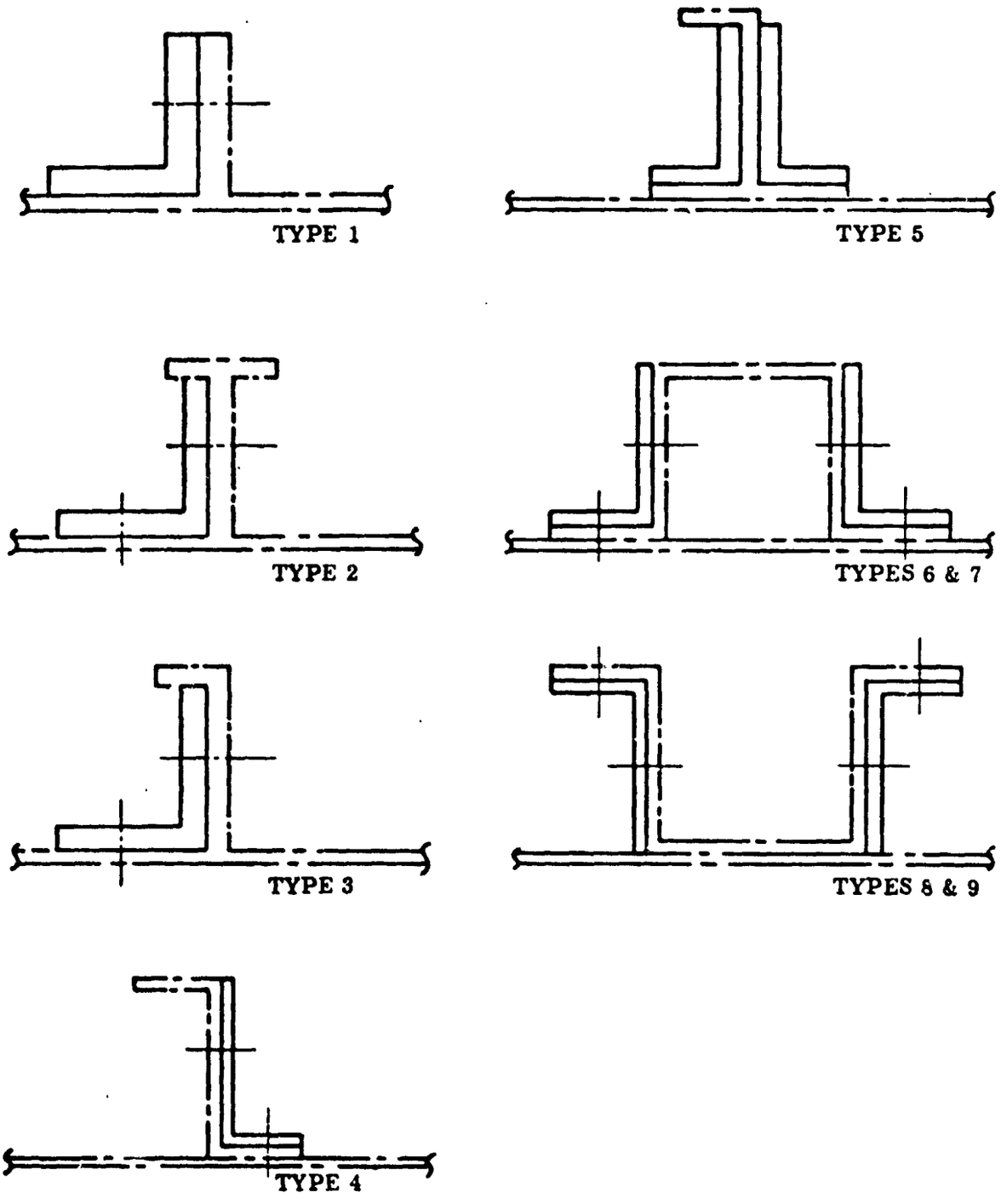

Figure 9-25 Stringer Splice Cross-Sections

NLGWT = .44 * QMAX ** .3 * SND
MLGWT = 3.223 * SMD ** 1.125
SLDWT = 9.0 * SDA

where

NLGWT	=	Nose landing gear door weight
QMAX	=	Maximum dynamic pressure
SND	=	Nose landing gear door area
MLGWT	=	Main landing gear door weight
SMD	=	Main landing gear door area
SLDWT	=	Side loading door weight
SDA	=	Side loading door area

The weight of floors and floor supports is computed as a function of the ultimate flight design load factor, a design floor loading, and the floor area. The equation is as follows (Reference 2).

FLRWT = 6.51 * (NZ * WF * AF/1000) **.924

where

FLRWT	=	Floor and floor support weight
NZ	=	Ultimate flight design load factor
WF	=	Design floor loading at 1.0 g
AF	=	Floor area

The floor and window areas can be computed from the fuselage shell geometry. Values for the maximum dynamic pressure and the ultimate load factor are brought across from the vehicle synthesis portion of the program. The user may input values for the design floor loading, and the nose gear, main gear, and side loading door areas. In the absence of an input, typical values for a passenger transport type of aircraft are utilized. The values are: design floor loading, 3591 N/m^2 (75 lb/ft^2); nose gear door area, 1.4 m^2 (15 ft^2); main gear door area, 7.4 m^2(80 ft^2), and side loading door area, 139 m^2 (1500 ft^2).

The manufacturing cost portion of the analysis is based on an average unit cost. The user may input a value, or in the absence of an input, a value of $176/kg ($80/lb) is assumed. The cost is derived by multiplying the weight previously computed by the appropriate average unit cost.

9.4 REFERENCES

1. Shanley, F. R., "Weight-Strength Analysis of Aircraft Structures," Dover Publications, Inc., New York, N. Y., March 1960.

2. Roland, H. L., Neben, R. E., "Aircraft Structural Weight Estimation Methods," Convair Aerospace Report GDC-ERR-242, September 1964 (Revised Sept. 1965).

SECTION 10

COST ANALYSIS

The cost analysis encompasses the manufacturing cost, material cost, engineering cost, tooling cost, total vehicle program cost, direct operating cost and airline return-on-investment. Manufacturing cost is determined as a function of the actual shop processes necessary to produce each part. From this the corresponding number of labor hours that are required can be computed, and hence, the manufacturing cost. An alternate method using cost estimating relationships is also provided.

Material cost is derived on the basis of the amount of raw material stock purchased, material type and form, and various extra cost items such as special lengths, widths, and tolerances. The detail material cost model is not used in the alternate mode since this data is included in the cost estimating relationship.

Engineering costs are derived on the basis of equations originally developed by G. S. Levenson and J. M. Barro in Reference 1 . Both initial and sustaining engineering costs are represented.

Tooling cost is derived on the basis of the number of dissimilar parts to be produced, and hence, the total number of tools required. Basic tooling, rate tooling and sustaining tooling costs are represented.

Total vehicle program costs are derived using primarily the cost estimating relationships developed by R. E. Kenyon in Reference 2. A learning curve approach is applied to adjust first unit cost to those of subsequent units.

A return-on-investment analysis utilizes computed aircraft performance parameters and the 1967 Air Transport Association formula to derive direct operating costs. Indirect operating costs and return-on-investment are derived on the basis of an input traffic route structure. All cost data are computed relative to a specified dollar reference year. Actual cost estimation methodology is discussed in detail in the following sections.

10.1 AIRFRAME MANUFACTURING COST (PROCESSES, STANDARD HOURS, AND RATES)

10.1.1 First Unit Manufacturing Cost. The technique being used to estimate first unit manufacturing costs basically is as follows. A breakdown of major vehicle components into their detail parts is accomplished through the use of vehicle synthesis, structural synthesis, and part definition operations. The actual manufacturing cost analysis is based on calculating the material, and direct and indirect labor costs associated with the fabrication and assembly of each detail part. For each part, in turn, a record of manufacturing and assembly operations required to produce that part and integrate it into the vehicle structure is established. For each operation specified the number of direct or actual labor hours required to perform the operation is derived,

and based on this, material costs are calculated. Figure 10-1 summarizes the steps necessary in determining the manufacturing cost from the detail part level.

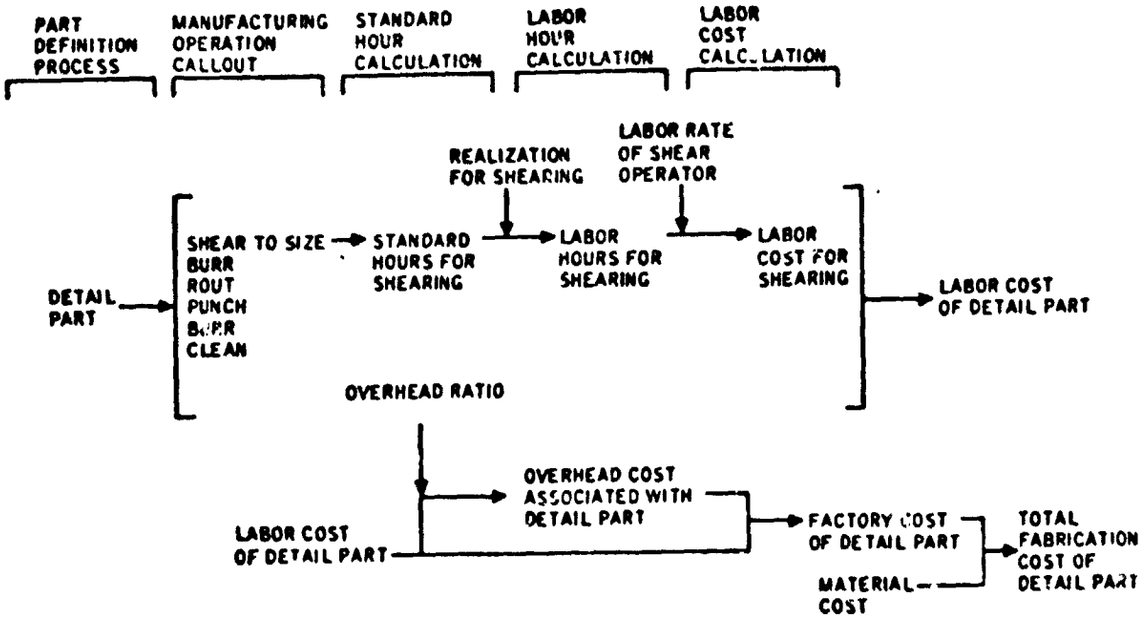

Figure 10-1 Cost Analysis Sequence Based at the Detail Part Level

The derivation of direct and indirect costs associated with the manufacture of each detail part involves the determination of the number of actual labor hours required for each production process, and the corresponding labor rates. The computation of actual labor hours is accomplished by multiplying a computed number of shop standard hours (discussed in the following section) by a shop efficiency (the so-called realization) factor. Labor costs then, are simply the actual labor hours multiplied by a representative labor rate. Overhead costs are computed by multiplying the direct labor costs by an overhead ratio that is derived from accounting practice. Each of these computations is discussed in detail in the following sections. The equations are:

$$LABHR = STDHR/REFCT$$
$$LACOST = LABHR * LARATE$$
$$VCOST = VRATE * LABHR * LARATE$$

where

LABHR = actual labor hours
STDHR = standard hours
REFCT = realization (efficiency) factor
LACOST = direct labor cost
LARATE = labor rate
VCOST = indirect overhead cost
VRATE = overhead ratio

10.1.2 Manufacture and Assembly Processes. The parts definition routines were designed to provide an accounting of the detail parts required to produce a complete airframe. Each detail part is looked at individually and analyzed in terms of the manufacturing and assembly processes associated with it. In order for this analysis to be performed it was necessary to be able to internally account for each of the required shop processes.

To develop the process lists associated with each part, a library of shop planning records was established from existing production articles. These documents were studied and used to identify the typical processes associated with each part. A method was developed to internally relate each part to its corresponding list of processes. It was the intent to provide a means of internally generating the equivalent of a shop planning order. A representative example of such an order is presented in Figure 10-2 . It is from this type of document that the specific planning for the production of an individual part can be implemented.

Currently, equations for a total of 33 manufacturing and assembly operations are represented within the program. It is the purpose of these equations to compute a value for the number of standard hours necessary to perform the specified tasks. While the equations for each of the operations are strictly valid only for the specified process, a reasonable number of standard hours may be obtained by applying the equations to related processes. Provision has been made in the program for the future addition of any new processes that might be needed to account for new production processes.

As each detail part, subassembly, and assembly is considered during the part definition portion of the program, a part index (KK) is assigned. This index is associated with a program block that calls, in turn, each of the applicable standard hour equations for the part. For example, a wing rib brace is given the part index KK=26, which is used to direct the program to the operations required to manufacture the brace. The operations specified might include the following depending on the structural mode:

SAWING:	saw the raw material stock to size
BURRING:	deburr the sized brace
DRILLING:	drill the required holes
CLEANING:	clean and degrease the finished brace
SURFACE TREATMENTS:	perform required surface treatments
PAINTING:	primer and paint finished part
IDENTIFY:	mark with identifying part number
INSPECTION:	inspect finished part

A value for standard hours is computed for each of these, and the sum is the total number of standard hours that manufacturing of this particular rib brace would be expected to require.

10.1.3 Standard Hours. Standard hours are, as the name implies, a standard time, measured in hours, which represents an optimum for the time required to perform a

GENERAL DYNAMICS CONVAIR — M-DAY 363 — LTR-NO D — PRJ 8 — PART NUMBER 4T11001-125A
SHOP ORDER PLANNING

PLANNER EBROLASKI — GRP 11 — CHG CD RC — ENGRG D/C OD — P/L — INSP CL — NO 26 — LTR-NO D — PRJ 8 — PART NUMBER 4T11001-125A

TITLE STIFFENER — MATERIAL PERCENT 3.000 — GRP NUMBER 12 120239 — A/Z D

M'L DESCRIPTION SEE NOTE A — GAU/DIA — WID/WALL — LENGTH 30.000 — SPECIFICATION CO-A-200/11 — COND NOTE 01 — PTS OP/END — PT-CL 2

DATE — STK RM — QTY — BY — SPARE — CUST — SHOP — INSP

-----OPERATIONS-----

INSP STNP	DEPT	CC	OPER NO	OP SCH	OPERATION DESCRIPTION / TOOL/SPEC NO	TOOL SEQ NO	TOOL SYMB	MACH CODE	SET-UP TIME	RUN TIME
			A		LS39048-1 7075T6511 EXTRU					
			B		STP63-001 STP58-208 STP57-301 STP53-201 DS30004 STP59-201					
	836	07	10		SAW TO LENGTH 1-1 4T11001-125A		SP	6880	0.12	0.0031
			15		INSPECT					
	01	03	20		ROUT 4T11001-125A 4T11001-125A		MAST SP	6455	0.08	0.025
	01	02	30		DRILL PILOT HOLES (74) PLCS 4T11001-125A		DLT	1552	0.25	0.1750
	01	12	40		BURR			2905		0.0155
	01	12	50		IDENTIFY (TAG) STP63-001 4T11001-125A		SP	2910	0.07	0.0006
			55		RW					
			65		INSPECT					
	02	05	70		ALK ETCH STP57-301			5845		0.0216
	02	11	80		SULF ANODIZE STP58-208			5807		0.0144
			85		INSPECT					
	02	03	90		(1) ZCP STP59-201			4815	0.10	0.0052
	02	03	100		IDENT R/S STP63-001 4T11001-125A		SP	2910	0.07	0.0032
			105		INSPECT					
			115		HPSI-00156 (PROJECT)					
						TOTAL			0.69	0.2644

Figure 10-2 Example of a Shop Planning Order for a Rib Brace

given task. They are the number of hours it would take for a normal person to do a normal job under normal conditions. They do not include allowances for fatigue, personal needs, rest breaks, machine adjustments or tool breakage, close tolerance work, etc. Thus, the standard hours are an idealized time scale against which actual time may be compared.

Standard hours are used industry-wide for estimating purposes. They are established by industrial engineering departments through the analysis of time and motion studies carried out for standard shop operations and procedures. They are used by industrial engineering departments to estimate the time required to perform production tasks, and by accounting departments to measure performance through comparison with actual times. By being able to estimate an optimum time in standard hours and then measuring a corresponding real or actual time, relative efficiency factors (or realization factors) can be established for various shop processes and tasks.

Included as a part of the shop planning order (Figure 10-2) is an estimate for the number of standard hours corresponding to each shop operation. The program, following a parallel logic, was designed with a capability to generate a number of standard hours corresponding to each of the internally generated shop processes. This is accomplished by a series of standard hour equations derived based on standards data acquired through the industrial engineering department.

An example of the initial form of a typical set of standards data is shown in Table 10-1 . The data presented is in table form and represents the standards for a HUFFORD A-12 extrusion stretch forming press, Convair machine code 8030. In this case the total standard hours are made up of two basic items, machine setup time (one increment per job or per die change), and machine run time (one increment per part for performing and one for finish forming). The run time increments are a function of the overall part length.

The development of the standard hour equations involved acquiring the general standards data and deriving an equation for each manufacturing operation based on the characteristic process and part parameters. For the example standards data (Table 10-1) a general equation would take the form:

$$STDHR = 0.52 + N * (f_1(L) + f_2(L)) \quad \text{(hours)}$$

where

0.52 represents the setup time (constant per job)
N represents the total number of parts to be produced
$f_1(L)$ represents preform time as a function of part length
$f_2(L)$ represents finish form time as a function of part length

Table 10-1 Example of Standards Data for Stretch Forming Press as Used by the Industrial Engineering Department

PRESS, EXTRUSION STRETCH FORM

SETUP 0.52 (ONCE PER DIE CHANGE) MACHINE CODE: 8030

PREFORM

LENGTH cm	0-38	39-76	77-114	115-152	153-191	192-229	230-267
(in.)	(0-15)	(16-30)	(31-45)	(46-60)	(61-75)	(76-90)	(91-105)
STD. HR	0.0255	0.0285	0.0315	0.0345	0.0375	0.0405	0.0435
LENGTH cm	268-305	306-343	344-381	382-419	420-457	458-495	496-533
(in.)	(106-120)	(121-135)	(136-150)	(151-165)	(166-180)	(181-195)	(196-210)
STD. HR	0 0465	0.0495	0.0525	0.0555	0.0585	0.0615	0.0645

FINISH FORM

LENGTH cm	0-38	39-76	77-114	115-152	153-191	192-229	230-267
(in.)	(0-15)	(16-30)	(31-45)	(46-60)	(61-75)	(76-90)	(91-105)
STD. HR	0.0595	0.0625	0.0655	0.0685	0.0715	0.0745	0.0775
LENGTH cm	268-305	306-343	344-381	382-419	420-457	458-495	496-533
(in.)	(106-120)	(121-135)	(136-150)	(151-165)	(166-180)	(181-195)	(196-210)
STD.HR	0.0805	0.0835	0.0865	0.0895	0.0925	0.0955	0.0985

NOTE: LENGTH IN INCHES IS BASED UPON THE BILL OF MATERIAL LENGTH OF PART.
ALL VALUES INCLUDE STOCK ALLOWANCE FOR VISE JAWS

The function of length $f_1(L)$ and $f_2(L)$ are determined by curve fitting the data in the standards table. In this case a linear curve fit is sufficient and the functions resulting are:

$$f_1(L) = 0.0002 * L + 0.058$$

$$f_2(L) = 0.0002 * L + 0.024$$

The resulting standard hour equation for this particular press forming operation then simplifies to:

$$STDHR = 0.52 + N * (0.0004 * L + 0.082)$$

A summary of the manufacturing and assembly operations currently represented by equations in the program is presented in Table 10-2

The standards data are usually derived for aluminum only. To apply the data to additional materials, material complexity factors are utilized. The material complexity factors account for the difference in manufacturing time requirements for performing identical tasks or operations on different materials. These factors are typically required only for those manufacturing operations associated with material removal such as drilling, milling, routing, burring, and cutting.

Table 10-2 **Library of Manufacturing and Assembly Operations Currently Available**

Boron epoxy layup	Graphite epoxy quality control	Press forming
Boron epoxy quality control	Heat treatment and straightening	Reaming or tapping
Clamping	Identification	Sawing, cutting
Cleaning, degreasing	Inspection (general)	Securing
Cleanup (of holes after drilling)	Inspection for assembly	Setup for assembly
Disassembly (removing clamps for cleaning)	Layout part (sheet)	Shearing
Drilling (general)	Layout holes (sheet)	Spray painting
Drilling for assembly	Layout part (machine shop)	Stretch forming
Edge burring	Layout holes (machine shop)	Surface treatment
Edge routing	Milling (chemical)	Turning (lathe)
Graphite epoxy layup	Milling (general)	Welding, brazing

Operations that usually do not require complexity factors are cleaning, layout, identification, painting, etc. Standard hours for operations performed on steel, titanium, and boron-aluminum are derived in the program using the material complexity factor approach. Table 10-3 summarizes the values for the factors and the processes for which they are applied. Aluminum represents the baseline of 1.0.

Table 10-3 **Summary of Material Complexity Factors Applied in the Computation of Standard Hours**

	Steel	Titanium	Boron-Aluminum
Burring	3.8	5.0	6.0
Drilling	3.8	5.0	1.2
Forming	3.8	8.0	10.0
Milling	3.8	4.2	1.26
Reaming	3.8	4.0	1.2
Routing	3.8	5.0	6.0
Sawing	3.8	1.1	1.5
Shearing	3.8	1.1	1.5
Turning	3.8	4.2	1.26

Analyses of fabrication processes with advanced composites are handled by assuming three material forms. These are boron-epoxy and graphite-epoxy layups from prepreg tape, and boron-aluminum sheet stock. In general, the advanced composite configurations are assumed to be comprised of the same detail parts, performing the same structural function, as the equivalent metallic configuration.

Boron-epoxy and graphite-epoxy parts are assumed to be layed up to finished form and cured, then bonded into final assembly form. Layup times are computed on the basis of actual hours per unit part weight and per unit part size for boron-epoxy, and on the basis of actual hours per unit part weight for graphite-epoxy. Quality control hours during layup and cure are computed based on hours per unit part size for boron-epoxy, and hours per unit part weight for graphite-epoxy. A realization factor of 1.0 is associated with composite fabrication processes.

A study was made of current data related to advanced composite fabrication operations. As a result of this study it was found that a thorough treatment of each operation in the layup and cure sequence would not be useful. This results from the very limited degree of breakdown of the data that is available, and the fact that much of the data corresponds to the fabrication of only a few actual parts, many of which are relatively simple and physically small. In other words, the data that is presently available is not really representative of a production situation involving actual aircraft components, and is, for the time being, treated in a more simplified manner.

The actual hour computation procedure that is in use for boron-epoxy and graphite-epoxy assumes that the sequence of processes can be combined into two, layup and quality control. These are treated on the basis of hours per unit size and weight. Expressions for actual hours are:

(4.18 * FFF * ACWT * CAREA) ** .5	boron-epoxy layup
.220 * CAREA	boron-epoxy quality control
9.6 * ACWT	graphite-epoxy layup
1.2 * ACWT	graphite-epoxy quality control

where

FFF is a factor corresponding to part configuration

ACWT is the part actual weight

CAREA is the characteristics part area

Boron-aluminum is assumed to be in the form of sheet stock. Standard hours are computed using the ordinary equations times a material complexity factor. These factors were summarized in Table 10-3 .

10.1.4 Rate Data: Labor, Overhead, and Realization. In the program standard hours are computed as an intermediate step in the process of deriving actual labor hours. The conversion is accomplished by making use of the realization factor, a measured value representing shop efficiency as discussed below. The equations for actual labor hours take the following form:

Actual Labor Hours = Standard Hours/Realization

Labor and overhead rates are used in the program to calculate labor and overhead costs, based on the number of actual labor hours required for each manufacturing and assembly process. Labor rates reflect the wages paid directly to the individual employees for each hour of clock time. The rates do not include fringe benefits or company contributions to retirement, social security, state unemployment, etc., which are considered part of the overhead cost. Also included as part of overhead are indirect labor costs, maintenance, supplies, taxes, insurance, depreciation, etc.

Labor rates are largely uncontrollable by management, being a function instead of union/management agreements and reflecting current labor supply and demand, general economic conditions, and inflation. Labor rates are a function of time and are readily predictable for the near future.

The overhead ratio is the ratio of overhead costs to direct labor costs. It is established based on historical accounting records, and is, in turn, often used by estimating departments. In the program, the overhead ratio is used to determine the overhead costs corresponding to the calculated labor costs where:

Overhead Cost = Labor Cost * Overhead Ratio

Realization is a measure of shop efficiency, and as such, it varies from department to department and from day to day within a department. Realization data for the various departments involved in production tasks at the San Diego operation has been collected, studied, and adapted for use with the program. Realizations can be specified either as a constant average value or as a time dependent equation. Some of the factors affecting realization are:

a. Worker personal needs.

b. Rest periods.

c. Inaccurate planning of the task.

d. Change in procedure, machines, or tools without corresponding change in manhour estimates.

e. Machine breakdown.

f. Tool breakage and part spoilage.

g. Availability of previous setups.

h. Use of special supervision.

i. Ability and effort level of individuals assigned the task.

Labor and overhead costs are computed directly for the first unit. A learning curve approach is applied to first unit costs to derive the cost of any subsequent unit or production lot. Labor (and overhead) costs are generated at the detail part level. For each manufacturing or assembly process specified for a given part, a value for standard hours, actual labor hours, labor cost, and overhead cost is computed. These are summed to obtain total costs for a given part, subassembly, assembly, etc.

Manufacturing and assembly processes have been divided into three groups: basic factory, quality control, and assembly. For each there is available in the program a corresponding labor rate that is computed from a base value as a function of time. Also available in the same manner are values for overhead ratio and realization factor.

For each, average industry values for 1970 are used as the base. Rate data for any year is computed by assuming a constant fractional annual rate of change. Any of the internal values for rate or annual rate of change may be overridden by direct input. In the absence of an input, values are computed. A summary of the rate data internal to the program is presented in Table 10-4 .

Table 10-4 Summary of Internal Program Rate Data

Description 1970 Base Year	Rate Data Fortran Name	Rate Data Value	Annual Rate of Change Fortran Name	Annual Rate of Change Value
Factory Labor Rate ($/hr)	FRATE	3.64	CLAR	0.055
Quality Control Labor Rate ($/hr)	QRATE	4.06	CLAR	0.055
Assembly Labor Rate ($/hr)	ARATE	3.48	CLAR	0.055
Overhead Ratio	VRATE	1.80	COVR	0.02
Realization Factor	REFCT	0.15	CRE	0.01

10.1.5 Material Cost. Material costs are computed based on the material type (aluminum, steel, etc.), material form (sheet, plate, bar, etc.), and the raw material purchase weight. The actual calculation of material cost takes the form:

MATCOS = AMUV * COSWT * MAWT

where

MATCOS is the material cost

AMUV is the manufacturing usage variance factor explained below

COSWT is the material unit cost

MAWT is the raw material purchase weight

The computation of material costs requires the derivation of a material unit cost and the definition of a manufacturing usage variance factor. The computation of the material purchase weight is done during the weight analysis portion of the program.

The material unit cost is, in general, a function of the material type, form, quantity of material bought, and special feature requirements such as special lengths, widths, thicknesses, alloys, tempers, tolerances, and marking. Computation of the material unit cost can be summarized as follows: a base price is computed as a function of material type and form; the base price is adjusted to account for the quantity buy p differential; the prices of appropriate special feature extra cost items are computed and summed to derive a total special feature penalty cost; a total material unit cost is determined by summing the adjusted base price and the special feature penalty cost; and finally, the resultant value for material unit cost is adjusted, if necessary, to correspond to dollars for the specified reference year.

Material type is specified by input of a value for MATLID, which represents the component structural material. The materials currently available in the program are:

MATLID = 1 Aluminum	MATLID = 4 Boron-Epoxy
MATLID = 2 Steel	MATLID = 5 Boron-Aluminum
MATLID = 3 Titanium	MATLID = 6 Graphite-Epoxy

Material form is specified by defining a value for KEY in the parts definition subroutines. Each detail part is assumed manufactured from and is thus associated with one of the following material forms:

KEY = 1 FASTENER
2 HONEYCOMB
3 FOIL, SHEET, PLATE
4 WIRE, ROD, BAR
5 EXTRUSION

For a given material type and form, a value for the total quantity of material purchased is computed by summing the values for raw material purchase weight for each detail part. A system of arrays is defined to categorize materials by type, form, and stock dimensions. The value derived for material weight for each detail part is added to one of the array elements as it is computed. After material purchase weights have been computed for all detail parts, the system of arrays is multiplied by the number of ship-sets to be produced. By this means a total quantity of required material is available for computing material costs as a function of quantity bought.

By specifying the material type the program is directed to one of two fundamental areas of material cost computation. The first encompasses the metallic materials aluminum, steel, and titanium, and the second encompasses the advanced composites boron-epoxy, boron-aluminum, and graphite-epoxy. The primary difference in methodologies reflected by the two areas is due to the assumptions made with respect to material form. For the metallics a material form is specified by the parts prediction routines, and the unit material costs are computed as a function of the form. For the advanced composites a material form is assumed, and all parts are considered to be fabricated of the assumed material form. The assumed material forms are 7.62-cm (3-in.) wide prepreg tape for boron-epoxy and graphite-epoxy, and cured sheet for boron-aluminum.

Unit costs for metallic materials are computed as a function of both material type and form. Price data for various materials and material forms were collected and curve fit as a function of nominal material stock sizes. Table 10-5 illustrates a typical base price schedule for alloy steel plate between 0.635 cm (0.25 in.) and 15.24 cm (6.0 in.) thick. The resulting equation for this particular material is:

Table 10-5 Part of Typical Material Price Schedule for Alloy Steel Plate (1970 Data)

Thickness (cm)	Thickness (in.)	E4340, AMS-6359 Hot Rolled Annealed ($/100 kg)	($/100 lb)
0.635	(0.250)	99.00	(45.00)
0.953	(0.375)	97.68	(44.40)
1.270	(0.500)	97.13	(44.15)
1.588	(0.625)	97.35	(44.25)
1.905	(0.750)	97.02	(44.10)
2.540	(1.000)	96.69	(43.95)
3.175	(1.250)	96.80	(44.00)
3.810	(1.500)	96.80	(44.00)
4.445	(1.750)	98.01	(44.55)
5.080	(2.000)	98.01	(44.55)
5.715	(2.250)	104.28	(47.40)
6.350	(2.500)	104.28	(47.40)
6.985	(2.750)	104.28	(47.40)
7.620	(3.000)	104.28	(47.40)
8.890	(3.500)	104.28	(47.40)
10.160	(4.000)	104.28	(47.40)
11.430	(4.500)	104.28	(47.40)
15.240	(6.000)	104.28	(47.40)

$$PBASE = 0.006 * THK + 0.439$$

where

PBASE is the unit base price

THK is the material thickness

Thus, by specifying MATLID = 2, KEY = 3, and THK equal to some characteristic or computed thickness, the program calculates a unit base price for the required size of alloy steel plate. In a similar manner, equations were derived to provide a means of computing base price data for the various forms of aluminum, steel, and titanium.

For some combinations of material type and form, such as titanium extrusions, specific price data was not available. For these cases a characteristic material base price was established, as MBASE = 8.50 for titanium. The specified material was then analyzed in terms of the equivalent aluminum material form (aluminum extrusions), and the resulting value of PBASE derived for the

Table 10-6 Summary of Values for the Characteristic Material Base Price Currently in Use in the Program

Aluminum	ALBASE = 0.80
Titanium	MBASE = 8.50
Alloy steel	MBASE = 0.40

equivalent aluminum form was ratioed using an aluminum base price (ALBASE = 0.80) and the specified material base price (MBASE). Table 10-6 is a summary of the values of MBASE currently being used in the program. Table 10-7 is a summary of the material type and forms currently available in the program.

A price differential based on the quantity of material purchased is computed and

Table 10-7 Summary of Material Type and Forms Currently Available in the COSTMA Subroutine

			Al	Steel	Ti
KEY =	1	fastener	●	●	●
	2	honeycomb	●	o	o
	3	foil, sheet, plate	●	●	●
	4	wire, rod, bar	●	●	●
	5	extrusion	●	o	o
	6	tubing	To be added at a future date		
	7	forging			
	8	casting			

● direct material price data available

o ratioed material price data available

used to adjust the unit base price. Equations defining the price differential were derived by curve fitting quantity purchased versus unit cost data. An example of data typical of the type utilized is presented in Table 10-8 .

A cost penalty is determined for required extra cost special features. Equations for each of the typical extra cost items have been generated from material vendor pricing handbooks. These equations include costs for protective coatings, identification, mechanical testing, packing, shipping, etc. (Table 10-9). The cost penalty is added to the adjusted material unit cost to provide a total material unit cost.

Table 10-8 Example of the Quantity Buy Price Differential for Aluminum Plate

Quantity per Item		Extra	
kg	(lb)	$/kg	($/lb)
13,636 and over	(30,000 and over)	Base	(Base)
13,635 - 9,091	(29,999 - 20,000)	0.022	(0.010)
9,090 - 4,545	(19,999 - 10,000)	0.044	(0.020)
4,544 - 3,636	(9,999 - 8,000)	0.110	(0.050)
3,635 - 1,818	(7,999 - 4,000)	0.154	(0.070)
1,817 - 1,364	(3,999 - 3,000)	0.275	(0.125)
1,363 - 909	(2,999 - 2,000)	0.627	(0.285)
908 - 682	(1,999 - 1,500)	0.990	(0.450)
681 - 455	(1,499 - 1,000)	1.705	(0.775)

Table 10-9 Summary of Extra Cost Items Available for Aluminum Plate

PRICING CHECK LIST

The following General Extras apply to sheet and plate products.

PLATE	
ACTUAL PIECE COUNT	PACKING
ALLOYS AND SPECIAL EXTRAS	PACKING PER MIL-STD 649- SHEET AND PLATE
CIRCLES	PROTECTIVE TAPE
CONVERSION COATINGS	QUANTITY
EXACT QUANTITY	TEST MATERIAL SAMPLES
IDENTIFICATION MARKING-STANDARD	TOLERANCES
IDENTIFICATION MARKING-SPECIAL	DIAMETER
INTERLEAVING AND OILING	FLATNESS
LENGTHS, LONG	LENGTH
LENGTHS, SHORT	THICKNESS
MACHINED SURFACE (TWO SIDES)	WIDTH
MECHANICAL TESTING	ULTRASONIC INSPECTION

Material unit costs for advanced composites are computed directly as a function of the reference year for boron-epoxy and boron-aluminum and as a combined function of the average single-ply thickness and reference year for graphite-epoxy. The equations were derived by curve-fitting actual and projected cost data acquired from the Convair Advanced Composites Laboratory and from typical material vendors. The equations are:

$$P = 225 - 16.5 * (YR - 70) \qquad \text{Boron-Epoxy}$$

$$P = 425 - 22.5 * (YR - 70) \qquad \text{Boron-Aluminum}$$

$$P = 115/(PLYT - 1.111) - 9.3 * (YR - 70) + 89 \qquad \text{Graphite-Epoxy}$$

where

P is the material unit cost

YR is the dollar reference year

PLYT is the average single-ply thickness

A plot of material cost versus year for boron-epoxy and boron-aluminum is presented in Figure 10-3 . Graphite-epoxy costs versus year for various single-ply thicknesses are presented in Figure 10-4 .

The value for average single-ply thickness (PLYT) is computed from material thickness. A range of from 0.013 to 0.051 cm (5 to 20 mils) is allowed. If the computed

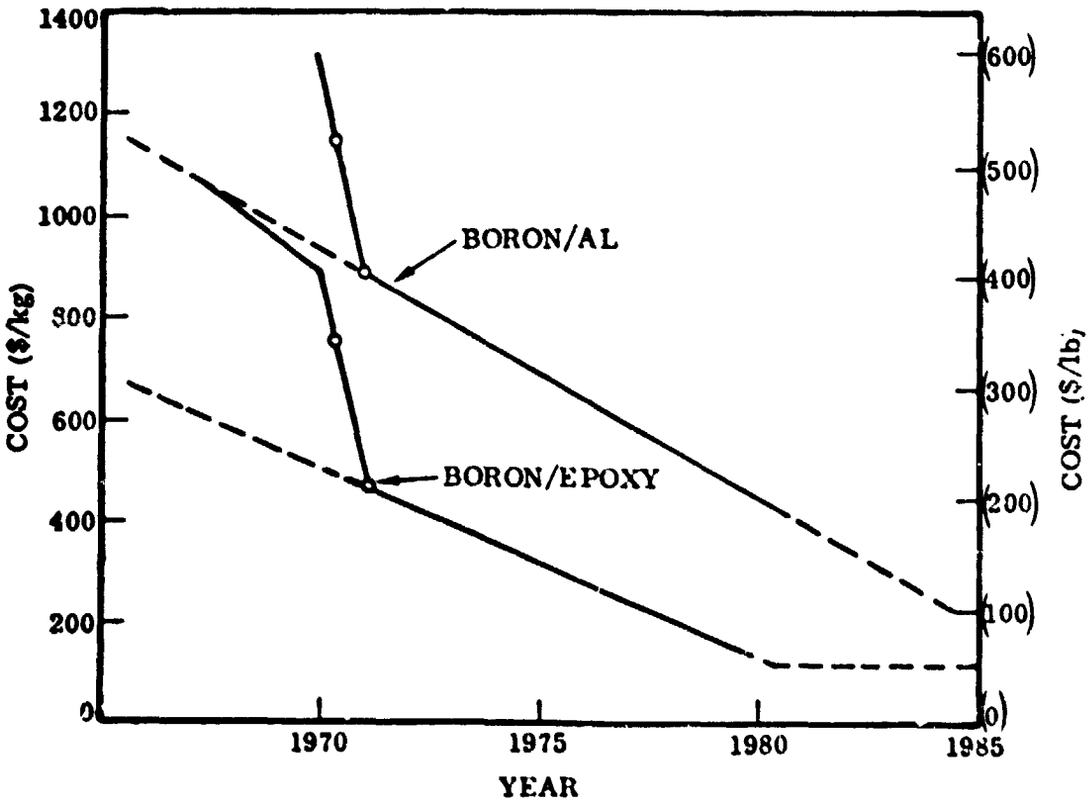

Figure 10-3 Projected Raw Material Costs for Boron-Aluminum and Boron-Epoxy

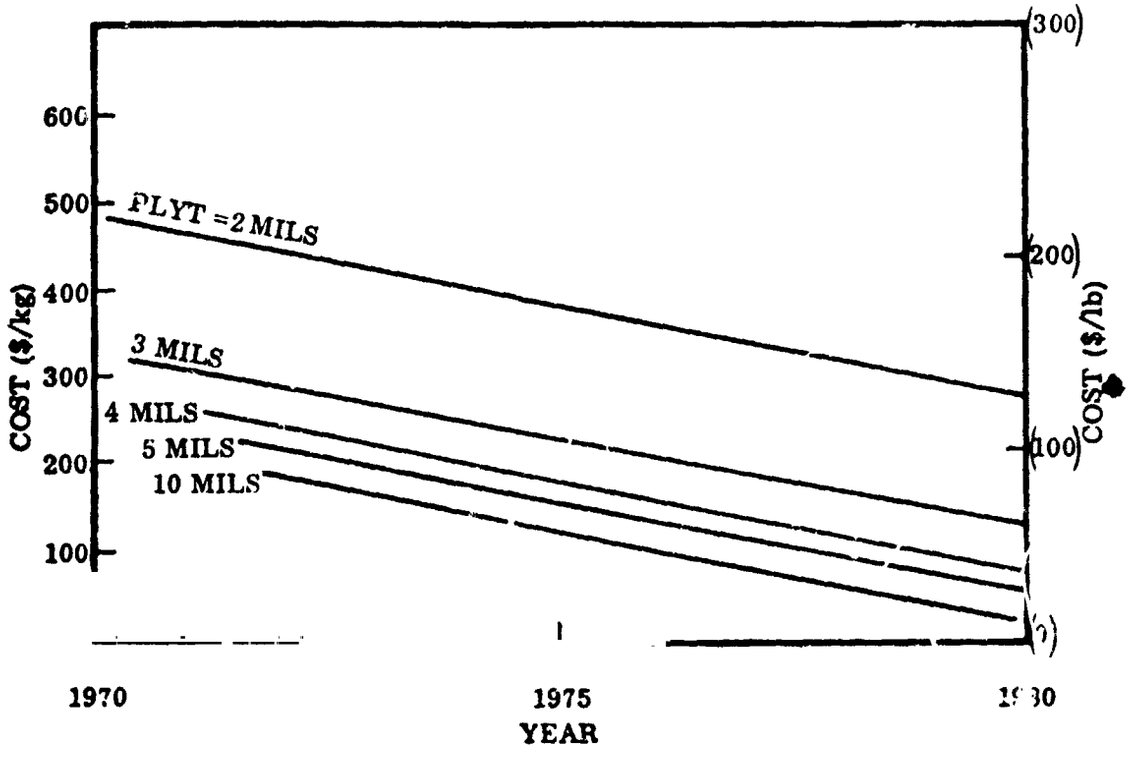

Figure 10-4 Projected Raw Material Costs for Graphite-Epoxy

value is outside this range, a value of 0.013 cm (5 mils) is set. A minimum value for each of the material unit costs has also been fixed. The unit costs, which override smaller computed values, are: $110/kg ($50/lb), boron-epoxy; $220/kg ($100/lb), boron-aluminum; and $22/kg ($10/lb), graphite-epoxy. It was determined that these were the minimum material prices that would be achieved in the foreseeable future. A price differential based on the total material quantity purchased was established as follows: a 10% penalty was added to the unit cost for purchases of 4545 to 45,455 kg (10,000 to 100,000 lb), 20% for purchases of 455 to 4545 kg (1,000 to 10,000 lb), 40% for purchases of 45 to 455 kg (100 to 1,000 lb), and 60% for purchases of less than 45 kg (100 lb).

While the unit material cost for advanced composites is computed as a function of the dollar reference year directly, the unit cost for metallics must be adjusted to the reference year. An adjustment is made assuming a constant annual rate of inflation. A value for the annual rate of inflation of material costs may be input directly by the user; in the absence of an input a nominal value of 0.03 is assumed.

Table 10-10 **Typical Manufacturing Usage Variance Factors for a Past Commercial Transport Program**

CONTRACT LOT NO.	ACTUAL MATERIAL COSTS A (millions of $)	ORIGINAL ESTIMATED MATERIAL COSTS E (millions of $)	PERCENT VARIANCE $\left(\frac{A - E}{A}\right) * 100$ (percent)	MANUFACTURING USAGE VARIANCE FACTOR
1	40.65	34.74	17.0	1.170
2	4.61	4.25	8.5	1.085
3	16.67	14.39	13.8	1.138
4	22.69	21.40	6.1	1.061
5	16.28	15.84	2.8	1.028
6	66.50	62.15	7.0	1.070
7	10.22	9.84	3.9	1.039
8	68.71	61.94	10.9	1.109

The manufacturing usage variance factor (AMUV) is the ratio of the actual amount of material purchased to the sum of the engineering net bill of materials plus the planning allowances for manufacturing. The factor is, in general, a function of material type (particularly in the case of advanced composites) and past material handling experience. The factor results from material and part overbuying to account for normal indirect material losses during the manufacturing phase of production. These losses include material and part spoilage, duplication, substitution, changes, waste, etc. These losses are to be differentiated from those resulting directly from manufacturing, such as trimming, routing, and milling, which are accounted for in the derivation of the material purchase weight.

The actual value for the manufacturing usage variance factor is determined by accounting procedures. Data from several past programs are presented in Table 10-10 . A nominal value of 1.10 is currently in use by the program for all material forms. This represents a 10% overbuy and is a fairly good average value for typical metallic aircraft construction. However, it is somewhat high for production involving the use of advanced composite materials.

10.2 AIRFRAME MANUFACTURING COST (CER-COST ESTIMATING RELATIONSHIPS). The airframe manufacturing costs in the methodology described in Section 10.1 uses a detailed manufacturing analysis to synthesize costs at the detail part level. This analysis approach requires a relatively large amount of aircraft definition and supporting factory manufacturing standards. To provide a simpler, more readily usable and accessible preliminary design tool, subsystem level cost estimating relationships (CER's) have been developed to provide a means for generating a theoretical first unit cost for any specific aircraft configuration under study. This alternate procedure develops airframe manufacturing costs on the basis of subsystem level cost estimating relationships (CER's) that include provisions for cryogenic tankage, insulation, and propellant feed and management subsystems . In addition, the engine development and production model has been modified based on the work performed by General Electric under NASA Contract NASA CR-120793 (Reference 3) and Pratt and Whitney under NASA Contract NASA CR-120862 (Reference 4).

10.2.1 Theoretical First Unit Cost. The theoretical first unit manufacturing cost has been broken down into the two major categories of structure and subsystems. Within the structure are the four basic elements of wing, body, empennage and nacelle. The subsystems are composed of landing gear, surface controls, environmental control, hydraulics/pneumatics, electrical, instruments, armament, engine associated equipment, fuel system, avionics provisions, furnishings and equipment and auxiliary power. For aircraft that use liquid hydrogen or methane for fuel the additional subsystems of tankage, insulation and propellant feed and management are required.

The first unit cost estimates are driven by equations that require differentiation between subsonic and supersonic aircraft and use the weight of the various elements of structure and subsystems as cost drivers.

For those aircraft configurations where there is more than one fuselage, the individual fuselages are treated as separate elements of structure and costs computed accordingly. This is also true for tankage where multiple tanks are used. Each tank is treated as a separate element and costs computed individually.

The equations used to generate first unit cost for JP-fueled aircraft have been tabulated and appear in Table 10-11. The additional equations required for those aircraft configurations that have liquid hydrogen and methane fuel systems have been tabulated and appear in Table 10-12. The CERs for JP aircraft are based on a sample of subsonic and supersonic fighter and bomber aircraft and subsonic commercial and military transports. The development of these cost estimating relationships is based on the

Table 10-11 Airframe TFU CERs

	Subsonic	Supersonic
1. Wing	$C = 1680\ W_W^{.70}$	$C = 3520\ W_W^{.70}$
2. Fuselage	$C = 2240\ W_F^{.70}$	$C = 4800\ W_F^{.70}$
3. Empennage	$C = 1680\ W_E^{.70}$	$C = 2320\ W_E^{.70}$
4. Nacelles	$C = 1680\ W_N^{.70}$	$C = 3360\ W_N^{.70}$
5. Landing Gear	$C = 1440\ W_L^{.70}$	$C = 1440\ W_L^{.70}$
6. Surface Controls	$C = 2240\ W_S^{.70}$	$C = 5760\ W_S^{.70}$
7. Hydraulics-Pneumatics	$C = 3200\ W_H^{.70}$	$C = 3200\ W_H^{.70}$
8. Electrical	$C = 2400\ W_{EL}^{.70}$	$C = 2400\ W_{EL}^{.70}$
9. Furnishings and Equipment	$C = 2000\ W_{FE}^{.70}$	$C = 2000\ W_{FE}^{.70}$
10. Environmental Control	$C = 1920\ W_A^{.70}$	$C = 2800\ W_A^{.70}$
11. Auxiliary Power	$C = 1520\ W_{AP}^{.70}$	$C = 1520\ W_{AP}^{.70}$
12. Instruments and Displays	$C = 6400\ W_I^{.70}$	$C = 6400\ W_I^{.70}$
13. Fuel System	$C = 2080\ W_{FU}^{.70}$	$C = 2080\ W_{FU}^{.70}$
14. Engine Associated Equipment	$C = 1600\ W_{EA}^{.70}$	$C = 1600\ W_{EA}^{.70}$
15. Armament	$C = 640\ W_A^{.70}$	$C = 640\ W_A^{.70}$
16. Avionics Provisions	$C = 1500\ W_{AV}^{.70}$	$C = 1500\ W_{AV}^{.70}$

Table 10-12 Cryogenic Fueled Aircraft TFU CERs

	Subsonic	Supersonic
Hydrogen:		
Tankage	$C = 3175\ W_{TH}^{.70}$	$C = 4762\ W_{TH}^{.70}$
Insulation	$C = 1905\ W_{IH}^{.70}$	$C = 2857\ W_{IH}^{.70}$
Propellant Feed & Management	$C = 11200\ W_{PH}^{.70}$	$C = 11200\ W_{PH}^{.70}$
Methane:		
Tankage	$C = 1587\ W_{TM}^{.70}$	$C = 2380\ W_{TM}^{.70}$
Insulation	$C = 952\ W_{IM}^{.70}$	$C = 1428\ W_{IM}^{.70}$
Propellant Feed & Management	$C = 5600\ W_{PM}^{.70}$	$C = 5600\ W_{PM}^{.70}$

Current year dollars modifier =

$$K(\text{Year}) = 1.273\ (C)\ (1.06)^{(\text{Year}-1974)}$$

analysis of historical first unit cost and weight data at the subsystem level. Each functional subsystem was analyzed separately and cost estimating relationships developed to differentiate between subsonic and supersonic aircraft. An example of the basic data and the developed relationships for the wing structure is shown in Figure 10-5 . The subsonic data points are represented by a square and the long lower line is the cost estimating relationship developed from these data. The supersonic data points are represented by a triangle and the long upper line is the cost estimating relationship developed from these data. The mathematical expression for these relationships are of the form:

$$C = aW^b$$

where

C = cost ($)
a = subsystem coefficient
W = subsystem weight (pounds)
b = weight scaling exponent

For the specific subsonic and supersonic wing first unit cost equations shown in Figure 10-5 , the costs are expressed in 1970 dollars.

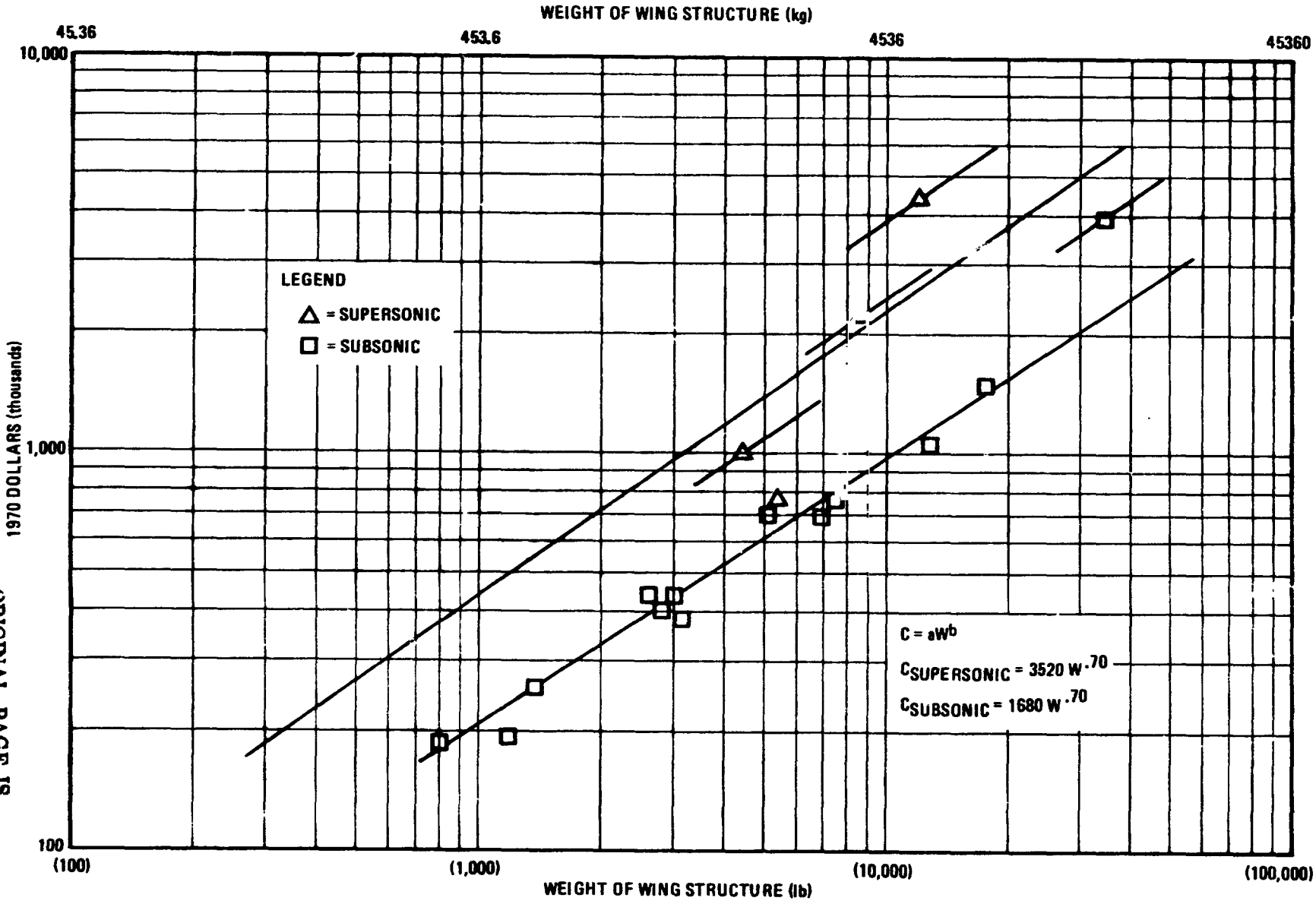

Figure 10-5 Wing First Unit Cost (Labor and Material)

The CERs for cryogenic fuel subsystems are based on Centaur and Space Shuttle experience with subjective weighting factors applied to differentiate between subsonic and supersonic applications. For those configurations where hydrogen or methane is used as a fuel, the fuel system weight is zero for the JP fuel system equation and all fuel system costs are generated by the propellant feed and management TFU equation.

The above theoretical first unit cost equations give results in terms of 1970 dollars. To convert these figures to current dollars the following modifier is used:

$$K_{(Year)} = 1.273\ (C)\ (1.06)^{(Year-1974)}$$

All of the equations for the separate functional pieces of hardware that make up the first unit cost have the same mathematical form and scale with weight to the .70 power. Developing the equations in this form has the advantage of providing additional visibility into the nature of the cost drivers at the TFU level. With both size (measured by weight) and scaling the same, the relative cost of different types of subsystems and structure can be determined from the equation coefficients. This information, coupled with the weight distribution among the elements of structure and subsystems for a specific configuration allows identification of high cost areas in terms of both absolute magnitude and in the more relative sense of dollars per pound.

The above formulation of first unit cost includes both the labor and material portions of manufacturing. As such, it replaces both the manufacturing labor and manufacturing material portions of the original cost model developed for NASA CR 132362 (Reference 5)

10.2.2 Engine Development and Production. There are three major areas of design that require development and/or testing for conversion of existing JP burning engines to cryogenic fuel. The turbopump bearings and seals have to be modified and a cryogenic pump throttling range of about 35 to 1 provided. In addition, heat exchangers to provide for vaporization of the cryogenic fuel need to be developed. Conversion of the existing engines will apparently not materially affect the pressure ratio, turbine inlet temperature, percentage of titanium and superalloys used in the engines, maximum thrust Mach numbers, or by-pass ratio. For the CF-6-50A and JTF22A-27A there is a weight increase of about 5% and 10%, respectively. A tabulation of CF-6-50A and JTF22A-27A engine data before and after conversion appears as Table 10-13.

Costs of conversion development, up to MQT (model qualification test) have been developed in two different ways. Point estimates based on the work of Pratt and Whitney and General Electric have been made and for the CF-6-50A and JTF22A-27A they can be used as through-puts in the model.

In terms of 1974 dollars, the conversion development cost through MQT is $53 million for the CF-6-50A and $39 million for the JTF22A-27A. These are ROM (rough order of magnitude) estimates and should be treated accordingly. For conversions where a parametric estimate is required the following CER was developed based on Centaur cryogenic propellant feed and management technology.

$$\text{Engine Cryogenic Conversion Cost (M\$)} = 2.1\ (\Delta W)^{.50}(1.06)^{(\text{Year}-1974)}$$

where

ΔW (lbs) = Weight after conversion - Weight before conversion
Year = Year when conversion takes place.

Production costs are based on the existing methodology with appropriate modification for changing to cryogenic fuel. The existing engine production equations is as follows:

$$TFU = 3270\ (FP)^{.60}\ CFENG$$

where

FP = maximum sea level thrust (lbs.)

CFENG = engine complexity factor

The new equation is modified by a factor in the following way:

$$TFU = 3270\ (FP)^{.60}\ CFENG\ (CRFM)$$

where

CRFM = cryogenic conversion factor for methane (CRFH is used for hydrogen cryogenic conversion factor)

The specific values for the cryogenic conversion factors are as follows:

	Turbofan	Turbofan with Afterburner
Hydrogen cryogenic conversion factor (CRFH) =	1.10	1.20
Methane cryogenic conversion factor (CRFM) =	1.05	1.10

These cryogenic modification factors are based on an assessment of the Pratt & Whitney and General Electric (References 3 and 4) studies and a parametric analysis of cryogenic cost differentials based on Centaur (Reference 6) historical cost data and the Aerospace Corporation space transport system cost model (Reference 7).

The above production costs are expressed in terms of 1970 dollars. To express them in current year dollars the following modifier is used:

$$\text{Current year dollars modifier} = K\ (\text{Year}) = 1.273\ (TFU)\ (1.06)^{(\text{Year}-1974)}$$

where

Year = year first production article is produced.

Table 10-13 Engine Conversion Data

Type	Original CF-6-50A Turbofan	Cryogenic Version CF-6-50A Turbofan	Original JTF22A-27A Turbofan (A.B.)	Cryogenic Version JTF22A-27A Turbofan (A.B.)
Pressure Ratio	29.9:1	29.9:1	23:1	23:1
Turbine Inlet Temp. °K(°R)	1547 (2325)	1547 (2325)	1616.5 (2450)	1616.5 (2450)
Percent Titanium	30%	30%	N.A.	N.A.
Percent Superalloys	40%	40%	N.A.	N.A.
Design Year	1970		1969	
Mach Number	0.90	0.90	2.3	2.3
Thrust (Max.) Kg (lbs)	22,226.4 (49,000)	22,226.4 (49,000)	10,813.4 (23,839)	10,813.4 (23,839)
Weight Kg (lbs)	3674.1 (8100)	3857.9 (8505)	1246.0 (2747)	1391.6 (3068)
By-Pass Ratio	4.4	4.4	.71	71
Development Cost (increase above existing eng.) (M 1974 $)		53		39

10.3 ENGINEERING COSTS. Engineering costs are derived by computing the number of engineering manhours required and multiplying this by a composite engineering labor rate. Engineering hours are computed as initial engineering hours - those hours utilized by the time the first airframe has been completed, and sustaining engineering hours - those hours occurring after the first airframe has been completed.

The actual computation of initial and sustaining engineering hours has as its basis equations developed by G. S. Levenson and J. M. Barro (Reference 1). For this reason their definiton of the engineering task was used. Engineering, then, was defined as including the following: design and integration studies, engineering for wind tunnel models, mockup and engine testing, test engineering, laboratory work on subsystems and static test items, development testing, board hours, release and maintenance of drawings, specifications, shop and vendor liaison, analysis and incorporation of changes, material and process specifications, and reliability. Hours not considered as engineering include those associated with flight test, planning, ground handling equipment, spares, mobile training units, and publications. Also not included as part of engineering cost are travel and computer time.

10.3.1 Engineering Cost Derivation. The intial engineering task is computed by first determining the number of hours to do the task and then applying an appropriate com-

posite engineering labor rate. The initial engineering hours represent those engineering hours expended to the point in time when the first airframe has been completed. The G. S. Levinson and J. M. Barro equation (Reference 1) develops the initial engineering hours required as a function of maximum aircraft speed at cruise altitude and total aircraft thrust at sea level. This equation provides for airframe development engineering and is based on a sample of fighter, bomber and cargo aircraft. To account for the unique features of a liquid hydrogen or methane fueled aircraft it is necessary to develop separate cost estimating relationships that provide for cryogenic fuel subsystems. Specifically, cost estimating relationships are developed that provide for design of cryogenic tankage, insulation and propellant feed and management. These cost estimating relationships were developed primarily on the basis of Centaur and Space Shuttle experience and are dealt with as add ons to the design of a more conventional aircraft. In addition, modifications are made to the JP cost methodology to provide for the reduction in the engineering task associated with the absence of a conventional fuel tankage and delivery system. The hydrogen and methand fueled aircraft have been dealt with separately to reflect the greater difficulty associated with the use of liquid hydrogen due to its lower liquefication temperature and greater permeability.

The total number of initial engineering hours computed is broken down and distributed among the various engineering disciplines based on percentages derived from studies of historical data. There are two basic breakdowns, one corresponding to a typical subsonic or transonic transport type aircraft and one corresponding to a typical high performance military type aircraft. Maximum Mach number is used to differentiate between the two breakdowns with a Mach number of 1.1 or greater corresponding to the military type aircraft.

The value for total initial engineering hours that is output is not the value that is computed directly, but is instead a value found by summing the hours for all of the various engineering disciplines. It is hoped that a future date each area of engineering can be looked at individually, and that for each, methods can be developed to derive hours directly by means of empirical relationships. As these methods are developed, the percentage based computation for a given discipline can be easily replaced by a direct computation, and the new equations will thus be represented in the final output value for initial engineering hours. In this way, an empirically based routine can be built up bit by bit while retaining the capability of generating a complete output during the development.

The total airframe initial engineering hours are developed as a summation of subsystem level initial engineering tasks and are developed from separate systems of equations that are dependent on type of fuel. For the JP fueled aircraft all the subsystem level inputs are available from the airframe initial design hours (DESIR) equations which are driven by the airframe initial engineering hours (ENGRIIR) equation. Values of ENGRIIR are developed by the G. S. Levinson and J. M. Barro equation which uses maximum aircraft speed at cruise altitude in knots and maximum total aircraft sea level thrust in pounds as independent variables. The total airframe initial engineering

hours are developed in a similar fashion for liquid hydrogen and liquid methane fueled aircraft but require, in addition, the weights of the cryogenic tankage, insulation and propellant feed and management subsystems. These weights are required as inputs to the subsystem level initial engineering hours equations. The above observations can be seen in the equation methodology that has been summarized below:

Initial Engineering Equations Summary

Airframe Initial Engineering Hours = ENGRHR

ENGRHR = 8.0 * (VELALT **0.55) *(FP**0.88)*CONFAK

where

VELALT = maximum aircraft speed at cruise altitude (knots)

FP = maximum total aircraft sea level thrust (pounds)

CONFAK = configuration complexity factor with a nominal value of 1.0

Airframe Initial Design Hours = DESHR

For Mach < 1.1

DESHR = 0.54 * ENGRHR

For Mach ≥

DESHR = 0.48*ENGRHR

For JP Fueled Aircraft

Airframe Initial Engineering Hours by discipline = ENGRJD

	Mach < 1.1	Mach ≥ 1.1
Structural/Mechanical Design		
Wing	0.14 DESHR	0.12 DESHR
Tail	0.07 DESHR	0.04 DESHR
Body	0.15 DESHR	0.20 DESHR
Furnishings	0.14 DESHR	0.08 DESHR
Gear	0.04 DESHR	0.04 DESHR
Propulsion	0.12 DESHR	0.10 DESHR
Controls	0.09 DESHR	0.09 DESHR
Environmental Control	0.05 DESHR	0.05 DESHR
Hydraulic Pneumatic	0.05 DESHR	0.06 DESHR
Reliability	0.01 DESHR	0.01 DESHR
Armament	0 DESHR	0.03 DESHR

Electrical/Electronic Design	0.14 DESHR	0.18 DESHR
Design Support		
Lines/ Loft	0.15 DESHR	0.15 DESHR
Drafting/Isometrics	0.02 DESHR	0.02 DESHR
Checking/ Release	0.06 DESHR	0.06 DESHR
Liaison/Support Design	0.02 DESHR	0.02 DESHR
Tec nical Support		
Stress	0.16 DESHR	0.16 DESHR
Weights	0.06 DESHR	0.06 DESHR
Aero	0.05 DESHR	0.05 DESHR
Dynamics	0.08 DESHR	0.08 DESHR
Therm	0.08 DESHR	0.08 DESHR
Test Lab	0.10 DESHR	0.10 DESHR
Electrical	0.06 DESHR	0.06 DESHR
Staff	0.01 DESHR	0.01 DESHR
Predesign	0.02 DESHR	0.02 DESHR
Standards/Specs. Publication	0.06 DESHR	0.06 DESHR
ENGRJD =	$\sum$	$\sum$

For Hydrogen Fueled Aircraft

Airframe Initial Engineering Hours by discipline = ENGRHD

	Mach < 1.1	Mach ≥ 1.1
Structural/Mechanical Design		
Wing	0.14 DESHR	0.12 DESHR
Tail	0.07 DESHR	0.04 DESHR
Body	0.15 DESHR	0.20 DESHR
Tankage	$6250\ (W_{TH})^{.50}$	$6250\ (W_{TH})^{.50}$
Insulation	$2700\ (W_{IH})^{.50}$	$2700\ (W_{IH})^{.50}$
Propellant Feed & Management	$25000\ (W_{PH})^{.50}$	$25000\ (W_{PH})^{.50}$
Furnishings	0.14 DESHR	0.08 DESHR
Gear	0.04 DESHR	0.04 DESHR
Propulsion	0.06 DESHR	0.05 DESHR
Controls	0.09 DESHR	0.09 DESHR
Environmental Control	0.05 DESHR	0.05 DESHR
Hydraulic Pneumatic	0.05 DESHR	0.06 DESHR
Reliability	0.01 DESHR	0.01 DESHR
Armament	0	0.03 DESHR

Electrical/Electronic Design	0.14 DESHR	0.18 DESHR
Design Support		
Lines/Loft	$K_H \times 0.15$ DESHR	$K_H \times 0.15$ DESHR
Drafting/Isometrics	$K_H \times 0.02$ DESHR	$K_H \times 0.02$ DESHR
Checking/Release	$K_H \times 0.06$ DESHR	$K_H \times 0.06$ DESHR
Liaison/Support Design	$K_H \times 0.02$ DESHR	$K_H \times 0.02$ DESHR
Technical Support		
Stress	$K_H \times 0.16$ DESHR	$K_H \times 0.16$ DESHR
Weights	$K_H \times 0.06$ DESHR	$K_H \times 0.06$ DESHR
Aero	$K_H \times 0.05$ DESHR	$K_H \times 0.05$ DESHR
Dynamics	$K_H \times 0.08$ DESHR	$K_H \times 0.08$ DESHR
Thermo	$K_H \times 0.08$ DESHR	$K_H \times 0.08$ DESHR
Test Lab	$K_H \times 0.10$ DESHR	$K_H \times 0.10$ DESHR
Electrical	$K_H \times 0.06$ DESHR	$K_H \times 0.06$ DESHR
Staff	$K_H \times 0.01$ DESHR	$K_H \times 0.01$ DESHR
Predesign	$K_H \times 0.02$ DESHR	$K_H \times 0.02$ DESHR
Standards/Specs./Publications	$K_H \times 0.06$ DESHR	$K_H \times 0.06$ DESHR
ENGRHD =	$\sum$	$\sum$

where

W_{TH} = weight of liquid hydrogen tankage

W_{IH} = weight of liquid hydrogen insulation

W_{PH} = weight of liquid hydrogen propellant feed and management

K_H = liquid hydrogen system multiplying factor and is derived by the equation:

$$K_H = 1.0 + \frac{12500\ (W_{TH})^{.50} + 5400 (W_{IH})^{.50} + 50000\ (W_{PH})^{.50}}{1.03\ \text{ENGRHR}}$$

For Methane Fueled Aircraft

Airframe Initial Engineering Hours by discipline = ENGRMD

	Mach < 1.1	Mach ≥ 1.1
Structural/Mechanical Design		
Wing	0.14 DESHR	0.12 DESHR
Tail	0.07 DESHR	0.04 DESHR
Body	0.15 DESHR	0.20 DESHR
Tankage	$4687(W_{TM})^{.50}$	$4687(W_{TM})^{.50}$
Insulation	$2025(W_{IM})^{.50}$	$2025(W_{IM})^{.50}$
Propellant Feed & Management	$18750(W_{PM})^{.50}$	$18750(W_{PM})^{.50}$
Furnishings	0.14 DESHR	0.08 DESHR
Gear	0.04 DESHR	0.04 DESHR
Propulsion	0.06 DESHR	0.05 DESHR
Controls	0.09 DESHR	0.09 DESHR
Environmental Control	0.05 DESHR	0.05 DESHR
Hydraulic/Pneumatic	0.05 DESHR	0.06 DESHR
Reliability	0.01 DESHR	0.01 DESHR
Armament	0	0.03 DESHR
Electrical/Electronic Design	0.14 DESHR	0.18 DESHR
Design Support		
Lines/Loft	$K_M \times 0.15$ DESHR	$K_M \times 0.16$ DESHR
Drafting/Isometrics	$K_M \times 0.02$ DESHR	$K_M \times 0.02$ DESHR
Checking/Release	$K_M \times 0.06$ DESHR	$K_M \times 0.06$ DESHR
Liaison/Support Design	$K_M \times 0.02$ DESHR	$K_M \times 0.02$ DESHR
Technical Support		
Stress	$K_M \times 0.16$ DESHR	$K_M \times 0.16$ DESHR
Weights	$K_M \times 0.06$ DESHR	$K_M \times 0.06$ DESHR
Aero	$K_M \times 0.05$ DESHR	$K_M \times 0.05$ DESHR
Dynamics	$K_M \times 0.08$ DESHR	$K_M \times 0.08$ DESHR
Thermo	$K_M \times 0.08$ DESHR	$K_M \times 0.08$ DESHR
Test Lab	$K_M \times 0.10$ DESHR	$K_M \times 0.10$ DESHR
Electrical	$K_M \times 0.06$ DESHR	$K_M \times 0.06$ DESHR
Staff	$K_M \times 0.01$ DESHR	$K_M \times$ DESHR
Predesign	$K_M \times 0.02$ DESHR	K_M 0.02 DESHR
Standards/Specs./Publications	$K_M \times 0.06$ DESHR	$K_M \times 0.06$ DESHR
ENGRMD =	$\sum$	$\sum$

where

W_{TM} = weight of liquid methane tankage

W_{IM} = weight of liquid methane insulation

W_{PM} = weight of liquid methane propellant feed and management

K_M = liquid methane system multiplying factor and is derived by the equation:

$$K_M = 1.0 + \frac{9375(W_{TM})^{.50} + 4050(W_{IM})^{.50} + 37500(W_{PM})^{.50}}{1.03\ ENGRHR}$$

Sustaining engineering hours are computed and output based on the total number of shipsets. G. S. Levenson and J. M. Barro found the sustaining hours were not systematically a function of aircraft physical or performance characteristics, and hence could be represented by the equation (Reference 1):

SUSEHR = ENGRHR * (SHPSET ** 0.20 - 1.0)

where

SHPSET is the total number of aircraft shipsets produced.

Sustaining engineering for a given production lot may be computed from:

SUSEH(N) = ENGRHR * (SHP(N) ** 0.20 - SHP(M) ** 0.20)

where

M+1 is the ship number of the first ship in the lot

and

N is the ship number of the last ship in the lot.

Engineering hours are assumed to be a function of aircraft performance and not directly a function of material or type of construction. Engineering hours for advanced composite structures, in particular, are assumed to be initially the same as for aluminum structures. However, the number of hours is expected to decrease later with learning (Reference 8). This assumption is based on the fact that composite structures are charcterized by fewer parts but by a higher degree of learning.

In general, adjustments to engineering hours to reflect unusual material or structural arrangements can be handled through the use of the engineering configuration complexity factor CONFAK. This factor has a nominal value of 1.0, which can be changed at the users option by direct input.

10.3.2 Engineering Labor Rate. Engineering labor rate may be input directly as a user option. If a value is not input a rate is computed based on the reference year. A single rate is applied to all engineering tasks.

To derive the equations for engineering labor rate, the rate data from several literature sources were plotted versus time (Figure 10-6). The data utilized were a composite rate composed of direct, indirect, general and administrative, and allocations charges. An average rate was derived for each of the years plotted and a smooth curve was faired through the average values in three segments. Equations were derived to fit each segment as a function of year, resulting in the following:

YR < 68	ERATE = .5129 * YR - 22.308
68 ≤ YR < 70	ERATE = 2 * YR - 123
YR ≥ 70	ERATE = 17 * (1 + EIFAC) ** (YR - 70)

where

EIFAC is an annual rate of inflation of the engineering labor rate, which has an estimated value of 0.06 but should be input based on prevailing conditions

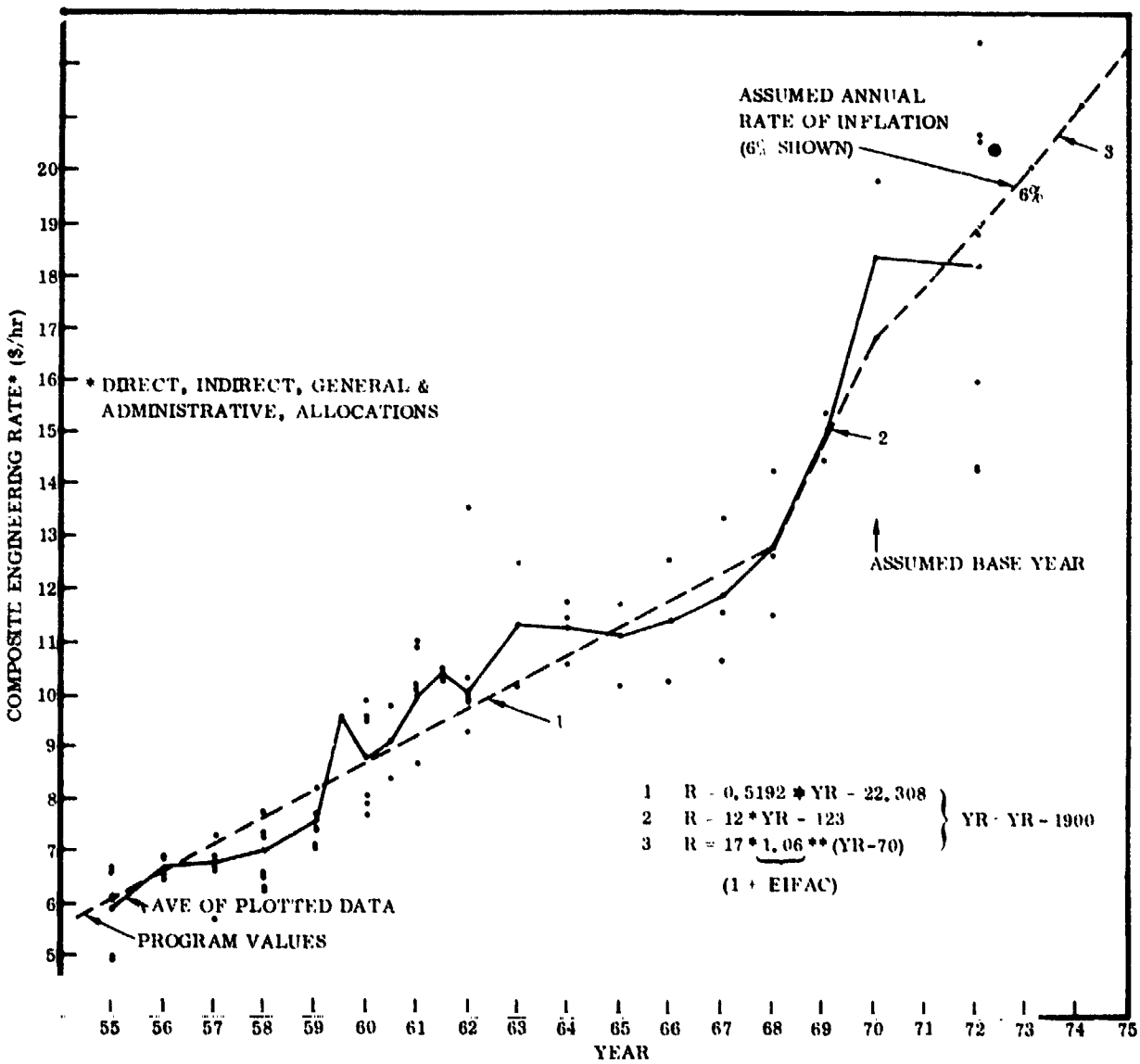

Figure 10-6 Engineering Labor Rate Versus Year

10.4 TOOLING COSTS

10.4.1 Tooling Cost Derivation. Tooling costs are comprised of three primary elements. They are: basic tooling, which is the first level of tooling designed to support the initial production lot at the initial production rate; rate tooling, which is the second level of tooling established to support the remainder of the production schedule at the maximum production rate; and sustained tooling, which is the tooling effort required to support the entire production schedule by providing for tool maintenance and producibility charges.

Each of the three tooling elements can, in turn, be broken down into manufacturing, engineering, and materials. Tool manufacturing includes the following: tooling machine shop, template shop, plastic pattern shop, foundry, jigs and fixtures, tool and die, form blocks, and plastics. Tool engineering includes tool design, tool and operations planning, tool project engineering, numerical control programming, tool liaison, production control, and proofing. Tooling materials include materials and graphic reproduction support. A summary of the tooling cost breakdown is listed in Table 10-14.

Table 10-14 Summary of the Tooling Cost Breakdown

Non Recurring Tooling
Basic Tooling
Manufacturing
Engineering
Material
Rate Tooling
Manufacturing
Engineering
Material
Recurring Tooling
Sustaining Tooling
Manufacturing
Engineering
Material

Tooling costs are computed as a function of the number of basic tooling manufacturing hours (BTMH), initial and sustaining production rates (RI and RS), and tool manufacturing and engineering labor rates (TRATEM and TRATEE). Following are the equations used (References 1 and 2):

Basic Tooling Costs

```
BMFGS  = 1.00 * BTMH * BTMH * TRATEM * RI ** .4
BENGRS =  .40 * BTMH * TRATEE * RI ** .4
BMATLS = 1.20 * BTMH * RI ** .4
```

Rate Tooling Costs

```
RMFGS  =  .10 * BTMH * TRATEM * (RS ** .4 - RI ** .4)
RENGRS = .015 * BTMH * TRATEE * (RS ** .4 - RI ** .4)
RMATLS = .120 * BTMH * (RS ** .4 - RI ** .4)
```

Sustaining Tooling Costs

```
SMFGS    = 1.00 * BTMH * SUMFAC * TRATEM * RS ** .4
SENGRS   =  .50 * BTMH * SUMFAC * TRATEE * RS ** .4
SMATLS   =  .90 * BTMH * SUMFAC * RS ** .4
```

where

SUMFAC is a production rate factor discussed below.

Basic tooling manufacturing hours are computed based on the number of dissimilar parts to be produced (DISPRT), the average number of tools required per dissimilar part (TOOLPP), and the average number of hours required to produce each tool (HRPTOO).

$$BTMH = CONFAC * DISPRT * TOOLPP * HRPTOO$$

where

CONFAC is a tooling configuration complexity factor discussed below.

A value for total number of dissimilar parts (DISPRT) can be input directly or in the absence of an input is calculated from the following (Reference 9):

$$DISPRT = 29.35 * AMPRWT ** 0.728$$

where

AMPRWT is the AMPR weight of the aircraft.

The equation is illustrated in Figure 10-7 . It is hoped that eventually the number of dissimilar parts can be derived directly from a parts count made in the parts definition portions of the program, rather than using a statistical derivation driven by weight.

A plot of total tools versus the number of dissimilar parts is shown in Figure 10-8 . A nominal value of 1.8 is used for the average number of tools required per dissimilar part (TOOLPP) in the absence of a direct input by the user. Figure 10-9 shows typical values of the average number of hours required to produce a tool (HRPTOO) plotted against numberof dissimilar parts. A nominal value of 49.0 is used by the program in the absence of a direct input. A summary of the data that was available for the analysis of tooling cost is presented in Table 10-15 .

The production rate factor (SUMFAC) represents a tool maintenance fraction, which is a function of the aircraft production rate and the number of shipsets produced. It is computed from the following:

$$SUMFAC = \sum_{i=LOTO}^{LOTS} (NOMO_i * Factor_i)$$

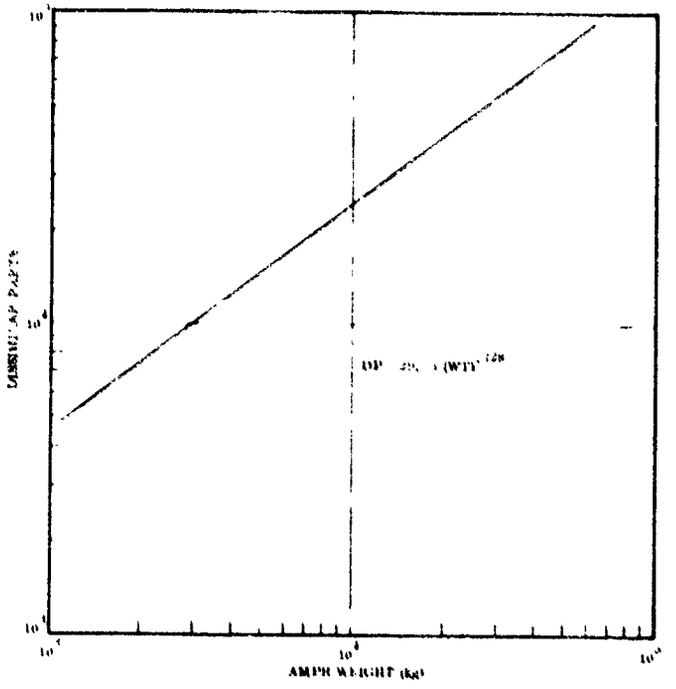

Figure 10-7 Number of Dissimilar Parts Versus AMPR Weight for the Complete Airframe

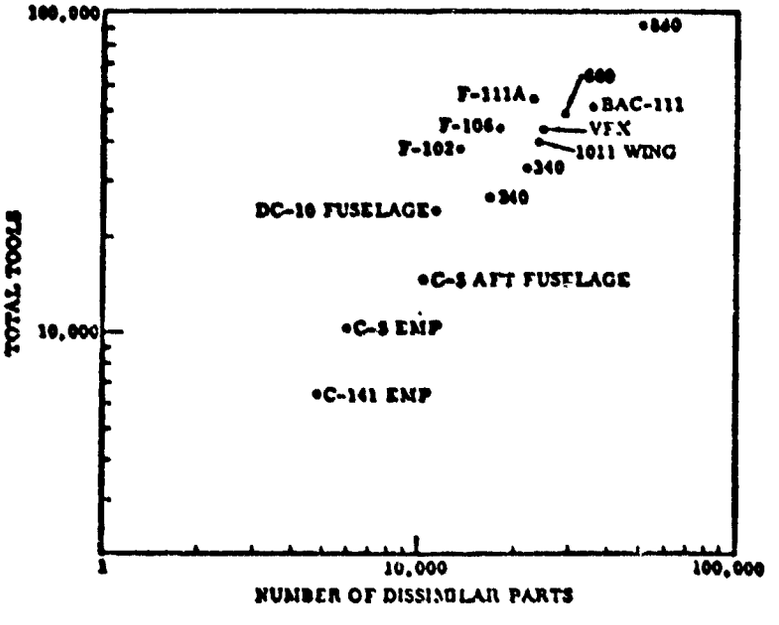

Figure 10-8 Number of Tools Required as a Function of Total Dissimilar Parts

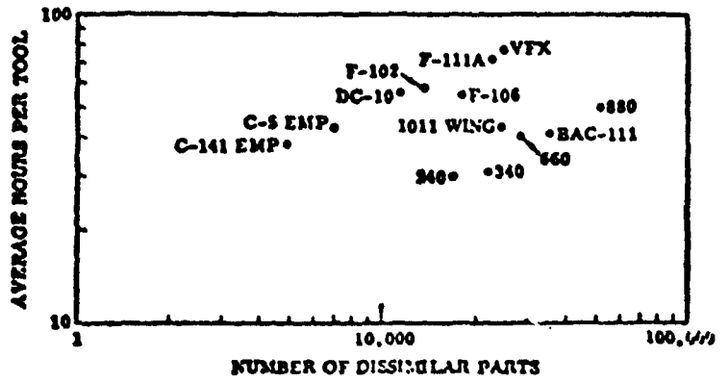

Figure 10-9 Average Number of Tooling Manufacturing Hours Required per Tool

Table 10-15 Summary of Tooling Cost Data used in the Analysis

Program	AMPR kg	Weight (lb)	Diss. Parts	Tools/ Part	Total Tools	Average Hr/Tool	Tool Mfg. Hr
A	9,017	(19,838)	16,785	1.51	25,400	29.6	751,734
B	9,851	(21,673)	22,000	1.51	33,200	31.0	1,029,820
C	29,864	(65,700)	51,000	1.77	90,181	50.2	4,526,110
D	39,614	(87,150)			66,154	45.0	2,986,930
E	5,488	(12,074)	13,815	2.62	36,191	58.0	2,099,772
F	6,835	(15,037)	18,166	2.31	42,060	55.7	2,341,320
G	14,923	(32,830)	35,866	1.44	51,751	40.6	2,100,000
H	2,767	(6,087)	4,871	1.30	6,315	38.4	242,363
I	5,381	(11,839)	6,077	1.72	10,439	41.4	432,059
J	19,268	(42,390)	24,020	1.69	40,506	43.8	1,772,730
K	13,000	(28,600)	28,800	1.70	48,960	40.0	1,958,400
L	8,301	(18,263)	10,709	1.36	14,569	31.8	559,440
M	14,795	(32,548)	22,741	2.34	53,000	71.0	3,775,000
N	11,530	(25,365)	24,300	1.7	42,200	77.0	3,250,000
O	15,075	(33,166)	11,367	2.13	24,174	55.0	1,314,467
P	7,045	(15,500)					2,165,600

where

$NOMO_i$ is the number of months required to produce the shipsets of LOT_i

$FACTOR_i$ is a factor computed from the curve of Figure 10-10

The number of months each lot is under production is computed by dividing the shipsets in each lot by the production rate corresponding to that lot. A value for FACTOR is taken from the curve of Figure 10-10 as follows: a value of 0.015 is

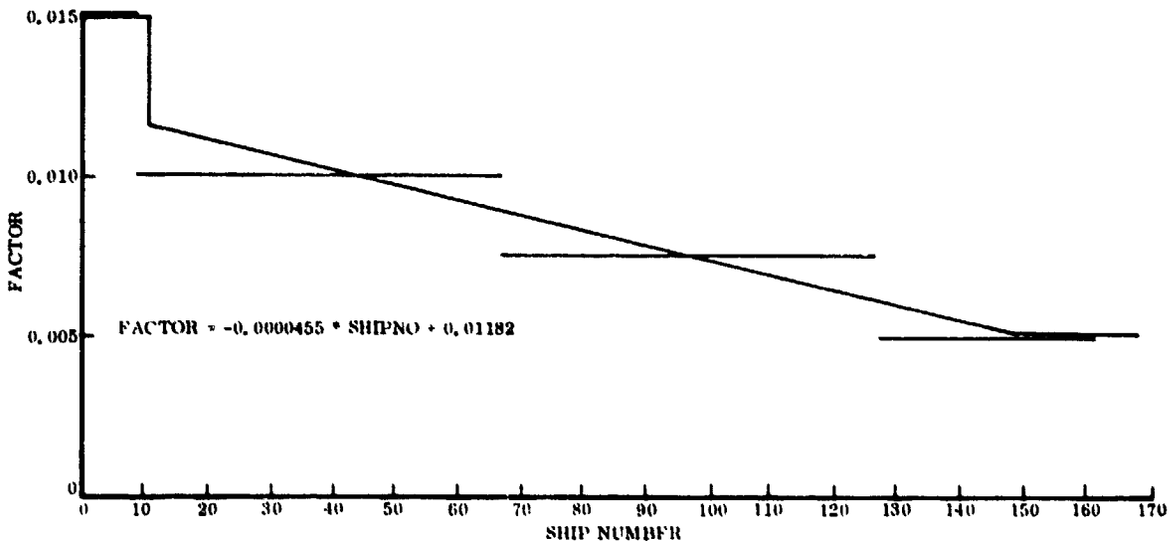

Figure 10-10 Plot of the Tooling Maintenance Factor per Month Versus Ship Number

used for the first lot, or the first 10 ships of the first lot if the total is greater than 10; for each successive lot up to ship number 150, and for the remaining ships of the first lot if the total is greater than 10, a value is computed using:

$$FACTOR_i = -0.0000455 * SHPNO_i + 0.01182$$

where

$SHPNO_i$ is the middle ship number of lot_i

For the remaining lots (above ship number 150) a value of 0.005 is used.

The tooling configuration complexity factor (CONFAC) was designed to account for different materials and structural arrangements. It has a nominal value of 1.0, which is used in the absence of a direct input. Table 10-16 lists some suggested values for the factor. It should be noted that an aircraft constructed of advanced composite materials was assumed to require 70% of the tooling necessary for a comparable metallic version (Reference 8).

Table 10-16 Suggested Input Values for Tooling Configuration Complexity Factor CONFAC

	Metallic	Combination Metallic/Composite	Composite
Simplified Design, Follow-on Subsonic	0.8	0.7	0.5
Regular Subsonic	1.0	0.9	0.7
Complex Subsonic; Simplified Design, Follow-on Supersonic	1.8	1.6	1.2
Regular Supersonic	2.2	1.9	1.5
Complex Supersonic	2.5	2.2	1.8

The initial and sustaining production rates (RI and RS) are given nominal values of 1.0 in the absence of a direct input. The initial production rate (RI) is assumed to encompass the production of the RDT&E (preproduction) and LOT1 ships, and the sustaining rate (RS) is assumed to encompass the remainder, LOT2 through LOT5. A summary of the tooling cost elements as related to the assumed production schedule is illustrated in Figure 10-11.

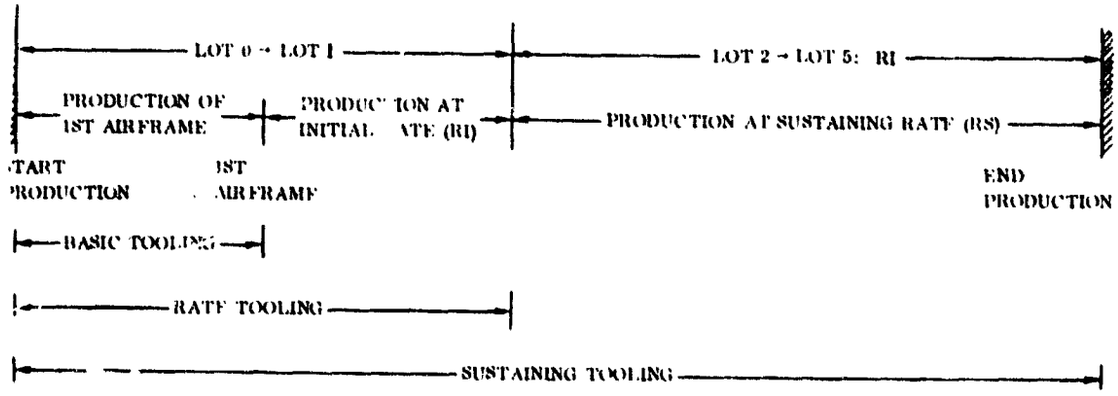

Figure 10-11 Summary of Tooling Cost Elements as Related to the Production Schedule

10.4.2 Tooling Labor Rates. Tool engineering and manufacturing labor rates may be input as a user option. If a value for either is not input, a rate is calculated based on the reference year.

To derive equations for tool engineering and manufacturing labor rates, rate data (combined average of engineering and manufacturing) from several literature sources

were plotted versus time (Figure 10-12). The data utilized were a composite rate composed of direct, indirect, general and administrative, and allocations charges. An average rate was derived for each of the years plotted and a smooth curve was

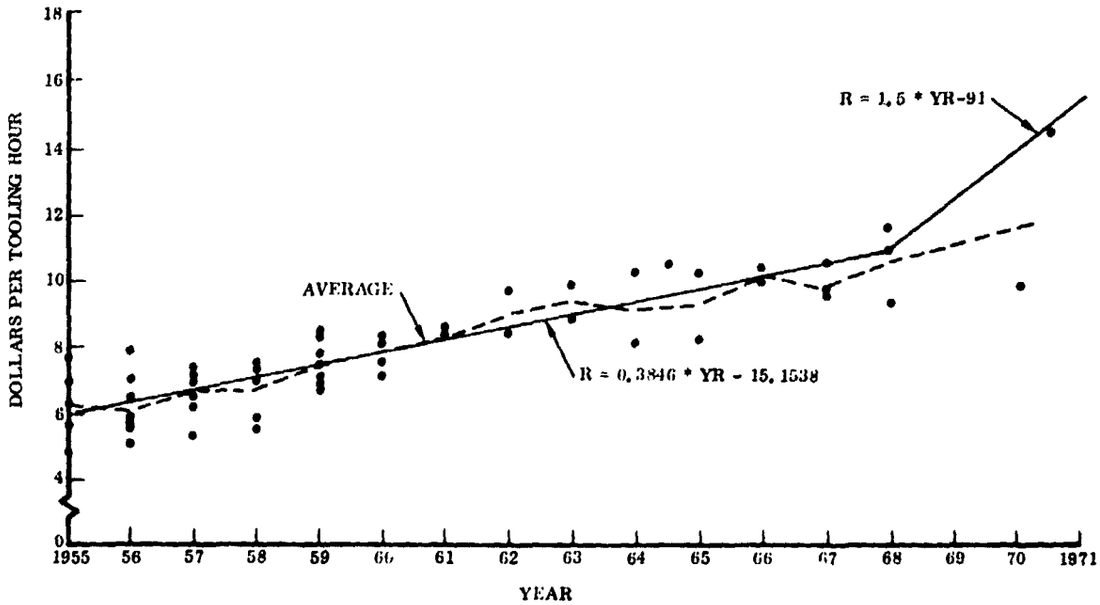

Figure 10-12 Tooling Labor Rate Versus Year

faired through the average values in three segments. Equations were derived to fit each segment as a function of year, resulting in the following:

YR < 68	RATE = 0.3846 * YR - 15.1538
68 ≤ YR ≤ 70	RATE = 1.5 * YR - 91
YR > 70	RATE = 14 * (1 + TIFAC) ** (YR - 70)

where

TIFAC is an annual rate of inflation of the tooling labor rate, which has a nominal value of 0.06 but may be input as an option

The resultant value for labor rate is then adjusted to correspond to either the engineering or manufacturing areas of tooling cost. It was found that tool engineering and tool manufacturing labor rates are usually separated by about 7%. For this reason the average calculated labor rate is increased by 3.5% to derive a tool engineering rate, and decreased by 3.5% to derive a tool manufacturing rate.

TRATEE = 1.035 * RATE

TRATEM = 0.965 * RATE

10.5 TOTAL VEHICLE PROGRAM COSTS. The total vehicle program costs are computed based on a cost model that was assembled primarily utilizing the work of R. E. Kenyon (Reference 2). The model incorporates a general format similar to that used by Kenyon although equations taken from the referenced literature have been substituted in several places. Where possible values for various cost elements that have been computed elsewhere in the program are brought across. These include first unit manufacturing costs (wing, body, horizontal, vertical, and nacelle), initial and sustaining engineering costs, basic tooling costs (basic tool engineering, manufacturing, and material) and rate and sustaining tooling costs. Table 10-17 summarizes the elements of the total vehicle program cost model.

Table 10-17 Total Vehicle Program Cost Model

NONRECURRING RDTE
- Precontract Funded Studies
- Airframe Development
  - Initial Engineering
  - Development Support
    - Engineering Material
    - Manufacturing Support and Material
    - Quality Control
  - Basic Tooling
    - Basic Airframe Tool Manufacturing
    - Basic Subsystem Tool Manufacturing
    - Basic Tool Engineering
    - Tooling Material
    - Manufacturing Development
    - Plant Engineering and Material
- Propulsion Development
- Avionics Development
- Systems Engineering and Management
- AGE Development and Procurement
- Training Equipment Development and Procurement
- Flight Test Operations
- Technical Data

Total Nonrecurring RDTE Costs

RECURRING RDTE AND PRODUCTION
- Production Airframe
  - Basic Structure
    - Wing
    - Body
    - Horizontal
    - Vertical
    - Nacelle
  - Subsystems
    - Gear
    - Surface Controls
    - Environmental Systems
    - Hydraulics/Pneumatics
    - Electrical/Electronics
    - Instruments
    - Armament
    - Engine Associated Equipment
    - Fuel System
    - Avionics Provisioning
    - Furnishings/Equipment
- Engine Production
- Avionics Production
- Armament
- Primary and Final Assembly
- Mission Equipment Installation
- Acceptance Operations
- Sustaining Engineering
- Rate Tooling
- Sustaining Tooling
- Spares for Test
- AGE for Test
- Technical Data
- Program Management

Total Flyaway Costs

- Support Costs
  - Initial Spares and Replenishment Parts
    - Airframe
    - Propulsion
    - Avionics
  - AGE for Production
  - Training Equipment
  - Test Aircraft Conversion
  - Category II and III Test Support

Total Support Costs

Total Program Costs

As part of the total vehicle cost derivation a learning curve approach is applied to first unit costs to compute the cost of any subsequent unit or production lot. The learning curve analysis assumes a constant slope for the cumulative unit average cost (cumulative total cost divided by cumulative number of shipsets) plotted against shipset. This, in effect, assumes that a percentage increase in production results in a constant percentage decline in the average unit cost. The cumulative average cost for all units through the Nth unit then can be presented as a function of the first unit cost (FUC) and the learning curve slope (S) as follows:

cumulative average cost = FUC * N ** B

where

B = ALOG (S)/ALOG (2)

The corresponding total cost of N units is N times the cumulative average cost through Nth unit. The actual unit cost for the Nth unit is:

unit cost = FUC * (N ** (B+1) - (N-1) ** (B+1))

≈ FUC * (B+1) * N ** B for N > 16

Total vehicle cost elements, which are input directly, are summarized in Table 10-18 The remaining items are computed by cost estimating relationships (CER's) or by a combination of detail hours and rates plus cost estimating relationships (CER's).

Table 10-18 Total Vehicle Cost Elements Established by Direct Input

Precontract Funded Studies
Systems Engineering and Management
Training Equipment Development and Procurement
Avionics Production
Program Management
Category II and III Test Support

The user has the option of developing the first unit manufacturing cost (wing, fuselage, empennage, and nacelles) utilizing the detailed approach described in Section 10.1 or by the cost estimating relationship (CER) method described in Section 10.2 .

The following vehicle program costs are accounted for by cost estimating relationships (CER's). These cost estimates are additive to the first unit manufacturing cost for wing, fuselage, empennage, and nacelles independent of how it was developed (detail or theoretical).

Engineering Material

C = FE2 (ENGRS)

where

FEC = Engineering material cost as a fraction of initial engineering cost.

ENGRS = Total initial engineering cost

Manufacturing Support and Material

$$C = 18.76\ (ENGRHR)\ (1 + EIFAC)^{(Year-1970)}$$

where

ENGRHR = Total number of initial engineering hours

EIFAC = Annual rate of inflation of engineering labor rates

YEAR = Actual year of cost projection

Quality Control

$$C = MRATE\ [FQ1\ (ENGRHR) + FQ2\ (TOOLHR)]$$

where

MRATE = Quality control labor rate

FQ1 = Quality control manufacturing support hours as a fraction of initial engineering hours

ENGRHR = Total number of initial engineering hours

FQ2 = Quality control tool inspection hours as a fraction of tool manufacturing hours

TOOLHR = Sum of basic tool manufacturing and rate tooling hours for airframe and subsystems

Basic Subsystem Tool Manufacturing

$$C = STF\ (CMT)(WTSYS)^{CS}$$

where

STF = Subsystem tool factor

CMT = Subsystem development complexity factor

WTSYS = Total vehicle subsystem weight

CS = Subsystem development scaling exponent

Manufacturing Development

$$C = FT4\ (TOOLHR)\ (MRATE)$$

where

FT4	=	Manufacturing development hours as a fraction of tool manufacturing hours
MRATE	=	Quality control labor rate
TOOLHR	=	Sum of basic tool manufacturing and rate tooling hours for airframe and subsystems

Plant Engineering and Material

$$C = FT3\ (TOOLHR)\ (MRATE + 2.00)$$

where

FT3	=	Plant engineering hours as a fraction of tool manufacturing hours
MRATE	=	Quality control labor rate
TOOLHR	=	Sum of basic tool manufacturing and rate tooling hours for airframe and subsystems

Propulsion Development

$$C = 29500000.0\ (FP/1000)^{0.55}\ (MACHND)^{0.66}\ (SHP(6))\ (QENG)\ (1 + SPRS)^{0.1}$$

where

FP	=	Total sea level thrust
MACHND	=	Mach number
SHP(6)	=	Total number of shipsets to be produced
QENG	=	Total number of engines per aircraft
SPRS	=	Engineering spares factor as a fraction of initial engineering unit required

Avionics Development

$$C = 55000000.0\ (WI)^{0.439} + 375000.0\ (WAV)^{0.439}$$

where

WI	=	Total weight of vehicle instruments
WAV	=	Total weight of vehicle avionics

AGE Development and Procurement

$$C = 0.05\ (ADDE) + 0.15\ (FV)$$

where

FV	=	Total aircraft production cost
ADDE	=	Sum of precontract funded studies and initial engineering costs

Flight Test Operations

$$C = 0.75\ (SHP(6))^{1.1}\ (TAKOFF)^{0.08}\ (VELALT)^{0.9}$$

where

SHP(6)	=	Total number of shipsets to be produced
TAKOFF	=	Vehicle gross takeoff weight
VELALT	=	Maximum velocity at cruise altitude

Technical Data

$$C = 0.02\ (FV)$$

where

FV = Total aircraft production cost

Subsystems	Subsonic	Supersonic
Landing Gear	$C = 1440\ W_L^{.70}$	$C = 1440\ W_L^{.70}$
Surface Controls	$C = 2240\ W_S^{.70}$	$C = 5760\ W_S^{.70}$
Hydraulics-Pneumatics	$C = 3200\ W_H^{.70}$	$C = 3200\ W_H^{.70}$
Electrical	$C = 2400\ W_{EL}^{.70}$	$C = 2400\ W_{EL}^{.70}$
Furnishings and Equipment	$C = 2000\ W_{FE}^{.70}$	$C = 2000\ W_{FE}^{.70}$
Environmental Control	$C = 1920\ W_{EC}^{.70}$	$C = 2800\ W_{EC}^{.70}$
Auxiliary Power	$C = 1520\ W_{AP}^{.70}$	$C = 1520\ W_{AP}^{.70}$

Instruments and Displays	$C = 6400\ W_I^{.70}$	$C = 6400\ W_I^{.70}$
Fuel System	$C = 2080\ W_{FU}^{.70}$	$C = 2080\ W_{FU}^{.70}$
Engine Associated Equipment	$C = 1600\ W_{EA}^{.70}$	$C = 1600\ W_{EA}^{.70}$
Armament	$C = 640\ W_A^{.70}$	$C = 640\ W_A^{.70}$
Avionics Provisions	$C = 1500\ W_{AV}^{.70}$	$C = 1500\ W_{AV}^{.70}$
Hydrogen:		
Tankage	$C = 3175\ W_{TH}^{.70}$	$C = 4762\ W_{TH}^{.70}$
Insulation	$C = 1905\ W_{IH}^{.70}$	$C = 2857\ W_{IH}^{.70}$
Propellant Feed & Management	$C = 11200\ W_{PH}^{.70}$	$C = 11200\ W_{PH}^{.70}$
Methane:		
Tankage	$C = 1587\ W_{TM}^{.70}$	$C = 2380\ W_{TM}^{.70}$
Insulation	$C = 952\ W_{IM}^{.70}$	$C = 1428\ W_{IM}^{.70}$
Propellant Feed & Management	$C = 5600\ W_{PM}^{.70}$	$C = 5600\ W_{PM}^{.70}$

where

W_L	=	Total weight of landing gear
W_S	=	Total weight of surface controls
W_H	=	Total weight of hydraulics-pneumatics
W_{EL}	=	Total weight of electrical
W_{FE}	=	Total weight of furnishings and equipment
W_{EC}	=	Total weight of environmental control
W_{AP}	=	Total weight of auxiliary power
W_I	=	Total weight of instruments and displays
W_{FU}	=	Total weight of fuel system
W_{EA}	=	Total weight of engine associated equipment

W_A = Total weight of armament

W_{AV} = Total weight of avionics provisions

W_{TH} = Total weight of hydrogen tankage

W_{IH} = Total weight of hydrogen insulation

W_{PH} = Total weight of hydrogen propellant feed and management

W_{TM} = Total weight of methane tankage

W_{IM} = Total weight of methane insulation

W_{PM} = Total weight of methane propellant feed and management

Engine Production

$$C = 3270\ (CFENG)\ (FP)^{0.60} \qquad \text{(for JP fuel)}$$

$$C = 3270\ (CFENG)\ (FP)^{0.60}(CRFH) \qquad \text{(for hydrogen fuel)}$$

$$C = 3270\ (CFENG)\ (FP)^{0.60}\ (CRFM) \qquad \text{(for methane fuel)}$$

where

CFENG = Engine complexity factor

FP = Maximum sea level thrust

CRFH = Cryogenic conversion factor for hydrogen (use 1.1 for turbofan and 1.2 for turbofan with afterburner)

CRFM = Cryogenic conversion factor for methane (use 1.05 for turbofan and 1.1 for turbofan and afterburner)

Primary and Final Assembly

$$C = FFA\ (CFUAF + CFUSS)$$

where

FAA = Ratio of mission equipment installation cost to the sum of first unit cost of avionics and armament

CFUAF = First unit cost of airframe

CFUSS = First unit cost of subsystems

Mission Equipment Installation

$$C = FAA\ (CFUAV + CFUAR)$$

where

FAA	=	Ratio of mission equipment installation cost to the sum of first unit cost of avionics and armament
CFUAV	=	First unit cost of avionics
CFUAR	=	First unit cost of armament

Acceptance Operations

$$C = FAO\ (CFUAF + CFUAV + CFUENG + CFUINS + CFUSS + CFUSSY)$$

where

FAO	=	Ratio of the acceptance operations cost to the sum of the airframe total cost minus acceptance operation cost plus propulsion system cost plus avionic cost
CFUAF	=	First unit cost of airframe
CFUAV	=	First unit cost of avionics
CFUENG	=	First unit cost of propulsion system
CFUINS	=	Cost of mission equipment installation
CFUSS	=	First unit cost of subsystems
CFUSSY	=	Total of primary and final assembly cost

Spares for Test

$$C = [F3\ (AFT) + F4\ (ENG) + A15\ (AV)]/(SHP(6))^{0.7}$$

where

F3	=	Factor for airframe spares for testing
AFT	=	Airframe production cost
F4	=	Factor for propulsion spares for testing
ENG	=	Propulsion system production cost
A15	=	Factors for avionics spares for testing
AV	=	Avionics production cost
SHP(6)	=	Total number of shipsets to be produced

Age for Test

$$C = P2\ (AGTA)\ (AFT) + P4\ (AGTP)\ (ENG) + P6\ (AGTV)\ (AV)$$

where

P2	=	Airframe age set cost as a fraction of airframe production cost
AGTA	=	Number of airframe age sets for testing
AFT	=	Airframe production cost
P4	=	Propulsion age set cost as a fraction of propulsion system production cost
AGTP	=	Number of propulsion age sets for testing
ENG	=	Propulsion system production cost
P6	=	Avionics age set cost as a fraction of avionics production cost
AGTV	=	Number of avionics age sets for testing
AV	=	Avionics production cost

Technical Data

$$C = F11\ (ATOT)$$

where

F11	=	Technical data cost factor as a fraction of the sum of airframe, avionics, and propulsion system production costs.
ATOT	=	Sum of airframe, avionics, and propulsion system production cost

Airframe Spares and Replenishment parts

$$C = F5\ (AFT)$$

where

F5	=	Airframe spares cost factor as a fraction of airframe production cost
AFT	=	Airframe production cost

Propulsion Spares and Replenishment Parts

$$C = F6\ (ENG)$$

where

F6	Propulsion spares cost factor as a fraction of propulsion system production cost
ENG	Propulsion system production cost

Avionics Spares and Replenishment Parts

$$C = F7\ (AV)$$

where

F7	Avionics spares cost factor as a fraction of avionics production cost
AV	Avionics production cost

Age for Production

$$C = F8\ (1 + F9)\ (ATOT)$$

where

F8	Age cost factor as a function of the sum of airframe, avionics, and propulsion system production cost
F9	Age spares cost factor as a fraction of primary age required for spares
ATOT	Sum of airframe, avionics, and propulsion system production cost

Training Equipment

$$C = F10\ (ATOT)$$

where

F10	Training equipment cost factor as a fraction of the sum of airframe, avionics, and propulsion system production cost
ATOT	Sum of airframe, avionics, and propulsion system production cost

Test Aircraft Conversion

C = F12 (ATOT)

where

F12	=	Test aircraft conversion cost factor as a function of the sum of airframe, avionics, and propulsion system production cost
ATOT	=	Sum of airframe, avionics, and propulsion system production costs

10.6 RETURN-ON-INVESTMENT ANALYSIS

10.6.1 Direct Operating Cost. The direct operating cost computation requires as input the aircraft price, as previously computed in the total vehicle cost module, and aircraft performance, defined principally as fuel and time required for various distance increments up to the operational range. The input when applied to the 1967 Air Transport Association formula (Reference 10) develops direct operating cost elements for specified distance increments. The Air Transport Association formula provides the basis to compute crew cost (primarily a function of the number in the cockpit crew), time to cover specified distances, and aircraft gross weight. Fuel and oil costs are computed directly from block fuel required. Insurance (hull insurance only, liability is an indirect cost) is computed as an annual percentage of the aircraft price. Maintenance is computed as a function of time, weight, thrust, and hardware cost. Depreciation is computed for a specified number of years, and includes depreciation of spares as well as primary flight equipment. The resultant output is direct operating cost per aircraft mile and per available seat block for various distances up to the operational range of the airplane.

The logic flow of the equations that make up the direct operating cost methodology can be described as shown in Figure 10-13. The direct operating cost, in terms of dollars/mile, is developed for a specific aircraft for various distances up to the operational range of the vehicle. As shown in Figure 10-13, the direct operating costs are determined basically by the original cost of the aircraft and the costs that are accrued on the basis of hours of use and passage of time. The aircraft cost is determined from other parts of the model that essentially define the vehicle based on specific performance criteria. The hourly costs that are the result of actually using the aircraft are made up of crew pay, fuel and oil and maintenance. The crew pay is determined by the block time expended from engine to start up to shut down. The fuel and oil costs are determined by the total quantity of block fuel required for a specific flight distance. The maintenance costs are determined primarily by flight hours and flight cycles. The longer flights have relatively lower maintenance costs per mile

Figure 10-13 Direct Operating Cost Logic Flow

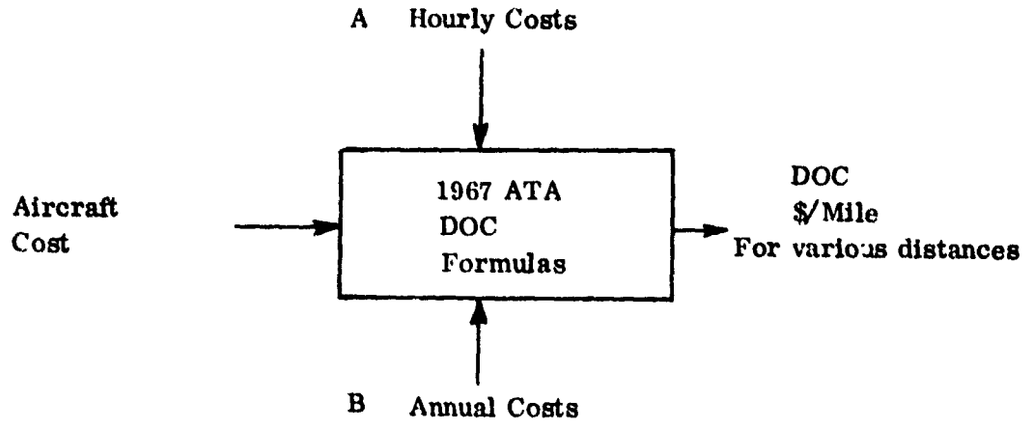

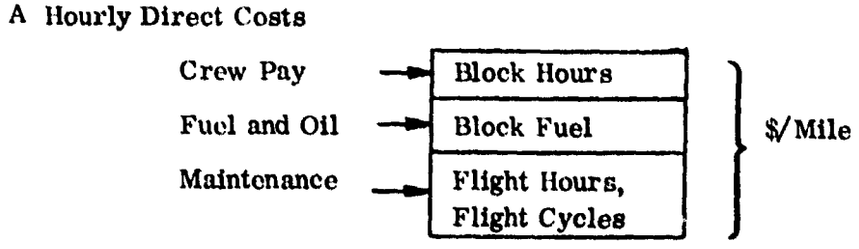

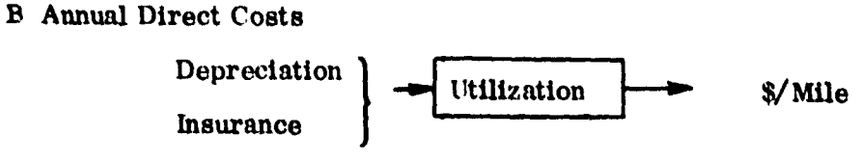

because of a smaller increment of cost associated with takeoff and landing. The annual direct costs which accrue, regardless of whether the aircraft is flown, are depreciation and insurance. By determining the annual utilization of an aircraft in terms of miles per year the annual costs can be dealt with on a dollars/mile basis.

In the direct operating cost area, the fuel cost and maintenance costs are affected by a decision to use methane or hydrogen fuel. The fuel costs in the ATA formulation are calculated from the block fuel and require as an input the unit fuel cost in $/gal. Projections of fuel costs into the 1980's time frame vary considerably. Specific values for JP, liquid methane or hydrogen can be input to the model, or sensitivity studies can be performed for various assumptions about unit fuel costs. Without other data, the following ranges of fuel cost for the 1980's time frame are appropriate.

1980's Time Frame

JP $/M^3 ($/gal)	31.7 - 95.11	(.12 - .36)
Methane $/M^3 ($/gal)	29.06 - 58.12	(.11 - .22)
H_2 $/M^3 ($/gal)	19.81 - 79.26	(.075 - .30)

The maintenance portion of the direct operating cost module is affected to some degree by the cleaner burning characteristics of hydrogen fuel engines. A detailed maintenance analysis would be needed to establish the extent of this cost impact. In contrast with the above decrease in maintenance costs, the cryogenic tankage and insulation systems would increase the maintenance associated with the airframe. Because of these counterbalancing uncertainties and the lack of any detailed analysis on which to presently make changes, the existing maintenance direct cost methodology has been left unchanged.

10.6.2 Indirect Operating Cost. In the indirect cost area, two cost elements are impacted by the choice of fuel. Aircraft servicing costs would be increased by the necessity for increased quantity and quality of personnel required to fuel aircraft with cryogenic fuels. The increased sophistication of cryogenic fuel technology requires additional manning for fuel handling and monitoring hardware due to the essentially different physical properties of cyrogenic fuels and increased safety requirements. In addition to the manpower to use the above equipment, provisions would have to be made for maintenance, depreciation and amortization of such equipment. The assessment of these effects in quantitative terms requires a maintenance and operations analysis that is beyond the scope of this current research effort. The current return on investment module continues to use the original Lockheed formulas (Reference 11) for determination of indirect operating costs by city pair for such factors as aircraft servicing, stewardess expense, food, reservations and sales, baggage handling, and general and administrative expenses.

10.6.3 Return-on-Investment. To compute return-on-investment data, a comparison is made between revenue and direct plus indirect operating costs. City pair traffic data, distances, and fare formula establish the revenue of interest. Aircraft capacity, frequency, and load factor constraints determine the required flight frequency, indirect costs, and fleet size.

To compute return-on-investment, total income minus total cost is compared to total investment as determined by fleet size, aircraft price, and spares factors. Return-on-investment is calculated as that percentage return on net invested capital (initial investment minus cash flow from depreciation) that would equal the same percentage return on fixed return investment, such as accrual savings deposit. Return-on-investment is computed for each city pair and for the entire system. In this way, it is possible to establish the traffic and distance requirements to make a given aircraft profitable and to make a meaningful comparison between two airplanes where seating capacity, performance, and price are different.

10.7 REFERENCES

1. Levenson, G. S., Barro, J. M., "Cost Estimating Relationships for Aircraft Airframes," Rand Report RM-4845-PR (Abridged), May 1966.

2. Kenyon, R. E., "Techniques for Estimating Weapon System Structural Costs," Air Force Report AFFDL-TR-71-74, July 1971.

3. Willis, William S., "Space Shuttle Airbreathing Engine Study," NASA CR-120793, September 1971.

4. Moore, H. G., Bucknell, R. L., "Space Shuttle Orbiter/Booster Air-breathing Engine Study," NASA CR-120862, PWA FR-4803, December 1971.

5. "Computer Program to Perform Cost and Weight Analysis of Transport Aircraft," (NAS 1-11343) NASA CR 132362, November 1973.

6. General-Dynamics/Convair Aerospace Division, "Centaur Cost-Technical and Programmatic Data Study," CASD-NAS73-007, Vol. I, II. Appendix, September 1973.

7. The Aerospace Corporation, "Space Transport System Cost Methodology", TOR-0059 (6759-04)-1, Vol. 1, August 1970.

8. "Study of the Application of Advanced Technologies to Long Range Transport Aircraft," NASA Report CR 112090, May 1972.

9. Benson, R. L., Seiden, E. I., "Cost Element Research, Convair Aerospace Report GDC-ERR-1379, December 1967.

10. "Standard Method of Estimating Comparative Direct Operating Costs of Turbine Power Aircraft", Air Transport Association of America, December 1967.

11. Lockheed Aircraft Corporation, "A Proposed Standard Method for Calculating Airline Indirect Operating Costs," Report LW-70-500R, May 1970.

SECTION 11

COMPUTER PROGRAM

11.1 PROGRAM CAPABILITIES

This program has been designed in a modular fashion to provide users application flexibility, as well as providing ease of update and modification. Each of the modules is composed of many subroutines coupled together to perform the required functions.

The program driver "WTSIZ" acts as the main control routine for the total program. It establishes a logic flow for the program from beginning to end. The breakdown for the detail analysis version is subdivided into six primary modules (driver, vehicle synthesis, external loads, structural synthesis, parts definition, and cost synthesis). The preliminary analysis version has three primary modules (driver, vehicle synthesis, and cost synthesis).

The users manual encompasses seventeen volumes and addresses USER INSTRUCTIONS AND OPERATING INSTRUCTIONS. Volume one is the summary, Volume Two through Volume Four covers Vehicle Sizing, Volume Five is for External Loads, Volume Six is for Structural Synthesis, Volumes Seven through Ten cover Parts Definition, and Volume Eleven through Volume Seventeen covers the Cost Synthesis.

11.2 USAGE INSTRUCTIONS

The Vehicle Design Evaluation Program currently has two batch versions in operational status. One version is the "Detailed Analysis" capability which uses the vehicle sizing, external loads, structural synthesis, parts definition, and cost modules. The other is a "Preliminary Analysis" version which uses the vehicle sizing and cost estimating relationships (CER) modules. In both program versions the user has the option of using a mini-performance or a detailed mission and performance approach.

The input required for executing these programs and options is discussed in Section 4 of each volume of the users manual.

11.3 OPERATING INSTRUCTIONS

This computer program runs at NASA/Langley under the Network Operating System (NOS 1.1). The program operates with Scope 3.4 at General Dynamics. The NASA/Langley and the General Dynamics programs have been written for the FTN compiler.

The program at General Dynamics Convair under Scope 3.4, operates with approximately 72K octal cells of core and needs 2000 octal seconds of CP time for the compiler detail analysis program. The same program under NOS 1.1 at NASA/LRC will use approximately 75K octal cells of core and needs less than 500 seconds of CP time. This reduced time at NASA/LRC is due to the high speed CYBER 175 fronting the CDC 7600.

Instructions for operating the program are shown in Control Card form in Section 5 of each volume of the users manual. These control cards are shown for operating the program and the setup for modifications for both NASA/LRC and General Dynamics Convair.